

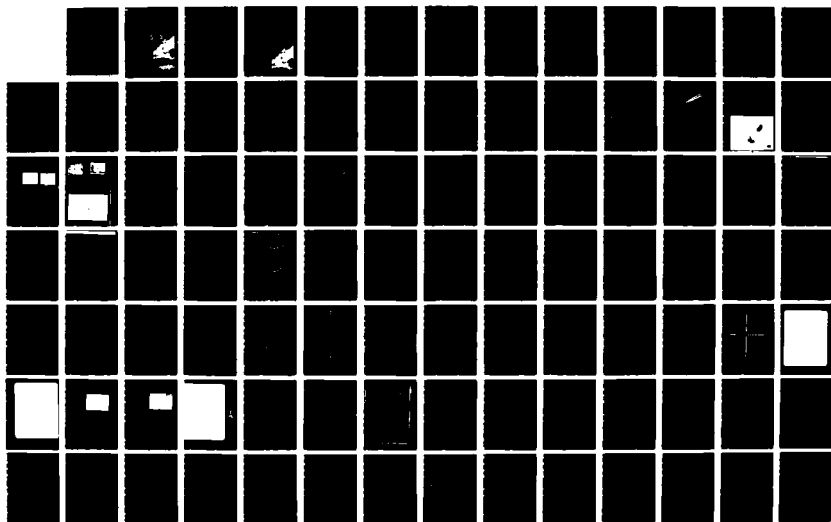
NO-A186 938

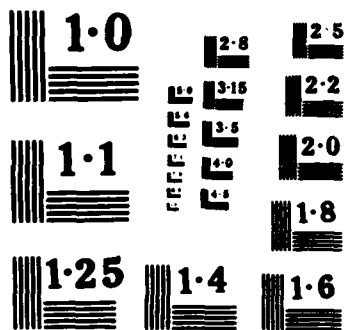
UNITED STATES - JAPAN SEMINAR ON QUANTUM MECHANICAL
 ASPECTS OF QUANTUM EL (U) MASSACHUSETTS INST OF TECH
 CAMBRIDGE RESEARCH LAB OF ELECTRON
 J H SHAPIRO ET AL OCT 87 N00014-87-G-0198 F/G 28/3

177

UNCLASSIFIED

NL





AD-A186 938

UNITED STATES - JAPAN SEMINAR
ON
QUANTUM MECHANICAL ASPECTS
OF QUANTUM ELECTRONICS

DTIC
ELECTE
NOV 25 1987
S H D

HILTON INN RESORT
MONTEREY, CALIFORNIA
JULY 21-24, 1987

J.H. SHAPIRO
H. TAKUMA
Coordinators



DISTRIBUTION STATEMENT A

Approved for public release;
Distribution Unlimited

87 11 10 052

**UNITED STATES – JAPAN SEMINAR
ON
QUANTUM MECHANICAL ASPECTS
OF QUANTUM ELECTRONICS**

**HILTON INN RESORT
MONTEREY, CALIFORNIA
JULY 21–24, 1987**

**J.H. SHAPIRO
H. TAKUMA
Coordinators**



Preface

The continuing rapid developments taking place in quantum electronics cut across a wide swath of research activities including atomic and solid-state physics, nonlinear optics and spectroscopy, and quantum light beams and quantum measurements. Strong research programs in these areas presently exist in the United States and Japan. These Proceedings represent summaries and viewgraphs from a U.S.-Japan Seminar entitled "Quantum Mechanical Aspects of Quantum Electronics," which was held from July 21 to July 24, 1987 at the Hilton Inn Resort in Monterey, California. The 1987 Seminar was the fourth in a series on quantum electronics which began in Hakone, Japan in 1977, with meetings in Maui, USA in 1980 and Nara, Japan in 1983. The previous seminars engendered valuable technical ties between researchers in the two countries, which were strengthened and expanded at the Monterey Seminar. The early meetings in the series were centered on the emerging techniques in nonlinear and high-resolution spectroscopy. At the Nara meeting, the emphasis shifted to include major consideration of quantum issues of coherence and incoherence. The 1987 Seminar focused on topics of very current interest, including: neutral atom trapping; ultrahigh stability sources and ultrahigh resolution spectroscopy; squeezed states of light; and nonlinear optics of semiconductors. The spirit and vibrancy with which these topics were discussed was a testimony to the vitality of the U.S.-Japan Seminars. We look forward to another such successful meeting in Japan in 1989.

Jeffrey H. Shapiro
Hiroshi Takuma

October 1987



DTIC TAB		<input checked="checked" type="checkbox"/>
Unannounced		<input type="checkbox"/>
Justification		
By _____		
Distribution/		
Availability Codes		
Dist	Avail and/or	
	Special	
A-1		

Acknowledgements

The 1987 U.S.-Japan Seminar on Quantum Mechanical Aspects of Quantum Electronics was principally supported by grants from the U.S. National Science Foundation and the Japan Society for the Promotion of Science. The preparation and distribution of these Proceedings was supported by the U.S. Office of Naval Research. Additional support for the Seminar arrangements came from the following Corporate Sponsors: Coherent Laser Products, Hoya Optics, IBM, Massachusetts Institute of Technology, Newport Corporation, and Spectra-Physics. Without the support obtained from all of these sources the 1987 Seminar would not have been so successful.

U.S.-JAPAN SEMINAR
Quantum Mechanical Aspects of Quantum Electronics

July 21 - July 24, 1987

Hilton Inn Resort
Monterey, California

PROGRAM

Tuesday July 21

Page No.

7:00 AM Continental Breakfast

Seminar Introduction

8:20 AM Welcoming Remarks
- J.H. Shapiro and H. Takuma

Session I - Manipulation and Spectroscopy of Atoms - J.L. Hall, Chairman

8:30 AM Optical Cooling and Trapping 13
- W.D. Phillips

9:10 AM Optical Trapping of Neutral Atoms and Dielectric Particles 36
by Radiation Pressure
- A. Ashkin, J.E. Bjorkholm, and S. Chu

9:50 AM Macroscopic Quantum Jumps in a Single Atom 70
- A. Schenzle and R.G. Brewer

10:30 AM Coffee Break

11:00 AM Laser Cooling of Neon Metastable States 90
- F. Shimizu, K. Shimizu, and H. Takuma

Session II - Nonlinear and Excitonic Optics I - D.S. Chemla, Chairman

11:40 AM Gigantic Optical Nonlinearity in Low Dimensional Systems 104
- E. Hanamura

12:20 PM Measurements of Optical Nonlinearities in MOCVD-Grown 117
GaAs/GaAlAs Multiple Quantum Wells
- E. Garmire

Session III - Stable Lasers - E. Garmire, Chairwoman

7:30 PM	Progress in Stabilized Lasers	128
	- J.L. Hall, D. Hils, C. Salomon, J.-M. Chartier, and N.C. Wong	
	Doppler-free Optical Multiplex Spectroscopy, with Stochastic Excitation	142
	- K.-P. Dinse, M. Winters, and J.L. Hall	
8:10 PM	Dynamic and Spectral Properties of Semiconductor Lasers with Quantum Well, Quantum Wire, and Quantum Box Structures	147
	- Y. Arakawa	
8:50 PM	Quantum Limited Linewidth of Semiconductor Lasers	
	- A. Mooradian	
9:30 PM	Ultrahigh Coherent Semiconductor Lasers and Their Applications to Rb Atomic Clocks	183
	- M. Ohtsu, K. Kuboki, and M. Hashimoto	

Wednesday July 22

7:00 AM Continental Breakfast

Session IV - Squeezed States I - Y. Yamamoto, Chairman

8:30 AM	Squeezed States in Degenerate Parametric Amplification Discussed by H. Takahasi in 1963	216
	- K. Shimoda	
9:10 AM	Squeezed States of Light	235
	- H.J. Kimble, R.J. Brecha, L.A. Orozco, M.G. Raizen, L.-A. Wu and, M. Xiao	
9:50 AM	Pulsed Squeezed Light	237
	- R.E. Slusher	
10:30 AM	Coffee Break	
11:00 AM	Quantum Nondemolition Detection and Squeezing in Optical Fibers	253
	- M.D. Levenson, R.M. Shelby, and S.H. Perlmuter	
11:40 AM	Quantum Nondemolition Detection	
	- N. Imoto	

Session V - Nonlinear and Excitonic Optics II - E.P. Ippen, Chairman

2:00 PM	Optical Properties of Quantum Well Structures with Electric Field: Lifetime-Free Switching of Luminescence Intensity and Virtual Charge-Induced Ultrafast Optical Nonlinearity - M. Yamanishi	268
2:40 PM	Why Lose Sleep Over II-VI Compound Semiconductor Superlattices? - S. Chang, Q. Fu, D. Lee, A. Mysyrowicz, A.V. Nurmikko, J.-W. Wu, R. Gunshor, and L. Kolodziejski	304
3:20 PM	Coffee Break	
3:50 PM	Enhanced Excitonic Optical Nonlinearity and Exciton Dynamics in Semiconductor Microstructures - T. Takagahara	321
4:30 PM	Free Carrier Nonlinear Optics - P.A. Wolff	327
7:00 PM	Cocktail Hour	
8:00 PM	Banquet	
9:30 PM	After-Dinner Presentation: Berry's Phase in Fiber Optics - R.Y. Chiao	344

Thursday July 23

7:00 AM Continental Breakfast

Session VI - Dynamic Studies in Semiconductors - E. Hanamura, Chairman

8:30 AM	High Density Femtosecond Excitation of Nonthermal Carrier Distributions in Intrinsic and Modulation Doped GaAs Quantum Wells - W.H. Knox, D.S. Chemla, and G. Livescu	364
9:10 AM	Dynamical Aspects of Carrier Tunneling in Semiconductor Superlattices - Y. Masumoto	377
9:50 AM	Experimental and Theoretical Studies of Coherent and Nonthermal Processes in Semiconductors Probed by Femtosecond Laser Techniques - N. Peyghambarian and S.W. Koch	396
10:30 AM	Coffee Break	

		<u>Page No.</u>
11:00 AM	Femtosecond Studies of Hot Carrier Relaxation in GaAs and AlGaAs - E.P. Ippen and J.G. Fujimoto	415
11:40 AM	Exciton Relaxation Phenomena in a Disordered System - M. Aihara	434
2:00 PM	Afternoon Outing: Tour of Monterey Bay Aquarium	

Session VII - Squeezed States II - M.D. Levenson, Chairman

7:30 PM	Generation of Number-Phase Minimum Uncertainty States - Y. Yamamoto, S. Machida, N. Imoto, M. Kitagawa, and G. Bjork	438
8:10 PM	Squeezing via Traveling-Wave Forward Four-Wave Mixing in Atomic Vapors: Comparison with Nondegenerate Theory - P. Kumar	451
8:50 PM	Generating Squeezed Microwave Radiation with a Josephson Parametric Amplifier - B. Yurke	476
9:30 PM	Detecting Squeezed States by Cross-Correlation - Z.Y. Ou, C.K. Hong, and L. Mandel	489

Friday July 24

7:00 AM Continental Breakfast

Session VIII - Spectroscopy, Instability and Multistability -

	- R.G. Brewer, Chairman	
8:30 AM	What Has Been Done and What Will Be Done by Subnatural Linewidth Spectroscopy - H. Takuma, K. Shimizu, and F. Shimizu	503
9:10 AM	Comprehensive Model for Laser Instability in a CO ₂ Laser with Gaseous Saturable Absorber - T. Shimizu, M. Tachikawa, and K. Tani	531
9:50 AM	Recent Progress in Optical Bistability and Tristability - T. Yabuzaki and M. Kitano	552
10:30 AM	Coffee Break	

Session IX - Quantum Light and Quantum Photodetection - B. Yurke, Chairman

11:00 AM	Nonclassical Lights - H.P. Yuen	575
11:40 AM	Quantum Statistics of Parametric Oscillators Above Threshold - D.F. Walls, M.J. Collett, A.S. Lane, M.D. Reid, and C.M. Savage	601
12:20 PM	Open Questions in Closed-Loop Photodetection - J.H. Shapiro	628

Principal Sponsors

National Science Foundation

Japan Society for the Promotion of Science

Proceedings Sponsor

U.S. Office of Naval Research

Corporate Sponsors

Coherent Laser Products

Hoya Optics

IBM

MIT

Newport Corporation

Spectra-Physics

Coordinators

J.H. Shapiro - U.S. Coordinator

D.S. Chemla - U.S. Co-Coordinator

H. Takuma - Japan Coordinator

U.S. — JAPAN SEMINAR

Quantum Mechanical Aspects of Quantum Electronics

July 21 - July 24, 1987

Hilton Inn Resort
Monterey, California

LIST OF PARTICIPANTS

Japanese Participants

M. Aihara	Department of Physics, Faculty of Liberal Arts, Yamaguchi University, Yamaguchi 753.
Y. Arakawa	Institute of Industrial Science, University of Tokyo Roppongi 7-22-1, Minato-ku, Tokyo.
E. Hanamura	Department of Applied Physics, University of Tokyo, 7-3-1 Hongo, Bunkyo-ku, Tokyo 113.
N. Imoto	NTT Basic Research Laboratories 3-9-7, Midori-cho, Musashino-shi, Tokyo 180.
S. Kano	Institute for Laser Science, University of Electro-Communications, 1-5-1, Chofugaoka, Chofu-shi, Tokyo 182.
Y. Masumoto	Institute of Physics, University of Tsukuba Sakura-mura, Niihari-gun, Ibaraki-ken, 305.
M. Ohtsu	Graduate School of Nagatsuta, Tokyo Institute of Technology, 1-15-42 Nagatsuta, Midori-ku, Yokohama 227.
F. Shimizu	Department of Applied Physics, University of Tokyo Bunkyo-ku, Tokyo 113.
K. Shimoda	Department of Physics, Keio University 3-4-1 Hiyoshi, Kohoku-ku, Yokohama 223.

Japanese Participants (contd)

M. Tachikawa Department of Physics, University of Tokyo
(T. Shimizu) 7-3-1 Hongo, Bunkyo-ku, Tokyo 113.

T. Takagahara NTT Electrical Communication Laboratories
 3-9-11 Midori-cho, Musashino-shi, Tokyo 180.

H. Takuma Institute for Laser Science,
 University of Electro-Communications, 1-5-1 Chofugaoka,
 Chofu-shi, Tokyo 182.

T. Yabuzaki Department of Physics, Kyoto University
 Sakyo-ku, Kyoto 606.

Y. Yamamoto NTT Electrical Communication Laboratories
 3-9-11 Midori-cho, Musashino-shi, Tokyo 180.

M. Yamanishi Department of Physical Electronics,
 Hiroshima University, Saijo-cho, Higashi-Hiroshima 724.

United States Participants

A. Ashkin AT&T Bell Laboratories, Holmdel, New Jersey 07733

R.G. Brewer IBM Almaden Research Center, 650 Harry Road,
 San Jose, California 95120.

R.Y. Chiao Department of Physics, University of California,
 Berkeley, California 94720.

D.S. Chemla AT&T Bell Laboratories, 4E418, Holmdel, New Jersey 07733

E. Garmire Center for Laser Studies, University of Southern
 California 1112, Los Angeles, California 90089.

United States Participants (contd)

J.L. Hall JILA National Bureau of Standards, 325 Broadway,
Boulder, Colorado 80303.

E.P. Ippen Department of Electrical Engineering and Computer Science,
Massachusetts Institute of Technology, Cambridge, Mass. 02139.

H.J. Kimble Department of Physics, University of Texas, Austin, Texas 78712.

S.W. Koch Optical Sciences Center, University of Arizona, Tucson,
Arizona 85721.

M.S. Kruger Laboratory for Physical Science, 4928 College Avenue,
College Park, Maryland 20740.

P. Kumar Department of Electrical Engineering and Computer Science,
Northwestern University, Evanston, Illinois 60201.

M.D. Levenson IBM Almaden Research Center, 650 Harry Road, San Jose,
California 95120.

M. Lindberg Optical Sciences Center, University of Arizona, Tucson,
Arizona 85721.

L. Mandel Department of Physics and Astronomy, University of Rochester,
Rochester, New York 14627.

A. Mooradian MIT Lincoln Laboratory, Lexington, Massachusetts 02173.

H. Nathel Lawrence Livermore National Lab, Mail Stop L-43, P.O. Box 807,
Livermore, California 94550.

A.V. Nurmikko Division of Engineering, Brown University, Providence,
Rhode Island 02912.

N. Peyghambarian Optical Sciences Center, University of Arizona, Tucson,
Arizona 85721.

United States Participants (contd)

W.D. Phillips National Bureau of Standards, Gaithersburg, Maryland 20899.
H. Pilloff Office of Naval Research, Code 1112L0, Arlington, Virginia
 22217.
B.L. Schumaker Jet Propulsion Laboratory, MS 200-122, 4800 Oak Grove Drive,
 Pasadena, California 91109.
J.H. Shapiro Department of Electrical Engineering and Computer Science,
 Massachusetts Institute of Technology, Cambridge, Mass. 02139.
R.M. Shelby IBM Almaden Research Center, 650 Harry Road, San Jose,
 California 95120.
R.E. Slusher AT&T Bell Laboratories 1D368, Murray Hill, New Jersey 07974.
P.A. Wolff Department of Physics, Massachusetts Institute of Technology,
 Cambridge, Massachusetts 02139.
N.C. Wong Research Laboratory of Electronics, Massachusetts Institute of
 Technology, Cambridge, Massachusetts 02139.
H.P. Yuen Department of Electrical Engineering and Computer Science,
 Northwestern University, Evanston, Illinois 60201.
B. Yurke AT&T Bell Laboratories 1C247, Murray Hill, New Jersey 07974.

Third Country Participants

D.F. Walls Physics Department, University of Waikato, Hamilton,
 New Zealand.
Ms. L.-A. Wu Department of Physics, University of Texas, Austin, Texas 78712.

OPTICAL COOLING AND TRAPPING

William D. Phillips, MET B258, National Bureau of Standards
Gaithersburg, MD 20899

(Summary of presentation at the U. S. - Japan Seminar on Quantum Mechanical Aspects of Quantum Electronics, Monterey, CA, July 1987)

Past and present collaborators on work done at NBS Gaithersburg are shown on the 1st slide. Many other groups throughout the world are active in this area and only a few are mentioned in this talk. The November 1985 issue of J. Opt. Soc. Am. B contains papers from many of these groups. A forthcoming article in Science by Phillips, Gould and Lett reviews much of the recent work.

Some of the motivations for the work are listed in slide 2. In particular, note that efforts to achieve Bose condensation in spin polarized hydrogen have been plagued by problems related to interactions between atoms at high density and atoms adsorbed on the walls of the container. Optical cooling and electromagnetic trapping may be able to address these problems because low temperatures can be achieved, allowing lower densities for Bose condensation, and in a container without material walls.

Slide 3 shows how the resolution of free-bound spectroscopy is limited by the kinetic energy spread of the free atoms. With laser cooled atoms, the free-bound spectroscopic resolution becomes about equal to bound-bound resolution. Slide 4 illustrates how the low energies of laser cooled atoms put collisions between them in a highly quantum mechanical regime, one which has not been investigated experimentally as yet.

The principle of laser cooling, proposed in 1975 and first demonstrated on trapped ions in 1978, is shown in slide 5. When the laser is tuned below resonance, the atoms absorb the light more strongly when they are moving toward the laser. This results in more absorptions that slow the atoms than ones which accelerate them. In a trap, such as an ion trap, the orbits of the atoms continually bring the atoms toward the laser, so they can be slowed down. In the absence of such trapping, symmetric illumination can accomplish the same thing, as shown in slide 6.

The problem is that the range of velocities over which the force is substantial is only a few meters per second. For a trapped atom going much faster than this, this is not too bad, since the small cooling rate can act over a long period of time. Ion traps hold ions at room temperature or higher energies, but neutral traps (slide 7) are all very shallow and can't hold atoms with energies above about 1 K. Therefore, one must slow the atoms down first, then trap or further cool them.

Slide 8 shows the basic idea of decelerating an atomic beam. A laser beam is directed against an atomic beam and the absorbed photons slow down the atoms. As the atoms slow, their Doppler shift changes and they go out of resonance with the laser. The two major solutions to this problem are to change the frequency of the laser to compensate the change in Doppler shift, and to change the frequency of the atoms (by for example a Zeeman shift).

Slide 9 shows the effect on an atomic beam velocity distribution when nothing is done to compensate the changing Doppler shift. A narrow feature is produced, but little deceleration occurs and only a small part of the distribution is affected. Slides 10 and 11 show the effects of using Zeeman tuning and frequency chirping. These techniques can actually bring the atomic beam virtually to rest. Slide 12 shows a view of our Zeeman tuned cooling apparatus, and the observer position for slide 13 which is a photograph of the stopped beam.

Once the atoms are stopped or going very slowly, the cooling scheme of slide 6 can be used. Slide 14 calculates the damping force on an atom with small velocity. Slide 15 calculates the limiting temperature, balancing the rate of dissipating energy by damping with the rate of gaining energy by the random heating caused by scattering of photons in random directions. Also illustrated is the fact that with a strong motional damping the atoms have a short mean free path and therefore a long diffusion time. This slow diffusion of atoms is the molasses effect. Note that the numbers will be quite different in three dimensions. Slide 16 shows the expected 1-D diffusion time as a function of detuning for this "classical" molasses.

Slide 17 shows our experimental arrangement for observing molasses: Atoms from the atomic beam, slowed by the laser, enter the molasses formed at the intersection of 3 orthogonal pairs of counterpropagating laser beams. Here they "stick" for a long time. Slide 18 is a photograph of the nearly stopped atomic beam and the molasses. Molasses was first observed at Bell Labs in 1985 in pulsed experiments. We achieve higher density by using a continuous process.

Slide 19 shows Phil Gould and Paul Lett making molasses in our lab, along with a picture of molasses so bright it can be easily seen in daylight. Another picture of molasses is in slide 20.

By sweeping the molasses laser frequency we can measure the molasses brightness as a function of frequency as shown in slide 21. The smooth curve is the predicted behavior of the molasses diffusion time, which should be directly related to the atomic density. Because of additional factors affecting molasses brightness, we also measured the molasses lifetime, the time for atoms to diffuse out of the intersection of the laser beams. The apparatus for this is shown in slide 22. The atomic beam and cooling laser are chopped off, turning off the slow atoms into the molasses, and the fluorescence from the molasses is observed as a function of time.

Slides 23 and 24 show typical loading and decay curves as the source of slow atoms to the molasses is turned on and off. Slide 24 shows a sequence of decay curves as the molasses frequency is scanned, and slide 25 plots the molasses lifetime as a function of frequency for two different powers. The solid curve is the theoretical prediction for classical molasses. The disagreement is strong.

Slide 26 derives the expected drift velocity of atoms in molasses if the laser beams are unbalanced. The exact result for classical molasses indicates a substantial reduction in the molasses lifetime for a 10% imbalance. Slide 27 shows the experimental results compared to the theory, again with a large disagreement, more than a factor of ten. Slide 28 summarizes possible reasons for the disagreement. Most significant is the

fact that at low power the experimental molasses acts nearly "normal", that is, like classical molasses. None of the possible explanations have given explicit predictions of the experimentally observed behavior.

We now turn to a consideration of dipole forces on atoms in laser fields. Slide 29 shows the origin of the dipole potential in the dressed atom picture. Starting with a ground and excited state g and e , we turn on the laser field, but not the interaction between atoms and laser. The energy levels of atom+field are a ladder of pairs of nearly degenerate states separated by the detuning from resonance. When the interaction is turned on the nearly degenerate states (ground state with $n+1$ photons and excited state with n photons in the field) are repelled and mixed, being separated by the generalized Rabi frequency. In slide 30 we see the case for both positive and negative detunings of the laser. The atom occupies both dressed levels, but is predominantly in the one which connects adiabatically to the ground state. This is illustrated by the bigger dot. Thus for negative detunings the atom is more often on the level which has its lowest energy at the strongest part of the field. Details of this approach can be found in Dalibard and Cohen-Tannoudji, J. Opt. Soc. B 2, 1701 (1985).

The dipole force can be exploited to make a trap. Slide 31 shows a design suggested by Ashkin in 1978 and recently realized in our laboratory for the first time. Two laser beams with Gaussian intensity profiles are focussed so that they are counterpropagating and diverging at the center of the trap. For negative detunings the dipole force provides a potential well perpendicular to the symmetry axis, while the radiation pressure or scattering force provides the potential well along the axis.

A number of refinements were needed before the original idea of Ashkin could be accomplished. Gordon and Ashkin realized that the trap beam alone could not provide the cooling needed to stabilize that trap and that separate cooling was needed (slide 32.) They also realized that the dynamic Stark shifts induced by the trap would inhibit proper cooling. Dalibard, Reynaud and Cohen-Tannoudji suggested alternating the trapping and cooling beams to eliminate this problem (slide 33.) It was also known that the standing wave resulting from the counterpropagating trap beams would cause additional heating due to fluctuations in the strong dipole forces. Dalibard and Cohen-Tannoudji proposed the alternation of the two trap beams to eliminate this effect (slide 34.) Finally, Chu et al. demonstrated the efficient loading of an optical trap from optical molasses. Combining all these ideas we were able to make such a trap, having a volume over which atoms could be captured, of about 10^{-4} cm^3 , and a density increase, averaged over the capture volume, on the order of 10^3 or 10^4 compared to the molasses density.

①

OPTICAL COOLING AND TRAPPING

Phillip Gould

Paul Lett

Alan Migdall

John Prodan

Harold Metcalf

Tom Bergeman

Ivan So

Jean Dalibard

W.D. Phillips

N.B.S. Postdocs

S.U.N.Y. Stony Brook

Ecole Normale Supérieure, Paris

NBS

②

Why Cool and Confine Atoms?

- Spectroscopy - reduce Doppler and Transit Effects

- Bose-Einstein Condensation

(Lower $T \rightarrow$ lower n ; no walls)

- Quantum Optics

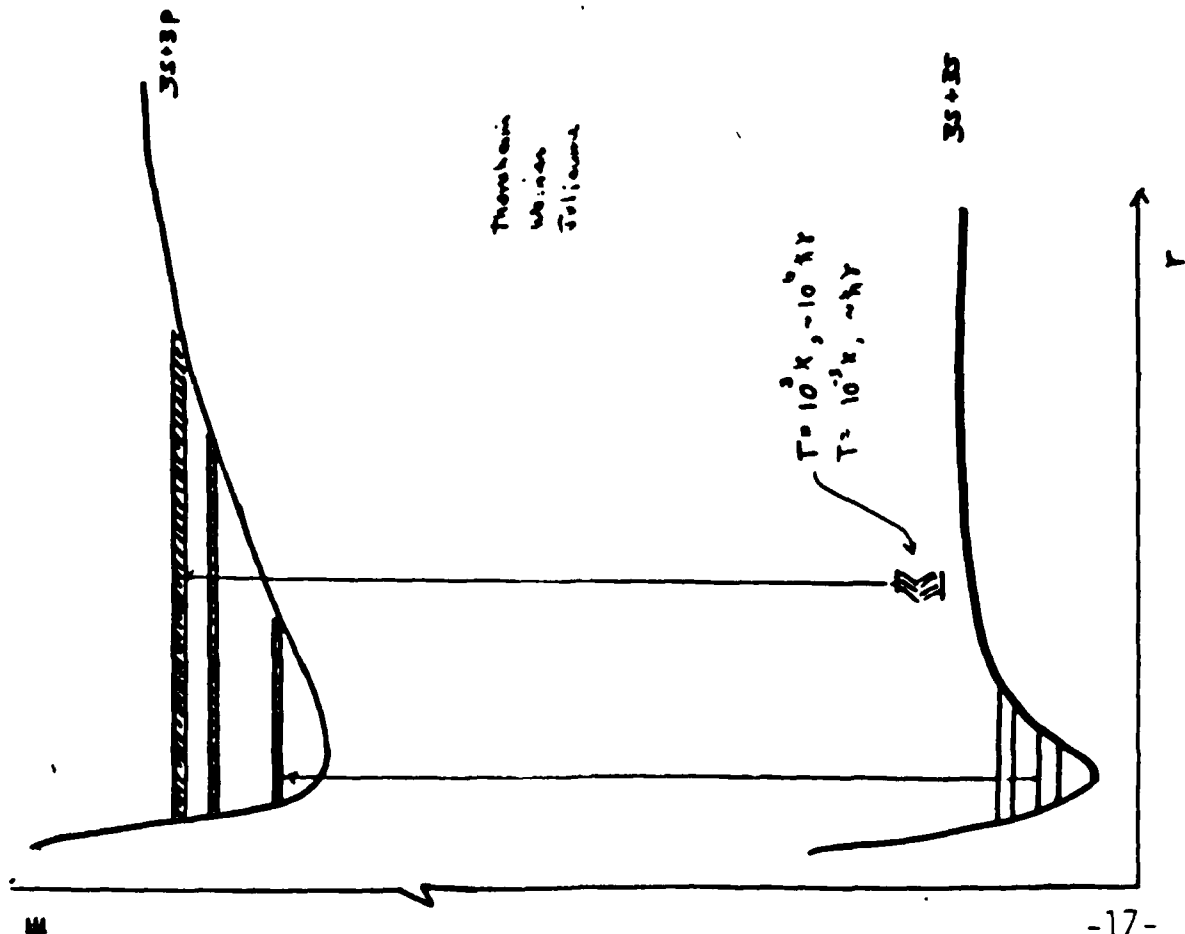
(trap, cooling physics; cavity QED; statistics)

- Collisions

(ultra-low energy, molecule and cluster formation)

- Antimatter

③



Phenol
Water
Toluene

④

de Broglie wavelength

$$\lambda_{dB} = \frac{h}{p}$$

for Na, 10^3 m/s ($1\pi 10^3 \text{ K}$) $\lambda \approx .15 \text{ \AA}$
 1 m/s ($1\pi 10^3 \text{ K}$) $\lambda = 150 \text{ \AA}$

Partial waves

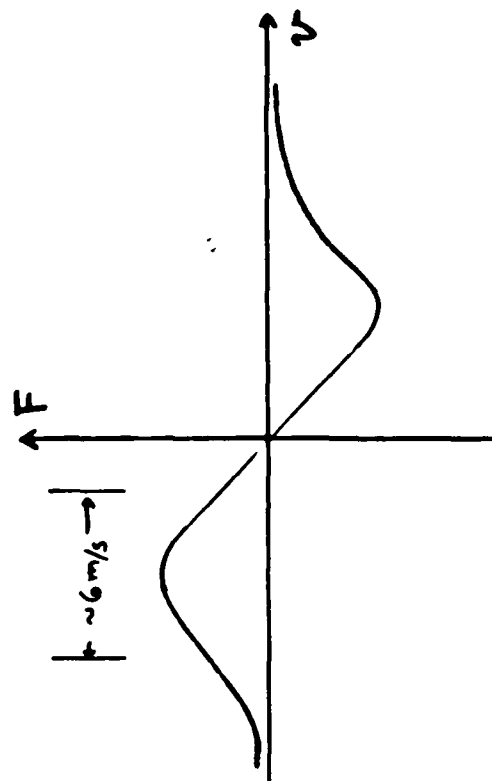
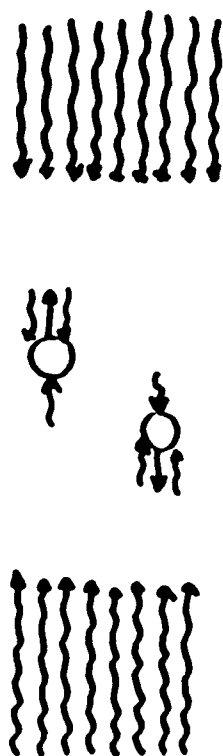
$$l \approx \frac{2\pi \cdot r_{eq}}{\lambda_{dB}}$$

Na^+ , $r_{eq} = 15 \text{ \AA}$, 10^3 m/s $l \sim 600$
 1 m/s $l \sim 1$

⑥

"Balanced" Cooling

(Hänsch • Schawlow 1975)

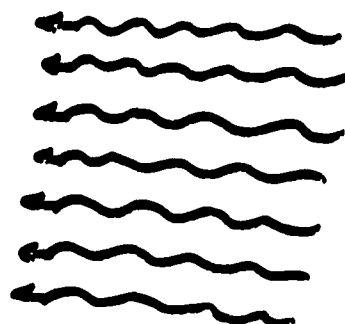
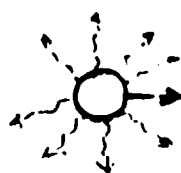


⑤

Laser Cooling (Doppler Cooling)

(SCATTERING FORCE)

Hänsch • Schawlow
Wineland • Dehmelt
1975



Wineland et al. 1978
Neuhauser et al.

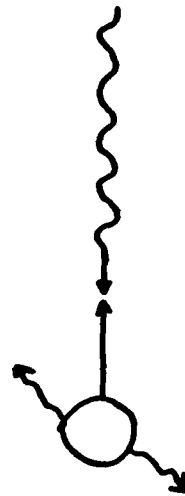
⑦

Neutral Atom Traps

- Magnetic
- Optical
 - Gradient Force
 - Radiation Pressure (scattering) Force
- Electrostatic
- Hybrid
- Stable Traps are too Shallow ($\approx 1 \times$)
to hold most thermal atoms!

⑧

Laser Deceleration (and Cooling) Atomic Beams



For Na: $\Delta v/\text{photon} = 3 \text{ cm/s}$

$$v_i \approx 10^5 \text{ cm/s}$$

$$N_{\text{phot}} \approx 3 \times 10^4$$

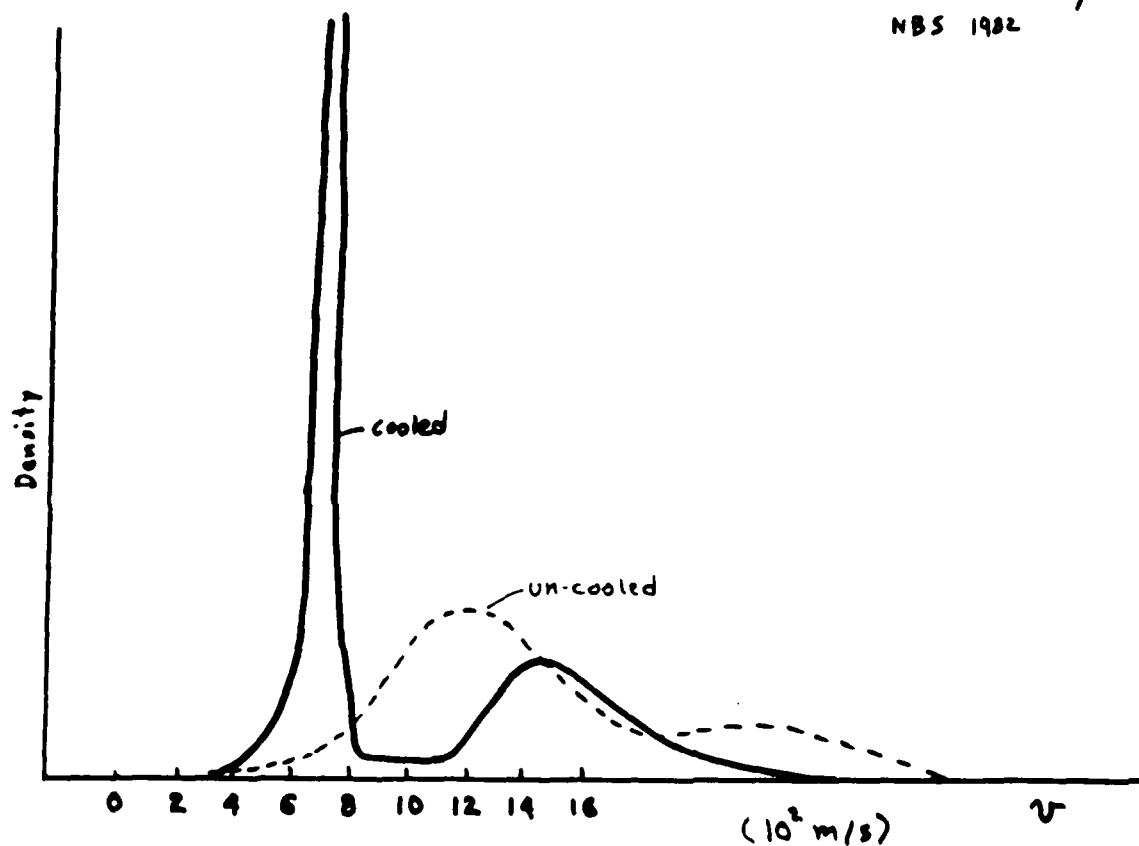
But! after 100 photons, Doppler shifts
off resonance

two solutions (among many)

- Change Laser Frequency (Moscow 1979)
- Change Atomic Frequency (NBS 1981)

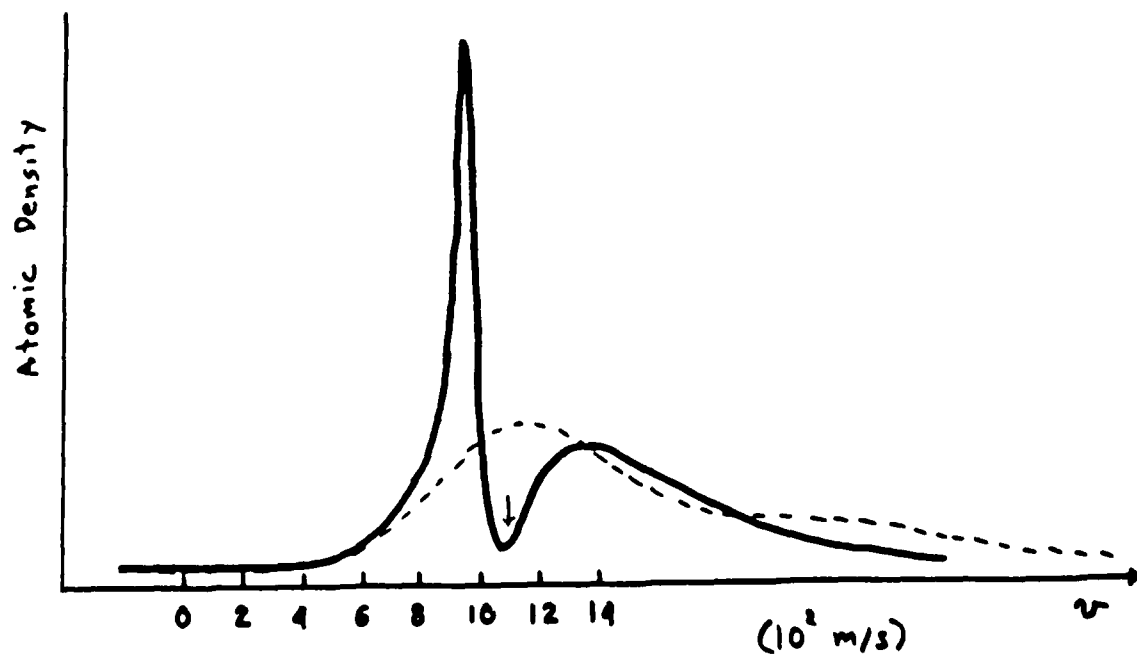
⑩

Zeeman-Tuned Cooling NBS 1982

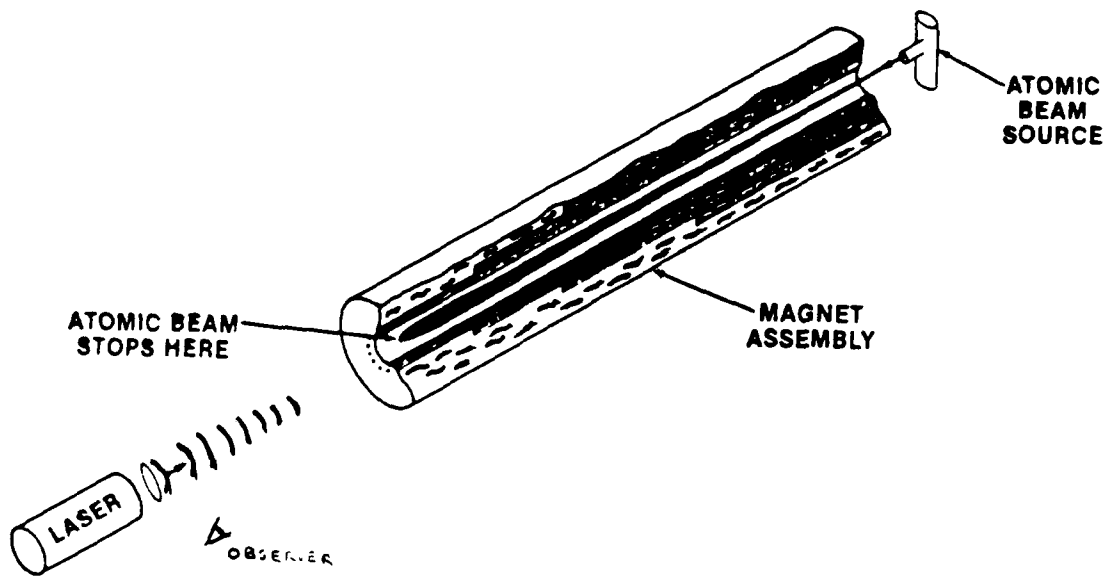


⑨

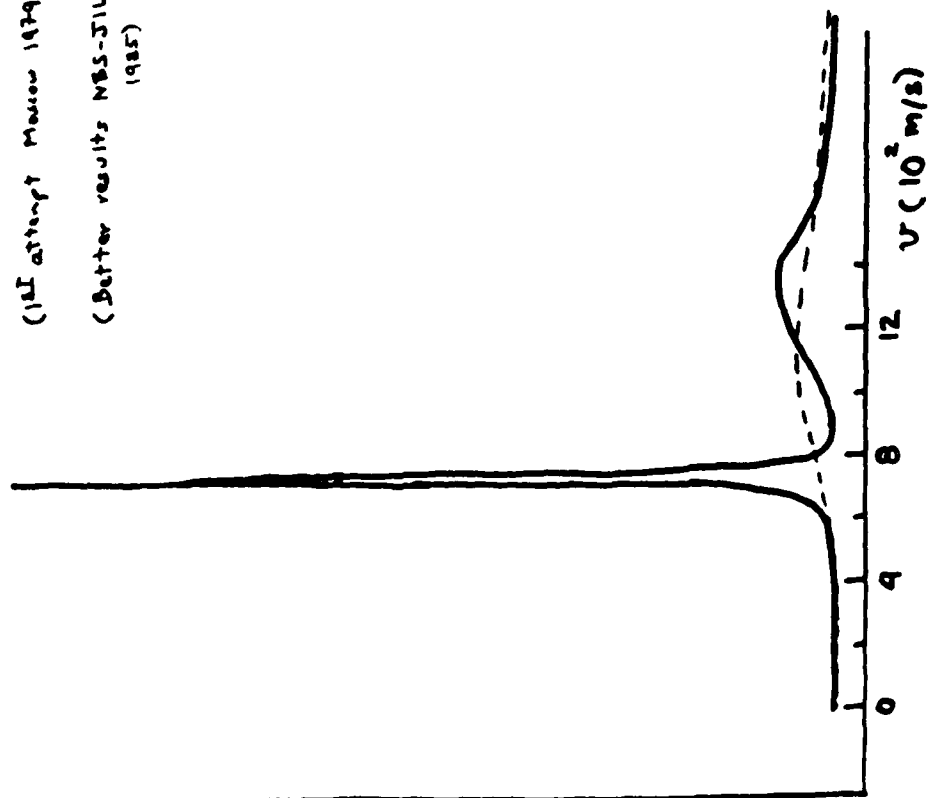
Non-Resonant Cooling (1st expt: Andrews et al 1981)



(12)

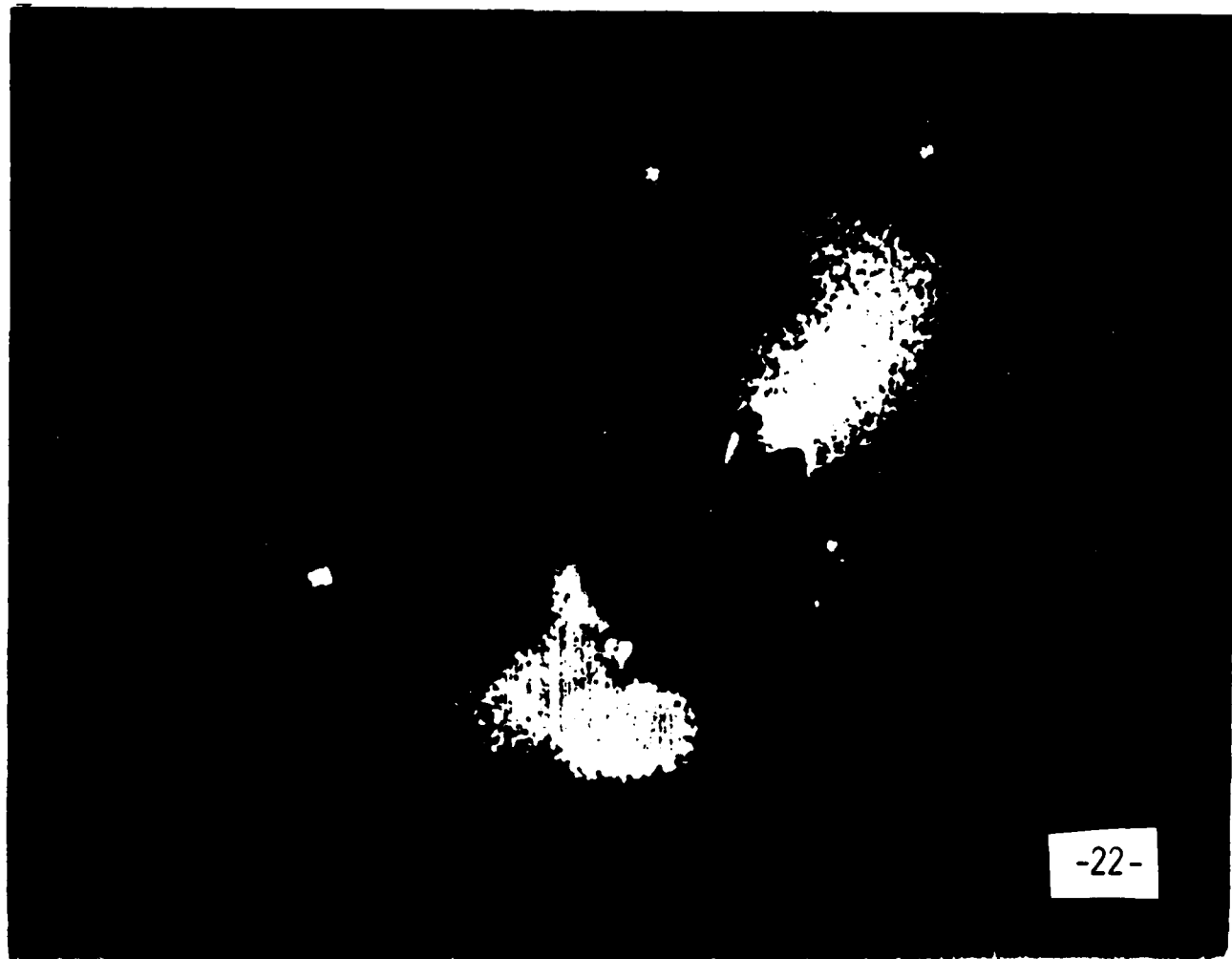


Chirp-Cooling NBS 1983
(1st attempt Moseley 1979)
(Better results NBS-JILA
1985)



(11)

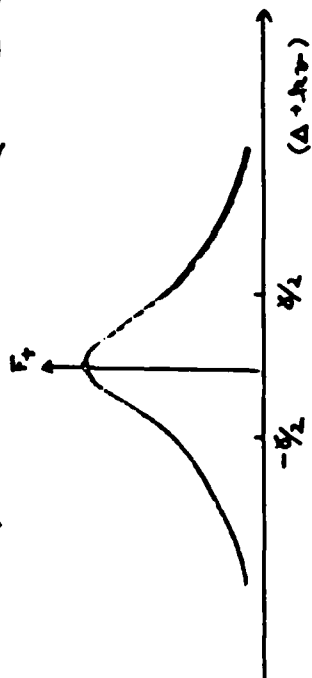
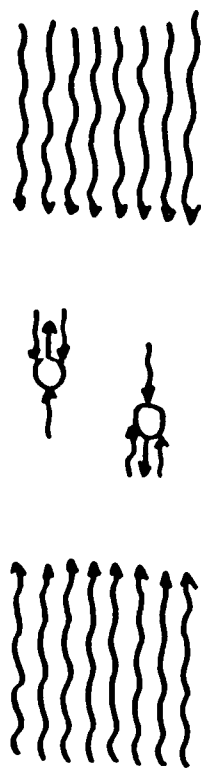
(13)



-22-

(14)

OPTICAL MOLASSES

 AT&T 1985
 MBS


$$F_z = \frac{\hbar \chi \hbar}{2} \frac{I/I_0}{1 + I/I_0 + \left(\frac{\Delta + \hbar\nu}{\hbar/2}\right)^2}$$

$$F_z - F_c = -\frac{4\hbar \hbar^2 I/I_0}{\left[1 + I/I_0 + \left(\frac{\Delta + \hbar\nu}{\hbar/2}\right)^2\right]^2} \left(\frac{\Delta + \hbar\nu}{\hbar/2}\right) \nu \quad \hbar\nu \ll \delta$$

$$F_{\max} = -\frac{1}{4} \hbar \hbar^2 \nu \quad (I/I_0 = 1, \Delta = \frac{\hbar}{2})$$

$$F = -\alpha \nu$$

$$(\text{For Na } \nu/\nu_0 \approx 13 \mu s = \tau_{\text{cool}})$$

(15)

COOLING LIMIT

$$F = -\alpha v$$

$$\dot{E}_{\text{cool}} = Fv = -\alpha v^2$$

$$\dot{E}_{\text{heat}} = \frac{\dot{p}^2}{2m} = \frac{\hbar^2 k^2}{m} \cdot R_{\text{scatt.}}$$

$$\text{set } \dot{E}_{\text{cool}} + \dot{E}_{\text{heat}} = 0, \quad \frac{1}{2} m v_{\text{th}}^2 = \frac{1}{2} \hbar^2 T$$

$$\hbar^2 T = \frac{\hbar^2}{4} \frac{1 + \frac{\hbar^2}{I_0} + (2\Delta/\hbar)^2}{(2\Delta/\hbar)}$$

$$\hbar^2 T_{\text{min}} = \frac{\hbar^2}{2} \quad \text{at } \Delta = \hbar/2, \quad \hbar/I_0 \ll 1$$

DIFFUSION (THE MOLASSES EFFECT)



$$\langle x^2 \rangle = \ell^2 \frac{t}{\tau_d}$$

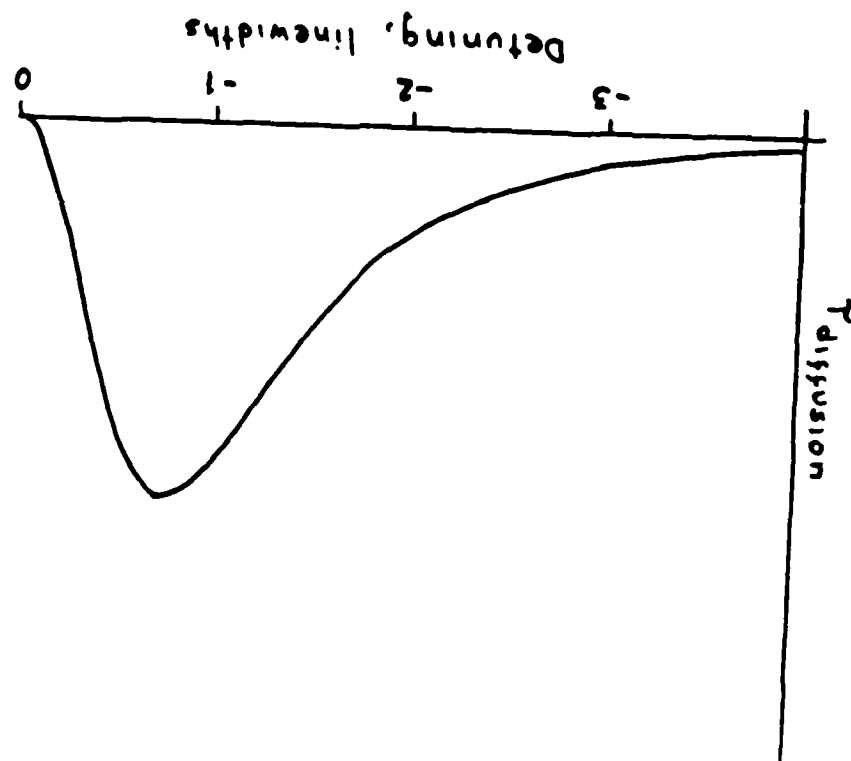
$$= v_{\text{th}}^2 \tau_{\text{cool}} \cdot \frac{t}{\tau_{\text{cool}}}$$

$$\tau_{\text{max}} = \frac{4}{27} \frac{\langle x^2 \rangle \hbar^2}{8}$$

$$D_x = \hbar^2 T / \alpha$$

$$\langle x^2 \rangle = 2 D_x t = \frac{2 \hbar^2 T t}{\alpha}$$

$$(7 \text{ sec at } 5 \text{ mK for Na})$$



(16)

optical molasses

source of ultra-slow atoms

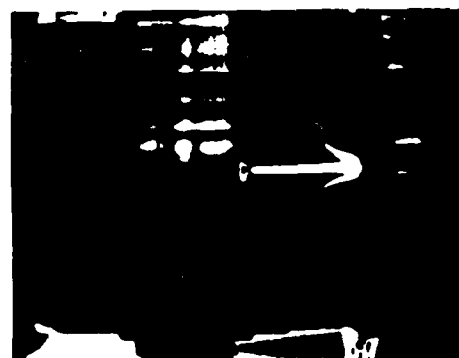
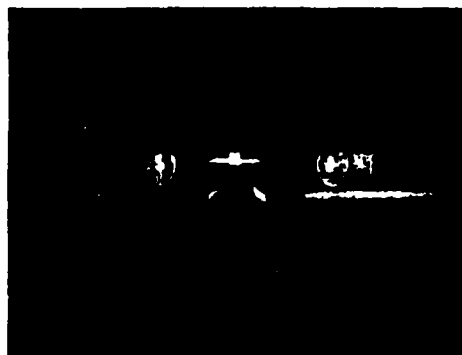
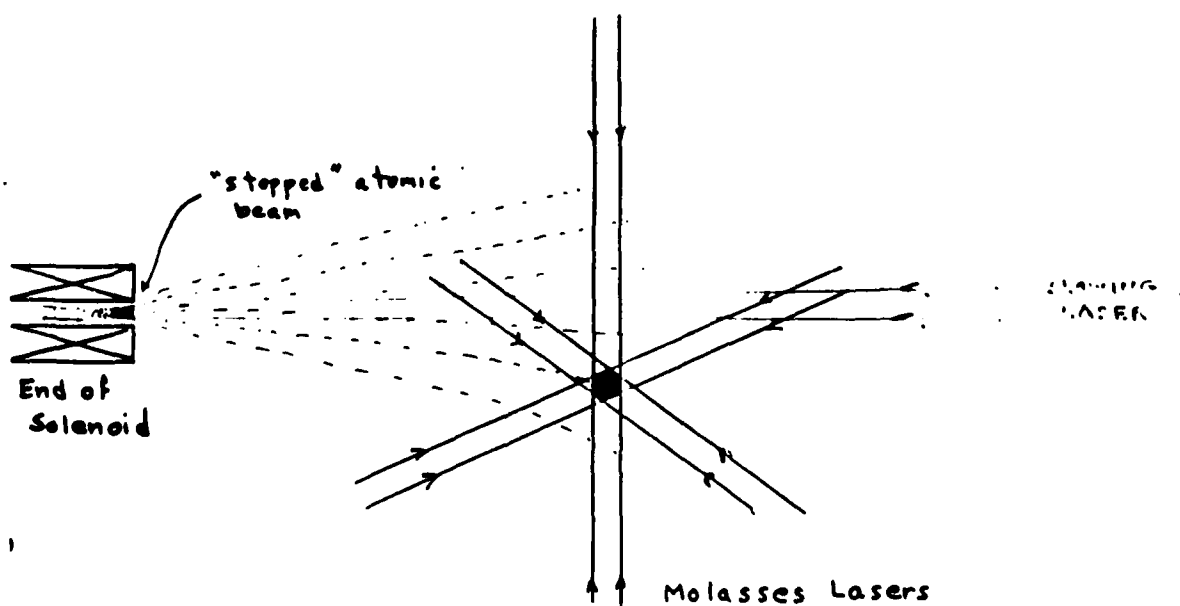


Fig. 9d

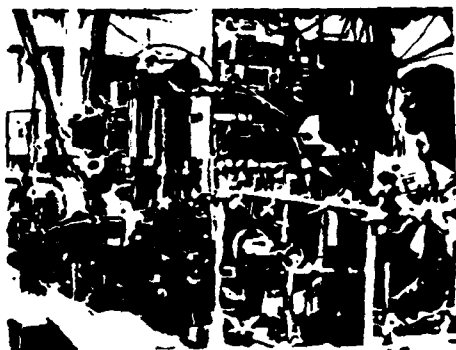
17

Experimental Arrangement For Observing Molasses

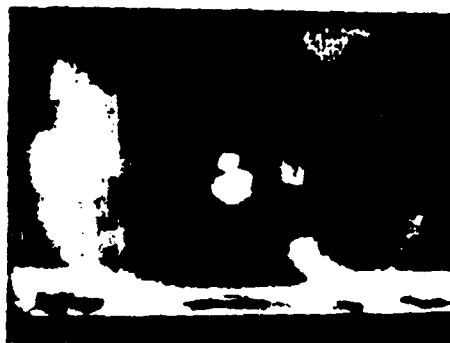


(19)

Molasses Apparatus

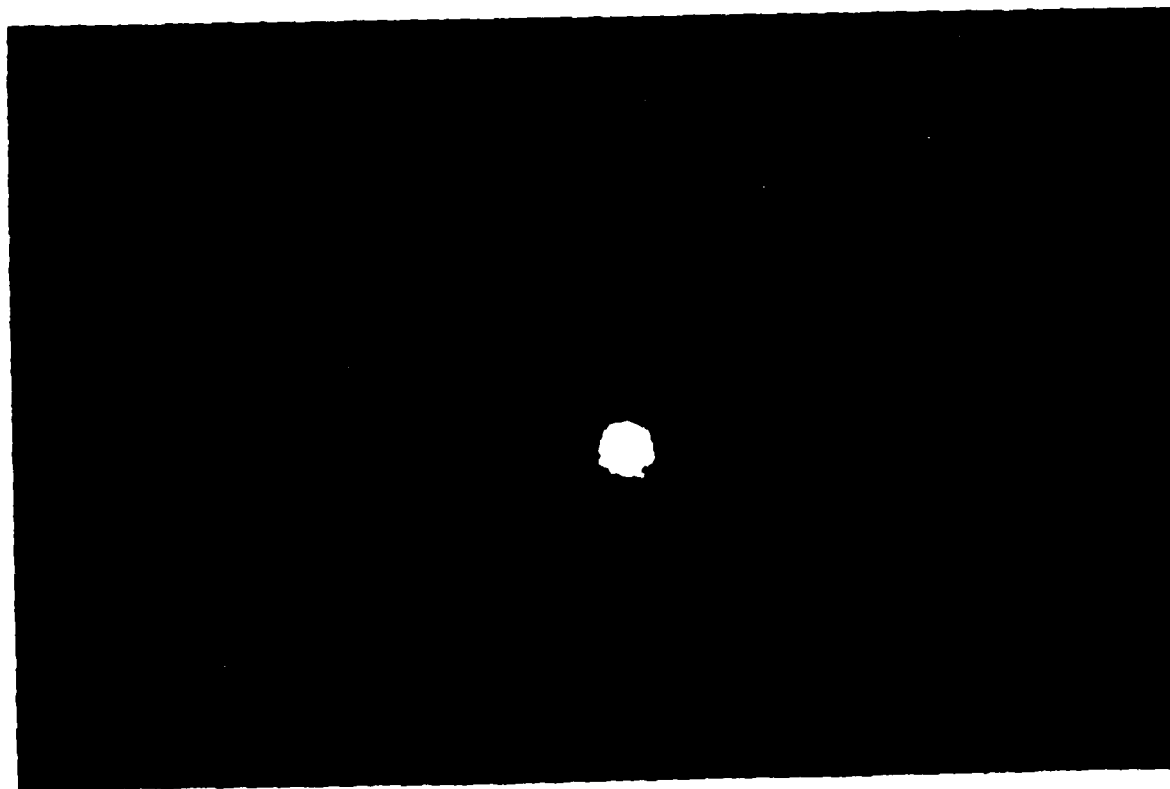


P.L. Gould and P.D. Lett



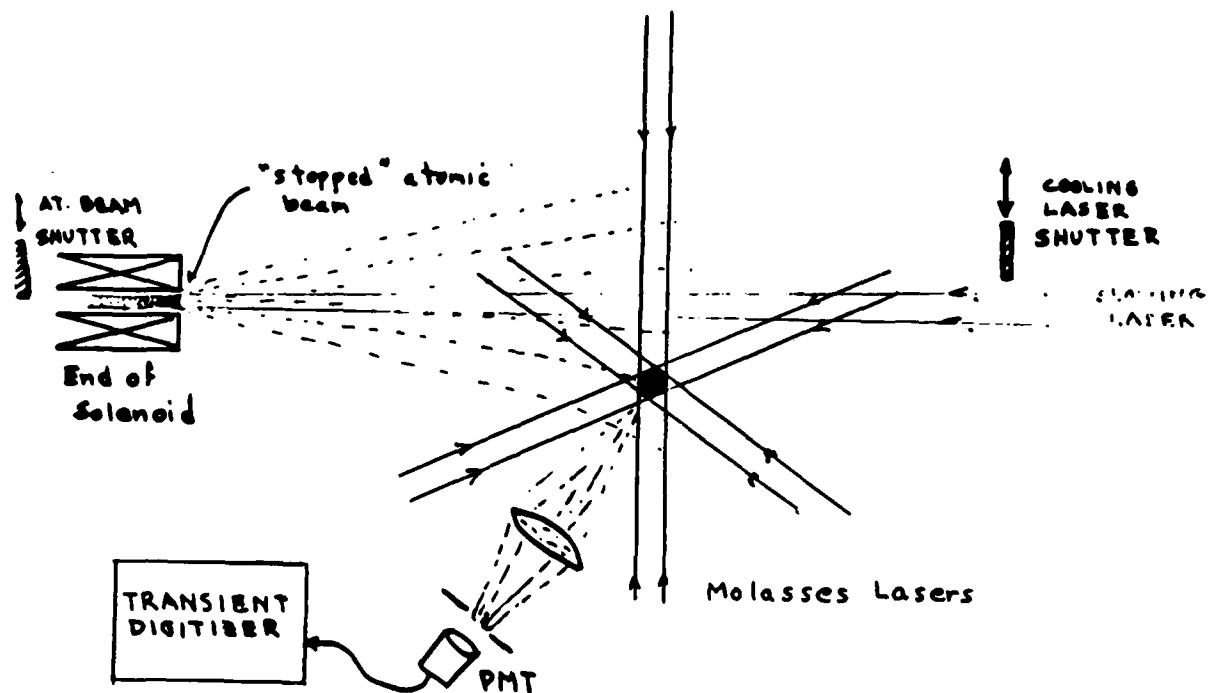
Optical Molasses in
Daylight

(20)



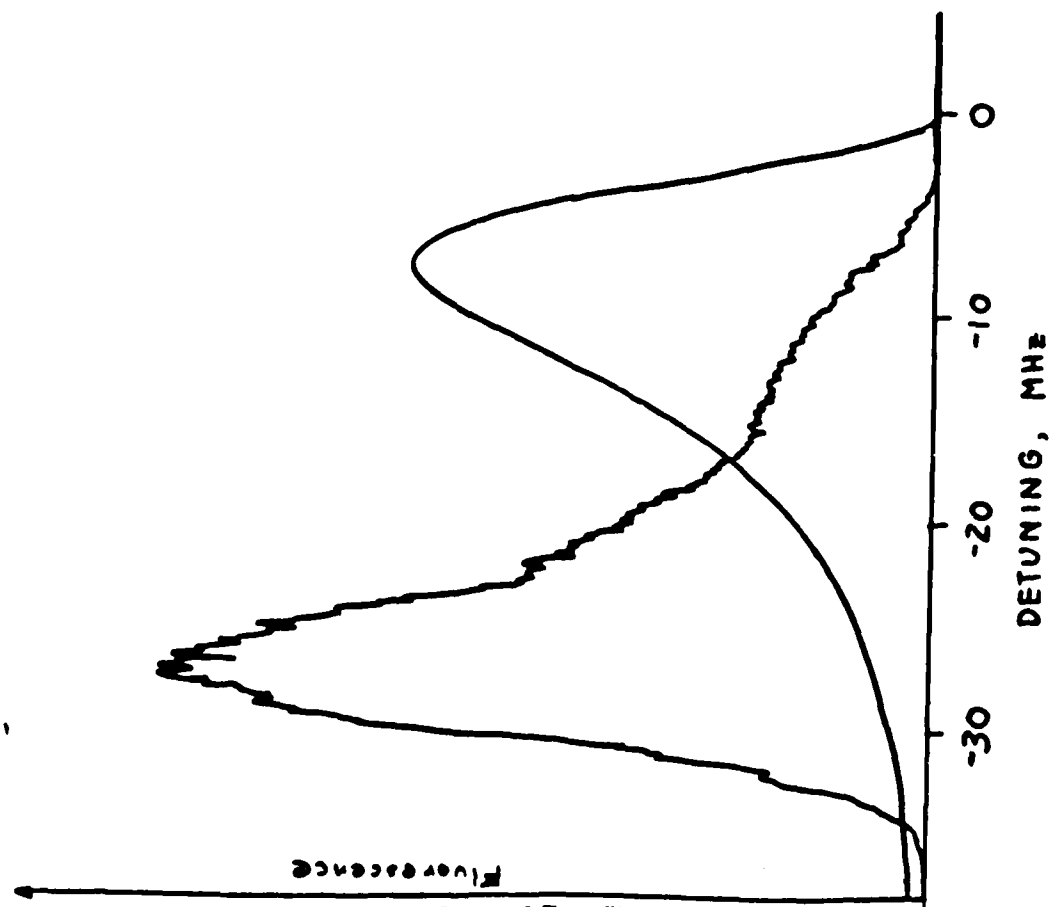
Experimental Arrangement For Observing Molasses

(22)

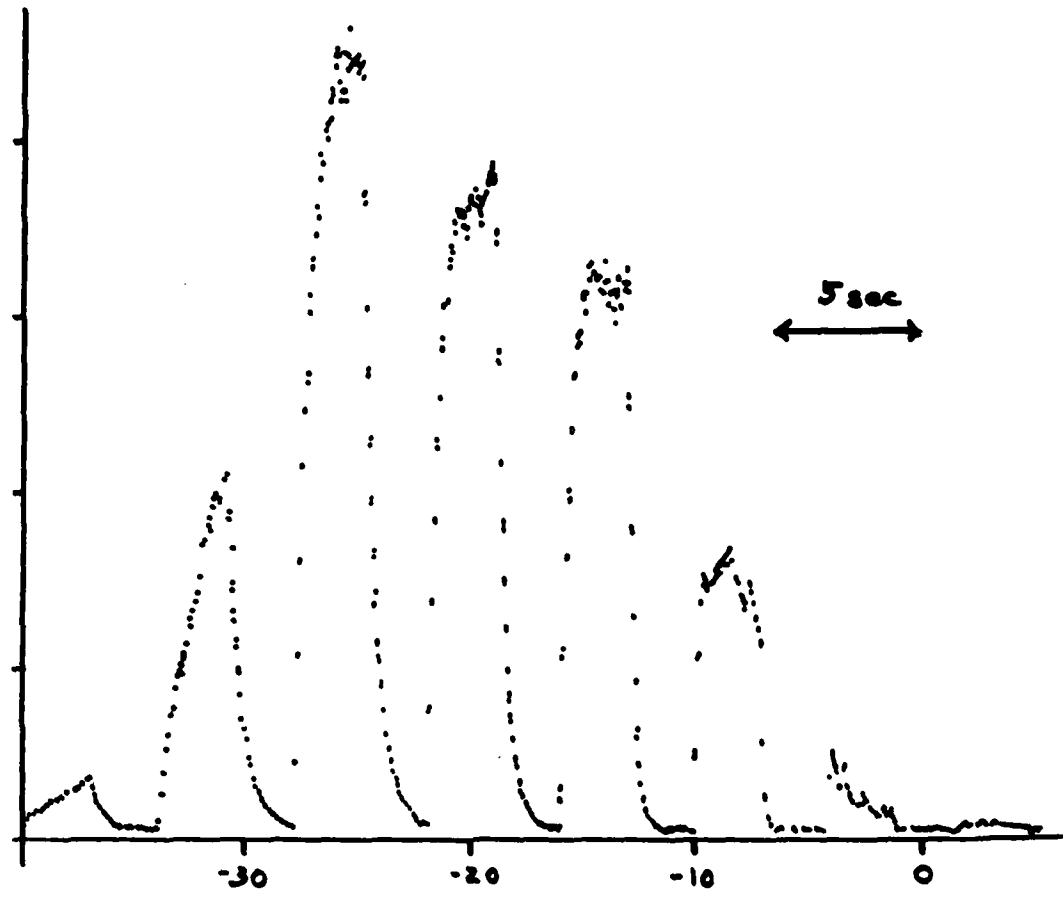


(Earlier, pulsed, expts: Bell Labs, 1985)

(21)



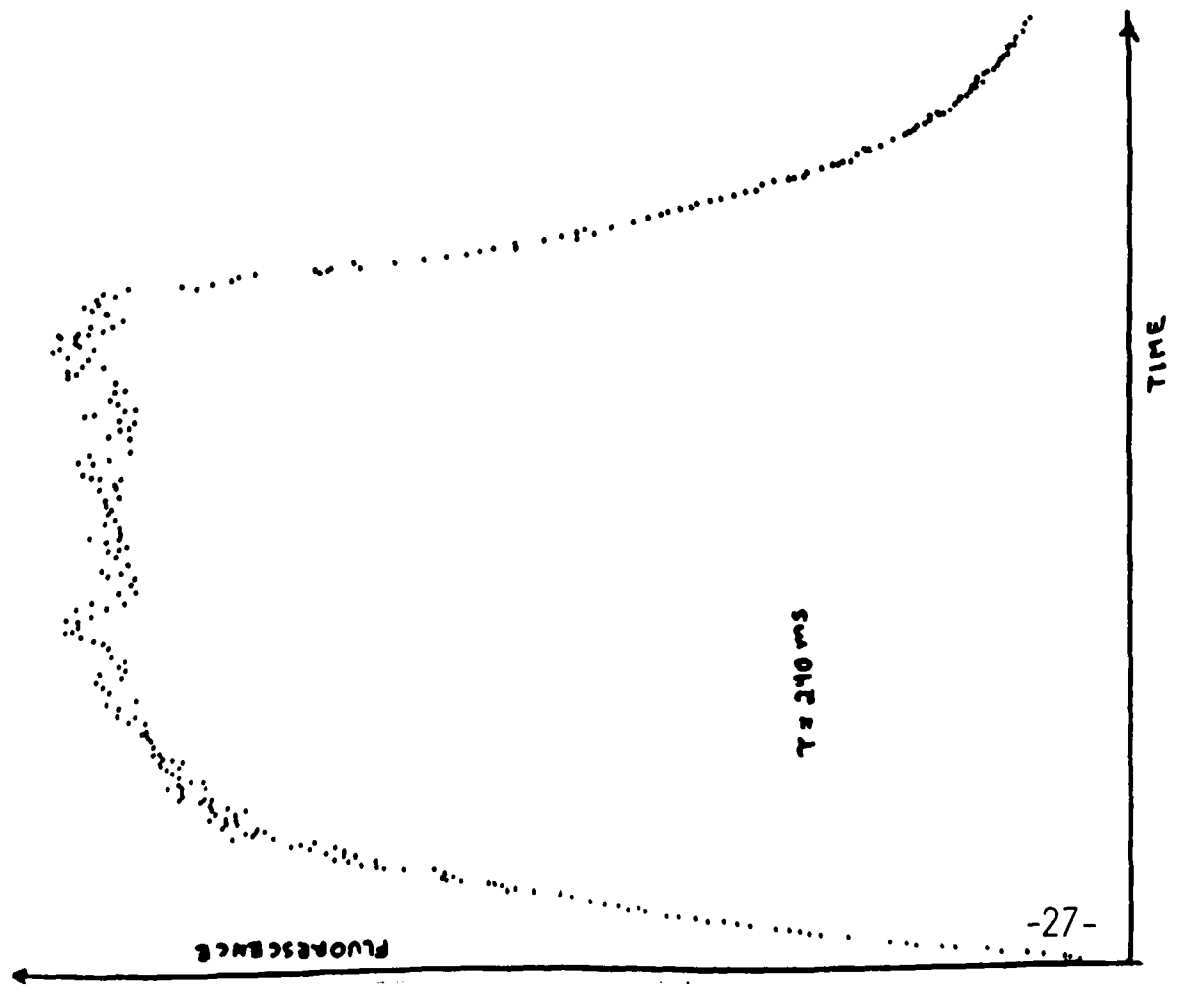
(24)



Jan 16 . 022 1987

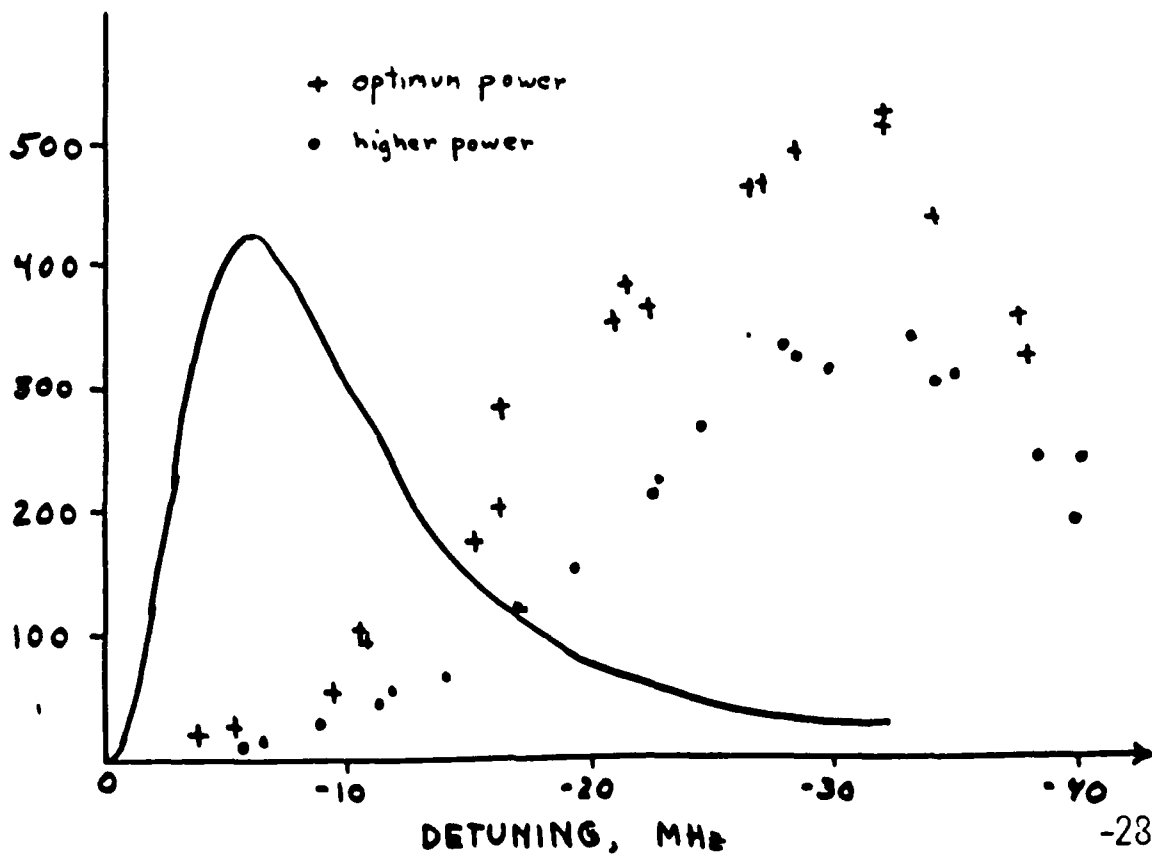
(23)

MOLASSES LOADING AND DECAY



25

LIFETIME, ms



DETUNING, MHz

-28-

26

Effect of Imbalance



estimate v :

$$F_{\text{unbal}} + F_{\text{grat}} = 0$$

$$d \frac{\hbar k \gamma}{4} - \frac{\hbar k^2 v}{4} = 0 \Rightarrow v = d \frac{\gamma}{k}$$

$$\gamma/k = 6 \text{ m/s}$$

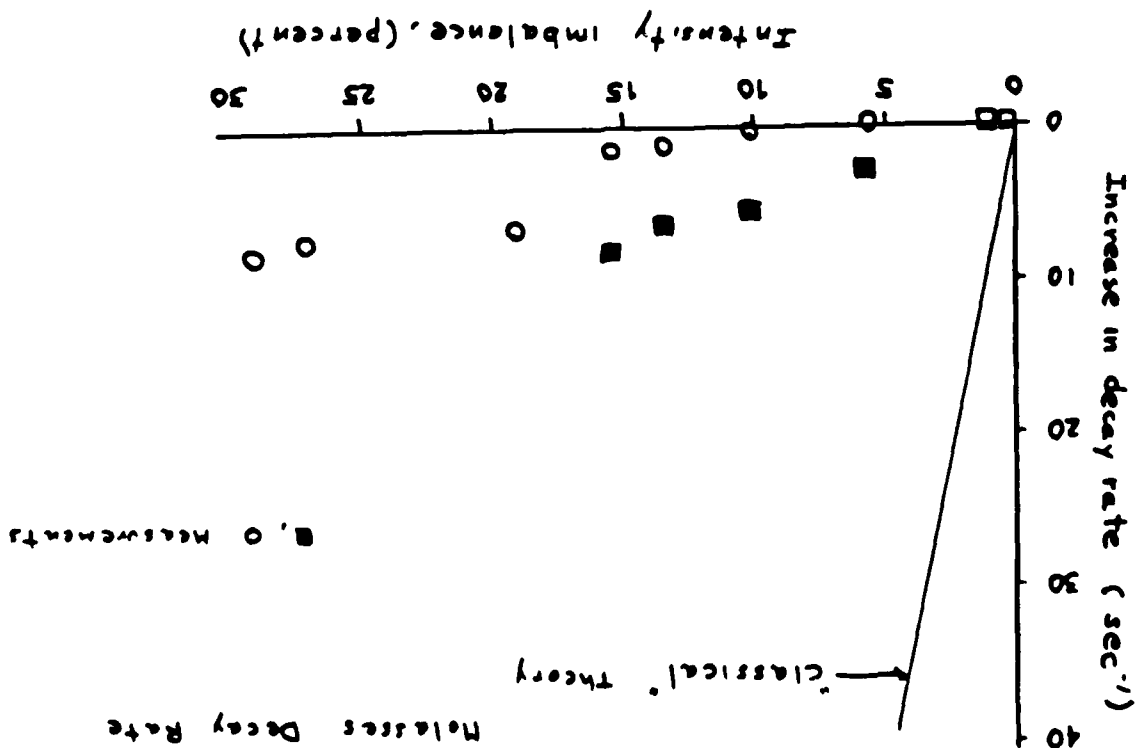
$$\text{exact: } v = \frac{\hbar \gamma}{4 \hbar} \frac{\frac{1}{4}(1 + \gamma/\gamma_0) + \Delta^2/\gamma^2}{\Delta/\gamma}$$

For optimum no losses ($\gamma/\gamma_0 = 1$, $\Delta = \gamma/2$)

$$v_{\text{opt}} = (2.2 \text{ m/s}) d$$

10% imbalance \Rightarrow 23 ms lifetime in 5 nm

Effect of Imbalance on
Molasses Decay Rate



IMBALANCE EFFECT ON MOLASSES LIFTING

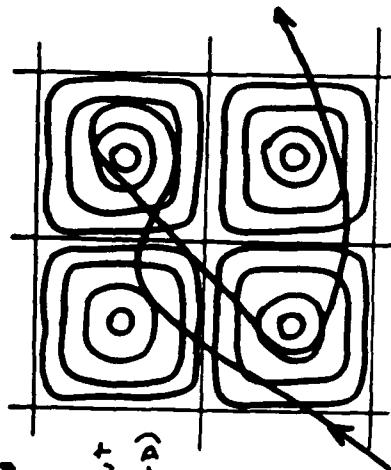
WHY IS EXPERIMENTAL MOLASSES SO STRANGE?

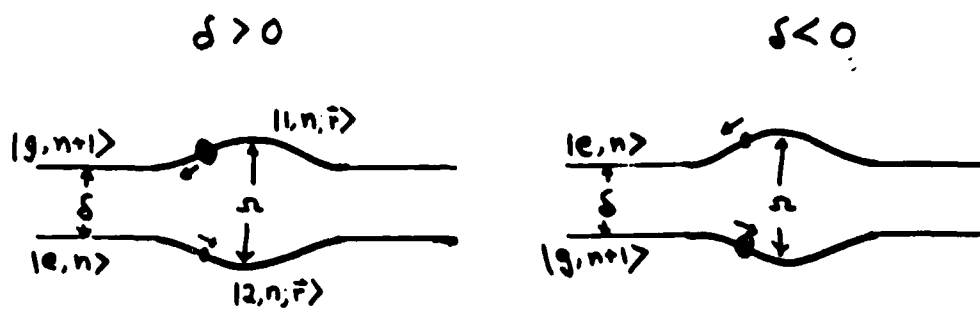
- At very low power - $I/I_0 \approx 0.01$ it is nearly "normal"
- Saturation and dipole forces not accounted for (but it doesn't help)
- Multiple Levels

$$F=3$$
- Multiple States (molasses is sensitive to field and polarization)

• Detailed Motion

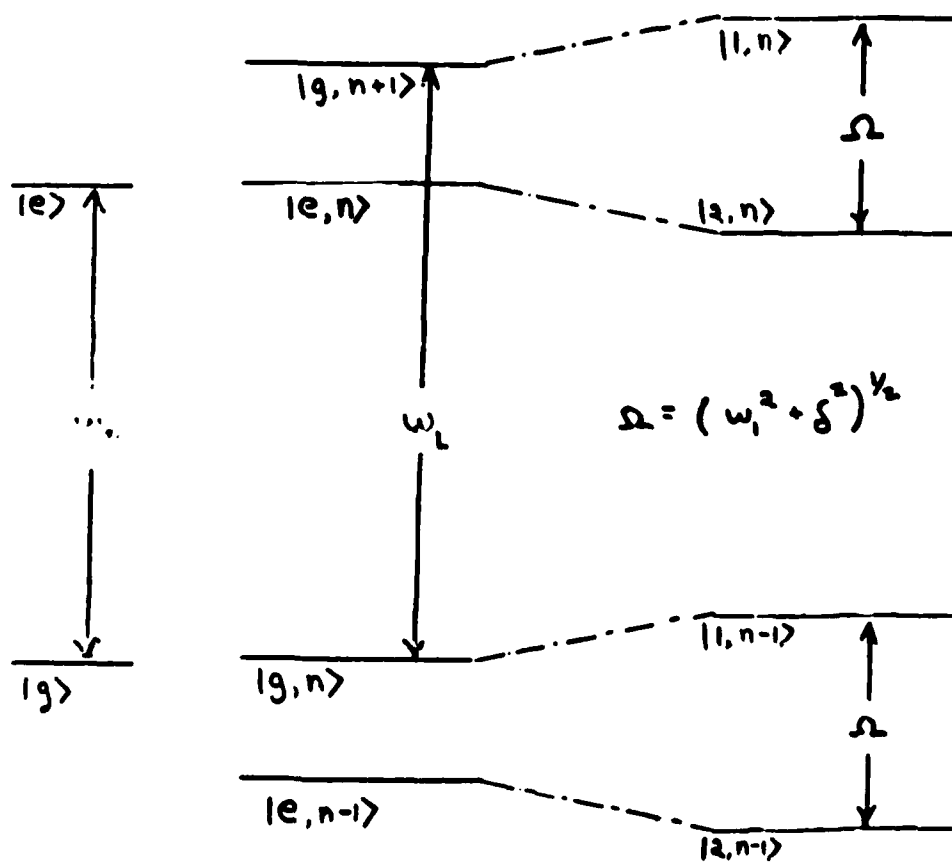
(Maybe, but not in 1-D)





$$\Omega = (\omega_L^2 + \delta^2)^{1/2}$$

for large δ : $\Omega \approx \delta + \frac{1}{2} \frac{\omega_L^2}{\delta}$



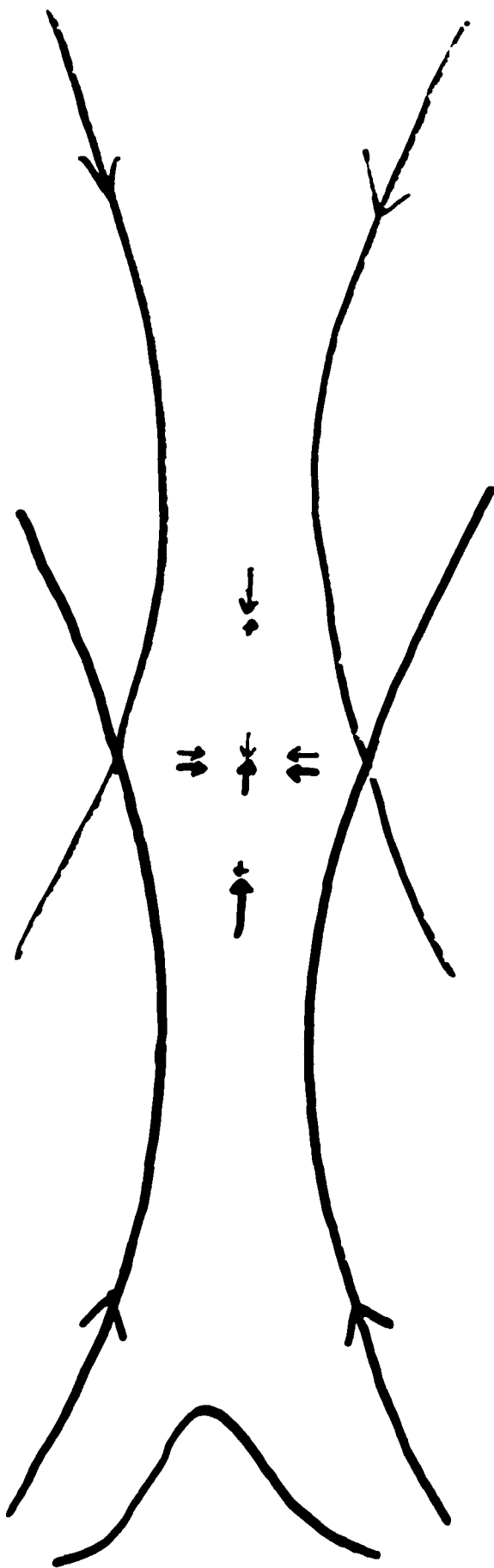
BARE ATOM

ATOM + PHOTONS
(NO COUPLING)

DRESSED STATES

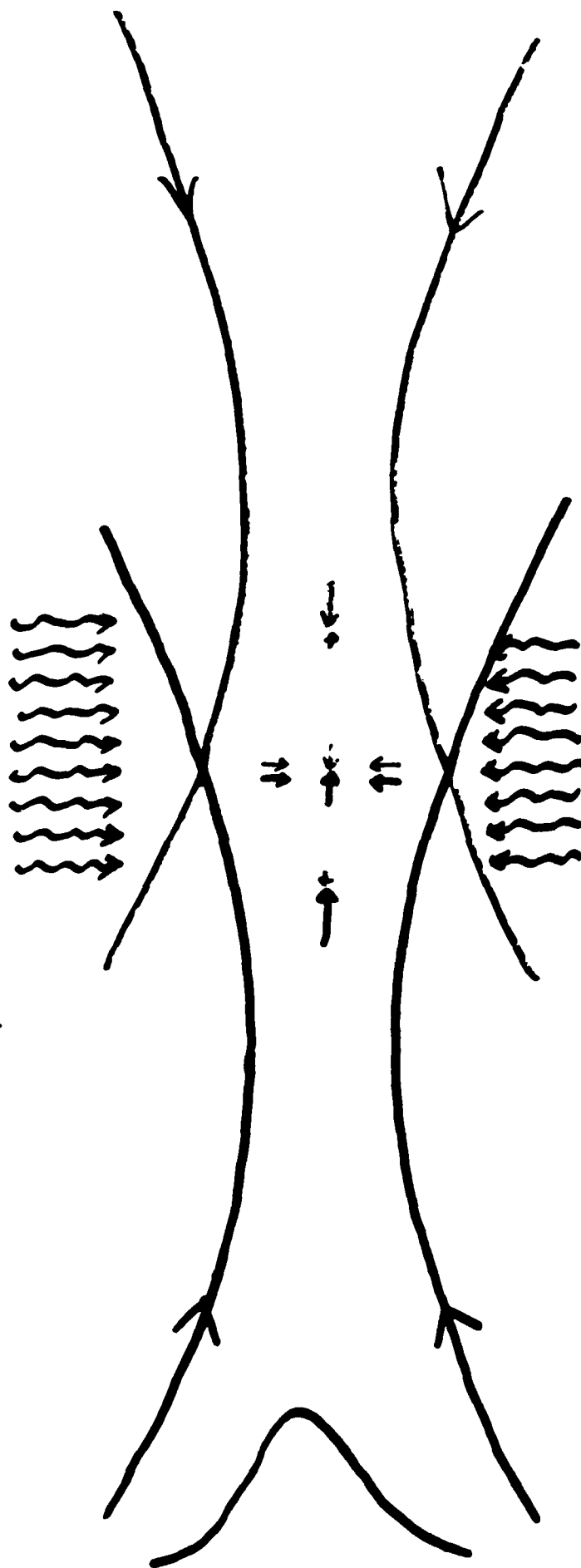
(31)

2-Focus Trap (Ashkin 1978) NBS 1987



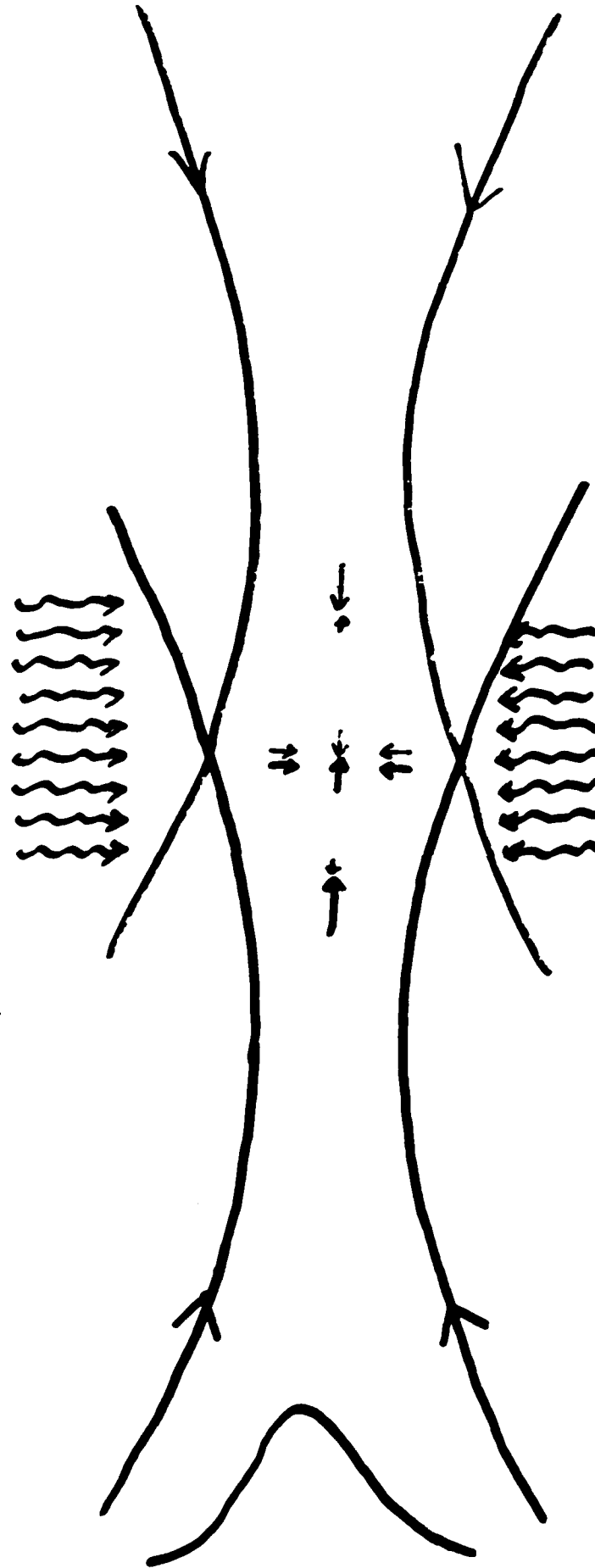
(32)

2- Focus Trap (Ashkin 1978) NBS 1987



• Separate Cooling Beams (Gordon & Ashkin)

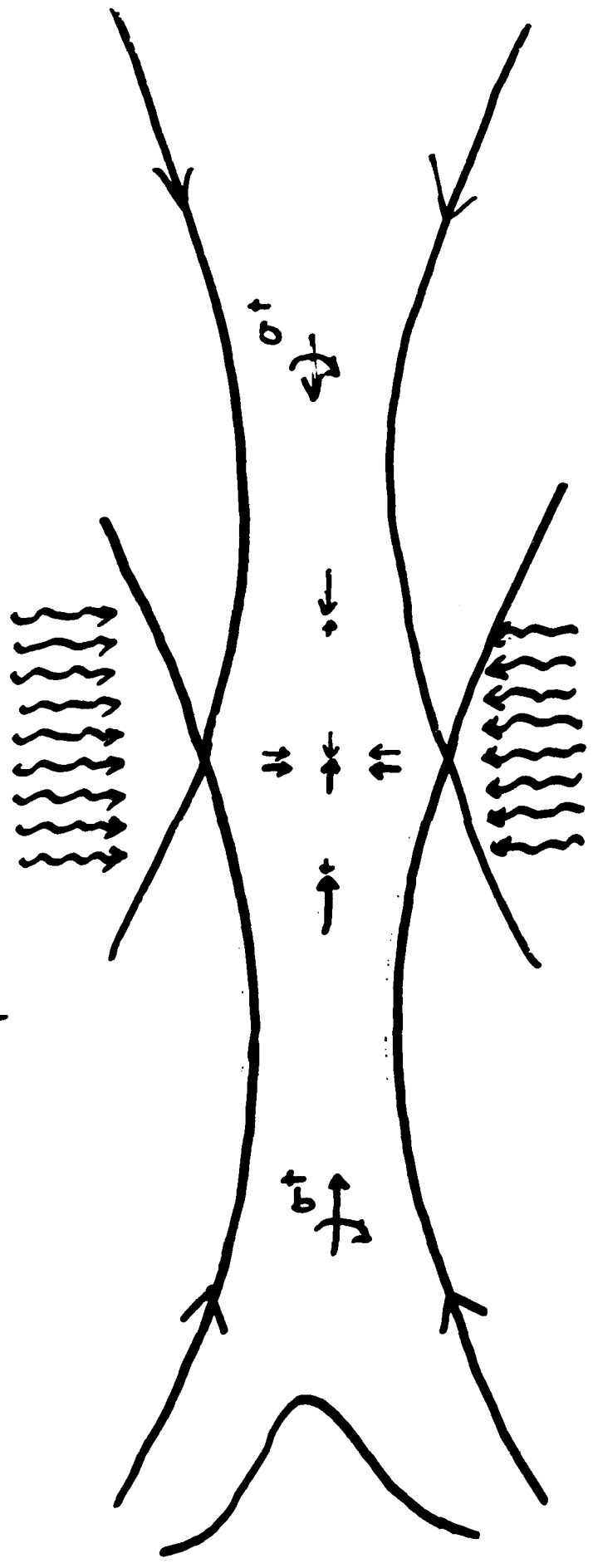
2- Focus Trap (Ashkin 1978) (33) NBS 1987



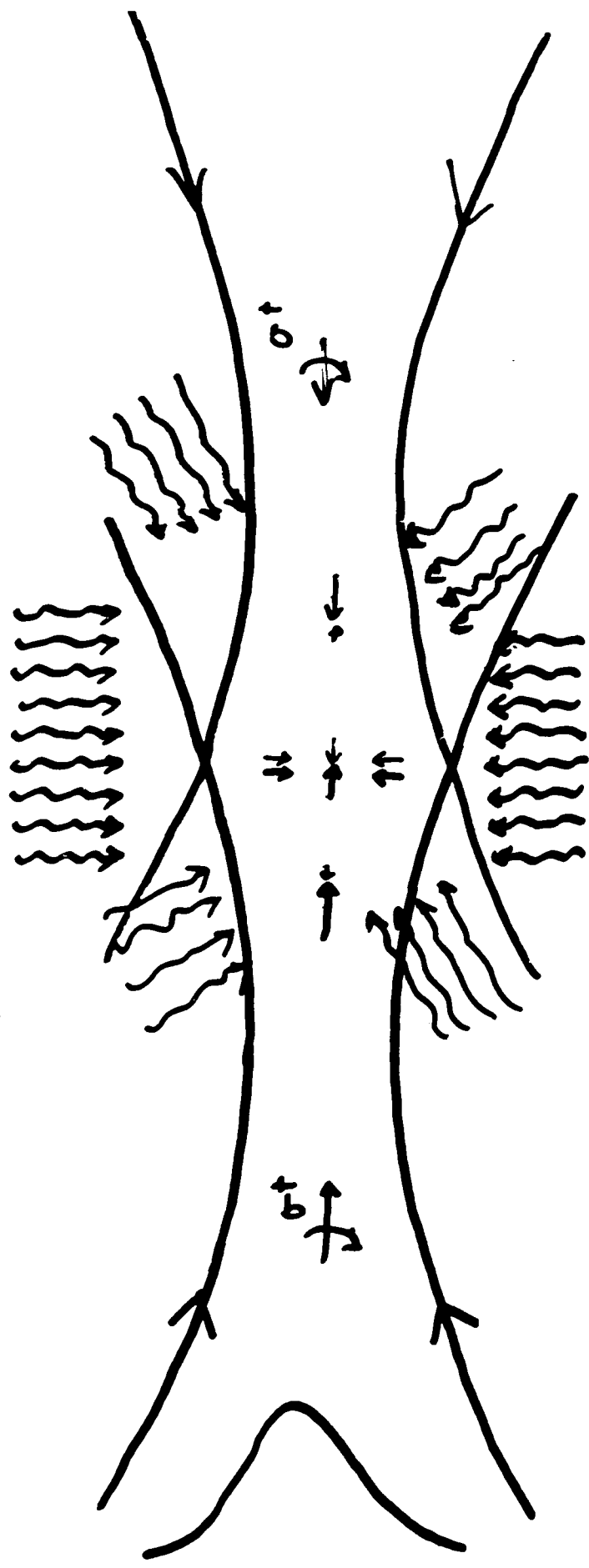
- Separate Cooling Beams (Gordon & Ashkin)
- Alternate Cooling and Trapping (Dalibard, Reynaud & Cohen-Tannoudji)

(34)

2-Focus Trap (Ashkin 1978) NBS 1987



- Separate Cooling Beams (Gordon + Ashkin)
- Alternate Cooling and Trapping (Dalibard, Reynaud + Cohen-Tannoudji)
- Alternate Trapping Beams (Dalibard + Cohen-Tannoudji)



- Separate Cooling Beams (Gordon & Ashkin)
- Alternate Cooling and Trapping (Dalibard, Reynaud & Cohen-Tannoudji)
- Alternate Trapping Beams (Dalibard & Cohen-Tannoudji)
- Load From Molasses (Chu et al.)

NBS: $\sim 10^{-4} \text{ cm}^3$, $\sim 10^4$ density increase in capture volume

Optical Trapping of Neutral Atoms and Dielectric Particles by Radiation Pressure

A. Ashkin, J. E. Bjorkholm and S. Chu
AT&T Bell Laboratories
Holmdel, NJ 07733

SUMMARY

Recently a number of exciting results have been achieved in the field of laser trapping and manipulation of small dielectric particles. Optical trapping and manipulation of Na atoms has been demonstrated at record low temperatures and record densities.

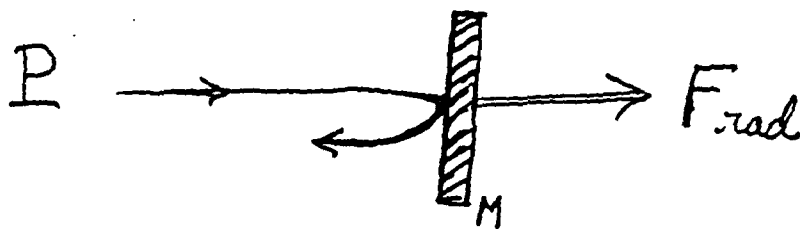
Trapping of submicron Rayleigh particles with diameters down to $\approx 250 \text{ \AA}$ has been achieved. Individual biological particles such as viruses, bacteria and small organisms have also been manipulated with light. The basic forces involved in trapping all these rather diverse particles are the forces of radiation pressure which come from the momentum of the light itself.

This talk briefly traces the history of the subject, gives some physical feel for the subject, mentions some of the principal results, and gives my perspective on the future. It concludes with a 5 minute tape showing trapping and manipulation of atoms and biological particles.

Force on a Reflecting Mirror

$$\text{momentum of photon} = \frac{h\nu}{c}$$

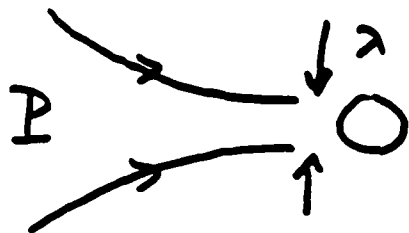
$$\text{\# photons/sec} = \frac{P}{h\nu}$$



$$F_{\text{rad}} = \frac{P}{h\nu} \left(2 \frac{h\nu}{c} \right) = \frac{2P}{c}$$

Forces

Laser Beam, $P = 1 \text{ watt}$, Focal Spot $\sim \lambda$



Dielectric Sphere:

$$\text{dia} \sim \lambda = 1/2 \mu\text{m}, m \approx 10^{-12} \text{ gm}$$

$$F_{\text{rad}} = \frac{2P}{c} \approx 10^{-3} \text{ dynes.}$$

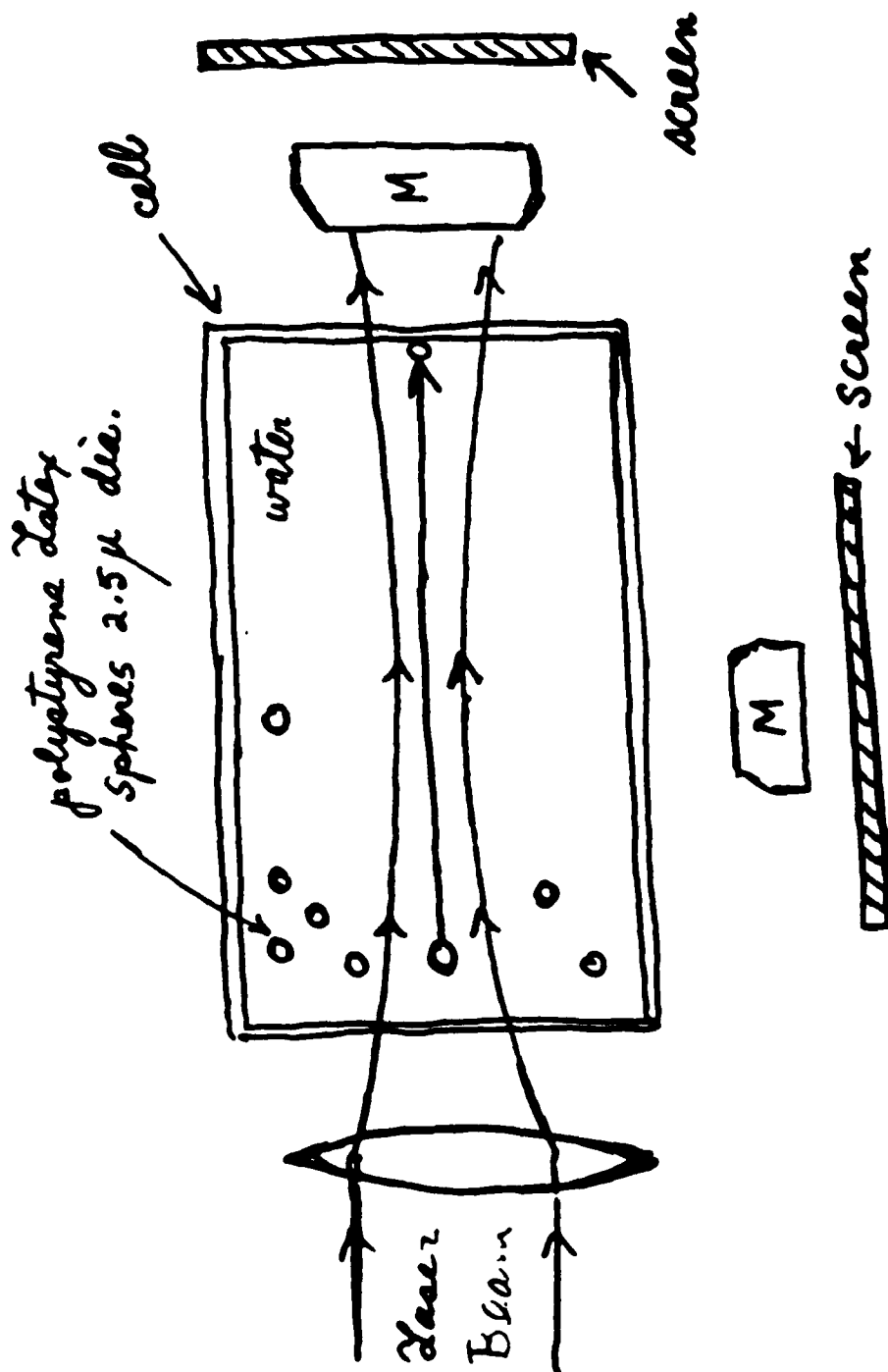
$$\text{Accel } A = \frac{F}{m} \approx 10^9 \text{ cm/sec}^2 = 10^6 g$$

Big !!

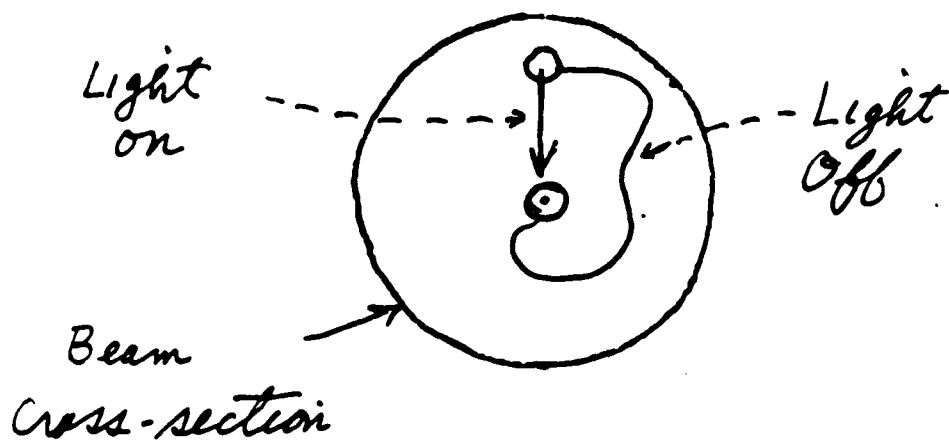
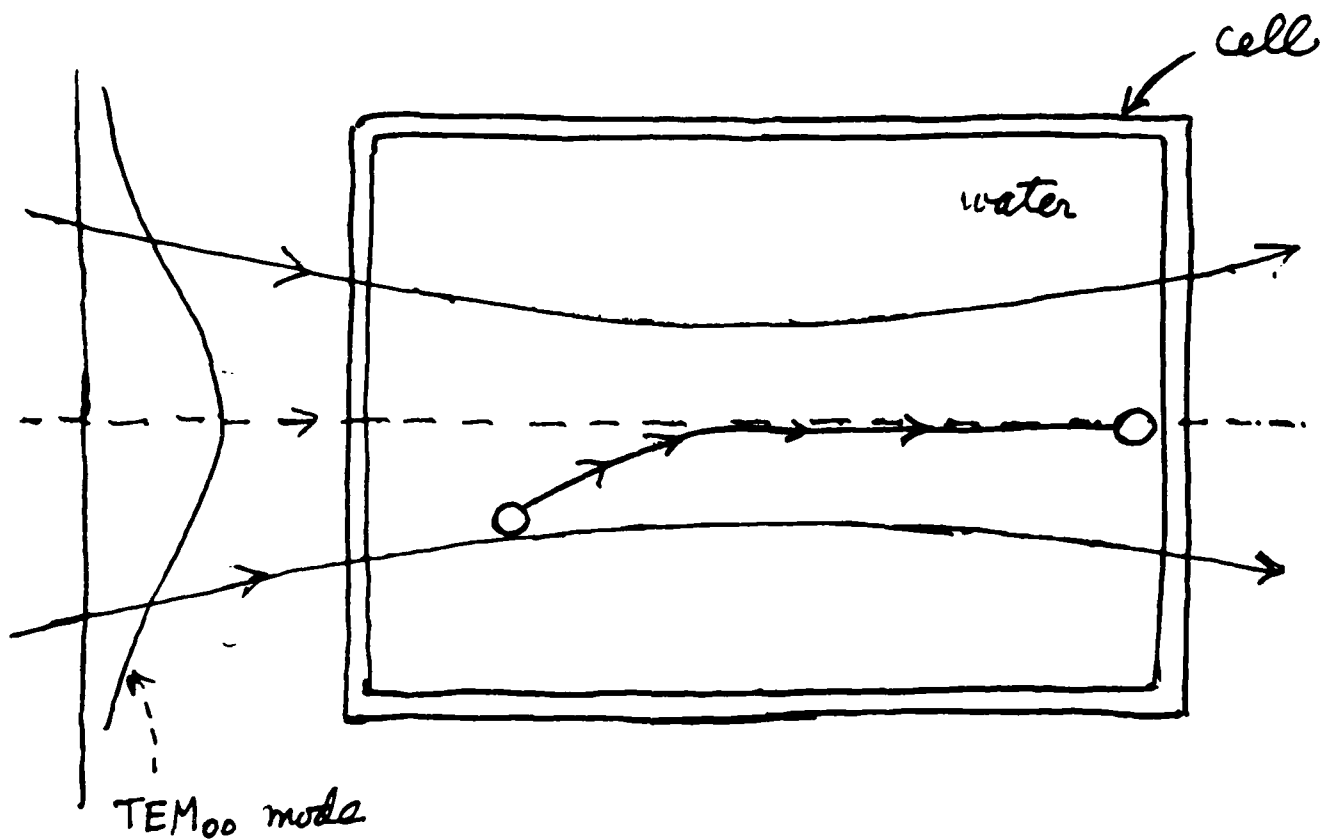
Atoms:

$$\sigma_{\text{sat}} \sim \lambda^2 \quad m_{\text{atom}} \sim 10^{10} \text{ smaller}$$

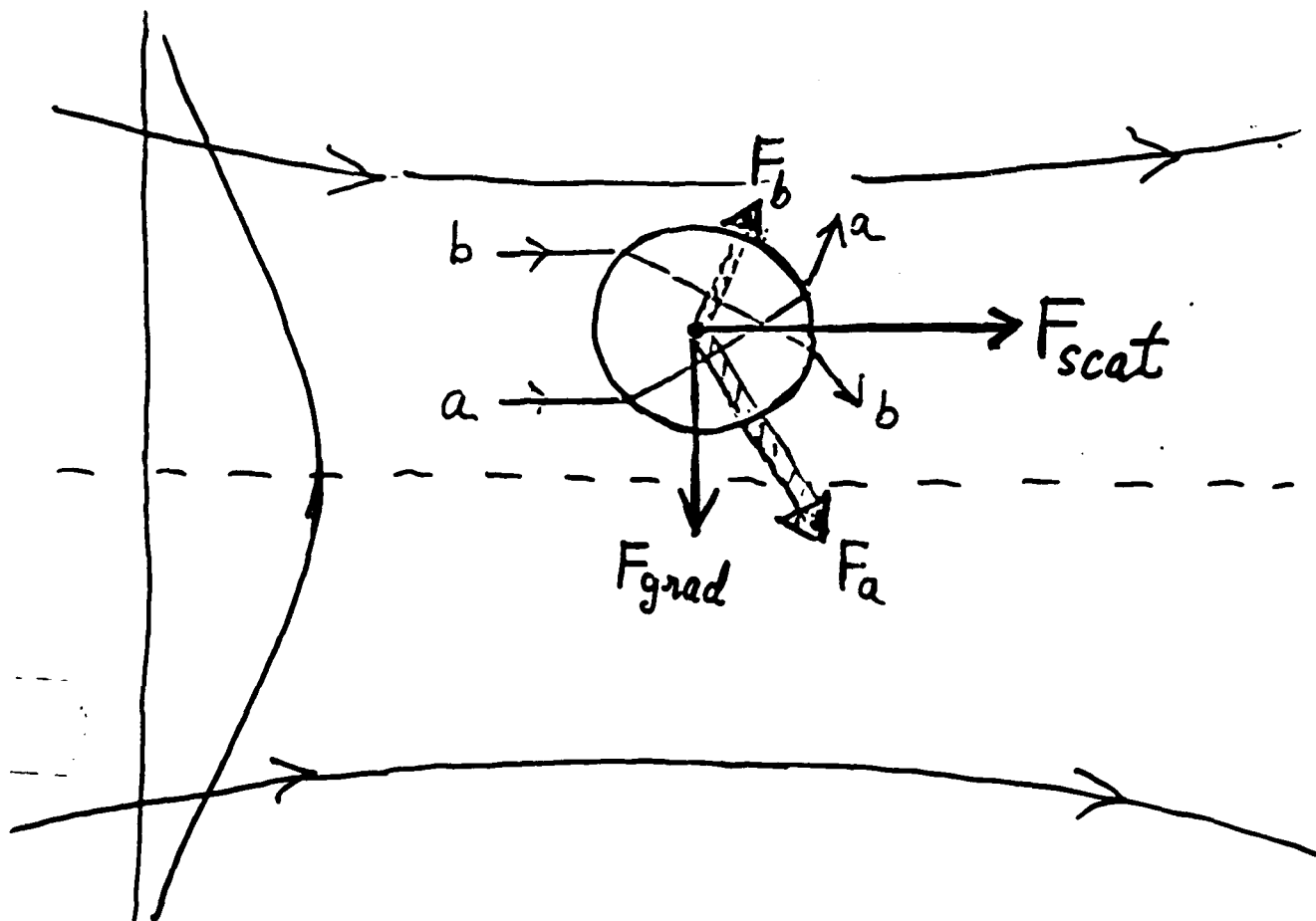
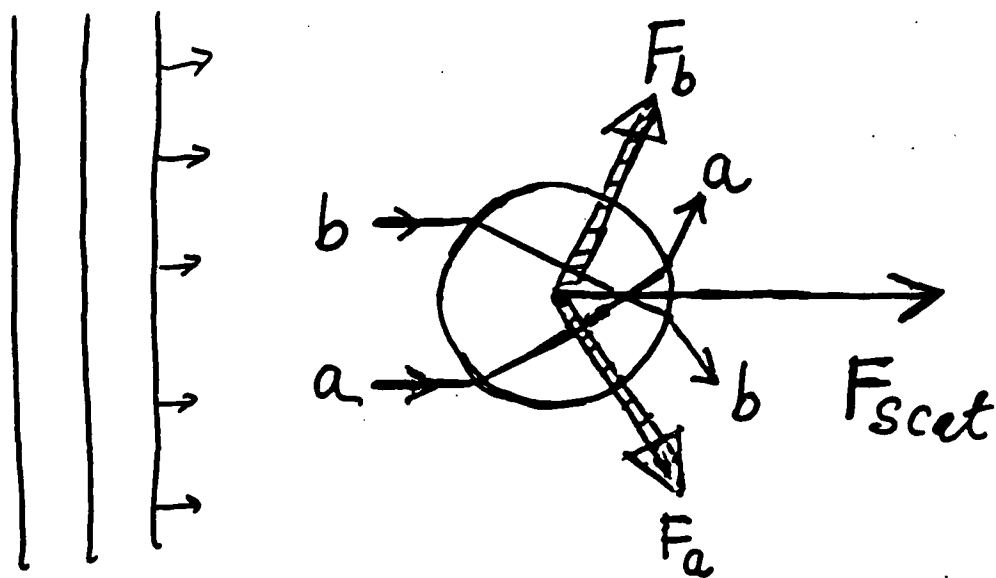
A large in spite of saturation



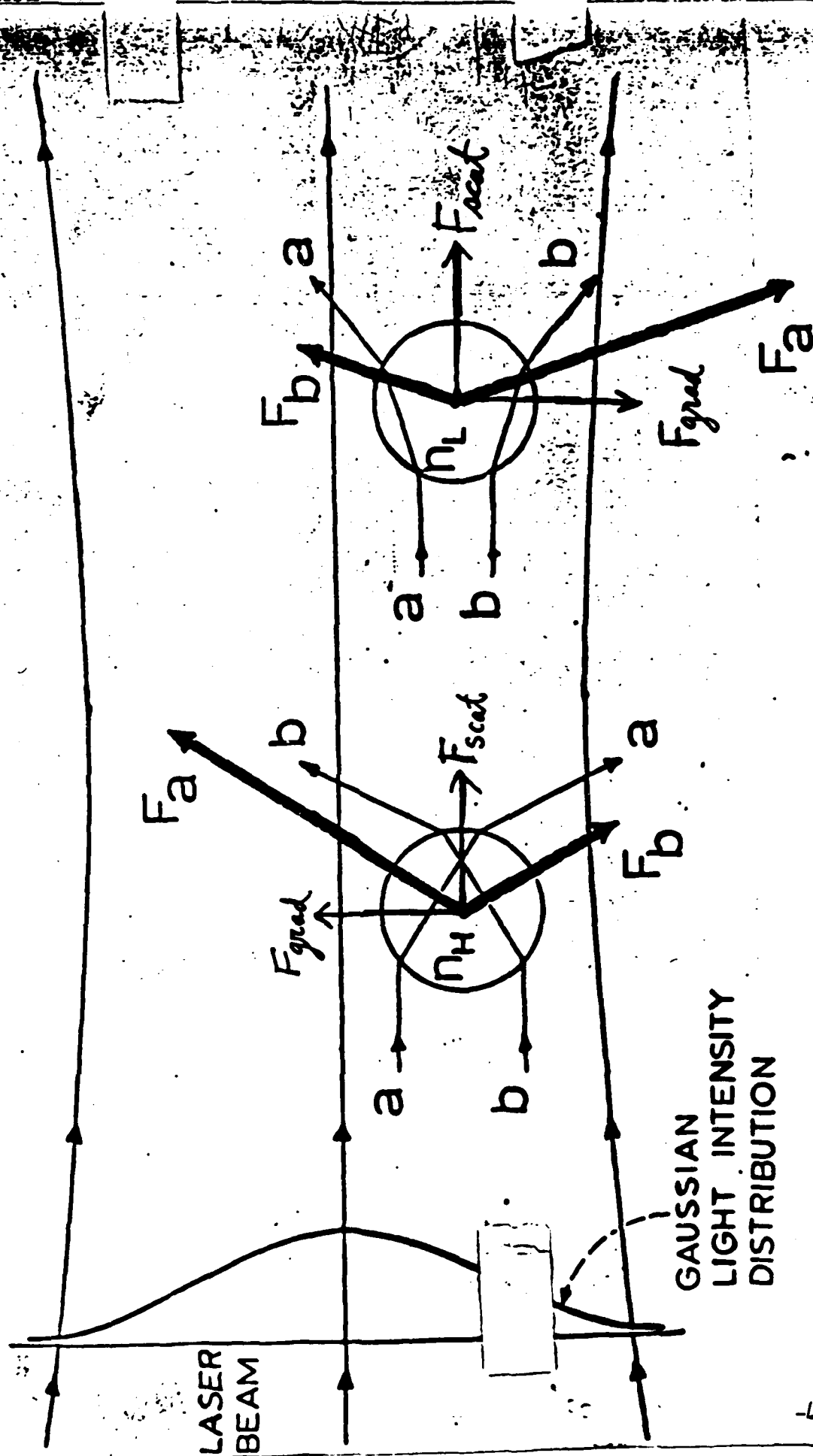
(3)



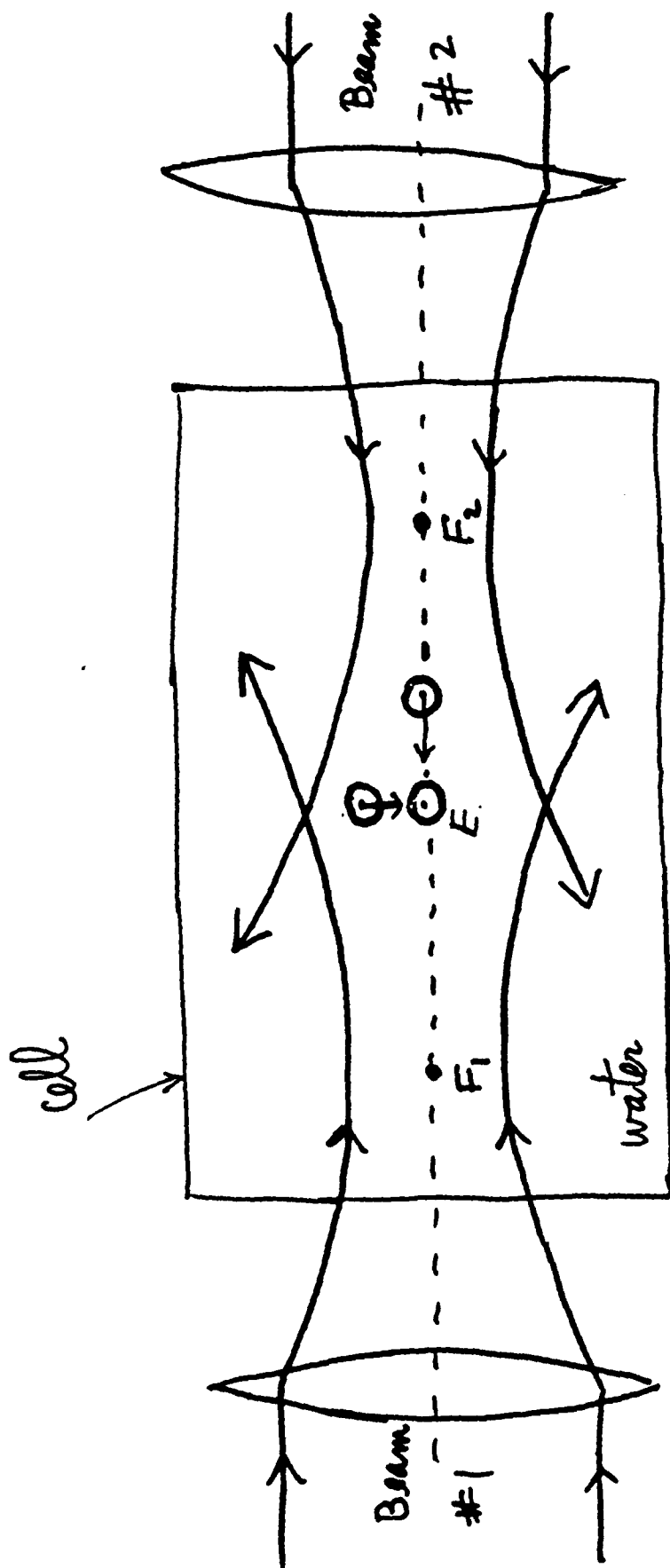
Mie Particles - $d \gg \lambda$



GRADIENT FORCE



Just Optical Trap

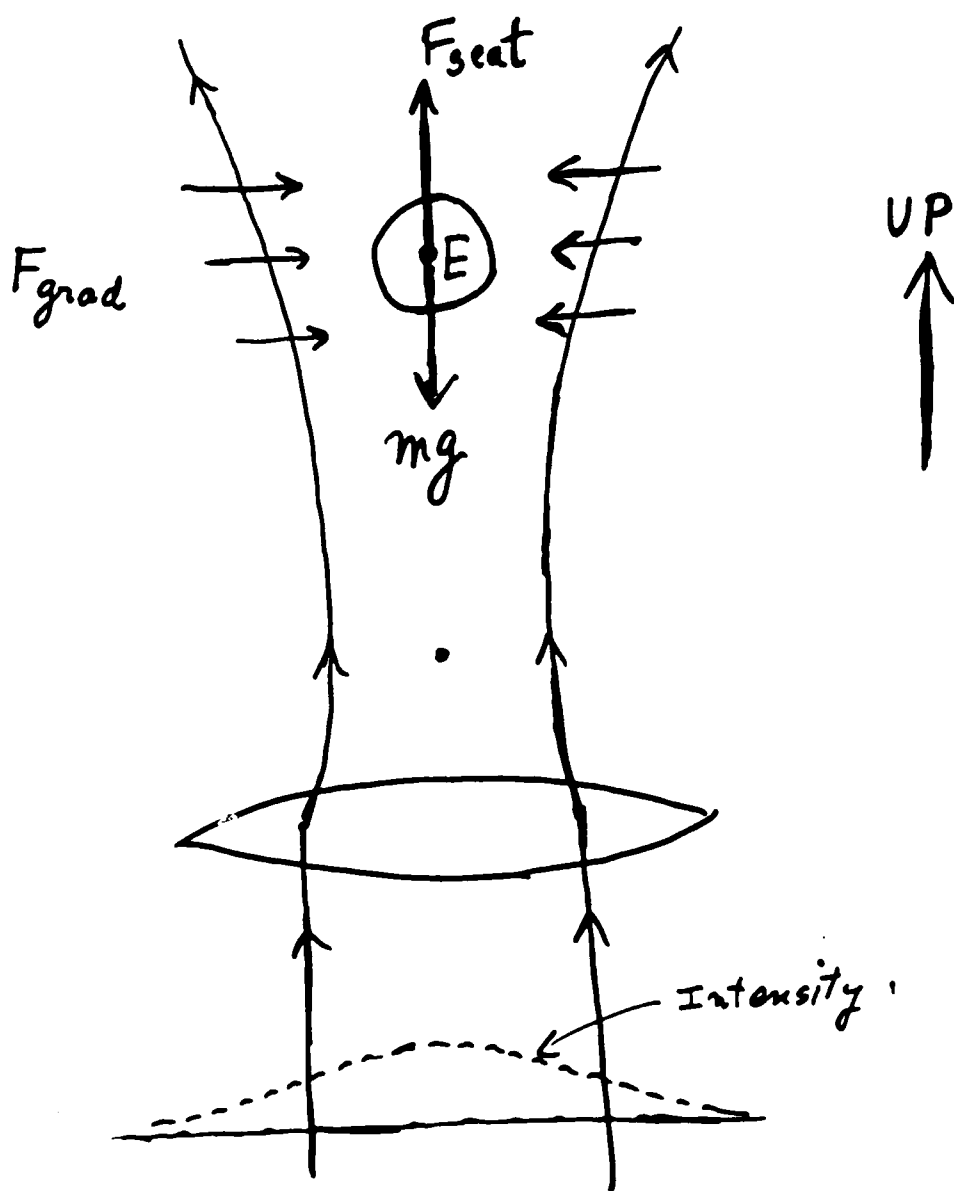


Microscope

Ashkin,

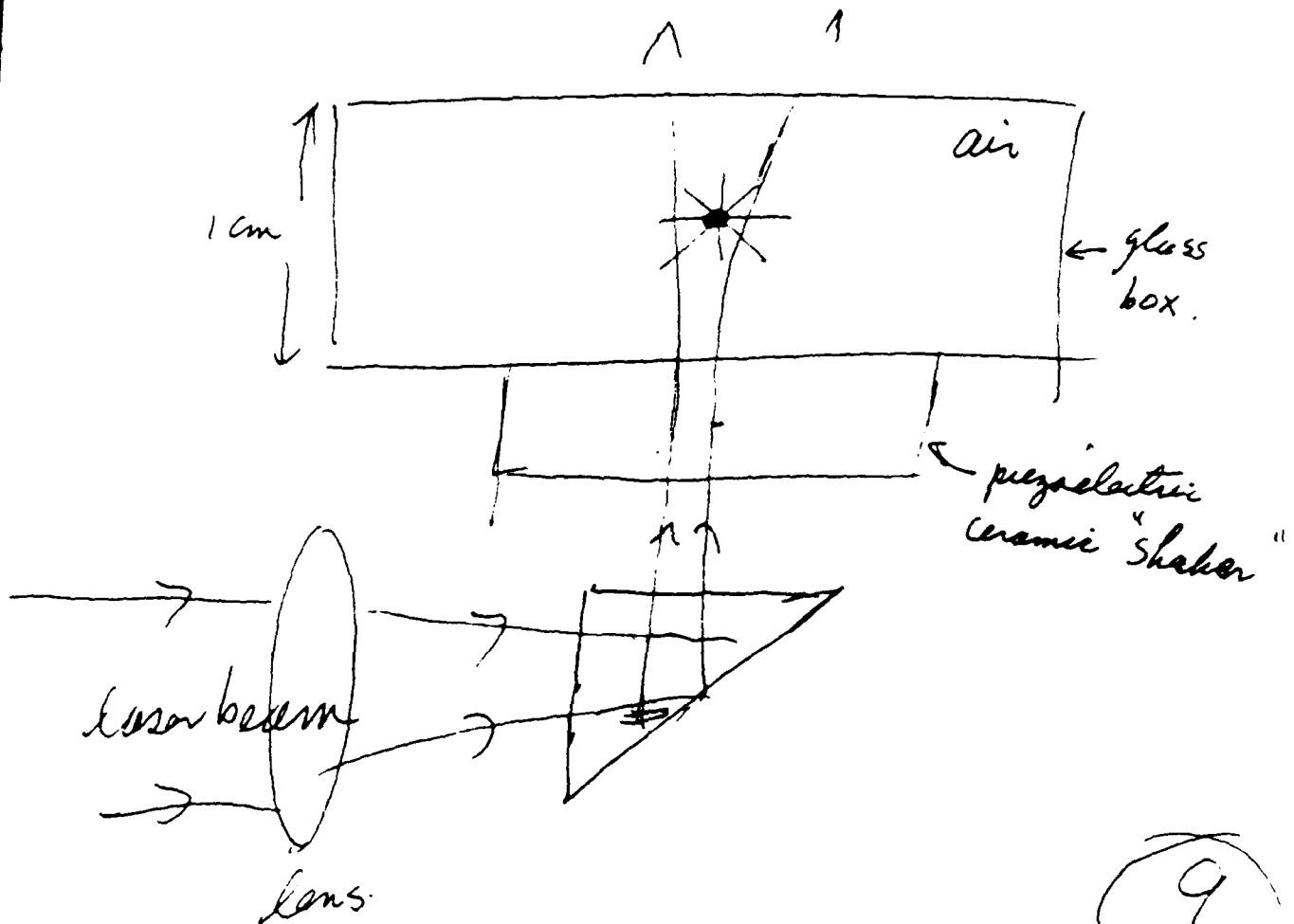
Phys. Rev. Lett. 24, 156 (1970).

Optical Levitation Trap -



Ashkin and Dziedzic, Appl. Phys. Lett. 25, 283 (1971)

Photo of Levitated Glass Sphere
 $25\mu\text{m}$ in diameter



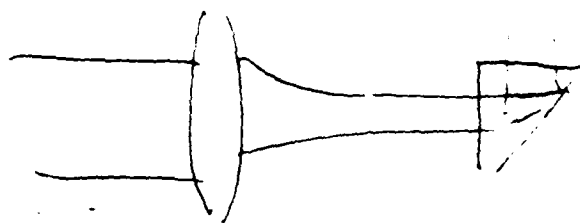
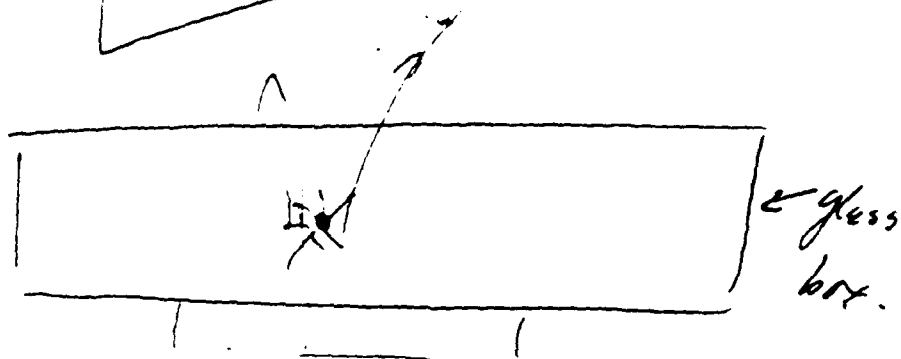
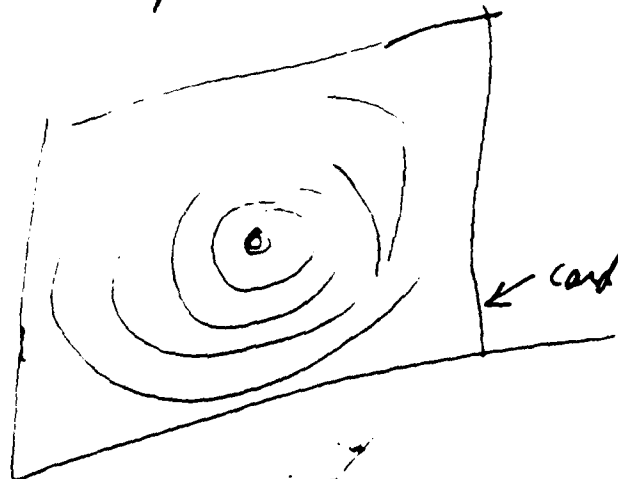
(9)

From Scientific American 226, 63 (1972)
 "The Pressure of Laser Light" A. Ashkin

-45-

DRAWN	ENGR	TITLE	BELL LABORATORIES	SHEET
	DRAWN			
NO. OF SHEETS PER SET				

Photo of "Mie" Scattering Rings from
levitated sphere



10

-46-

DESIGN	ENGR	TITLE	BELL LABORATORIES
	SPAWN		NO. OF SHEETS PER SET

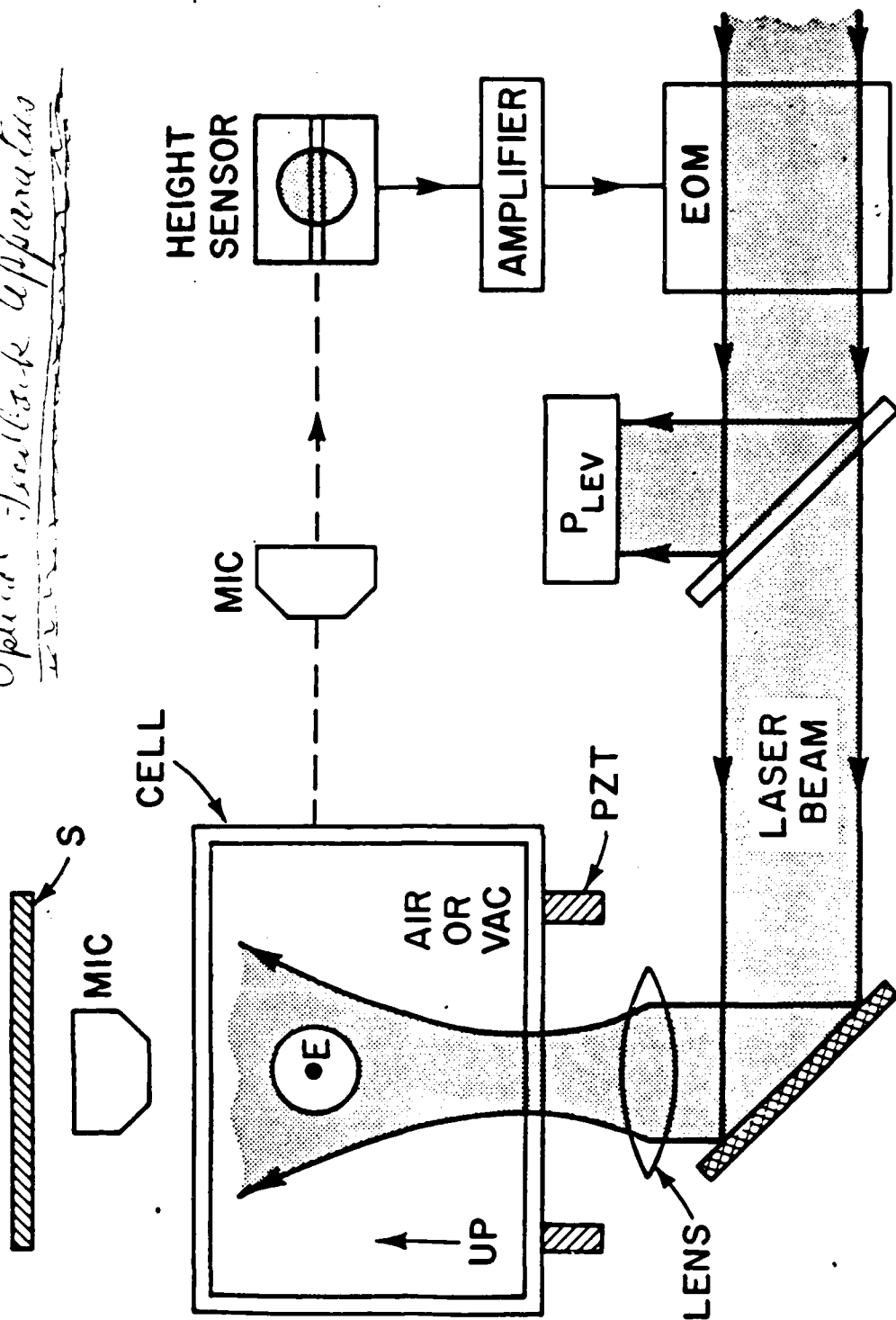
Levitation + Manipulation of Mie Particles

- Assembly of New Particles - Ashkin + Dziedzic
Appl. Opt. 19, 660 (1980)
using 2 beams
- Levitation in Vacuum - { Ashkin + Dziedzic
Appl. Phys. Lett. 28, 333 (1976)
+ Appl. Phys. Lett. 30, 202 (1977)
using optical feedback damping
- Spectroscopy on Single Particles
 λ dependence of Force + Scattering
(First Observation of hi Q Mie Surface-Wave Resonances)

↑
Ashkin + Dziedzic
Phys. Rev. Lett. 38, 1331 (1977).

Ashkin, Science 210, 1081 (1980)
Review Article

Optical Levitation Apparatus

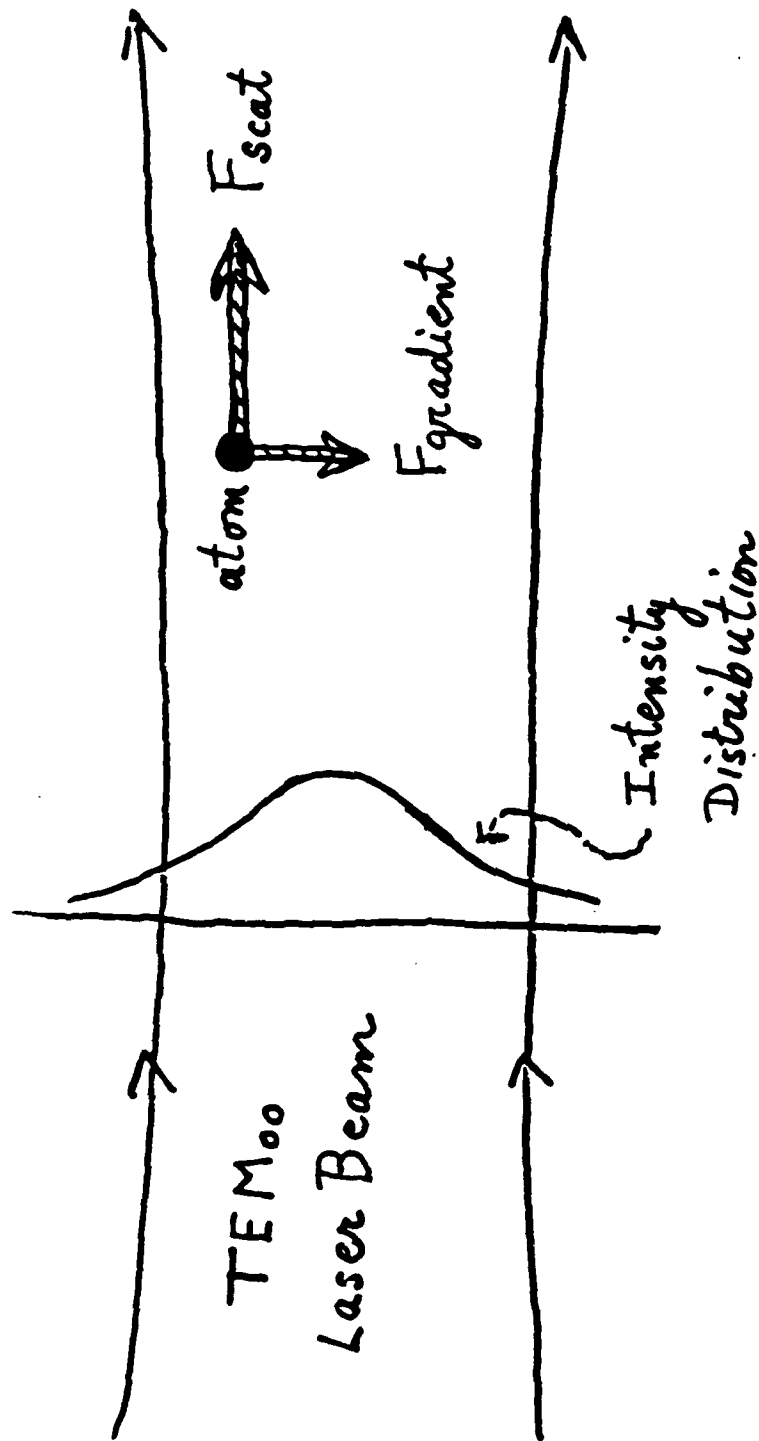


FEEDBACK APPARATUS

BASIC
LEVITATION APPARATUS

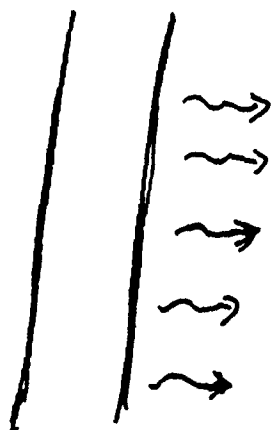
[Oodkin & Dziedzic
Appl. Phys. Lett. 30, 202 (1977).]

Radiation Pressure Forces on Atom
In "Parallel" Gaussian Laser Beam

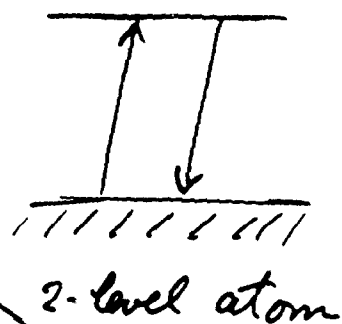
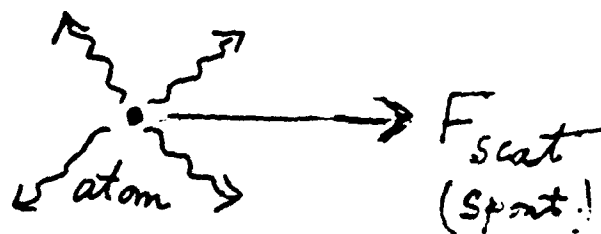


MM

Atoms - Scattering Force



plane wave
resonant light



$$F_{scat} = \left(\frac{h}{\lambda} \right) \left(\frac{1}{\tau_n} f \right)$$

\swarrow mom. photon \searrow # phot/sec scattered

f = fraction of time spent in excited state

low power $f \propto I$

high power $f \rightarrow 1/2$ saturation

Ashkin, Phys. Rev. Lett. 25, 1321 (1970).

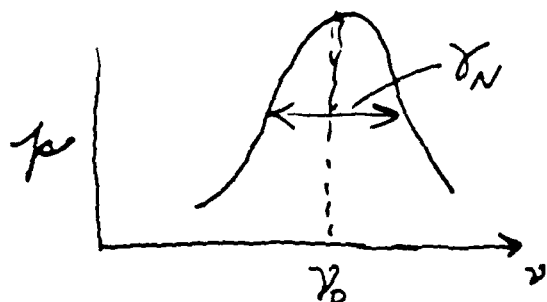
Saturation - Use rate equations

$$F_{\text{sat}} = \frac{h}{\lambda} \frac{1}{\tau_N} f$$

$$f = \frac{1}{2} \frac{p}{1+p}$$

$$p \equiv \text{Sat. parameter} = \frac{I}{I_{\text{sat}}} \frac{(\gamma_N/2)^2}{(\nu - \nu_0)^2 + (\gamma_N/2)^2}$$

↪ line shape.



$$\left. \begin{array}{l} \gamma_N = 10 \text{ MHz} \\ I_{\text{sat}} = 20 \frac{\text{mW}}{\text{cm}^2} \end{array} \right\} \text{Na}$$

$$p = 1 \quad I = I_{\text{sat}} \quad f = \frac{1}{4}$$

$$p = \infty \quad f = \frac{1}{2}$$

$$A_{\text{sat}} = \frac{F_{\text{sat}}}{m} \cong 10^8 \text{ cm/sec}^2.$$

Ashkin, Phys. Rev. Lett 25, 1321 (1970).

Gradient Force
or Dipole Force

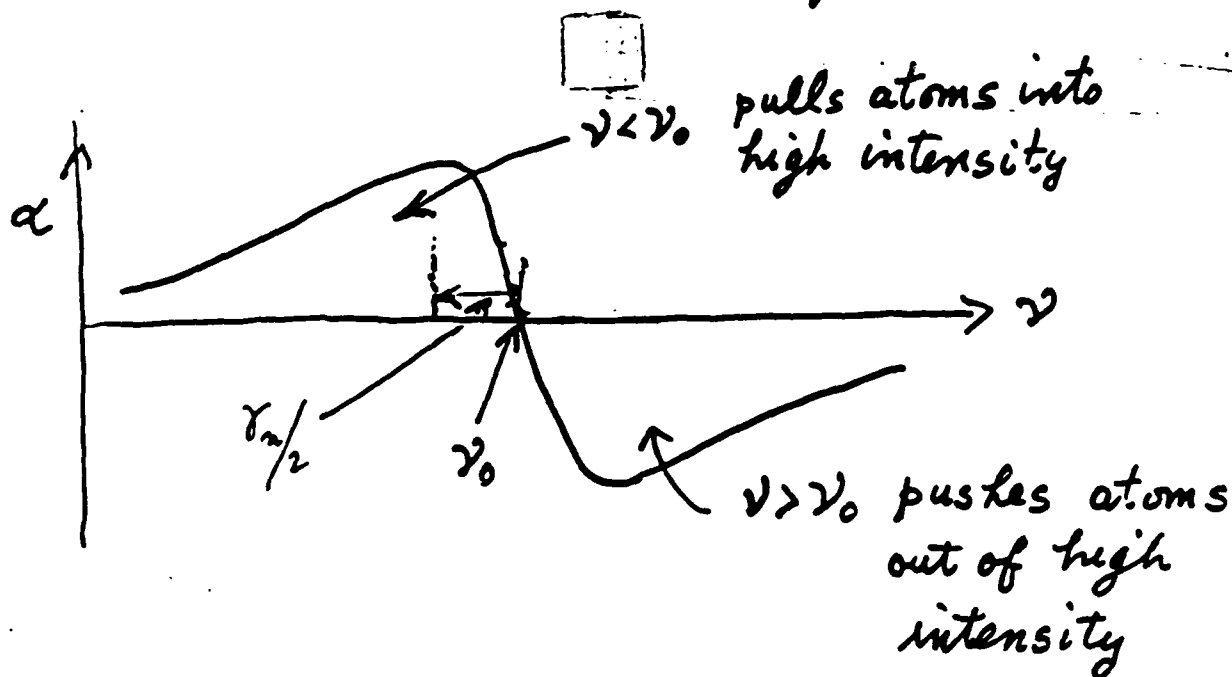
induced dipole moment $d = \alpha E$

α = polarizability of atom

$$\vec{F}_{dip} = -\frac{1}{2} \alpha \vec{\nabla} E^2$$

$$\alpha = \alpha_0 \frac{\nu - \nu_0}{(\nu - \nu_0)^2 + \gamma_n^2/4} \left(\frac{1}{1 + f_p} \right)$$

← saturates to zero
dispersive

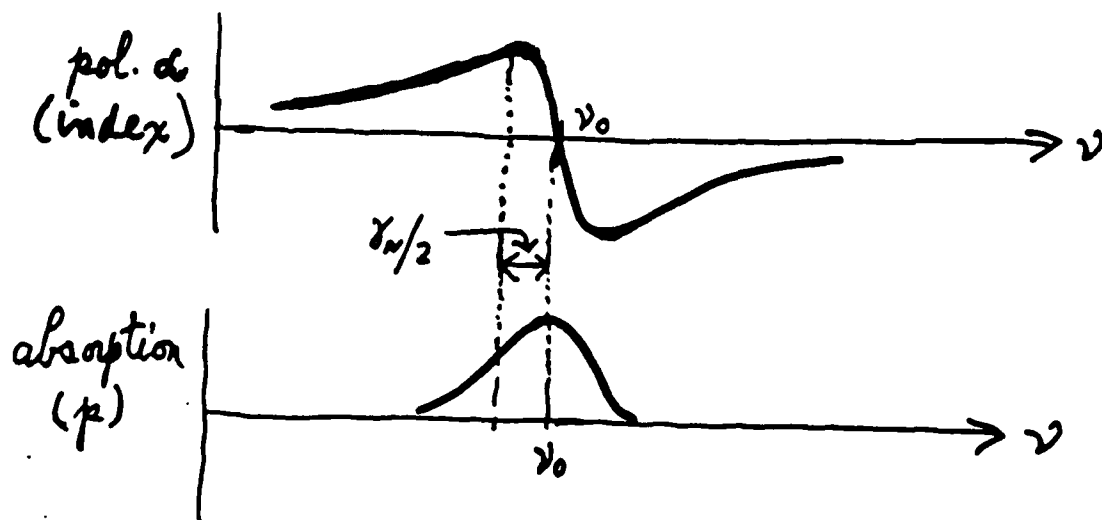


Saturation of F_{dip}

$$\vec{F}_{\text{dip}} = -\frac{\alpha}{2} \vec{\nabla} E^2 = -\vec{\nabla} U$$

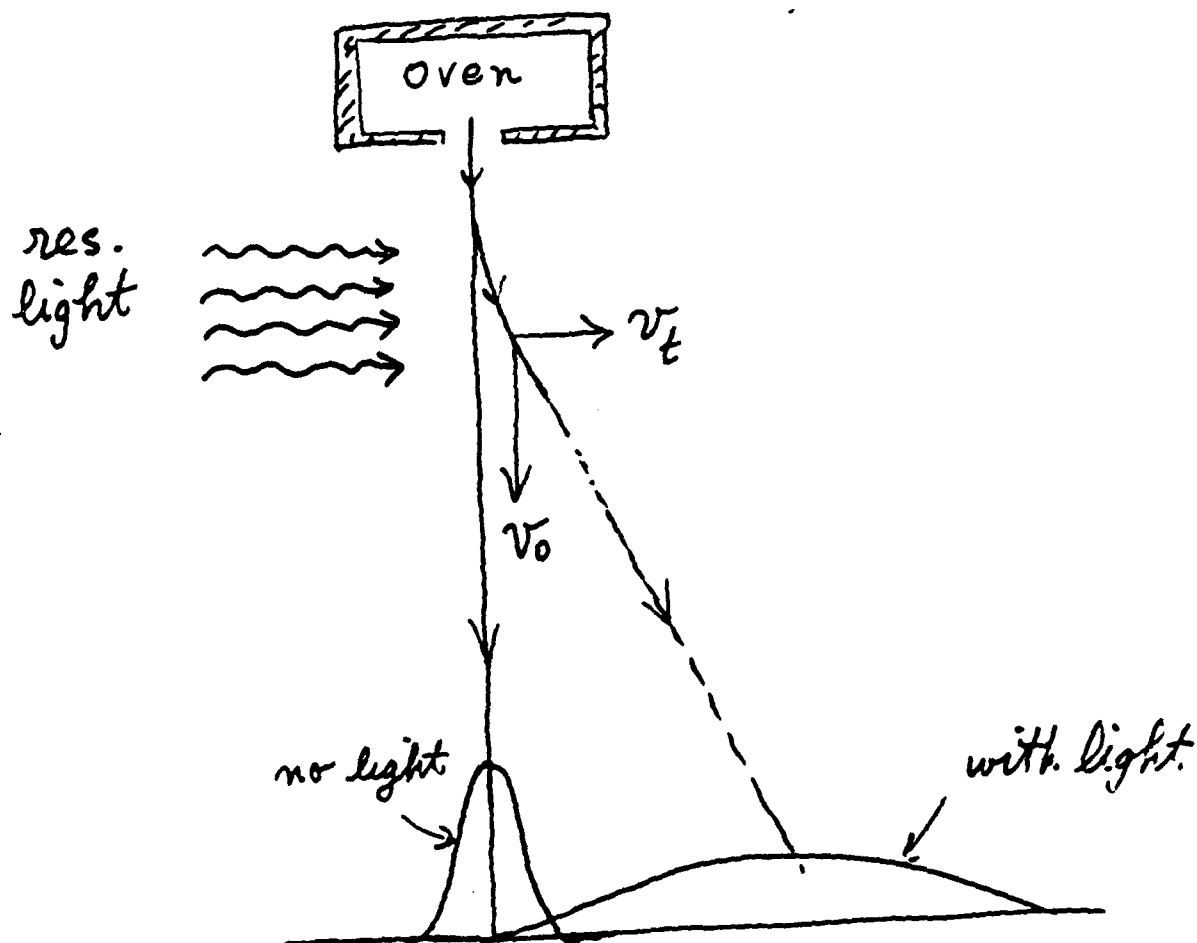
$$U = \frac{\hbar}{2} (\nu - \nu_0) \ln(1+p)$$

same power $\left\{ \begin{array}{l} \nu - \nu_0 = \frac{\gamma_n}{2}, \quad p = 5 \times 10^{-7}, \quad U \approx 4 \hbar \gamma_n \\ \nu - \nu_0 = 5 \times 10^3 \gamma_n, \quad p = 1, \quad \underbrace{U \approx 1.7 \times 10^3 \hbar \gamma_n}_{\sim 400 \times \text{larger!}} \end{array} \right.$



Ashkin, Phys. Rev. Lett. 40, 729 (1978).

Atomic Beam Deflection

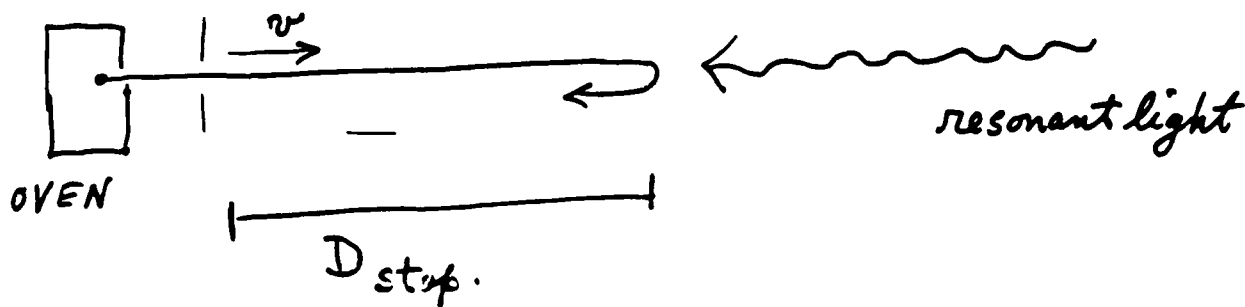


Björkholm et. al. Phys. Rev. A. 23, 491 (1981).

18

-54-

Stopping Atoms -



If $v \sim 2 \times 10^4 \text{ cm/sec}$

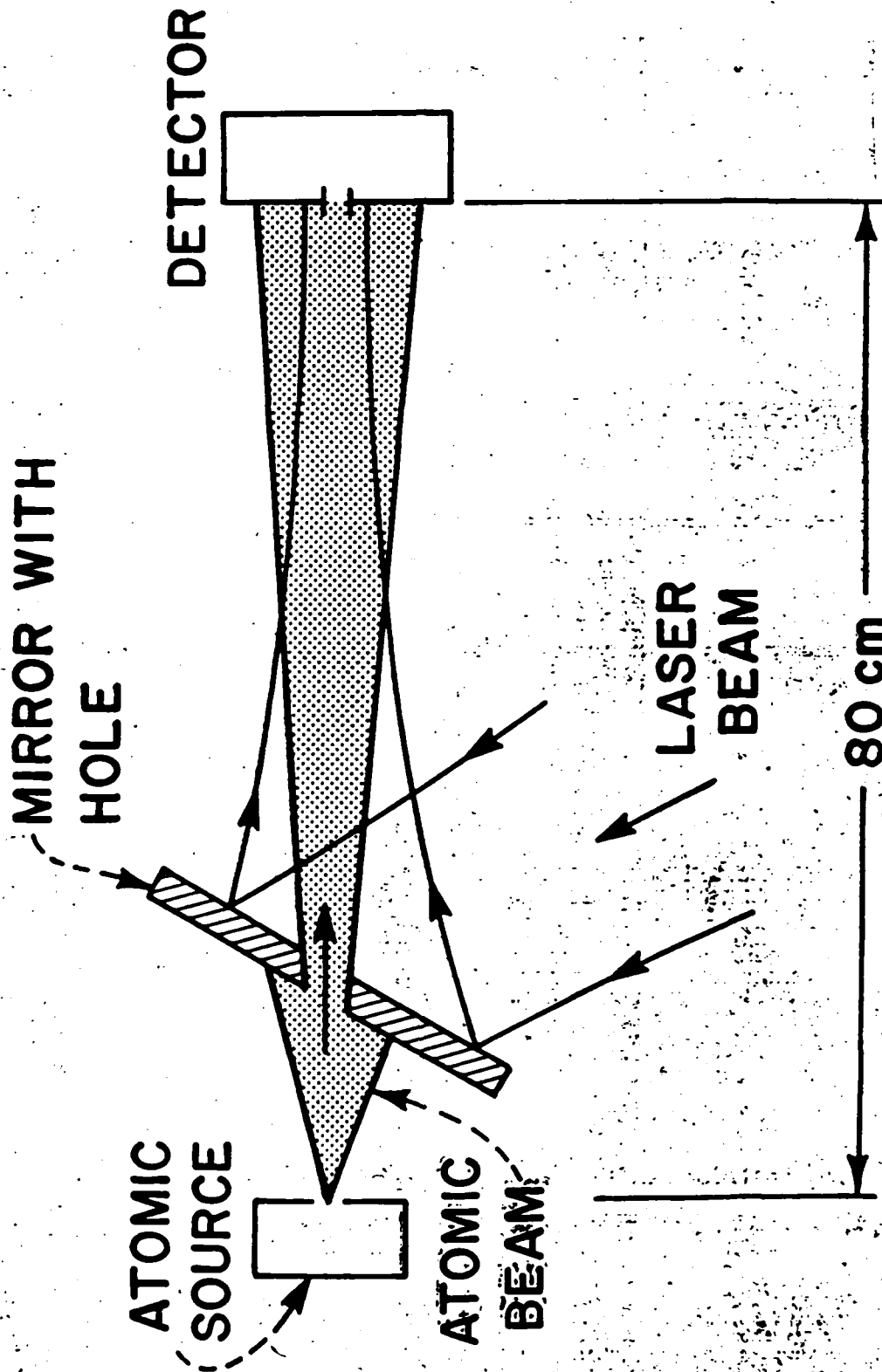
$D_{\text{stop}} \sim 5 \text{ cm.}$

If continuously applied

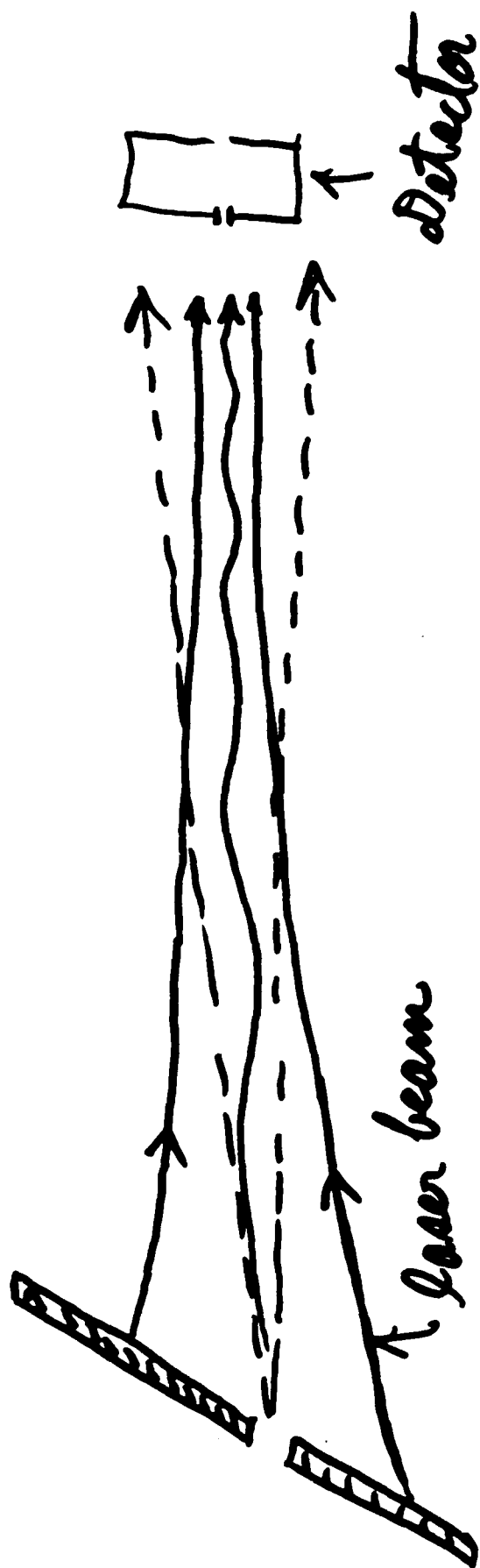
- Doppler Shift -
- Chirp -

Prodan et. al., Phys. Rev. Lett. 54, 992 (1985).

Ertmer et. al., Phys. Rev. Lett. 54, 996 (1985).

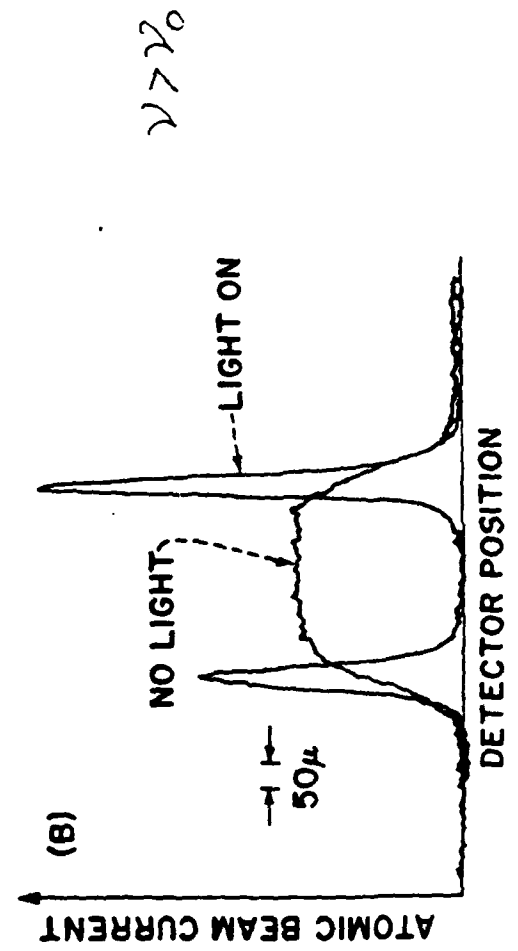
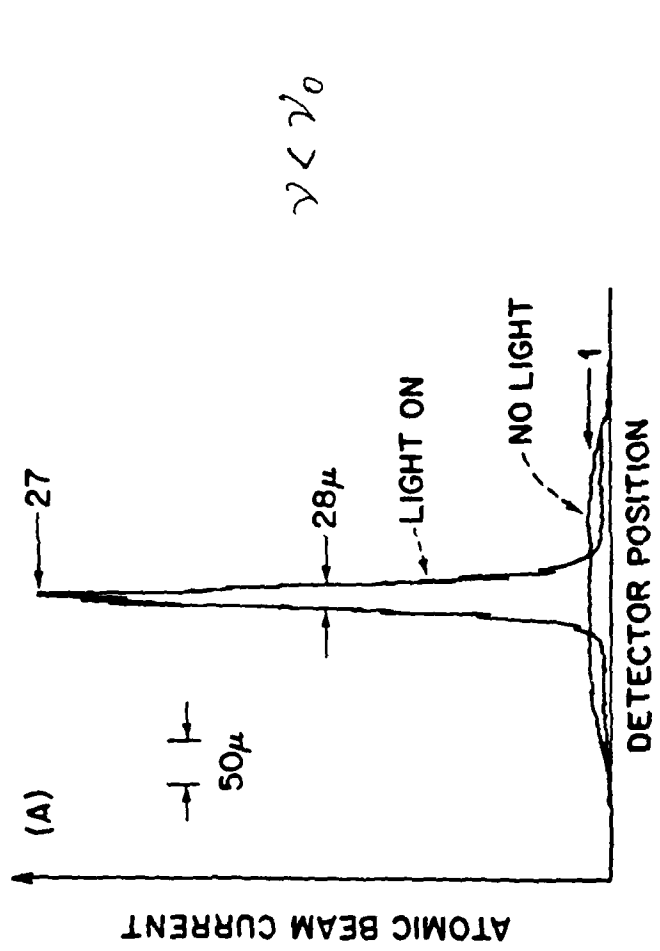


Bjorklein, Frieman, Ashkin, Pearson,
Phys. Rev. Lett. 41, 1364 (1978).

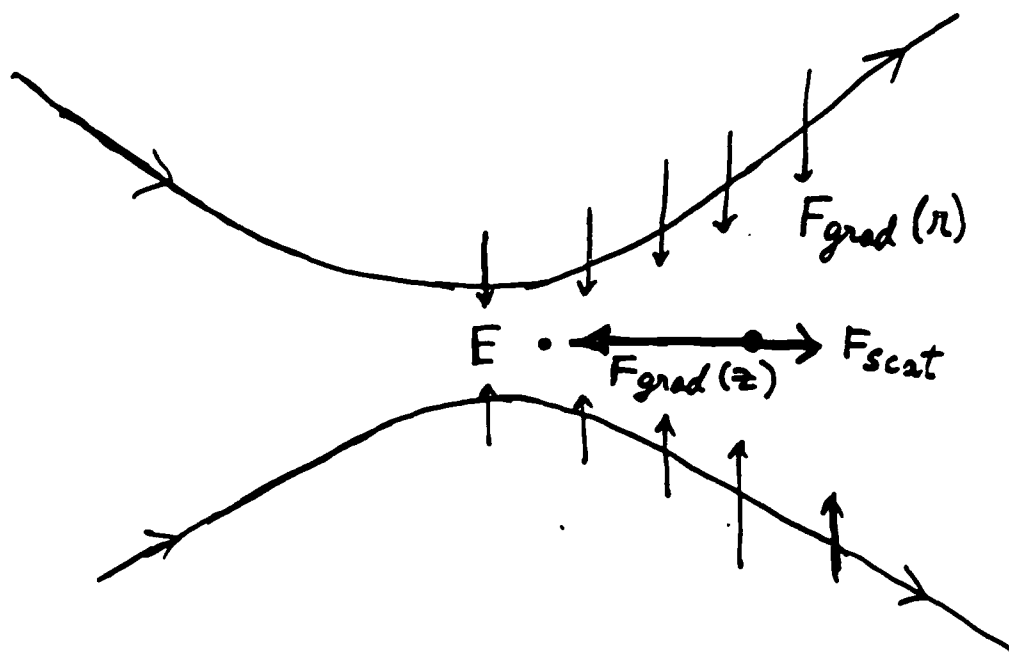


(21)

22



Single-Beam Gradient Trap



$$\underline{U \cong 10^3 h \gamma_n \sim 0.3 \text{ K}}$$

$$v_{\text{escape}} \sim 2 \times 10^3 \text{ cm/sec.}$$

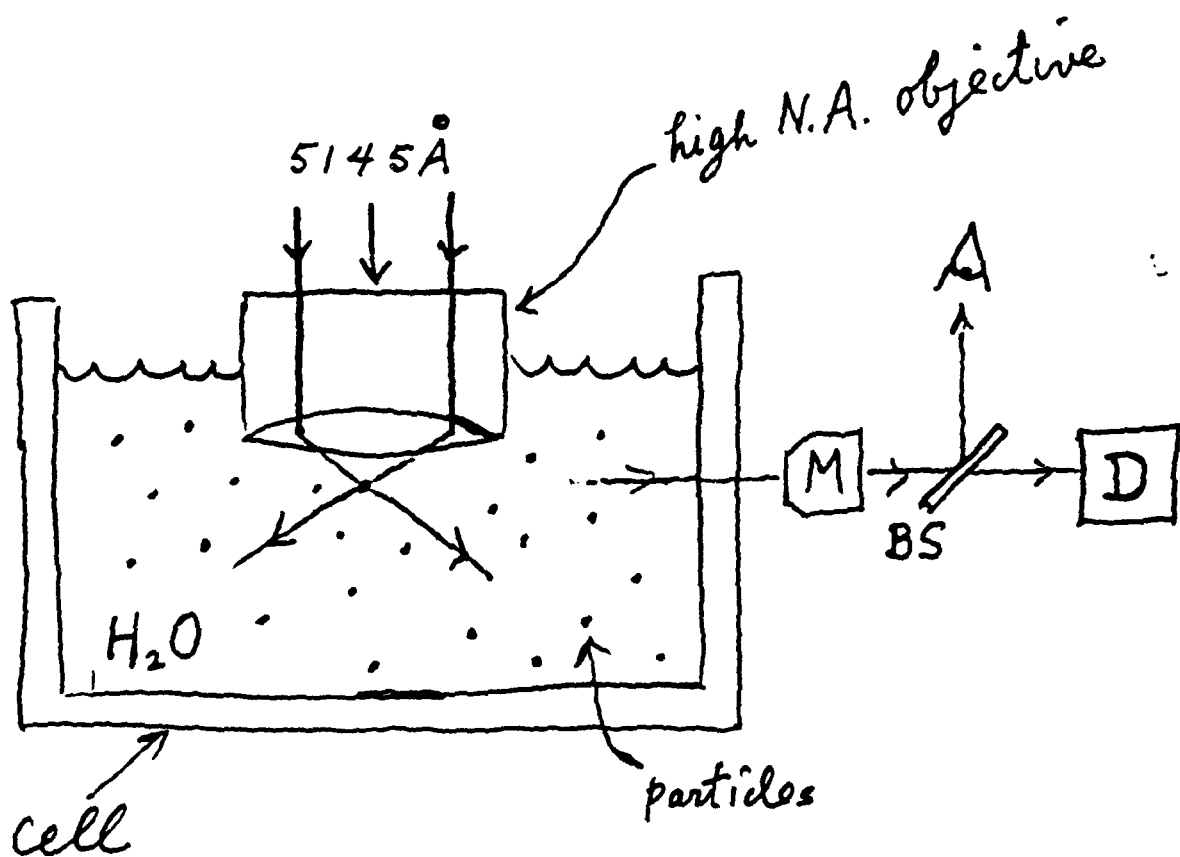
$$\underline{\text{Trapping Volume} \sim 200 \mu^3}$$

$$\left(\begin{array}{l} P = 100 \text{ mW} \\ w_0 = 1.2 \mu \quad \mu \approx 0.2 \end{array} \right)$$

Ashkin, Phys. Rev. Lett. 40, 729 (1978).

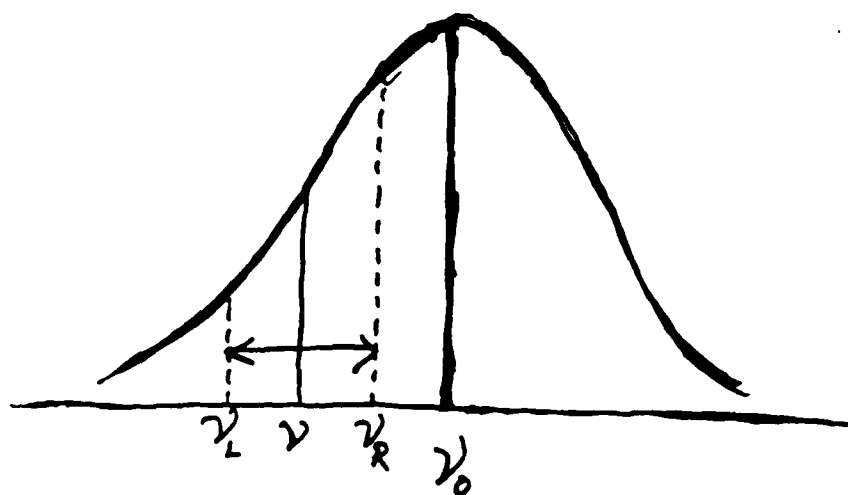
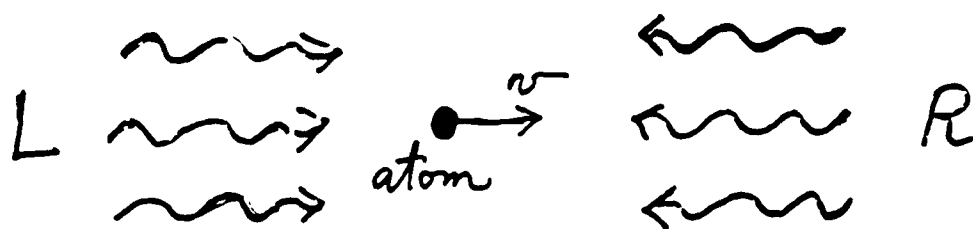
Trapping of Submicron Rayleigh Particles

Apparatus -



Ashkin, Dziedzic, Bjorkholm, Chu
Opt. Lett. 11, 288 (1986).

Optical Damping of Atomic Motion



$$\nu < \nu_0$$

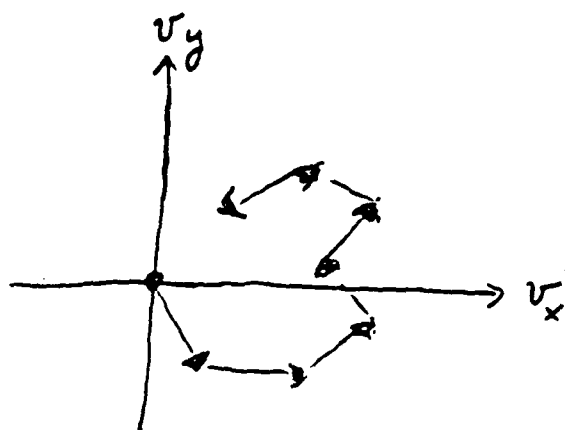
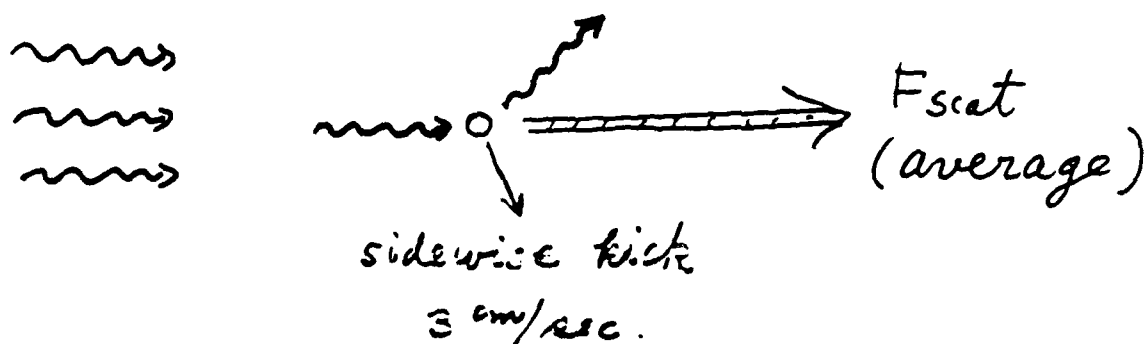
$$F = -\gamma v$$

In 3 dimensions \rightarrow Optical Molasses

Hänsch & Schawlow, Opt. Comm. 13, 68 (1975)

Heating

Quantum Fluctuations in F_{scat}



Random Walk in
Velocity space -

$$\langle \Delta v \rangle = 0 \text{ in milliseconds.}$$

$$\langle \Delta v^2 \rangle \sim t$$

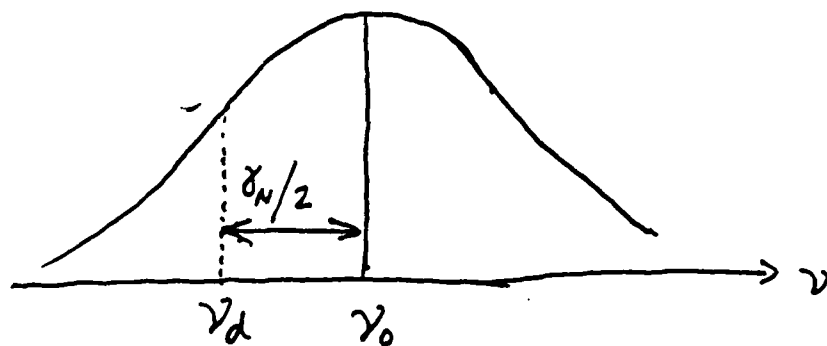
$$\overline{KE}_{\text{random}} \sim \langle \Delta v \rangle^2 \sim t$$

linear heating rate -

Letokhov et. al. JETP 39, 698 (1977).

Ashkin + Gordon, Opt. Lett. 4, 161 (1979).

KE_{equilib} - Balance of Heating + Cooling -



For optimum damping $\nu_d = \nu_0 - \delta_N/2$

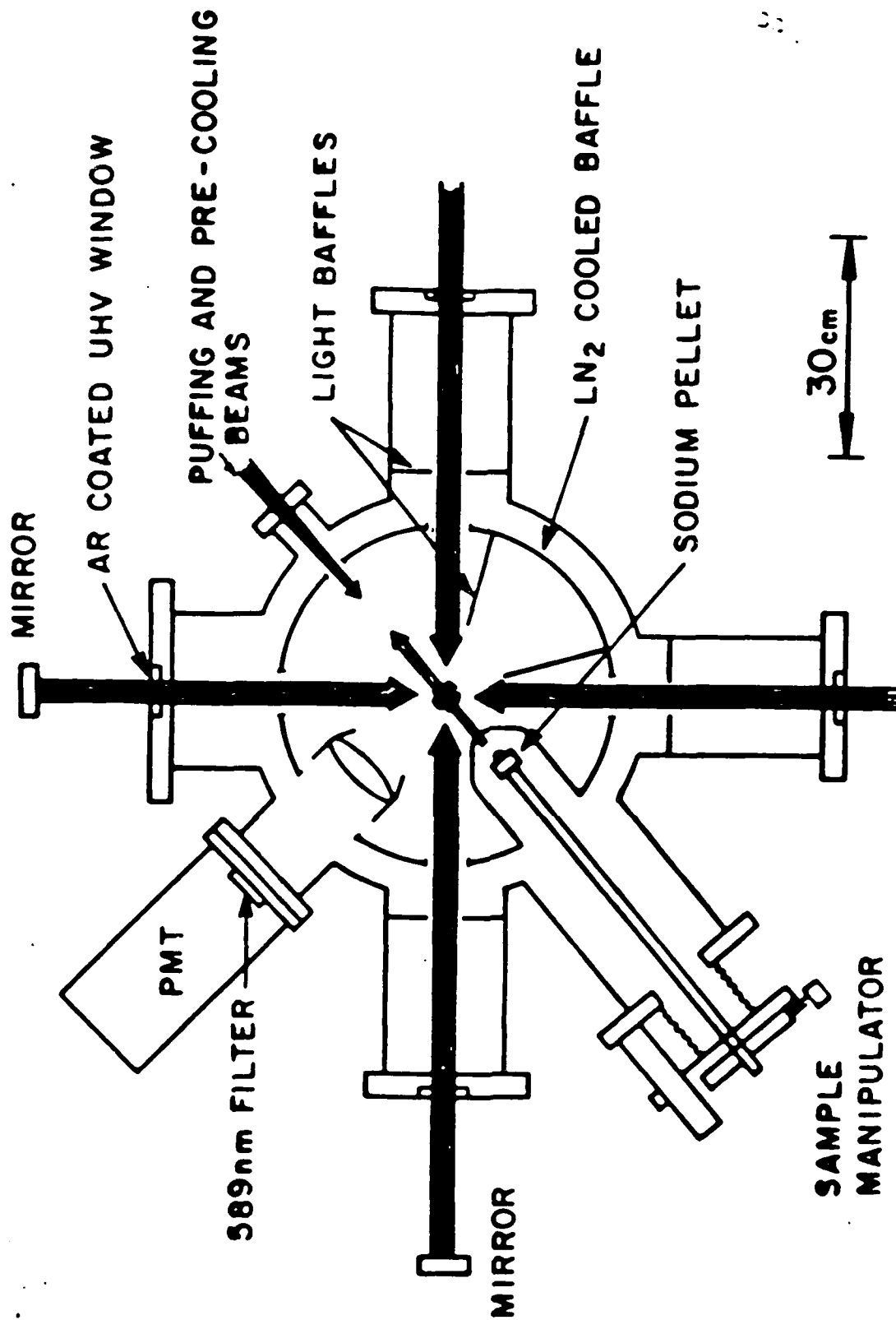
$$KE_{\min} = \frac{\hbar \delta_N}{4} + \frac{\hbar \delta_N}{4} \quad \begin{array}{l} \text{From Scat Force} \quad \text{From Dipole Force} \end{array}$$

$$KE_{\min} = \frac{\hbar \delta_N}{2}$$

$$T_{\min} \cong 240 \mu K.$$

$$v_{\text{av}} \cong 60 \text{ cm/sec}$$

Gordon & Ashkin
Phys. Rev. A 21, 1606 (1980).



E-9148 (10-83)

Chu, Hallberg, Björkholm, Cable, Gashkin

Phys. Rev. Lett. 55, 48 (1985).



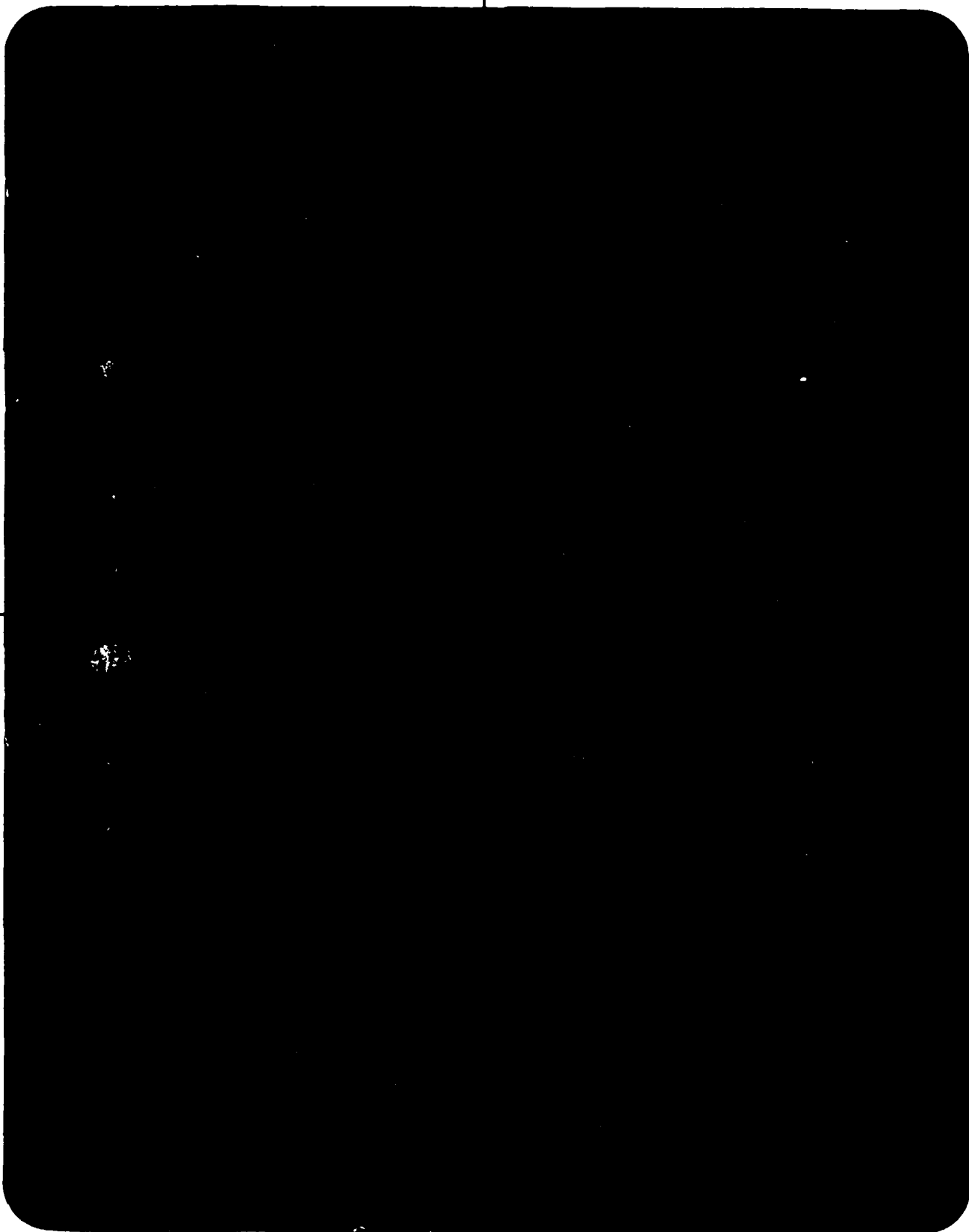
AT&T
Bell Laboratories

28

VG. NO. _____

10p

DO NOT AFFIX OVERLAYS ALONG THIS SURFACE



E-9148 (6-85)

AT&T BELL LABORATORIES



Photo of Apparatus for Motion

29

TOP
DO NOT AFFIX OVERLAYS ALONG THIS SURFACE



1000
1000
6 in
-2.50
6000
(10000)
from
mean
range
Hand
in 10
atom
to 20

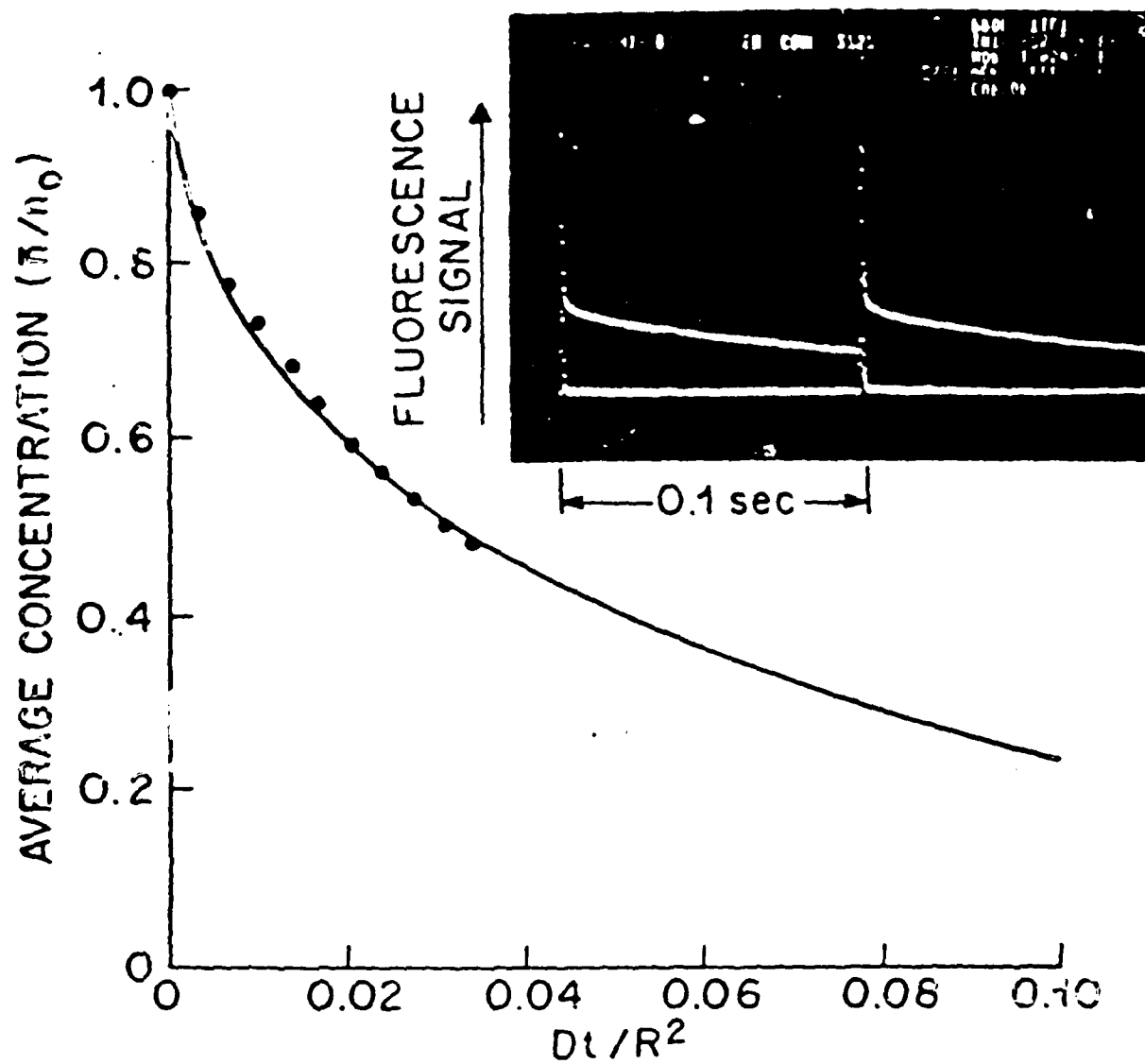


Fig 2.

Time of Flight Temperature Measurement

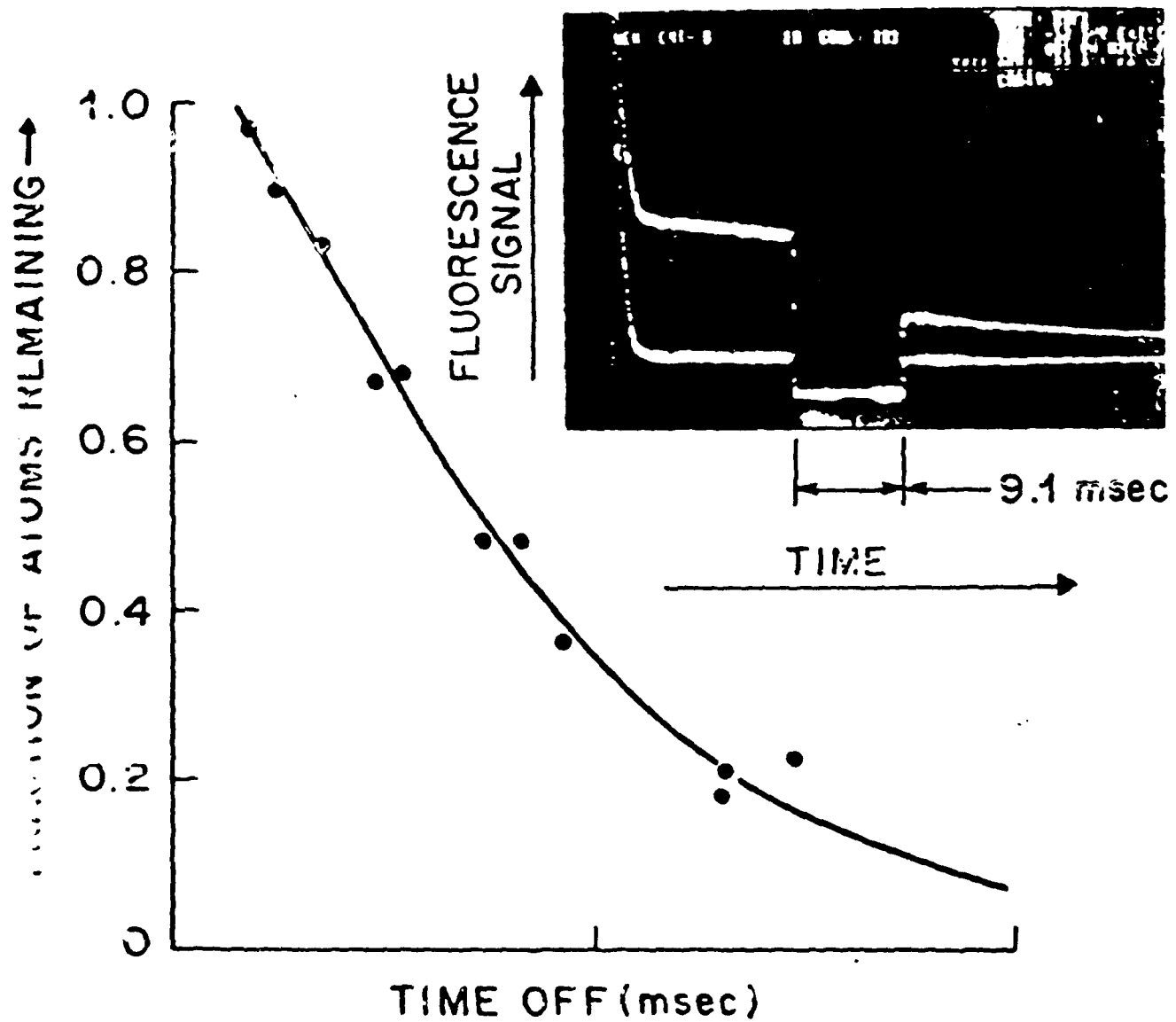


Fig 3.

33

SEQUENCE NO.

VG. NO.

AT&T BELL LABORATORIES

Photo of Atom Trap in Molasses -



AT&T

MACROSCOPIC QUANTUM JUMPS IN A SINGLE ATOM

Axel Schenzle

University of Essen
4300 Essen
West Germany

Richard G. Brewer

IBM Almaden Research Center
650 Harry Road
San Jose, California 95120-6099

ABSTRACT: A single atom optical clock proposed over 10 years ago utilizes an amplification scheme which only recently was recognized as a novel problem in quantum statistics. The atom, a three state system, has two coupled transitions that are driven continuously by two external fields, one being an allowed transition ($1 \leftrightarrow 3$) and the other a forbidden transition ($2 \leftrightarrow 3$) where $|3\rangle$ is the lowest state. It has been argued that the weak transition, which is difficult to detect, could be monitored by the presence or absence of spontaneous emission of the strong transition. Thus, when the atom is shelved in the metastable state $|2\rangle$, the strong transition is extinguished, but when the atom executes a single quantum jump ($2 \rightarrow 3$), it triggers a succession of perhaps a million quantum jumps (macroscopic quantum jumps) in the strong transition, an amplification that can be detected easily. This intuitive argument for alternating bright and dark intervals assumes, however, that the atom is always in an eigenstate. Should the atom be in a superposition state, because of coherent excitation, one could imagine that the weak transition would merely reduce the intensity of the strong transition slightly. This issue is resolved, in favor of the first intuitive argument, by calculating the photon counting statistics, the probability $W(n,T)$ of observing precisely n photon counting events in a collection T in a quantum mechanically consistent way. The results cannot

be described by classical statistics. A compact analytic form is obtained for $W(n,T)$ by considering the entire hierarchy of correlation functions where the emission interval peaks sharply about a particular n with a Poisson distribution and can be comparable in length to the darkness interval ($n = 0$) while the other values of n display vanishingly small probabilities.

The British Journal for the Philosophy of Science

VOLUME III

AUGUST, 1952

No. 20

ARE THERE QUANTUM JUMPS?

PART I*

E. SCHÖNBERGER

"... cominciati a credere, che uno, che faccia un'opinione imbecille
coll'istesso, e seguita da infiniti, per venire in un' altra da pochissimi seguita,
e seguita da tutte le scuole, e che veramente scriba un'opinione grandissima,
bisognante per necessità, che fosse nuova, per non dir famosa, da ragioni
più efficaci." Galileo, *Dialogue on the Two Great World Systems*, 2nd Day.

1. *The Cultural Background*

PHYSICAL science, which aims not only at devising fascinating new experiments, but at obtaining a rational understanding of the results of observations, incurs at present, so I believe, the grave danger of getting severed from its historical background. The innovations of thought in the last 50 years, great and momentous and unavoidable as they were, are usually overrated compared with those of the preceding century; and the disproportionate foreshortening by time-perspective, of previous achievements on which all our enlightenment in modern times depends, reaches a disconcerting degree according as earlier and earlier centuries are considered. Along with this disregard for historical linkage there is a tendency to forget that all science is bound up with human culture in general, and that scientific findings, even those which at the moment appear the most advanced and esoteric and difficult to grasp, are meaningless outside their cultural context. A theoretical science, unaware that those of its constructs considered relevant and momentous are destined eventually to be

* Revised 22. iv. 52

Are there quantum jumps?

J.S. Bell¹⁾

Geneva, 19 June 1986

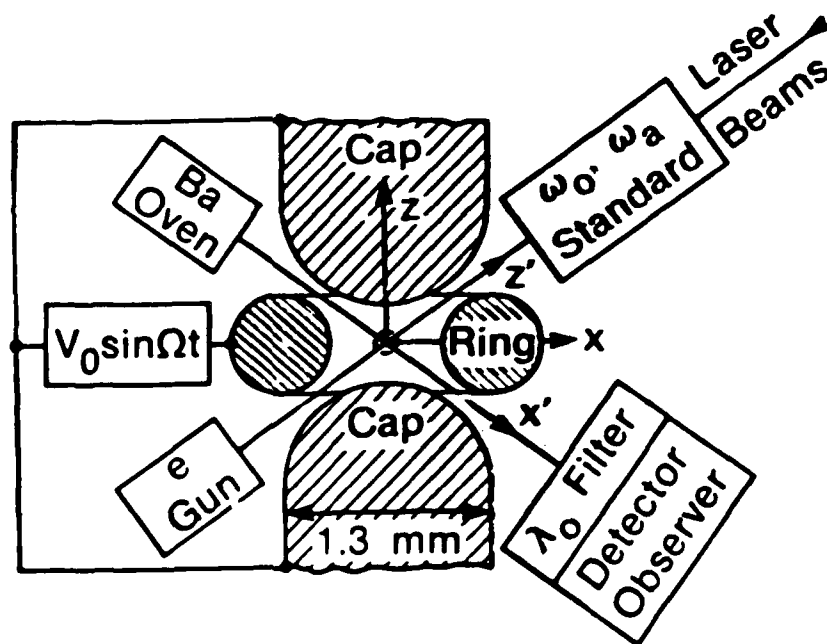
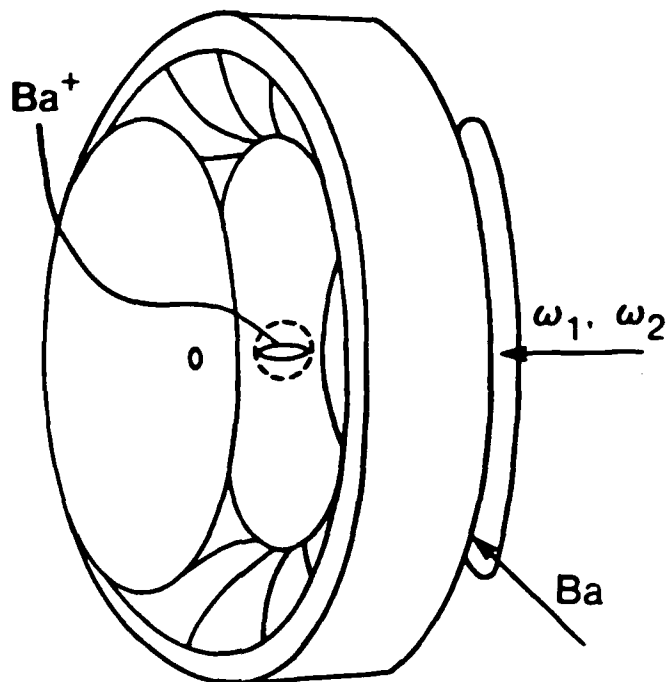
If we have to go on with these damned quantum jumps, then I'm sorry that I ever got involved. E. Schrödinger.

1. Introduction

I have borrowed the title of a characteristic paper by Schrödinger (Schrödinger, 1952). In it he contrasts the smooth evolution of the Schrödinger wavefunction with the erratic behaviour of the picture by which the wavefunction is usually supplemented, or 'interpreted', in the minds of most physicists. He objects in particular to the notion of 'stationary states', and above all to 'quantum jumping' between those states. He regards these concepts as hangovers from the old Bohr quantum theory, of 1913, and entirely unmotivated by anything in the mathematics of the new theory of 1926. He would like to regard the wavefunction itself as the complete picture, and completely determined by the Schrödinger equation, and so evolving smoothly with-

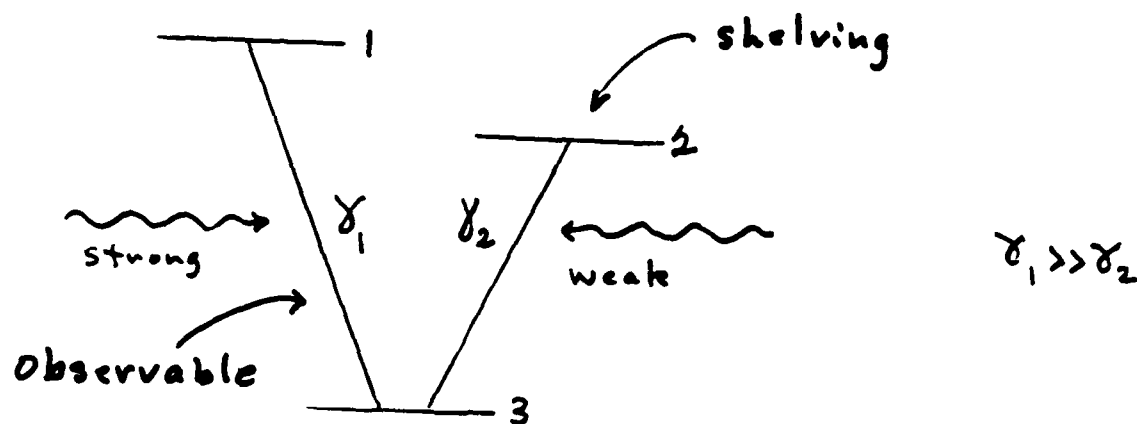
¹⁾ CERN - TH, 1211 Geneva 23, Switzerland

Trapping and Cooling a Single Ba⁺ Ion



W. Neuhauser, H. Hohenstatt, P.E. Toschek
and H.G. Dehmelt, Phys. Rev. Lett. 41, 233 (1978)

Dehmelt proposal: single atom clock - $1/10^8$

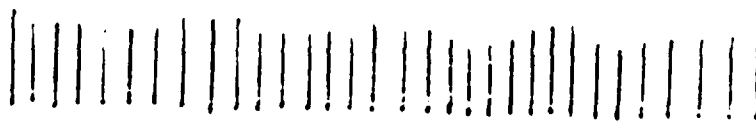


"Macroscopic Quantum Jumps" ?

Does weak transition switch strong transition on and off ?



Or is intensity of strong transition just slightly reduced ?



Macroscopic Quantum Jumps in a Single Atom

Proposal

H.G. Dehmelt, Bull. Am. Phys. Soc. 20, 60 (1975)

Theory

R.J. Cook and H.J. Kimble, Phys. Rev. Lett. 54, 1023 (1985)

F.T. Arecchi, A. Schenzle, R.G. DeVoe, K. Jungmann and

R.G. Brewer, Phys. Rev. A 33, 2124 (1986)

A. Schenzle, R.G. DeVoe, and R.G. Brewer,

Phys. Rev. A 33, 2127 (1986)

A. Schenzle and R.G. Brewer, Phys. Rev. A 34, 3127 (1986)

J. Javanainen, Phys. Rev. A 33, 2121 (1986)

C. Cohen-Tannoudji and J. Dalibard, Europhysics
Letters 1, 441 (1986)

D.T. Pegg, R. London and P.L. Knight,

Phys. Rev. A 33, 4085 (1986)

P. Zoller, M. Marte and D.F. Walls,

Phys. Rev. A 35, 198 (1987)

Experiments

W. Nagourney, J. Sandberg and H. Dehmelt,
Phys. Rev. Lett. 56, 2727 (1986)

R.G. Hulet, J.G. Bergquist, W.M. Itano and
D.J. Wineland, Phys. Rev. Lett. 57, 1699 (1986)

Th. Santer, W. Neuhauser, R. Blatt and
P.E. Toschek, Phys. Rev. Lett. 57, 1696 (1986)

M.A. Finn, G.W. Greenlees and D.A. Lewis
(to be published)

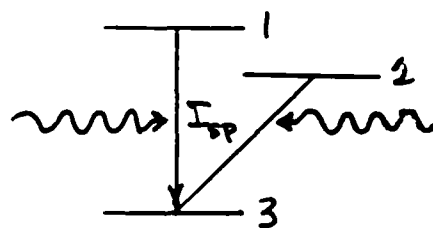
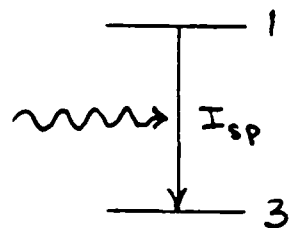
Object of this Talk

Describe a quantum statistical theory which predicts the existence of "macroscopic quantum jumps" and other details of a 3 state atom beginning with

- (1) the Heisenberg equation of motion
- (2) modeling spontaneous emission as a Markov process

Intuitive Arguments

Assume single atom, saturation and steady state



$$I_{sp}^{ss} = \gamma_1 \rho_{11}^{ss}$$

$$\langle I_{sp}^{ss} \rangle = \frac{1}{2} \gamma_1$$

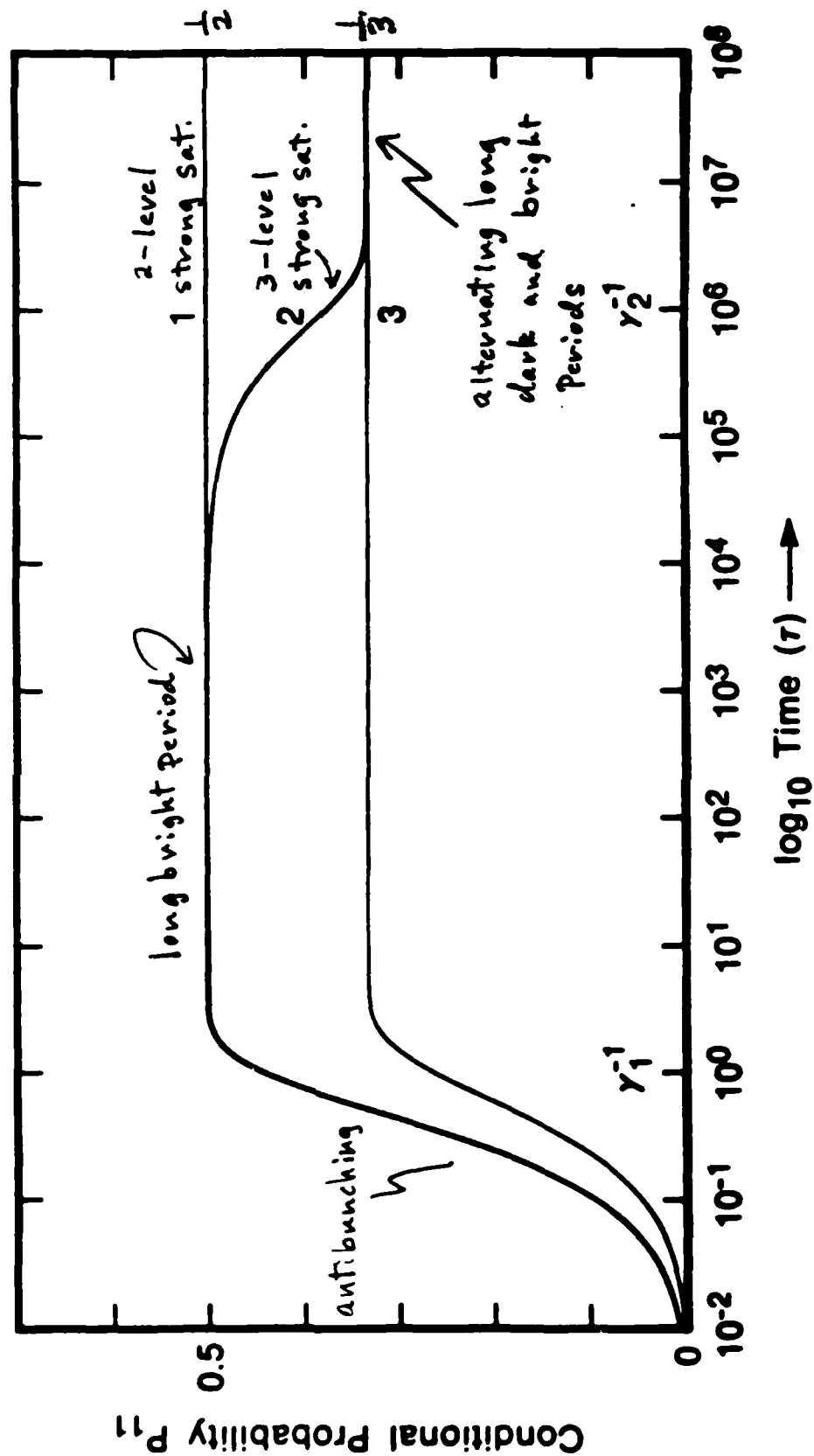
$$\langle I_{sp}^{ss} \rangle = \frac{1}{3} \gamma_1$$

Assume atom is always in an eigenstate in 3-level case

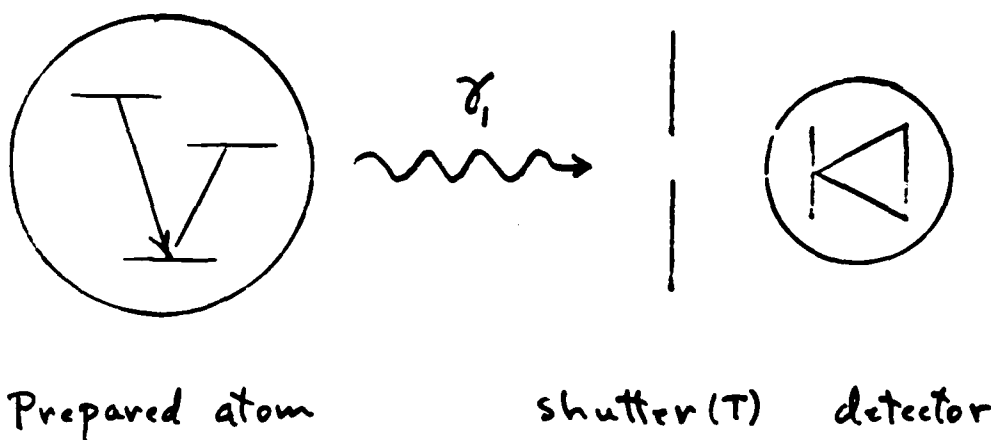
- $2/3$ probability of occupying $|1\rangle$ and $|3\rangle \Rightarrow$ bright period
- $1/3$ probability of being shelved in $|2\rangle \Rightarrow$ dark period
- $\tau_B / \tau_D = 2$
- During bright period, $I_{sp} = \frac{1}{2} \gamma_1$ as in two-level problem, but time average $\langle I_{sp}^{ss} \rangle = \frac{1}{3} \gamma_1 = \frac{1}{2} \gamma_1 \frac{\tau_B}{\tau_D + \tau_B}$

Assume 3 levels in superposition

Intensity is constant in time with $\langle I_{sp}^{ss} \rangle = \frac{1}{3} \gamma_1 - \epsilon$



More general treatment



What is the probability $W(n, T)$ of detecting
 n photons in a collection time T ?

Classical Photon Statistics

$$W(n, T) = \left\langle \frac{1}{n!} \left(\eta \int_0^T I(t) dt \right)^n e^{-\eta \int_0^T I(t) dt} \right\rangle$$

η : detector quantum efficiency

$\int_0^T I(t) dt \sim$ Probability of detecting 1 photon in time T

$$W(0, T) \rightarrow 0 \quad \text{for } I = \frac{1}{2}\delta, \text{ and } T \approx \delta_2^{-1} \\ \neq \frac{1}{3}$$

Quantum Statistics

$$W(n, T) = \text{tr} \rho \left\{ \hat{T} \frac{1}{n!} (\gamma, \eta \int_0^T b^\dagger(t) b(t) dt)^n e^{-\gamma, \eta \int_0^T b^\dagger b dt} \right\}^*$$

$$= \sum_{\ell=0}^{\infty} (-1)^\ell (\gamma, \eta)^{n+\ell} \binom{n+\ell}{\ell} \int_0^T dt_1 \int_0^{t_1} dt_2 \dots \int_0^{t_{n+\ell-1}} dt_{n+\ell}$$

$$\times G_{n+\ell}(t_{n+\ell} - t_{n+\ell-1}, \dots, t_2 - t_1)$$



Photon correlation function

* P.L. Kelley and W.H. Kleiner, Phys. Rev. 136, A316 (1964)

$$W(0,T) = \frac{1}{S+2} \left\{ S e^{-(R_2+\gamma_2)T} + 2 e^{-\frac{1}{2}\eta\gamma_1 T} \right\}$$

$$W(n,T) = \frac{2}{S+2} \frac{\left(\frac{1}{2}\eta\gamma_1 T\right)^n}{n!} e^{-\frac{1}{2}\eta\gamma_1 T}, \quad n=1,2,3-\dots$$

$$S = R_2 / (R_2 + \gamma_2)$$

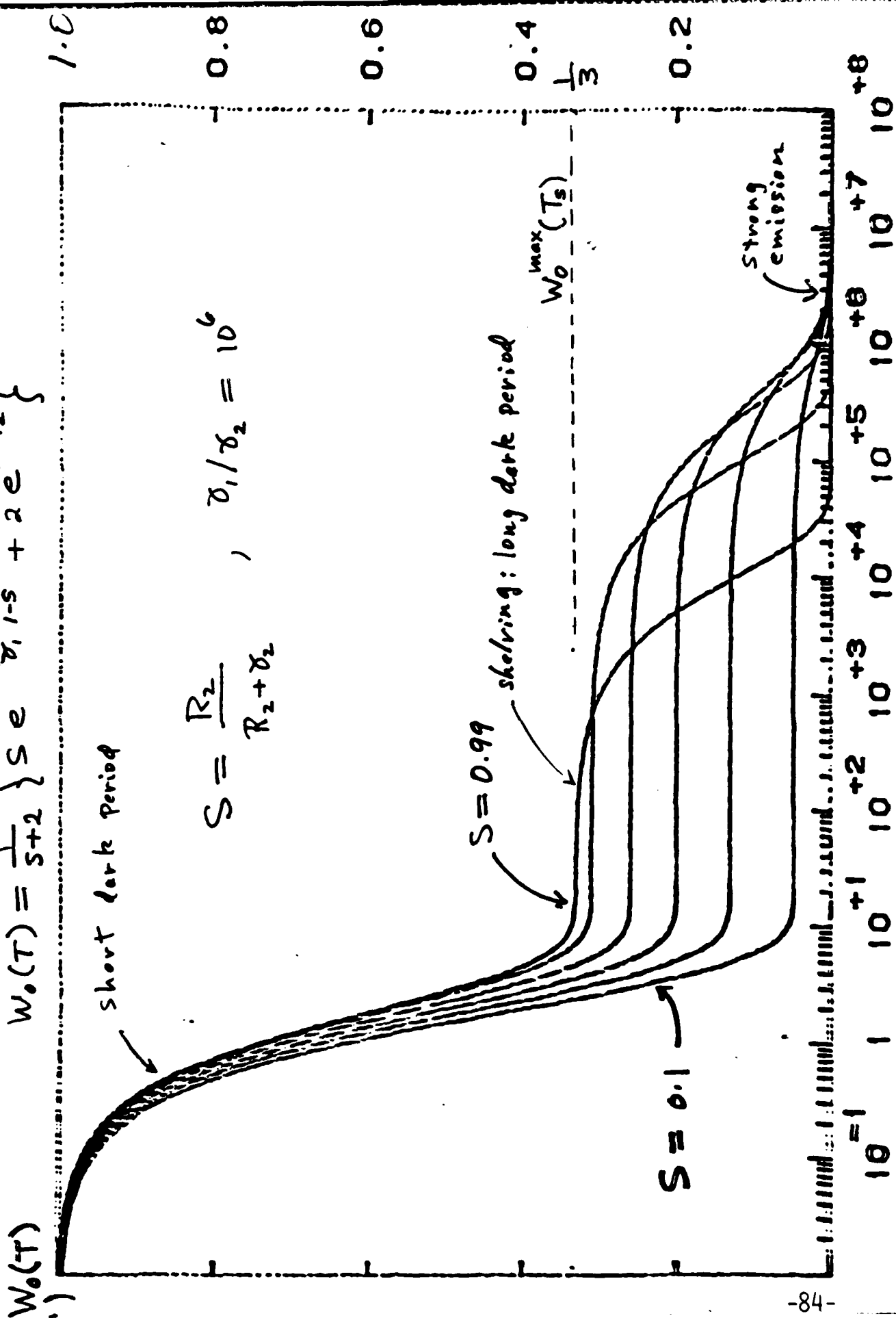
$$\left. \begin{array}{l} \tau_D = \frac{1}{R_2 + \gamma_2} \\ \tau_B = \frac{2}{R_2} \end{array} \right\} \begin{array}{l} S=1 \Rightarrow \\ \frac{1}{3} \text{ of the time dark} \\ \frac{2}{3} \text{ of the time bright} \end{array}$$

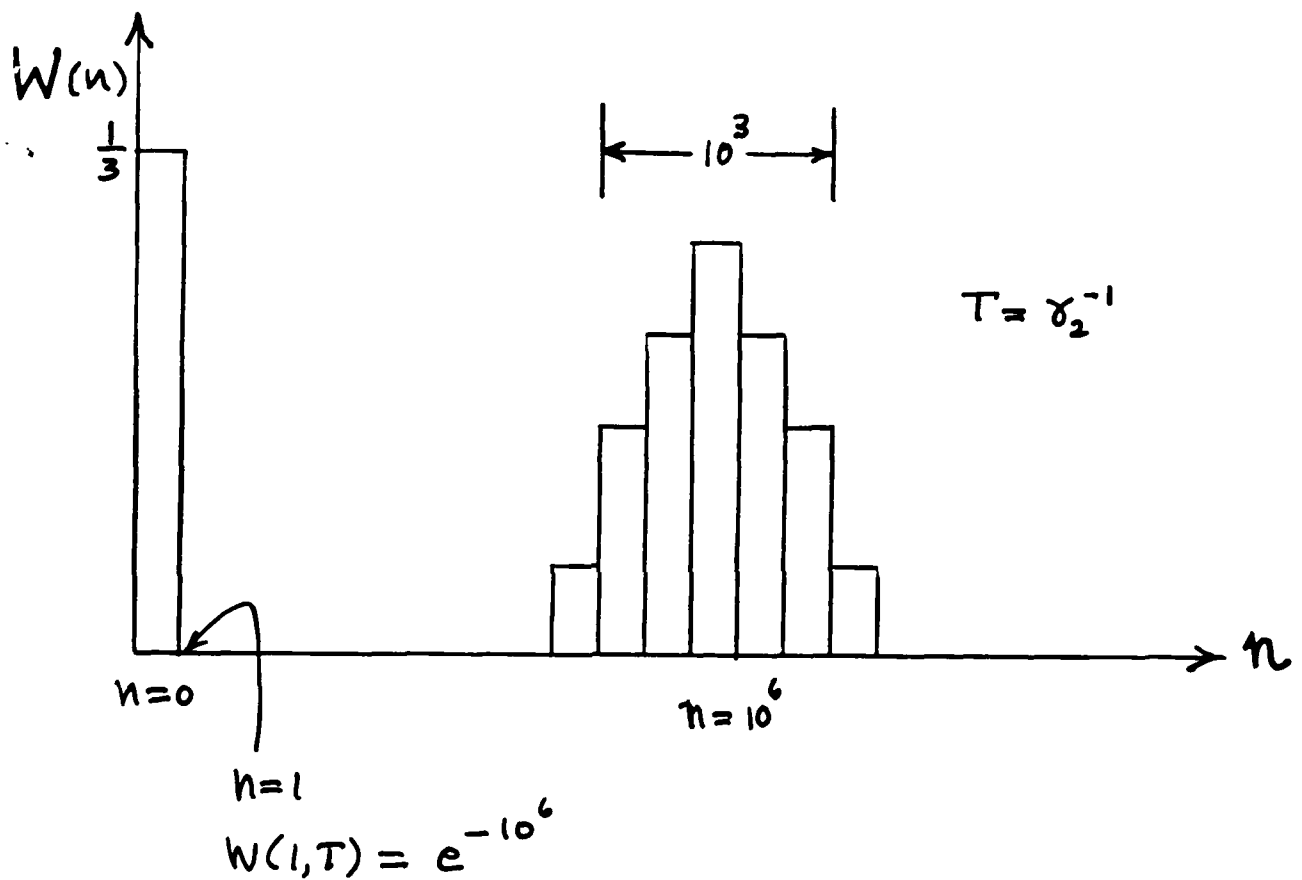
Wavelengths

$$W_0(T) = \frac{1}{S+2} \left\{ S e^{-\frac{\delta_2}{\delta_1} T} + 2 e^{-T/2} \right\}$$

slow fast

$$S = \frac{R_2}{R_2 + \delta_2}, \quad \delta_1/\delta_2 = 10^6$$





Thus, for an observation time $T \approx \gamma_2^{-1}$,
 We have either

$$n=0 \quad \text{or} \quad n=10^6$$

but not $n=1, 2, 3 \dots$!

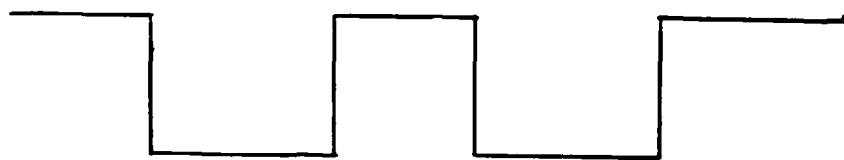
Many Atoms

Joint probability for n atoms not radiating in an interval T :

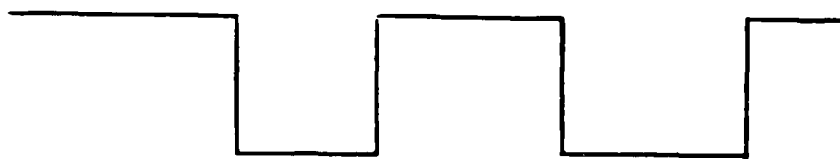
$$W(0, T)_n = W(0, T)^n$$

Average darkness interval:

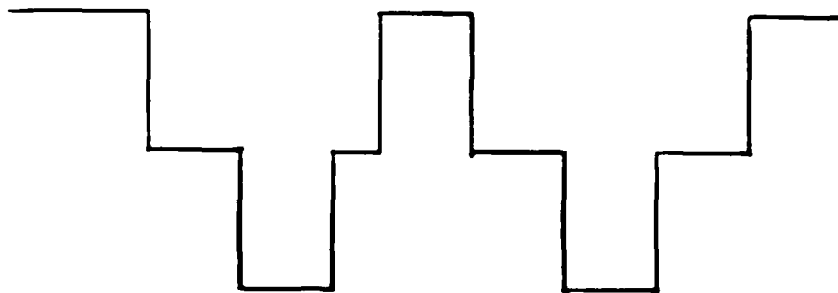
$$\langle T \rangle_n \cong \frac{1}{n(R_2 + \gamma_2)}, \text{ slowly varying part}$$



Atom #1



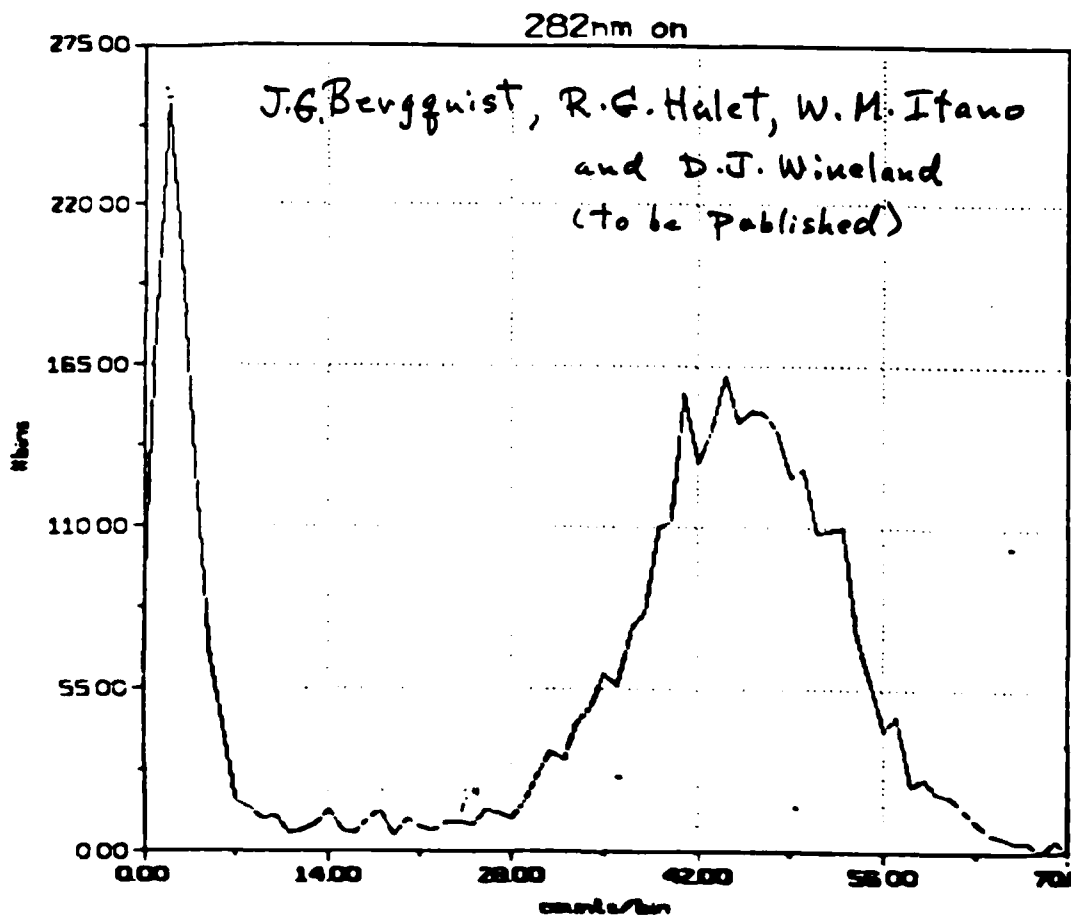
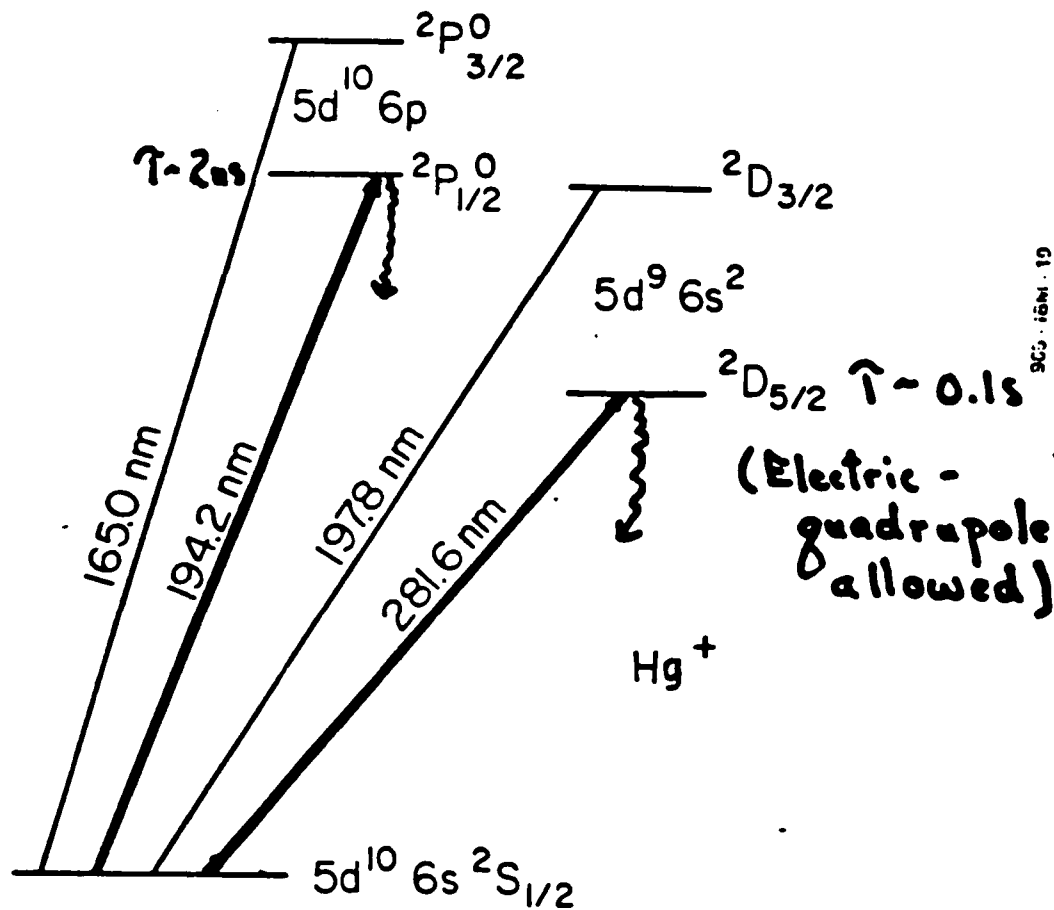
Atom #2



Sum

For an ensemble

$$\lim_{n \rightarrow \infty} \langle T \rangle_n = 0$$



Conclusions

- A quantum statistical theory of a single three-state atom shows that quantum jumps of a macroscopic kind occur where the strong transition fluctuates between a state of strong spontaneous emission to a state of no emission when the electron is shelved in the metastable state. Thus, even though the atom is excited continuously, the emission is not continuous.
- Remarkably, this single atom quantum evolution can be seen by the naked eye.
- Like a Stern-Gerlach experiment, the three-level problem demonstrates how quantum measurements work.

Laser cooling of neon metastable states

Fujio Shimizu, Kazuko Shimizu and Hiroshi Takuma

We report the first demonstration of the laser cooling of a neutral atomic beam other than alkali atoms. A neon beam was cooled by using the 640nm transition between the metastable state $1s_5$ ($J=2$) and $2p_9$ ($J=3$). We further transferred this cooled $1s_5$ metastable atoms to another metastable state $1s_3$ ($J=0$). The population in $2p_9$ can decay only to the metastable state $1s_5$. Therefore, this metastable atoms can be cooled by the same technique as used for the cooling of alkali beams. The cooled atoms can be transferred to another metastable state $1s_5$, or to the ground state, by pumping $1s_9$ population to one of four $J=1$ levels of $2p$ state followed by spontaneous decay to $1s$ state, then to the ground state by emitting 70nm VUV photon. The heating in this process is very small, because the kinetic energy gain by the recoil momentum is very small even for the VUV photon.

The experimental setup is basically the same as the sodium cooling by Phillips et al. The metastable atoms are created by a dc discharge, and are extracted through a pinhole on the anode. The beam passes through a solenoid, which produces a nonuniform axial field. The deceleration laser with 640nm is sent from the opposite direction towards the Ne beam source. It is usually circularly polarized, and its frequency is 100 to 200MHz below the resonance without magnetic field. The velocity distribution of the decelerated atom emerging from the solenoid is monitored through the Doppler profile of $1s_5-2p_7$ and $1s_3-2p_5$ transitions, by detecting 70nm spontaneous photon by an electron multiplier. To transfer the cooled $1s_5$ atoms, to $1s_3$ level, a 588nm laser is crossed perpendicular to the Ne beam approximately 1cm upstream of the Doppler analysis point.

The result shows that a large fraction of the $1s_5$ atoms can be slowed 100m/s suitable for the further deceleration and trapping by standing wave lasers or by magnetic field. Neon atoms in the beam is expected in either one of $1s_5$, $1s_3$ and ground states. Because $J=2$ for $1s_5$ while for others $J=0$, one can separate $1s_5$ atoms by nonuniform magnetic field. It is also possible to produce pure $1s_3$ or ground state atoms from $1s_5$ atoms by various laser pumping schemes. Therefore, by combining the above cooling technique, we can produce cooled atoms in single metastable or ground state. Those cooled atoms are of interest for studying lifetime and dynamics of metastable states.

number of allowed levels

Z

1

10

20

30

Z

1

10

20

30

Z

1

10

20

30

Z

1

10

20

30

Z

1

10

20

30

Z

1

10

20

30

Z

1

10

20

30

Z

1

10

20

30

Z

1

10

20

30

Z

1

10

20

30

Z

1

10

20

30

Z

1

10

20

30

Z

1

10

20

30

Z

1

10

20

30

Z

1

10

20

30

Z

1

10

20

30

Z

1

10

20

30

Z

1

10

20

30

Z

1

10

20

30

Z

1

10

20

30

Z

1

10

20

30

Z

1

10

20

30

Z

1

10

20

30

Z

1

10

20

30

Z

1

10

20

30

Z

1

10

20

30

Z

1

10

20

30

Z

1

10

20

30

Z

1

10

20

30

Z

1

10

20

30

Z

1

10

20

30

Z

1

10

20

30

Z

1

10

20

30

Z

1

10

20

30

Z

1

10

20

30

Z

1

10

20

30

Z

1

10

20

30

Z

1

10

20

30

Z

1

10

20

30

Z

1

10

20

30

Z

1

10

20

30

Z

1

10

20

30

Z

1

10

20

30

Z

1

10

20

30

Z

1

10

20

30

Z

1

10

20

30

Z

1

10

20

30

Z

1

10

20

30

Z

1

10

20

30

Z

1

10

20

30

Z

1

10

20

30

Z

1

10

20

30

Z

1

10

20

30

Z

1

10

20

30

Z

1

10

20

30

Z

1

10

20

30

Z

1

10

20

30

Z

1

10

20

30

Z

1

10

20

30

Z

1

10

20

30

Z

1

10

20

30

Z

1

10

20

30

Z

1

10

20

30

Z

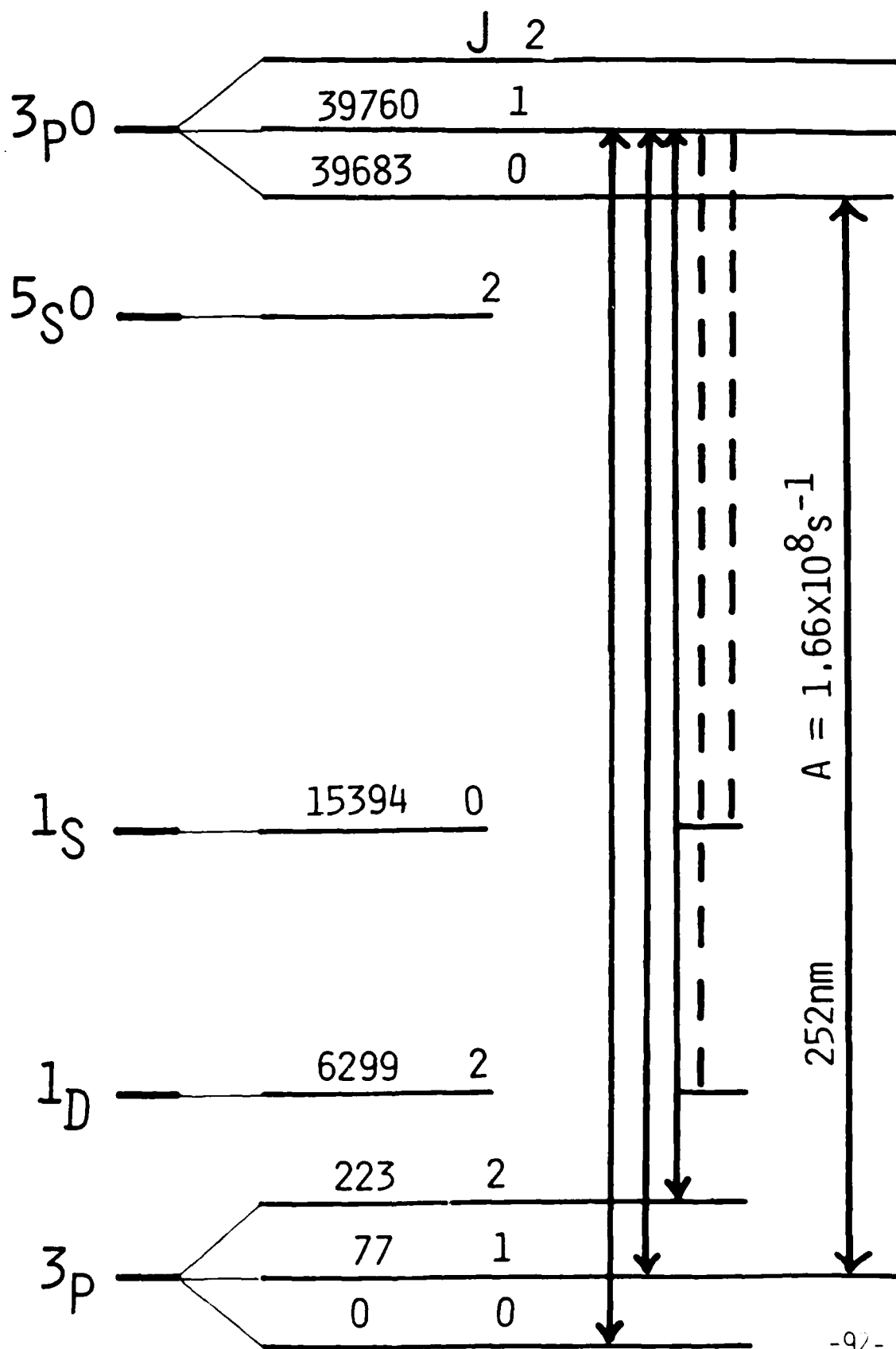
1

10

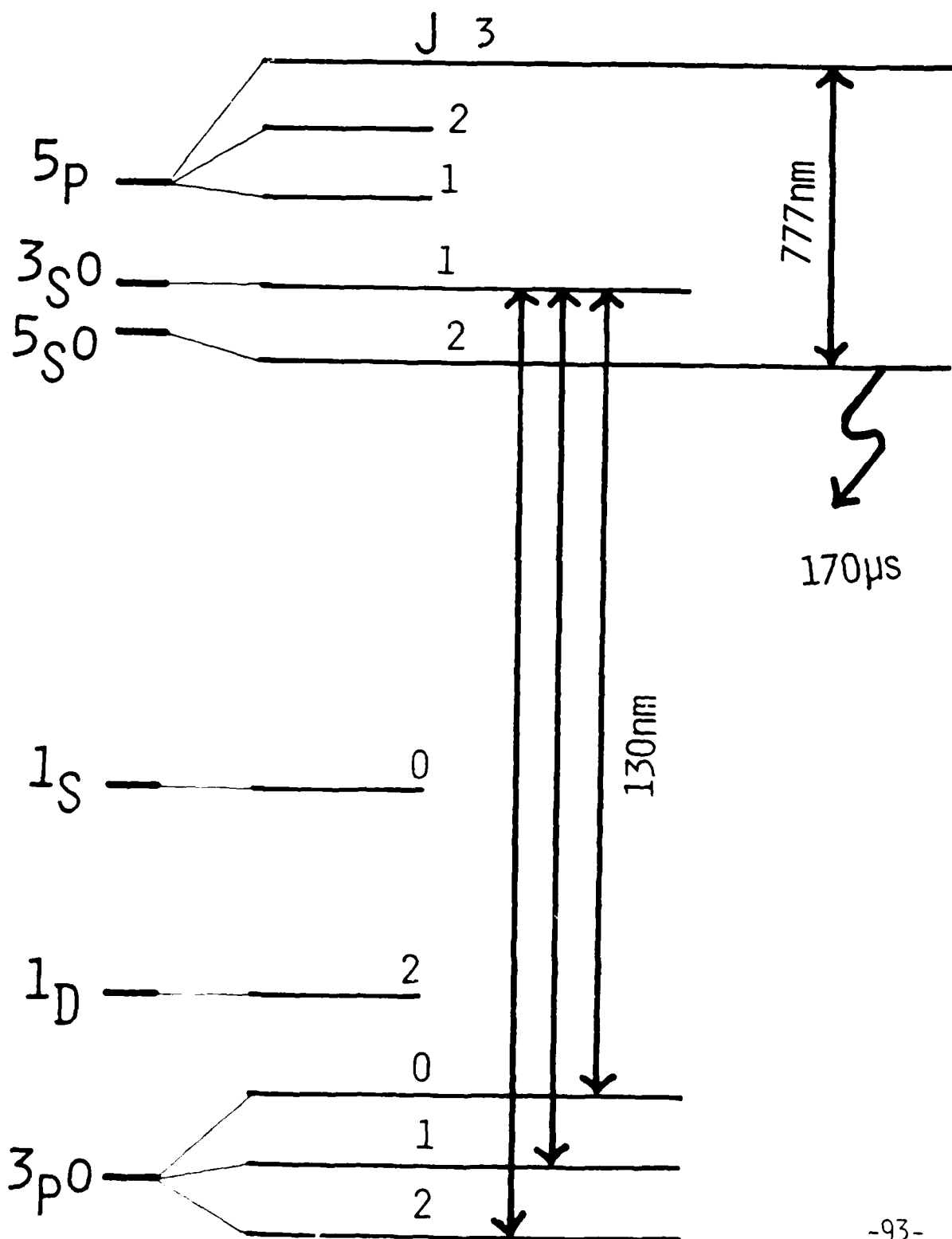
20

30

Silicon energy levels



Oxygen energy levels

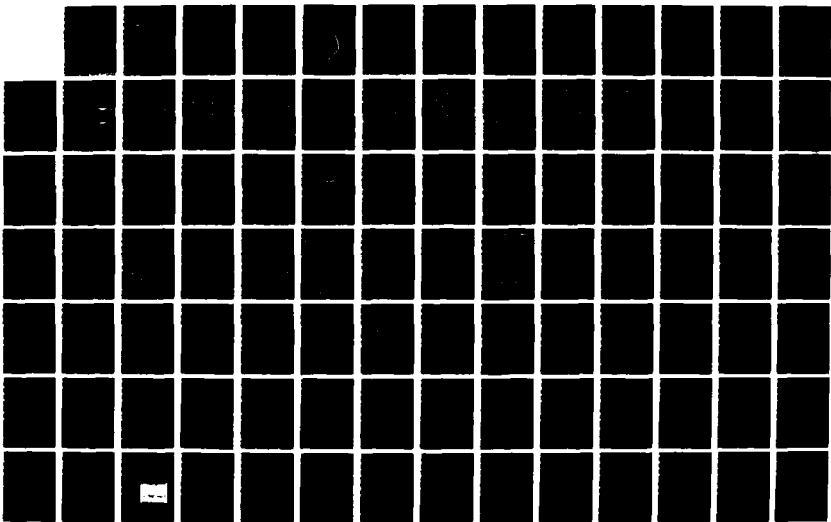


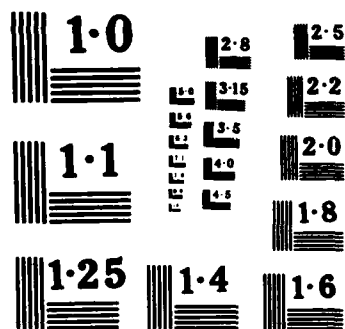
UNCLASSIFIED

UNITED STATES - JAPAN SEMINAR ON QUANTUM MECHANICAL
ASPECTS OF QUANTUM EL (U) MASSACHUSETTS INST OF TECH
CAMBRIDGE RESEARCH LAB OF ELECTRON
J H SHAPIRO ET AL OCT 87 N00014-87-G-0198 F/G 20/3

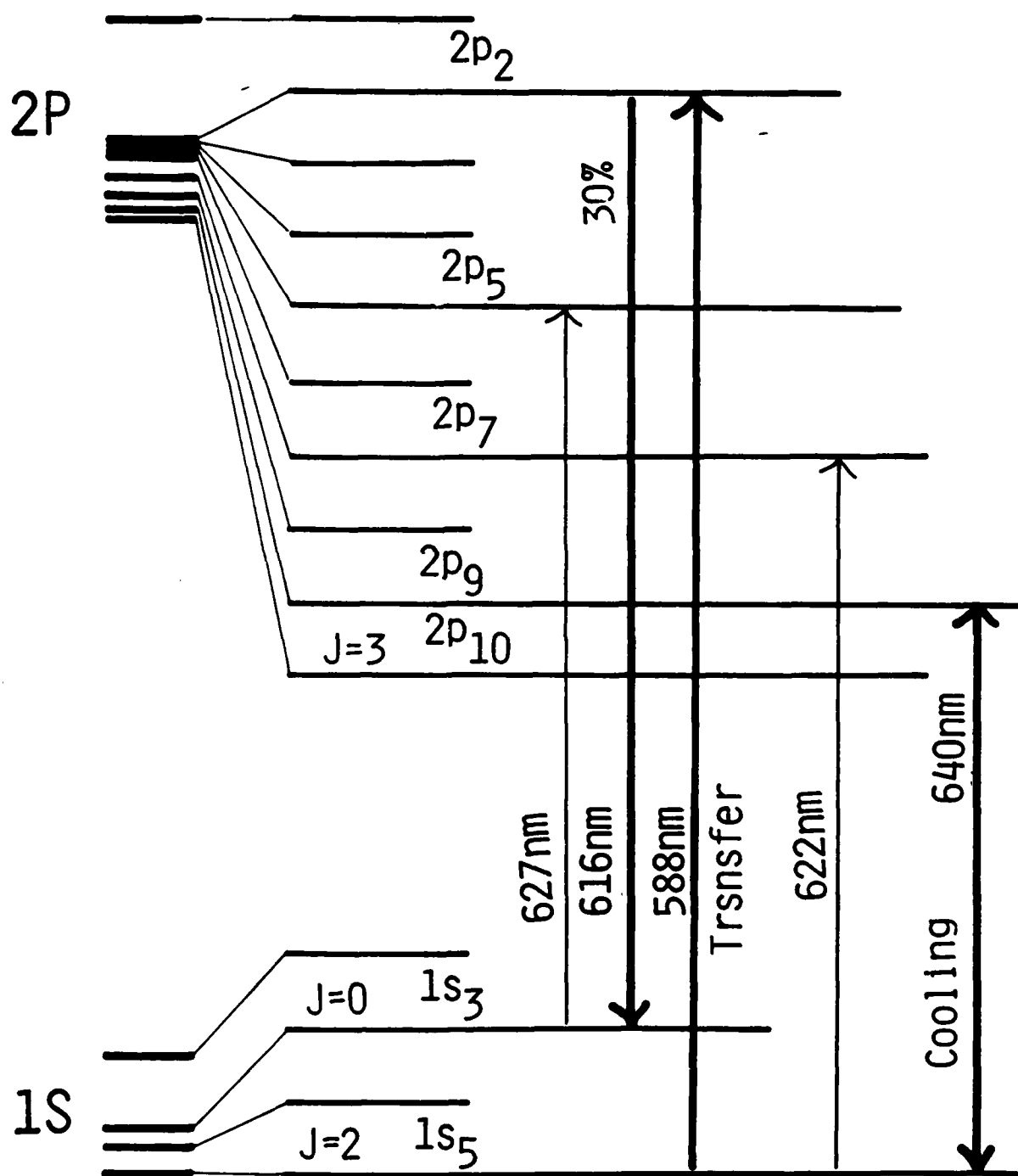
217

ML

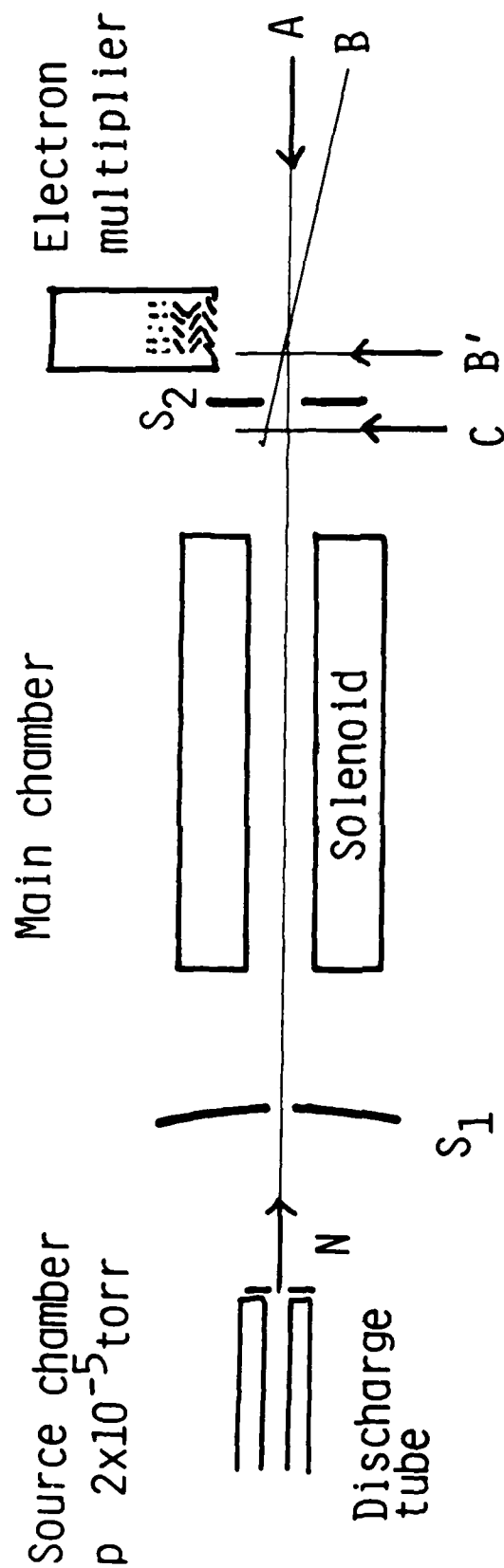




Neon energy levels



Experimental configuration



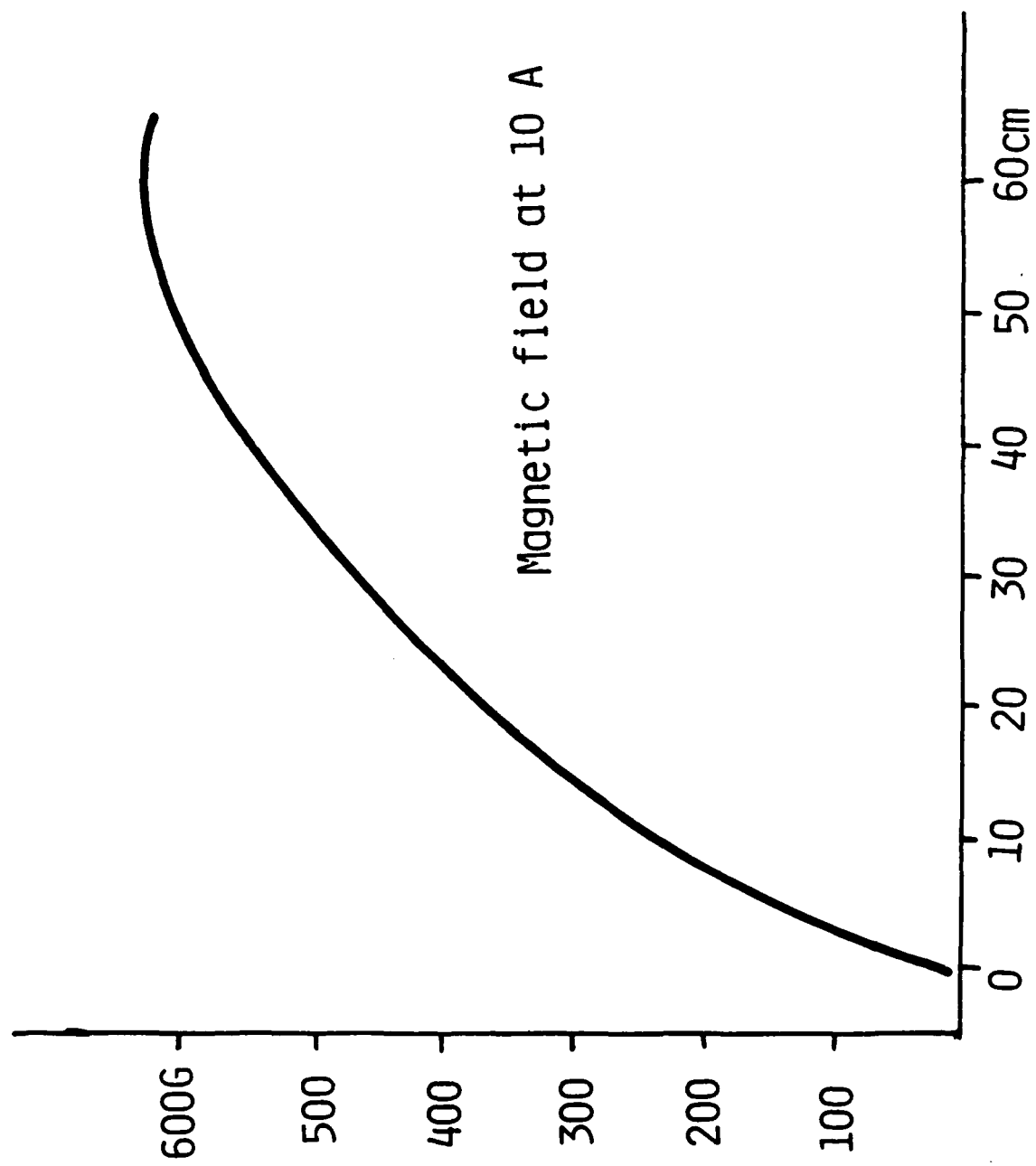
A: Deceleration laser

B : Laser for velocity analysis

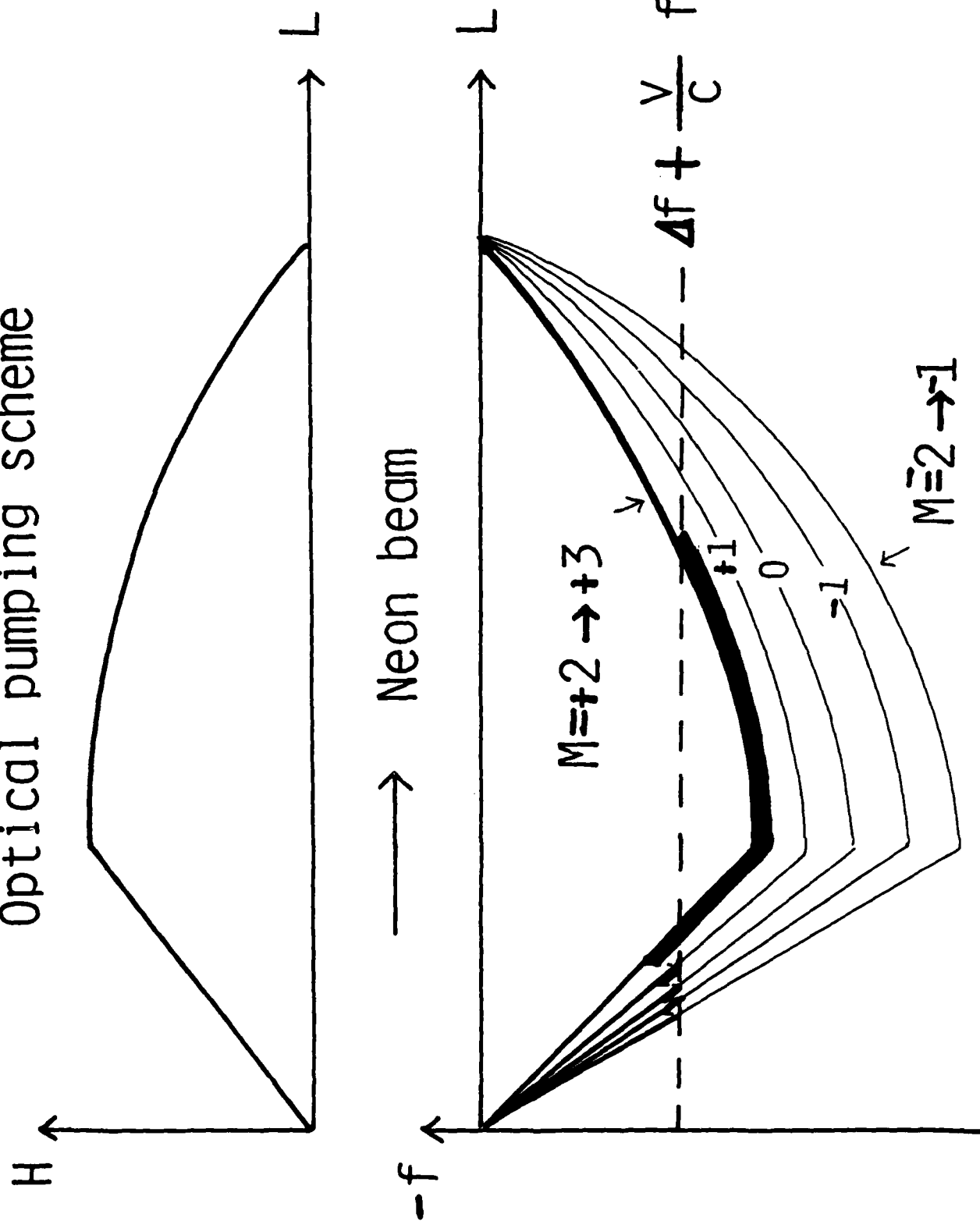
N: Neon beam

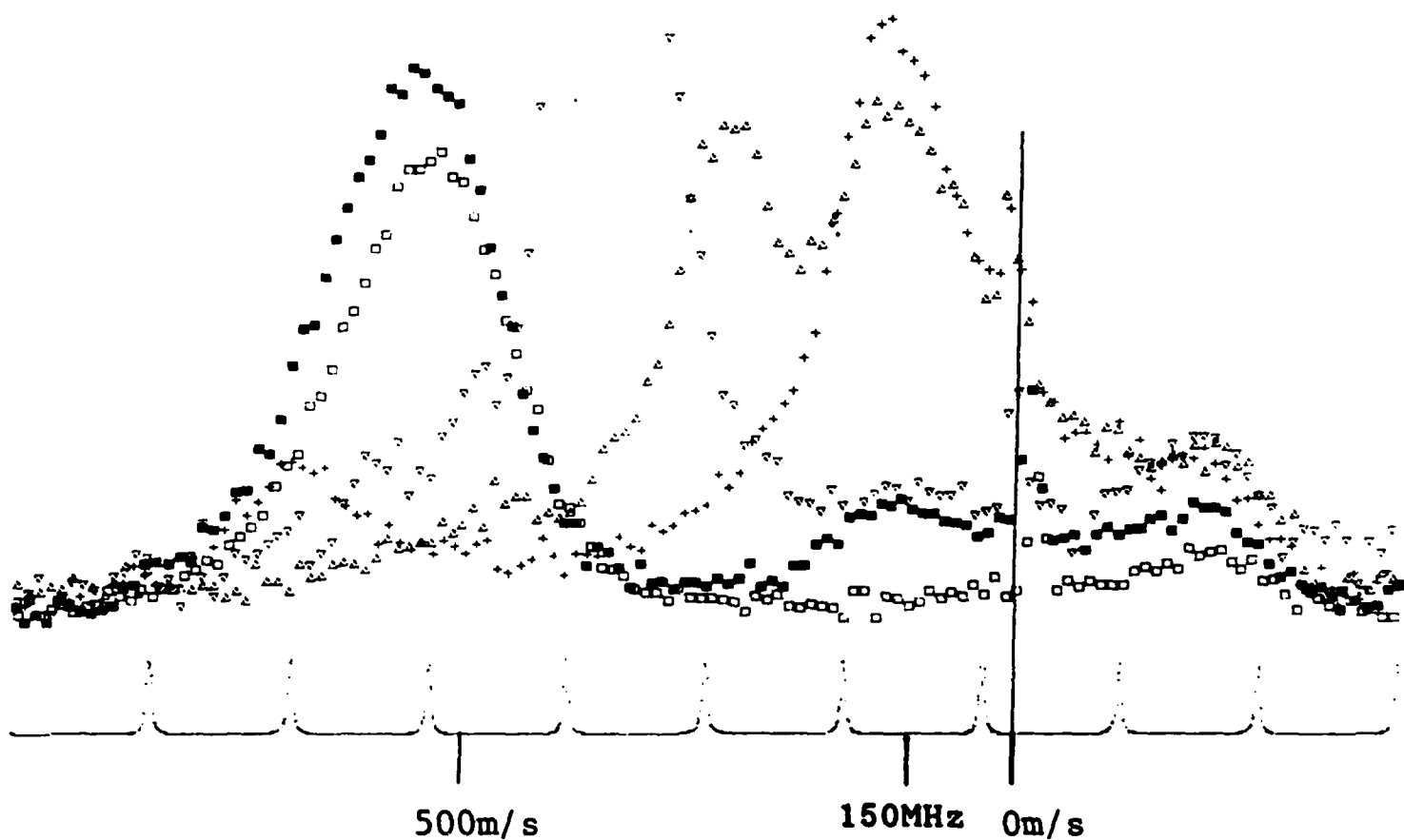
C: Transfer laser

B' : Laser for $v=0$ marker



Optical pumping scheme



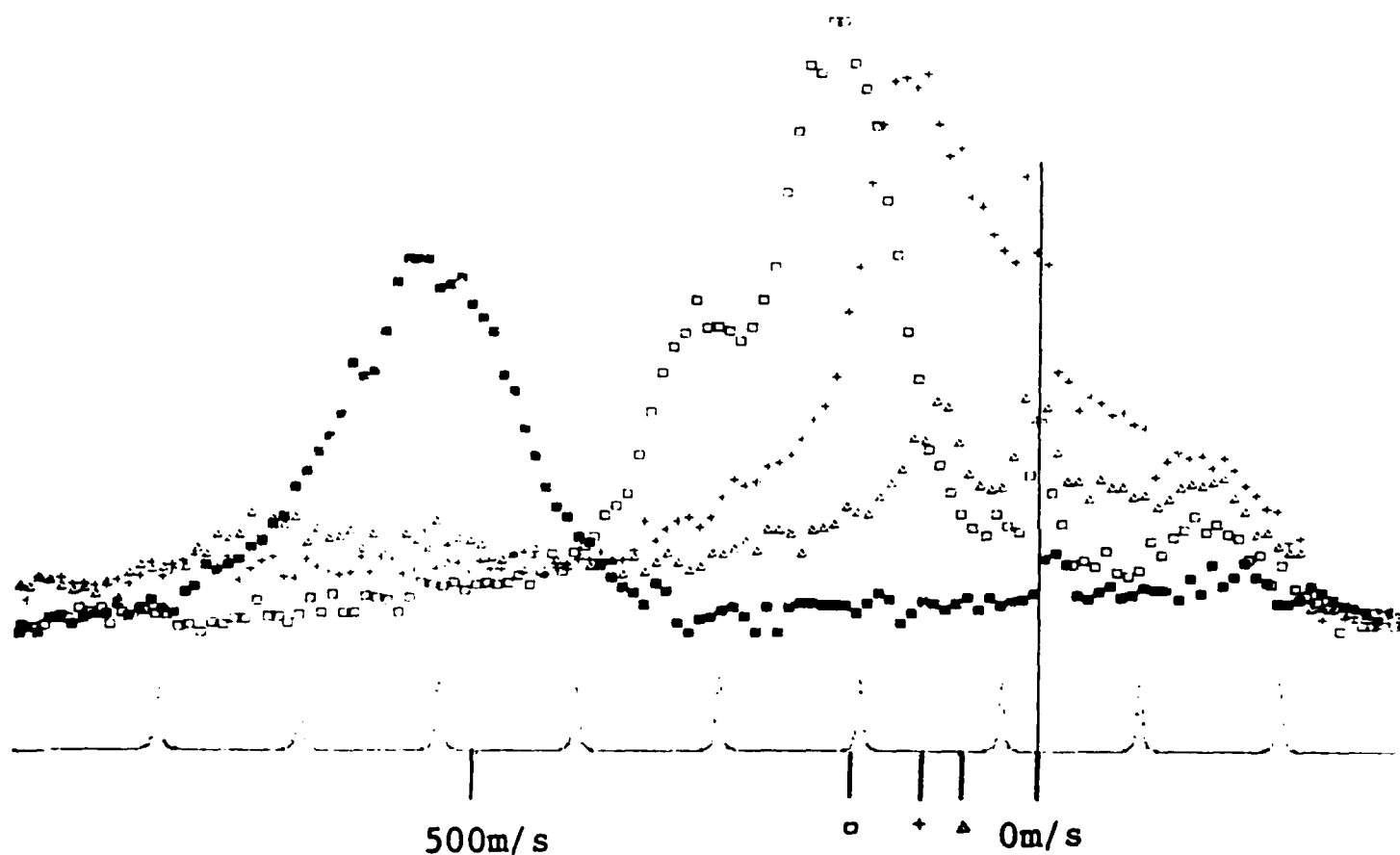


Circular polarization

$\Delta f = -150\text{MHz}$

□ No deceleration laser
 ■ H=260G
 + 460G
 △ 610G
 ▴ 790G

Magnetic field dependence

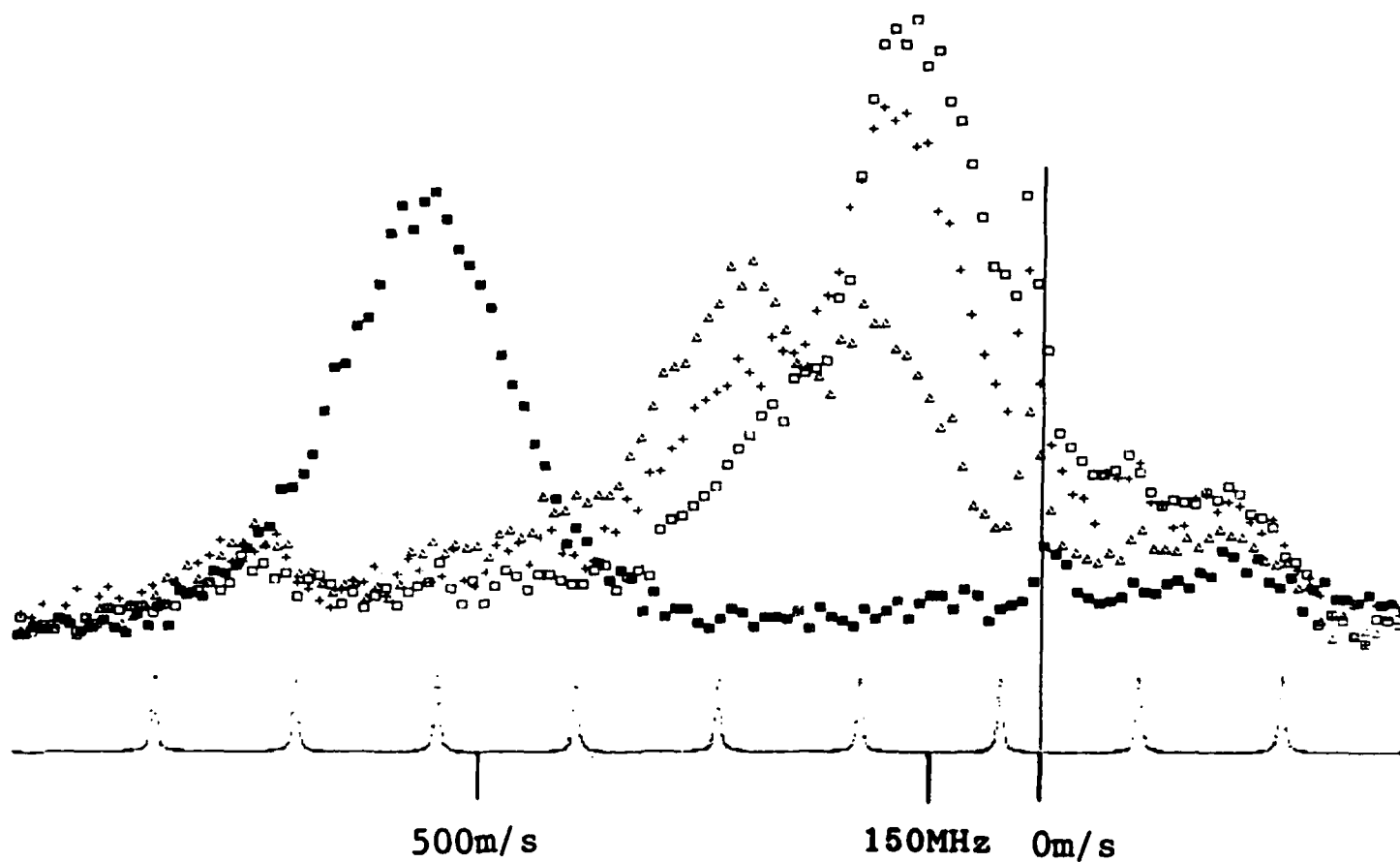


Circular polarization

H=470G

- No deceleration laser
- ▲ $\Delta f = -100\text{MHz}$
- + -150MHz
- -250MHz

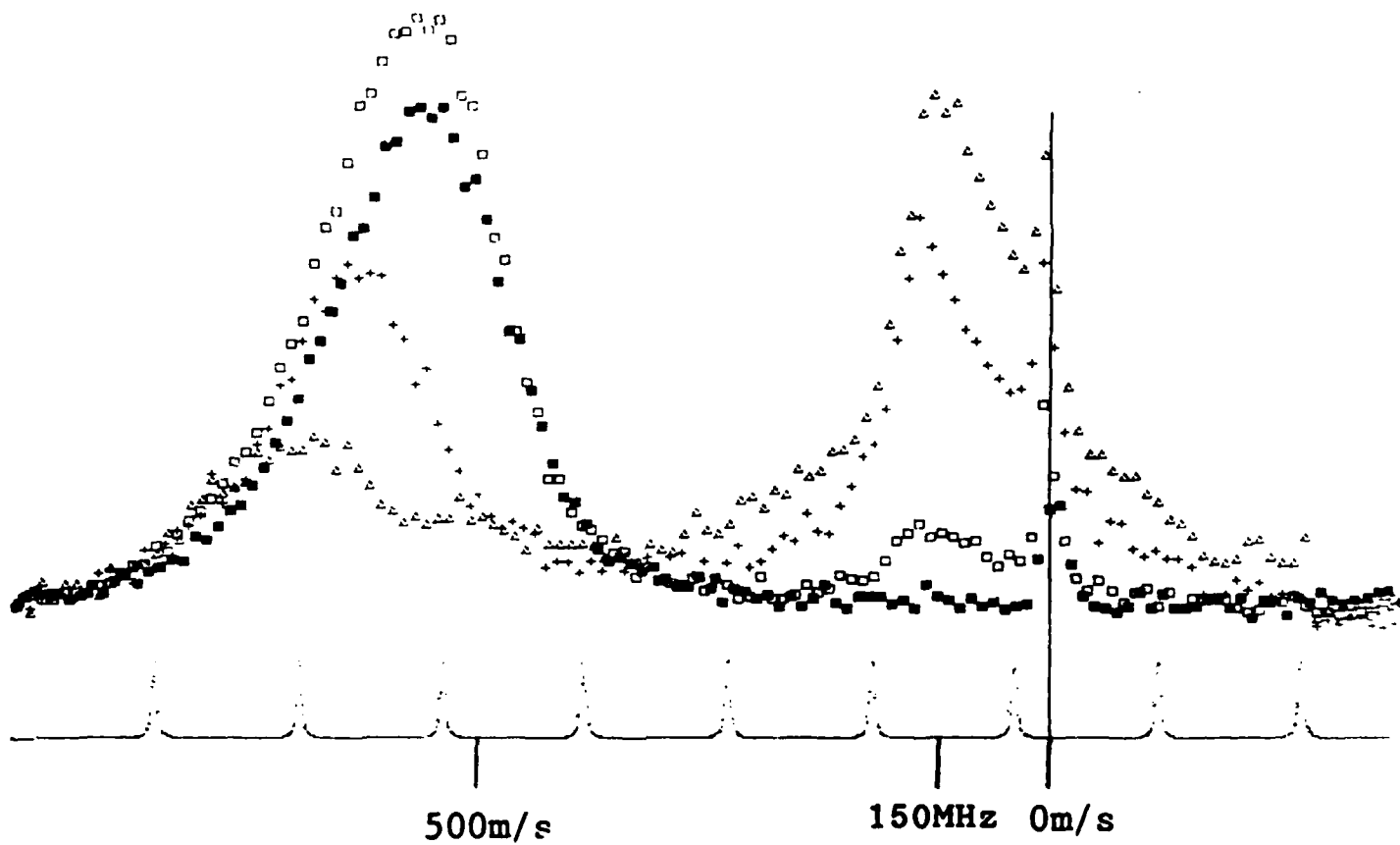
Detuning dependence



Circular polarization
 $H=470G$
 $\Delta f=-150MHz$

■ No deceleration lase
 □ 35mW
 + 15mW
 △ 5mW

Power dependence

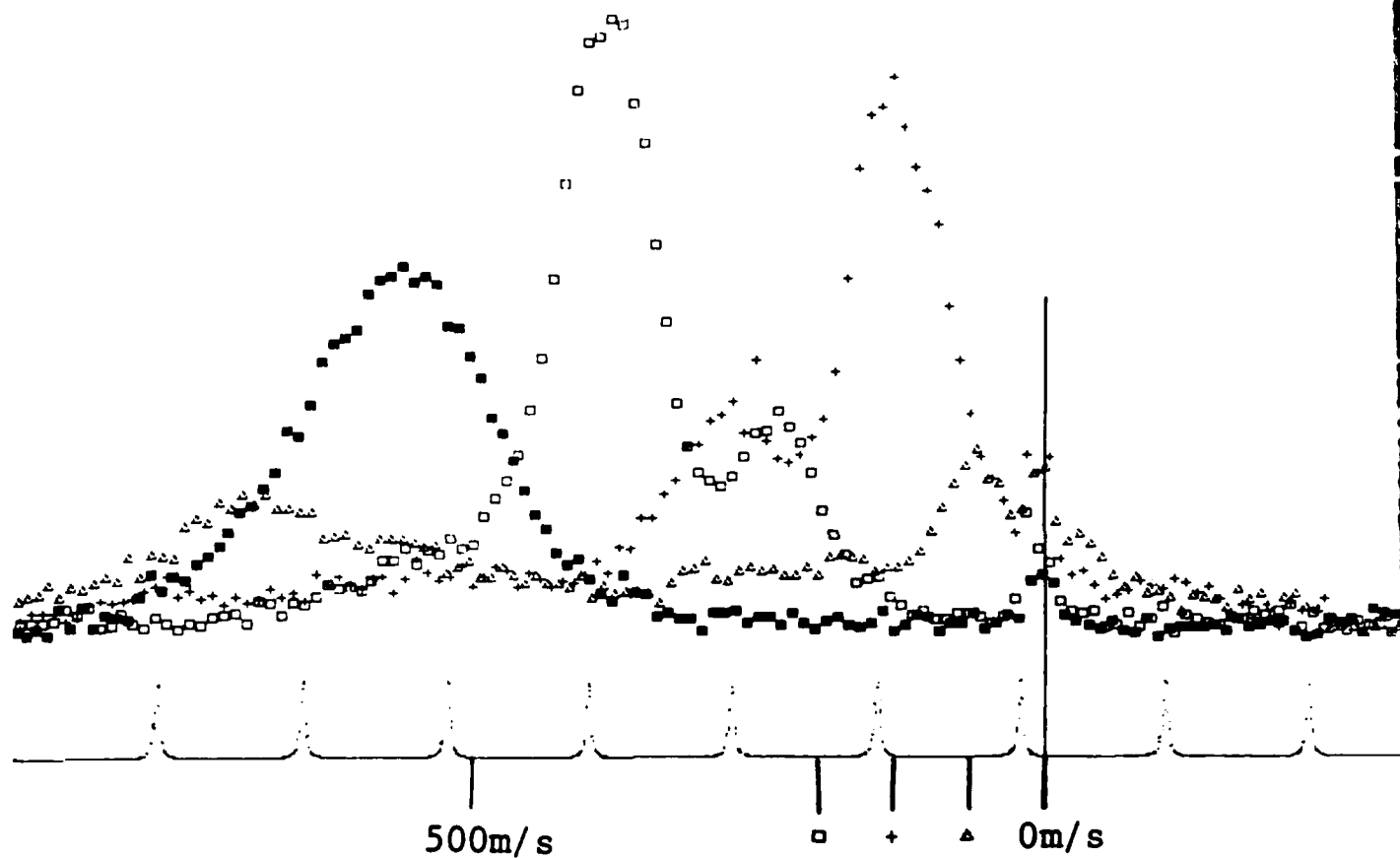


Linear polarization

$\Delta f = -150\text{MHz}$

- No deceleration laser
- H=260G
- + 350G
- △ 440G

Magnetic field dependence

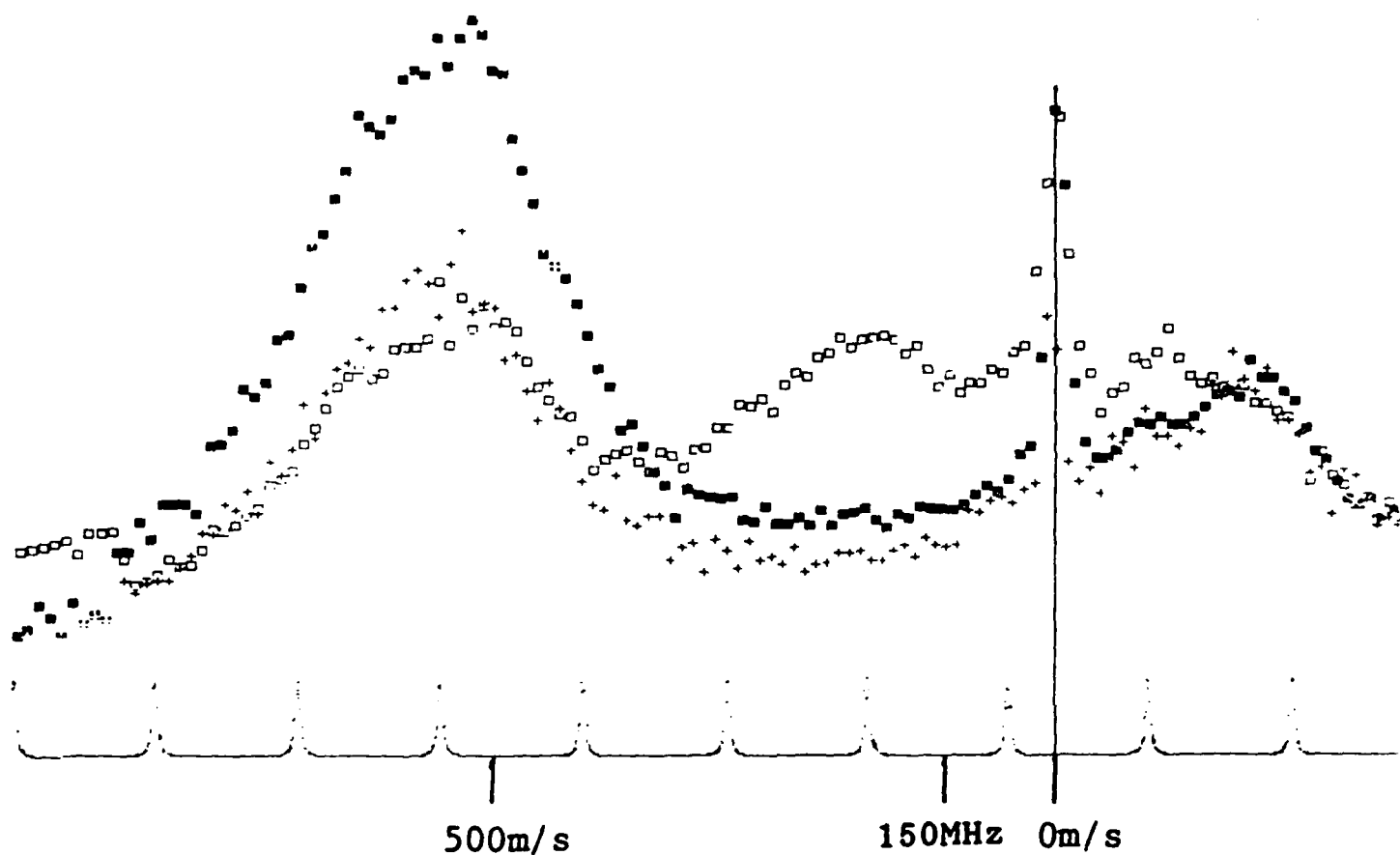


Linear polarization

H=470G

- No deceleration laser
- ▲ $\Delta f = -100\text{MHz}$
- + -200MHz
- -300MHz

Detuning dependence



Transfer 150MHz

H=470G

- + No transfer, no deceleration laser
- With transfer, but no deceleration laser
- With transfer and deceleration lasers

Transfer of cooled atoms from $J=2$ to
 $J=0$ metastable state

Gigantic Optical Nonlinearity
in Low Dimensional Systems

Eiichi Hanamura

Department of Applied Physics, University of Tokyo,
Hongo, Bunkyo-ku, Tokyo 113, Japan

Artificial as well as natural low-dimensional materials are now available in addition to bulk crystals. The material system with larger nonlinear optical susceptibility, e.g., $\chi^{(3)}(\omega; -\omega, \omega, -\omega)$ the third order optical susceptibility, is being looked for to realized more effective optical information processor.

First, we discuss the dimensional effects on $\chi^{(3)}$ and how $\chi^{(3)}$ increases when we proceed from the bulk system of 3-dimension into the 2- and 1-dimensional systems. Here the larger $\chi^{(3)}$ comes from the enhanced oscillator strengths due to the stronger confinements of particles and the stronger exciton effect in lower dimensional system.

Second, the nonlinear optical susceptibility is shown to be extremely enhanced for an assembly of microcrystallites as 0-dimensional systems. This is because the exciton is quantized due to the confinement effect and the excitons in a single microcrystallite interact enough strongly to make the excitons deviate from ideal harmonic oscillators.

Gigantic Optical Nonlinearity in Low Dimensional Systems

E. HANAMURA

- 3-D : bulk crystal
- 2-D : quantum well
layered-structure
semiconductor (GaSe, ...)
- 1-D : quantum wire
polydiacetylene crystal
- 0-D : quantum box
semiconductor microcrystallites
in glass
colloid particles of semiconductors



large $\chi^{(3)}(\omega; -\omega, \omega, -\omega)$



optical information processor

$$P^{(3)} = \chi^{(3)}(\omega_4; -\omega_1, \omega_2, -\omega_3) E_1 E_2^* E_3$$

$\omega_1 = \omega_2 = \omega_3 = \omega_4$: degenerate 4-wave mixing

$$\chi^{(3)}(\omega; -\omega, \omega, -\omega) \\ = \sum_{\alpha, \beta, \gamma} \frac{P_{\gamma\gamma} P_{\gamma\beta} P_{\beta\alpha} P_{\alpha\gamma}}{\hbar^3 (\omega_{\gamma g} - \omega) (\omega_{\beta g} - 2\omega) (\omega_{\alpha g} - \omega)}$$

α, γ : lowest Wannier exciton

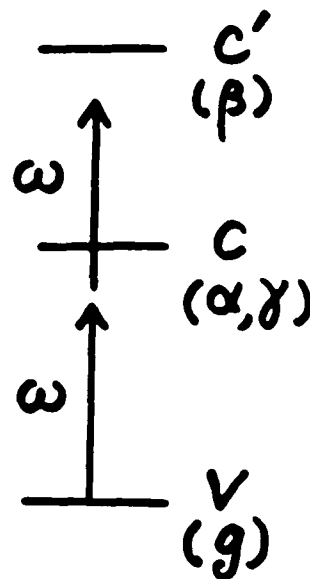
$$P_{\alpha g} = P_{g\gamma} = \sqrt{\frac{N u^3}{\pi a_\alpha^3}} P_{cv}$$

u^3 : unit cell volume

a_d : exciton Bohr radius

N : number of unit cells in the crystal

$$P_{\beta\alpha} = 8 \left(\frac{\sqrt{a_\alpha a_\beta}}{a_\alpha + a_\beta} \right)^3 P_{c'c}$$



Dimensional Effects

3D-oscillator strength per unit cell

$$f_{\alpha}^{(3)} = \frac{2m\omega_{\alpha}}{\hbar e^2} |P_{\alpha g}|^2 \frac{1}{N}$$

$$= \frac{2m\omega_{exc}}{\hbar e^2} |P_{cv}|^2 \frac{u^3}{\pi a_{\alpha}^3}$$

$$E_{exc}^b = \frac{\mu e^4}{2\hbar^2 \epsilon_0^2}$$

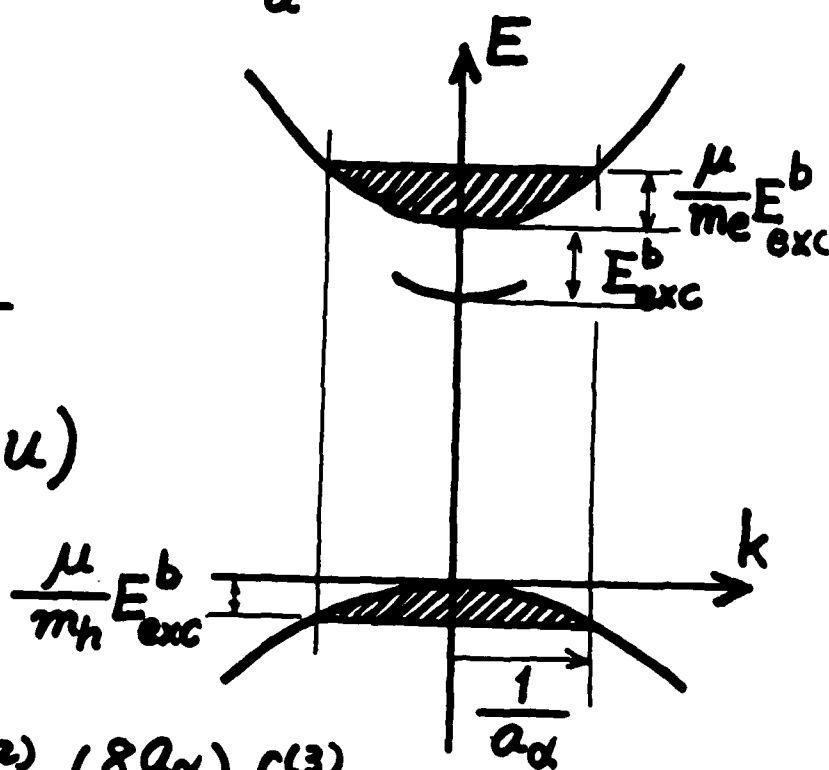
$$a_{\alpha} (\gg u)$$

2D: $4E_{exc}^b, a_{\alpha}/2$

1D: $\infty, 0$

$$f_{\alpha}^{(2)} = \left(\frac{8a_{\alpha}}{u} \right) f_{\alpha}^{(3)}$$

in the effective mass appr.

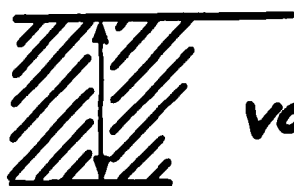


polydiacetylene crystal (1-D)



β \downarrow 0.55 eV A_{1g} exciton $f_{\beta\alpha} = 3.88$
 α \downarrow 1.33 eV B_{1u} exciton $f_{\alpha g} = 2.44$ (3.2) (1.5)

c.f. $f_{\alpha g} = 10^{-4}$ GaAs (3-D)
 $= 3.2 \times 10^{-3}$ CdS (3-D)



valence band width 3.1 eV

sum rule : $\sum_{\alpha} f_{\alpha g} = 4$

$\chi^{(3)} \sim 10^{-8}$ esu for $\hbar\omega = 1.33$ eV —
 2-photon resonant
 to A_{1g} exciton

$\hbar\Gamma = 0.01$ eV

Size Effects

larger $\chi^{(3)}(\omega; -\omega, \omega, -\omega)$

- ① enhanced transition dipolemoments
- ② resonant energy denominators

under nearly resonant condition to the free exciton, ① and ② are satisfied.

excitons as almost ideal bosons

→ no nonlinear optical response

Reducing the size of microcrystallites the transition dipolemoment is reduced but the exciton interactions make excitons deviate from ideal bosons.

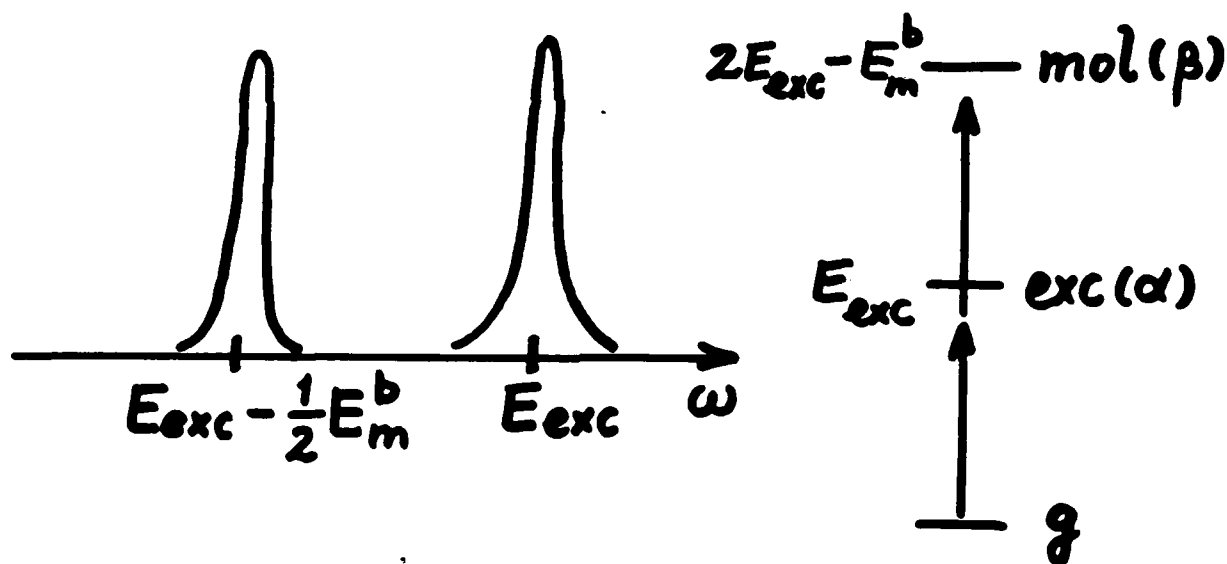
⇒ optimum size for largest $\chi^{(3)}$

two excitons are bound \rightarrow excitonic molecule

$$P_{\beta\alpha} = P_{cv} \frac{u^3}{\pi a_\alpha^3} \sum_R G(R)$$

R : separation between two excitons

$\sqrt{N_m} \rightarrow$ giant oscillator strength



$$\chi^{(3)} \sim 4 \times 10^{-8} \text{ esu (for } 2E_{exc} - E_m^b - 2\hbar\omega = 3 \text{ meV)}$$

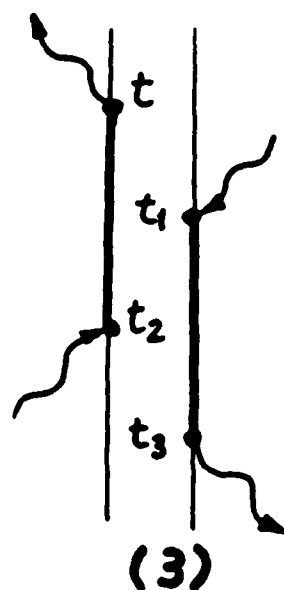
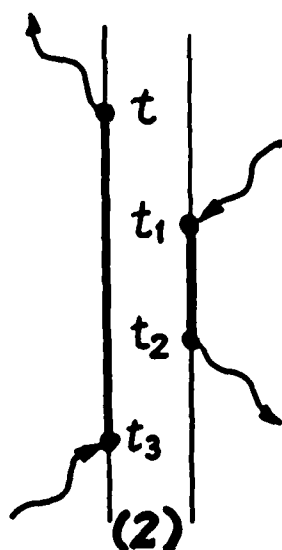
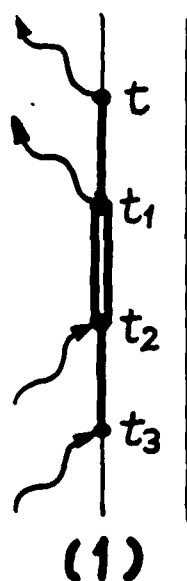
When the bound state of two excitons is not relevant and under resonant excitation,

$$\langle P^{(3)}(t) \rangle = \left(\frac{-i}{\hbar} \right)^3 \int_{-\infty}^t dt_1 \int_{-\infty}^{t_1} dt_2 \int_{-\infty}^{t_2} dt_3 \times \langle P(r,t) [H'(t_1), [H'(t_2), [H'(t_3), P_0]]] \rangle$$

$$H'(t) = -P \cdot E(t)$$

$$P^{(3)} e^{-i\omega t} = \chi^{(3)}(\omega; -\omega, \omega, -\omega) E(t) E(t)^* E(t)$$

$$E(t) = E e^{-i\omega t}$$



$$\gamma, \gamma' \ll |\omega - \omega_{exc}|, \quad \omega_{int} \ll |\omega - \omega_{exc}|$$

\Rightarrow excitons as harmonic oscillators

$$\Rightarrow \chi^{(3)}(\omega; -\omega, \omega, -\omega) = 0.$$

- under near resonance to the lowest exciton ω_0 in the
- microcrystallites $L, R \gg a_\alpha$

$$\chi^{(3)} = \frac{N_c |P|^4}{\hbar^3 (\omega - \omega_0 + i\Gamma)^2 (\omega - \omega_0 - i\Gamma)} \cdot \frac{\gamma'}{\gamma} + \frac{N_c |P|^4}{\hbar^3 (\omega - \omega_0 + i\Gamma)^2 (\omega - \omega_0 - i\Gamma)} \frac{\omega_{int} - 2i\Gamma}{(\omega_0 - \omega + \omega_{int} - i\Gamma)}$$

$$\Gamma = \gamma + \gamma'$$

$$P_n = \left(\frac{2\sqrt{2}}{\pi} \right)^3 P_{cv} \sqrt{\frac{u^3}{\pi a_\alpha^3}} \frac{N^{3/2}}{n_x n_y n_z}$$

for a cubic box with $L = uN$.

$$1 \leq n_x, n_y, n_z \leq N$$

$$P_{n00} = 2\sqrt{\frac{2}{\pi}} P_{cv} \sqrt{\frac{u^3}{\pi a_\alpha^3}} \frac{N^{3/2}}{n}$$

for a sphere with $R = uN$

$$1 \leq n, \ell=0, m=0$$

$$\gamma = \gamma_0 N^3 \Rightarrow \gamma'/\gamma \ll 1 \quad (N \gg 1)$$

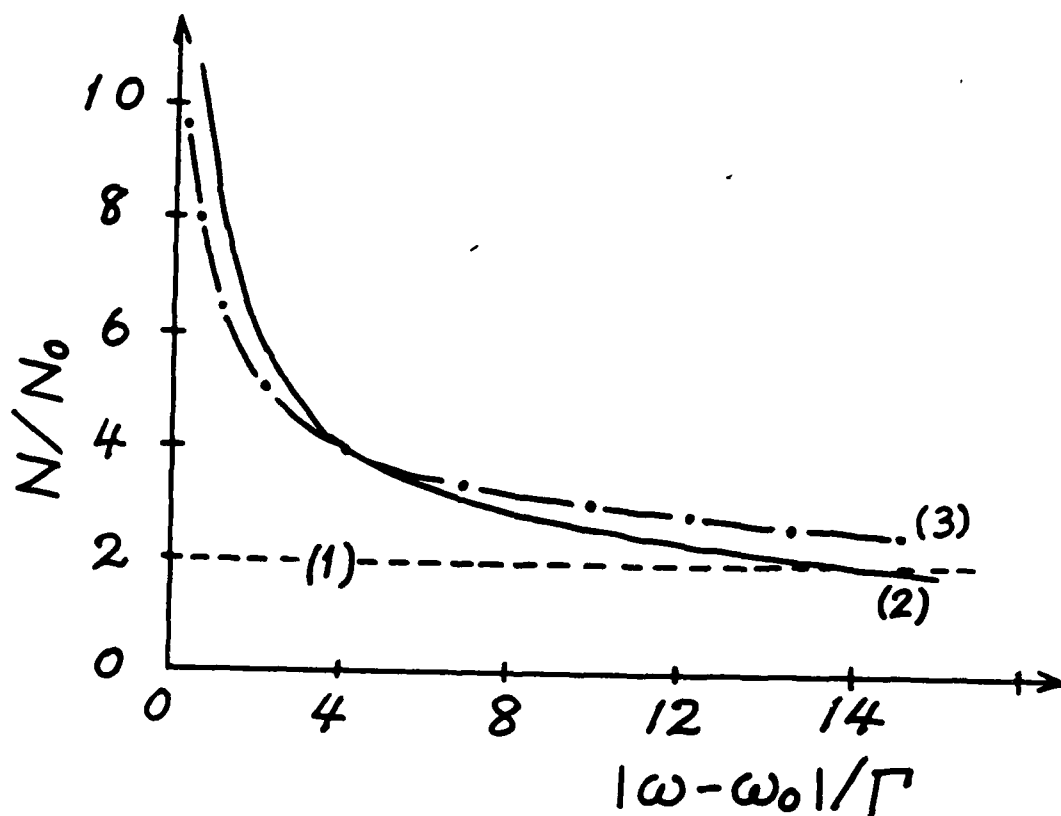
$$\omega_{int} \gg |\omega - \omega_0| :$$

$$\chi^{(3)} \sim \frac{N_c |P|^4}{\hbar^3 (\omega - \omega_0)^3} \sim N^3$$

$$N_c \sim \frac{1}{N^3}, \quad |P| \sim N^{3/2}$$

Conditions for gigantic $\chi^{(3)}$

- (1) Exciton binding energy \gg ele. & hole quantization energies
 $a_a(\text{exciton Bohr radius}) \ll L, R$ (size)
- (2) Exciton interaction energy $\hbar\omega_{\text{int}} \equiv 8\pi E_{\text{exc}}^b \frac{m_e m_h}{(m_e + m_h)^2} \frac{a^2 f_0}{L^3} \gg \hbar|\omega - \omega_0|$
- (3) Exciton quantization energy $\equiv \frac{3\pi^2 \hbar^2}{2(m_e + m_h)L^2} \gg \hbar|\omega - \omega_0|$



(1) CuCl microcrystallites

$$E_{\text{exc}}^b = 213 \text{ meV}, \quad m_h = 2m, \quad m_e = 0.5m$$

$$\hbar\omega_{\text{exc}}^l = 3.2079 \text{ eV}, \quad \hbar\omega_{\text{exc}} = 3.2022 \text{ eV}$$

$$\frac{3.6(1-\hbar)}{7.2(1-e)} \ll N \leq \left[\frac{4.4 \text{ eV}}{\hbar|\omega - \omega_0|} \right]^{1/2} \sim 30 \quad (3)$$

$$\left[\frac{24.8 \text{ eV}}{\hbar|\omega - \omega_0|} \right]^{1/3} \sim 17 \quad (2)$$

$$\chi^{(3)} = 7 \times 10^{-7} N^3 \text{ esu} \leftarrow \hbar|\omega - \omega_0| \uparrow$$

$$\sim 4 \times 10^{-4} \text{ esu for } N=17, \quad = 5 \text{ meV}$$

(4900 unit cells) ⁻¹¹⁴⁻

(2) CdS and II-VI semiconductors

$$E_{exc}^b = 30 \text{ meV}, \quad m_h = 1.6 m, \quad m_e = 0.25 m$$

$$\hbar\omega_{exc}^2 = 2.5546 \text{ eV}, \quad \hbar\omega_{exc} = 2.5546 \text{ eV}$$

$$\frac{10(1-\kappa)}{25(1-\epsilon)} \ll N \leq \sqrt{\frac{4.96 \text{ eV}}{\hbar|\omega - \omega_0|}} \sim 32 \quad (3)$$

$$\left[\frac{183 \text{ eV}}{\hbar|\omega - \omega_0|} \right]^{1/3} \sim 33 \quad (2)$$

$$\uparrow \hbar|\omega - \omega_0| = 5 \text{ meV}$$

$$\chi^{(3)} = 1.2 \times 10^{-10} N^3 \text{ esu} \leftarrow$$

$$\sim 3.2 \times 10^{-6} \text{ esu} \quad (N \sim 30)$$

(3) GaAs and III-V semiconductors

$$E_{\text{exc}}^b = 5.1 \text{ meV}, m_h = 0.475 m, m_e = 0.0665 m$$

$$u = 3.56 \text{ \AA}, a_d = 107 \text{ \AA}$$

$$\epsilon_0 = 12.53$$

$$\frac{114 (1-e)}{43 (1-h)} \ll N < \sqrt{\frac{16.4 \text{ eV}}{\hbar |\omega - \omega_0|}} \sim 57 \quad (3)$$

$$10 \left[\frac{72.4 \text{ eV}}{\hbar |\omega - \omega_0|} \right]^{1/3} \sim 200 \quad (2)$$

$$\uparrow$$

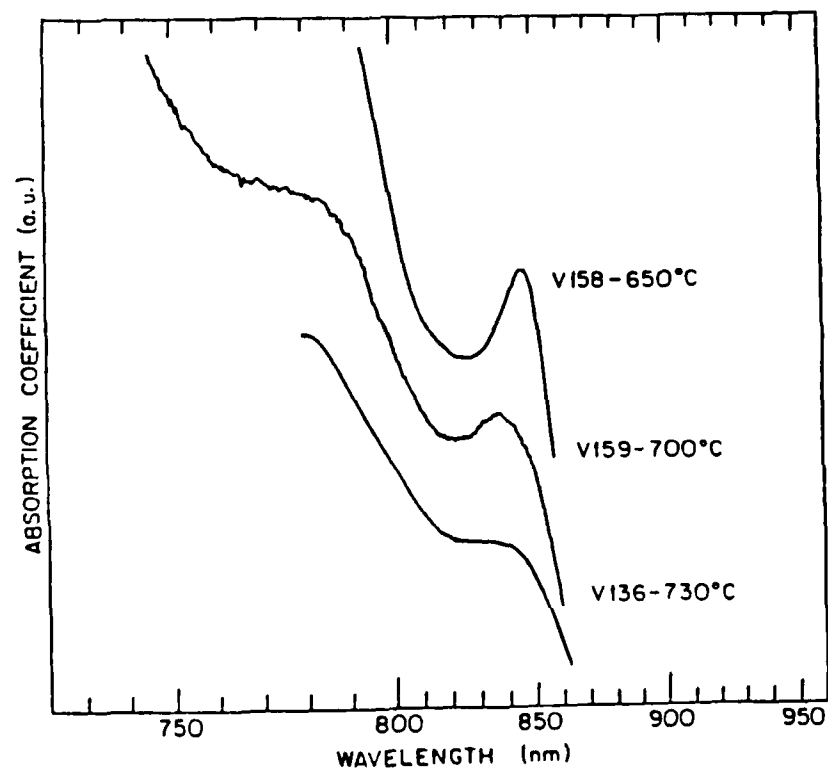
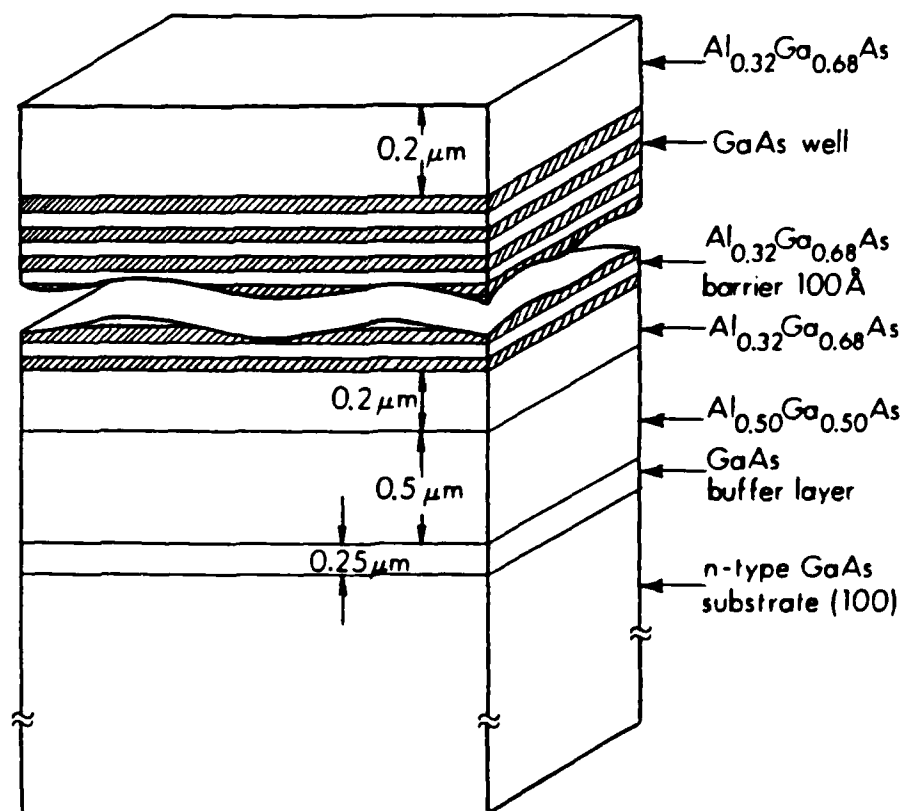
$$\hbar |\omega - \omega_0| = 5 \text{ meV}$$

MEASUREMENTS OF OPTICAL NONLINEARITIES
IN MOCVD-GROWN GaAs/GaAlAs MULTIPLE QUANTUM WELLS

E. Garmire
Center for Laser Studies
University of Southern California
Los Angeles, CA 90089-1112

This paper reports on measurements of nonlinear absorption made by A. Kost and M. Kawase in material provided by H. C. Lee, A. Hariz and P. D. Dapkus. The work was supported by AFOSR, ARO and NSF. Five samples with differing well thicknesses were compared. By fitting measurements of saturable absorption at particular wavelengths to excitonic bleaching (at low intensity levels) and background absorption saturation (at higher intensity levels), we are able to infer the separate contributions to the absorption. The well dependence of the height of the absorption contributions and also of the saturation intensities were measured.

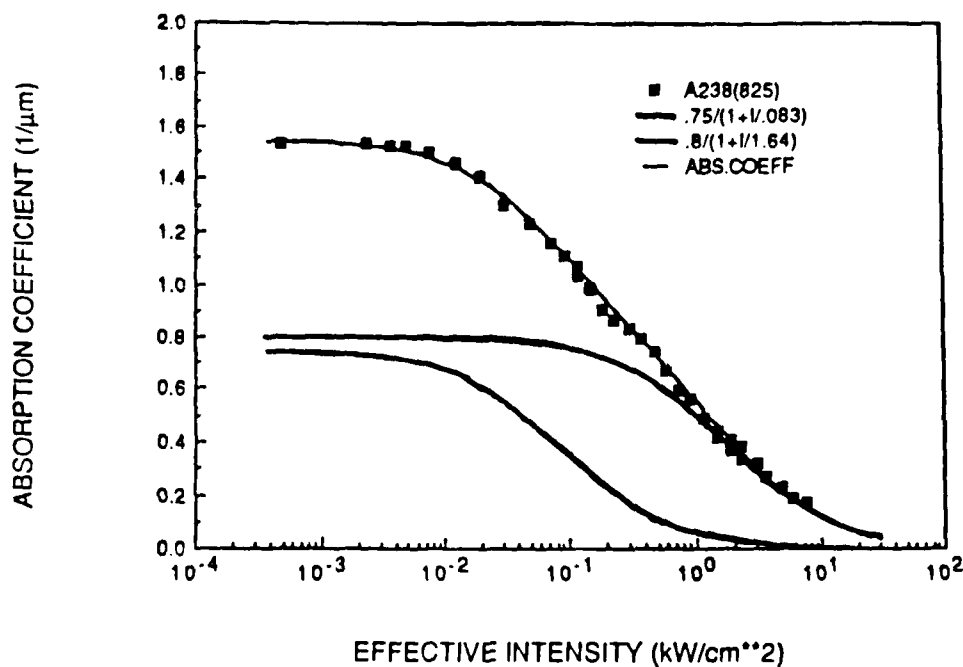
From measurements of the wavelength dependence of the saturable absorption, calculations were made of the wavelength dependence of the change in refractive index. The dependence of the change in index with intensity on or near resonance is sublinear.



$$\alpha = \frac{\alpha_E}{1 + I/I_{0E}} + \frac{\alpha_{B0}}{1 + I/I_{0B0}}$$

INTENSITY-DEPENDENT
ABSORPTION

MQW 238 - 54 Å (825nm, hh) CW



ABSORPTION

EXCITON (n,m)

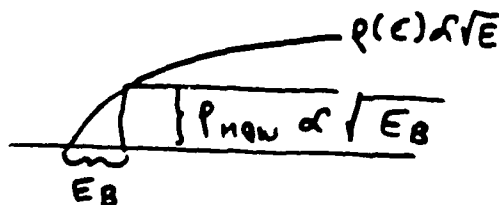
$$n = Q_u \cdot N_u(e) \\ m = Q_u \cdot N_u(h)$$

$$\alpha_{n,m} = \frac{4\pi^2 e^2 k F_{n,m}}{nm^2 c L_z} \mathcal{L}(\hbar\omega - E_{n,m})$$

↳ LORENTZIAN
↳ WELL WIDTH

BAND-TO-BAND

$$E_B = \frac{\hbar^2}{2m^*} \left(\frac{\pi n}{L_z} \right)^2$$

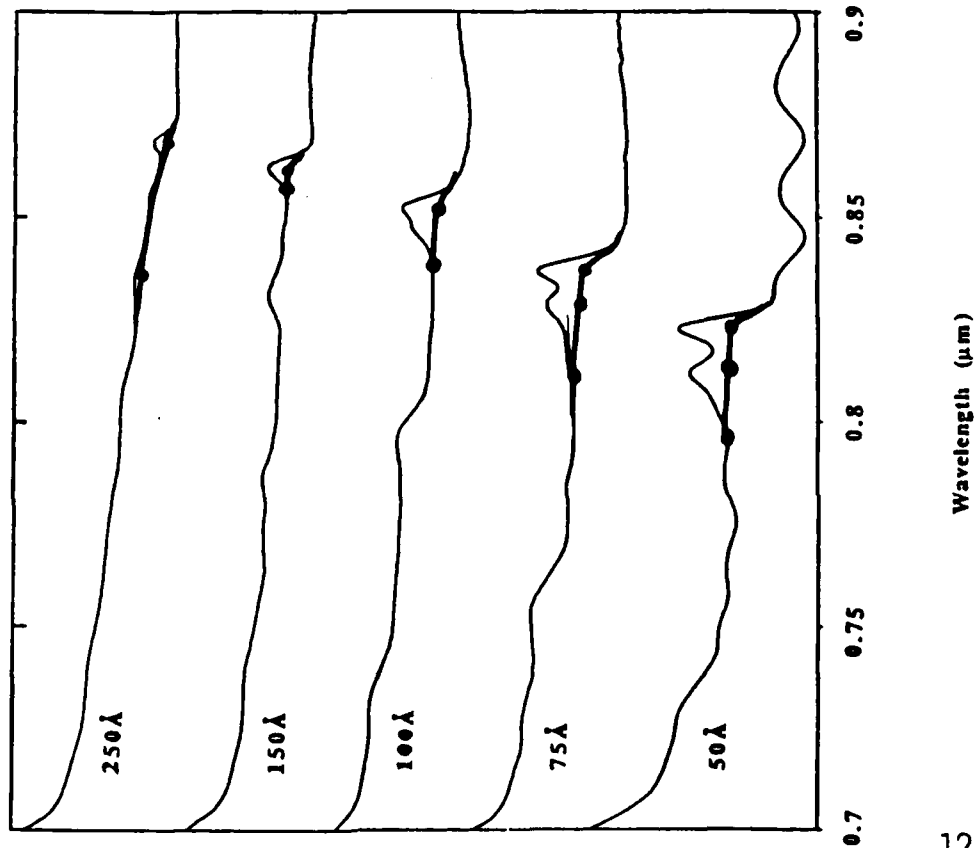


$$\alpha(E) \propto p(E) \propto \frac{\hbar}{\sqrt{2m^*}} \left(\frac{\pi n}{L_z} \right)$$

GaAs/GaAlAs MQW's GROWN

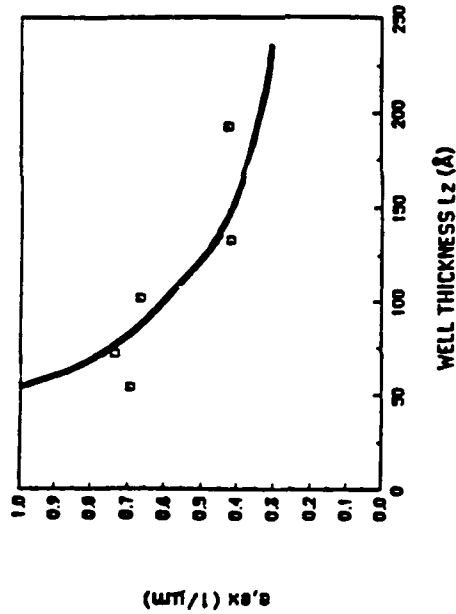
BY MOCVD; DARRUS et.al.

ABSORPTION OF MQW'S



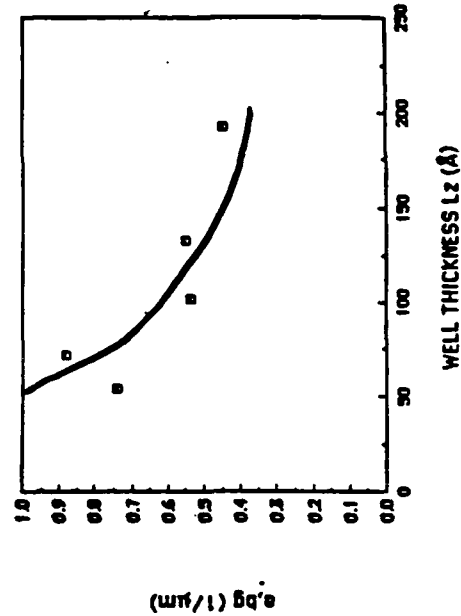
-120-
GARM
4

EXCITONIC LINEAR ABSORPTION ON hh



$$\alpha_e \propto \frac{1}{L_z}$$

BACKGROUND LINEAR ABSORPTION ON hh



$$\alpha_B \propto \frac{1}{L_z}$$

SATURATION INTENSITY

EXCITON

$$I_s \tau \approx \frac{\hbar \omega}{2} \left(\frac{1}{a_{n,m} L_z} \right) \left(\frac{1}{A_x} \right)$$

L_z EXCITON AREA

CARRIER DIFFUSION

$$I = \frac{P_{cw}}{\pi (4D\tau + \omega_0^2)} \quad \text{WHEN} \quad \omega_0 \tau \gg \omega_0$$

$$I \propto P_{cw}$$

ALSO

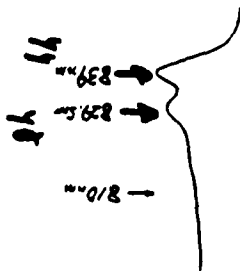
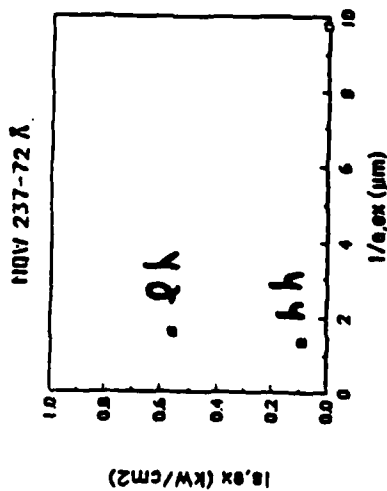
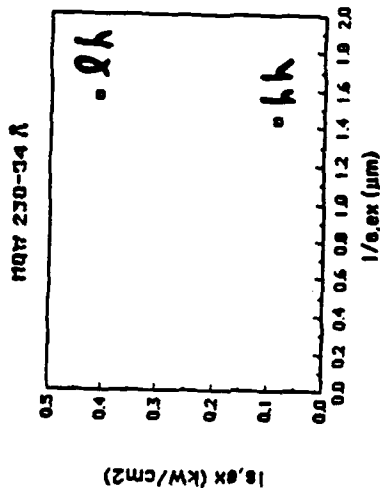
$$a_{n,m} \propto \frac{1}{L_z}$$

THUS

$$P_{s,cw} \propto \frac{1}{A_x} \propto \frac{1}{L_z^2} \quad \text{INDEP. OF } L_z$$

$$\gamma_B = \frac{\hbar^2 \epsilon}{e^2 \mu^+} \quad \frac{1}{\mu^+} = \frac{1}{m_0^+} + \frac{1}{m_h^+}$$

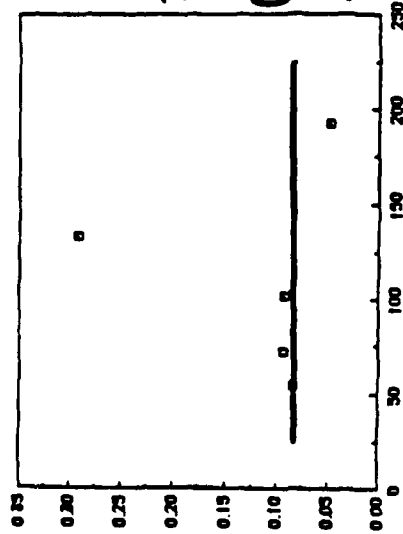
$$\frac{P_s(2h)}{P_s(1h)} = \left(\frac{\mu_{hh}^+}{\mu_{2h}^+} \right)^2 = 2.3$$



$$\frac{I_s(2h)}{I_s(1h)} = 5.42 \quad \text{EXPERIMENTALLY}$$

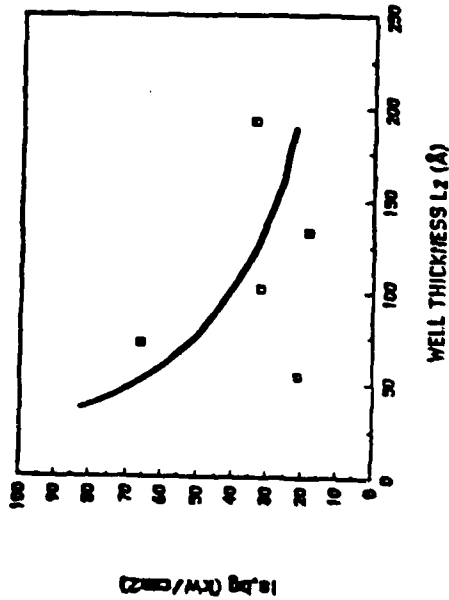
$$\sim \left(\frac{\mu_{hh}^+}{\mu_{2h}^+} \right)^4$$

EXCITONIC SATURATION INTENSITY ON hh



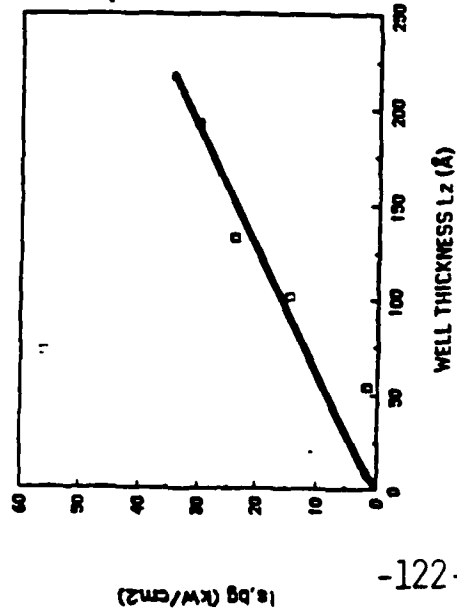
$$I_{se} \propto \frac{1}{(\Delta L) A x} \sim \text{CONST.}$$

BACKGROUND SATURATION INTENSITY ON c



$$\begin{aligned} \rho(\epsilon) &\sim \sqrt{\epsilon_0} \\ \rho(\epsilon) &\sim \frac{1}{L_z} \\ \rho(\epsilon) &\sim \frac{1}{L_z} \end{aligned} \quad E_0 \text{ h}\nu \rightarrow$$

BACKGROUND SATURATION INTENSITY ON hh



$$I_{se} \propto L_z$$

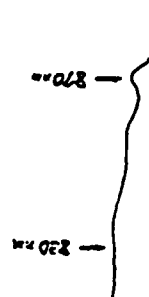
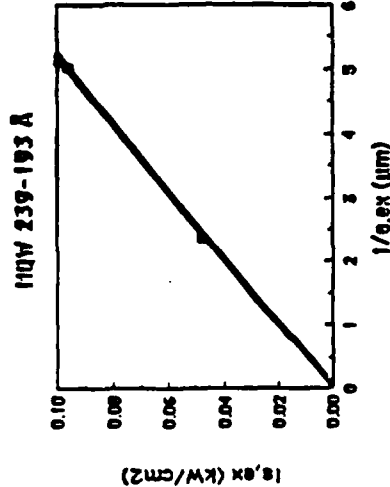
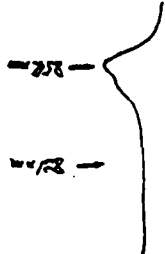
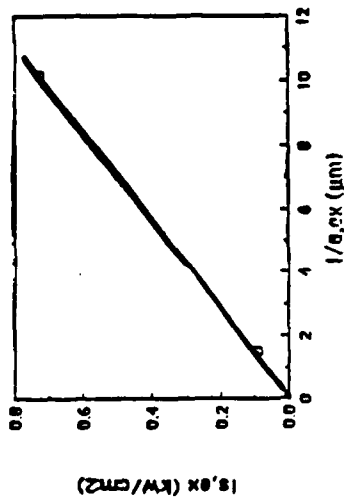
$\rho(\epsilon)$ IN BAND TAIL



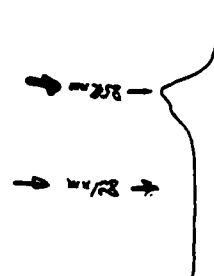
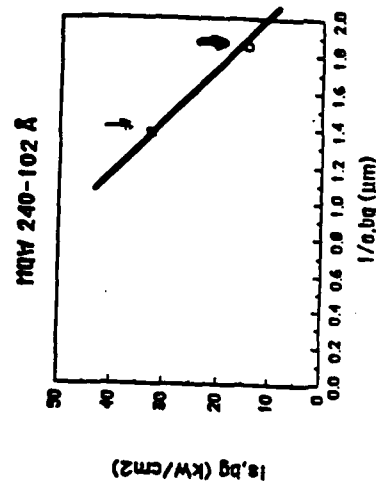
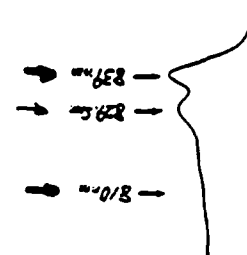
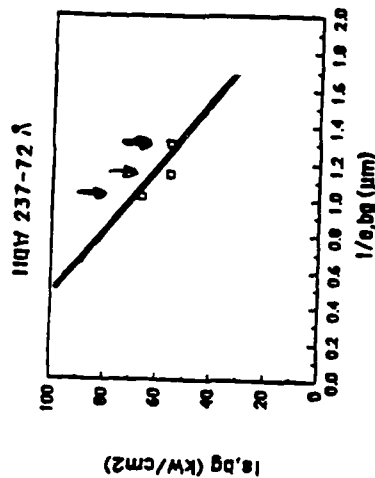
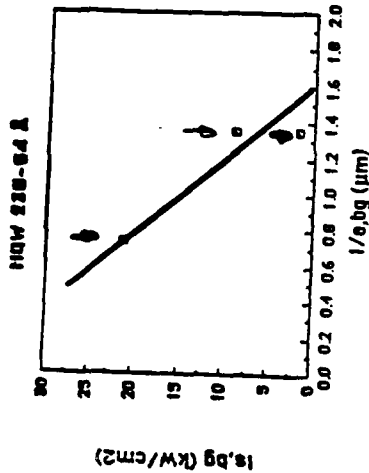
$$\rho \sim \frac{1}{(\Delta E)^2} \text{ IN TAIL}$$

$$\rho_B \propto \frac{\sqrt{E_0}}{E_0^2} \propto \frac{1}{L_z^2} \cdot \frac{L_z^2}{1} \sim L_z^2$$

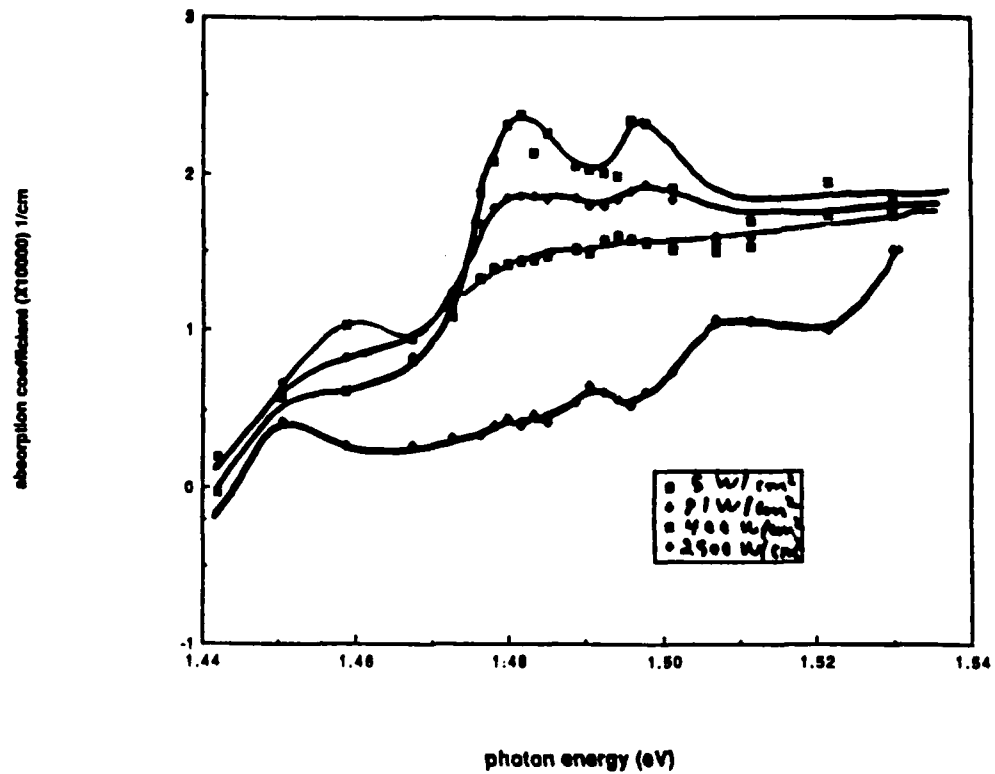
WAVELENGTH DEPENDENCE OF SATURATION INTENSITY



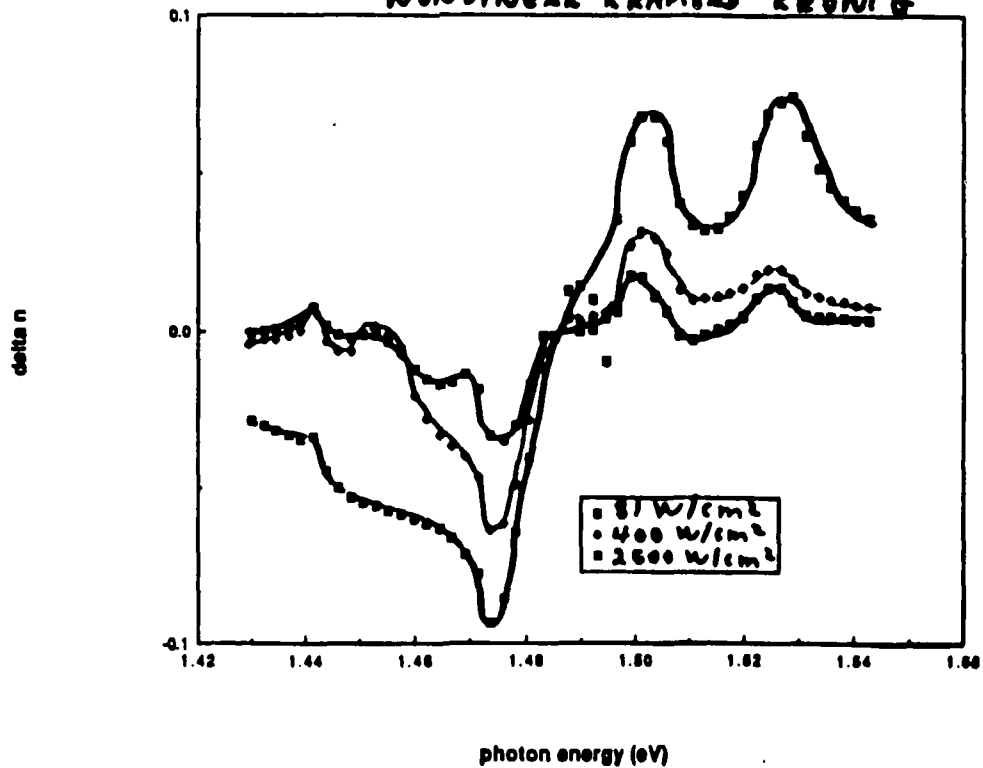
$I_{s,e} \propto \frac{1}{\alpha}$ for L constant



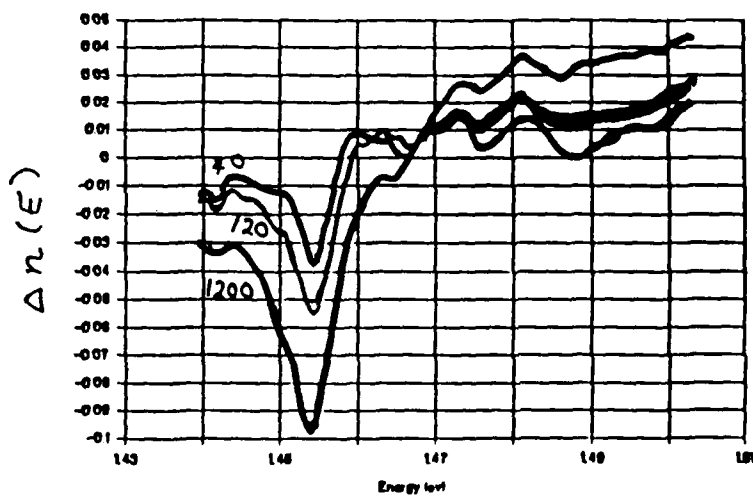
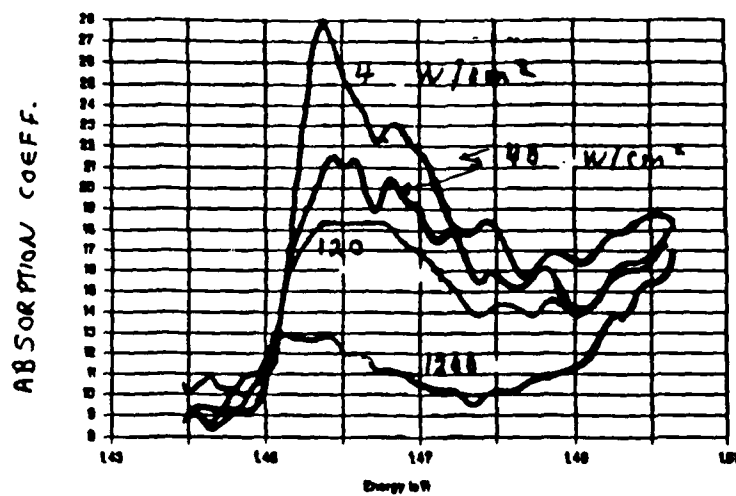
absorption coefficient for various intensities



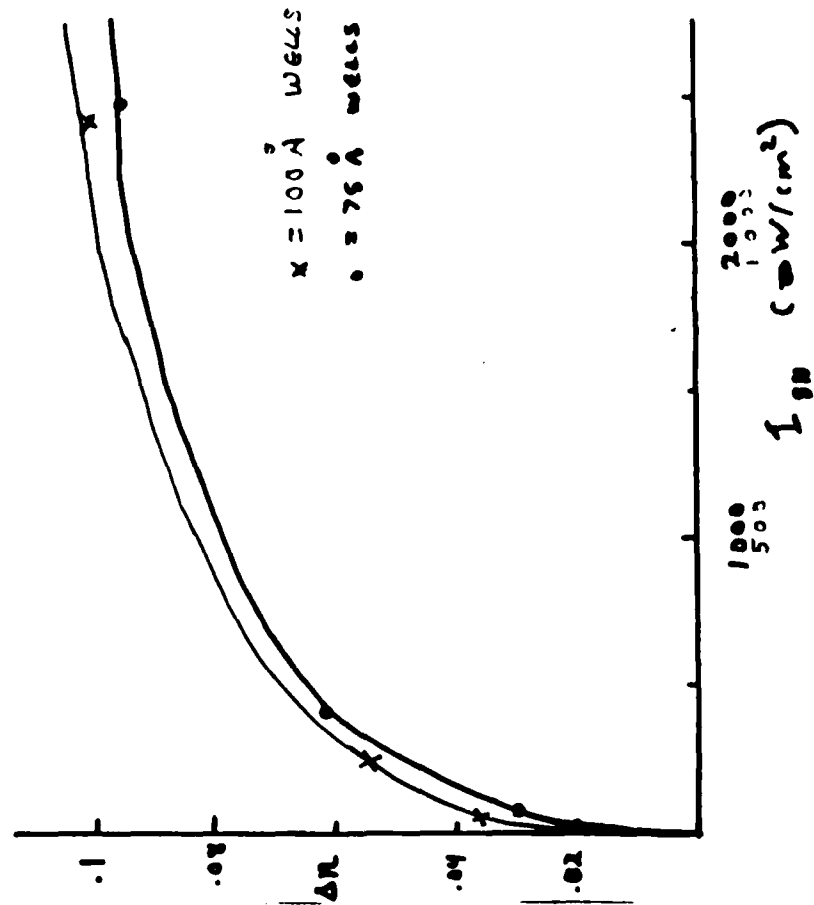
delta n for various intensities $\Delta n(E) = \frac{\hbar c}{\pi} p \int_0^\infty \frac{\alpha(E') dE'}{E'^2 - E^2}$
 USING
 NONLINEAR KRAMERS KRONIG



100 Å SAMPLE

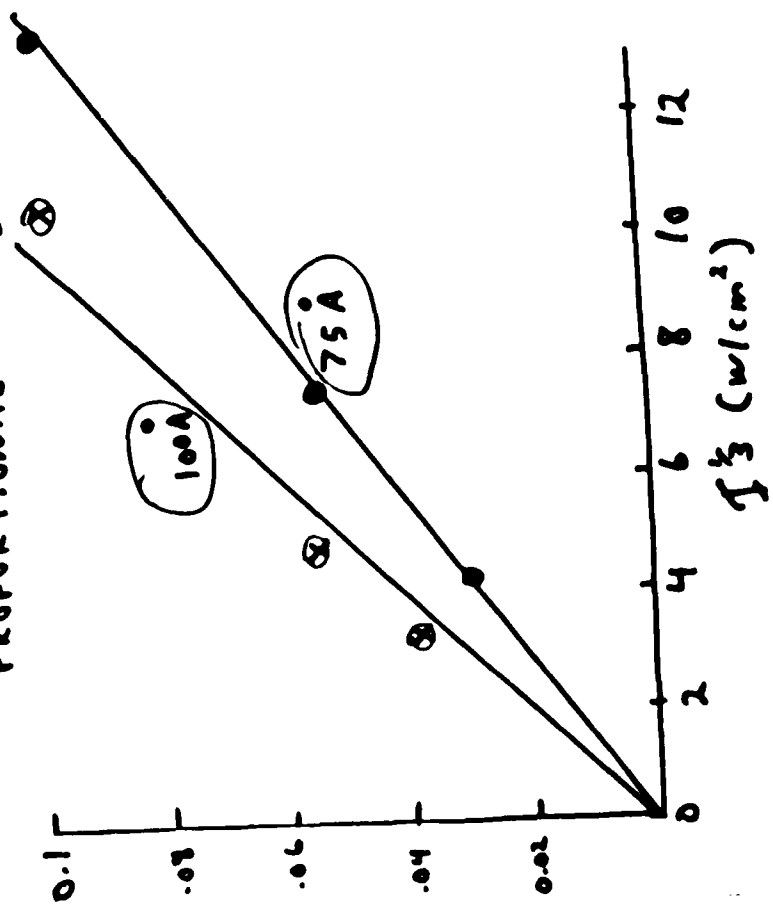


INTENSITY DEPENDENCE OF THE NONLINEAR INDEX



THIS IS NOT AN n_2 EFFECT

NONLINEAR INDEX PROPORTIONAL TO $I^{1/3}$



CONCLUSIONS

EXCITON AND BAND-TO-BAND

NONLINEAR ABSORPTIONS HAVE
BEEN SEPARATED

MEASUREMENTS OF ABSORPTION PULSE
WITH THEORY

MEASUREMENTS OF SATURATION INTENSITIES
ARE REASONABLE

CALCULATIONS OF THE NONLINEAR INDEX
FROM KRAMERS-KRONIG SHOW LARGE
DEVIATIONS FROM n_2]

Progress in Stabilized Lasers

John L. Hall

Dieter Hils

Christophe Salomon

Jean-Marie Chartier

Franco Wong

SubDoppler Optical Multiplex Spectroscopy, with Stochastic Excitation

Klaus-Peter Dinse

Mike Winters

John L. Hall

Joint Institute for
Laboratory Astrophysics
Boulder, Colorado

Slow Atoms and Stable Lasers

j hall, d h/s

JKA

{ University of Colorado
{ National Bureau of Standards

Some Interesting experiments REQUIRE a laser's frequency to be stable for a long time (seconds - years)

- Rydberg constant
- * QED Tests - positronium vs hydrogen
- operational frequency/wavelength standards
- * sources for long baseline interferometry
 - space gravity-wave antenna
 - space synthetic aperture astronomy
- * tests of cherished fundamental ideas
 - ex - isotropy of c

$$g_1 = g_0 \quad \text{in} \quad ds^2 = g_1 dx^2 + g_2 (dy^2 + dz^2) - g_0 c^2 dt^2$$

Estimating the Laser Linewidth w feedback

1. Residual FM of Laser - vibration

suppose $\delta\Omega_{\text{laser}} = a \cos \omega_v t$

linewidth is $\sim 2a$ if $a \gg \omega_v$

large excursions at low freq \sim Gaussian shape

Many sidebands



Apply servo control. Gain (ω_v) = G

$$\text{then } \delta\Omega_s \approx \frac{\delta\Omega_{\text{laser}}}{1+G} \sim \frac{2a}{1+G}$$

\rightarrow linewidth less by factor $G+1$

At high Gain, phase modulation index $\rightarrow 0$

sidebands disappear for $\frac{a}{\omega_v} \lesssim 1$

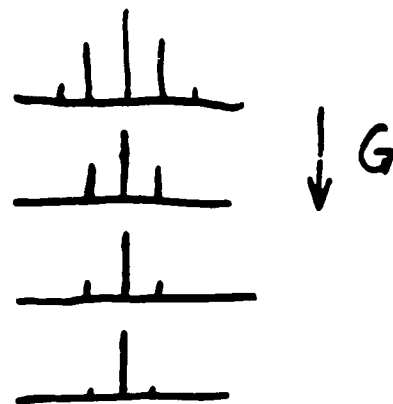
ie for $G > \frac{a}{\omega_v}$

Conclusion: if servo

feedback gain is high

enough, INTRINSIC

laser FM $\rightarrow 0$ effectively



\rightarrow What new effect keeps real linewidth non-zero?

Shot-Noise - Induced Laser FM



$$\rightarrow | \leftarrow \Delta$$

$$i_{\text{shot noise}} = \sqrt{2e i B}$$

$$\frac{\text{Sig}}{\text{Noise}} \sim \frac{i}{i_{\text{shot noise}}}$$

$$\delta \Omega_s \approx \frac{\Delta}{\text{Sig/Noise}} \sim \Delta \cdot \frac{\sqrt{2e i B}}{i}$$

→ Residual Frequency Excursion ←

What is the laser linewidth?

$$\begin{aligned} \delta \Omega_{1/2} &= \pi \frac{(\delta \Omega_s)^2}{B} = \pi \Delta^2 \frac{2e}{i} \\ &= \pi \cdot (\text{frequency noise spectral density})^2 \end{aligned}$$

valid in High S/N limit: $B \gg \delta \Omega_s$ D Elliott et al P.R.A (82)

ex:

$$\delta \Omega_s \approx 100 \text{ Hz in } 3 \text{ MHz BW}$$

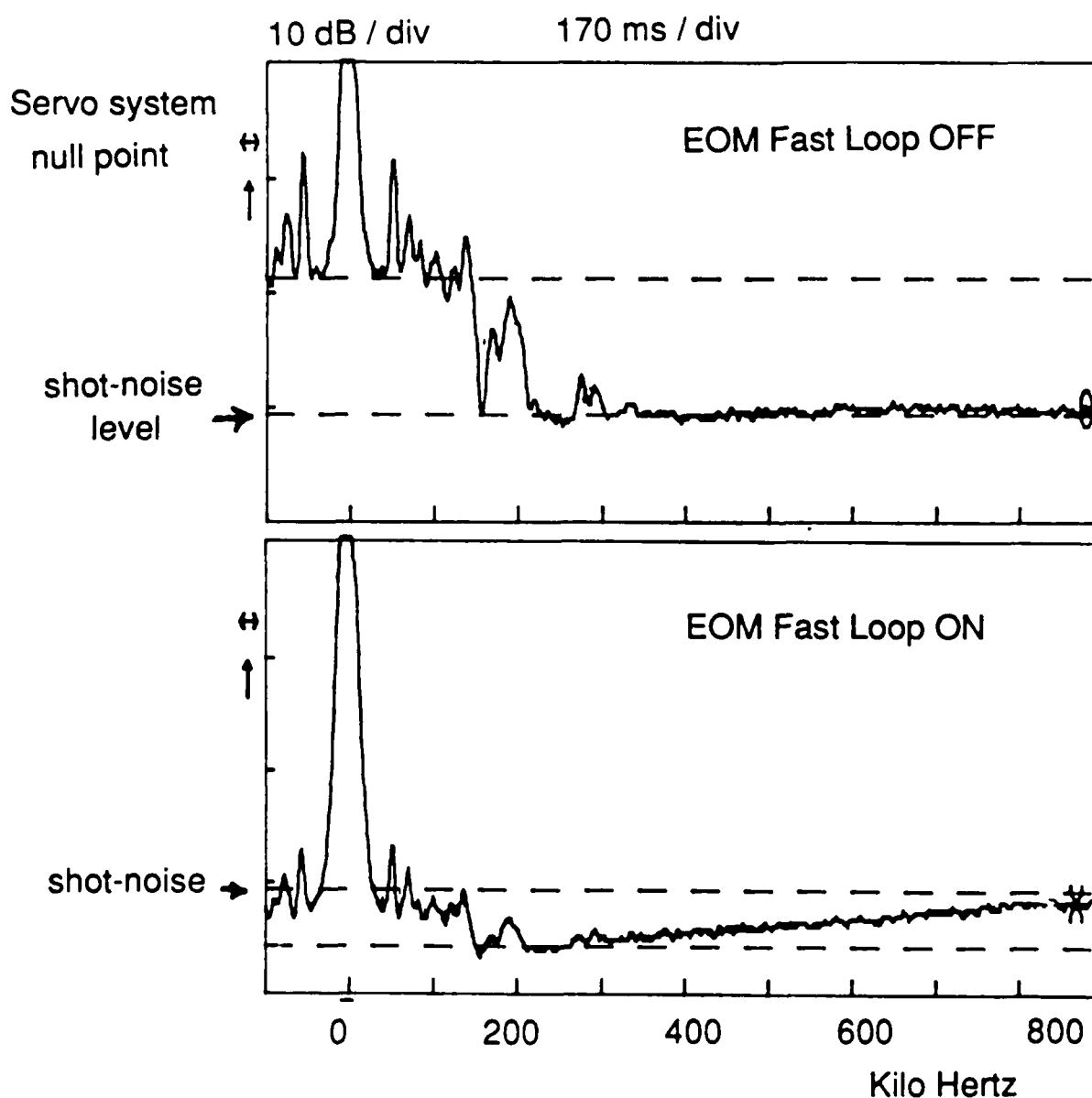
$$\delta \Omega_{1/2} \approx 100 \text{ milli Hertz}$$

Sig/Noise grows $\propto \sqrt{T}$
cycles grows $\propto T$

> we run out of S/N at
-131- long times

High Performance Frequency Servo

A frequency Servo system using a Reflection-mode phase/frequency optical discriminator and an "outside - the-laser" frequency transducer can achieve excellent closed loop performance. Here an Argon laser is stabilized tightly above 200 kHz so that measurement shot-noise is converted into a corresponding FM excursion, ie the servo null point goes 6 dB below the shot-noise level. The remaining FM noise at 100 kHz is near the shot-noise level and can be drastically reduced with additional low frequency gain.



Limiting Narrow Laser Linewidth

Servo Gain is very large \rightarrow laser intrinsic noise totally suppressed
only measurement noise important

$$\frac{\partial I}{\partial V} \times \delta V + \text{shot noise} = 0 \quad \text{Servo Eq.}$$

gives a frequency excursion density

$$\frac{\Delta}{\sqrt{B}} = \frac{\sqrt{2e i_d}}{i_{sig}} \times \Delta V_c \propto \frac{\text{Hz deviation}}{\sqrt{\text{Hz bandwidth}}}$$

$$\text{Lorentz Linewidth} \quad \delta f = \pi \Delta^2 \quad \text{Elliott '82}$$

$$\text{Ex: } F = 6500 \quad \nu_{2L} = 500 \text{ MHz} \quad \Delta V_c = 80 \text{ kHz}$$

$$\frac{\text{noise}}{\text{signal}} \sim 0.2 \text{ ppm in 1 Hz BW}$$

$$\rightarrow \Delta = 15 \text{ mHz} / \sqrt{\text{Hz}} \times \sqrt{5 \text{ kHz}} = 1 \text{ Hz}$$

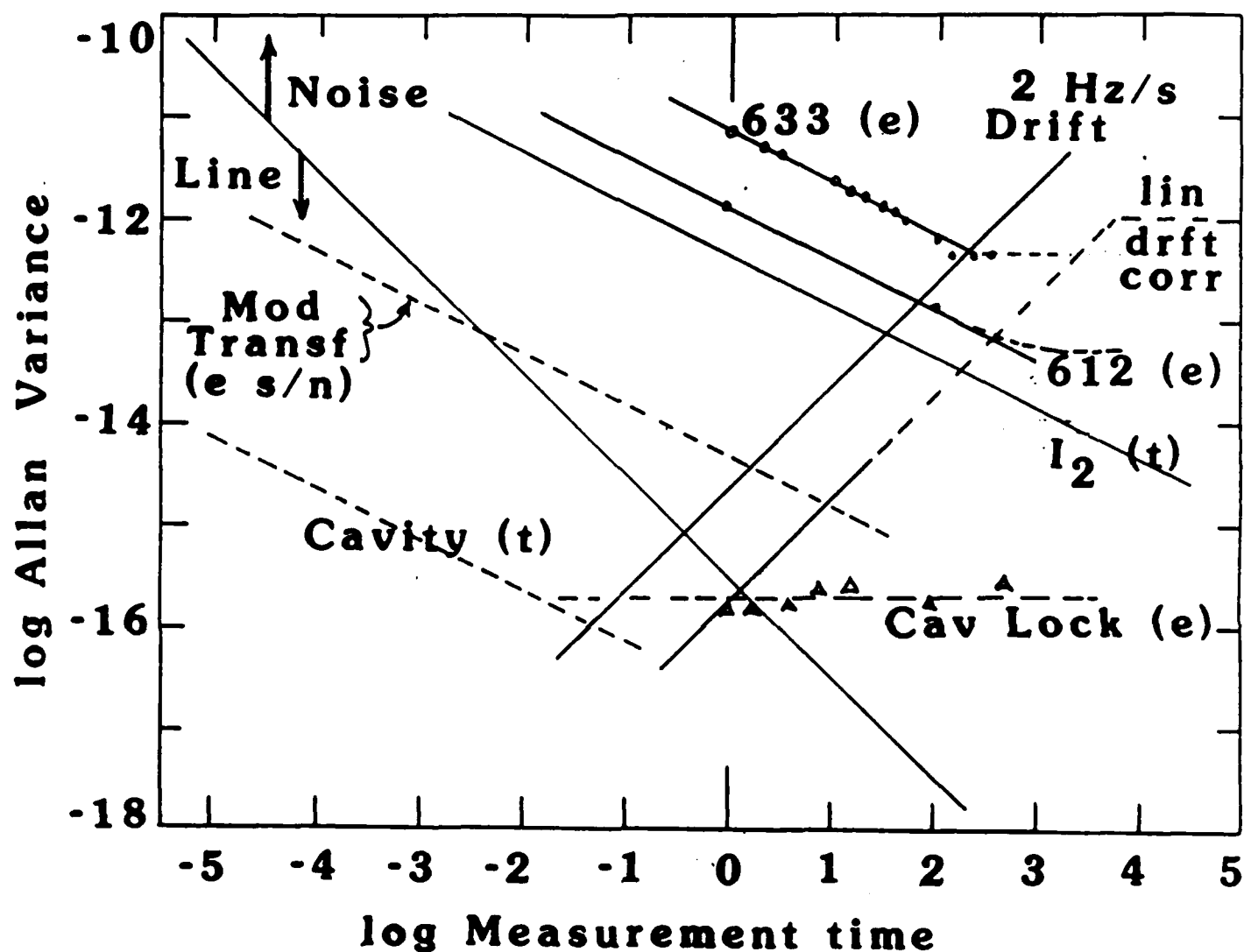
$$\text{so } \delta f = \pi \Delta^2 = \pi \cdot \left(.015 \frac{\text{Hz}}{\sqrt{\text{Hz}}} \right)^2 = 700 \mu\text{Hz}$$

$$\text{coherence time } 1/(2\pi \delta f) = 225 \text{ sec} !$$

"typical" time for ± 1 radian now $\sim 15-20 \text{ sec}$

$$\frac{10^{-2} \text{ Hz}}{5 \times 10^{14}} \sim 2 \times 10^{-17} \text{ at 15 sec} !$$

Distinguishing a Spectral Line from Filtered Noise



In the lower-left sector the fast laser phase-noise is below one radian, so the source looks like a spectral line which is (slowly) drifting in frequency. In the upper-right triangle, the phase noise exceeds one radian, and so no appreciable sharp carrier component is left. Thus the field has only a short time-coherence and looks like white noise which has been spectrally filtered, in our case by the resonance filter represented by the frequency servo loop. Note that the present cavity-locked results offer a line spectrum out to a few seconds, while the Iodine resonances are too broad and / or too weak to give good short-term locking.

Cavity Mirrors: $R = 575 \text{ cm}$
 $R = \infty$

are optically contacted to End Faces of
Zerodur Spacers : $15 \times 30 \text{ cm}^2$

$$F \sim 6,600$$

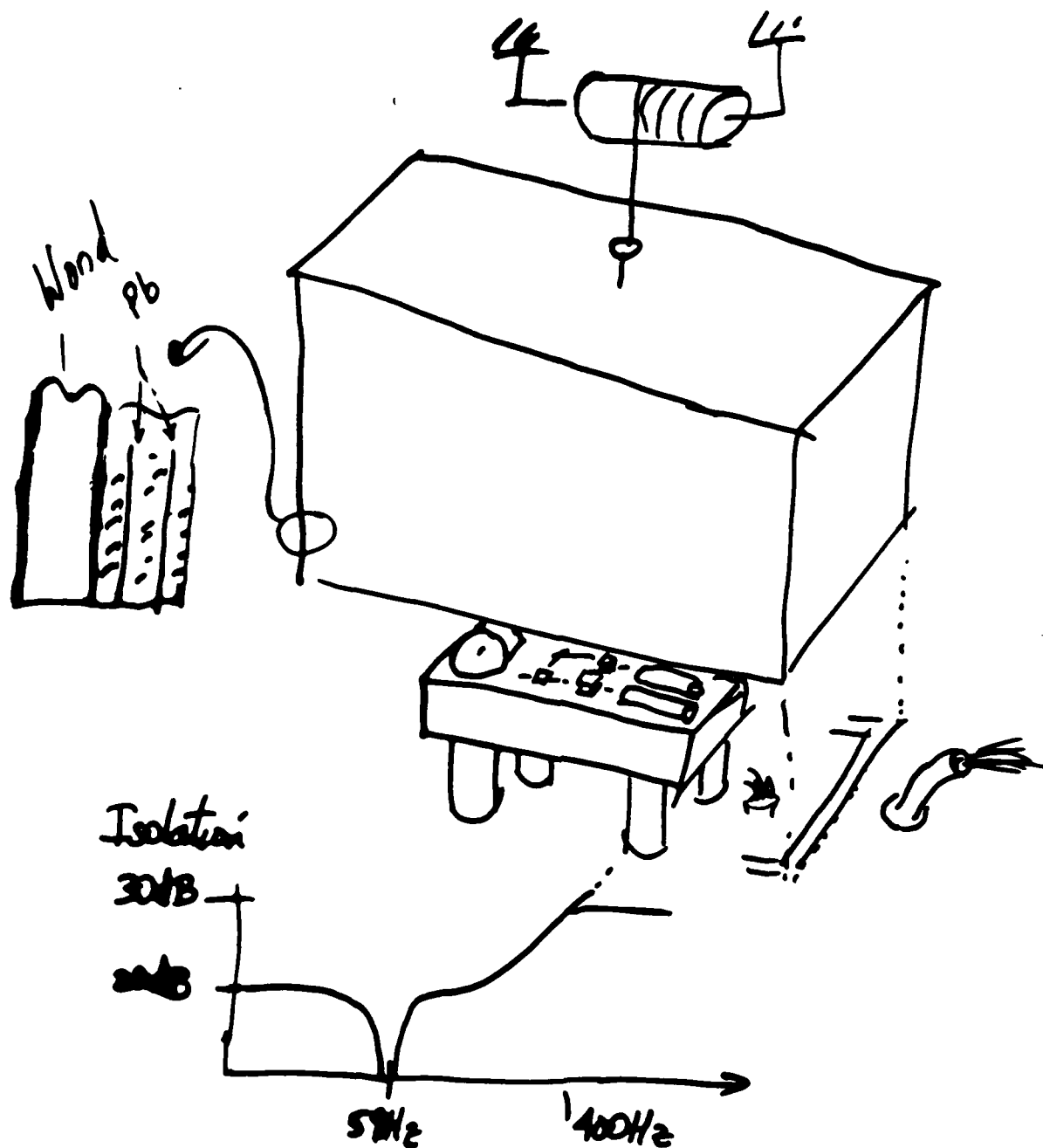
$$\text{FSR} = 480 \text{ MHz}$$

$$\Delta \nu_c = 72 \text{ kHz}$$

Cavity is located in sealed Aluminum Can.
Alu-Walls are temperature controlled

$$\text{Vac Pressure} < 8 \times 10^{-8} \text{ Torr}$$

Optical Set up is located inside Q-House
for Acoustic Isolation ($\sim 40 \text{ dB}$) and
Temperature Isolation ($\sim \text{mK}$).



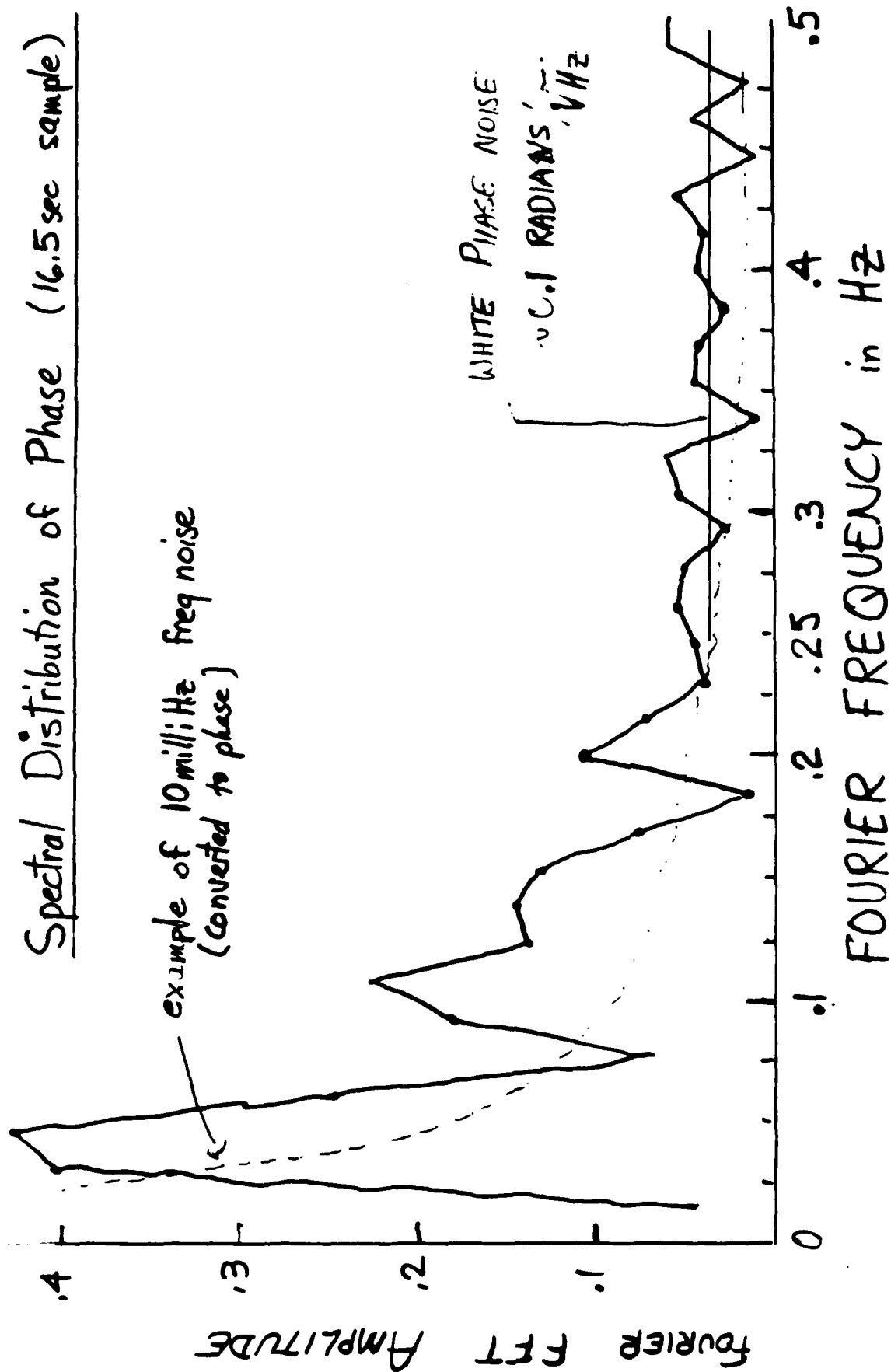
the JILA « QUIET HOUSE »

d hils, j fuller, j. hall

RSI sub 1986

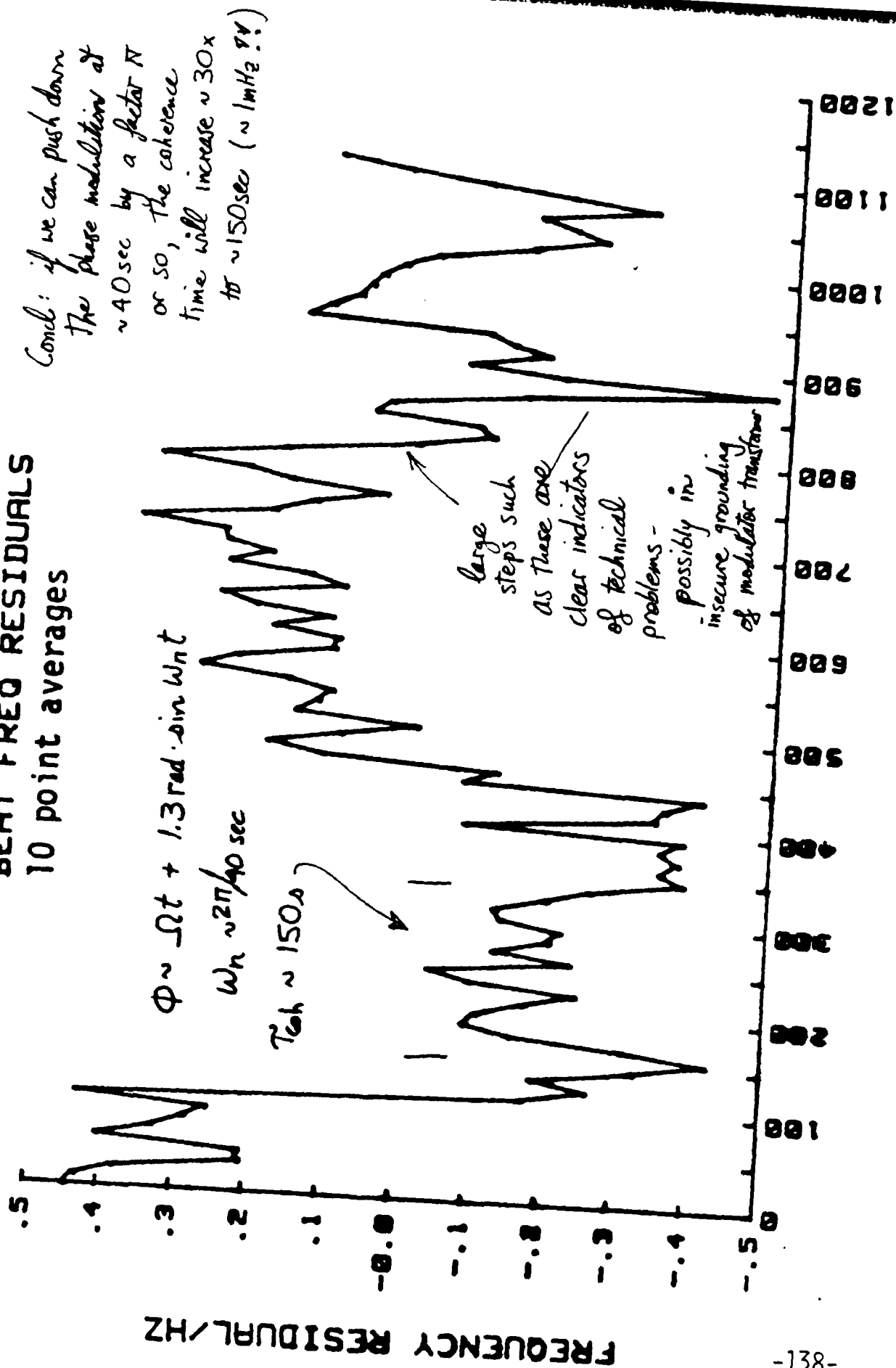
-136- 57 2532 (1986)

Spectral Distribution of Phase (16.5 sec sample)



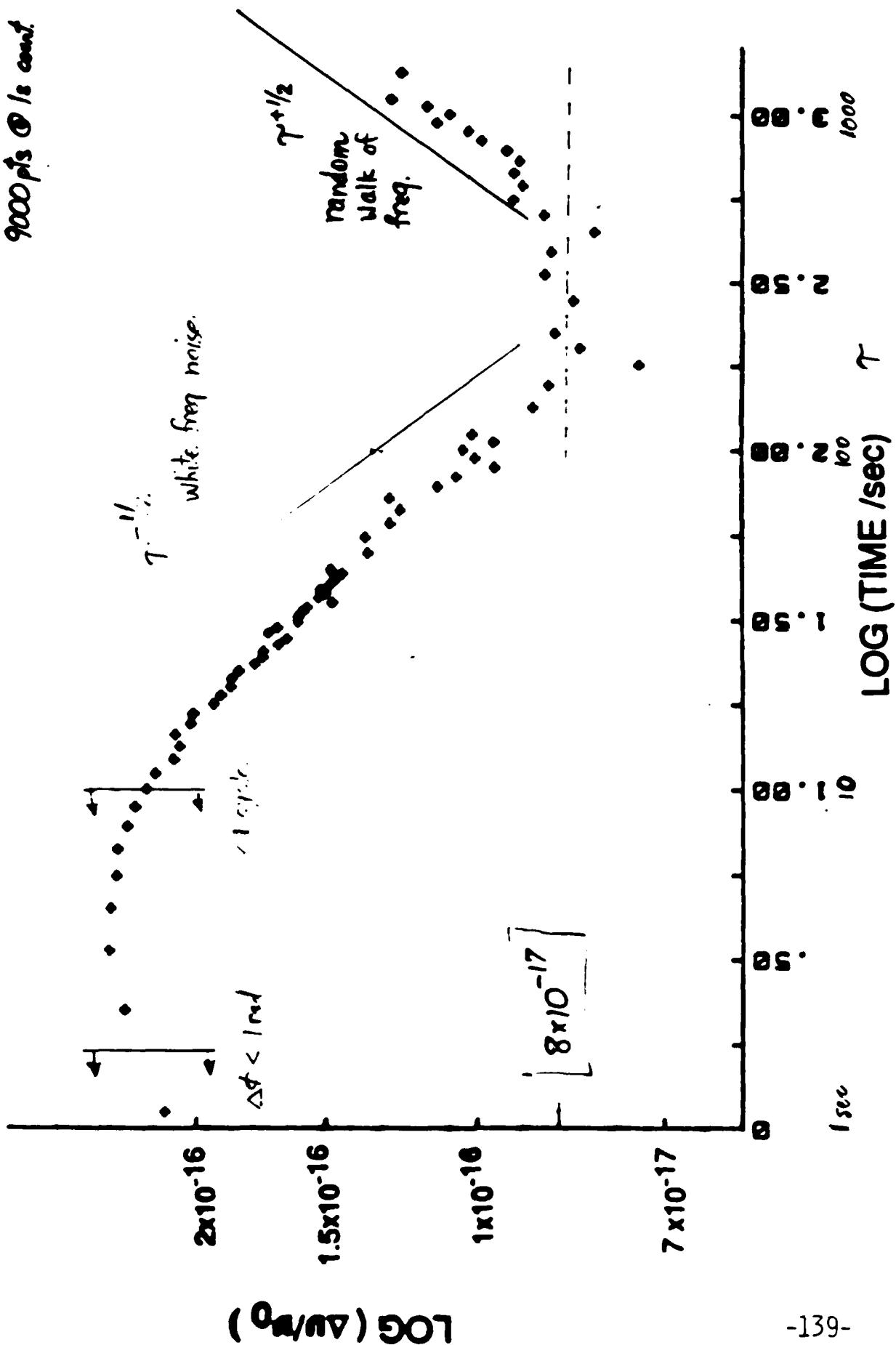
Hils & HALL Summer-87

BEAT FREQ RESIDUALS 10 point averages



ALLAN VARIANCE OF CAVITY LOCKED HENE LASER

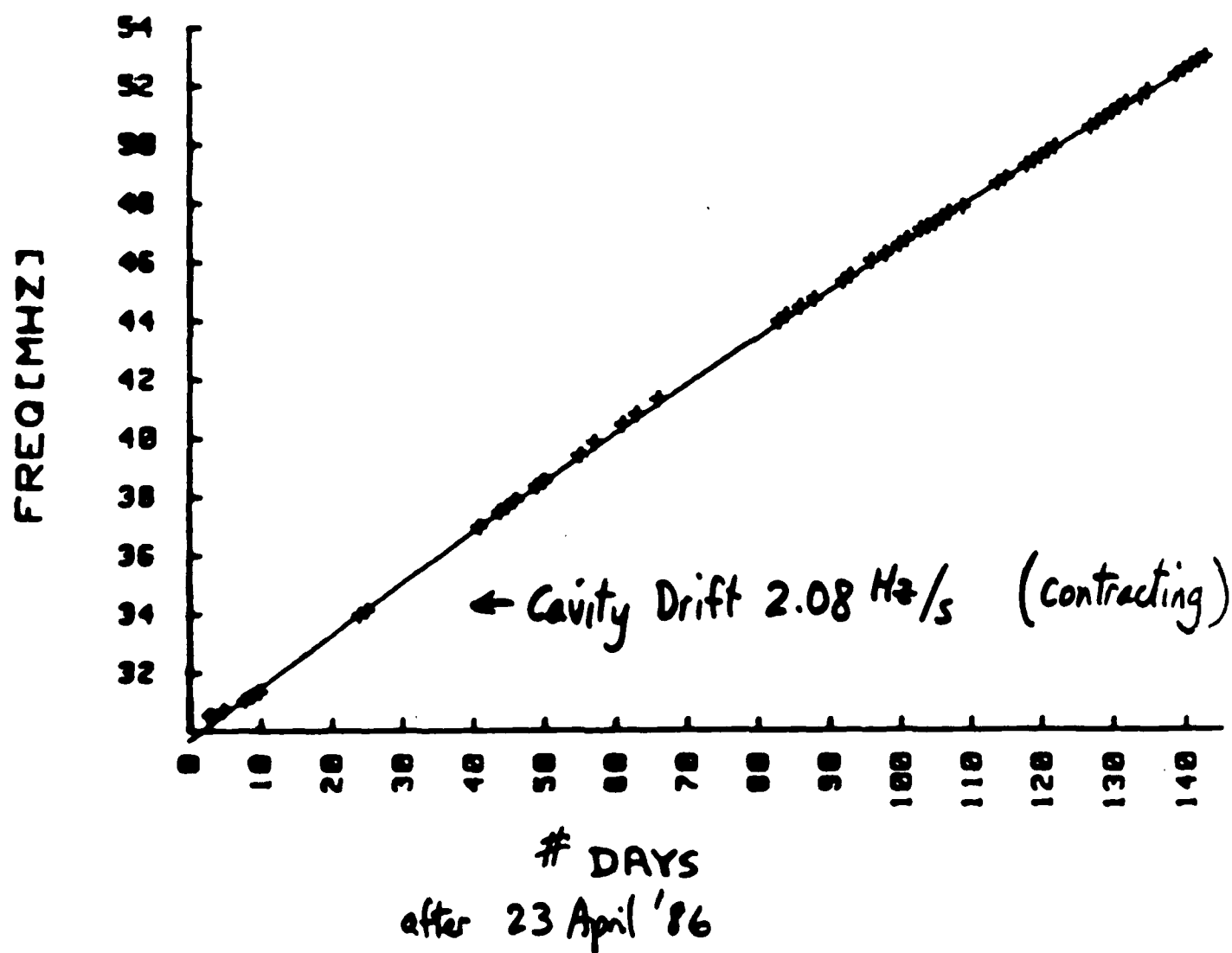
9000 p/s @ 1 s count



LONG-TERM STABILITY (CAVITY)

Cavity-Stabilized He/Ne vs I₂-Stabilized He/Ne

BEAT FREQUENCY [REF IS h-PEAK]



Strategy for Laser Locking

Tight lock to good cavity
+ SLOW lock to atoms

assume 30cm cavity, $F = 10,000$ } \rightarrow $SD < 1$ millihertz
 $\eta = 10\%$ due to shot noise
(theory)

expt'l $SD < 0.1$ Hz
limit was drifting of cavity - thermal?

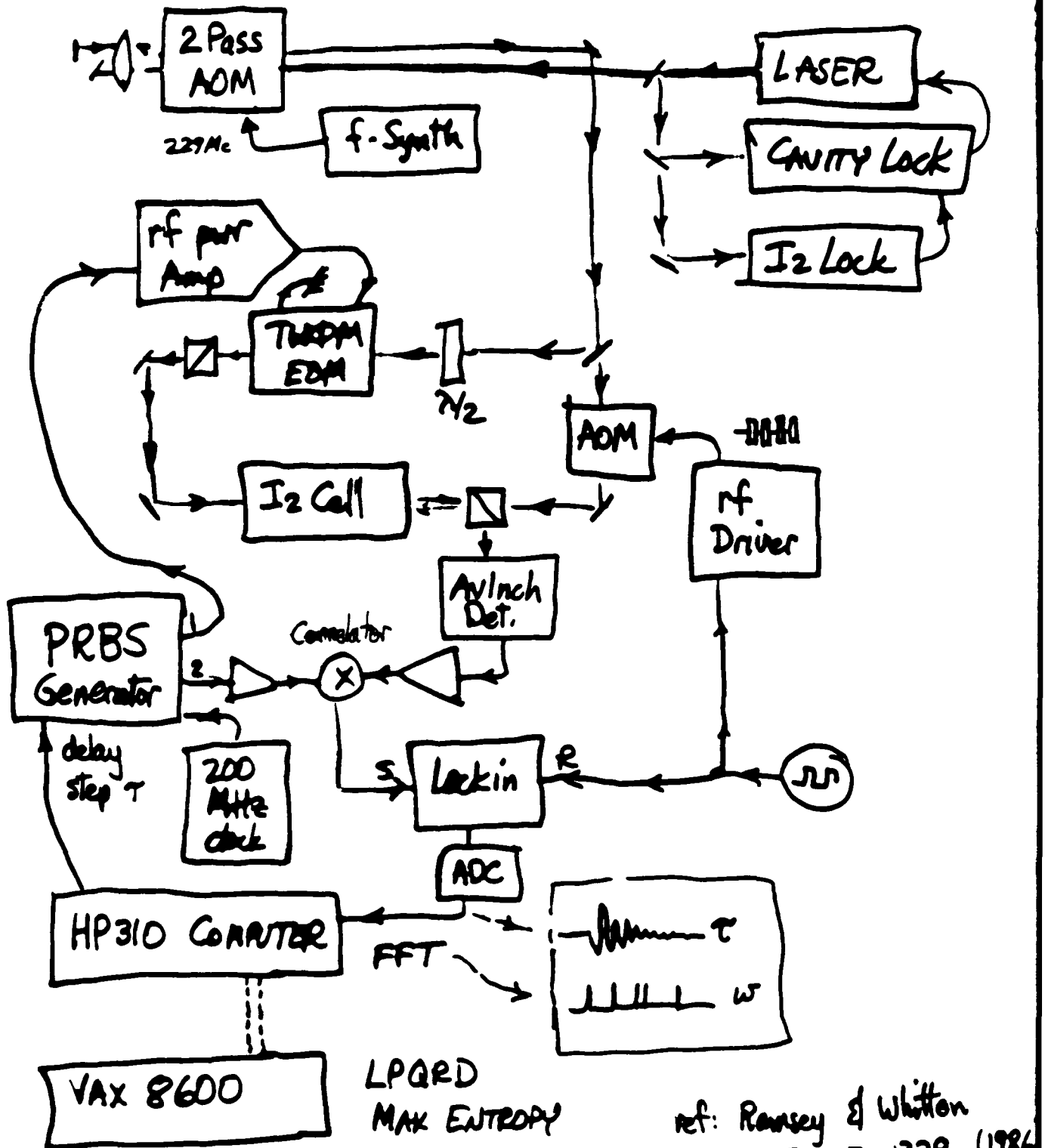
Compare I_2 - stabilized laser vs cavity-stabilized
drift rate $+2.08$ Hz/sec
rms deviations ~ 100 Hz in 24 hours

\rightarrow ready for ATOMS! (with sub-Hz linewidths)

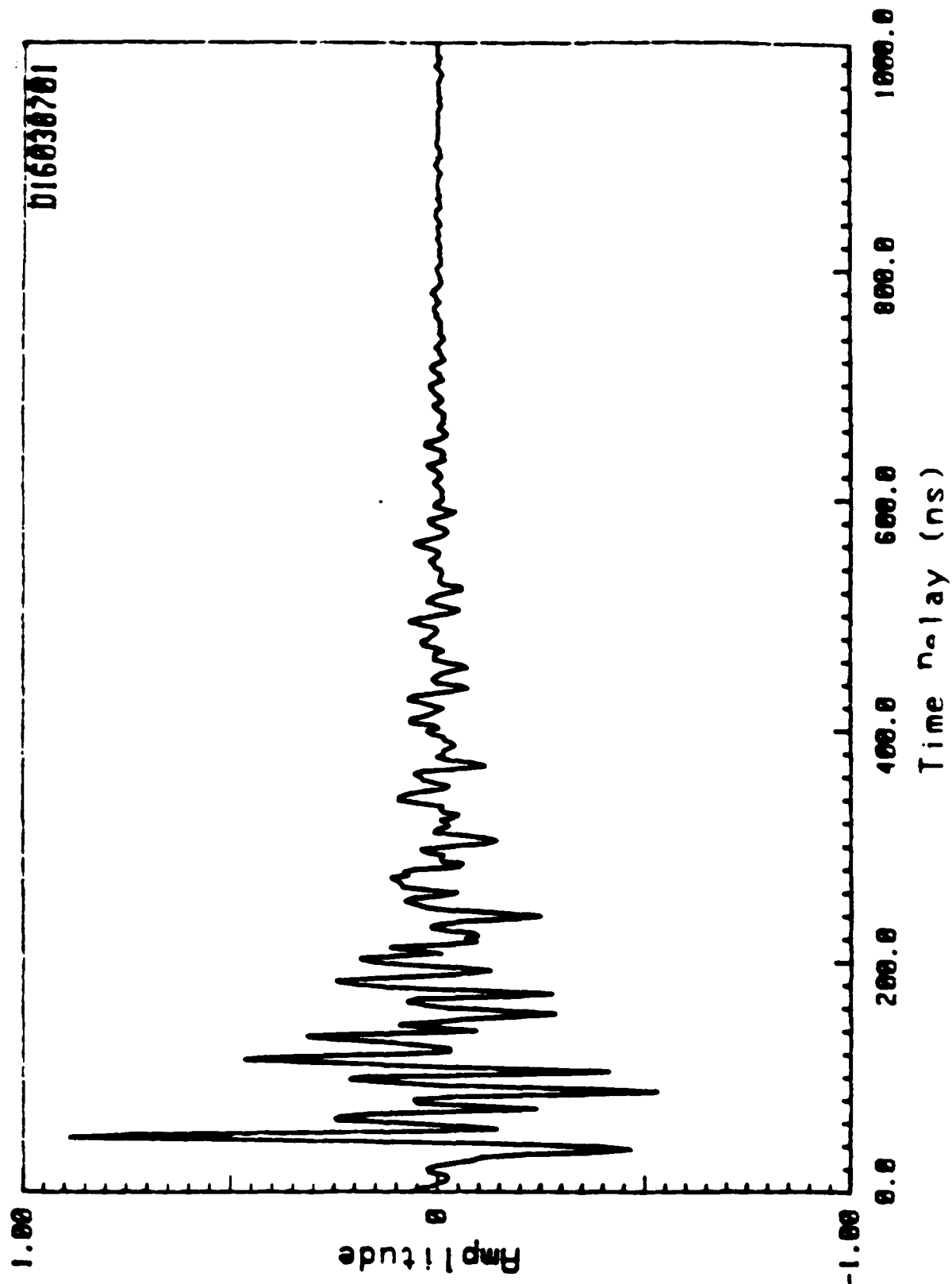
$SD_{FW} = 50$ mHz
drift predictable to 0.1 Hz for 30 sec

Doppler-free Optical Multiplex Spectros. with Stochastic Excitation

P. DINSE, M. WINTERS, j hall

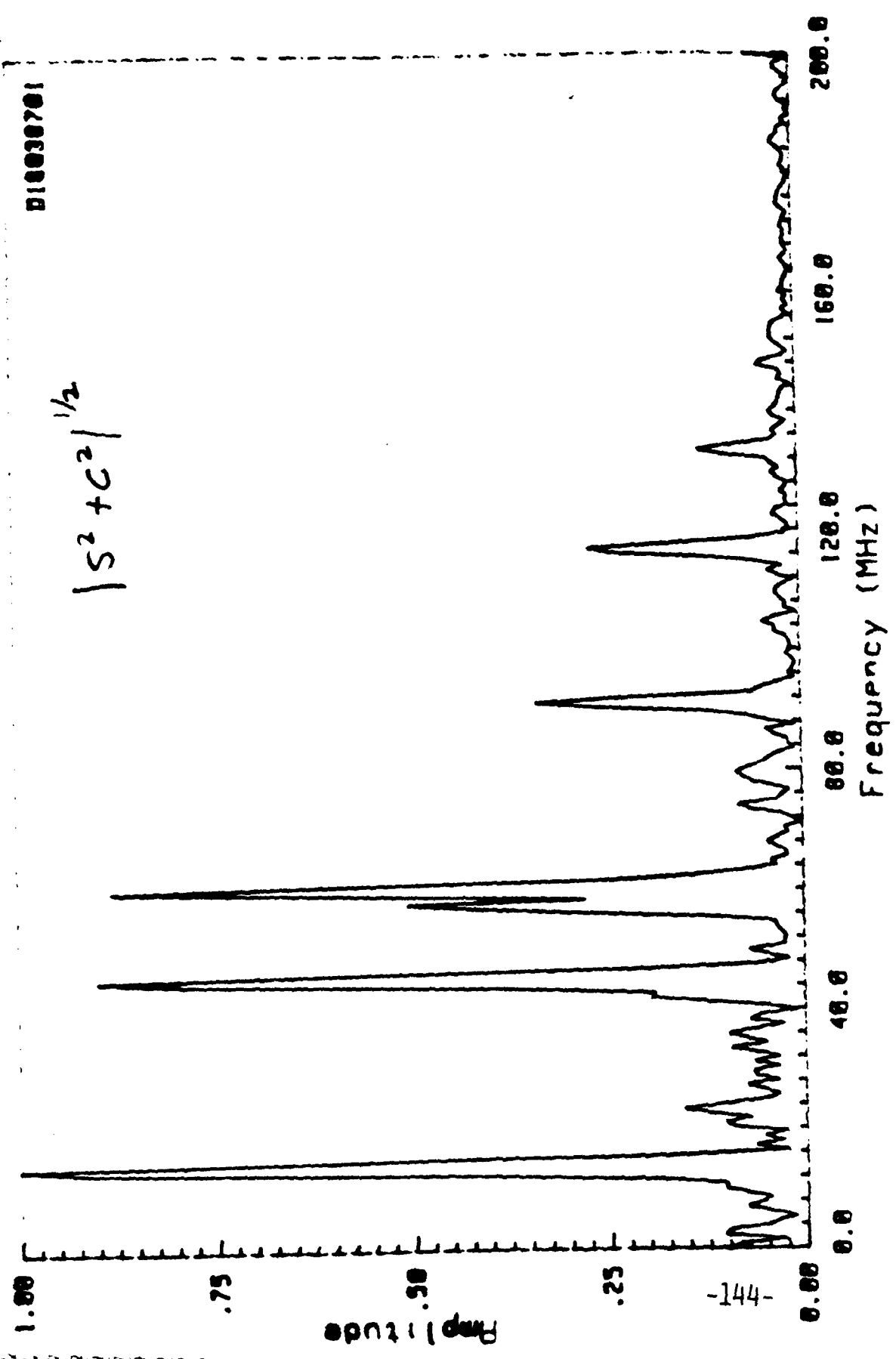


PRBS Signal (400 pts)



$\gamma = 1/4$
 $N = 0.5$

Fourier Transform (512 pts)



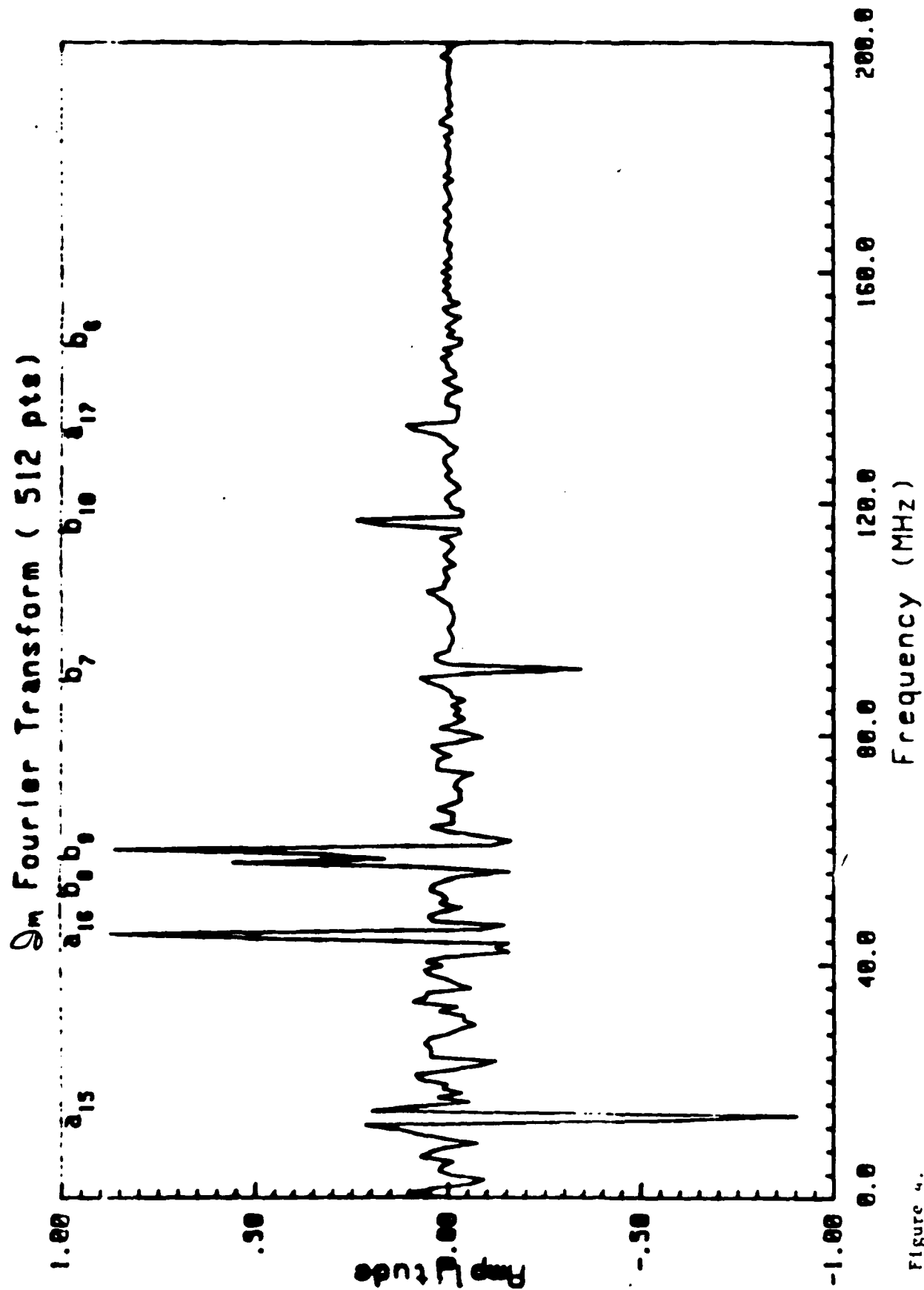


Figure 4.

Doppler-Free Spectroscopy with Multiplex Detection & Stochastic Ex

The present: idea demonstrated

paper ready for JOSA-B

K.P. Dinse, M. Winters, J. Hall

The future:

1. Servo-control phase modulator to produce pure FM
→ correlation at $t=0$ vanishes
→ only molecules give signal
2. Digital filtering to whiten $\sin x/x$ modulation
→ flat to $\sim 0.9 \times f_c$
3. Try bigger beams for I_2 at 507 \AA
 $20 \mu\text{s} = T_n \rightarrow < 20 \text{ kHz linewidth}$
with 200 MHz excitation width
 $N \sim 10^4$ multiplex factor $\sqrt{10^4}$ S/N
4. GaAs chips - 1 GHz BW covers most Dopplers

the Advantages:

1. S/N win by \sqrt{N}
2. Freq. axis is accurate
3. lineshape involves single intense field \rightarrow calculable

Dynamic and Spectral Properties of Semiconductor Lasers with Quantum Well, Quantum Wire, and Quantum Box Structures

Yasuhiko Arakawa

University of Tokyo, Roppongi, Minato-ku, Tokyo 106 Japan

Abstract

Effects of reduced dimensionality of electron motion alter various properties of semiconductor lasers. In fact, quantum well structures have brought significant improvements in semiconductor laser characteristics. In 1982, Arakawa et. al. proposed the concept of the quantum box laser as well as the quantum wire lasers. In an ideal quantum box structures, electrons and holes have highly localized wavefunctions and the state space in each box is discrete as opposed to the quasi continuum of the bulk. The contribution to gain from each ideal quantum box arises from a pair of two level systems. In this case, the overall active layer would much like a gas laser in which the quantum boxes are analogous to the atoms in the gas.

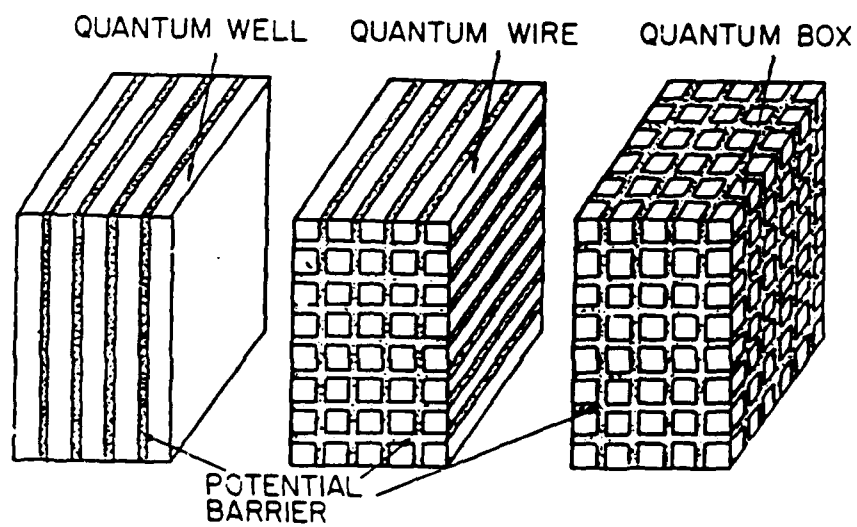
In this paper, we discuss dynamic and spectral properties of semiconductor lasers having such quantum-mechanical micro-structures, with emphasis on the quantum box lasers. The theoretical analysis indicates that laser characteristics are significantly improved in low-dimensional electronic gas systems. In order to demonstrate the quantum box effects experimentally, we place a quantum well laser in a high magnetic fields, in which zero-dimensional electronic systems are formed by both Lorentz force and the quantum well potential effects. In addition, recent progresses of picosecond pulse generation in quantum well lasers are also discussed.

DYNAMIC AND SPECTRAL PROPERTIES OF SEMICONDUCTOR LASERS WITH
QUANTUM WELL, QUANTUM WIRE, AND QUANTUM BOX STRUCTURES

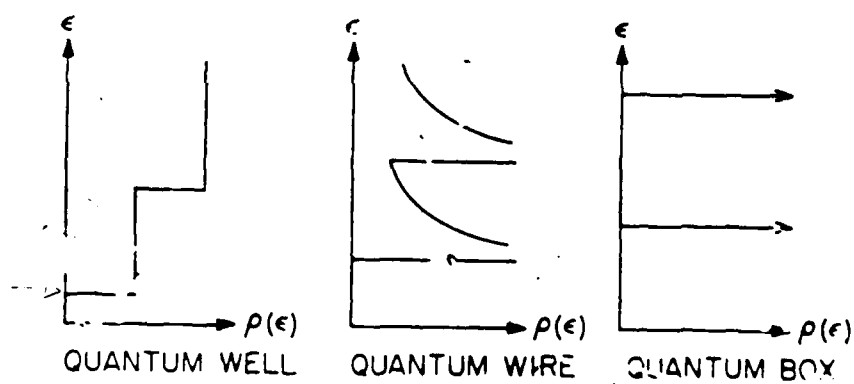
Y. ARAKAWA

UNIVERSITY OF TOKYO, TOKYO, JAPAN

-
1. BASIC PROPERTIES OF ELECTRONS IN QUANTUM-WELL(2D) STRUCTURES, QUANTUM-WIRE(1D) STRUCTURES, AND QUANTUM-BOX STRUCTURES(0D)
 2. MODULATION DYNAMICS
 3. FIELD SPECTRAL PROPERTIES
 4. EXPERIMENTAL DEMONSTRATION USING HIGH MAGNETIC FIELD
 5. PICOSECOND PULSE GENERATION IN QUANTUM WELL LASERS



(a)



(b) DENSITY OF STATES

FABRICATION OF QUANTUM-WIRE AND QUANTUM-BOX STRUCTURES

(GaAs/AlGaAs and InP/InGaAs)

ELECTRON BEAM LITHOGRAPHY

(1986 Worlock et al., 1987 Temkin et al.)

ETCHING THROUGH THE USE OF ANISOTROPIC PROPERTIES OF CRYSTALS

(1982 Petroff)

USE OF DISORDERING EFFECTS IN QUANTUM-WELL STRUCTURES

(1986 Petroff et al., 1986 Hirayama et al.)

GROWTH ON VICINAL SURFACES

(1984 Petroff)

(HIGH MAGNETIC FIELDS
 (1982 Arakawa et al.))

DEVICE PHYSICS

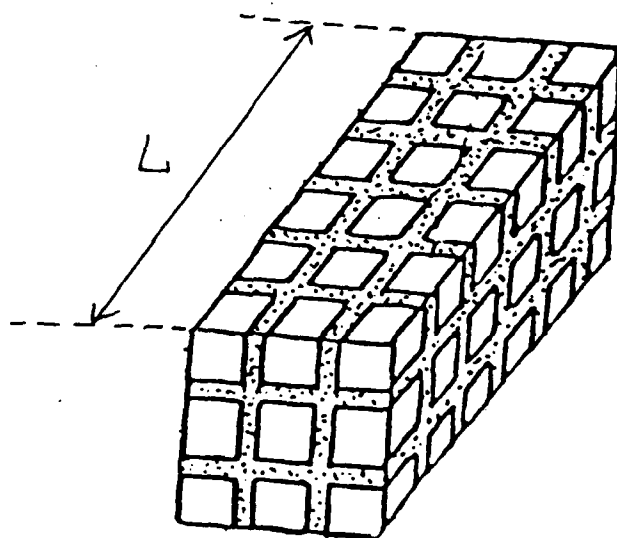
ANALYSIS OF ELECTRON TRANSPORT IN QUANTUM-WIRE STRUCTURES

(1980 Sakaki)

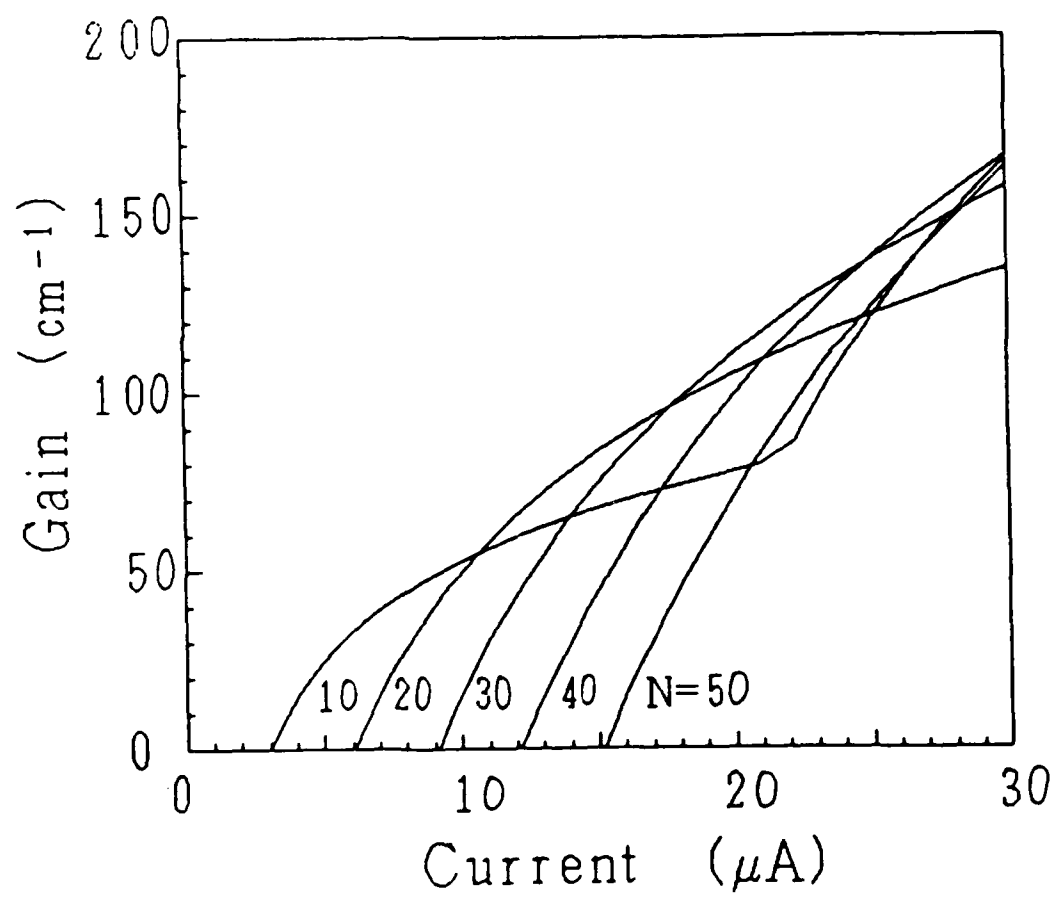
PROPOSAL OF QUANTUM-WIRE LASERS AND QUANTUM-BOX LASERS

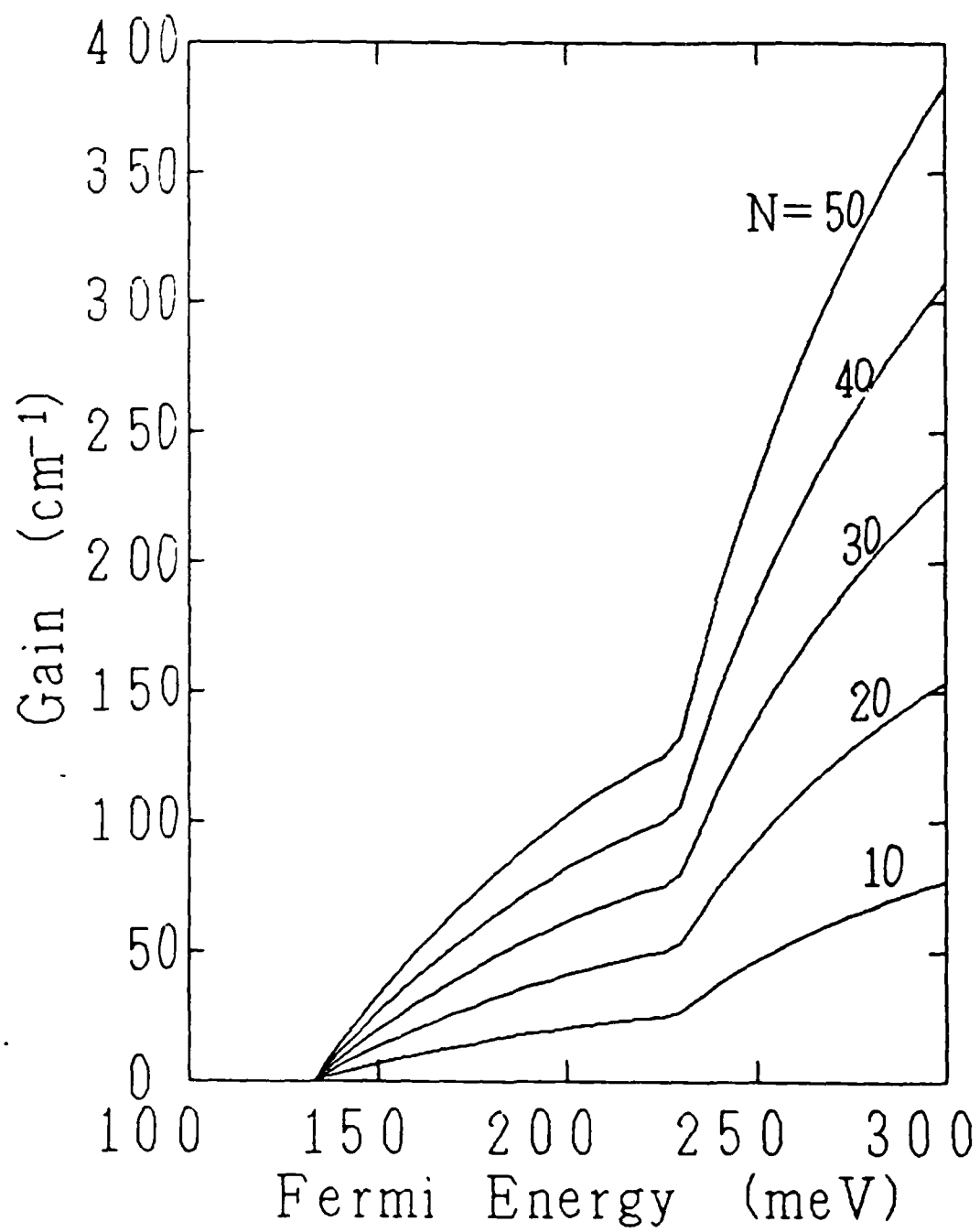
(1982 Arakawa et al.)

.....



$$N = 9$$

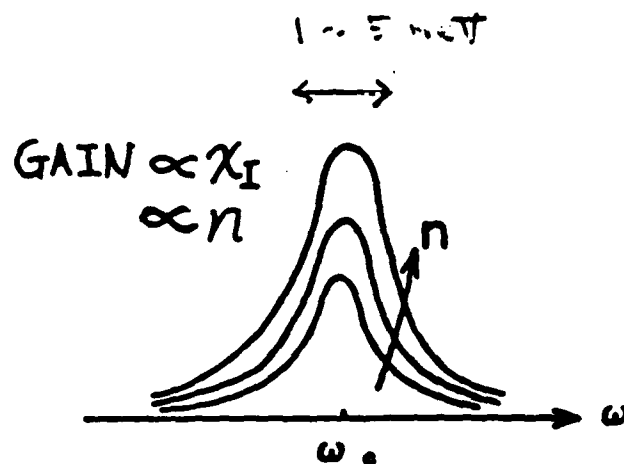
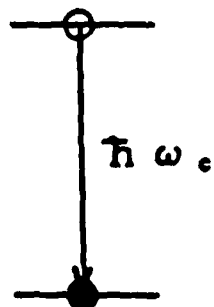




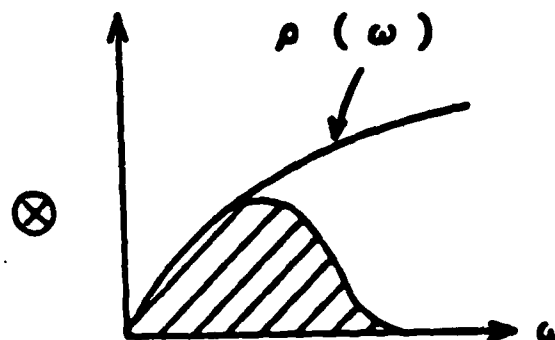
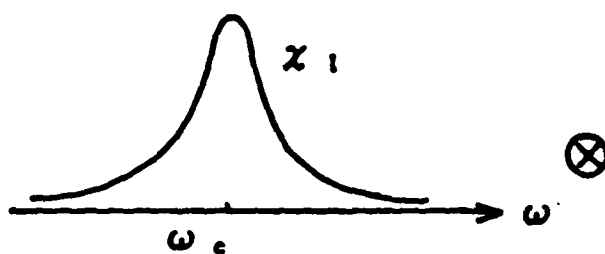
GAIN

$$x = x_r + j x_i$$

OD SYSTEM

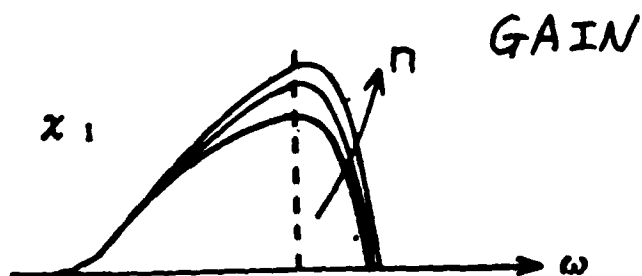


3D SYSTEM

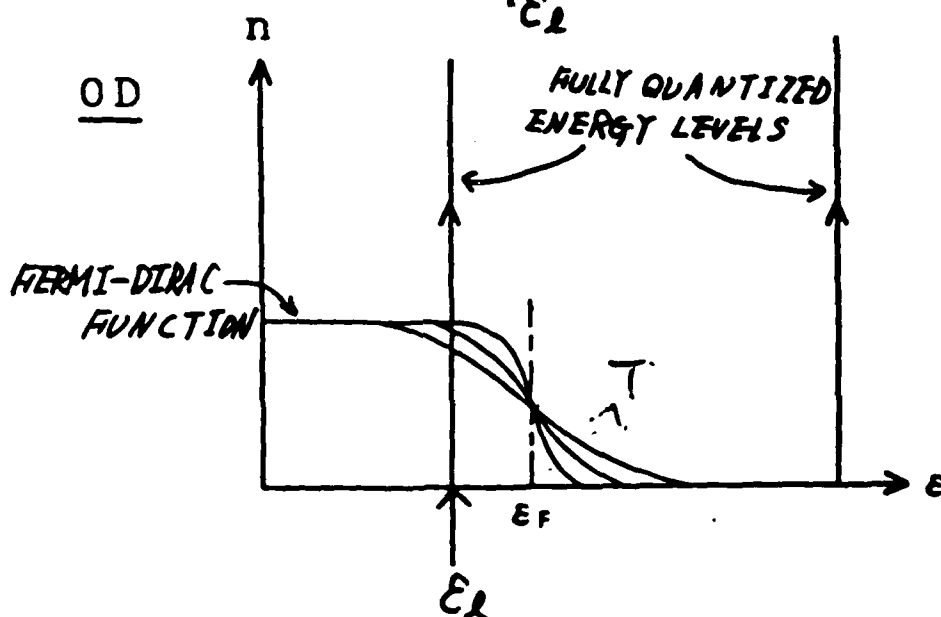
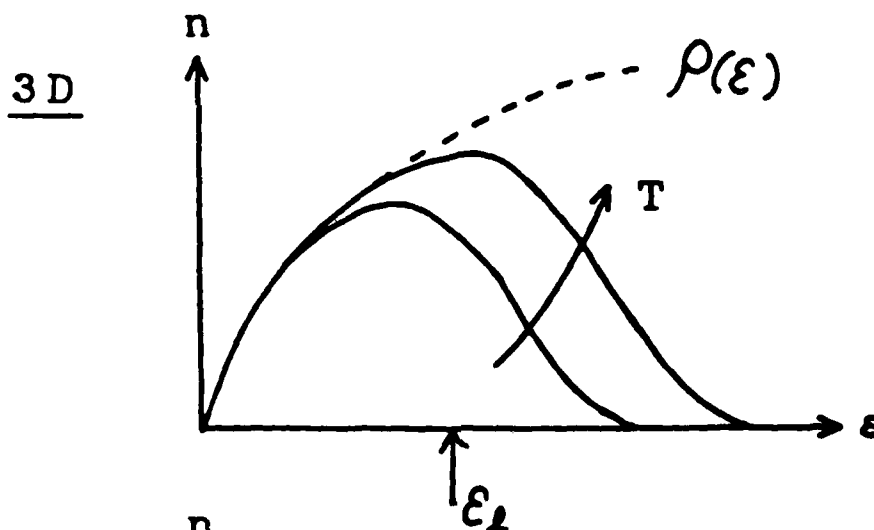


GAIN DUE TO ONE
ELECTRON-HOLE PAIR

CONVOLUTION



TEMPERATURE DEPENDENCE OF THRESHOLD CURRENT



Resonance Frequency f_r

$$\frac{dn}{dt} = \frac{J(t)}{eL_z} - \frac{c}{n_r} g(n)P - \frac{n}{\tau_s}$$

$$\frac{dP}{dt} = \Gamma \frac{c}{n_r} g(n)P + \beta \frac{n}{\tau_s} - \frac{P}{\tau_p}$$

Small Signal Analysis

$$n = n_0 + \Delta n; \quad P = P_0 + \Delta P$$

$$f_r = \frac{1}{2\pi} \sqrt{\frac{c}{n_r} \frac{g' P_0}{\tau_p}}$$

$$g'(n, E) = dg(n, E)/dn$$

: Differential Gain

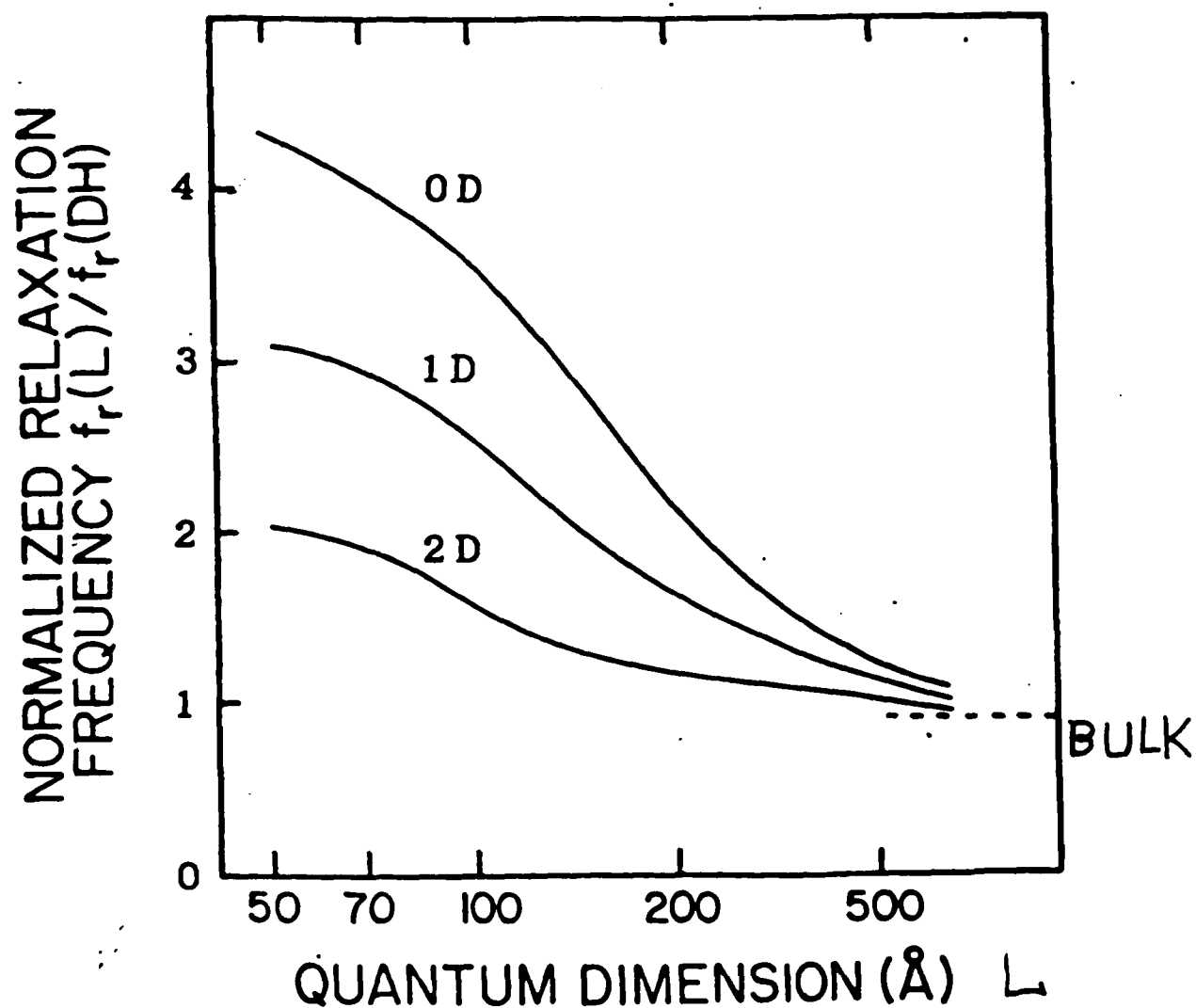
P_0 : Photon Density

τ_p : Photon Lifetime

$$f_r \uparrow \leftrightarrow \begin{cases} g' \uparrow & \text{Low Temperature} \\ P_0 \uparrow & \text{Window Type} \\ \tau_p \downarrow & \text{Short Cavity} \end{cases}$$

RELAXATION RESONANT FREQUENCY

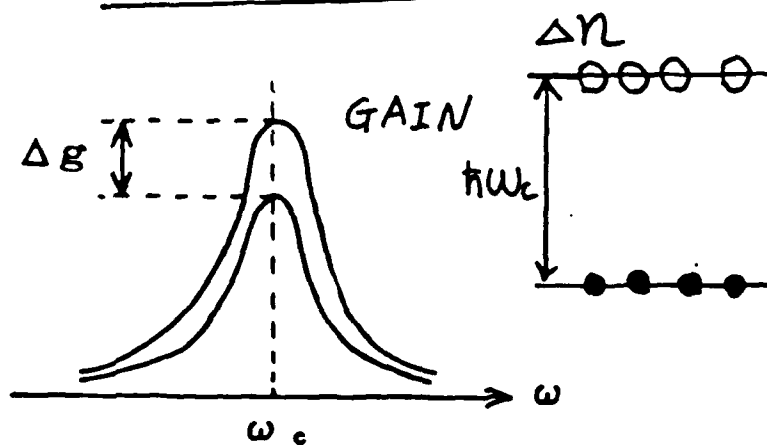
$$f_r(L) / f_r(L \rightarrow \infty)$$



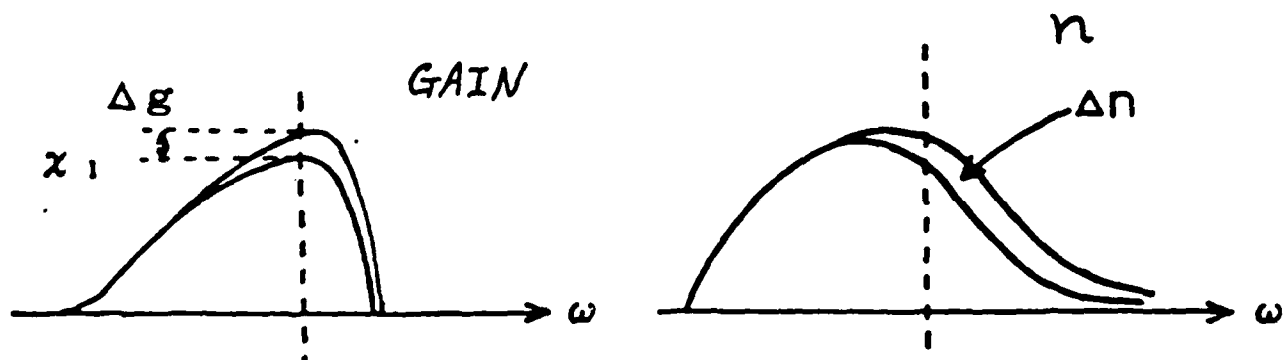
DIFFERENTIAL GAIN

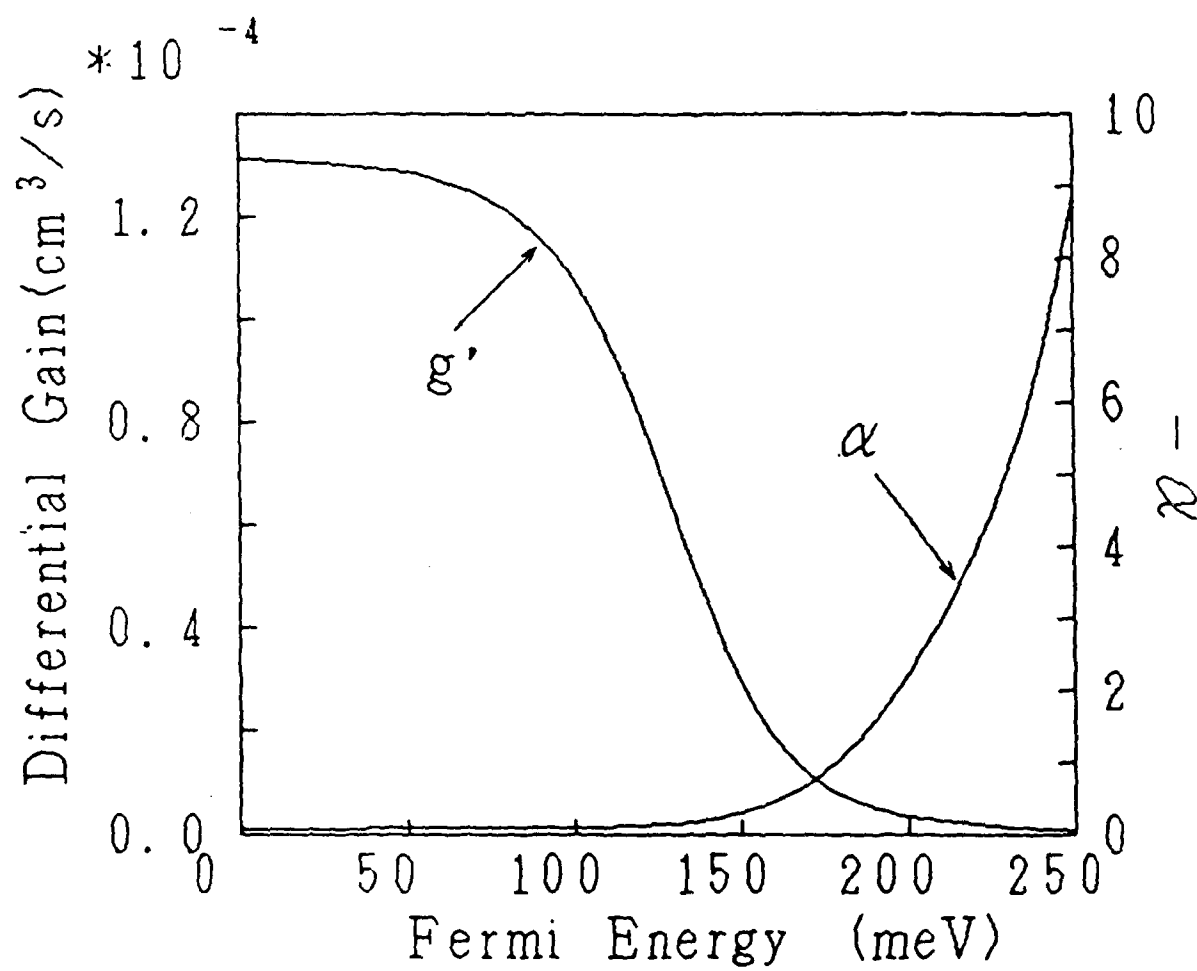
$$g' = \Delta g / \Delta n$$

OD SYSTEM

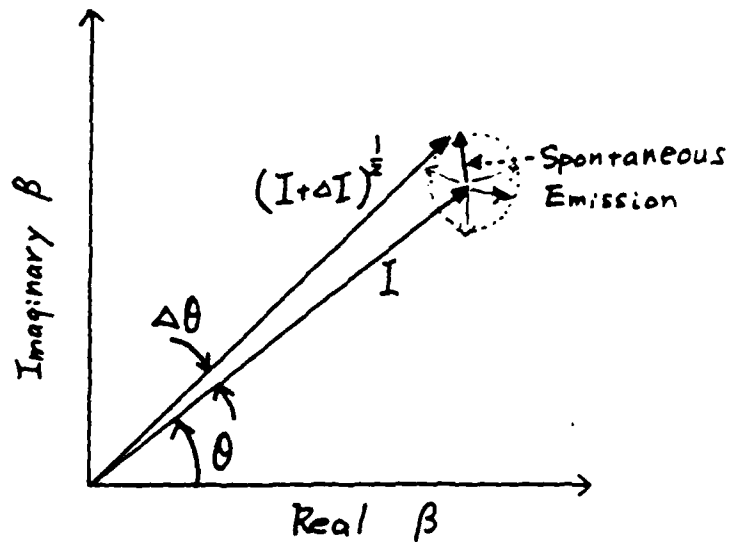


3D SYSTEM





$$\Delta\nu = \Delta\nu_{ST} + \Delta\nu_{AF}$$



$\Delta\nu_{ST}$: Shawlow-Townes Linewidth

Spontaneous Emission $\rightarrow \Delta\theta \rightarrow \Delta\nu_{ST} \propto 1/I$

$\Delta\nu_{AF}$: Phase Noise due to AM/FM Coupling

Spontaneous Emission $\rightarrow \Delta I \rightarrow \Delta n \rightarrow \Delta n_r$

$\rightarrow \Delta\theta_{AF} \rightarrow \Delta\nu_{AF}$

$$\Delta\nu_{AF} = \alpha^2 \Delta\nu_{ST}; \quad \alpha = \frac{d\chi_R/dn}{d\chi_I/dn}; \quad \chi = \chi_R + i\chi_I$$

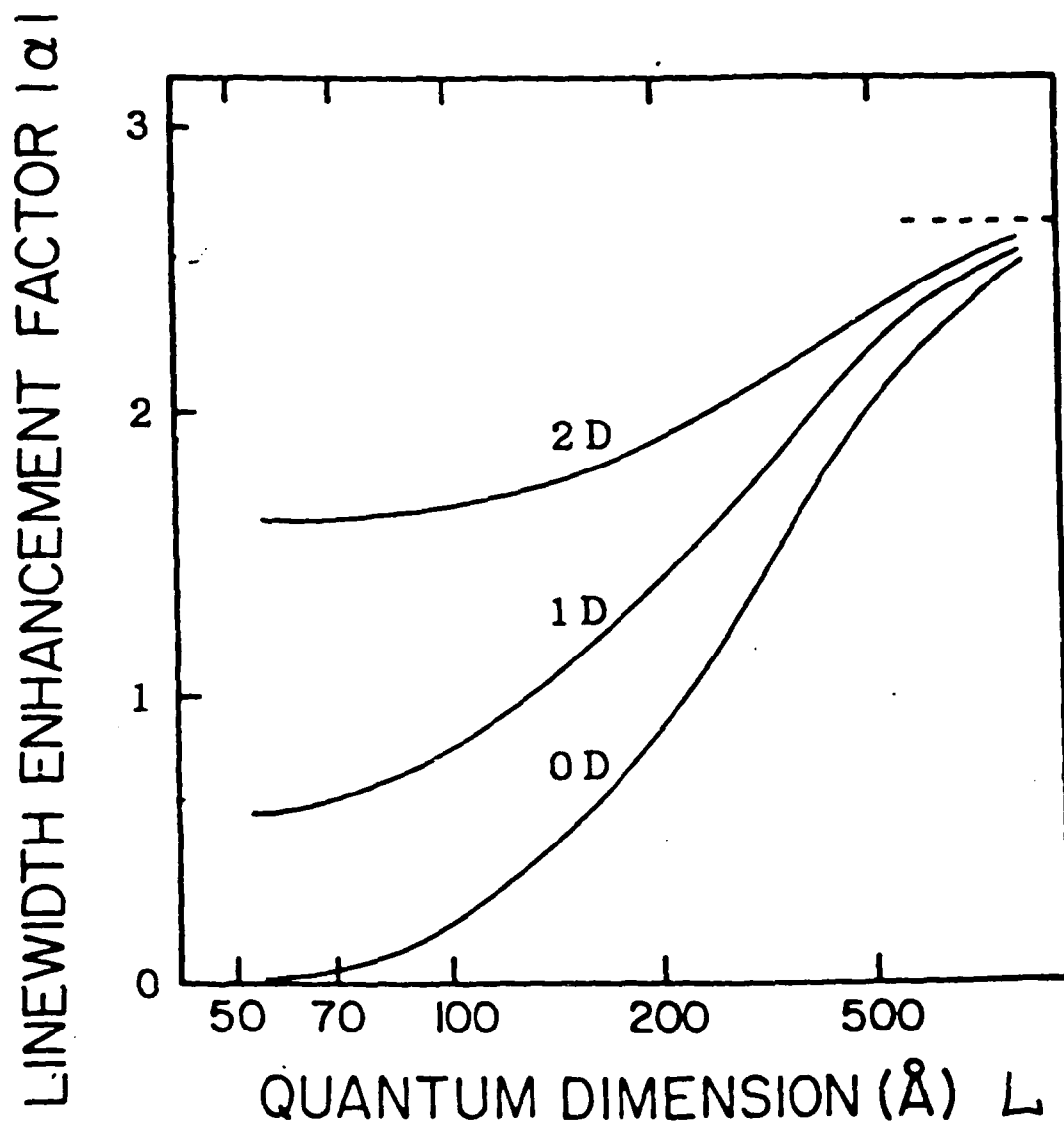
$$\Delta\nu = (1 + \alpha^2) \Delta\nu_{ST}$$

χ depends on ρ

$\rightarrow \alpha$ is improved by the use of quantum well and quantum wire structures

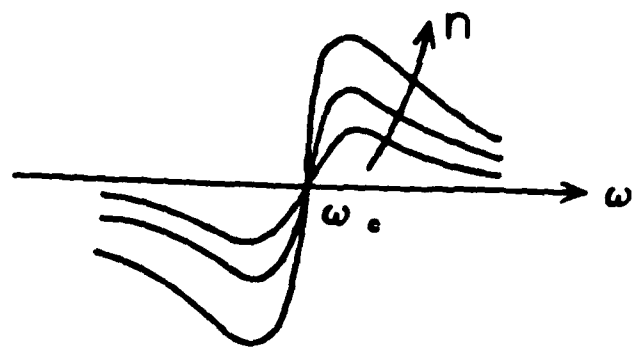
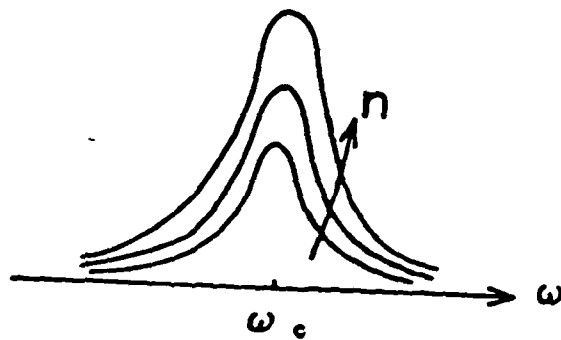
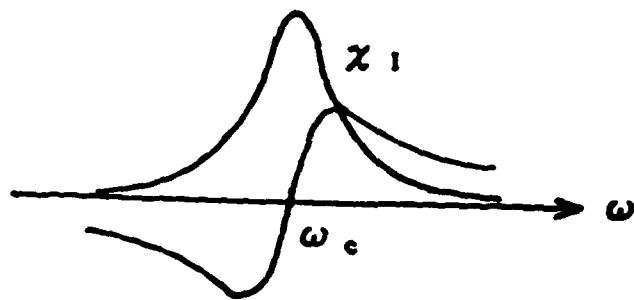
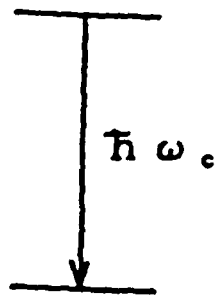
LINEWIDTH ENHANCEMENT FACTOR

$|\alpha|$

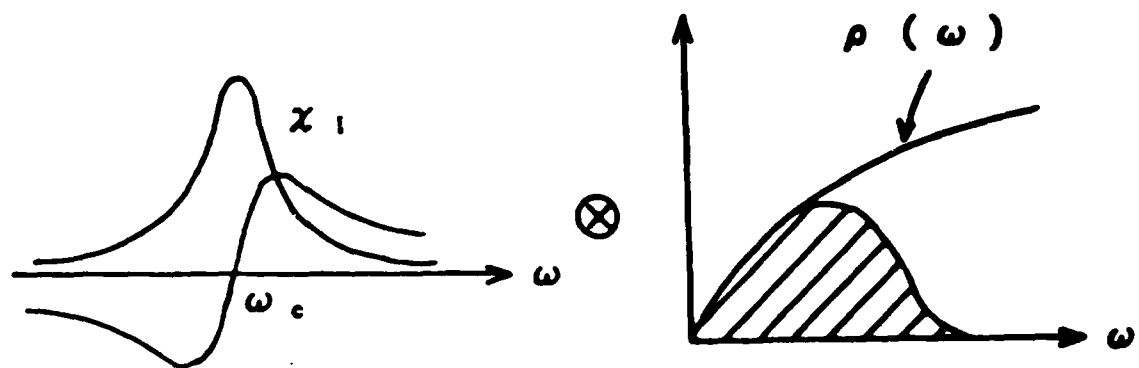


OD SYSTEM

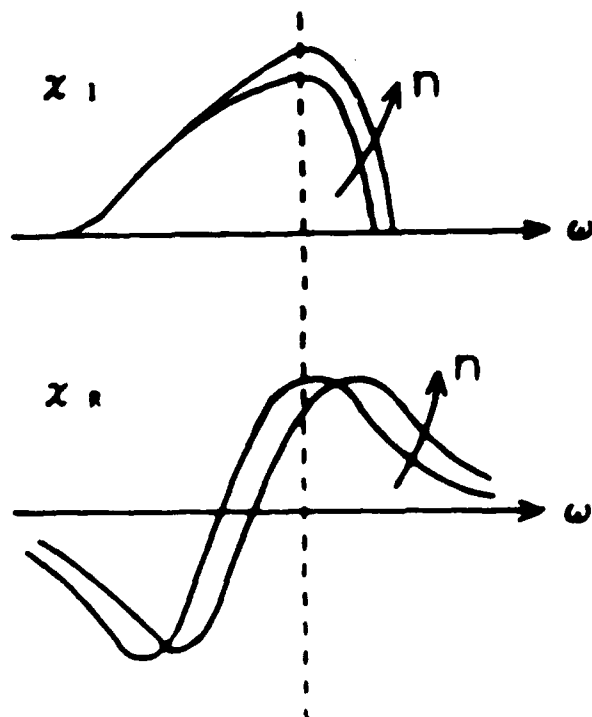
$$x = x_r + j x_i$$

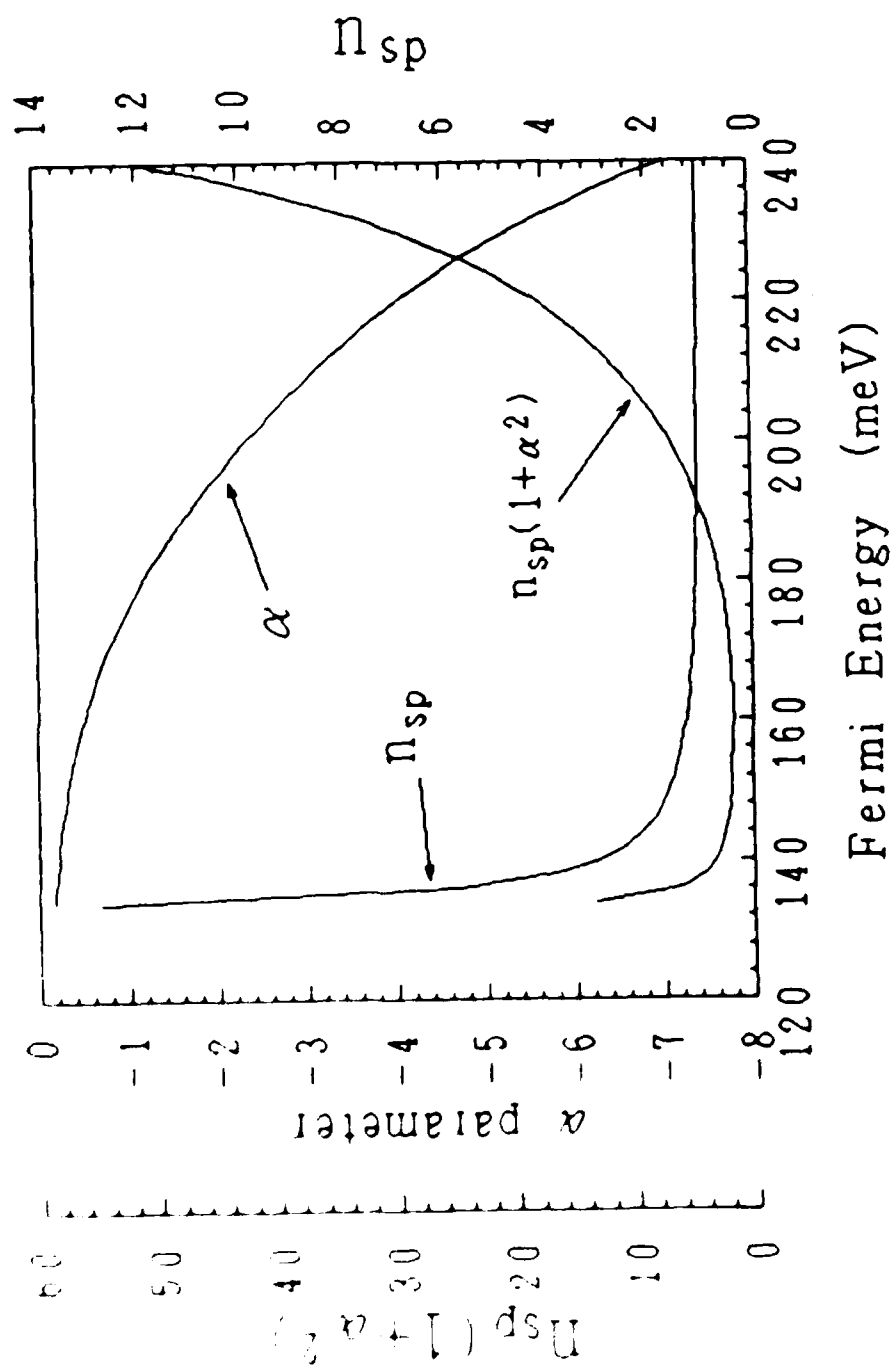


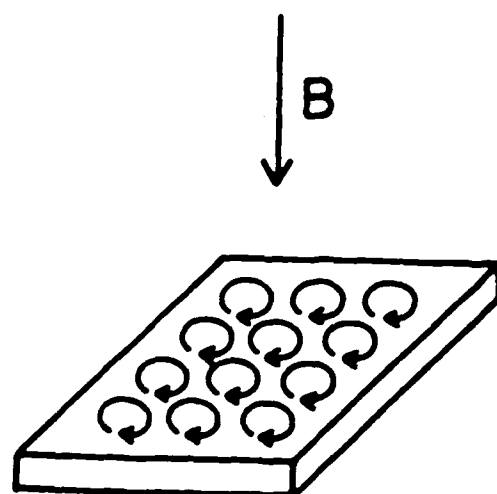
3D SYSTEM



CONVOLUTION



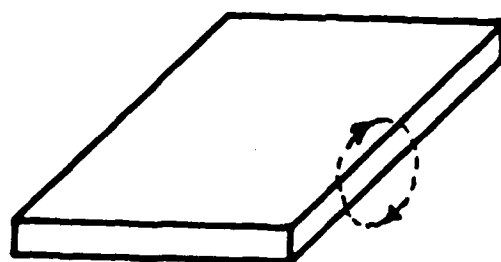
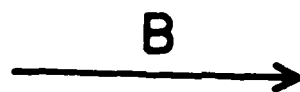




$B \perp \text{QW plane}$

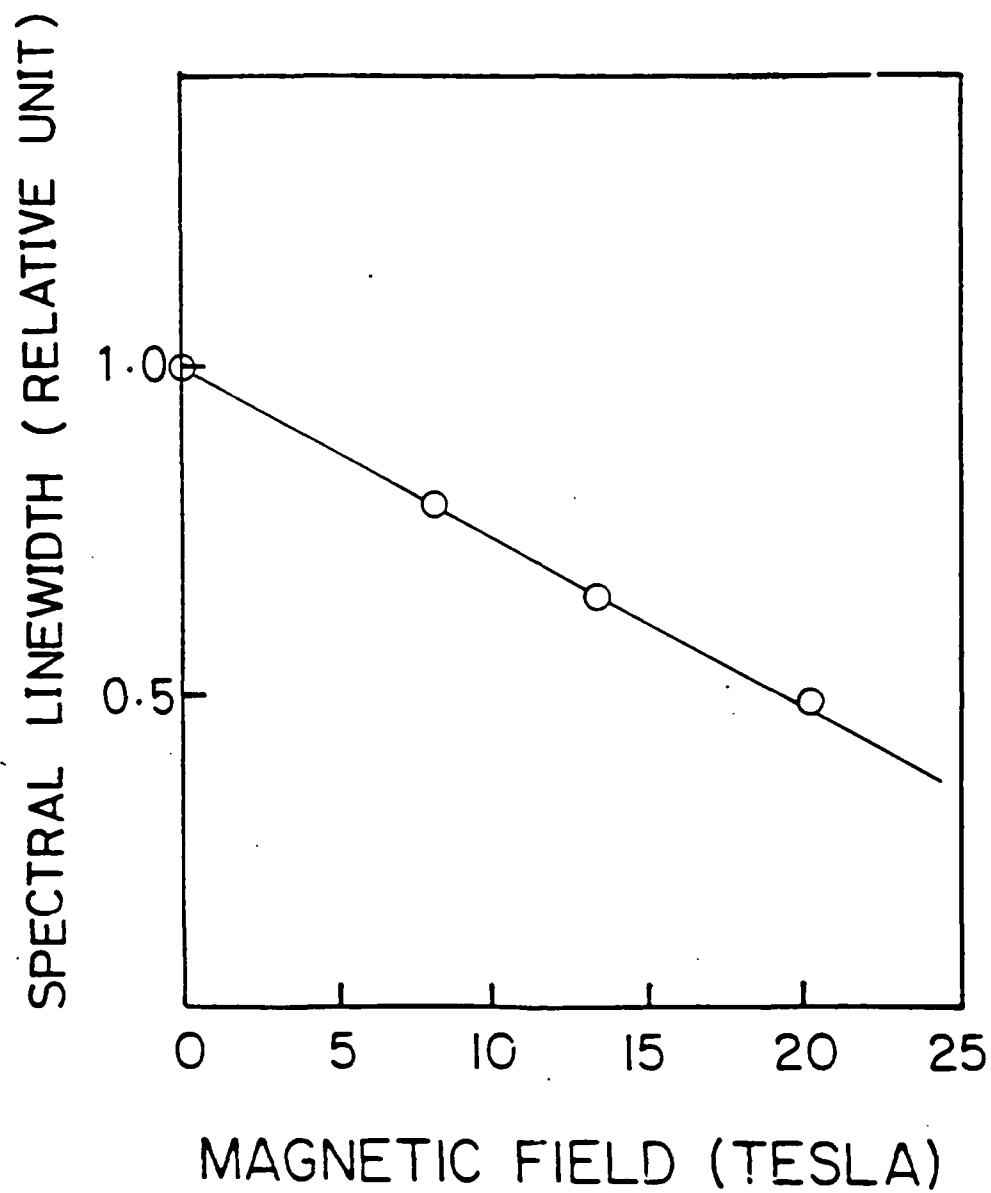
$$2\hbar - 2\hbar = 0\hbar$$

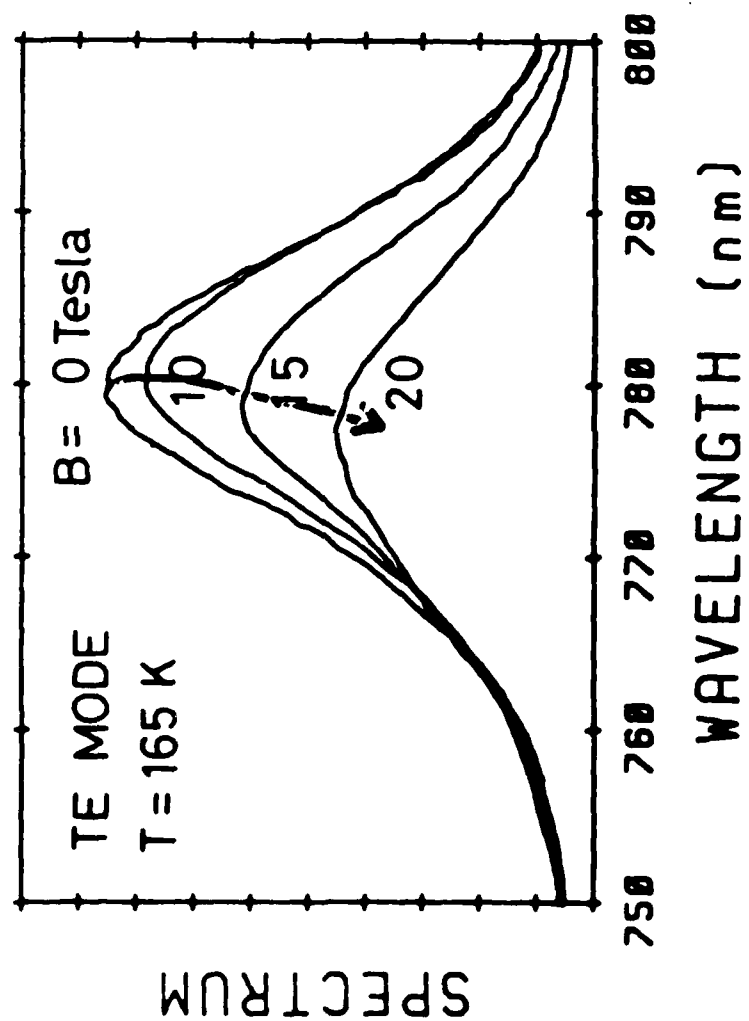
\uparrow \uparrow
 QW MAGNETIC
 EFFECT FIELD

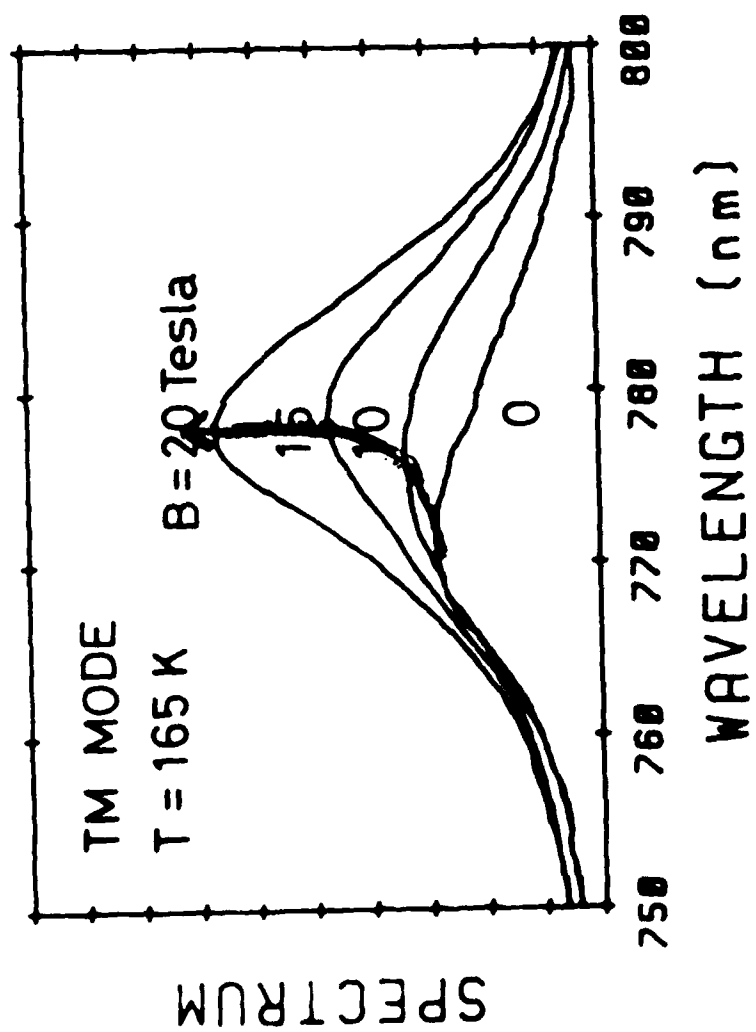


$B // \text{QW plane}$

$$2\hbar$$







SUMMARY

1. BASIC PROPERTIES OF ELECTRONS IN QUANTUM-WIRE (1D) STRUCTURES AND QUANTUM-BOX (0D) STRUCTURES

2. MODULATION DYNAMICS

$$4 \times f_R(\text{QUANTUM-BOX}) \quad 3 \times f_R(\text{QUANTUM-WIRE})$$

3. FIELD SPECTRAL PROPERTIES

$$\alpha \sim 0(\text{QUANTUM-BOX}) \quad \alpha \sim 0.8(\text{QUANTUM-WIRE})$$

4. EXPERIMENTAL DEMONSTRATION USING HIGH MAGNETIC FIELD

B~20TESLA

SIGNIFICANT IMPROVEMENTS IN MODULATION DYNAMICS AND SPECTRAL PROPERTIES ARE OBSERVED

PICOSECOND PULSE GENERATION IN QUANTUM WELL LASERS

GAIN SWITCHING METHOD

PULSE CURRENT INJECTION
MATRIX ELEMENT MODULATION

MODE LOCKING METHOD

ACTIVE
PASSIVE

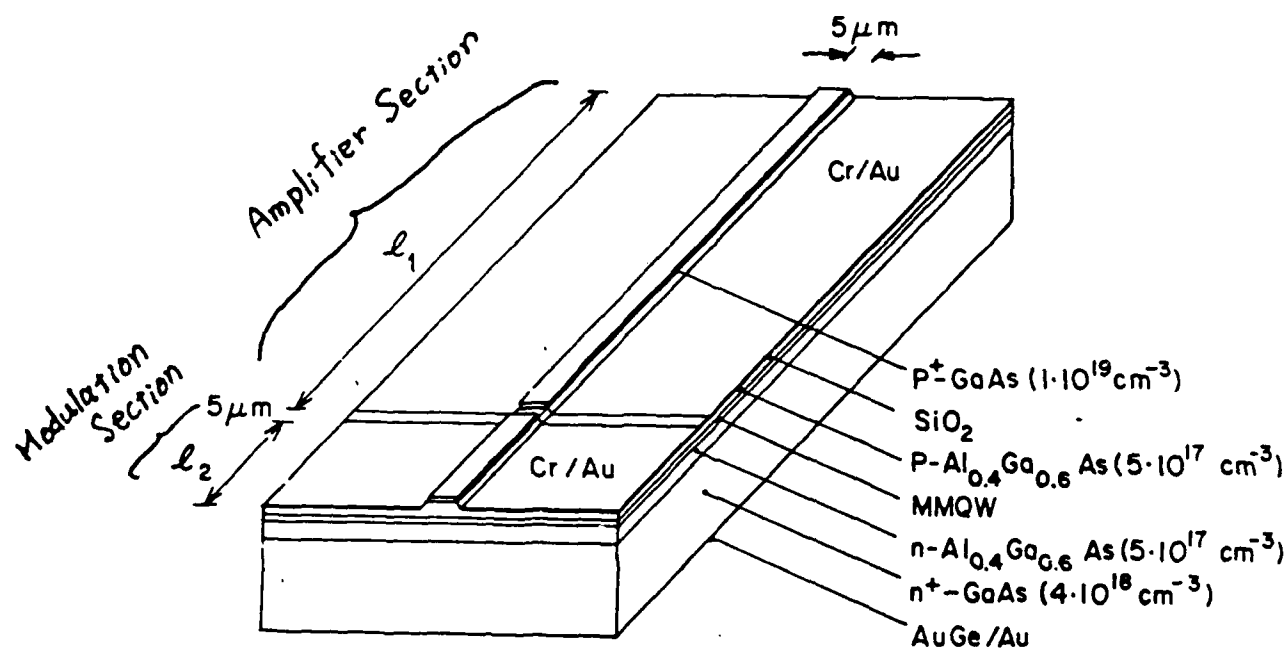
Q-SWITCHING METHOD

ACTIVE
PASSIVE

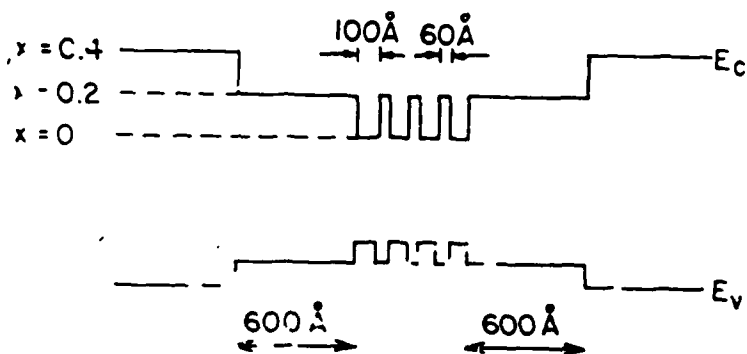
IN THIS TALK

ACTIVE Q-SWITCHING IN MULTI-QUANTUM WELL LASERS
WITH INTRACAVITY MONOLITHIC LOSS MODULATOR (18.6psec)

GAIN SWITCHING IN MULTI-QUANTUM WELL LASERS (1.8psec)

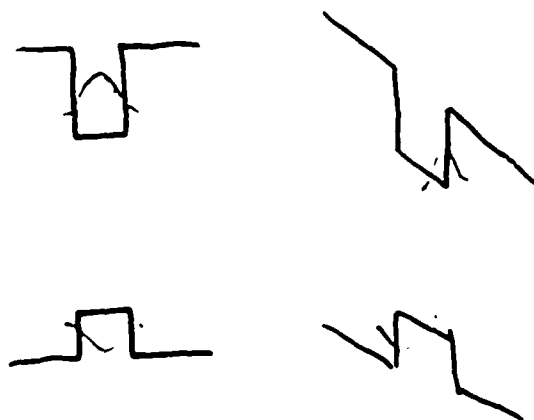
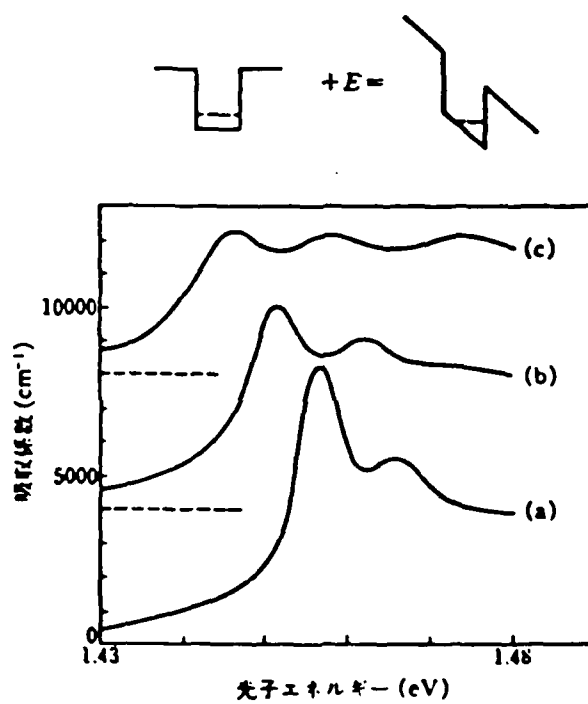


(a)

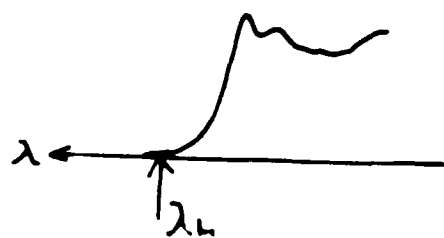


(b)

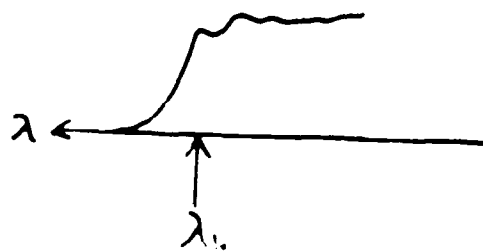
ENHANCED BAND SHRINKAGE EFFECTS
QUANTUM CONFINED STARK EFFECTS

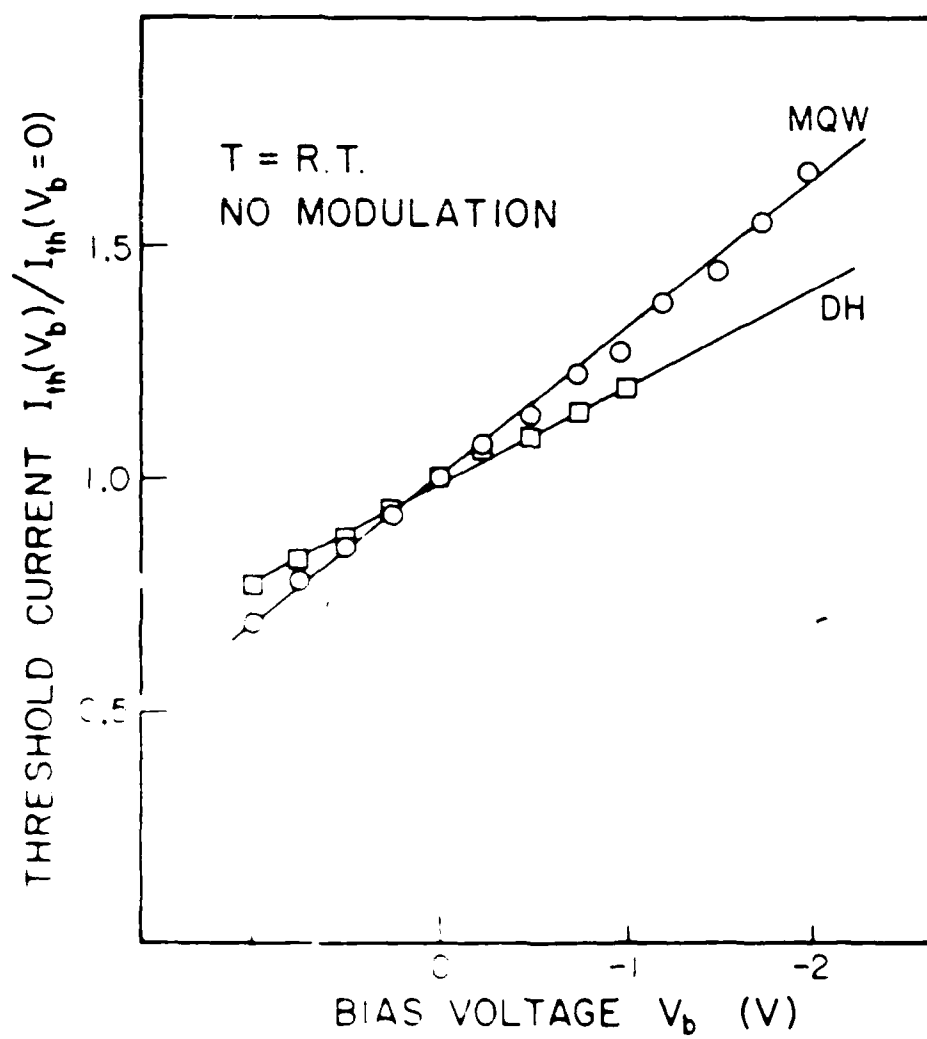


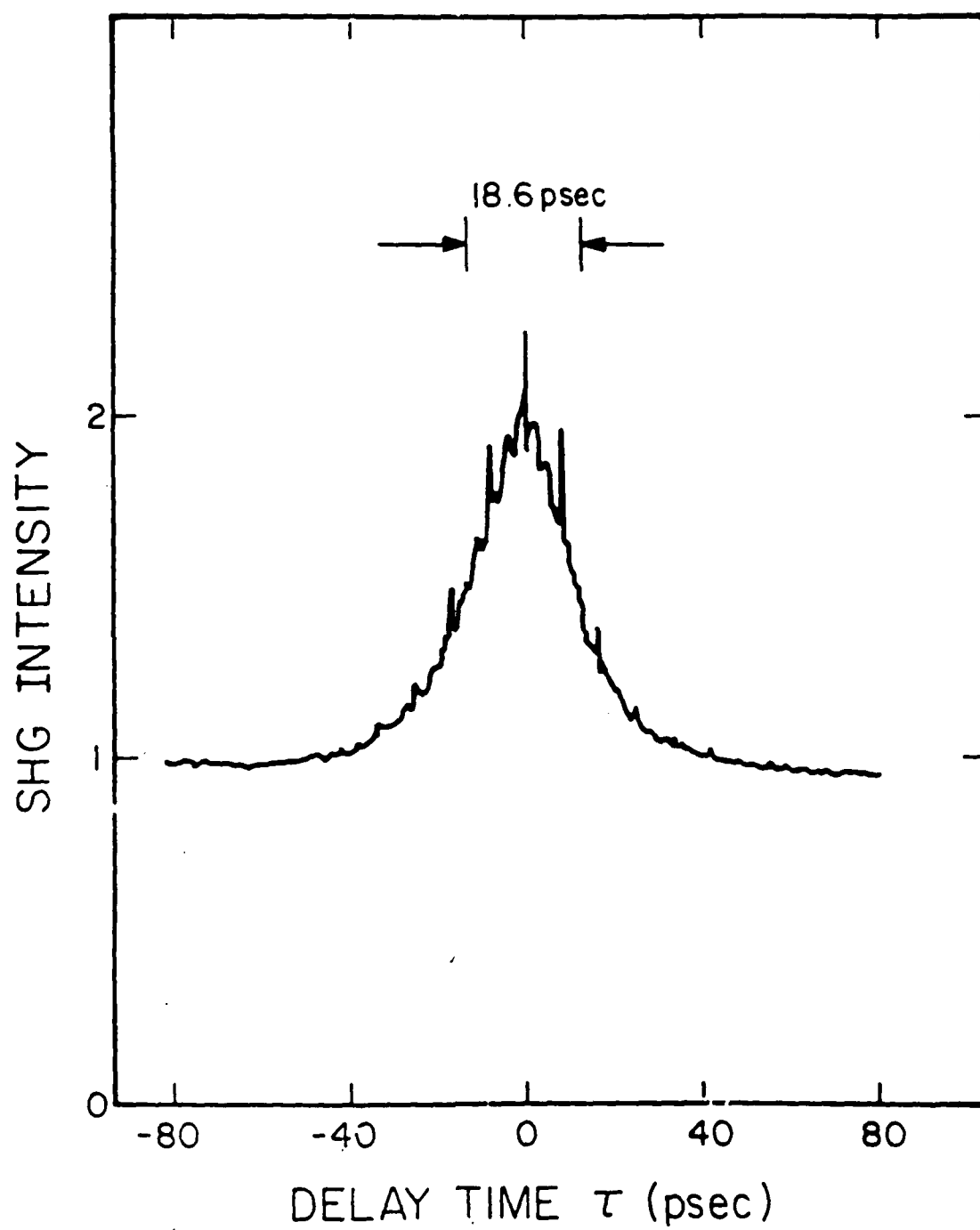
Without Electric Field

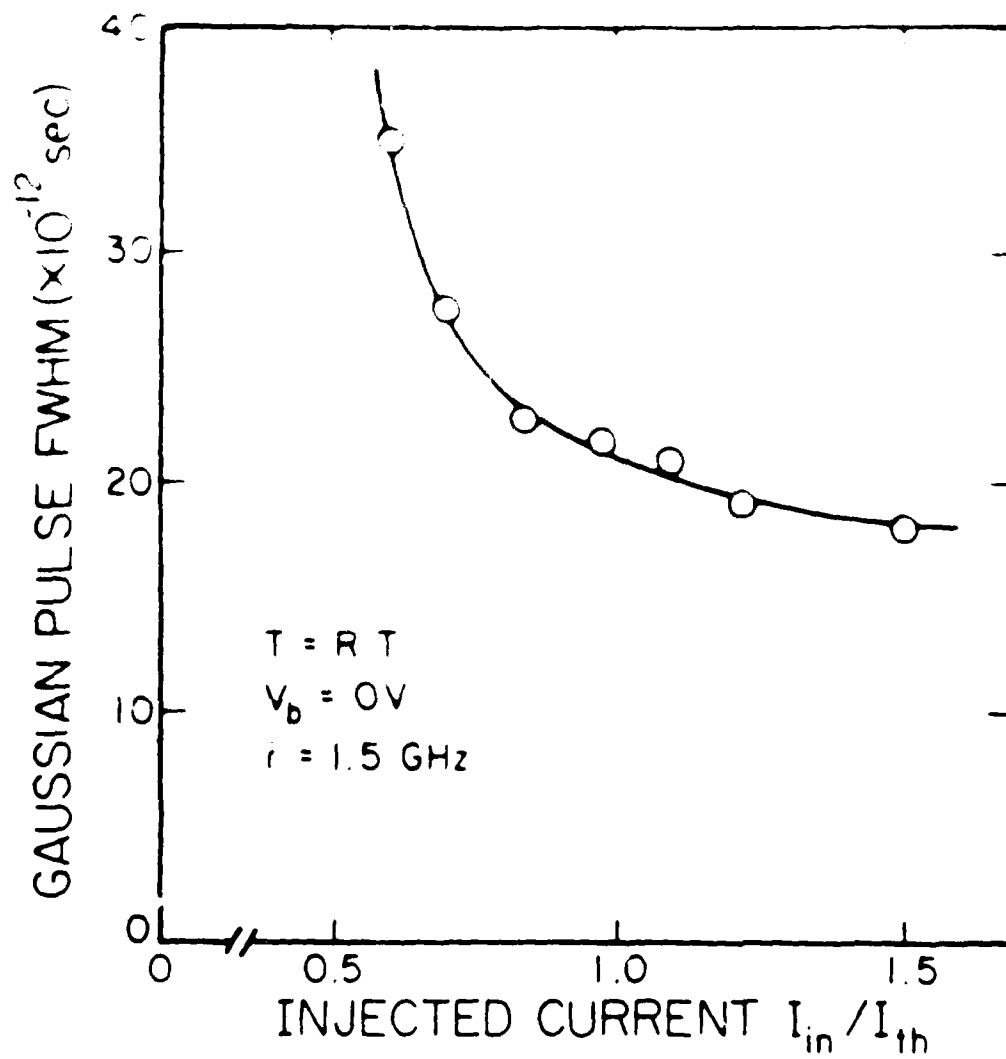


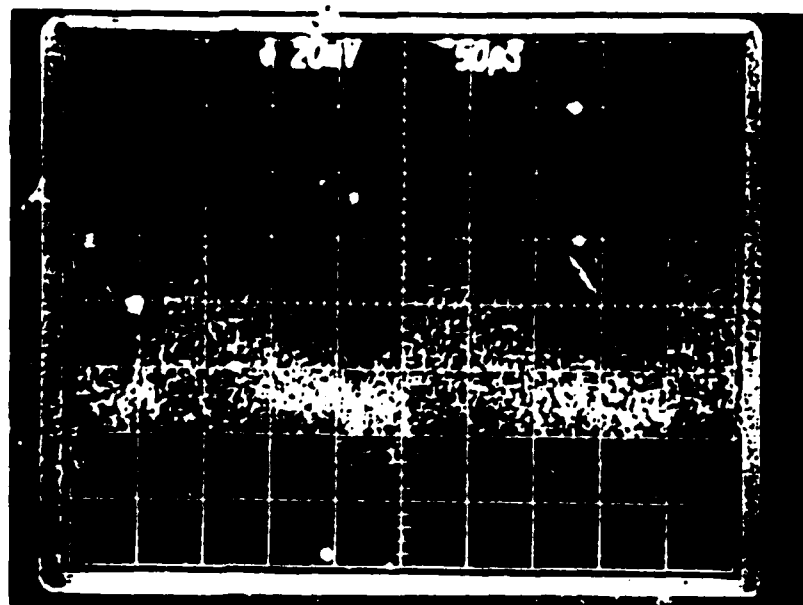
With Electric Field







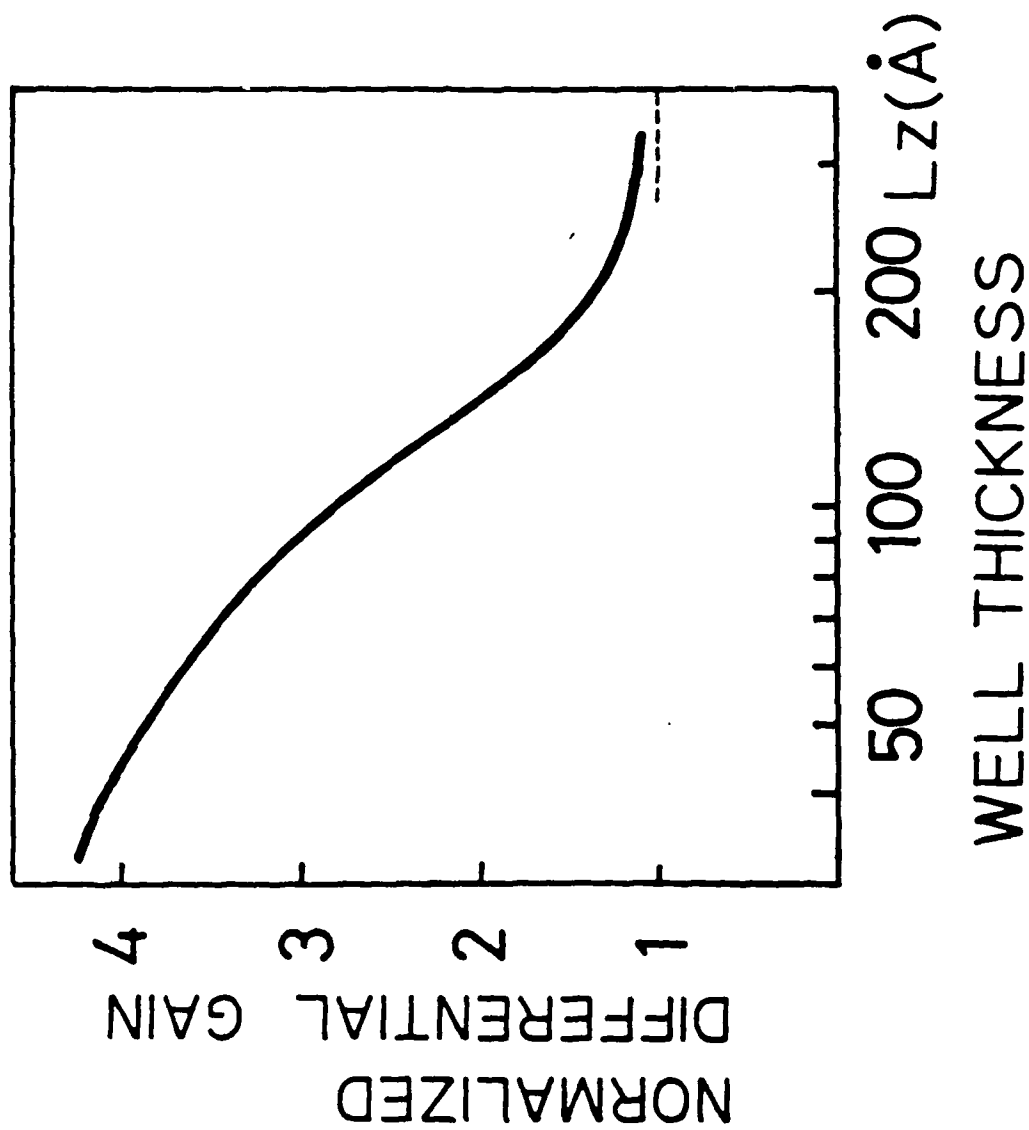


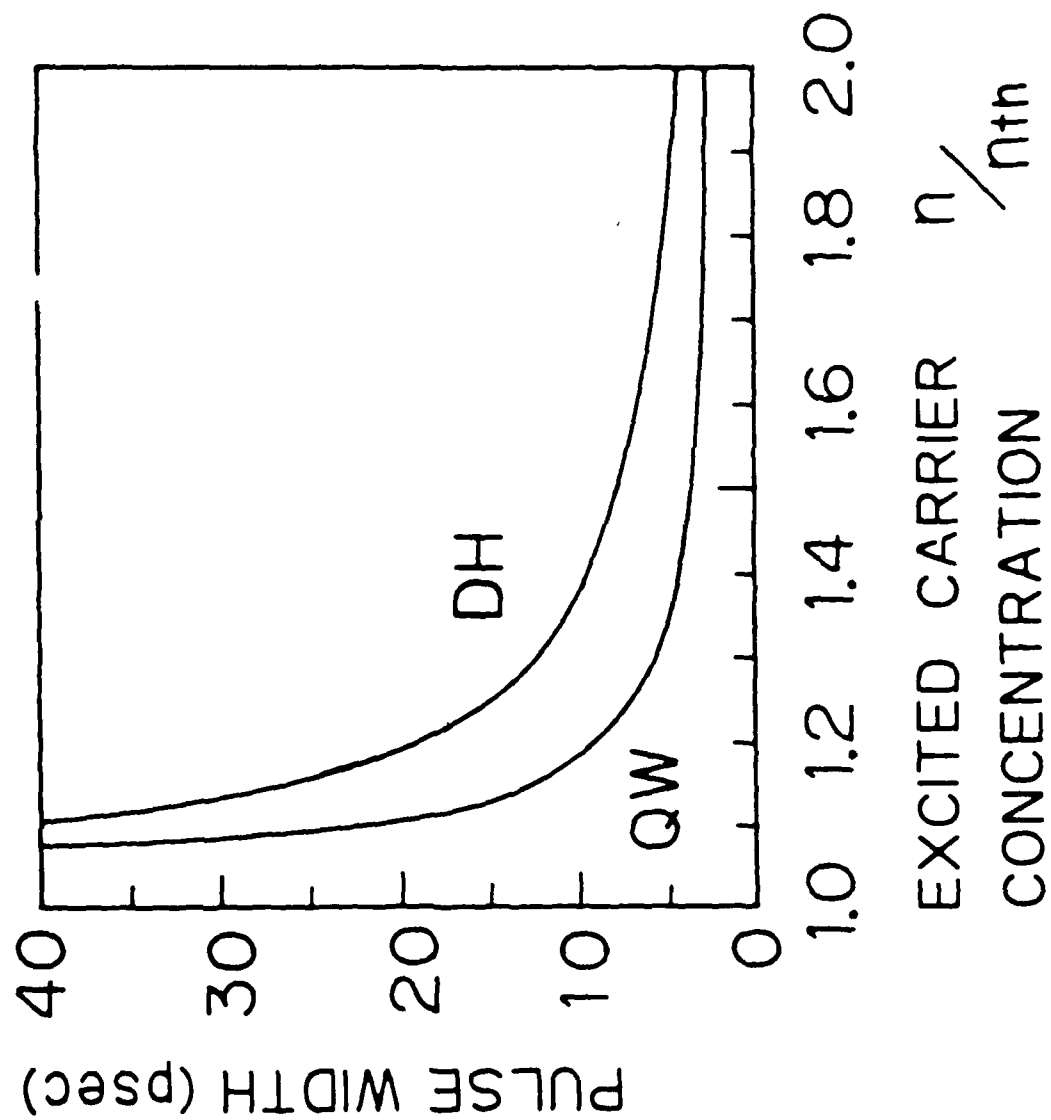


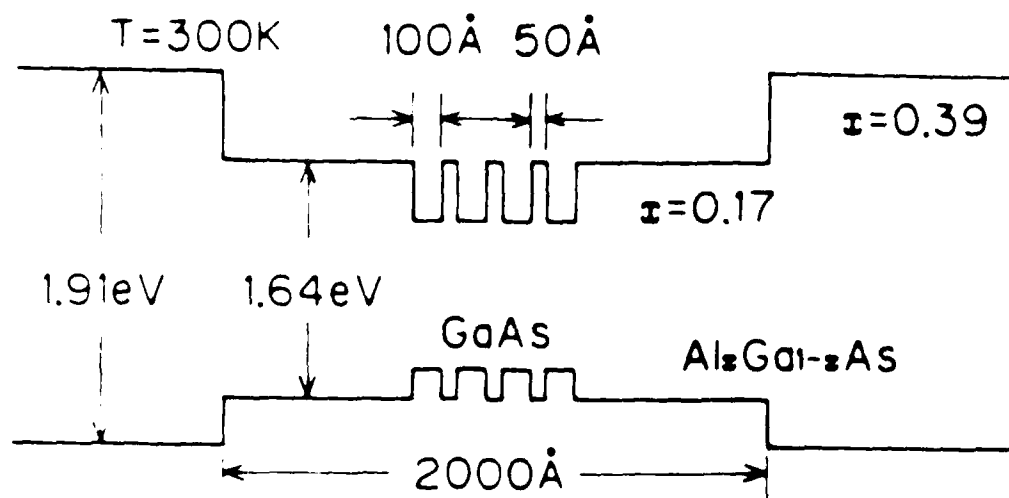
IN QUANTUM WELL LASERS

GAIN SWITCHING

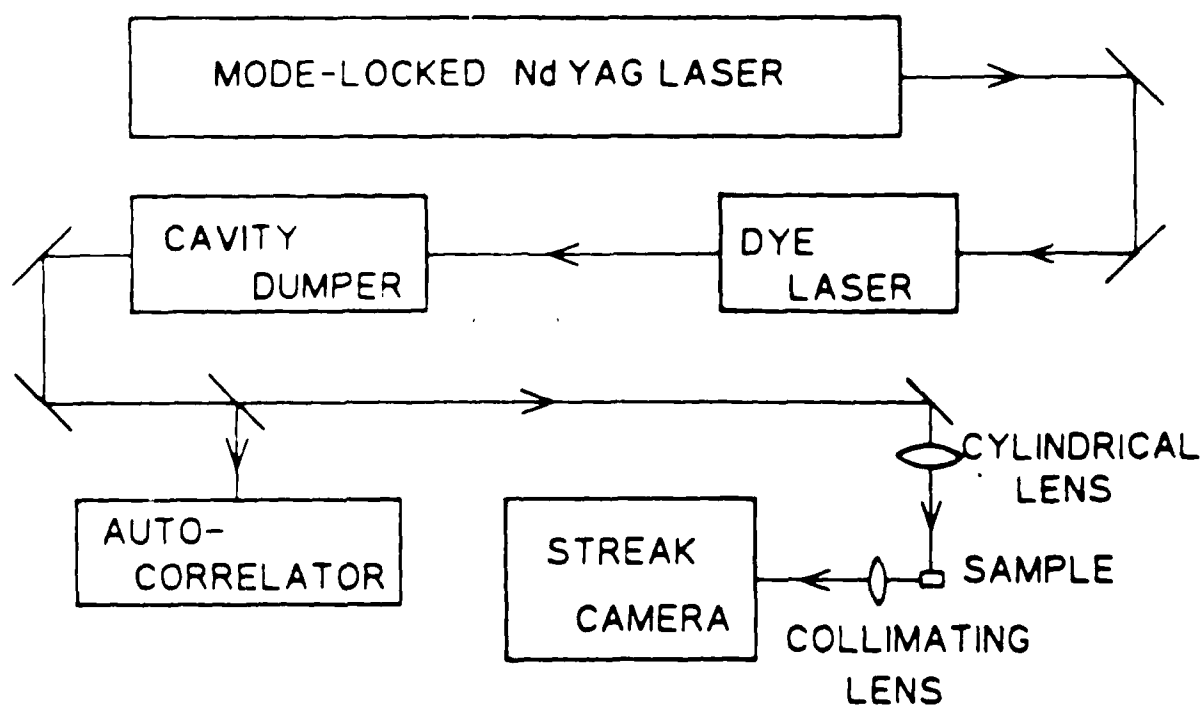
-179-



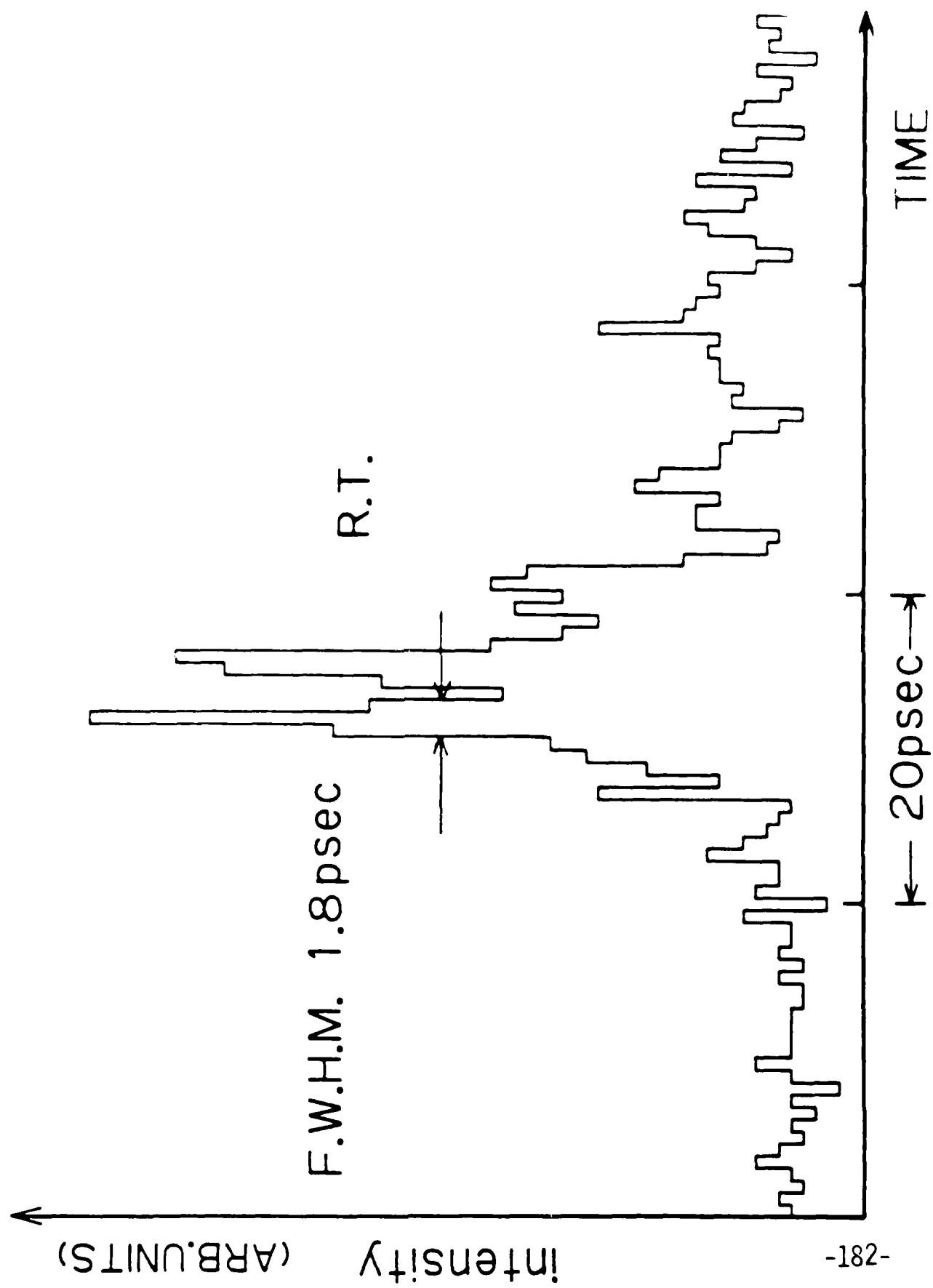




(a)



(b)



Frequency Stabilization of Semiconductor Lasers
At the AT&T Bell Laboratories, Red Bank, New York

Authors: * K. Kurokawa and M. Hashimoto

† Tokyo Institute of Technology
4259 Nagatsuta, Midori-ku, Yokohama, Kanagawa 227, Japan

*Presently: AT&T Bell Laboratories
600 Mountain View, Holmdel, NJ 07733, USA

ABSTRACT

We demonstrate that the FM noise in semiconductor lasers can be reduced to a value lower than the quantum noise limit by using negative electrical feedback. A synthesized method of electrical feedback (Fig. 1) is proposed to realize such ultrahigh temporal coherence of semiconductor lasers. The center frequency fluctuations of the field spectrum are reduced as low as 2×10^{-7} by this feedback. The linewidth of the field spectrum is reduced to 100 kHz, which is narrower than the value given by the quantum noise limit of the free-running laser (Fig. 2). Optical phase-locked loop realizes a frequency tracking accuracy of 3×10^{-8} , capture range of 1.2 GHz, and locking range of 53 GHz.

As an alternative scheme to realize ultrahigh coherence in semiconductor lasers, we present a novel experimental method for accurate frequency tracking using the correlated spontaneous emission between the two longitudinal modes [1,2]. We employ a method of resonant coupling between the two optical transitions via optical sidebands produced by parametric modulation of the laser gain. By this modulation, the linewidth of the heterodyned signal was reduced to 25 kHz (Fig. 3. The minimum of the linewidth obtained is limited by resolution of our linewidth measurement system). This value corresponds to suppression of the relative phase noise between the two modes to less than one-twentieth of the quantum noise limit of the free-running laser.

As an application of these ultrahigh coherent lasers, we have used them as optical pumping sources for Rb atomic clock of 6.8 GHz frequency. A novel optical-microwave double resonance spectral shape with the linewidth as narrow as 20 Hz is demonstrated by utilizing FM sidebands of the laser induced by nonlinear susceptibility of the three-level Rb atoms (Fig. 4). Theoretical analysis shows that by optimizing the modulation parameters one can realize ultra-sensitive microwave frequency discrimination, which is about 7500 times more sensitive than a conventional Rb atomic clocks.

REFERENCES

- (1) M. O. S. J. V. Phys. Rev. Lett. 55, 2802 (1980)
- (2) P. E. Toschek and J. L. Hall, Technical Digest of 15th International Quantum Electronics Conference, April 1987, Baltimore, WDD2

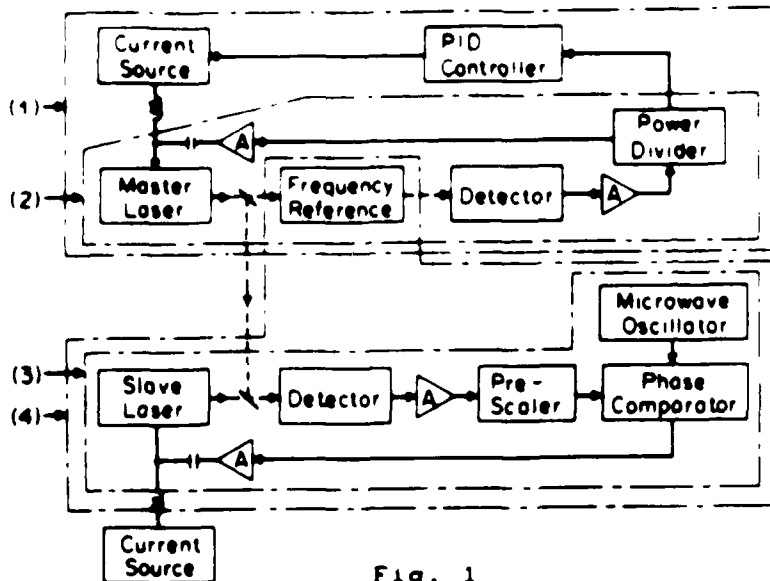


Fig. 1

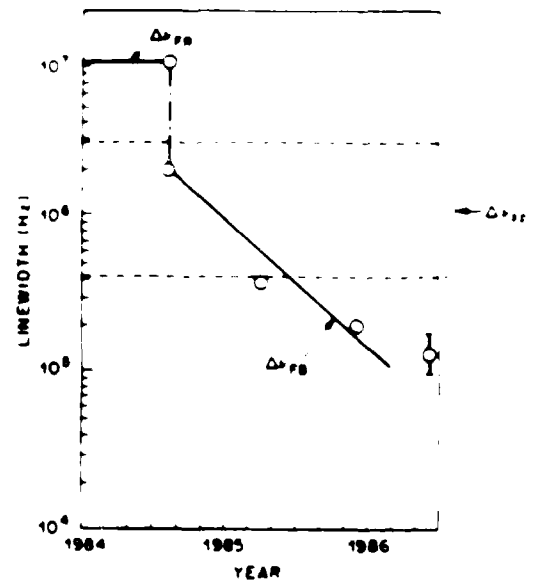


Fig. 2

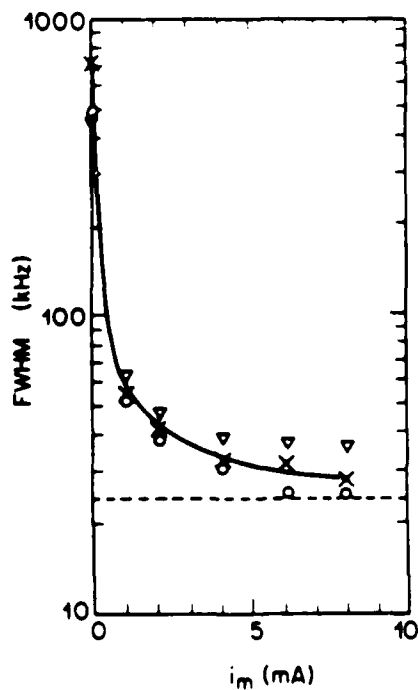


Fig. 3

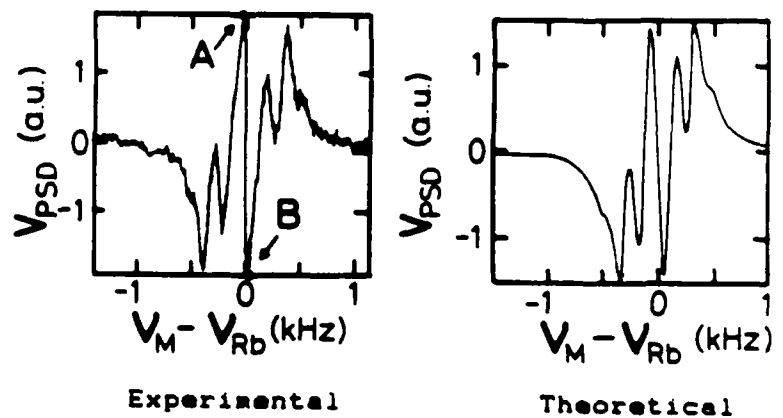


Fig. 4

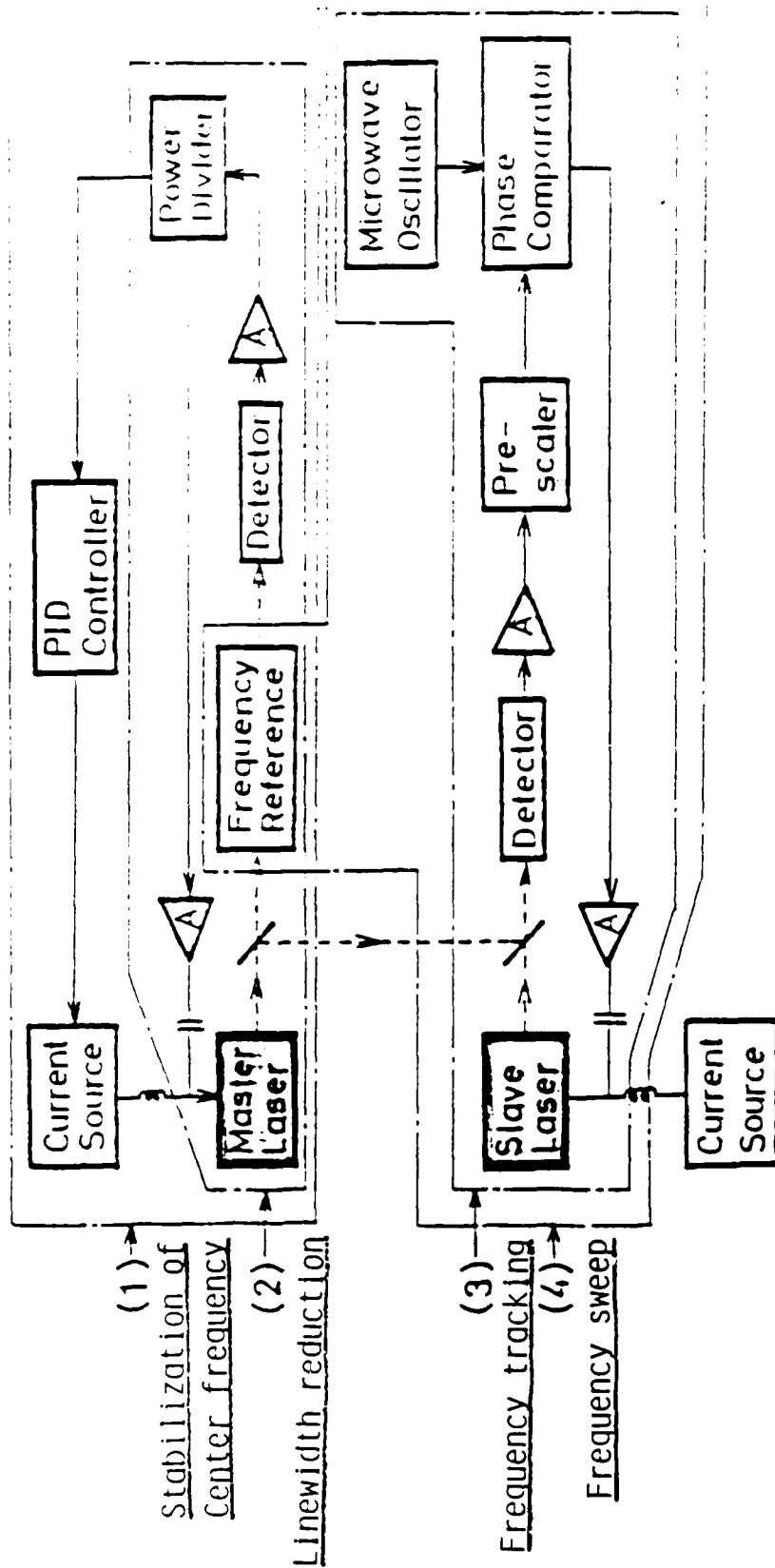
Ultrahigh Coherent Semiconductor Lasers, and Their Application to Rubidium Atomic Clock

M. OHTSU*, K. KUBOKI, & M. HASHIMOTO

Tokyo Institute of Technology

* Presently, AT&T Bell Laboratories
Crawford Hill Laboratory

- (1) Reduction of FM noise to a value lower than
quantum noise limit by
 - (a) negative electrical feedback
 - (b) correlated spontaneous emission
- (2) Application to optical pumping of
a Rb atomic clock



[Assumptions]

- (1) Quantum FM noise can be measured by classical electro-optical techniques.
- (2) Frequency can be countermodulated by modulating a macroscopic quantity.

(3) Infinite Feedback Bandwidth

[Y. Yamamoto, et. al.: IEEE J. Quantum Electron., QE-21 (1985) p.1919]

$$\delta v(t) = \frac{1}{2\pi} \frac{d}{dt} (\delta \phi) = \Gamma_S(t) + \Gamma_C(t) \leftarrow \text{spontaneous emission carrier } (\alpha\text{-parameter})$$

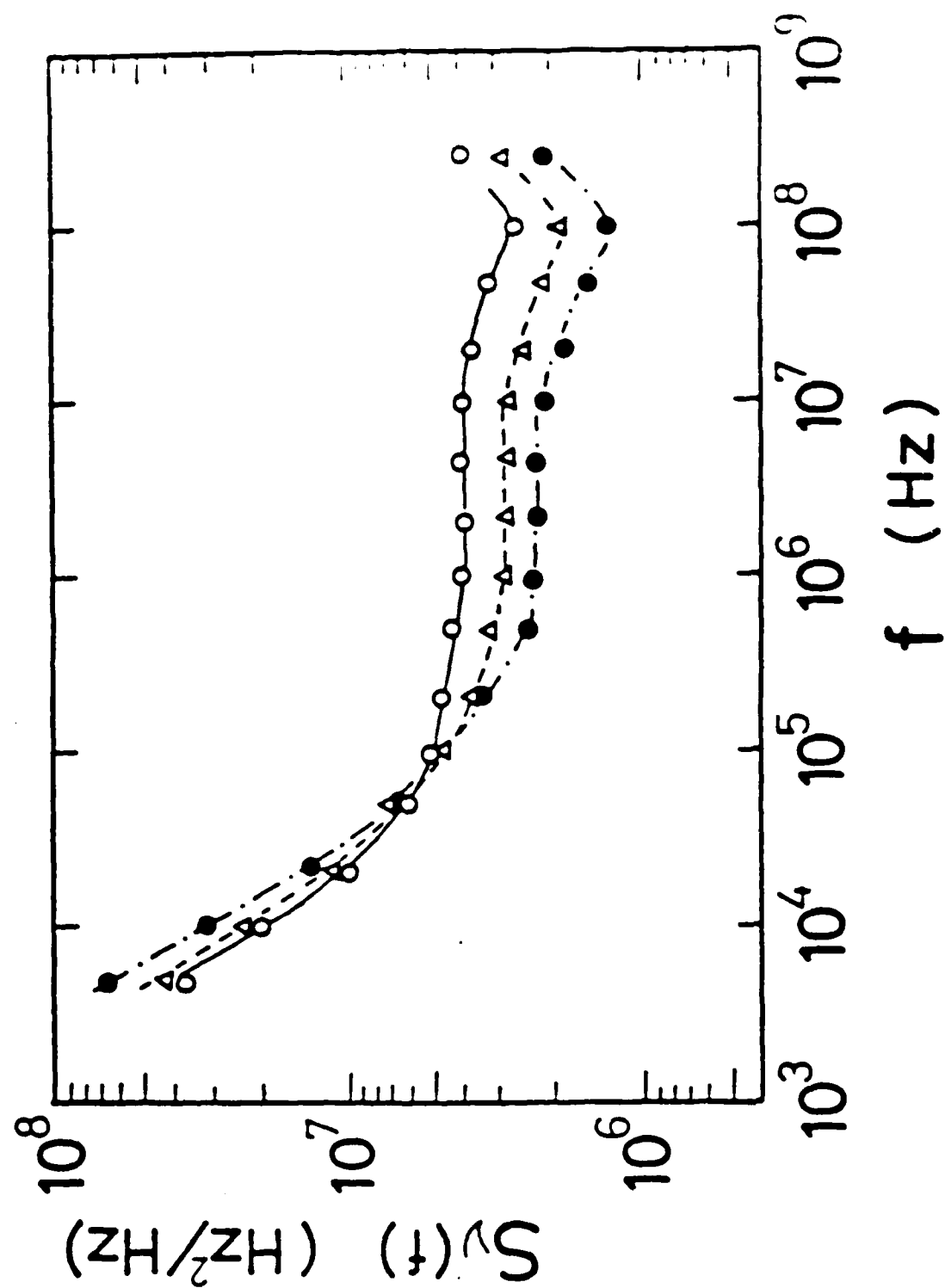
$$- \int_0^\infty h_F(t) [\delta v(t-\tau) + \Gamma_n(t-\tau)] d\tau$$

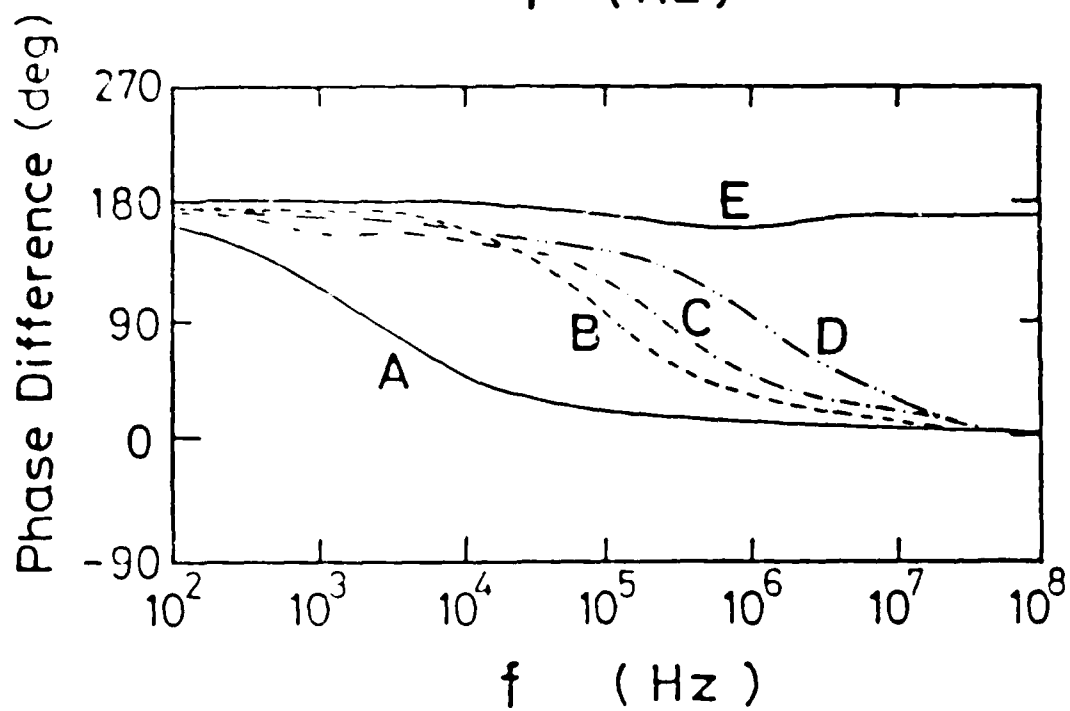
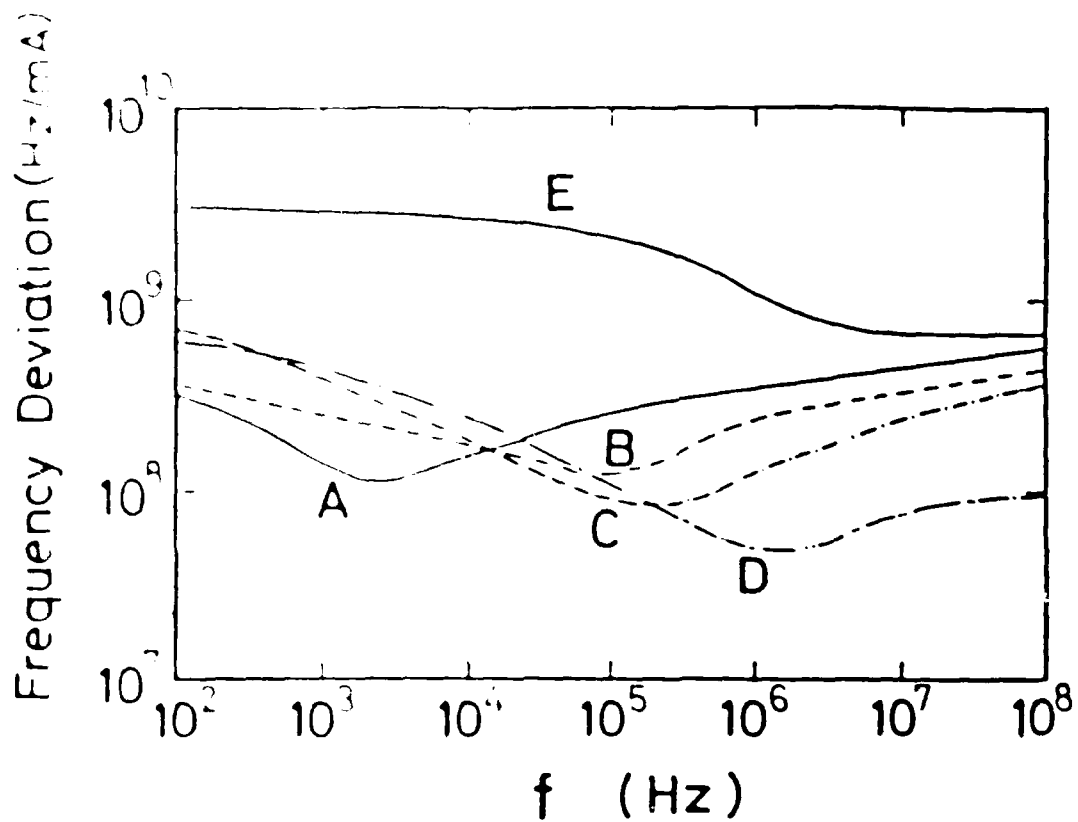
\downarrow impulse response \uparrow noise in feedback loop
 Fourier transform Fourier transform

$$F(f) = \frac{W_S(f)}{1 + H(f)} + \frac{W_C(f)}{1 + H(f)} - \frac{H(f)}{1 + H(f)} \frac{W_n(f)}{W_n(f)}$$

$(|H| \rightarrow \infty) \quad \downarrow \quad \downarrow \quad \downarrow$
 $\quad \quad \quad 0 \quad \quad \quad 0 \quad \quad \quad \frac{W_n(f)}{W_n(f)}$

Real quantities	Fourier transform
$\delta v(t)$	$F(f)$
$h_F(t)$	$H(f)$
$\Gamma_i(t)$	$W_i(f)$





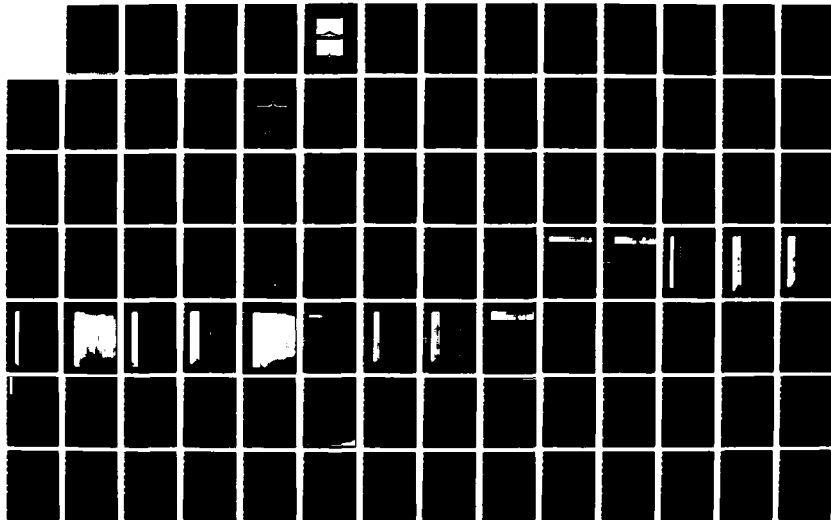
ND-A186 938

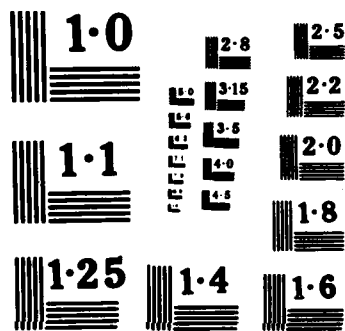
UNITED STATES - JAPAN SEMINAR ON QUANTUM MECHANICAL
ASPECTS OF QUANTUM EL (U) MASSACHUSETTS INST OF TECH
CAMBRIDGE RESEARCH LAB OF ELECTRON
J H SHAPIRO ET AL OCT 87 N80014-87-G-0198 F/G 20/3

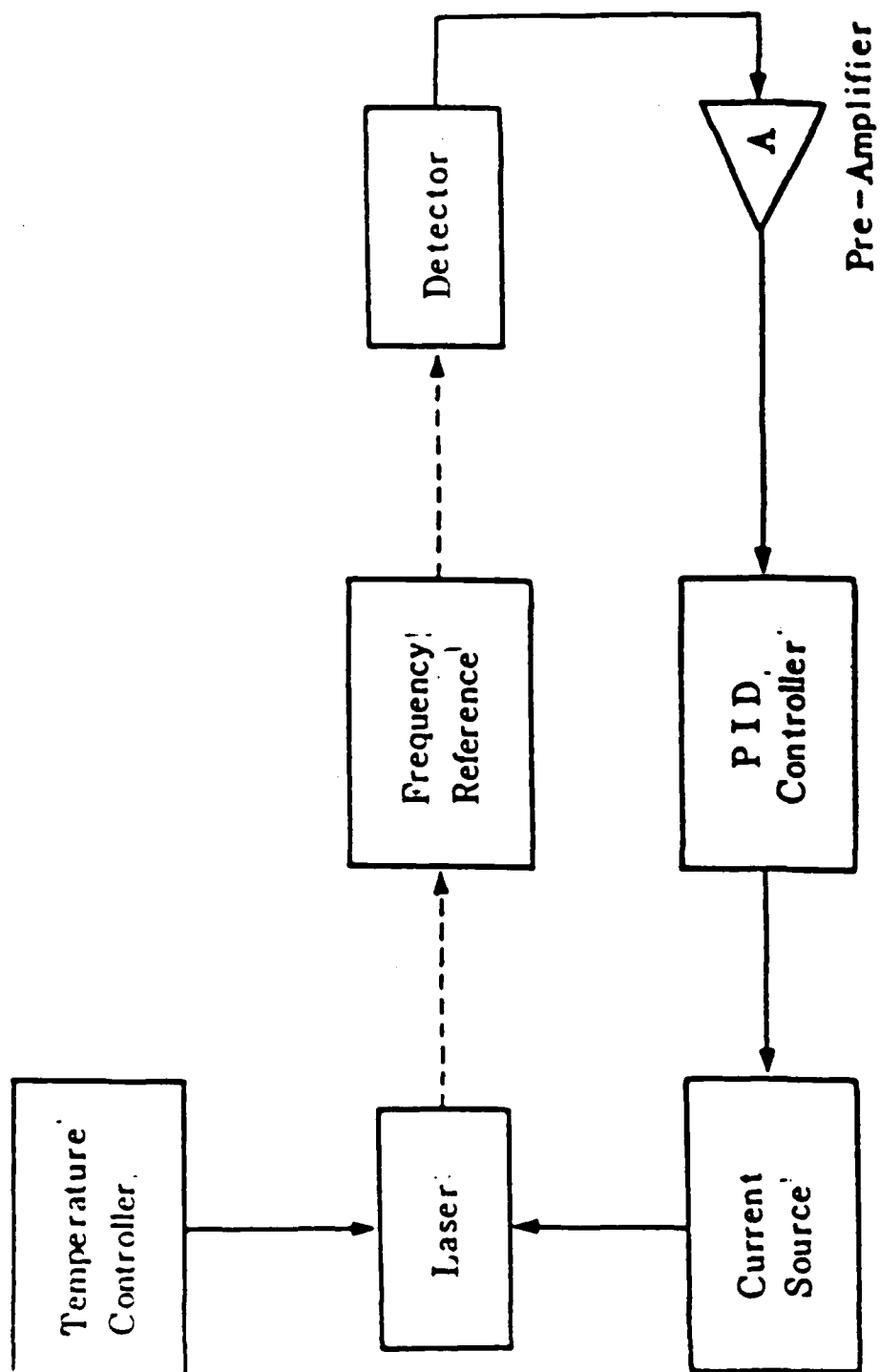
3/7

UNCLASSIFIED

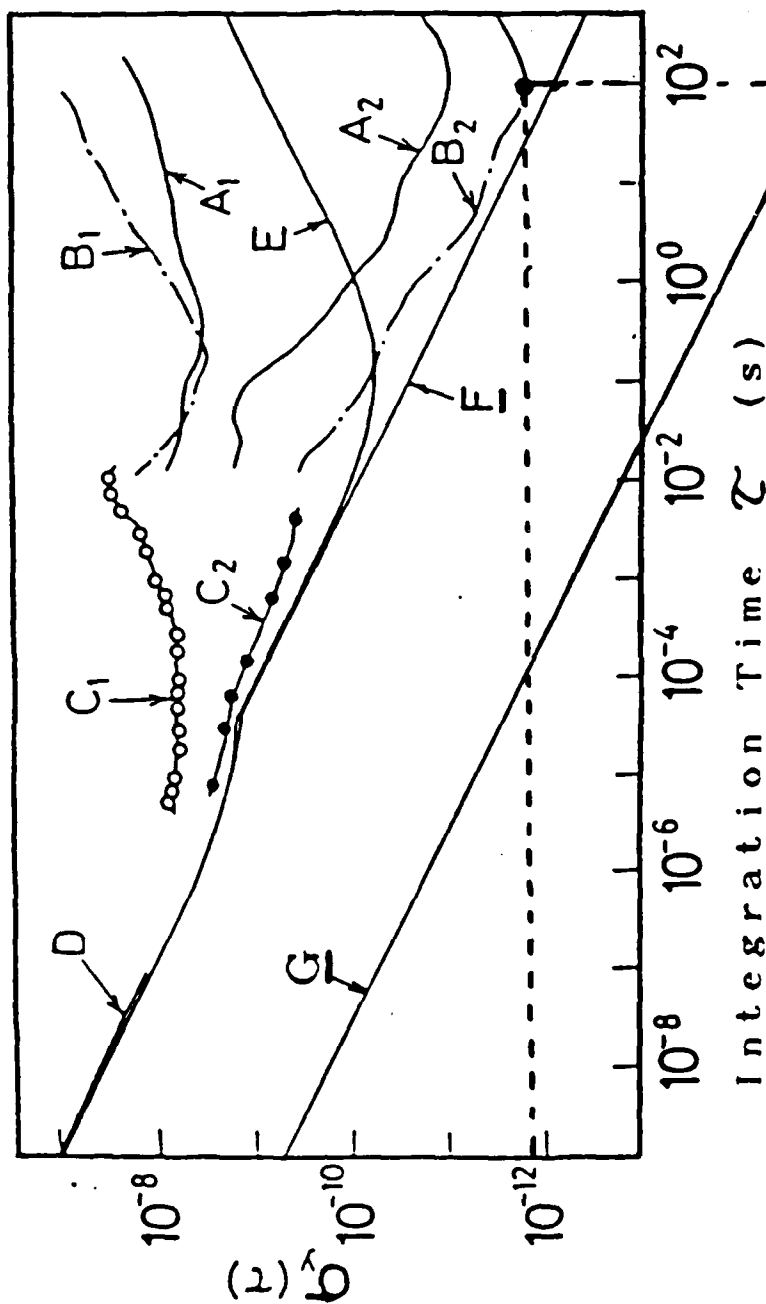
NL







Square Root of Variance



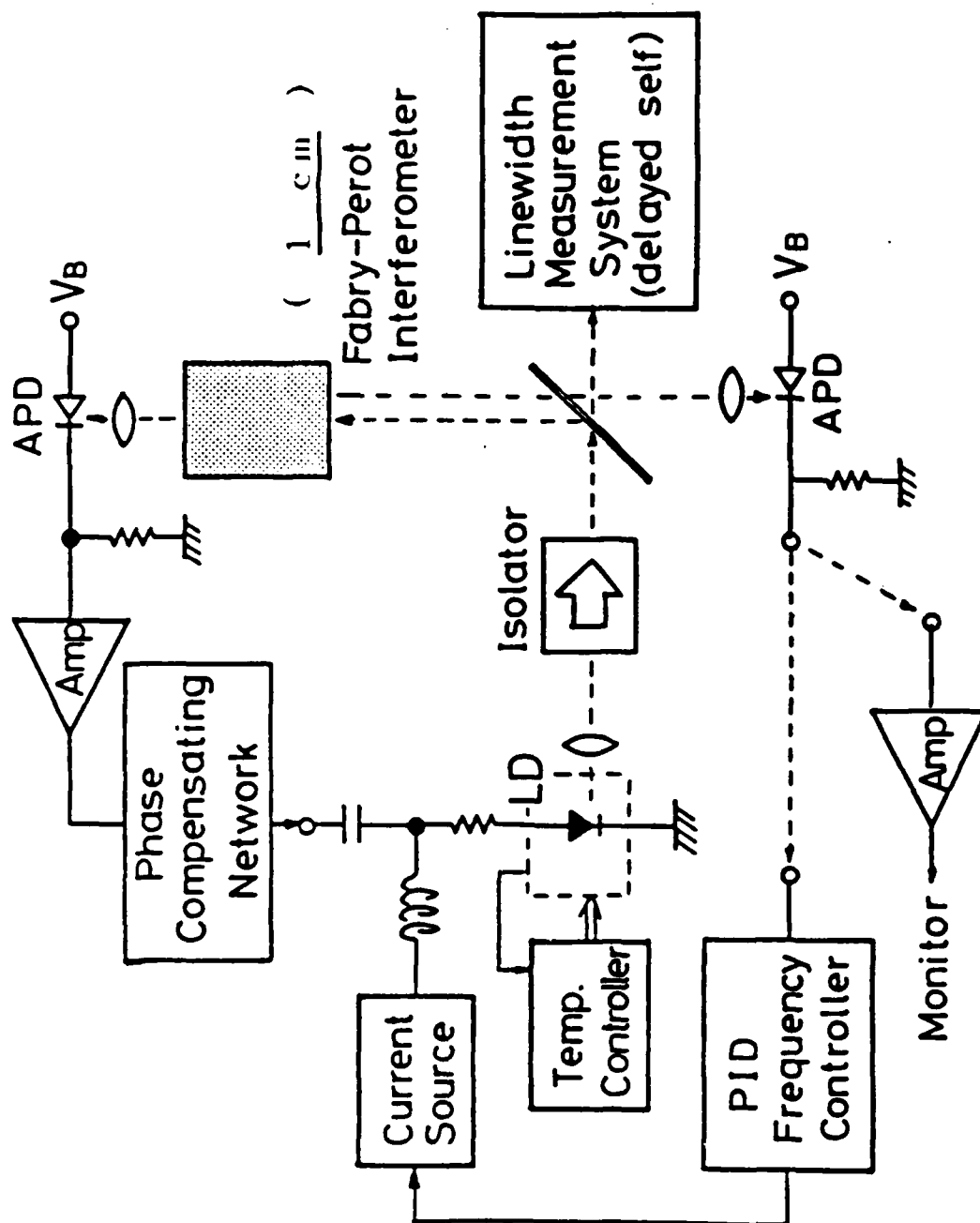
A₁, B₁, C₁, D : Free-running
 A₂ : Stabilized by H₂O B₂ : Stabilized by ⁸⁵Rb
 C₂ : Stabilized by a rigid Fabry-Perot
 interferometer

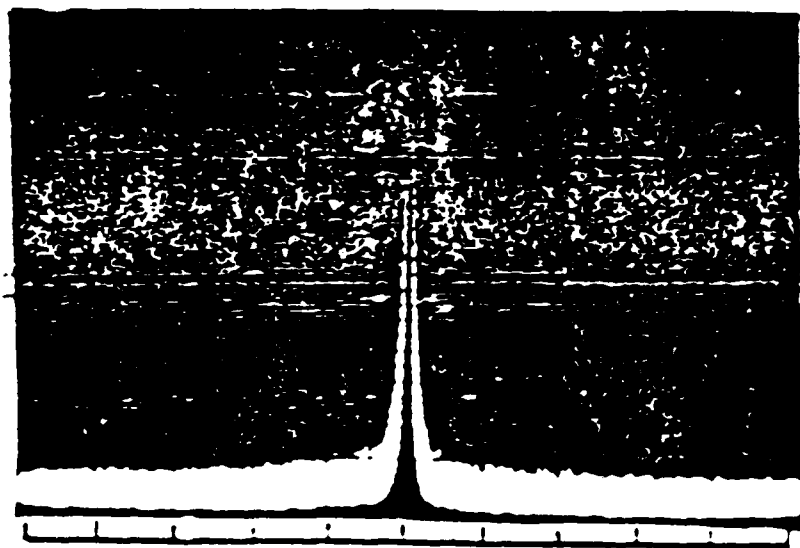
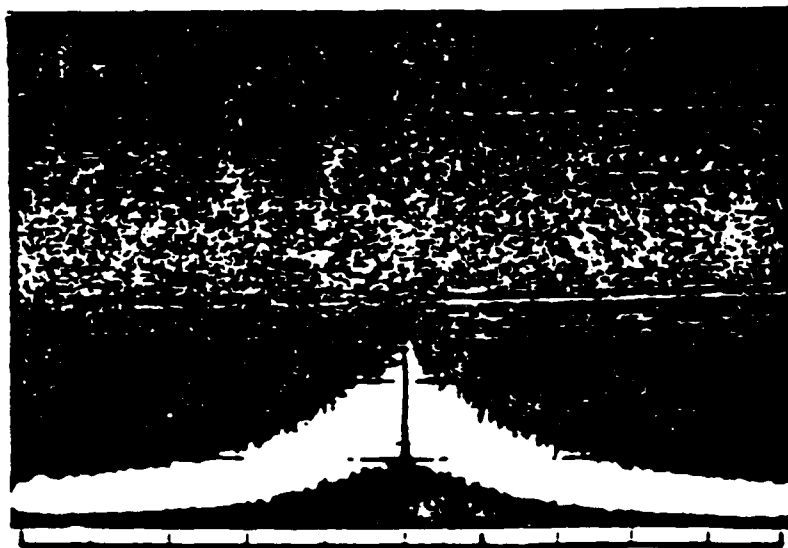
E : Free-running laser including external noises
 F : Quantum noises in free-running laser

[M. Ohtsu, et. al. : Jpn. J. Appl. Phys., 22 (1983) p.1157]

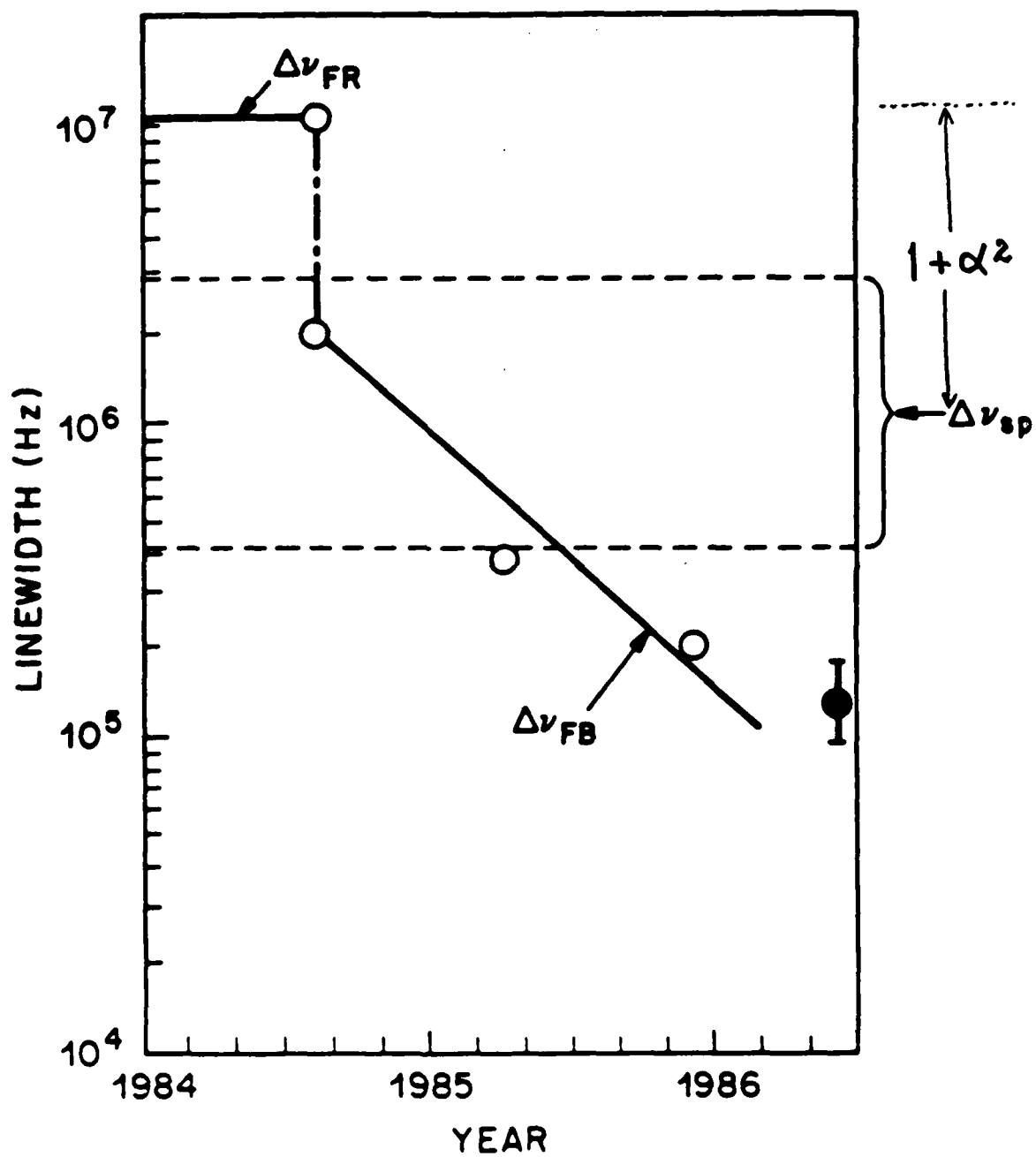
G : Detector noise limited

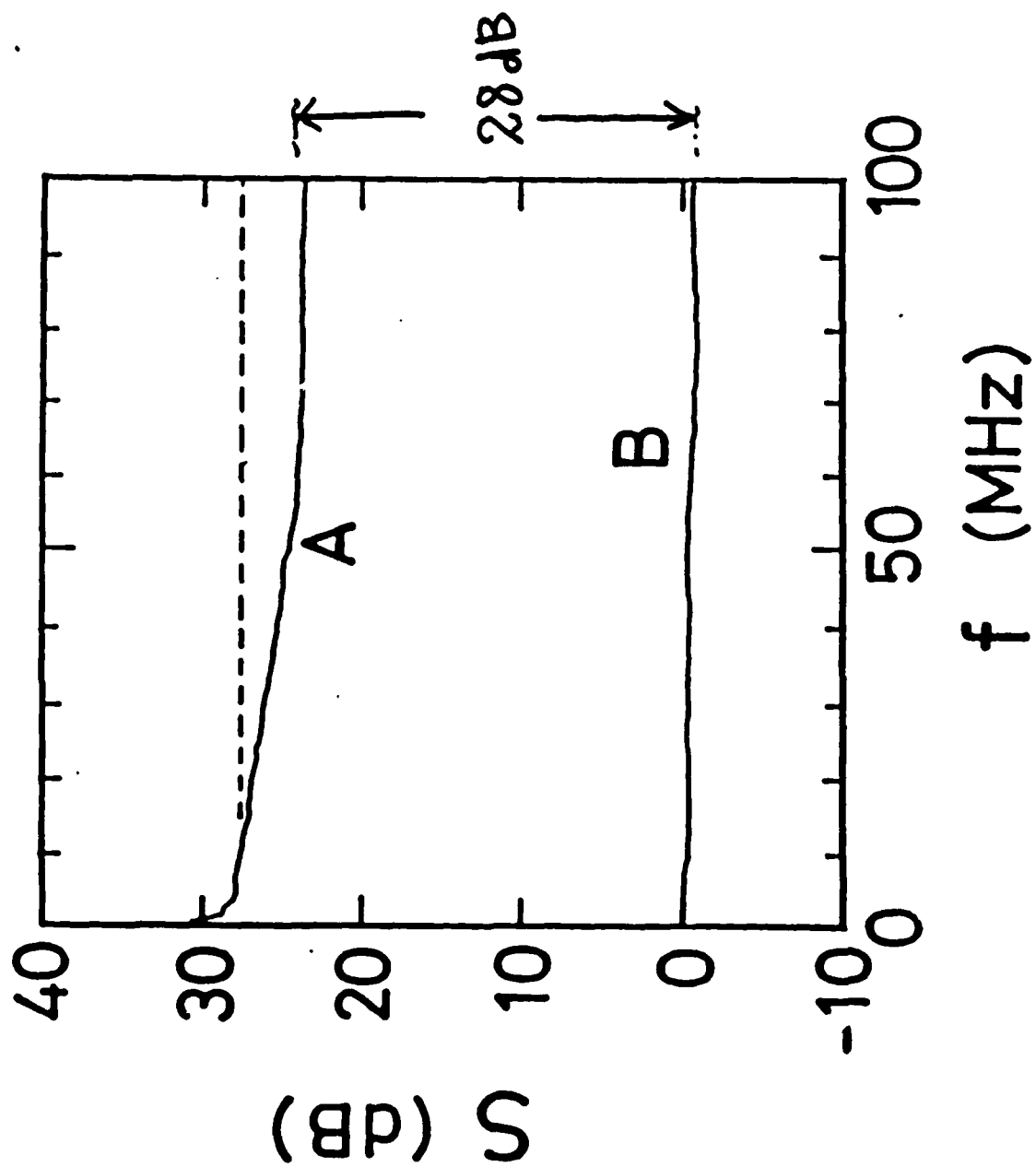
[2] Linewidth reduction





10MHz/div

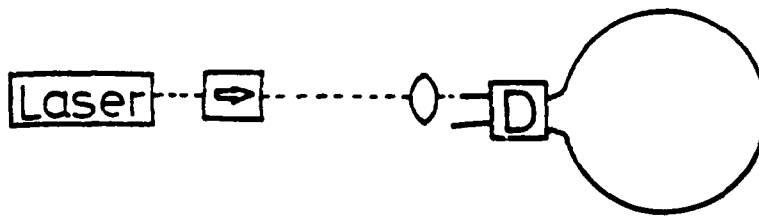




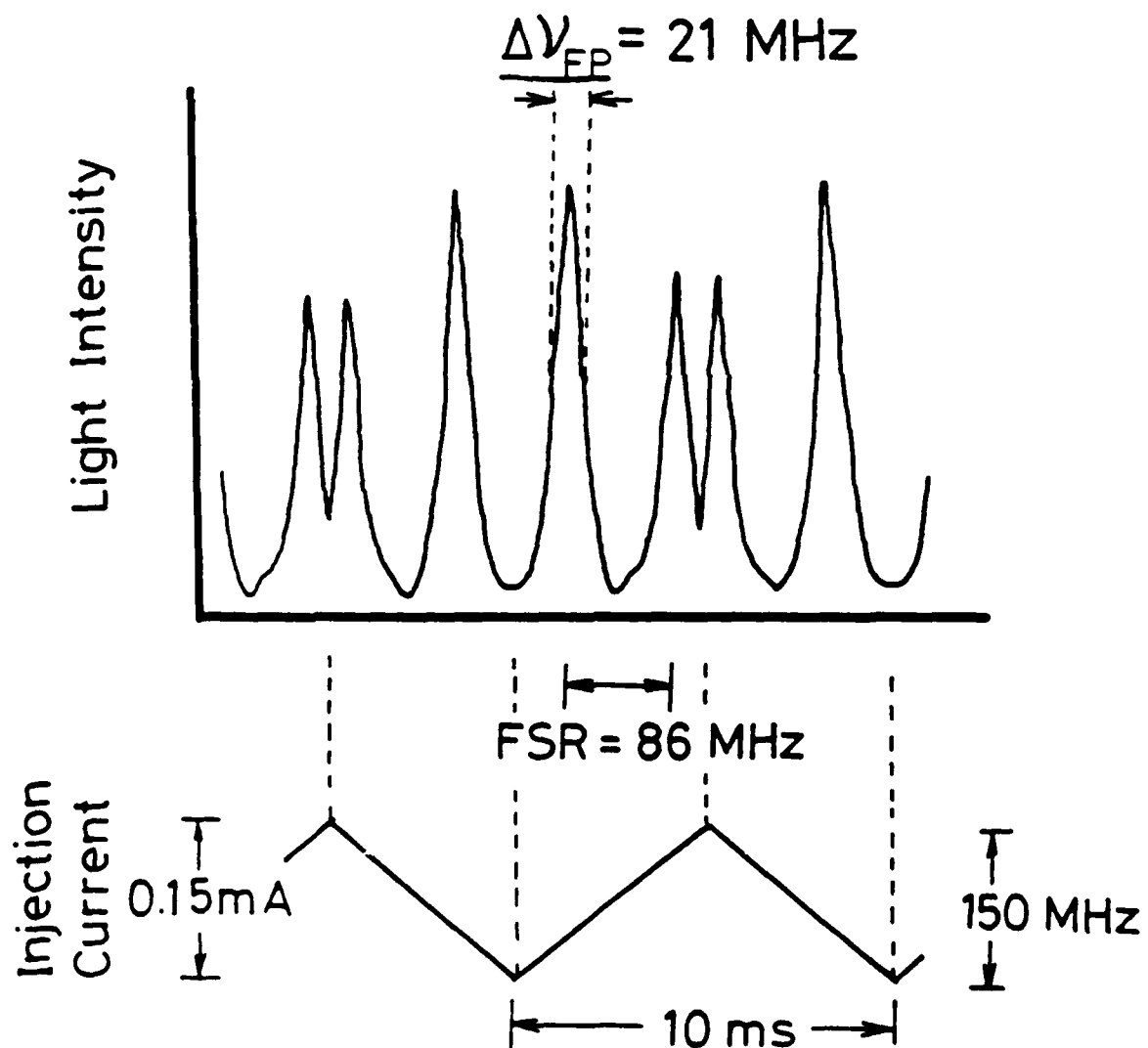
Network Analysis

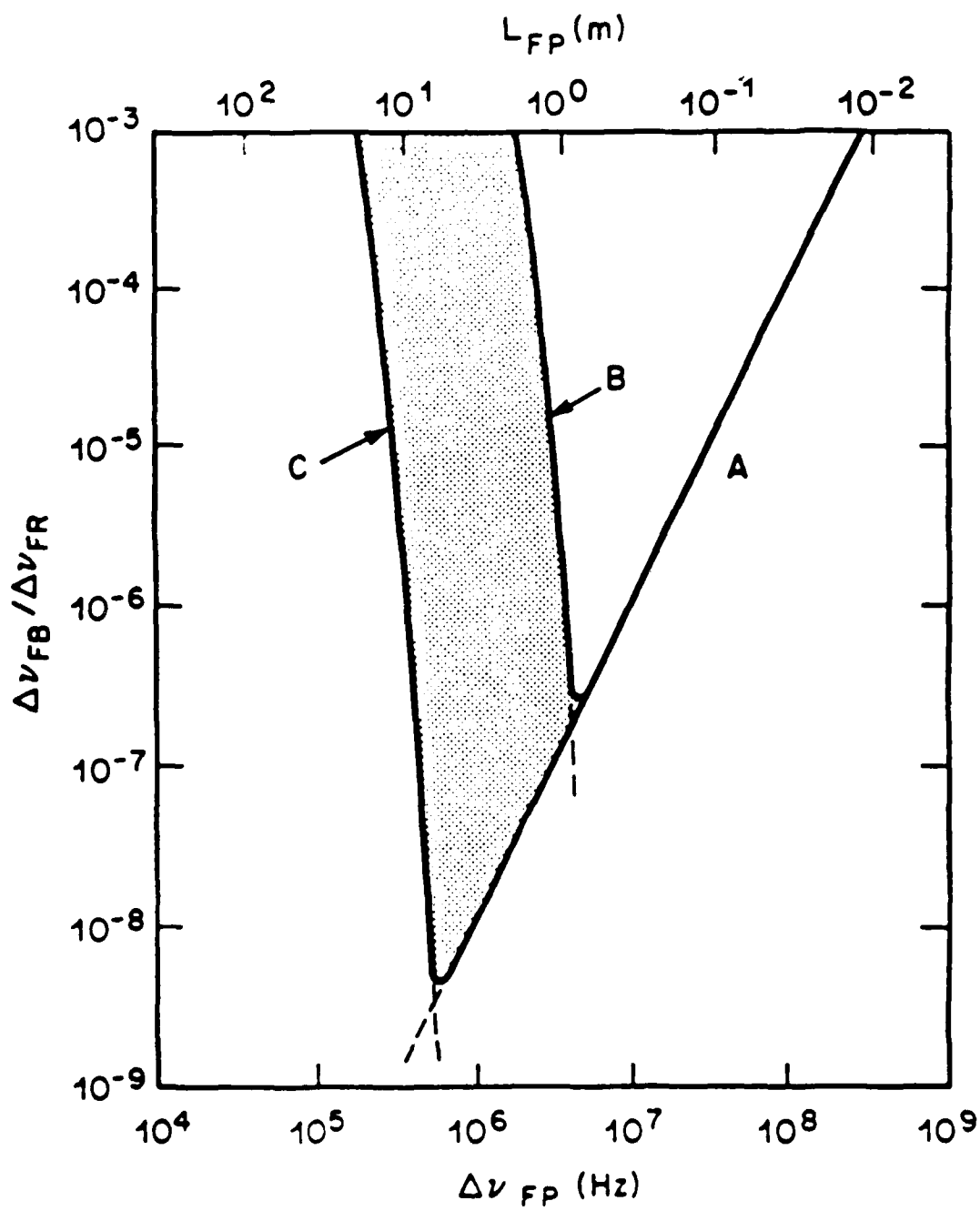
↓ Delay Time $\tau_d \approx 0.6 \text{ ns}$

- 0.2 ns : GaAs IC Servo-amplifier
- 0.4 ns : Optical & electrical path length $\approx 12 \text{ cm}$



Fiber Ring Cavity



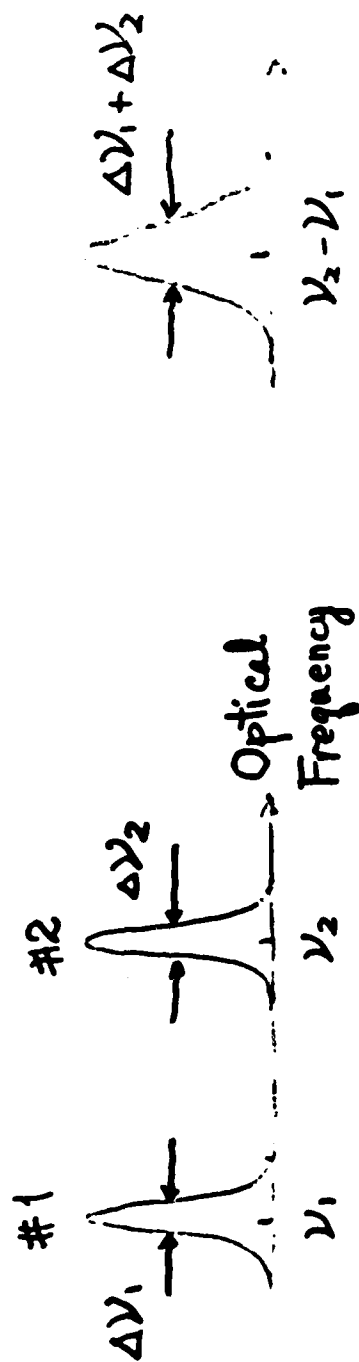


[Summary]

	Experimental Results	Theoretical Limits
(1) Frequency Stabilization	2×10^{-12}	1×10^{-15} (at $\tau = 100 \text{ s}$)
(2) Linewidth Reduction	100kHz	1 Hz
(3) Frequency Tracking	3×10^{-14}	2.7×10^{-16} (at $\tau = 100 \text{ s}$)
(4) Frequency Sweep	53.4GHz	1 THz

- (1) High stability and reproducibility
- (2) Degree of coherence is varied by varying the feedback gain, without modifying laser cavity structure
- (3) Analogy with electronic circuits is employed for design of feedback system
- (4) Compatible with opto-electronic IC
- (5) Applicable to sensing. low~medium bit rate coherent optical communication

Correlated Spontaneous Emission Between the Two Longitudinal Modes in a Semiconductor Laser

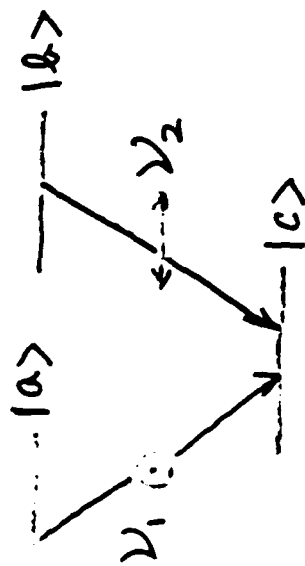


Two-Mode Laser

Heterodyned Signal

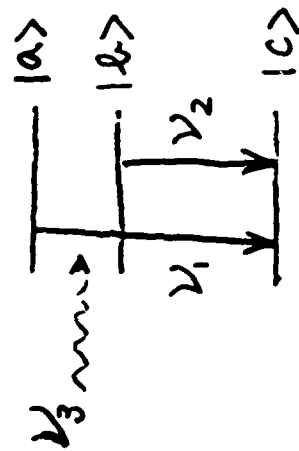
© M.O. Scully: Phys. Rev. Lett., 55 pp 2802-2805 (1985)

« Hanle Effect Laser »



Polarization Induced
Coherence

« Quantum Beat Laser »



Microwave Induced
Coherence

© Toschek & Hall: IQEC'87, Baltimore, WDD2

He-Ne Zeeman Laser

$$\Delta\nu \rightarrow (\text{Schawlow-Townes Limit}) \times 1/10$$

The state vector of the three-level atoms :

$$|\psi\rangle = \alpha e^{-i\phi_a} |a\rangle + \beta e^{-i\phi_b} |b\rangle + \gamma e^{-i\phi_c} |c\rangle \quad (1)$$

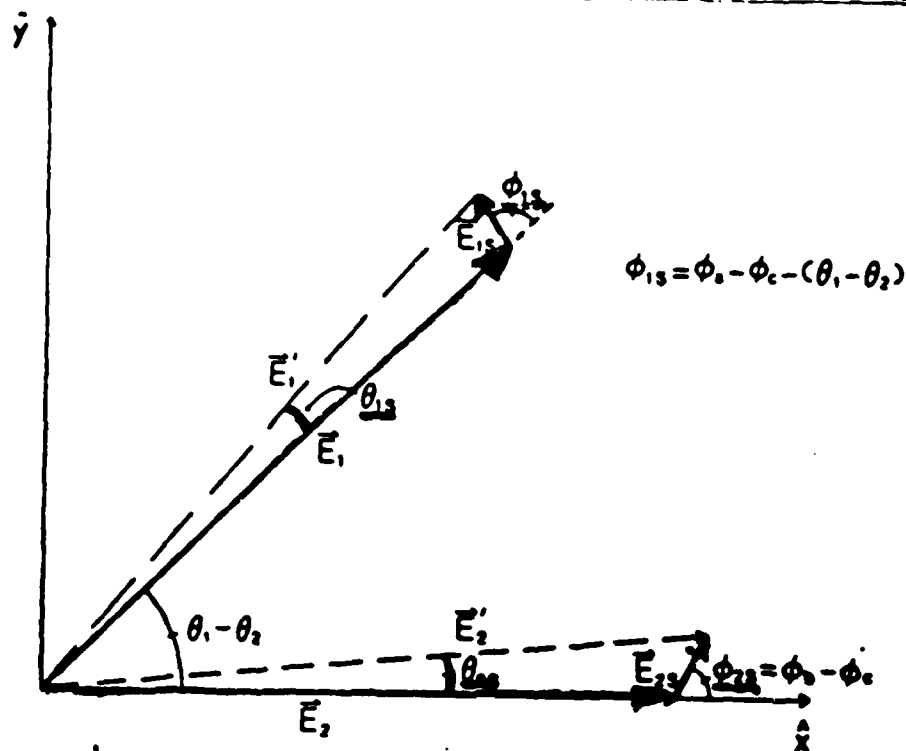


Spontaneously emitted fields :

$$E_{1s} = \varepsilon_1 e^{-i(\phi_a - \phi_c) - i\nu_1 t}$$

$$E_{2s} = \varepsilon_2 e^{-i(\phi_b - \phi_c) - i\nu_2 t}$$

(2)



Phase difference between the laser field and spontaneously emitted field :

$$\left. \begin{aligned} \underline{\phi_{1s}} &= \phi_a - \phi_c - (\theta_1 - \theta_2) \\ \underline{\phi_{2s}} &= \phi_a - \phi_c \end{aligned} \right\} \quad (3)$$

Fluctuations in the phase of laser field :

$$\left. \begin{aligned} \underline{\theta_{1s}} &= \frac{|\vec{E}_{1s}|}{|\vec{E}_1|} \cdot \sin \underline{\phi_{1s}} \\ \underline{\theta_{2s}} &= \frac{|\vec{E}_{2s}|}{|\vec{E}_2|} \cdot \sin \underline{\phi_{2s}} \end{aligned} \right\} \quad (4)$$

For quenching the phase noise in heterodyned signal:

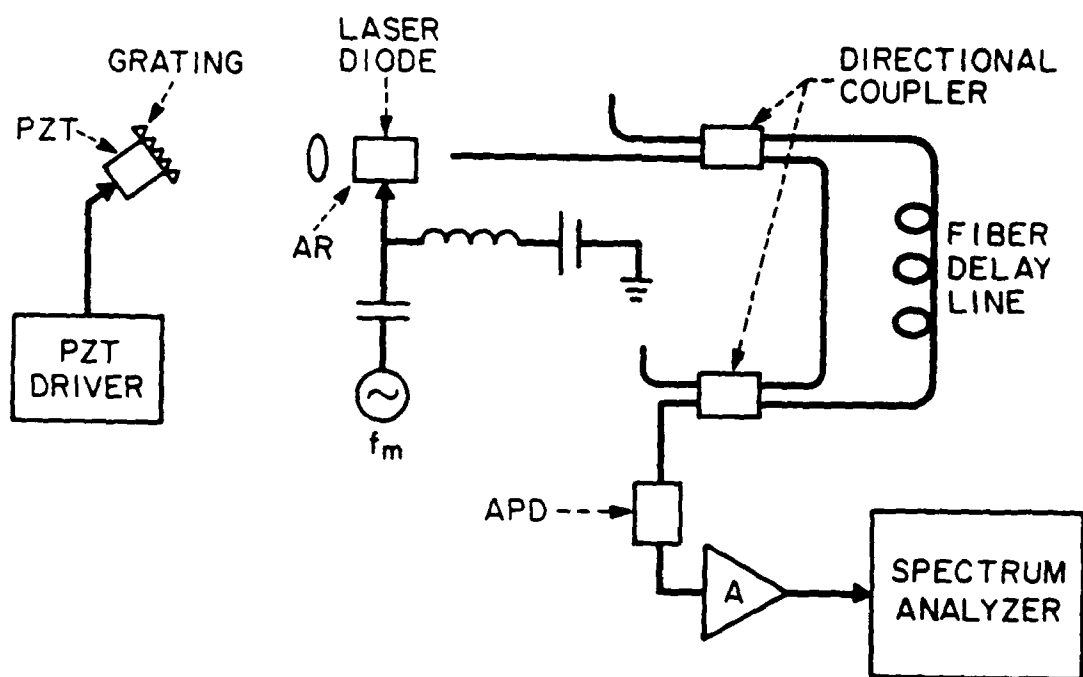
$$\theta_{1s} = \theta_{2s} \quad (5)$$

From eqs. (3), (4), this is met if

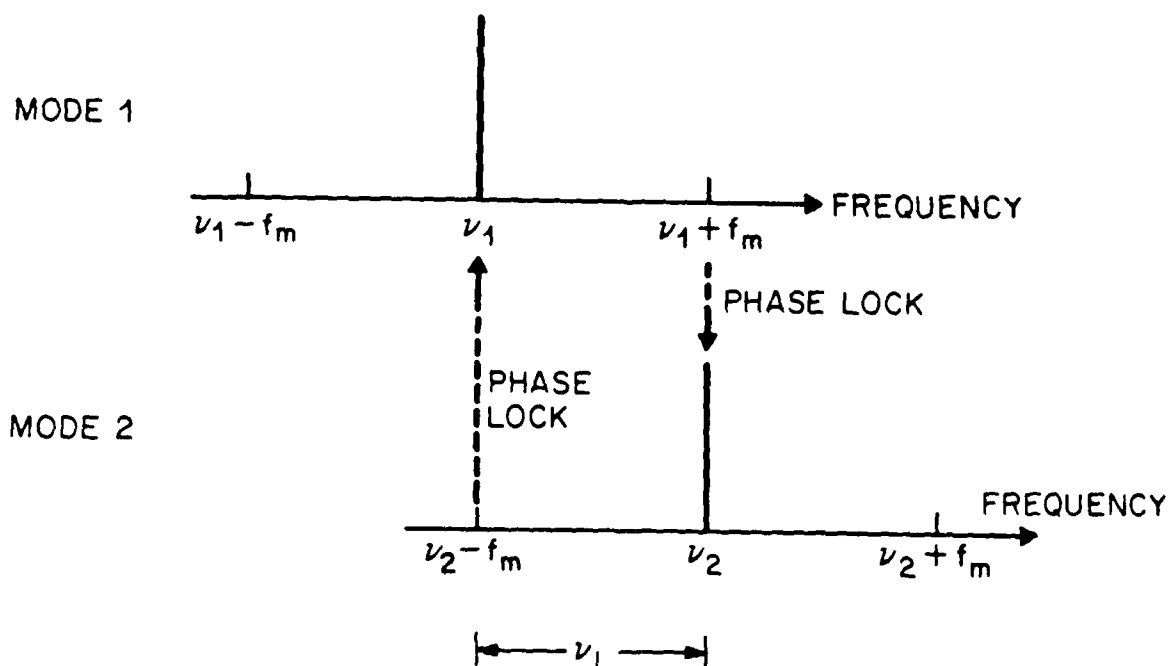
$$\theta_1 - \theta_2 - (\phi_a - \phi_e) = 0 \quad (6)$$

By applying microwave, $\phi_a - \phi_e = \phi_\mu$,
then the condition to be satisfied is

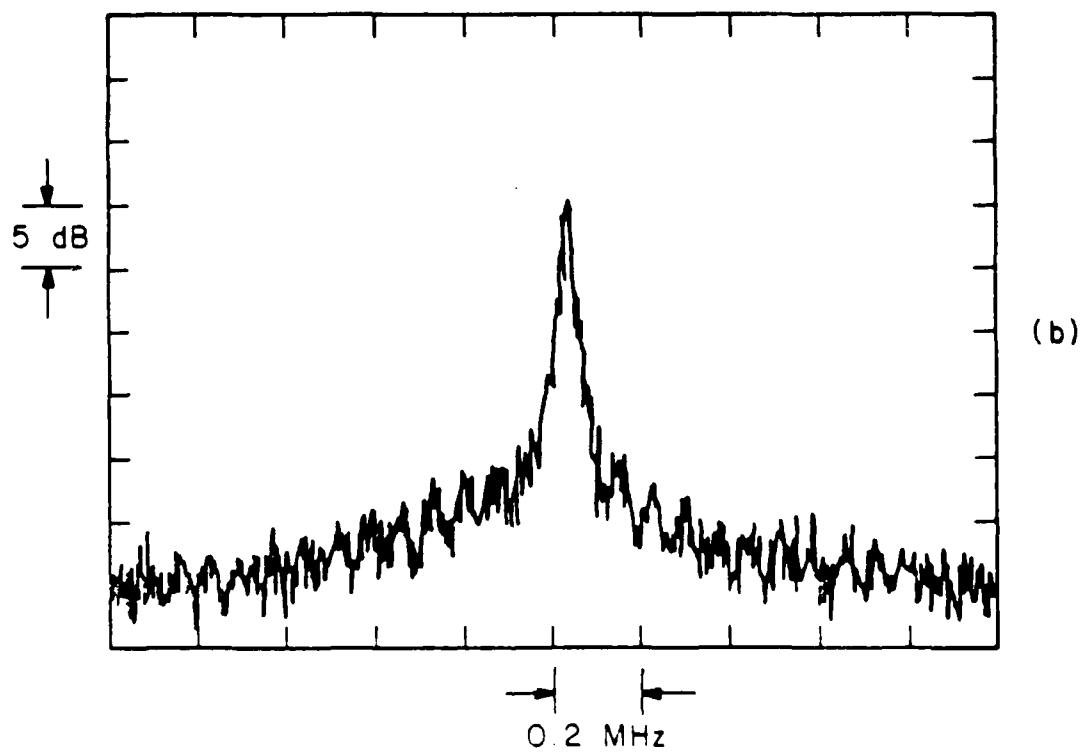
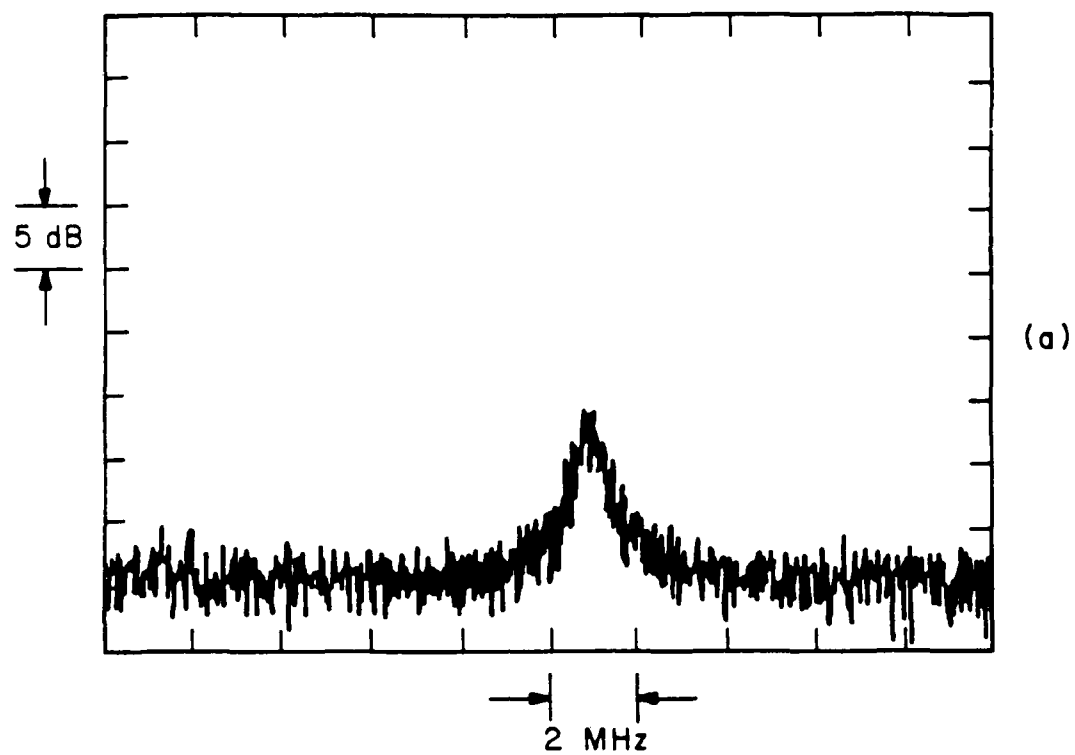
$$\underline{\theta_1 - \theta_2 = \phi_\mu} \quad (7)$$

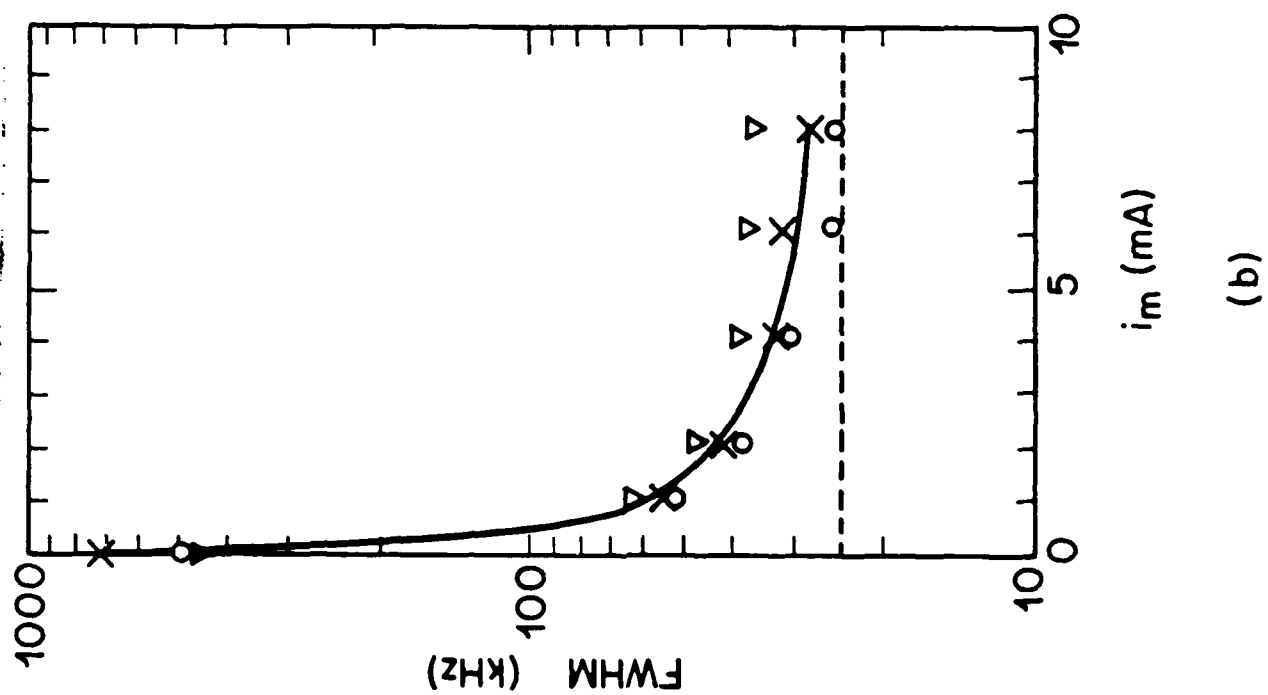
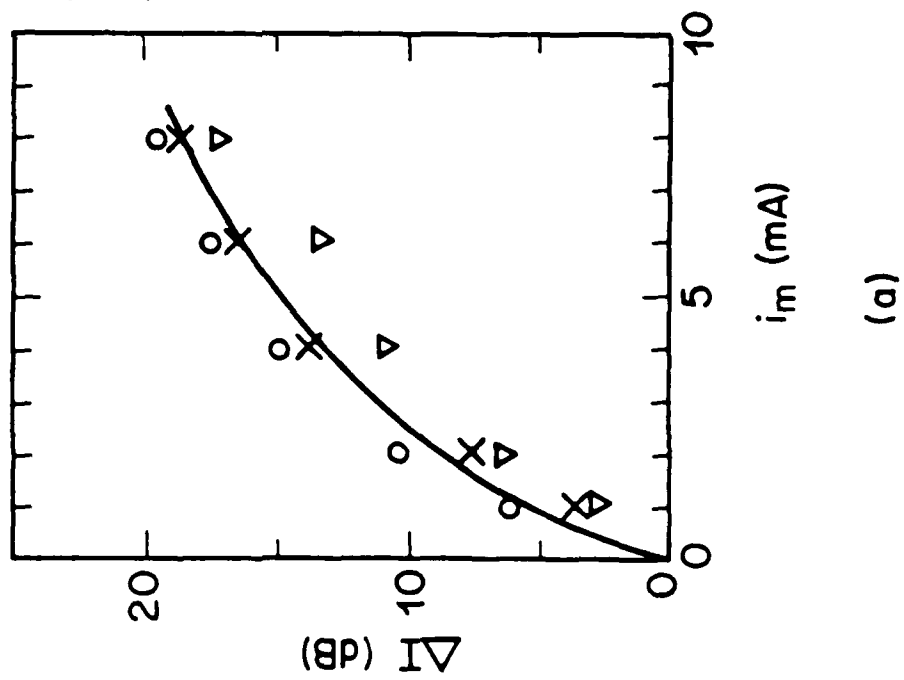


(a)

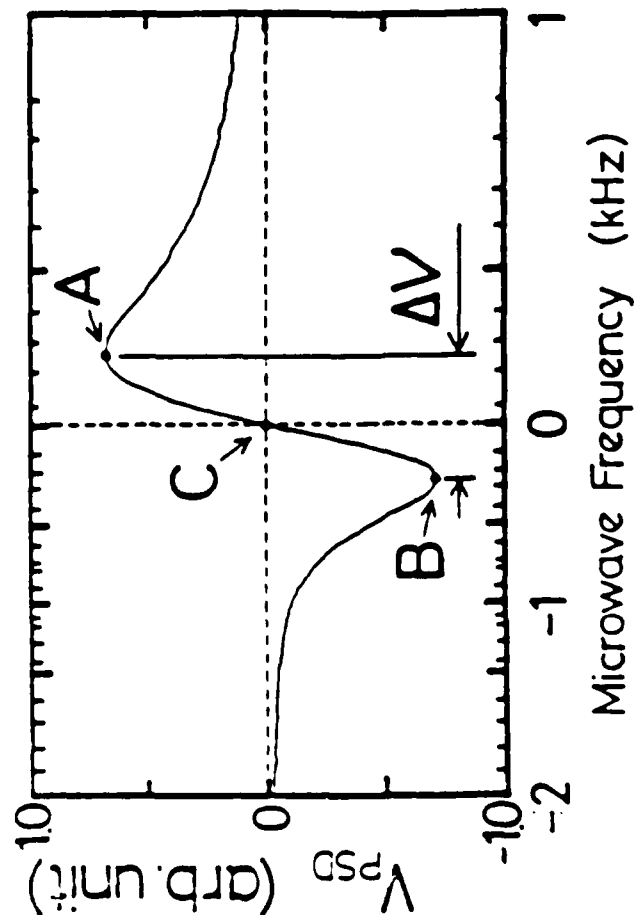
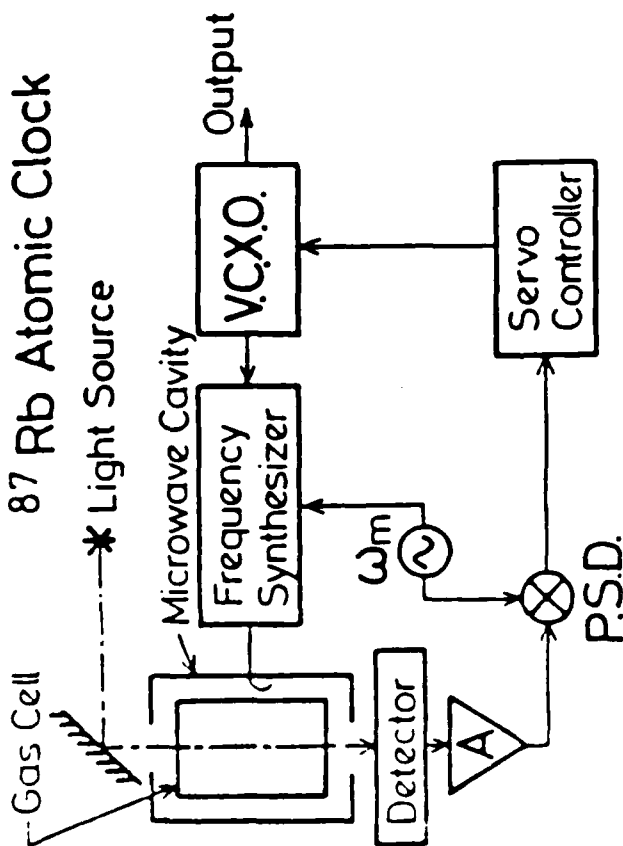


(b)

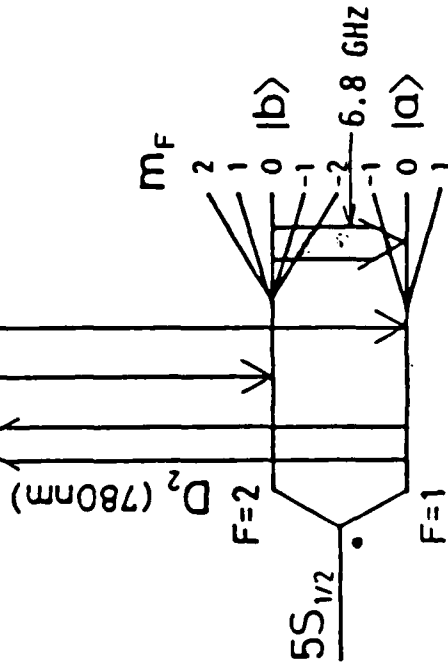




87 Rb Atomic Clock



5P_{3/2} |c>



Laser Pumping
 Spontaneous Emission
 Microwave Transition

Frequency Stability

$$\sigma_y(\tau) = \frac{1}{\sqrt{2\pi}(\nu_M/\Delta\nu)} \tau^{-1/2}$$

$$= \frac{N}{\sqrt{2\pi} \nu_M (S/\Delta\nu)} \tau^{-1/2}$$

Slope

Reference Signal

$$\cos(\omega_m t - \theta)$$

PSD Output

$$V_{PSD} = V_0[(B/2)\cos\theta + (C/2)\sin\theta]$$

Experimental

$$M = 1.8$$

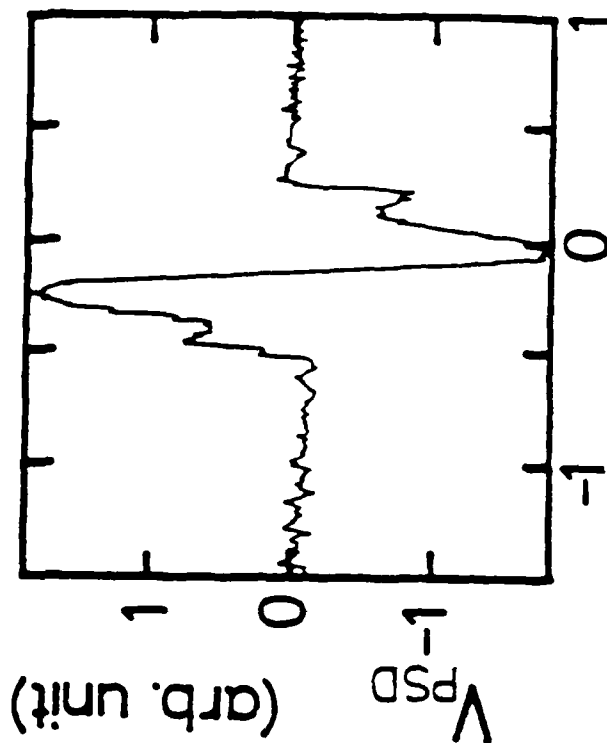
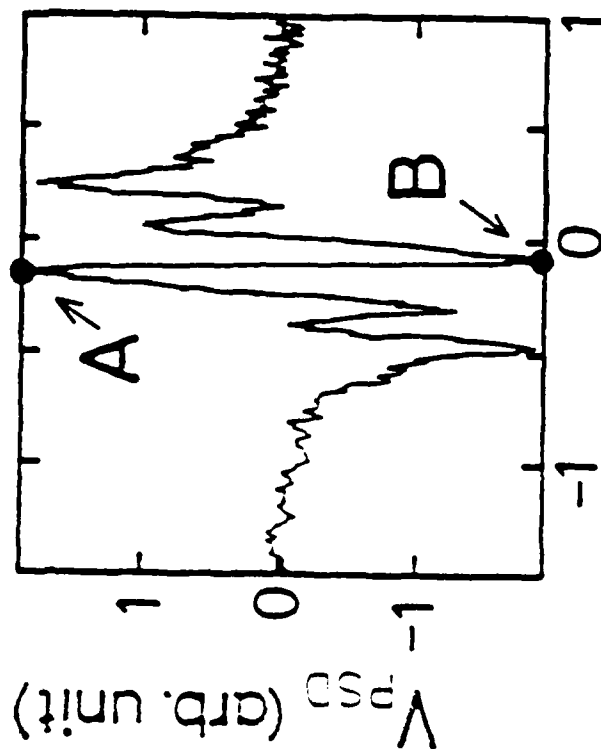
$$f_m/\gamma_{db}' = 2.3$$

$$\theta = 234^\circ$$

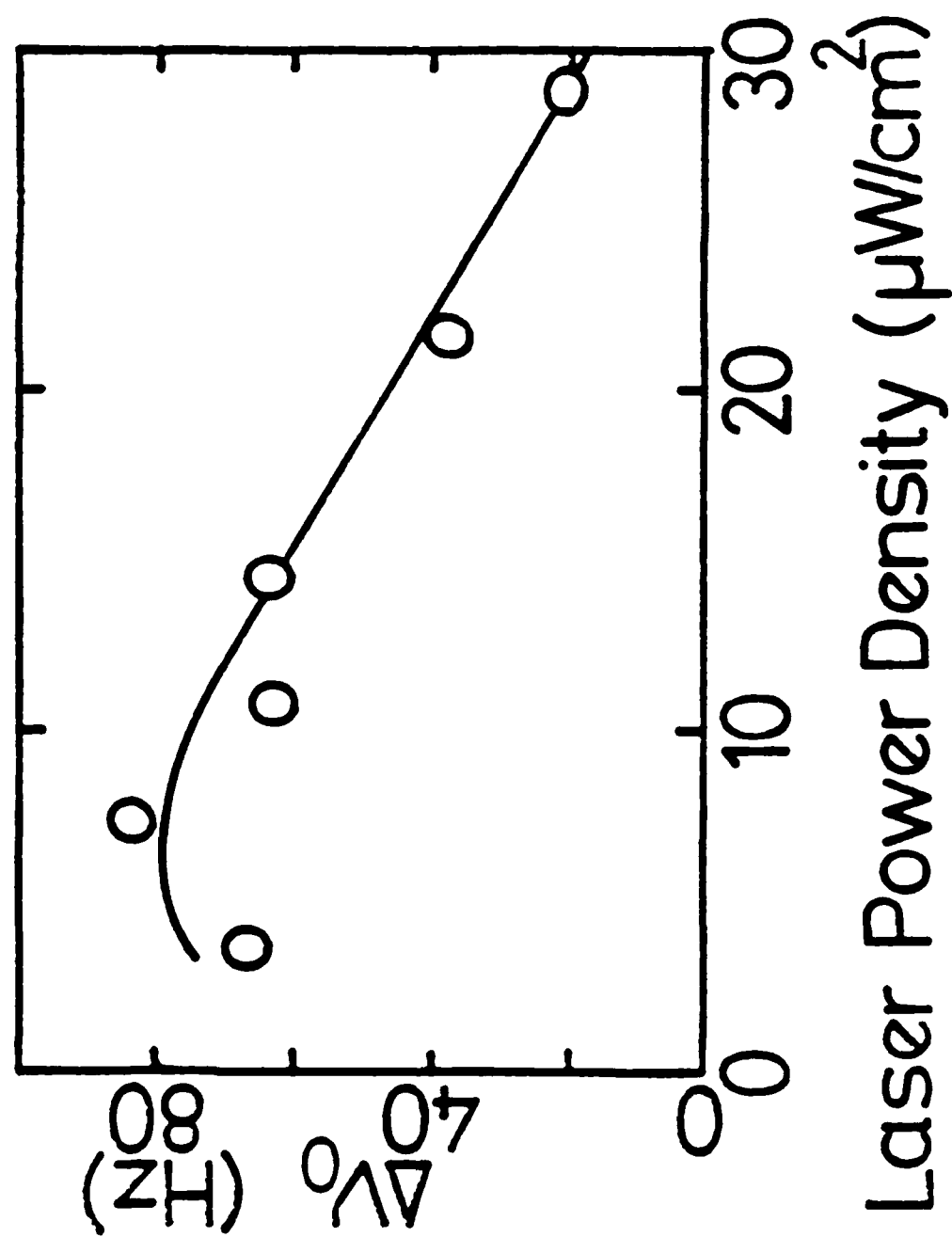
$$M = 1.6$$

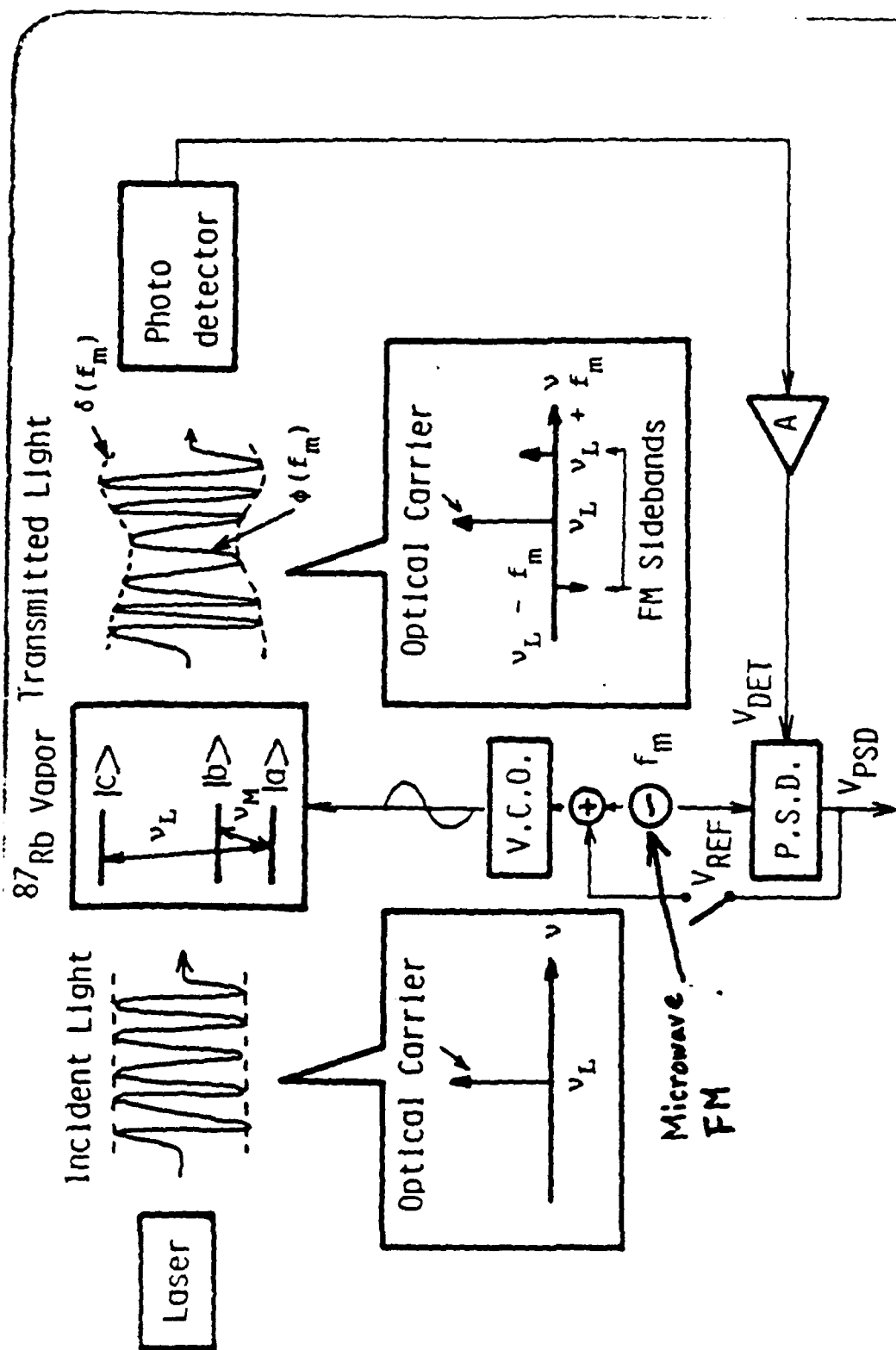
$$f_m/\gamma_{db}' = 2.9$$

$$\theta = 270^\circ$$



Microwave Frequency (kHz)





Detector Output $V_{\text{DET}} = V_0 [A + B \cos(2\pi f_{\text{nt}}) + C \sin(2\pi f_{\text{nt}})]$

Reference Signal $V_{\text{REF}} = \cos(2\pi f_{\text{nt}} - \theta)$

PSD Output $V_{\text{PSD}} = (B/2) \cos \theta + (C/2) \sin \theta$

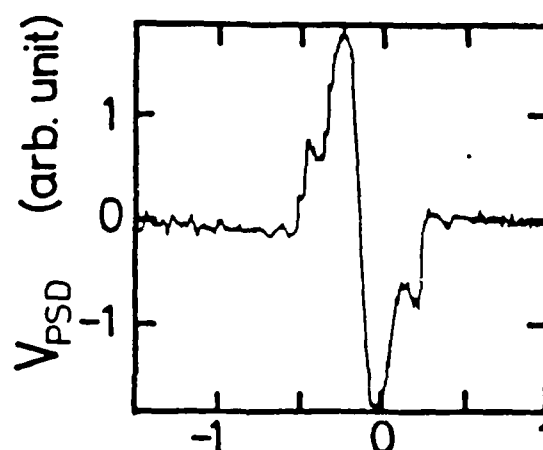
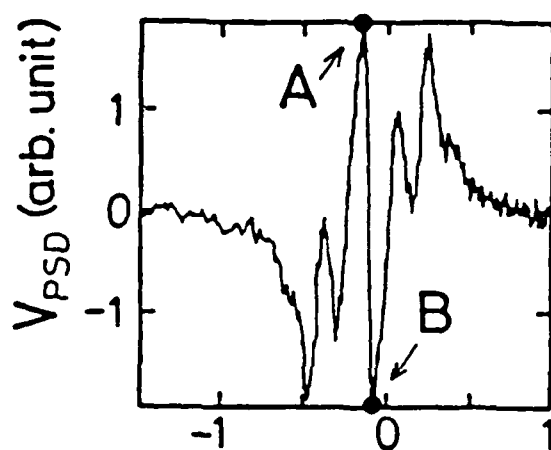
Reference Signal $\cos(\omega_m t - \theta)$

PSD Output $V_{PSD} = V_0[(B/2)\cos\theta + (C/2)\sin\theta]$

Experimental

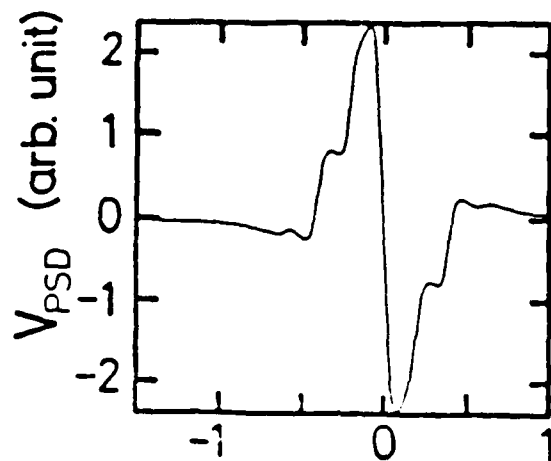
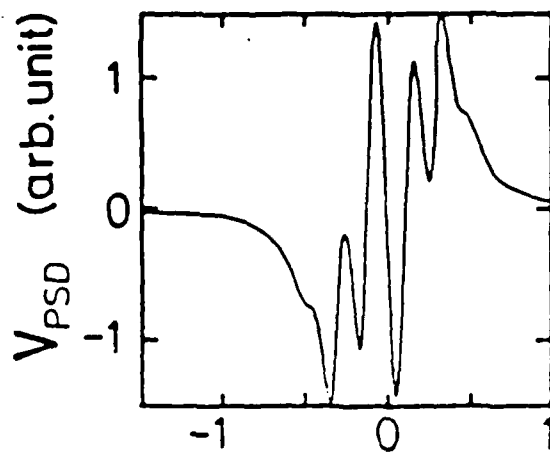
$M = 1.8$
 $f_m/\gamma_{ab'} = 2.3$
 $\theta = 234^\circ$

$M = 1.6$
 $f_m/\gamma_{ab'} = 2.9$
 $\theta = 270^\circ$

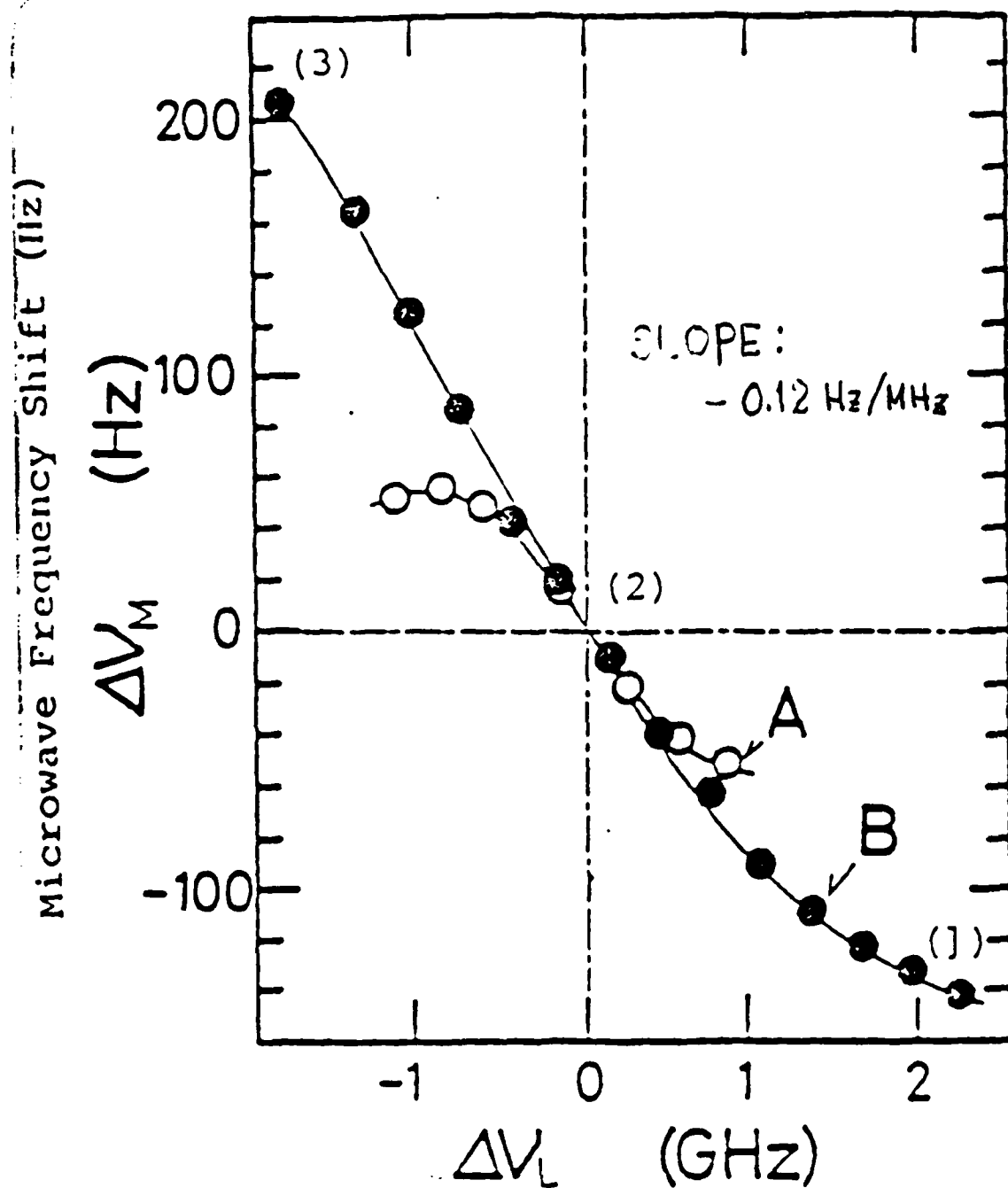


Microwave Frequency (kHz)

Theoretical

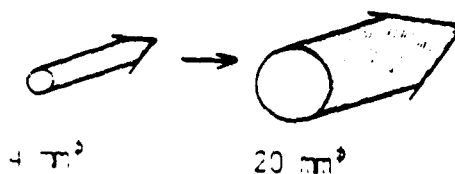
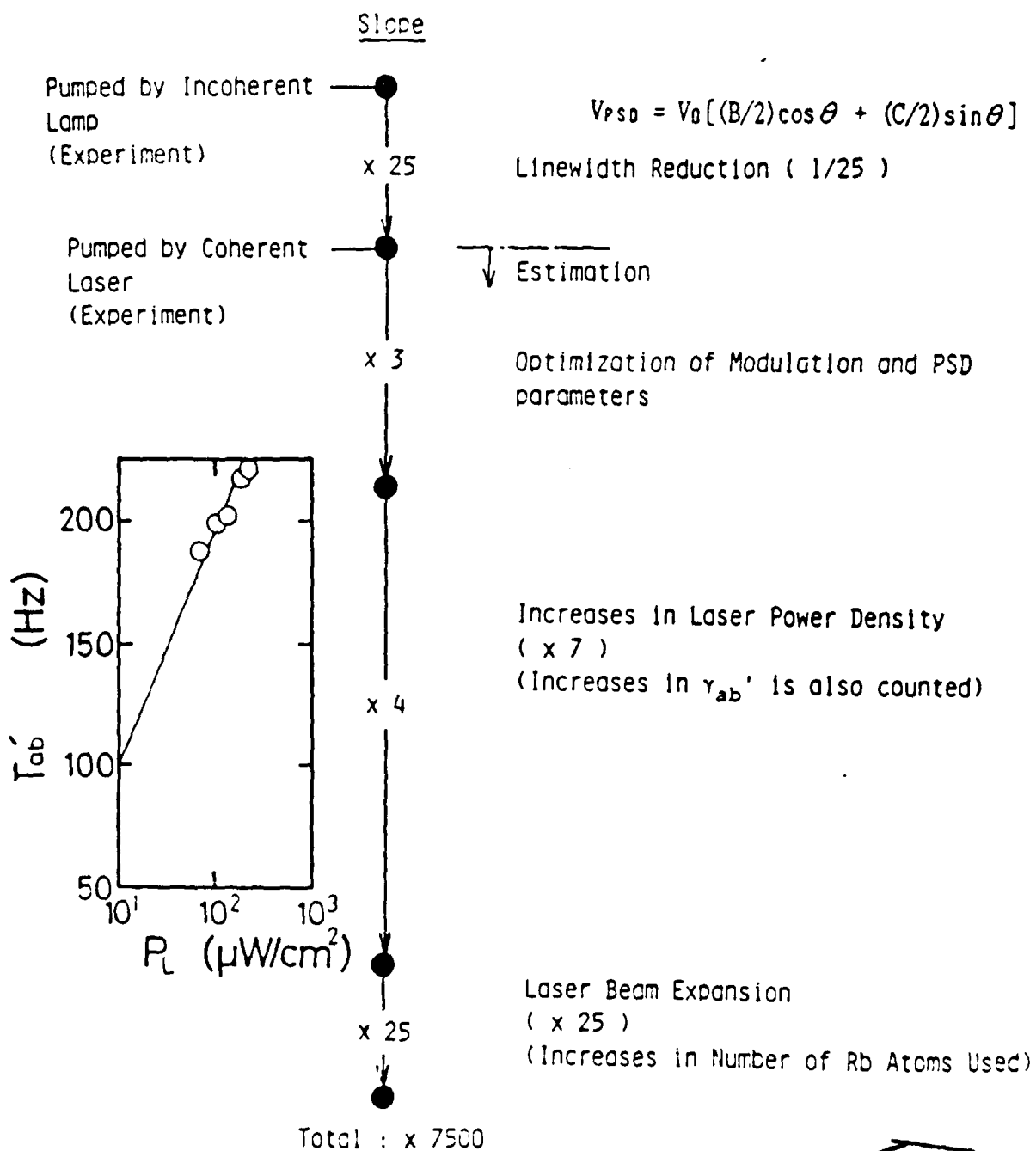


Microwave Frequency (kHz)



Laser Frequency Detuning (GHz)

A: Laser Power Density $57.6 \mu \text{ W/cm}^2$
 B: Laser Power Density $2880 \mu \text{ W/cm}^2$



[Summary]

- (1) Novel FM detection technique for double resonance spectral shape
- (2) Sensitivity of frequency discriminator : x 7500
- (3) Improve the frequency accuracy . (under optimum condition)

Squeezed State in Degenerate Parametric Amplification

Discussed by H. Takahasi in 1963

Koichi Shimoda

Department of Physics, Keio University

3-14-1 Hiyoshi, Kohokuku, Yokohama 223

Professor Hidetosi Takahasi who died in 1985 had developed a theory of quantum noise in 1963 by appropriately applying the quantum mechanics to a general theory of communication channels.

He discussed the quantum-mechanical coherent state of a harmonic oscillator, and subsequently developed a quantum theory of parametric amplifiers, in which the squeezed state in degenerate parametric conversion was particularly emphasized.

§1. Introduction

On January 14, 1963 Professor Hidetosi Takahasi, who died on June 30, 1985, gave a talk on "Semiclassical theory and quantum theory of photon noise" at a colloquium in the Department of Physics, University of Tokyo. He presented his conception of the coherent photon state and discussed that the "squeezed state" would be produced in parametric amplification. These works were first published in August, 1963 in Japanese.¹⁾ His paper in English entitled "Information Theory of Quantum-Mechanical Channels" which included these considerations was published in 1965.²⁾

It is the purpose of the present paper to reveal his early consideration of the squeezed state in degenerate parametric amplification. He developed the theory in a quite general way so that it could be applied to either mechanical, acoustic, electric, microwave, or optical systems. In particular, the Schrödinger equation of a parametric oscillator was treated with natural units. In the present paper, however, some of his terminologies and notations have been replaced by more familiar ones.

Although the full treatment in the present paper follow those in ref.1) and 2), almost faithful quotations from ref.2) will be accompanied by quotation marks.

§2. Quantum Noise in Linear Systems

Quantum noise is essentially different from classical noise.

Classical noise such as thermal noise is a definite physical quantity that varies stochastically with time. Quantum noise, on the other hand, is the result of uncertainties ⁱⁿ quantum-mechanical measurements which depend how we observe what in quantum-mechanical terms. Even without any classical noise in a system, we still have a statistical relation between transmitted and received signals, which arises from the intrinsic nature of quantum-mechanical observations.

We consider a linear system, either an attenuator or an amplifier, with a black-box model. It is important to see that we deal exclusively with transmission of discrete samples of signals with angular frequency ω rather than a continually varying function of time.

A simple classical relation between the input x and the output y of a linear system is

$$y = kx \quad (2.1)$$

where x and y represent the strength of oscillating fields, so that $|x|^2$ and $|y|^2$ give respectively the input and output energies of the observed mode. However, the relation (2.1) should be modified in order to take the effect of external systems into consideration.

Consider an attenuator for which $k < 1$. Then the absorbed power must be deposited to a heat reservoir, external space, or elsewhere. Likewise many external systems are coupled to the attenuator so that they may bring in noise. A number of such external systems are represented in our black-box treat-

ment as shown in Fig. 1, where a lossless channel (a beam splitter, for example) is coupled with four external systems.

Here the classical input-output relations should be

$$\begin{aligned} y &= kx + k'x' \\ y' &= -k'x + kx' \end{aligned} \quad (2.2)$$

where the coefficients have been made real by adjusting the time origins of x , x' , y , and y' . The energy conservation requests that

$$k^2 + k'^2 = 1 \text{ or } k' = \sqrt{1 - k^2}. \quad (2.3)$$

In quantum-mechanical measurements, x' includes zero-point fluctuations even in the ground state of the lowest energy.

"If we further assume that x' and y' are coordinates of harmonic oscillators having the same natural frequency, the pair of coordinates (x, x') may be thought of as representing a two-dimensional (isotropic) oscillator. Likewise (y, y') may represent the coordinates of a two-dimensional oscillator. We now see that actually these two two-dimensional oscillators are identical and that (2.2) is a coordinate transformation relating these two pairs of coordinates."

In quantum mechanics x , x' , y , and y' are regarded as annihilation operators, while their hermitian conjugates are creation operators. They satisfy commutation relations:

$$[x, x^\dagger] = 1, \quad [x', x'^\dagger] = 1, \quad [x', x^\dagger] = 0$$

and similar commutation relations for y , and y' . These relations are inconsistent with (2.1) except when $k = 1$, so that we should use (2.2) and (2.3).

Now an amplifier is represented by assuming that k is larger than 1. Thus k' must be imaginary from (2.3), since $k^2 > 1$. If we shift time origins for x and y by $\pi/4\omega$ and those of x' and y' by $-\pi/4\omega$, the relations for an amplifier can be written with real coefficients k and k' in the form

$$\begin{aligned} y &= kx + k'x' \\ y' &= k'x + kx' \end{aligned} \tag{2.4}$$

and

$$k^2 - k'^2 = 1, \text{ or } k' = \sqrt{k^2 - 1}. \tag{2.5}$$

Quantum-mechanical interpretation for (2.4) requires that, while x and y are annihilation operators, x' and y' are not annihilation but creation operators. This situation is related to the negative temperature in the laser and the effective negative energy quanta in the amplifier.

§3. Wave Packet for a Parametric Oscillator

"The characteristic property of a degenerate parametric amplifier is its phase-locking property. In other words, it amplifies one vector component, say, the cosine component of a sinusoidal input signal, while it attenuates the quadrature (sine) component. This unique property of degenerate parametric amplification will be discussed from a quantum-mechanical standpoint.

Instead of employing the more customary approach using a molecular model of the nonlinear optical system based on the higher-order perturbation theory, we will take a simple classi-

cal model of a harmonic oscillator having a time-varying force constant and to try to solve the corresponding Schrödinger equation. While such a model seems to have little resemblance to the multiple quantum transition scheme of parametric action, the property of wave equations obtained for such a variable parameter system would be an interesting problem in quantum mechanics which can be solved rigorously."

The Schrödinger equation for a harmonic oscillator with an effective mass m is expressed as

$$i\hbar \frac{\partial \psi}{\partial t} = -\frac{\hbar^2}{2m} \frac{\partial^2 \psi}{\partial x^2} + \frac{K}{2} x^2 \psi \quad (3.1)$$

where $K = m\omega^2$ will be modulated in a parametric oscillator. Equation (3.1) is known to have a solution which represents a wave packet in the form

$$\psi = \exp(-ax^2 + bx + c) \quad (3.2)$$

where a, b , and c are functions of time. We find

$$|\psi|^2 = \exp[-2(\text{Re } a)x^2 + 2(\text{Re } b)x + 2(\text{Re } c)] \quad (3.3)$$

so that the width of this Gaussian distribution is

$$\Delta x = (4\text{Re } a)^{-1/2} \quad (3.4)$$

and the position of the maximum probability is given by

$$x_m = \frac{\text{Re } b}{2 \text{Re } a} \quad (3.5)$$

Let us put (3.2) into the Schrödinger equation (3.1). Then we obtain

$$2i\hbar m(-\dot{a}x^2 + \dot{b}x + \dot{c}) = -\hbar^2(4a^2x^2 - 4abx + b^2 - 2a) + mKx^2.$$

Since both sides are polynomials of the second order in x , we obtain a set of equations as follows:

$$2i\hbar m \dot{a} = 4\hbar^2 a^2 - mK \quad (3.6)$$

$$2im \dot{b} = 4\hbar ab \quad (3.7)$$

$$2im \dot{c} = \hbar(2a - b^2) \quad (3.8)$$

Now if we write

$$a = -\frac{im}{2\hbar} \frac{\dot{\xi}}{\xi} \quad (3.9)$$

we obtain

$$m \ddot{\xi} = -K\xi \quad (3.10)$$

which is exactly the classical equation of harmonic oscillation when K is constant.

To obtain x_m and ψx , we have to calculate $\text{Re } a$ and $\text{Re } b$. We find

$$\text{Re } \dot{a} = \frac{\hbar}{im} a^2 + \text{c.c.} = \frac{4\hbar}{m} (\text{Re } a)(\text{Im } a) \quad (3.11)$$

from (3.6), and

$$\frac{1}{4i} \frac{d}{dt} |\xi|^2 = \dot{\xi} \xi^* + \text{c.c.} = \frac{2i\hbar m}{m} \xi^2 + \text{c.c.} = -\frac{4\hbar}{m} \xi^2 \text{Im } a \quad (3.12)$$

from (3.9). Equations (3.11) and (3.12) give

$$\frac{d}{dt} (|\xi|^2 \text{Re } a) = 0$$

so that

$$|\xi|^2 \text{Re } a = C_1 \quad (3.13)$$

where C_1 is a constant.

Equation (3.7) is solved by using (3.9)

$$\frac{\dot{b}}{b} = -\frac{\dot{\xi}}{\xi}$$

to give

$$b = C_2 / \xi. \quad (3.14)$$

Here the integration constant C_2 is related to the unit for measuring the magnitude of $\dot{\xi}$.

Equation (3.5) is then written as

$$x_m = \frac{C_1 \operatorname{Re} \dot{\xi}}{|\xi|^2 \operatorname{Re} a} = \frac{C_2}{2C_1} \operatorname{Re} \xi.$$

If we take $2C_1 = C_2$ for convenience, the center of the oscillating wave packet is given by

$$x_m = \operatorname{Re} \dot{\xi}. \quad (3.15)$$

Now a parametric oscillator can be represented by using

$$K(t) = m\omega^2[1 + 2q\cos 2\omega't] \quad (3.16)$$

where ω is the natural frequency of oscillation for $q = 0$. We will treat the simplest case of resonant excitation from $t = 0$ to t_1 , when $\omega' = \omega$ and $q \ll 1$. The general solution of (3.10) for $q = 0$, when $t < 0$ or $t_1 < t$, is written in the form

$$\xi = A_1 e^{i\omega t} + A_2 e^{-i\omega t}. \quad (3.17)$$

We obtain

$$\begin{aligned} (\Delta x)^2 &= \frac{k}{m} \left(\frac{\dot{\xi}}{\xi} - \text{c.c.} \right)^{-1} \\ &= \frac{k}{2m\omega} \frac{|A_1|^2 + |A_2|^2 + A_1 A_2^* e^{2i\omega t} + A_1^* A_2 e^{-2i\omega t}}{|A_1|^2 - |A_2|^2} \end{aligned} \quad (3.18)$$

from (3.4) and (3.9).

We see that harmonic oscillation of a wave packet with a constant width corresponds to the case $A_2 = 0$ and

$$\dot{\xi} = A_1 e^{-\omega t} \quad (3.19)$$

so that the locus of ξ becomes a circle.

"The form (3.17) obviously applies to the part $t < 0$ as well as to the part $t > t_1$. If we use A_1, A_2 to denote the coefficient values valid before amplification (i.e., $t \leq 0$) and B_1, B_2 to denote the values valid after amplification ($t \geq t_1$), then we must have a linear relation

$$\begin{aligned} B_1 &= k_{11}A_1 + k_{12}A_2 \\ B_2 &= k_{21}A_1 + k_{22}A_2 \end{aligned} \quad (3.20)$$

which completely describes the characteristics of the amplification. Here we note that the relation (3.20) must give real final values of ξ if we give real initial values for ξ , since the differential equation has only real coefficients. Since real values of ξ correspond to the conditions $A_1^* = A_2$ and $B_1^* = B_2$, we put these in (3.20) and get the conditions

$$k_{22} = k_{11}^*, \quad k_{21} = k_{12}^* \quad (3.21)$$

for the transformation coefficients.

By properly shifting the time origins in both input and output independently, we can make the coefficients real and positive, so that (3.20) may become

$$\begin{aligned} B_1 &= kA_1 + k'A_2 \\ B_2 &= k'A_1 + kA_2 \end{aligned} \quad (3.22)$$

Invariance of the Wronskian, $|B_1|^2 - |B_2|^2 = |A_1|^2 - |A_2|^2$, requires that condition

$$k^2 - k'^2 = 1, \quad (3.23)$$

The relation (3.22) can be thought of as a canonical form of the input-output relation for a degenerate parametric amplifier. It is not only gives the relation for the center of distribution (mean value) but also gives the relation for the width (or variance)."

Let us apply (3.22) to an input wave packet corresponding to the coherent state of an optical signal as given by

$$\xi_0 = A_0 e^{i\omega t}. \quad (3.24)$$

From (3.18) its width is

$$\Delta x_0 = \sqrt{\frac{\hbar}{2m\omega}}. \quad (3.25)$$

Then the output is given from (3.22) by

$$\xi = kA_0 e^{i\omega t} + k'A_0 e^{-i\omega t} \quad (3.26)$$

and the width of the output wave packet is calculated from (3.18) to be

$$\Delta x = \Delta x_0 \sqrt{k^2 + k'^2 + 2kk' \cos 2\omega t}. \quad (3.27)$$

This shows how the width varies with time. Since $k' = \sqrt{k^2 - 1}$, we find that

$$\Delta x_{\max} / \Delta x_0 = k + \sqrt{k^2 - 1}$$

$$\Delta x_{\min} / \Delta x_0 = k - \sqrt{k^2 - 1} = \Delta x_0 / \Delta x_{\max}$$

The center position of the wave packet is obtained from

(3.15) to become

$$x_m = |\xi| \cos \phi \quad (3.28)$$

where ϕ is the phase angle of $\xi = |\xi| e^{i\phi}$. From (3.26) we obtain

$$|\xi|^2 = |A_0|^2 (k^2 + k'^2 + 2kk' \cos 2\omega t) \quad (3.29)$$

The signal-to-noise ratio of the output is hence written in the form

$$(S/N) = \frac{x_m}{\Delta x} = \frac{|A_0|}{\Delta x_0} \cos \phi \quad (3.30)$$

from (3.27, 28, and 29). Since $|A_0| = |\operatorname{Re} \xi|$ is the amplitude of the input signal and Δx_0 the input noise, the S/N of the output is equal to that of the input signal, provided that the output is observed at an instant when ξ becomes real ($\phi = 0$). It is ~~note~~ noted that the instant for the maximum value of S/N does not in general coincide with the instant of maximum deviation (maximum of $\operatorname{Re} \xi$).

"If we take a limit $\xi \rightarrow 0$, we obtain a pulsating wave packet whose center is at rest. In classical oscillators, parametric excitation has no effect whatever if it is initially at rest. In quantum-mechanical oscillators, on the contrary, the wave function can make a natural pulsating oscillation at a frequency twice the natural frequency of translatory oscillation, and application of parametric excitation at the frequency of this natural pulsating oscillation results in the

building-up of the pulsation, quite independently of the existence of translatory oscillation. The pulsation of wave packet may somehow be regarded as amplification of the zero-point fluctuation.

If there is a translatory oscillation, this will also build up (Fig. 2), and the ratio of the amplification of this translatory oscillation is just equal to the amplification of zero-point fluctuation if it has a proper phase, as we have shown.

If we use q_0 and p_0 instead of A_1 and A_2 , and q and p instead of B_1 and B_2 , using the relations

$$\begin{aligned} q_0 &= A_1 + A_2, & p_0 &= i\omega m(A_1 - A_2) \\ q &= B_1 + B_2, & p &= i\omega m(B_1 - B_2), \end{aligned} \quad (3.31)$$

then (3.22) are transformed to

$$\begin{aligned} q &= (k + k')q_0 \\ p &= (k - k')p_0. \end{aligned} \quad (3.32)$$

Obviously, q_0 and q have the meaning of the coordinates, and p_0 and p the velocities or momenta, at the specified instant.

It would be appropriate at this point to make some remarks from the standpoint of quantum-mechanical measurement.

In quantum mechanics, measurements of the cosine and sine components of oscillation may be regarded as the measurement of coordinate q and the momentum p , respectively. In fact a harmonic oscillator is a system in which the roles of q and p are constantly being interchanged, but we can define a measurement of q and p by specifying a fixed time point to make the

measurement.

Our results are in good accord with the uncertainty principle. The input-output relations (3.22) satisfy

$$\Delta q \Delta p = \Delta q_0 \Delta p_0 \quad (3.33)$$

since $k^2 - k'^2 = 1$. In the absence of input signal we have $\Delta q_0 = \Delta x_0$ and $\Delta p_0 = \omega m \Delta x_0$, where Δx_0 is given by (3.25) so that we can find

$$\Delta q \Delta p \geq \omega m (\Delta x_0)^2 = \hbar/2 \quad (3.34)$$

which is exactly the uncertainty relation.

From what has been said, we may regard the degenerate parametric amplifier as a practical method of observing either q or p with arbitrary accuracy. We have seen that, in the degenerate parametric amplifier, the minimum noise just equals the zero-point fluctuation multiplied by the amplification factor, so that no deterioration of S/N ratio results. This is in contrast to the case of an ordinary amplifier where noise was $\sqrt{2k^2 - 1}$ times the zero-point fluctuation, and for large k we have a 3-dB deterioration of the S/N ratio, and it is of some interest to study this point in some detail.

Apparently, this 3-dB difference may be regarded as a compensation for the loss of information on the quadrature component in the degenerate parametric amplifier. In order to make the argument convincing we take the following model (Fig. 3).

We have two degenerate parametric amplifiers, the q -amplifier and p -amplifier, which will be used for amplifying the two com-

ponents separately. The input signal coming into a waveguide is divided using an ideal branch and is fed into these amplifiers. Their outputs are again combined using another branch, so that we have an output which would appear as if an output of an ordinary amplifier. What would be the overall S/N ratio of this whole system?

Let the input power S/N be a^2 (with respect to quantum noise). At the input of each amplifier, we would have an S/N ratio of $a^2/2$, since the signal power is halved by the branching, while the noise remains the same. Or we can say that noise power is also halved, but the same amount of noise power is added that comes from the blind guide. The output branch would also cause a minimum power loss of 3dB, but this is immaterial for the S/N consideration since we now have a sufficiently strong signal. Hence we see that over-all S/N ratio is 3dB less than a single phase-locking amplifier, that is, just equal to an ordinary amplifier."

§4. Conclusion

We have seen that the degenerate parametric oscillator allows us to measure either the cosine component q or the sine component p of a coherent wave with any accuracy within the limit of the uncertainty relation $\Delta q \Delta p = \hbar/2$.

Furthermore, photon interpretation of parametric excitation and the probability distribution of photon numbers in the case of a degenerate parametric amplifier were discussed in detail in ref. 1), pp. 284-291.

At the time when Professor Takahasi proposed in 1963 that the quantum noise could be squeezed in degenerate parametric oscillation, no optical parametric oscillation had been achieved. Although the optical parametric oscillator was believed to be realizable, the required driving power was believed to be too high at that time to consider any application to low-noise measurements.

References

- 1) H. Takahasi: *Kagaku* 33(1963)434-439. (in Japanese)
- 2) H. Takahasi: *Advances in Communication Systems*, vol. 1 (1965) pp. 227-310.

Figure Captions

Fig.1 Schematic diagram of an attenuator or a linear amplifier

Fig.2 Parametric amplification of a wave packet. Note that S/N ratio is unchanged at the peak points.

Fig.3 Combination of two phase-locking amplifiers; equivalent to an ordinary amplifier.

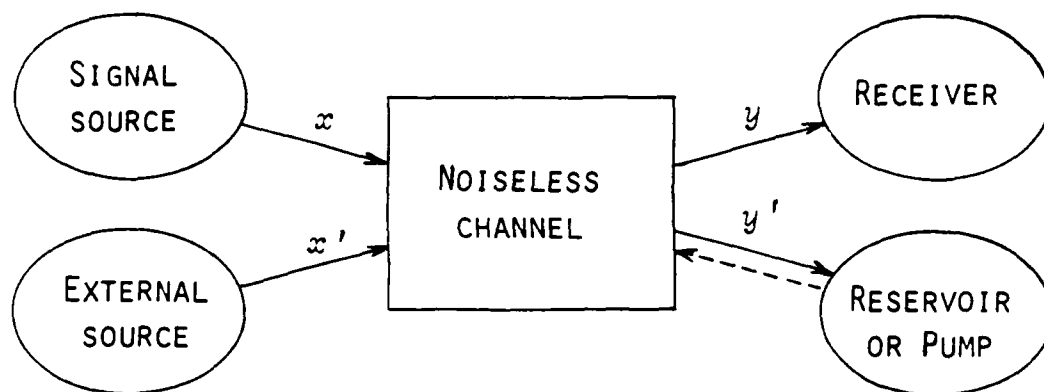


Fig.1 Schematic diagram of an attenuator
or a linear amplifier

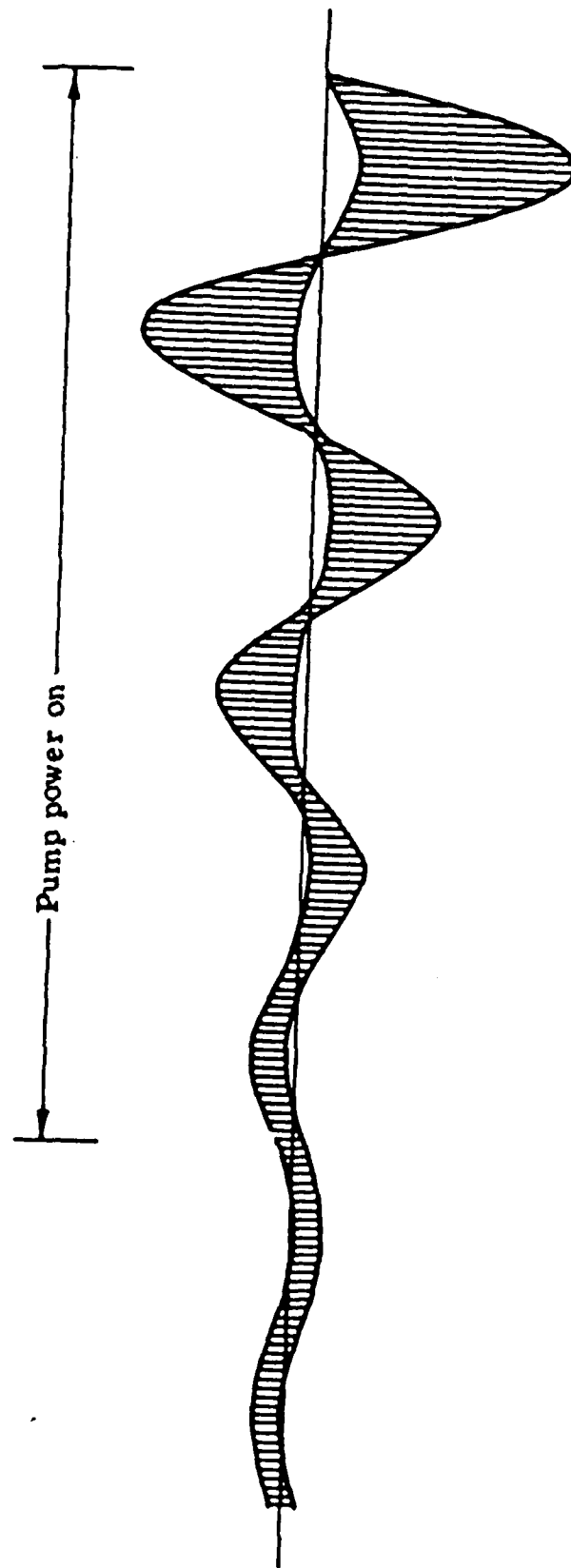


Fig.2 Parametric amplification of a wave packet. Note that S/N ratio is unchanged at the peak points.

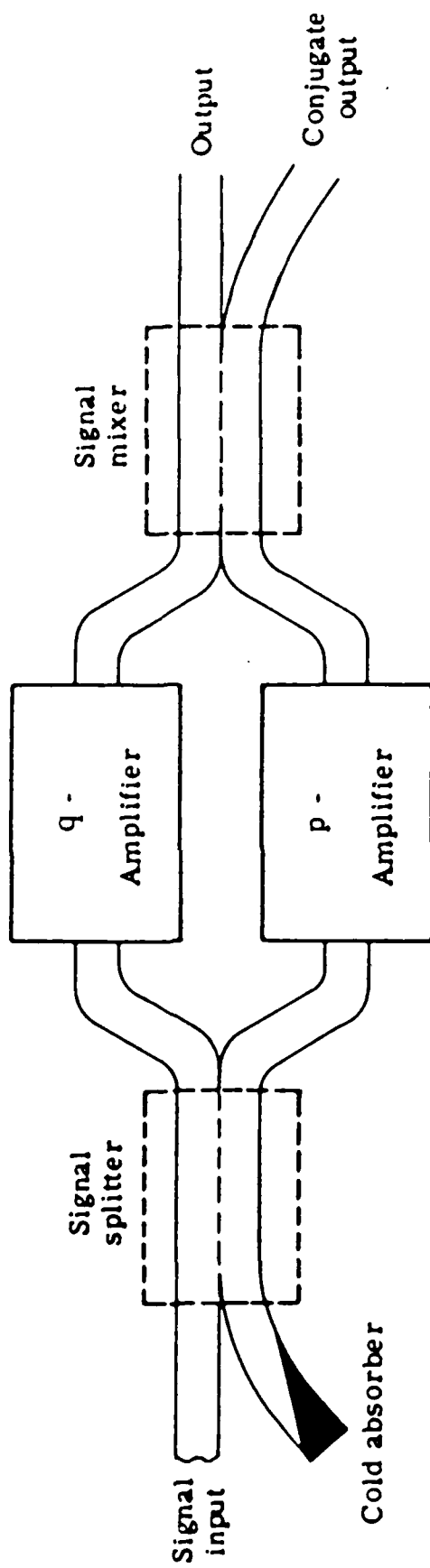


Fig.3 Combination of two phase-locking amplifiers; equivalent to an ordinary amplifier.

Squeezed States of Light

H.J. Kimble, R.J. Brecha, L.A. Orozco, M.G. Raizen,
L.A. Wu, and M. Xiao
Department of Physics
University of Texas at Austin
Austin, Texas 78712

Summary

In our laboratory squeezed states of light have been generated in two distinct physical systems. The first experiment investigates squeezing for two-level atoms coupled to the intracavity field of a high quality optical resonator. For large coupling of the atoms to the cavity field, there is a mode splitting in the eigenvalue structure of the system analogous to the splitting found when two otherwise independent pendulums are coupled by a spring. We employ the coupling-induced structure of the composite system to generate squeezing (1-3). The second experiment involves the process of degenerate parametric down conversion in which a photon of frequency 2ω is split into a correlated pair of photons at the subharmonic frequency ω . While we have observed noise reductions of greater than 60% relative to the vacuum-state limit, a quantitative analysis of the various propagation and detection losses in the current apparatus indicates that the field would in fact be squeezed more than ten-fold in the absence of these losses. Quite recently we have made use of the squeezed light to demonstrate that precision measurements can be made with a sensitivity greater than that given by the vacuum-state or shot-noise limit.

References

1. M.G. Raizen, L.A. Orozco, Min Xiao, T.L. Boyd, and H.J. Kimble, "Squeezed-state Generation by the Normal Modes of a Coupled System", Phys. Rev. Letter 59, 198 (1987).
2. L.A. Orozco, M.G. Raizen, Min Xiao, R.J. Brecha, and H.J. Kimble, "Squeezed State Generation in Optical Bistability", J. Opt. Soc. Am. B (October, 1987).
3. Min Xiao, H.J. Kimble and H.J. Carmichael, "Squeezed State Generation for Two-Level Atoms in a Spatially Varying Field Mode", J. Opt. Soc. Am. B (October, 1987).
4. L.A. Wu, H.J. Kimble, J.L. Hall, and Huifa Wu, "Generation of Squeezed States by Parametric Down Conversion", Phys. Rev. Lett. 57, 2520 (1986).
5. L.A. Wu, Min Xiao, and H.J. Kimble, "Squeezed States of Light from an Optical Parametric Oscillator", J. Opt. Soc. Am. B (October, 1987).
6. Min Xiao, L.A. Wu, and H.J. Kimble, "Precision Measurement Beyond the Shot-Noise Limit", Phys. Rev. Lett. 59, 278 (1987).

PULSED SQUEEZED LIGHT

Talk by R. E. Slusher
U.S./Japan Conference
7/22/87

Generation of interesting quantum states of light, including squeezed states and number states, requires a large nonlinear interaction (or nonlinear phase shift $\Delta\phi_{NL}$). At the same time, the length of the nonlinear generating medium must be short enough so that there is very small loss, $\alpha\ell \ll 1$ where α is the linear absorption constant and ℓ is the effective length of the nonlinear medium. A pulsed pump field can be used in many nonlinear systems to obtain high peak powers and the nonlinear phase shifts $\Delta\phi_{NL} \sim 1$ required for quantum light states in media which are sufficiently short to obtain $\alpha\ell \ll 1$. There is also a broader range of high-intensity laser pump sources available in a pulsed mode. This talk describes an extension of standard generation and homodyne detection experimental techniques to the pulsed case. An earlier paper referenced in VU-1 described the theory upon which these experiments are based. It is expected that by using mode-locked pulse trains as the pump laser and a portion of the pulse train as the local oscillator for the homodyne detector that squeezing can be observed which is comparable to the CW case but which corresponds to generation by the **peak** laser pump intensity in the pulse train. No cavity is required in cases where the peak pump intensity is sufficiently large. This allows squeezing over very large bandwidths limited only by phase-matching conditions in the nonlinear medium.

A number of interesting quantum phenomena may be associated with pulsed conditions including quantum noise on soliton pulses propagating in optical fibers, free electron nonlinearities, pulsed communications or data processing systems and short time scale measurements. An example of short time scale measurements is interferometry where the shot noise limit will be a dominant limitation at very short times (\sim ps or fs) when there are very few photons per pulse.

Viewgraphs 3 through 6 describe the analysis of pulsed squeezing. As shown in VU-6, the optimum noise reduction in the Gaussian pulse envelope approximation is only slightly reduced from the CW case or the case when the local oscillator pulse length $\tau_{LO} \ll \tau_p$ the pump pulse length.

Viewgraphs 7 and 8 describe a pulsed LO homodyne detector which is working at present. Limits due to amplifier and photodiode saturation restrict the dynamic range of this detector. A balancing network between the photodiodes and the amplifier reduces the amplifier saturation problem.

Experiments in progress are described in VU 9-12. GAWBS noise in the glass fiber experiment is still a problem in the pulse case, since this extra phase modulation noise scales with the peak pump power. A parametric down-conversion experiment using KTP will probably allow a demonstration of pulsed squeezing but the noise reduction is not expected to be spectacular.

The talk concludes with a short discussion of pulsed measurement of interference in phase space (VU 13) and a summary. A paper on this topic is in preparation and will be available this fall.

PULSED SQUEEZING

- I. Why Pulsed?
- II. Generation of Pulsed Squeezed Light
- III. Homodyne Detection
- IV. Experiments
 - A. Detector
 - B. Glass Fiber
 - C. Bananas
 - D. KTP

Collaborators: Experiment – Philippe Grangier
Arthur LaPorta

Theory – Bernard Yurke
Mary Potasek

PRA 35, 3586 (1987)

TOP
DO NOT AFFIX OVERLAYS ALONG THIS SURFACE

VU-1



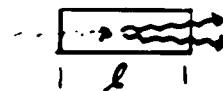
AT&T BELL LABORATORIES

SEQUENCE NO. _____

VG. NO. _____

I. Nonlinear-Gain/Linear-Loss Increased

→ More Squeezers



$$\alpha l \ll 1$$

$$\Delta\phi_{NL} \sim \frac{2\pi l}{2} \Delta n$$

$$\propto E_p$$

II. More Laser Pumps Achieve

$$\Delta\phi_{NL} \sim 1$$

III. No Cavity Required

→ Broad Band Squeezing

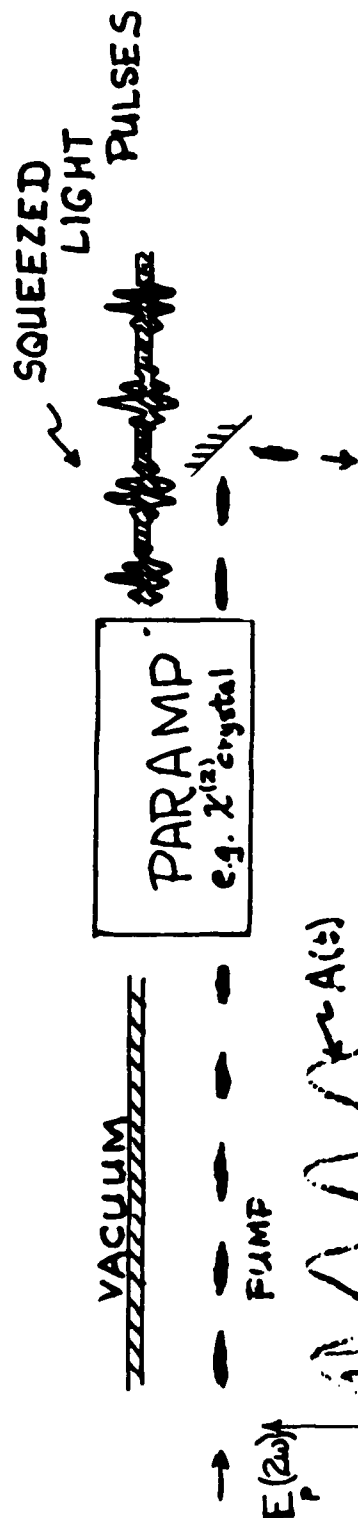
IV. Interesting Pulsed Phenomena

- Quantum Noise on Solitons In Optical Fibers
- FEL, TOK, etc.
- Atomic Radiation
- Communications Systems & Data Processing
- Short Time Scale Measurements

VU-2

TOP
DO NOT AFFIX OVERLAYS ALONG THIS SURFACE

GENERATION OF PULSED SQUEEZED LIGHT



VU-3

SQUEEZED FIELD: $E_s^{(+)}(0,t) = \epsilon_0 \int a(\omega) e^{-i\omega t} d\omega$

$$E_s^{(+)}(x,t) = \cosh \left[\frac{2K(t-x/v)x}{v} \right] E_s^{(+)}(0,t-x/v) - e^{-i\theta} \sinh \left[\frac{2K(t-x/v)x}{v} \right] E_s^{(-)}(0,t-x/v)$$

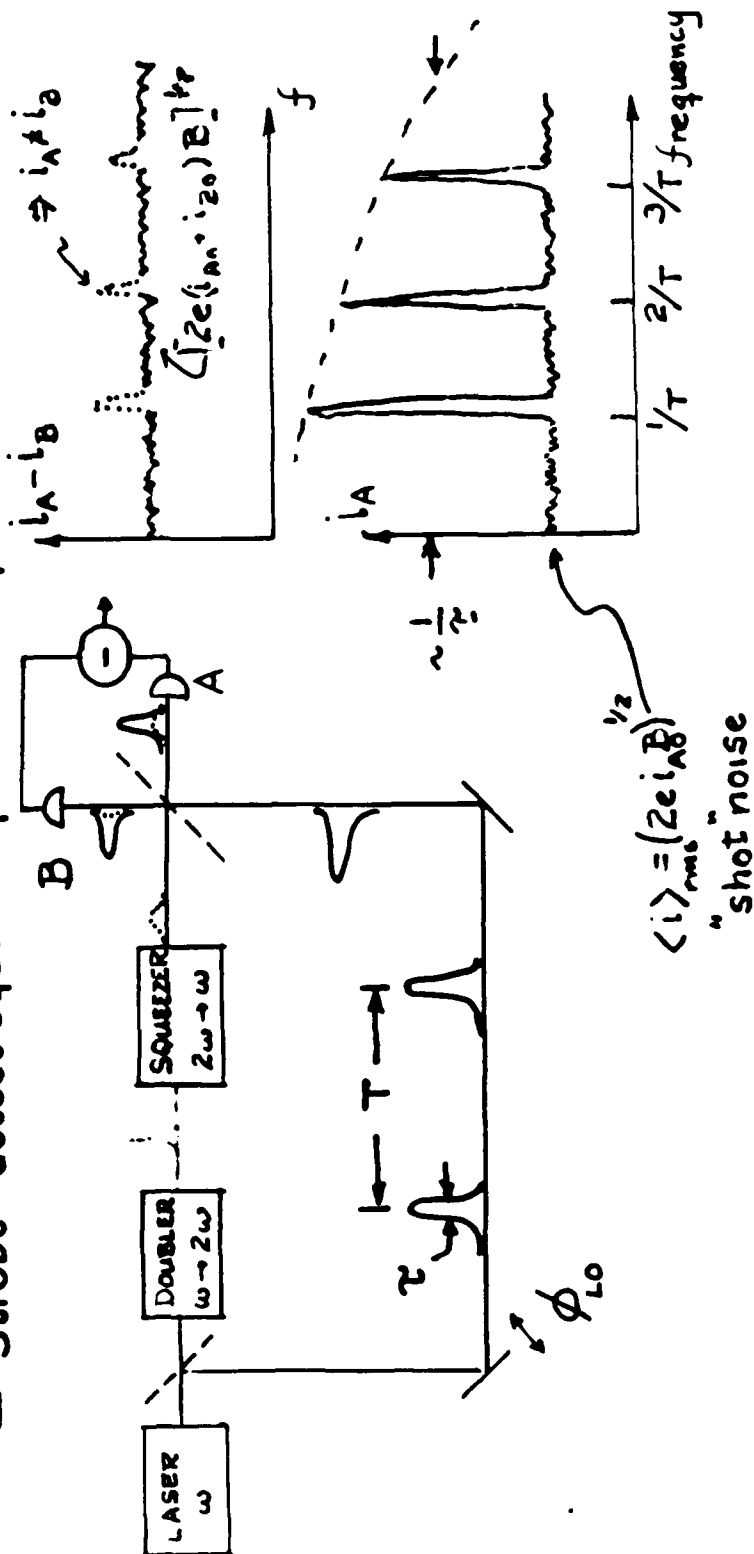
WHERE NONLINEAR PHASE SHIFT:

$$\Delta\phi_{NL}(t) \sim \omega_0 K(t) \sim \chi_{NL} A(t) \sim 1 \Rightarrow \text{LARGE SQUEEZING}$$

TOP
DO NOT AFFIX OVERLAYS ALONG THIS SURFACE

HETERODYNE DETECTION FOR PULSED SQUEEZED LIGHT

— "Strobe" detect squeezed pulses with pulsed local oscillator



- VU-4

TOP
DO NOT AFFIX OVERLAYS ALONG THIS SURFACE

NOISE POWER SPECTRUM FOR PULSED SQUEEZED LIGHT

$$S_n(\omega)_{\text{Max Min}} = \frac{\int_{-T/2}^{+T/2} F_{L_0}^2(t) \exp[i2\Delta\phi_{NL}(t)] dt}{\int_{-T/2}^{+T/2} F_{L_0}^2(t) dt}$$

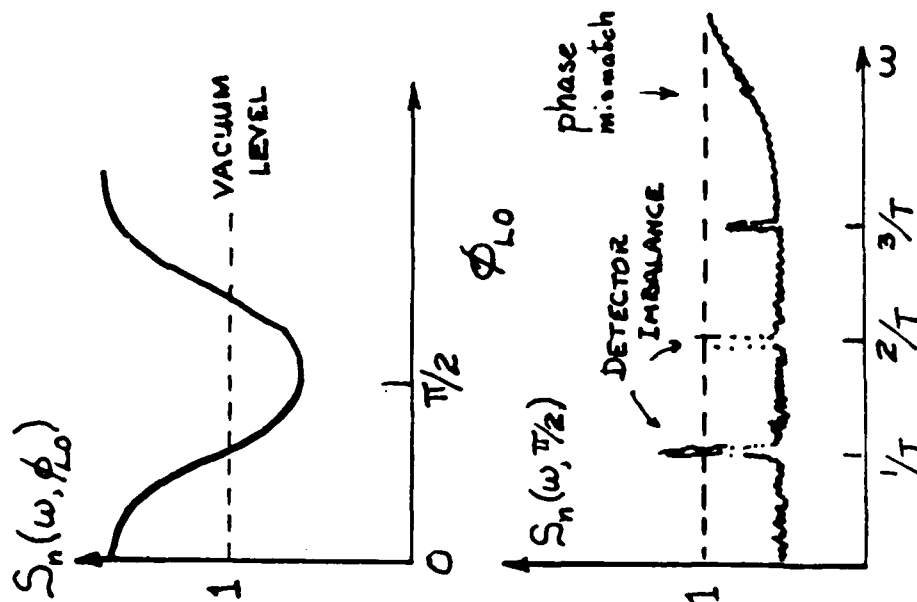
$$\Delta\phi_{NL}(t) = \Delta\phi_{NLO} \frac{A_P(t)}{A_{P0}}$$

PUMP AMPL. ENVELOPE

e.g. $F_{L_0}(t) = F_{L_0}(0) \exp(-t^2/2\sigma^2)$

Double for Pump

$$A_P(t) = A_{P0} \exp(-t^2/\sigma^2)$$

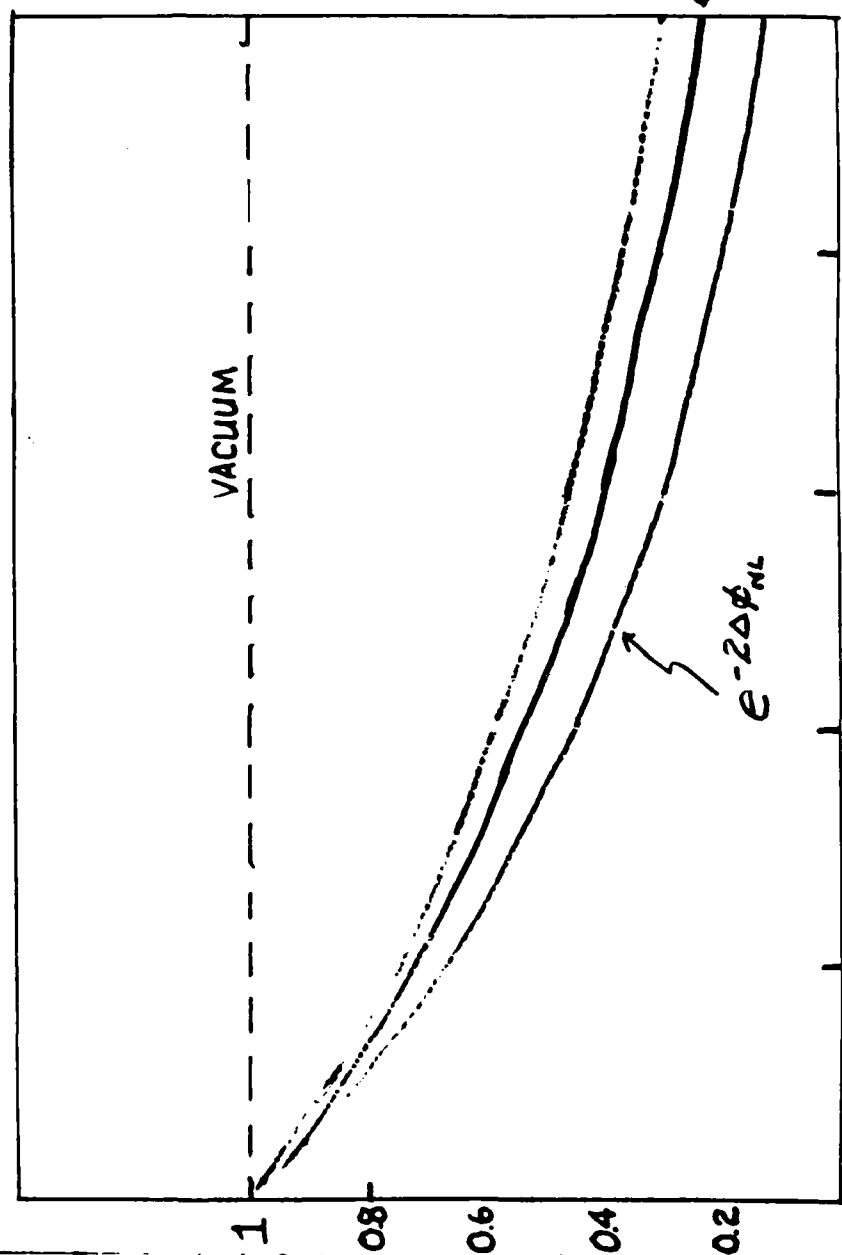


VU-5

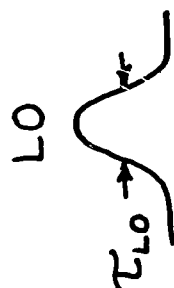
TOP
DO NOT AFFIX OVERLAYS ALONG THIS SURFACE

NOISE SQUEEZE

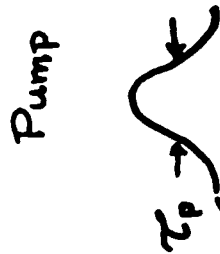
Noise
Power
 S_{min}



Pulse Shapes



VU-6



CW
or
 $\tau_{LO} \ll \tau_P$

$\tau \sim 160 \mu s$

100

$\langle P \rangle = 0.5 \text{ W}$

$P_0 = 20 \text{ mW}$

0.4

1

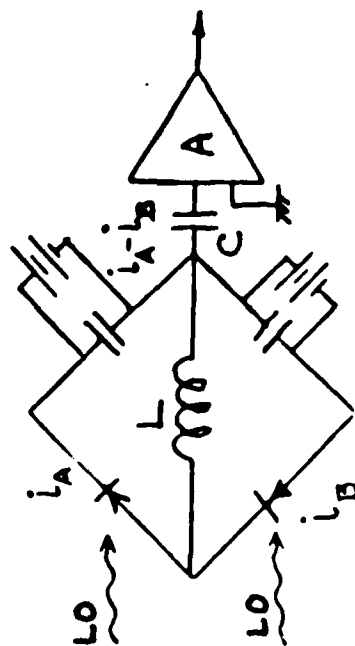
IND:YAG

LIMITS

- NO. 1000
- AMPLIFIER
- AMPLIFIER NOISE

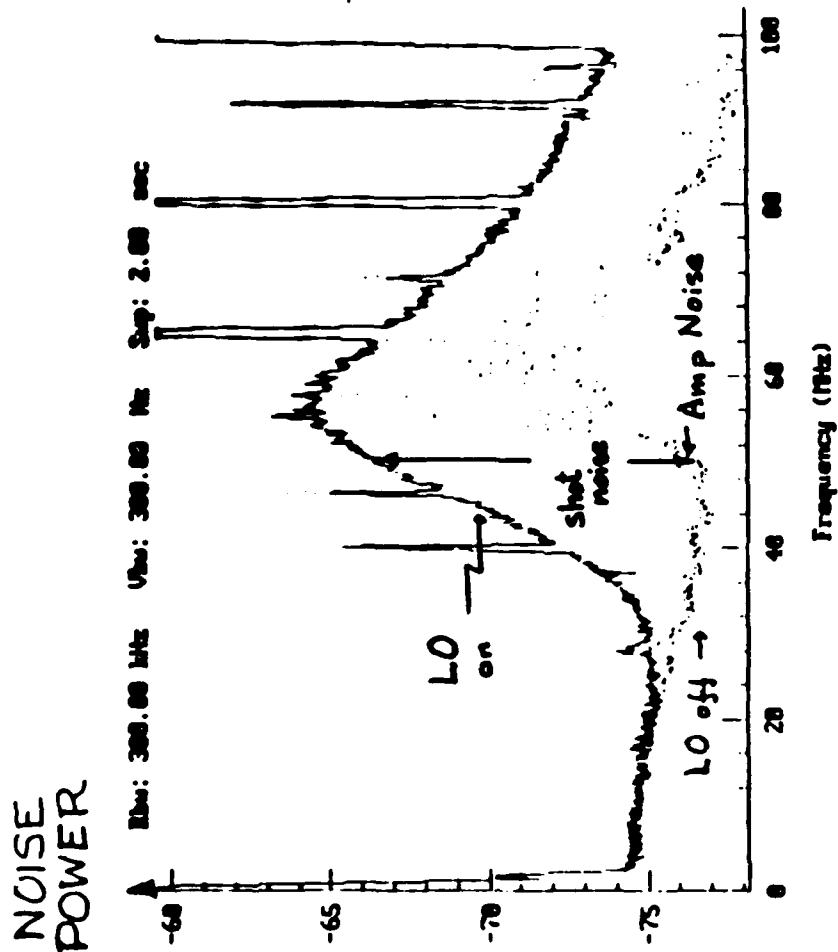
100/100

TOP
DO NOT AFFIX OVERLAYS ALONG THIS SURFACE



$$\omega_r \sim \frac{1}{\sqrt{LC}} \sim 50 \pm 10 \text{ MHz}$$

200 MHz pulse train
suppressed

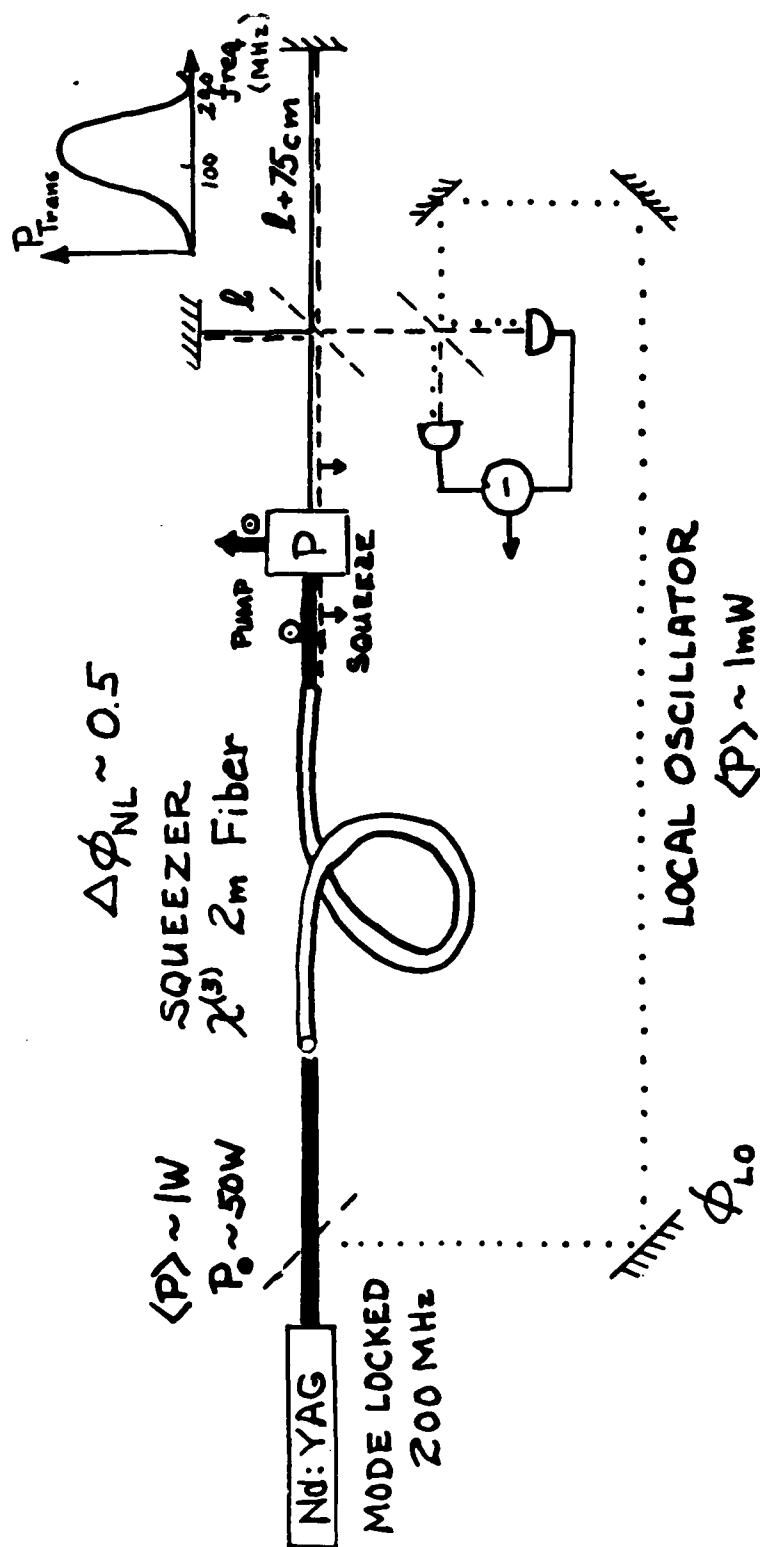


TOP
DO NOT AFFIX OVERLAYS ALONG THIS SURFACE

PHASED NOISE

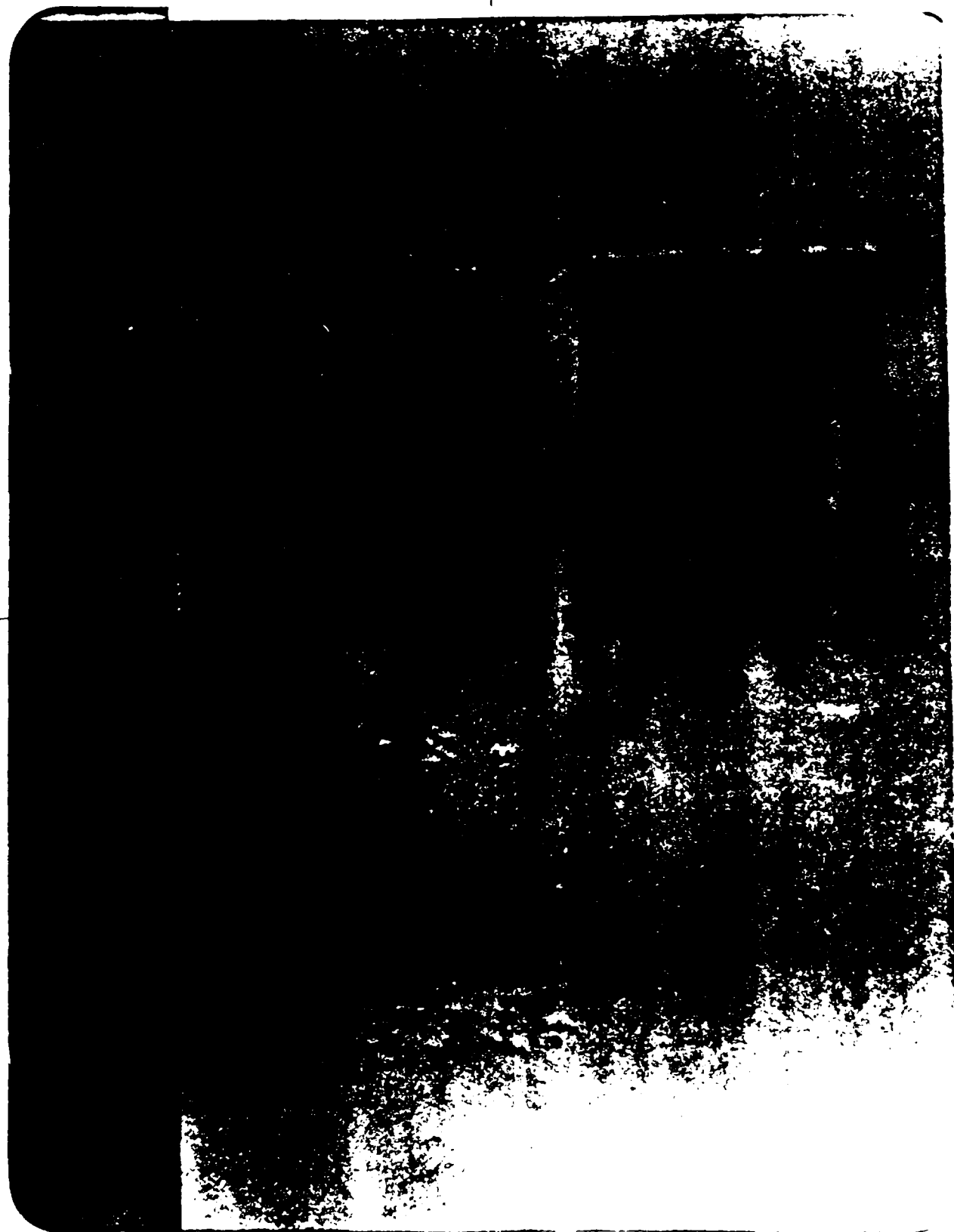
IN

GLASS FIBERS



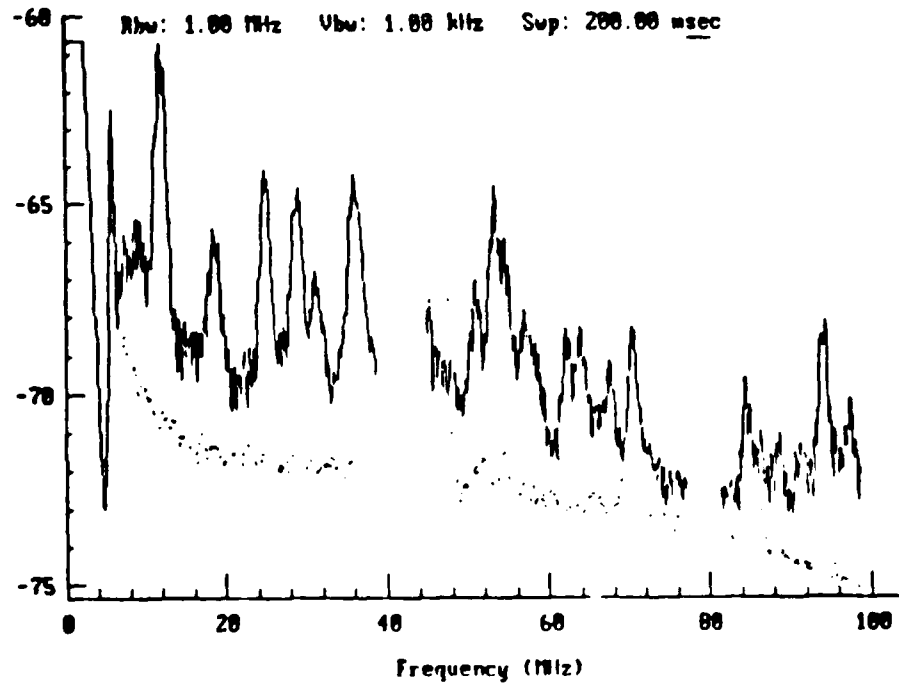
Top
DO NOT AFFIX OVERLAYS ALONG THIS SURFACE

(VU-10)

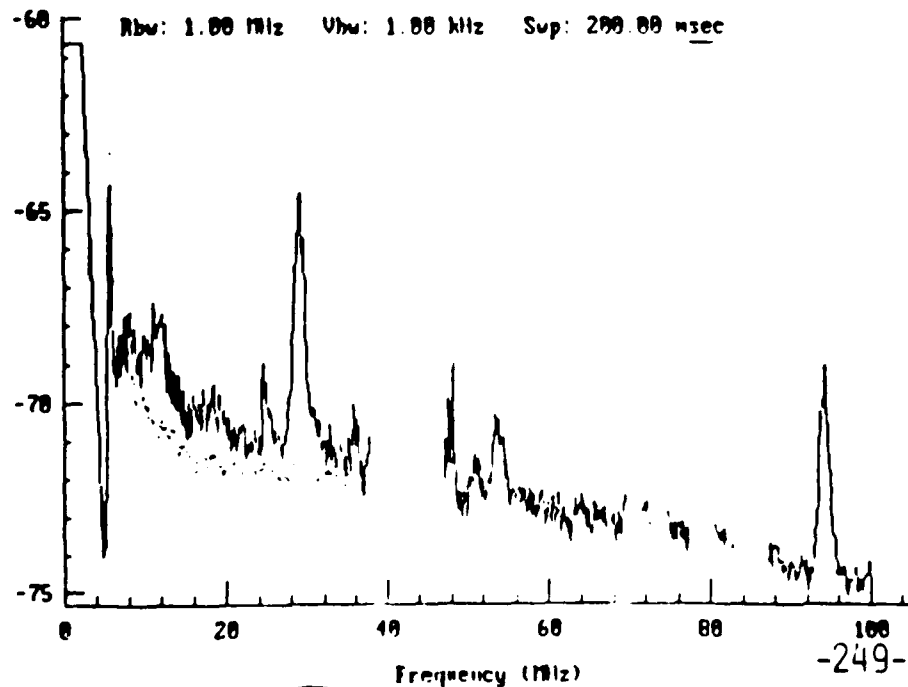


GLASS FIBER NOISE

PULSED



"CW"

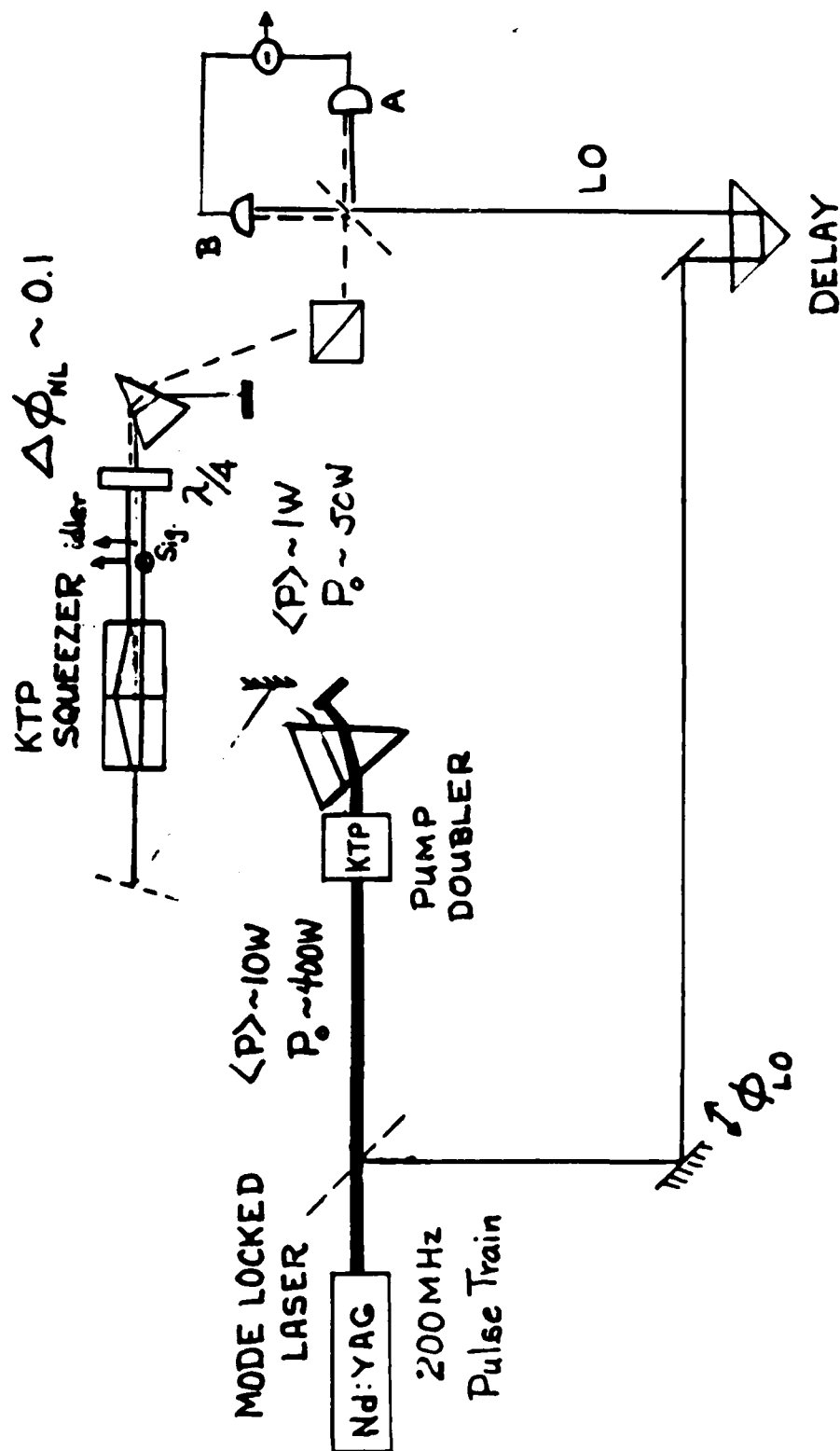


SEQUENCE NO. _____

(VU-11)

TOP
DO NOT AFFIX OVERLAYS ALONG THIS SURFACE

PRESENT EXPERIMENT



VU-12

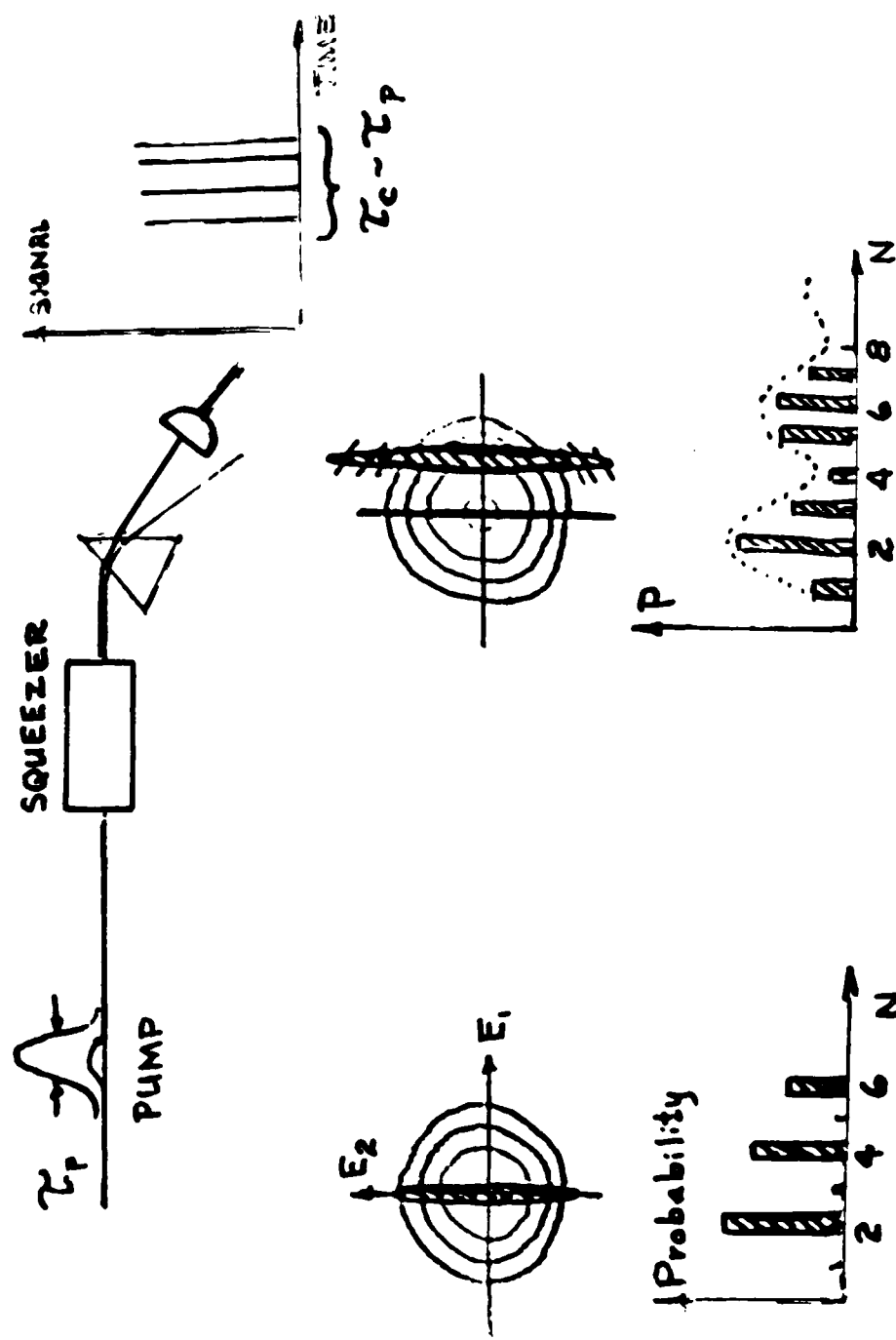
10-20% SQUEEZED NOISE REDUCTION
"POSSIBLE"



SEQUENCE NO. _____
 VG. NO. _____
 AT&T RESEARCH LABORATORIES

DIRECT DETECTION PULSED SQUEEZED LIGHT

VM-13



PULSED SQUEEZING SUMMARY

- I. Broader Spectral & Materials Range
 Accessible for Squeezed Light
- II. Homodyne Detection Works
- III. No Cavity \longrightarrow Broadband Squeezing
- IV. Applications
 - A. Quantum Noise on Solitons
 - B. Relativistic Electron Squeezing
 - C. Pulsed Atomic Excitation
 - D. Pulse Trains In Data Storage or Communications
 - E. Short Time Scale Precision Measurement

SEQUENCE NO. _____

VII-14

Quantum Nondemolition Detection and Squeezing in Optical Fibers

M.D. Levenson, R.M. Shelby, and S.H. Perlmuter

IBM Almaden Research Center
650 Harry Road
San Jose, CA 95120

The nonlinear optical interactions in an optical fiber permit the amplitude of one wave to be inferred from the phase of a coupled wave, and the partial suppression of quantum noise.

Conventional light detectors must destroy the quantum state of the electromagnetic field in order to measure its amplitude. They are Quantum Demolition detectors. The nonlinear index of refraction of an optical fiber permits one to infer the amplitude of one wave by measuring the light induced phase shift of a nonlinearly coupled wave. This process has been termed Quantum Nondemolition Detection or Back Action Evading Measurement. The amplitude of the first wave is unchanged by the interaction. That amplitude is the QND variable; the phase of the second wave is the QND readout. The uncertainty which quantum mechanics requires to be added to a system being measured appears in the phase of the first beam, not its amplitude, thus the back action is evaded.

We have demonstrated this effect by correlating the QND readout with a subsequent QDD measurement of the QND variable (1). We have demonstrated back action evasion by showing that the QND variable at the output of the detector has no greater noise than at the input - which was at the vacuum noise level.

When the correlated noise on two coupled laser beams is made to subtract coherently, the net noise level can be below the vacuum noise level. This effect has been termed "four-mode squeezing" since the fluctuations involve two sidebands of each of two strong pump waves (2). The noise on each beam can separately be above the vacuum noise level, but strong four mode correlations can lower the sum of the noise at two detectors to a value below the vacuum. Indeed, the correlations can be so strong that the noise on the two detectors can be less than that on one of them (3).

It is necessary to cool the optical fiber to 2K to suppress phase noise caused by light scattering in the optical fiber. The stimulated Brillouin effect must be suppressed by phase modulating the light to broaden the spectrum. The modulation frequency must be exactly equal to the mode spacing of the Fabry Perot interferometer needed to phase shift the carrier wave. Other experimental innovations are necessary to accurately measure the vacuum level and to maximize the effective quantum efficiency.

The same nonlinear interactions in an optical fiber give rise to conventional two-mode squeezing (4). The fluctuations in the amplitude of the beam cause correlated phase fluctuations of that beam. The nonlinear index of refraction cannot alter the amplitude of a wave. The correct superposition of amplitude and phase quadratures has been shown to have a noise level 12.5% below the vacuum level.

Squeezed light has the property that the ratio of noise to intensity rises as the light is attenuated (5). The squeezed light generated in an optical fiber is not a minimum uncertainty state as light scattering adds phase noise.

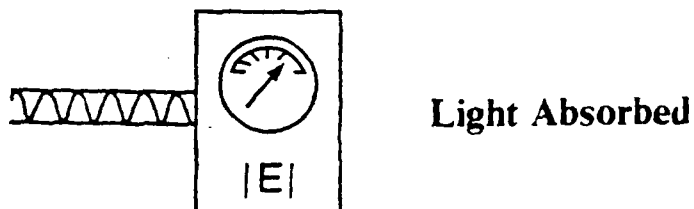
References:

1. M.D. Levenson, R.M. Shelby, M. Reid, and D.F. Walls, Quantum Nondemolition Detection of Optical Quadrature Amplitudes, *Phys. Rev. Lett.* 57, 2473 (1986).
2. B.L. Schumaker, S.H. Perlmuter, R.M. Shelby and M.D. Levenson, Four-Mode Squeezing, *Phys. Rev. Lett* 58, 357 (1987).
3. M.D. Levenson and R.M. Shelby, Four-Mode Squeezing and Applications, *Optica Acta* (to be published).
4. R.M. Shelby, M.D. Levenson, S.H. Perlmuter, R.G. DeVoe, and D.F. Walls, Broad-Band Parametric Deamplification of Quantum Noise in an Optical Fiber, *Phys. Rev. Lett* 57, 691 (1986).
5. G.J. Milburn, M.D. Levenson, R.M. Shelby, and D.F. Walls, On Optical Media for Squeezed State Generation, *J. Opt. Soc. Am* (to be published).

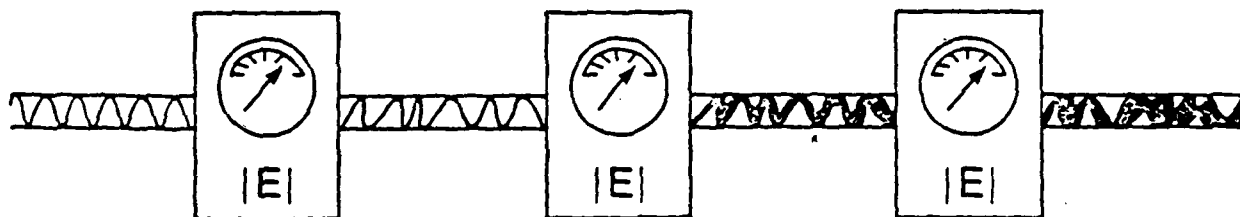
2

Conventional light detectors measure the amplitude of a light beam by absorbing photons and thus destroying the quantum state. They are QUANTUM DEMOLITION devices.

Quantum Demolition Detector (QDD)

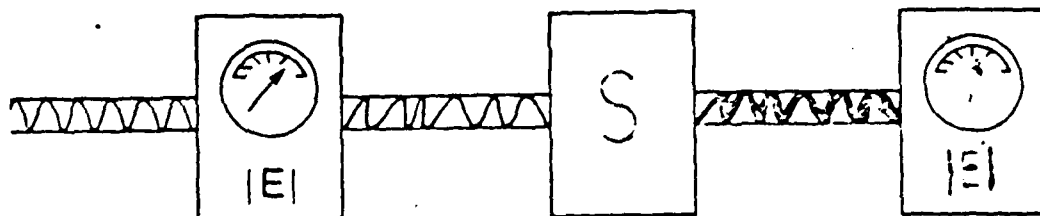


Quantum Nondemolition Detectors (QND)



No Absorption. Phase becomes more uncertain after each measurement.

Quantum Nondemolition Measurement System



A QND measurement system would allow small amplitude changes due to a sample to be determined by comparing before and after amplitudes. Such measurements can be more accurate than the shot noise limit.

3

Nonlinearity:

$$n(E) = n_0 + n_2 |E|^2$$

Phase:

$$\Phi(\ell) = 2\pi n(E)\ell/\lambda$$

Some Phase Fluctuations are Correlated With Amplitude Fluctuations

$$\delta\Phi_x(\ell) = \delta\Phi(0) + 4\pi n_2 |E_x| \delta E_x \ell / \lambda$$

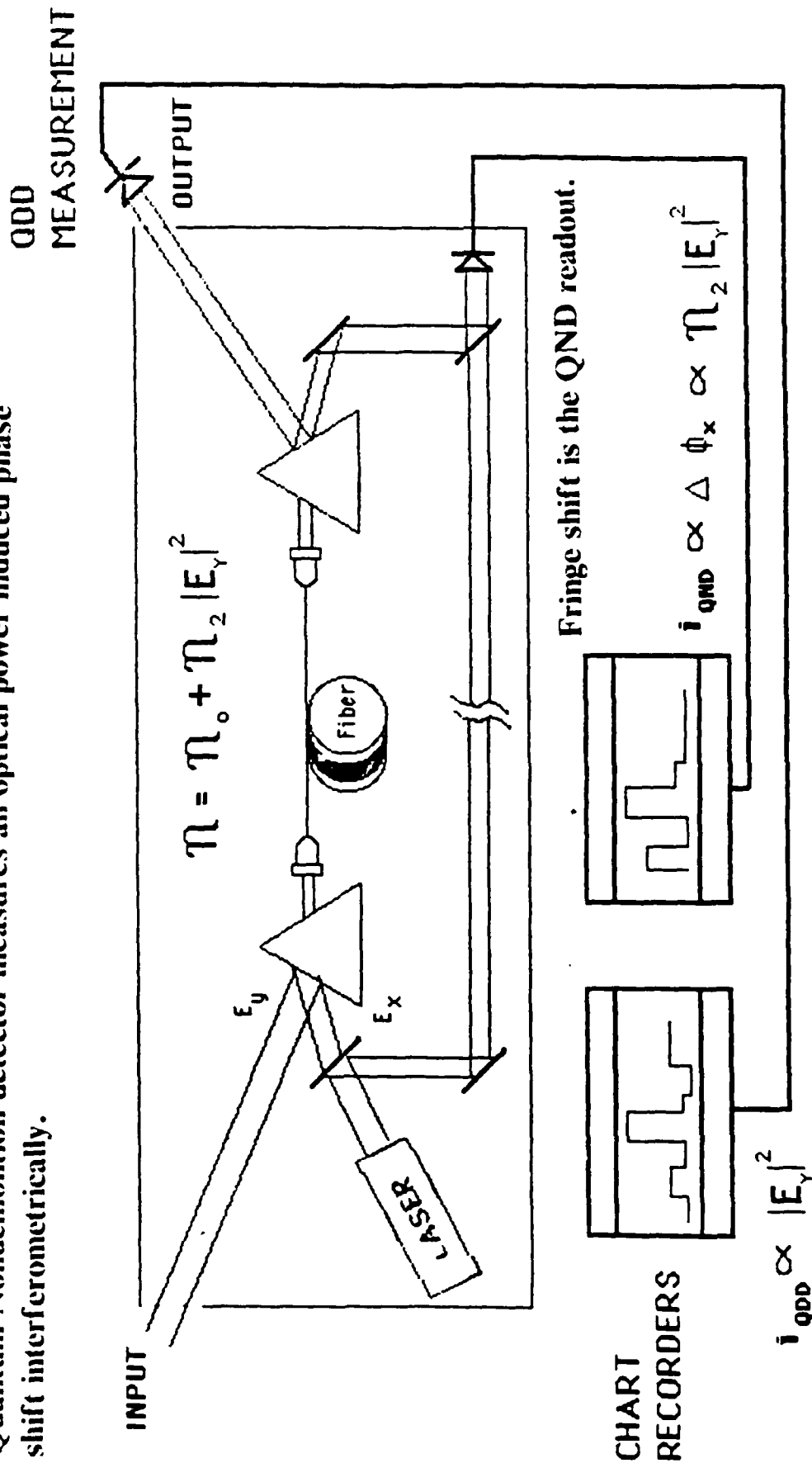
QND Experiments - There is Another Term

$$\delta\Phi_{xy}(\ell) = \delta\Phi_x(\ell) + 8\pi n_2 |E_y| \delta E_y \ell / \lambda$$

This Last Term is QND Readout

4

Quantum Nondemolition detector measures an optical power induced phase shift interferometrically.

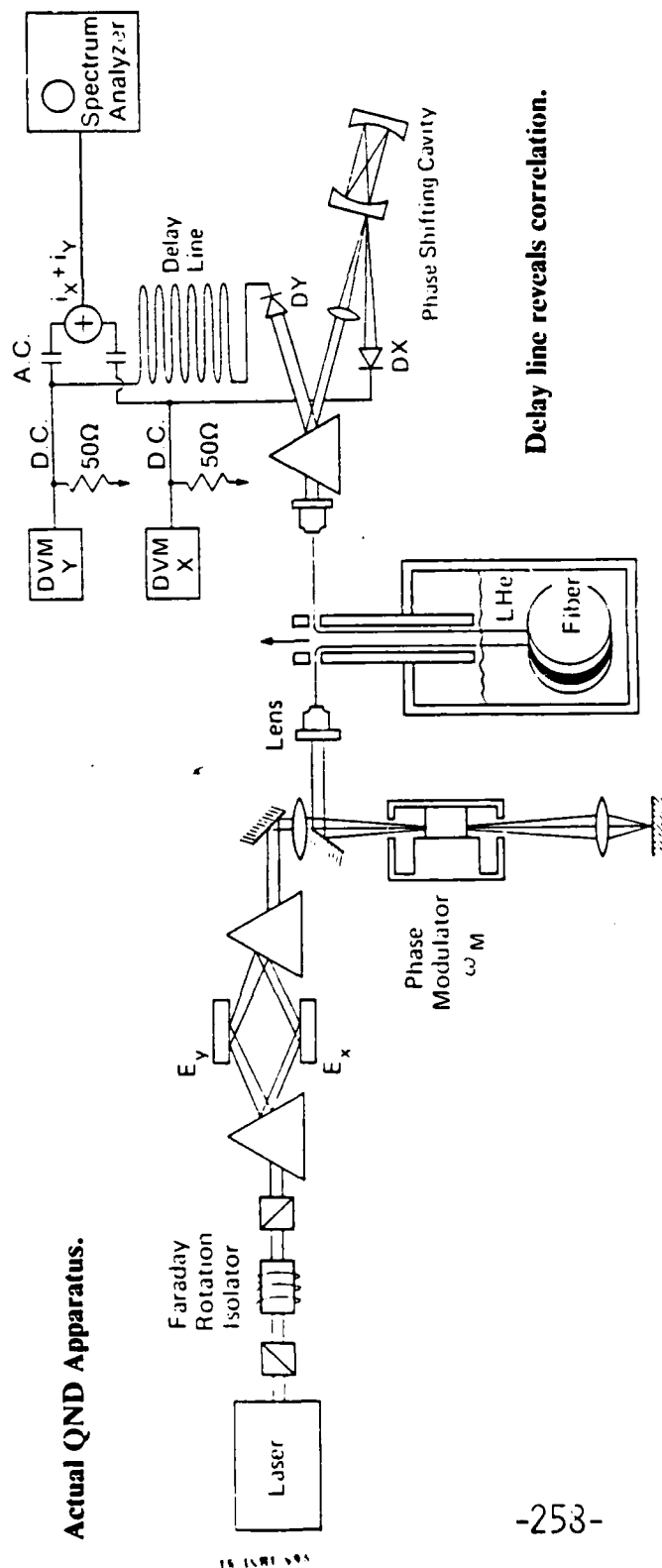


DO THEY CORRELATE ?

To verify that a QND measurement is valid, one must prove that it correlates with a quantum demolition measurement. To prove back action evasion, one must show that the fluctuations of the QND variable are no larger at the output of the QND meter than at the input. We have done both

The actual apparatus uses a coil of optical fiber as the nonlinear medium. It must be cooled to 2K to suppress phase noise caused by light scattering. The inputs must be phase modulated to suppress the stimulated Brillouin effect. At the output, the phase fluctuations of one beam are converted to amplitude fluctuations by a phase shifting cavity. Summing the delayed output of the QND readout detector DX with that of a QDD detector DY produces a signal level that varies sinusoidally with frequency - if the two signals correlate. The results are shown in the next figure.

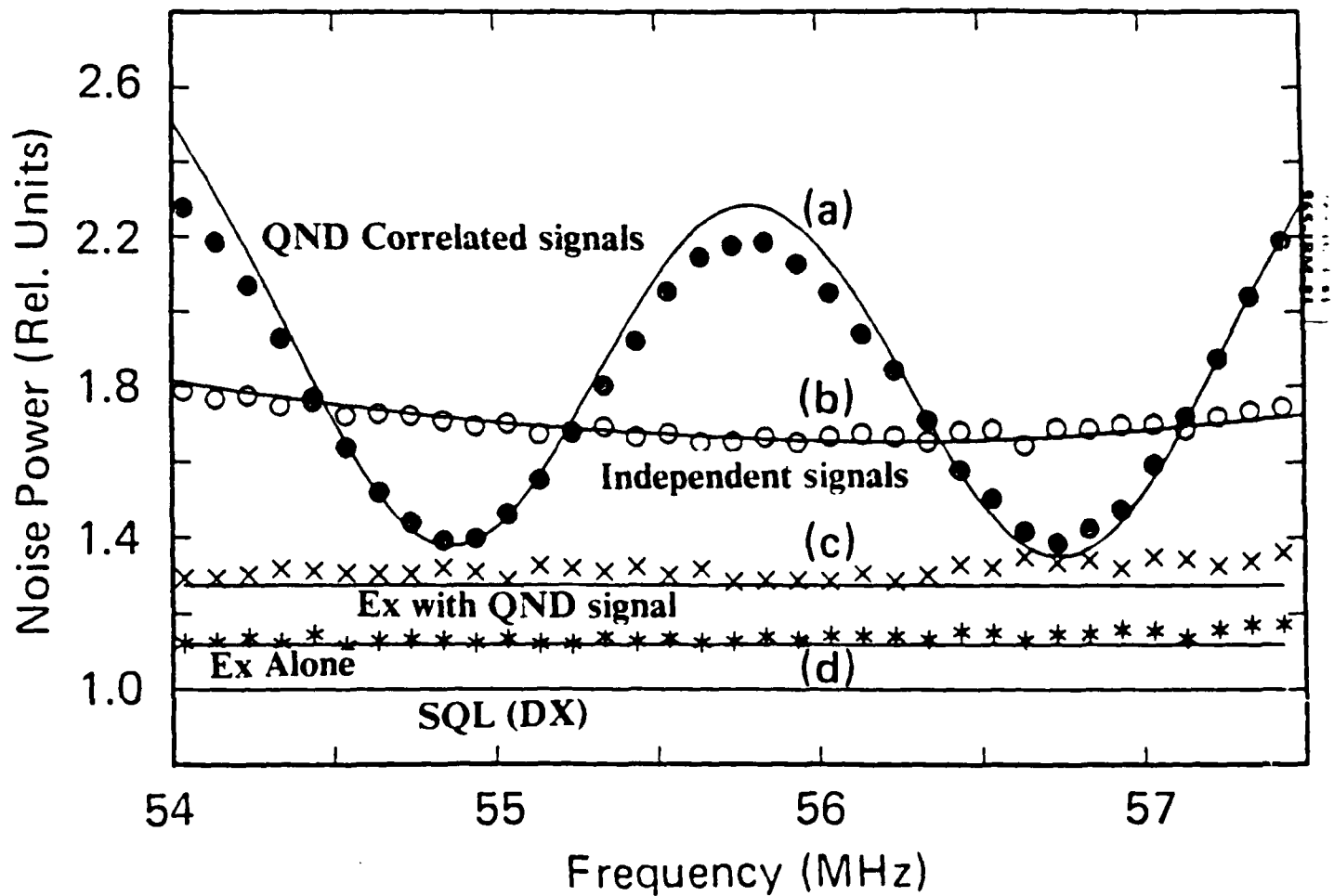
Actual QND Apparatus.



Delay line reveals correlation.

6

Sinusoidal Power Level shows interference between DX and DY signals.

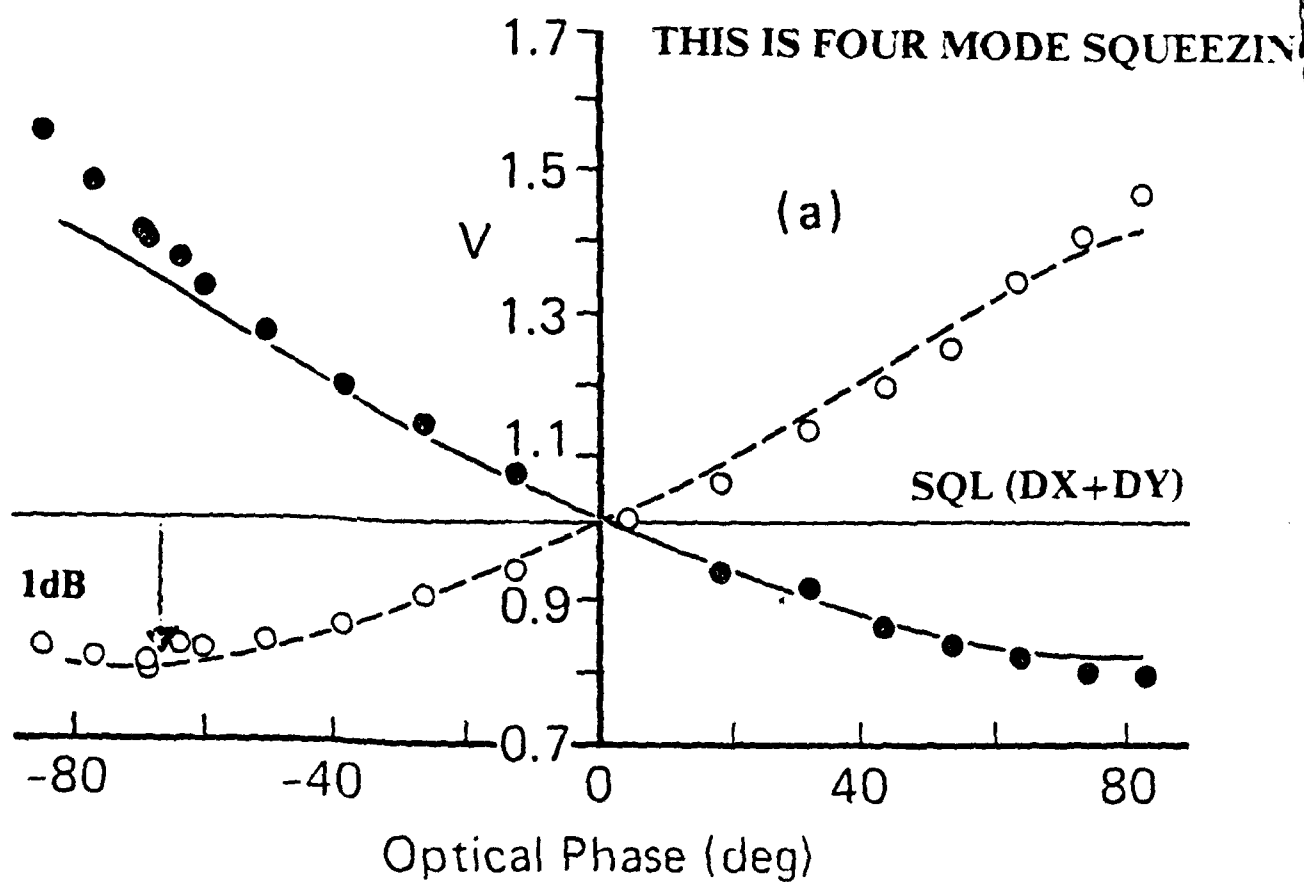


Noise below the sum of independent noises at two detectors shows quantum correlations in the QND signal.

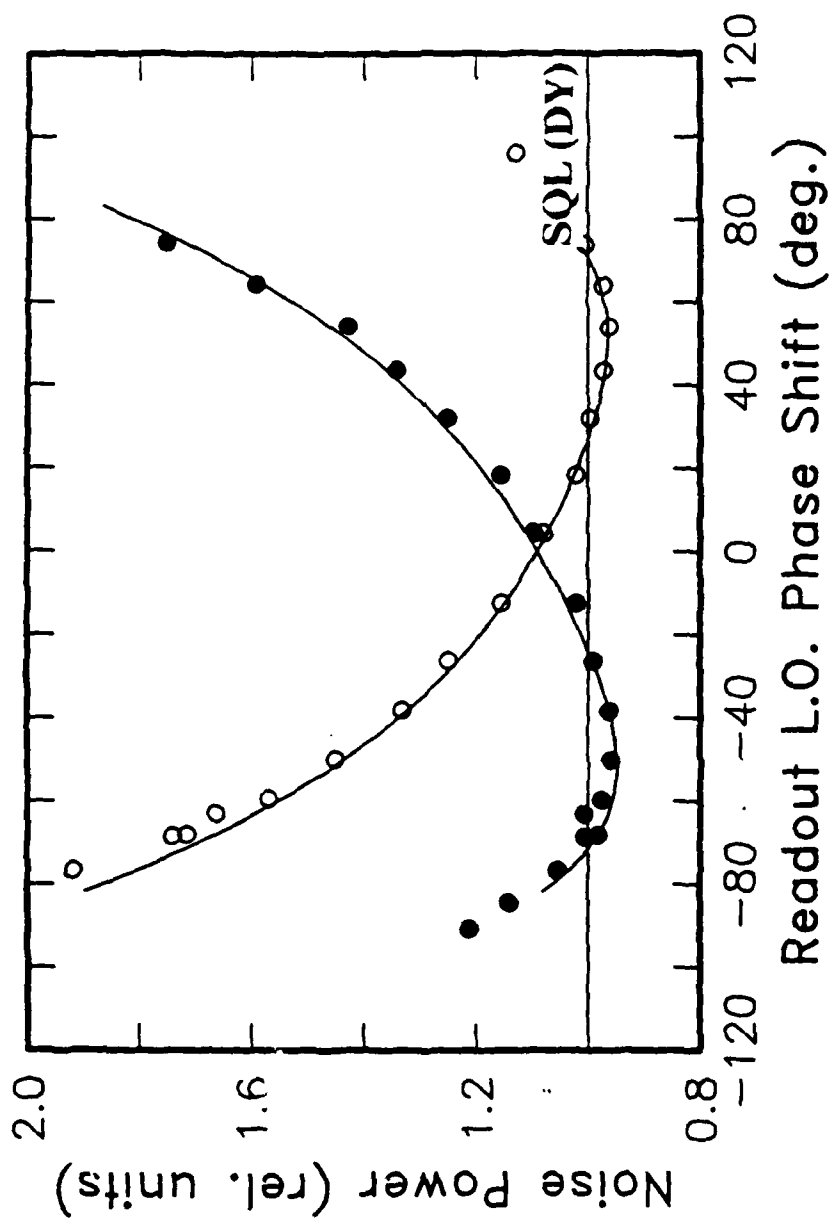
Difference between traces (b) and (d) is the standard quantum limit noise level on detector DY.

7

Minima of sinusoid is 1 dB below sum of vacuum noise levels on two detectors.

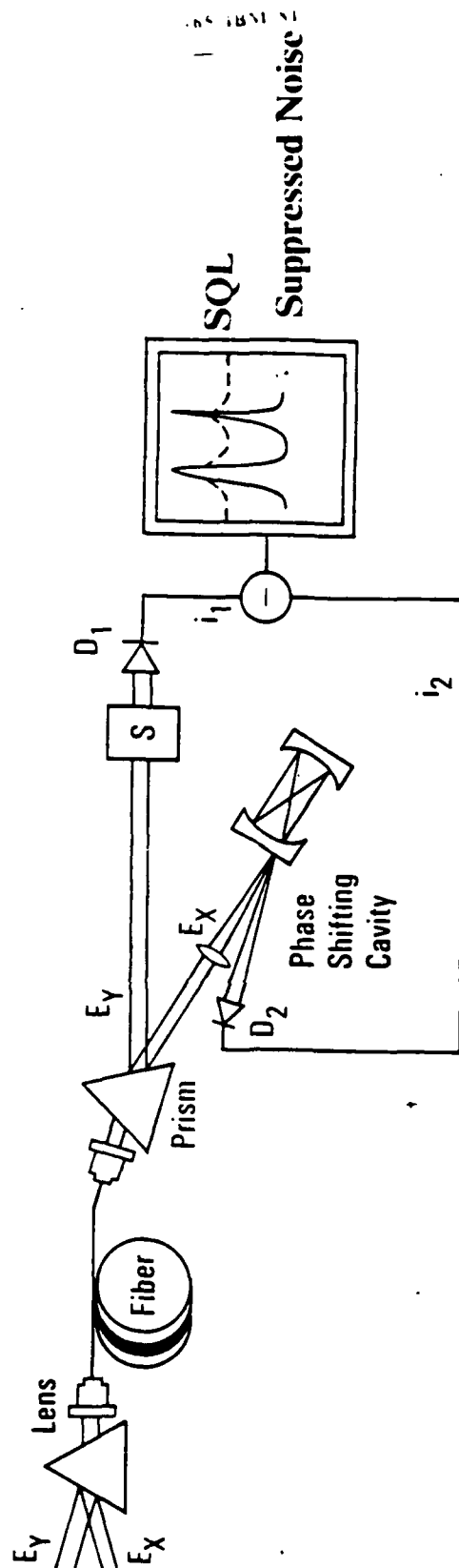


965-10M-01
DY noise is at the Standard Quantum Limit, DX noise level is above, BUT with correct gains, the sum of the noise is below the quantum level on detector DY.

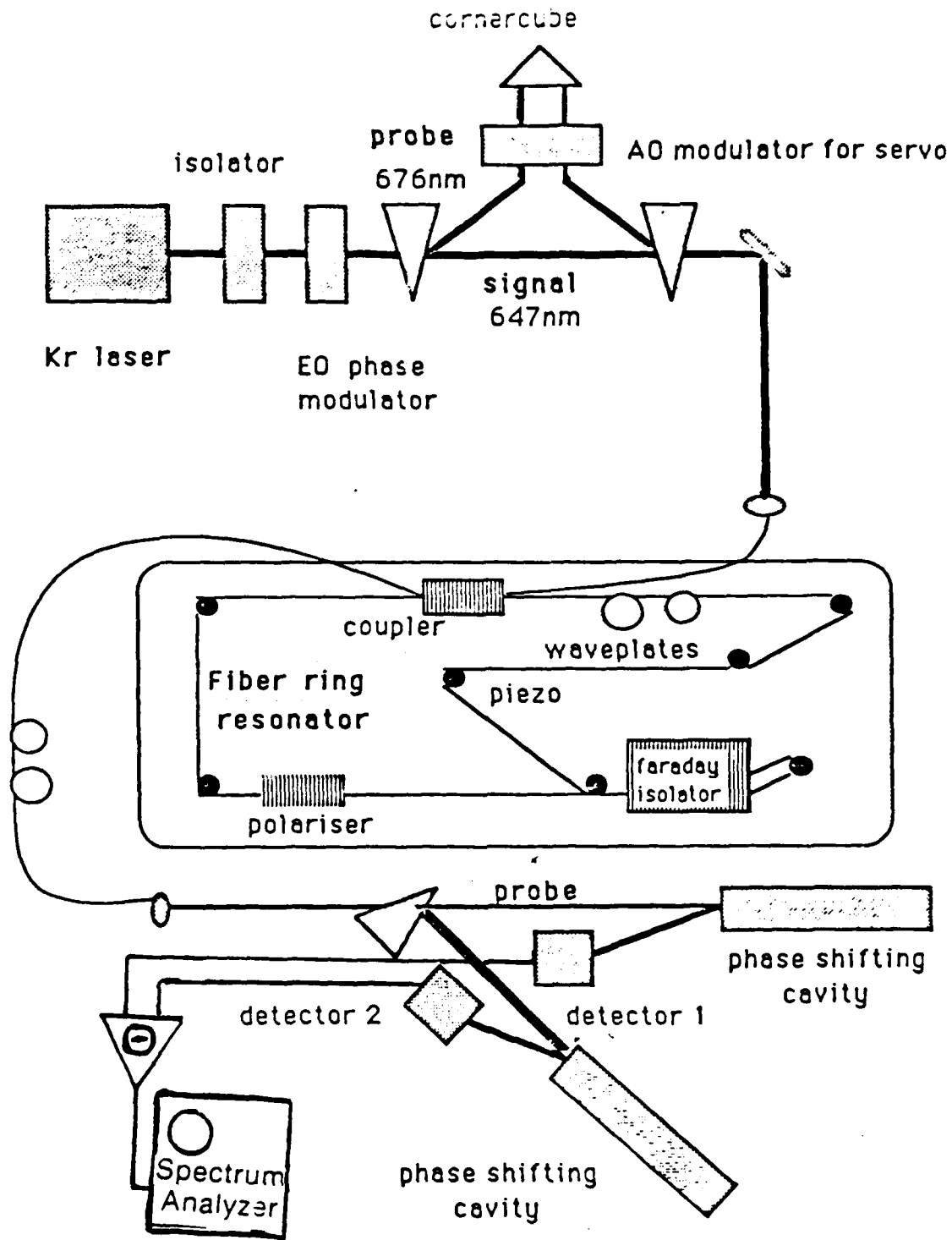


9

Quantum Cary 14 Dual Beam Spectrometer

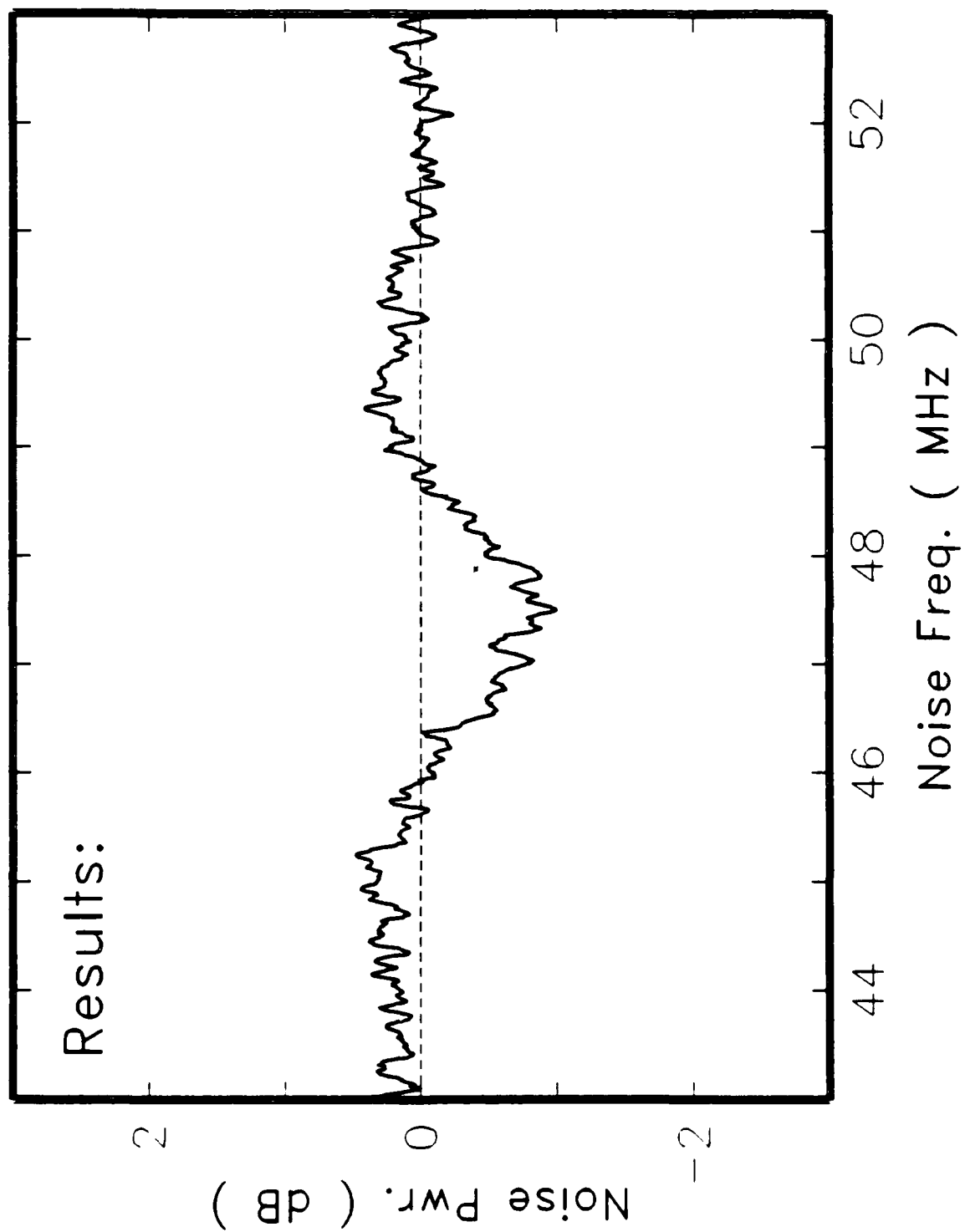


A QND detector can measure the amplitude fluctuations of a tuneable beam. That beam could then pass through a sample that absorbs weakly. A QDD detector then records the output. The fluctuations of the input can be subtracted off, resulting in an absorption spectrometer with the sensitivity of fluorescence spectroscopy.

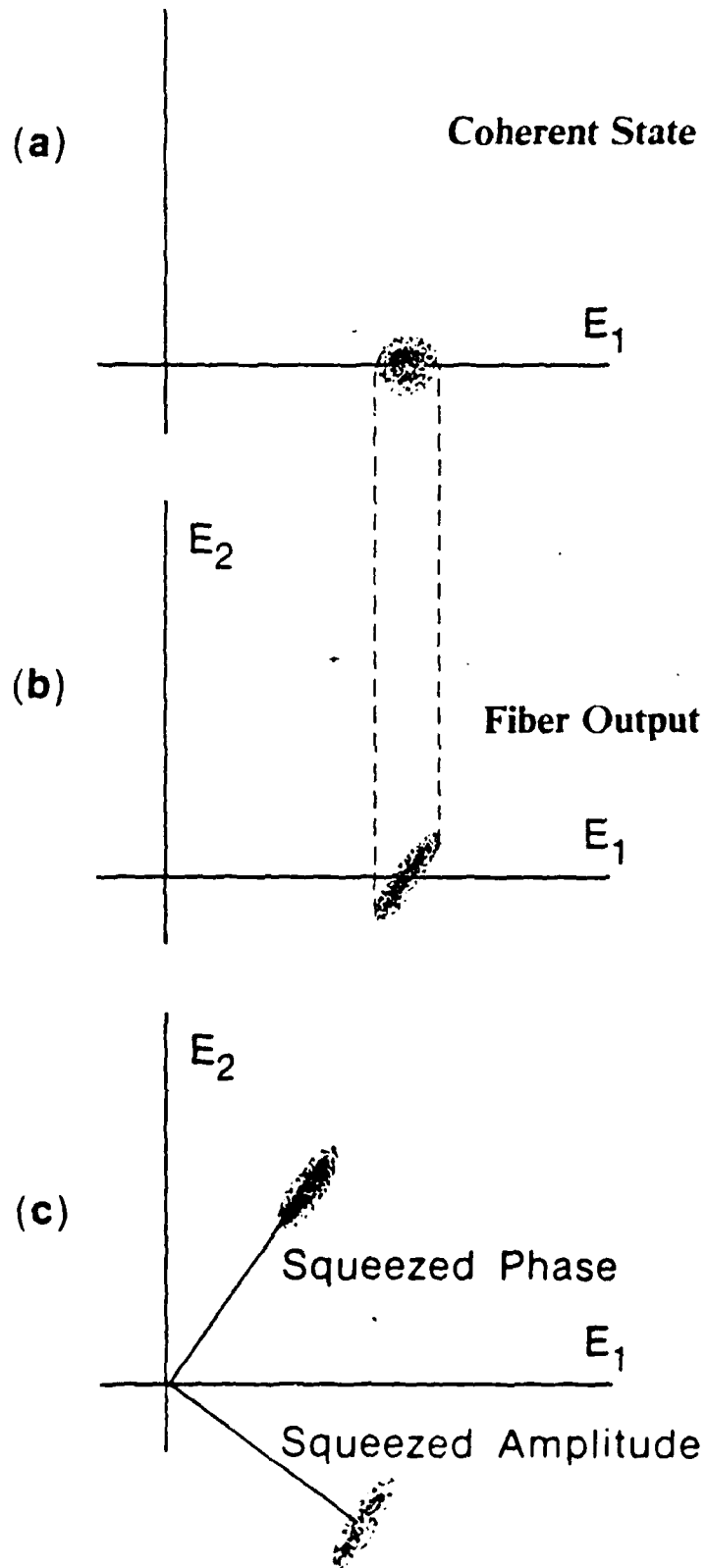


965-IBM-81

Ring Cavity 4 Mode Squeezing Experiment



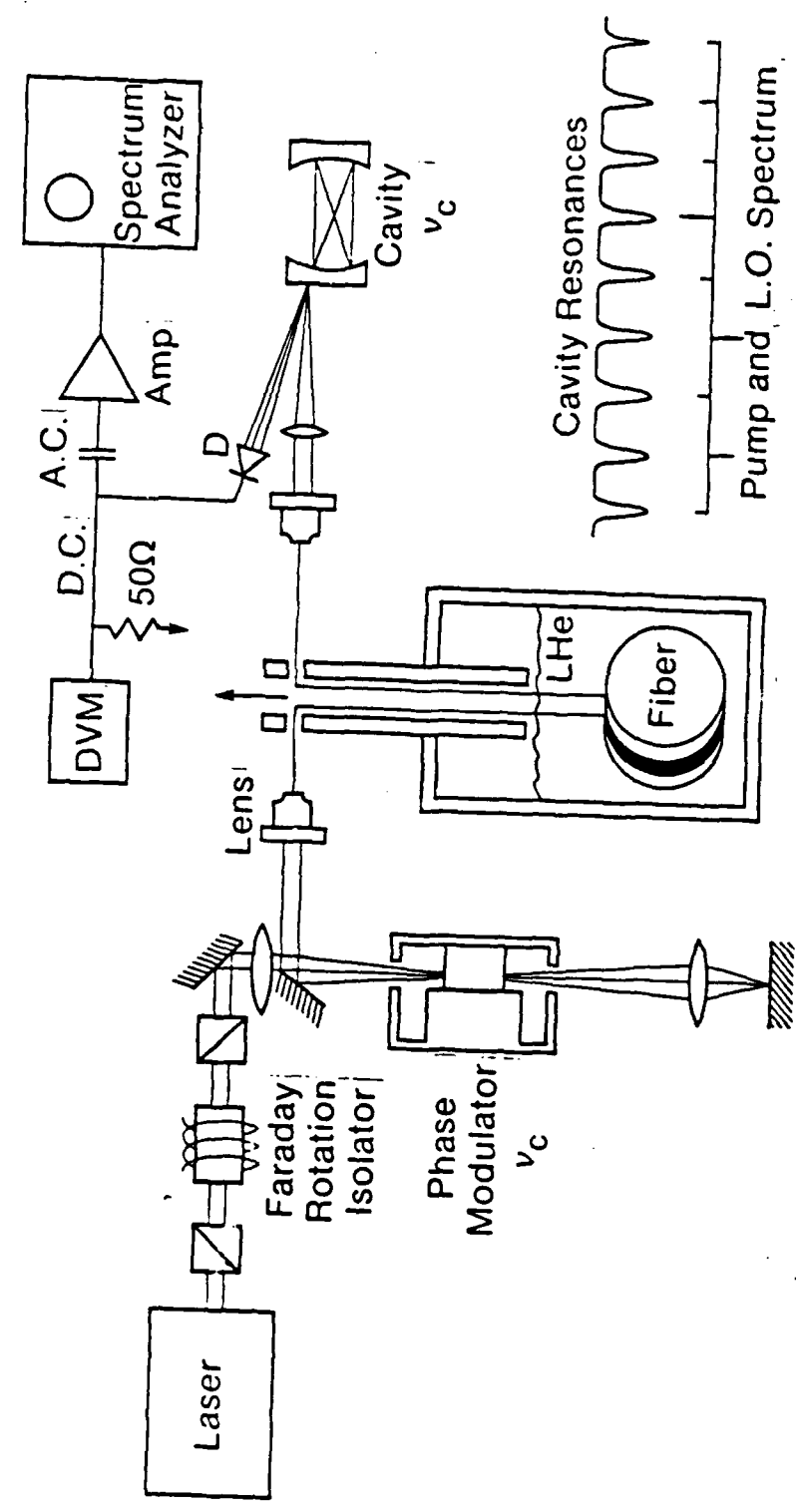
The same nonlinearity can give rise to a squeezed state of light. The amplitude fluctuations of the beam cause correlated fluctuations of the phase of that wave. The amplitude fluctuations are unaffected. The uncertainty circle characteristic of a coherent state is converted to the ellipse of a squeezed state. Phase shifting the average amplitude permits the creation of a strong beam with suppressed amplitude or phase noise.



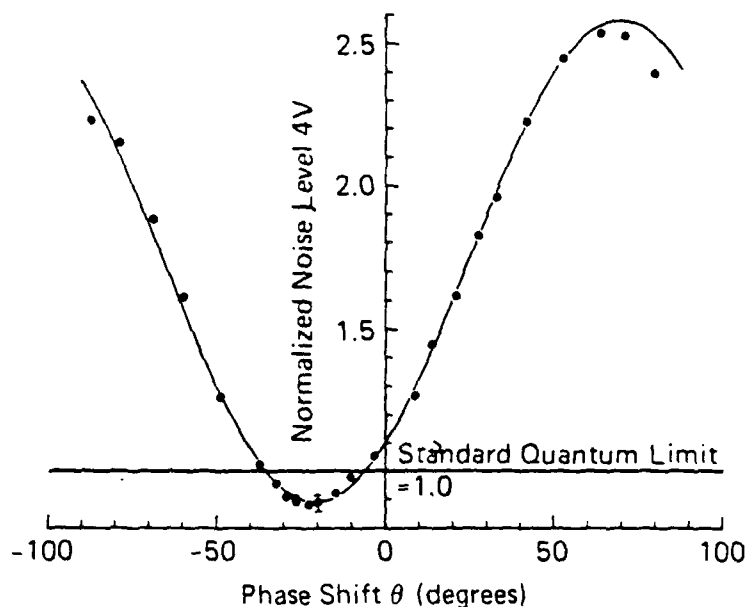
11

The apparatus is very similar to that used for QND, but only one beam is necessary.

Apparatus for Squeezing

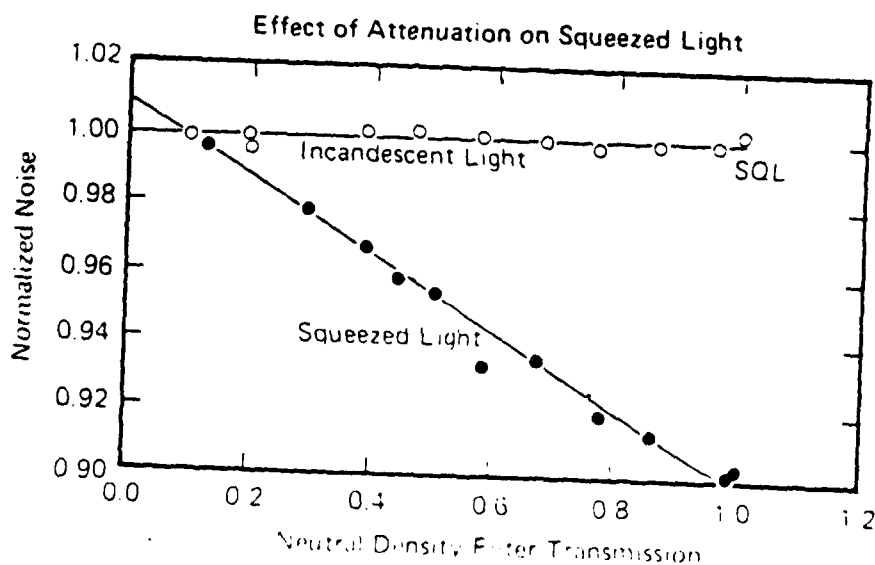


The phase modulation is at the cavity mode separation frequency.



The noise level depends upon phase and falls 12.5% below the vacuum noise level or SQL. This beam is not a minimum uncertainty state because of excess phase noise added by light scattering in the fiber - even at 2K.

When the squeezed beam is attenuated, the noise level rises towards the noise level characteristic of coherent light.



Optical Properties of Quantum Well Structures with Electric Field
: Life Time Free Switching of Luminescence Intensity
and Virtual Charge-Induced Ultrafast Optical Nonlinearity

Masamichi Yamanishi

Department of Physical Electronics,
Hiroshima University
Saijocho, Higashi-Hiroshima, 724 Japan

New modulation schemes for luminescence intensity and for attaining an ultrafast optical nonlinearity are discussed, pointing out possibilities of field controlled light emitters and of ultrafast control of quantum states.

(a) Dynamics of field control of luminescence intensities in GaAs/AlGaAs quantum well structures.

High speed photoluminescence (PL) switching by electric field-induced carrier separation inside the Quantum Well (QW), combined with carrier escaping out from the well to the barrier layer is demonstrated to be free from carrier life time limitation. A new technique for evaluating radiative life time is also shown.

Figure 1 shows the PL response for a short pulsed voltage applied to a p-i-n diode with a GaAs(100Å)/AlAs(300Å) multi-QW

structure. The 300psec delay of PL from the pulsed voltage was observed to be much shorter than the life time (30nsec). However, for a consecutive input pulse train, the PL response was degraded with the increasing number of the input pulses as shown in Fig.2(a) as long as the radiative recombination dominates over nonradiative processes under the condition of a constant generation rate. In order to solve this problem, we examined a modulation scheme in which a field-induced increase in radiative life time is combined with a field-induced decrease in nonradiative life time due to the carrier leakage at a high field. One of the examples of such a modulation is shown in Fig.2(b), indicating a significant improvement of the PL responses for the consecutive pulses. Figure 3 shows overall life time and radiative life time of the carriers obtained with the transient response of PL for pulsed electric field, as functions of the applied field. The new technique will be, in more detail, discussed at the presentation.

The obtained result can convince us of the realization of the proposed light emitter.¹⁾

b) Ultrafast optical nonlinearity by virtual charge polarization in DC biased quantum well structures

A new concept on field-induced optical nonlinearity due to virtual transitions in QW structures²⁾ will be proposed, showing some examples of theoretical result on the nonlinearity. In a QW structure subjected to DC electric field E_0 , negative and posi-

tive electric charges of which spatial profile are given by wave function at the subbands ($1e$, $2e$, ..., and $1hh$, $2hh$, ..., $1lh$, $2lh$, ...) induced by the virtual transitions due to an intense pump light with a photon energy $\hbar\omega_p$ far below the band gap may produce a screening field E_s , cancelling out, to some extent, the external bias field E_0 (see Fig.4). As a result, one may expect a blue shift of the energy gap and changes in oscillator strengths for a weak signal light with a photon energy $\hbar\omega_s$. The switching times of the nonlinearity should be very short, ~ 100 femtosec., both for the ON- and OFF-processes because the electric charges are induced by the virtual processes and the field cancellation results from the internal charges inside the QWs. In other words, the switching characteristic is free from life time limitation, in a contrast with those due to real excitation processes, and from C-R-time constant limitation.

As a consequence of numerical estimations, the following result is obtained for a $\text{Ga}_{1-x}\text{Al}_x\text{As}$ graded gap ($x=0 \rightarrow 0.3$, $L_z=200\text{\AA}$) QW structure. An increase in the $1e$ - $1hh$ transition oscillator strength, 1.5%, and a blue shift of band gap, 0.05meV are expected for a pump power density of 10^7W/cm^2 with a photon energy, 50meV below the energy gap and for an electric field E_0 of $9 \times 10^4\text{V/cm}$. Effective four-wave-mixing $\chi^{(3)}$ parameter was estimated to be $1 \times 10^{-9}[\text{esu}]$ for the graded gap QW biased by the DC field, 90KV/cm and for the detuning energy, 35meV. The variation in the oscillator strength is significantly larger than that (bleaching) due to conventional phase space filling mechanism. The amount of blue shift is comparable to that due to dressed

exciton mechanism.³⁾ The field-induced optical nonlinearity seems to be observable and quite useful for designing an ultra-fast optical gate.

References

- 1) M.Yamanishi and I.Suemune : Japan. J. Appl. Phys. 22 (1983) L22.
- 2) The basic idea of the proposed nonlinearity was discussed by the author and by D.S.Chemla et al., independently of each other.

M.Yamanishi, presented at technical meeting on Optics and Quantum Electronics of Inst. Electronic and Communication Engineers of Japan, paper No. OQE86-167, January 27, 1987 and at spring meeting of Japan Society of Applied Physics, abstract No.31p-ZH-7, March 31, 1987 : submitted to Phys. Rev. Letters, and, also, to be presented at 3rd Int. Conf. on Superlattices, Microstructures and Microdevices, Chicago, Aug.17-20, 1987.

D.S.Chemla, D.A.B.Miller and S.Schmitt-Rink, presented at a post dead line paper session, '87IQEC, paper No.PD-4, April 28,1987 : submitted to Phys. Rev. Letters.

- 3) S.Schmitt-Rink and D.S.Chemla, Phys. Rev. Letters, 57 (1986) 2752.

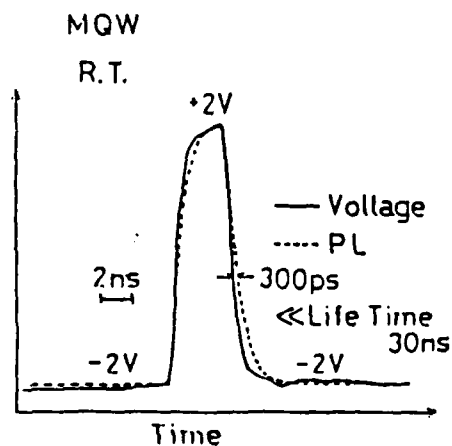


Fig. 1

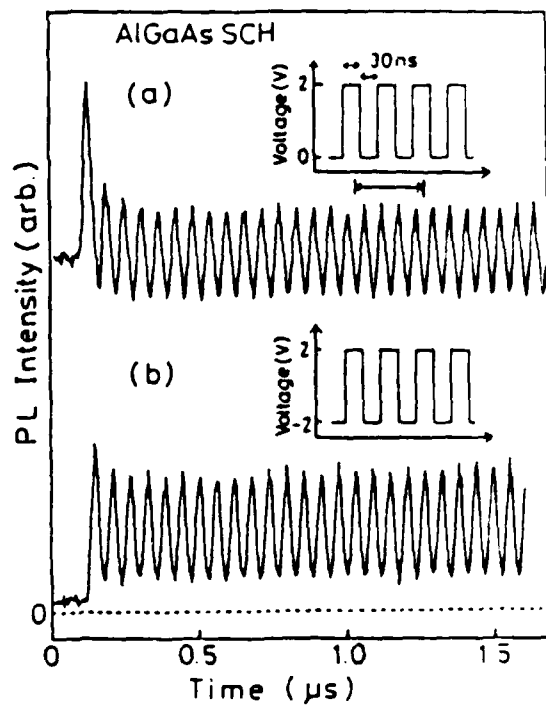


Fig. 2

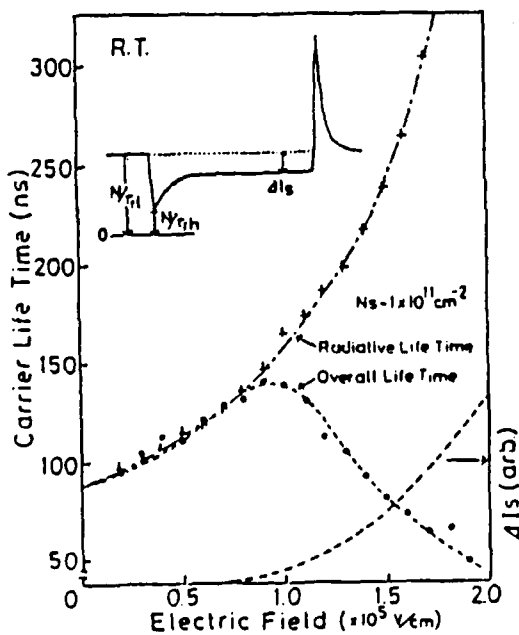


Fig. 3

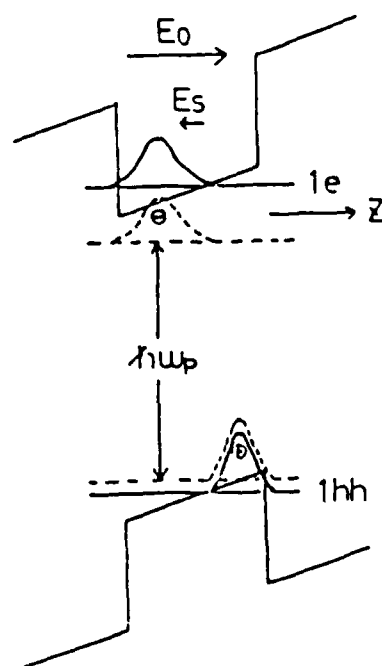


Fig. 4

Optical Properties of Quantum Well Structures biased by DC Electric Field

Masamichi Yamanishi

(Hiroshima University)

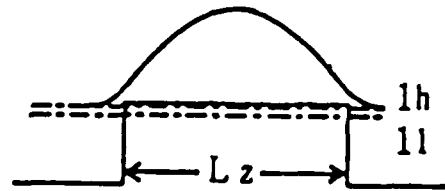
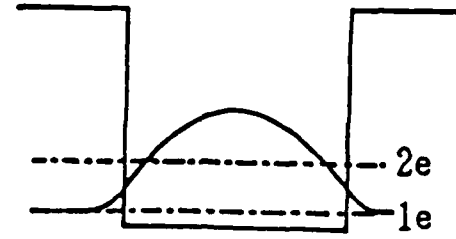
- Field effects on optical properties of QWs : High Speed Switching
- Life-Time-free switching of PL in AlGaAs QWs
- Proposal of Ultrafast optical nonlinearity

Outline of Presentation

1. Dynamics of field control of PL from AlGaAs QWs
 - Completely life-time-free switching of PL by field induced polarization of carriers, combined with carrier escapings.
 - Response time of PL ~ 300 psec, limited by a C-R time constant
2. New mechanism for ultrafast optical nonlinearity in QWs biased by D.C. electric field
 - Response time, ~ 100 fsec
 - Virtual charge polarization, life-time free and free from C-R time constant

Field induced Optical Phenomena in QWs

Energy ↑

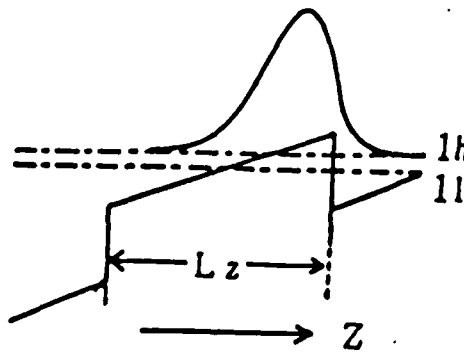
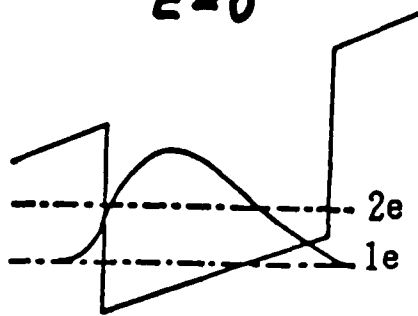


→ Z

(a)
 $E = 0$

Decreasing M^2
and $E_{g,eff}$.

Energy ↑



(b)

$E \neq 0$

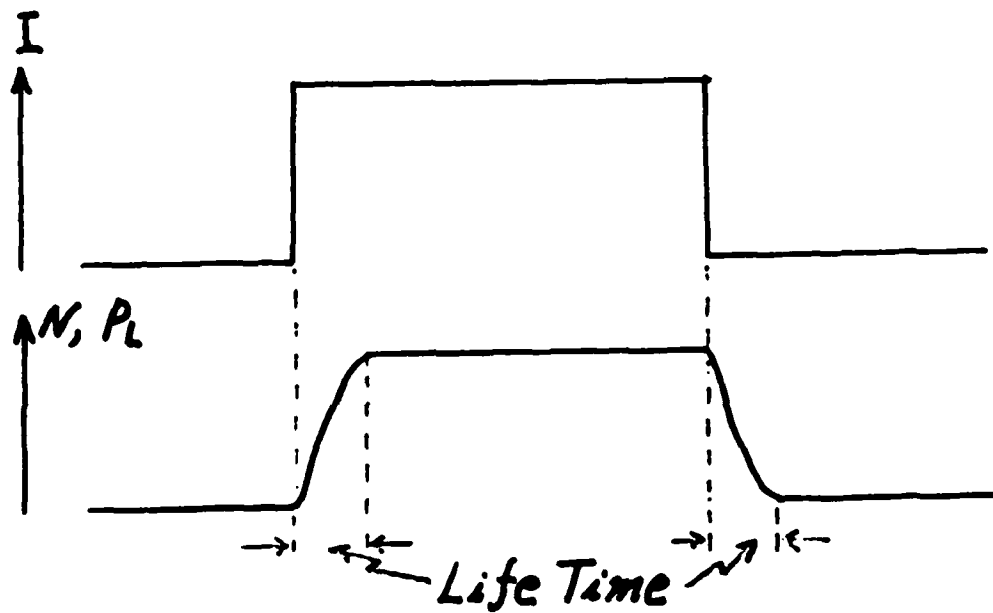
For exciton,
decrease
in E_{ex}

Changes in γ_B

⇒ Additional
Changes in
Oscillator
Strength

Quantum Confined
Stark Effect

- Modulations of Light Output from Laser Diodes and LEDs
by changes in injection current
, i.e., changes in carrier density



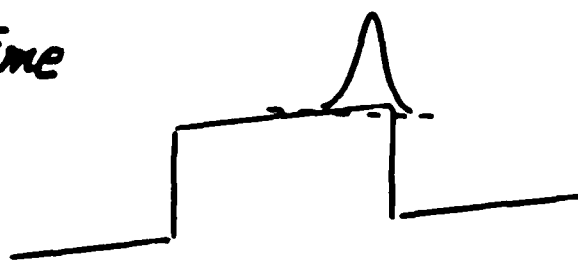
- Control of Oscillator Strength (Matrix Element) by Static Electric Field
 - * not depend on changes in carrier density
 - * fast switching, free from life time limitation

Field Control of Luminescence from QWs

$$\frac{\partial N}{\partial t} = G - N/\tau_r - N/\tau_{nr}$$



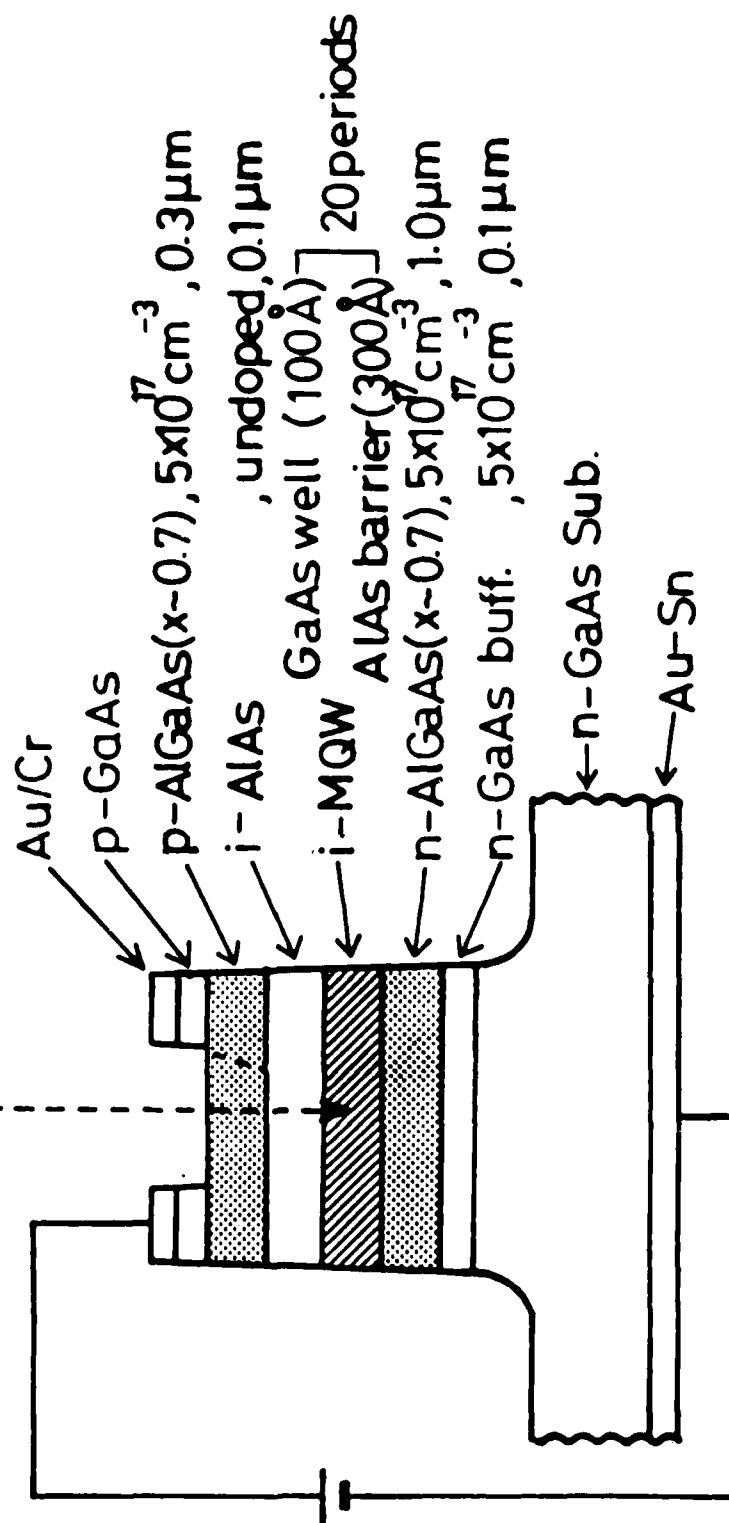
τ_r : Radiative life time
controlled by E.



τ_{nr} : none-radiative
life time

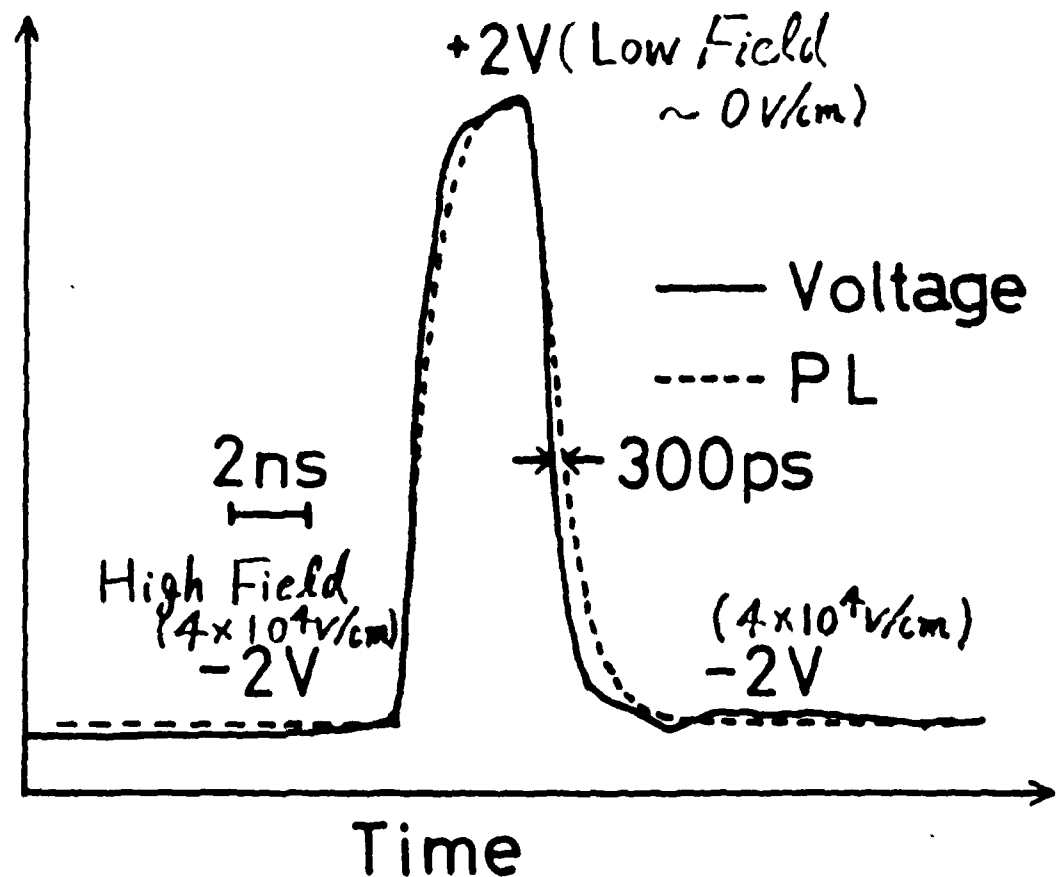
- For quick change in electric field, PL switching is free from life-time limitation.
- If $N/\tau_r \gg N/\tau_{nr}$ and unchanged G , emission rate $N/\tau_r = G$ (unchanged) under steady state condition

He-Ne Laser Beam
 $\lambda \sim 6328 \text{ \AA}$



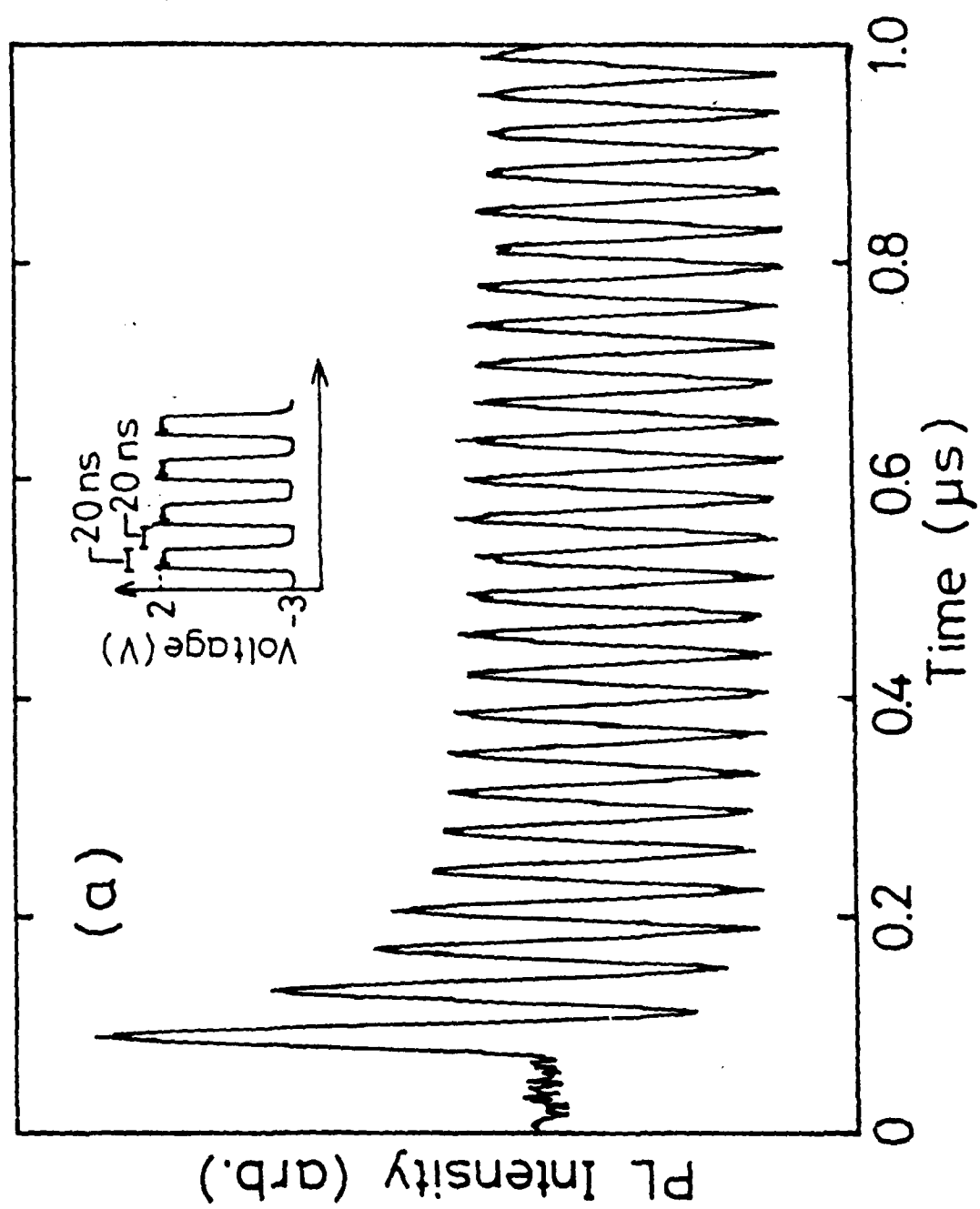
20 periods MQW. GaAs (100Å)/AlAs (300Å)

$T = 300 \text{ K}$



Switching time

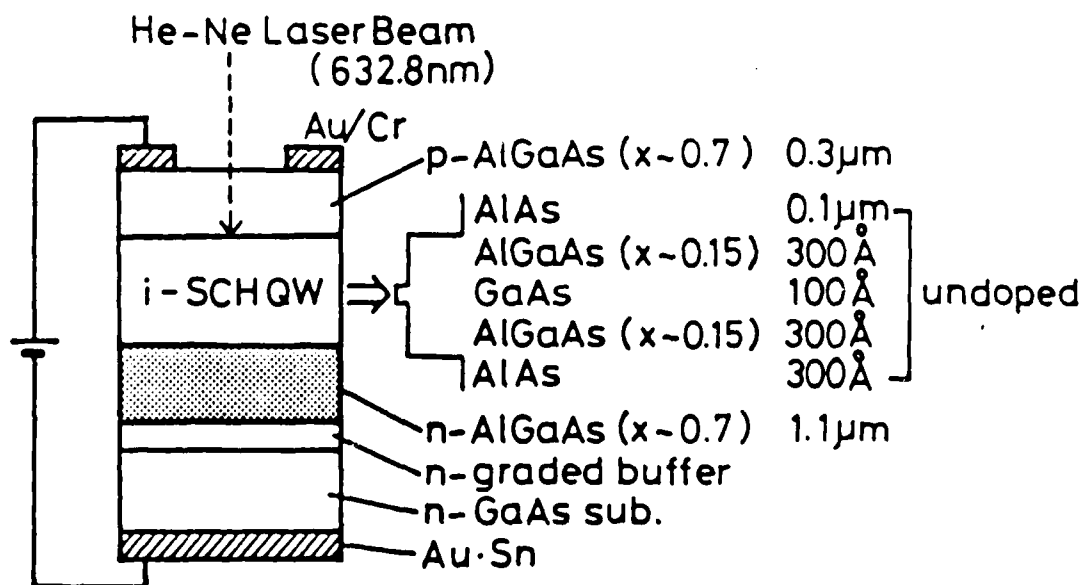
$300\text{psec} \ll \text{Recombination life time} \sim 30\text{nsec}$

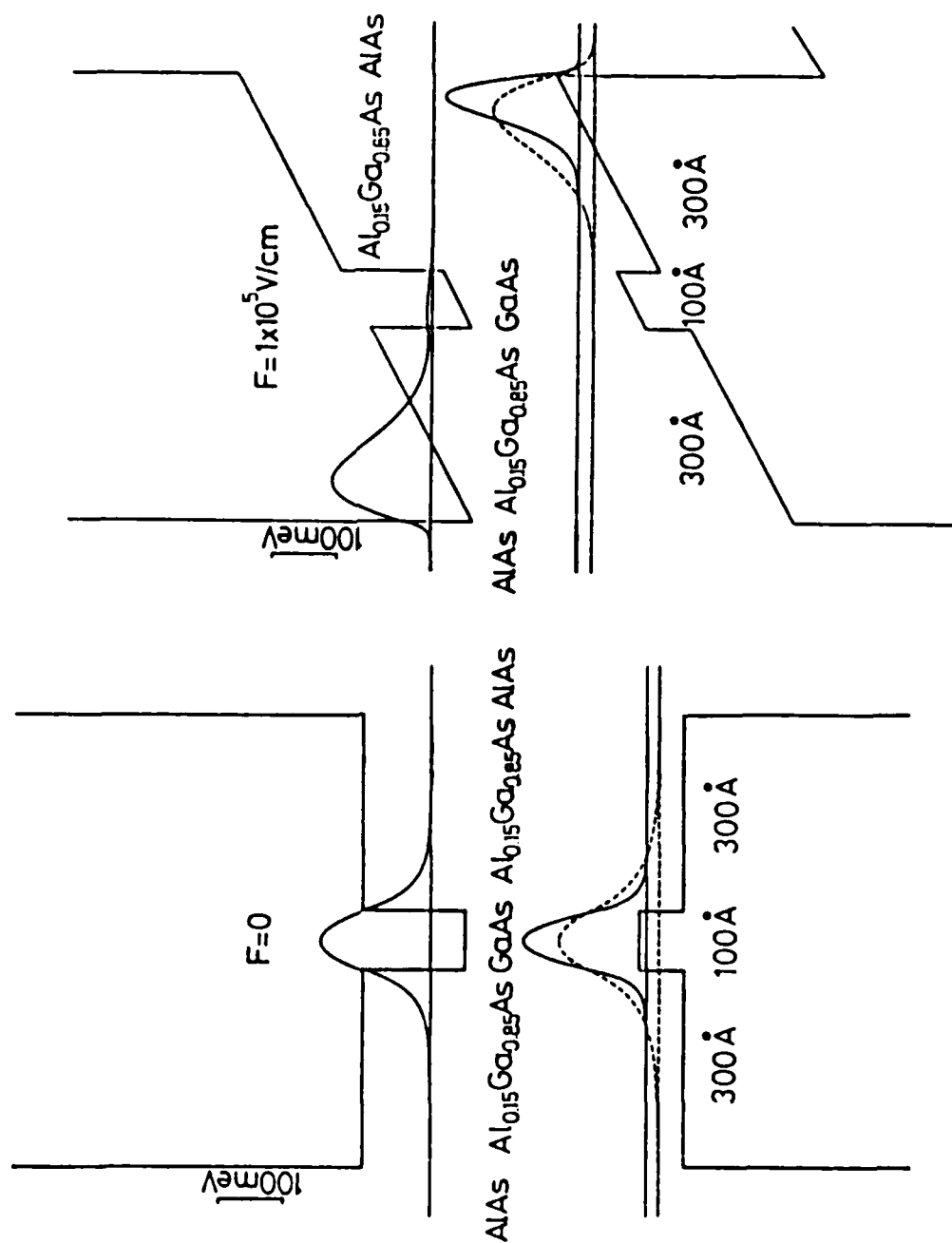


Problems

1. ON/OFF aspect ratio of PL intensities
 modification of QW structure
 \Rightarrow SCH/QW

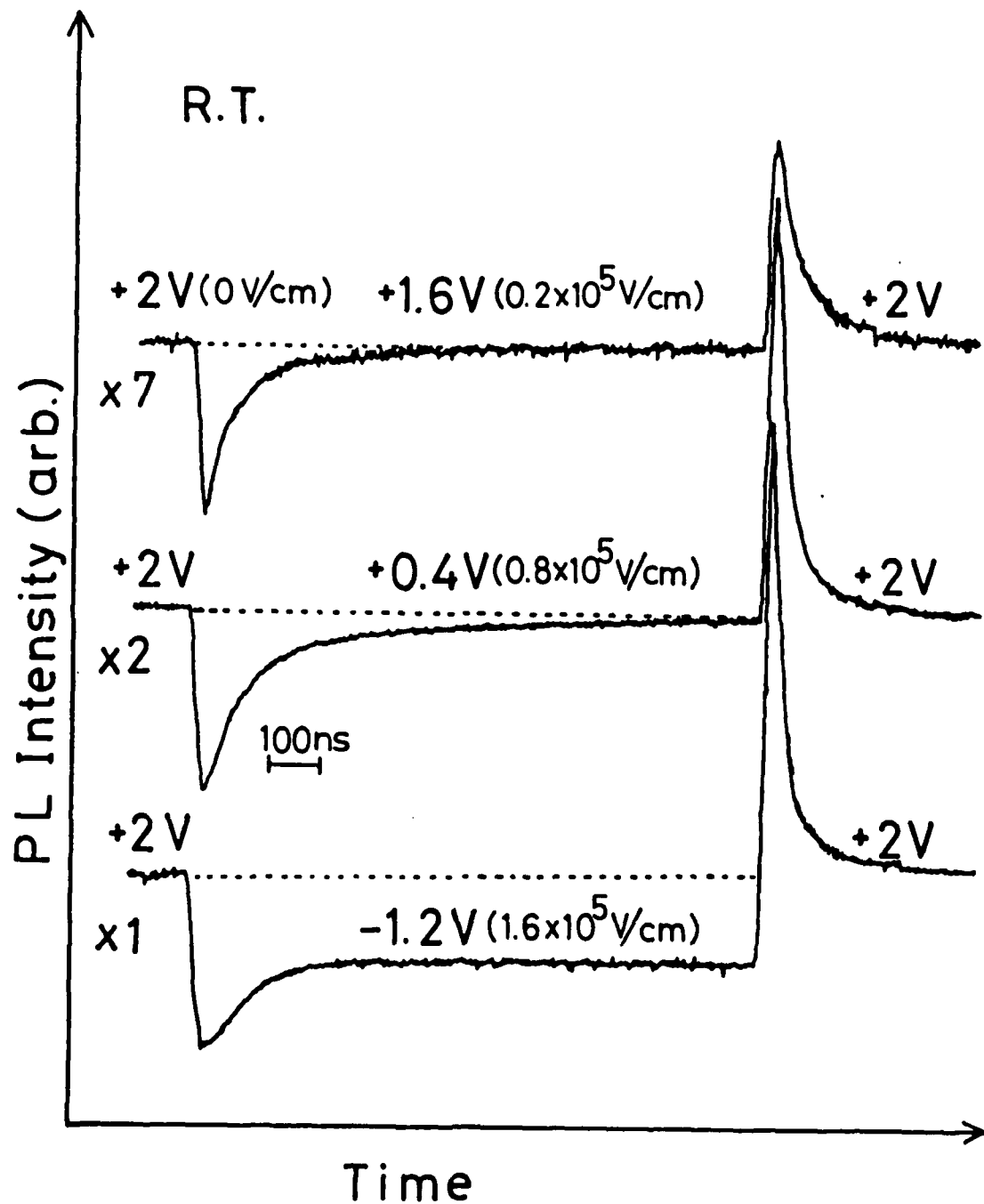
2. Unchanged PL intensity at steady state, i.e. degradation of PL response for consecutive input pulses
 carrier leakage at high field

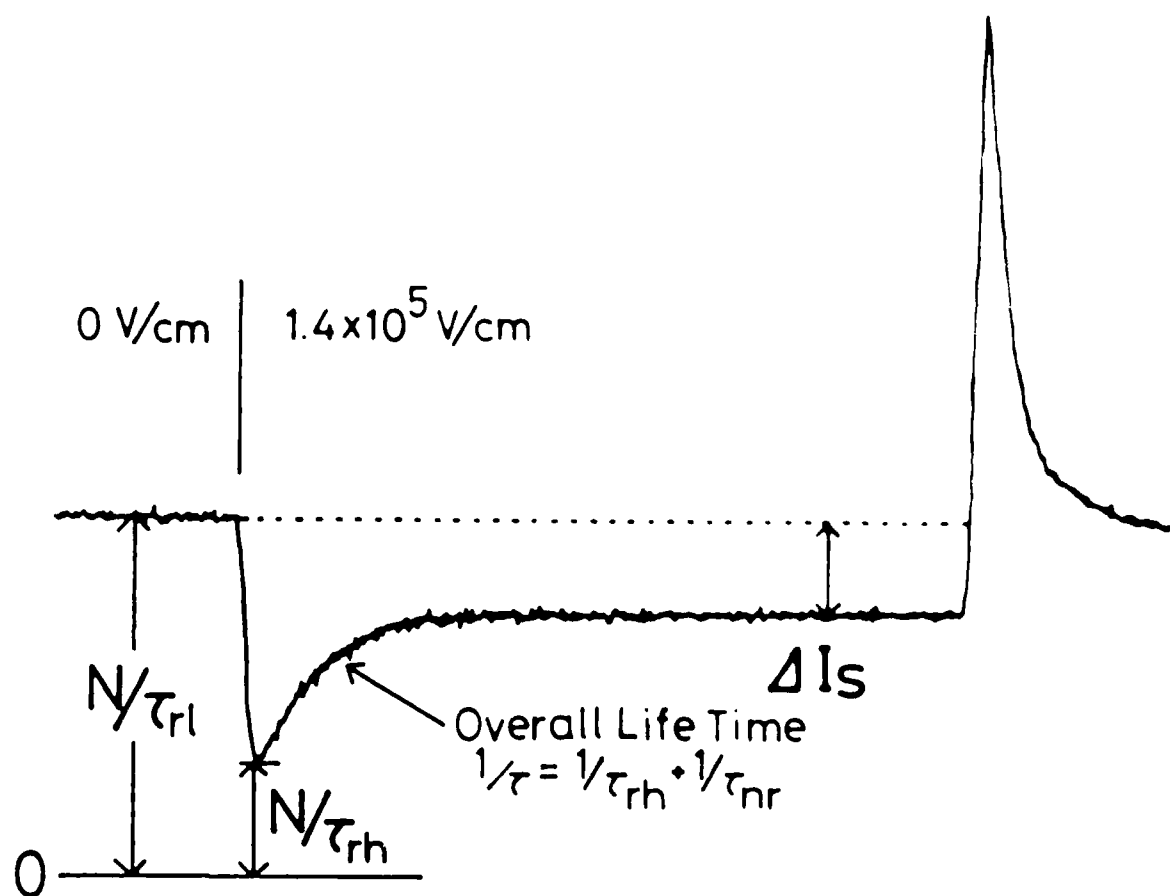




◦ Enough spatial separation

SCH/QW

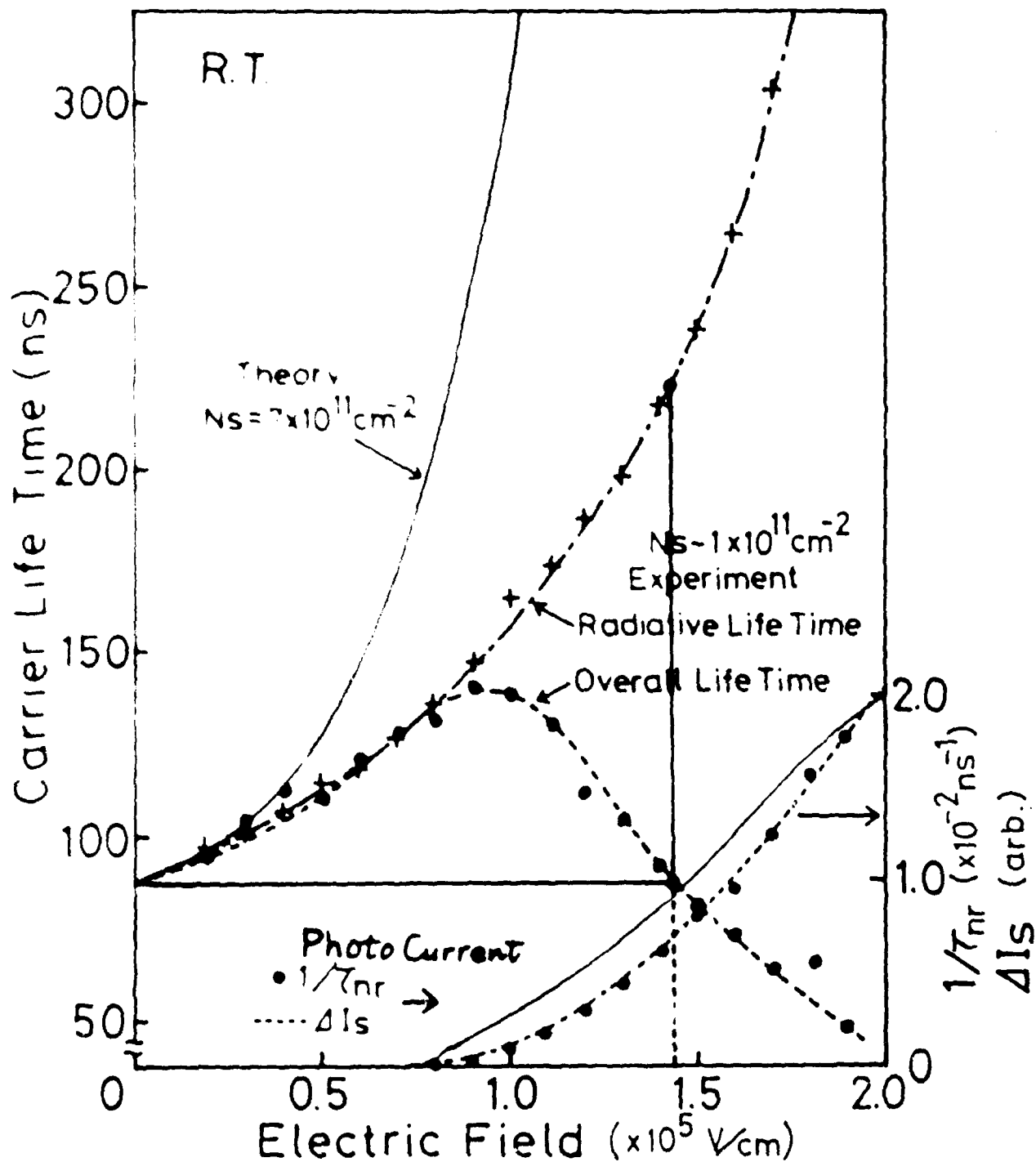




$$\frac{\text{PL at } E=0}{\text{PL at } E=1.4 \times 10^5 \text{ V/cm}} = \frac{N/\tau_{rl}}{N/\tau_{rh}} = \frac{\tau_{rh}}{\tau_{rl}}$$

- Carrier density is kept constant on a sudden change of life time.

SCH/QW



$$1/\tau_{nr} = 1/\tau(\text{overall}) - 1/\tau_r$$

AD-A186 938

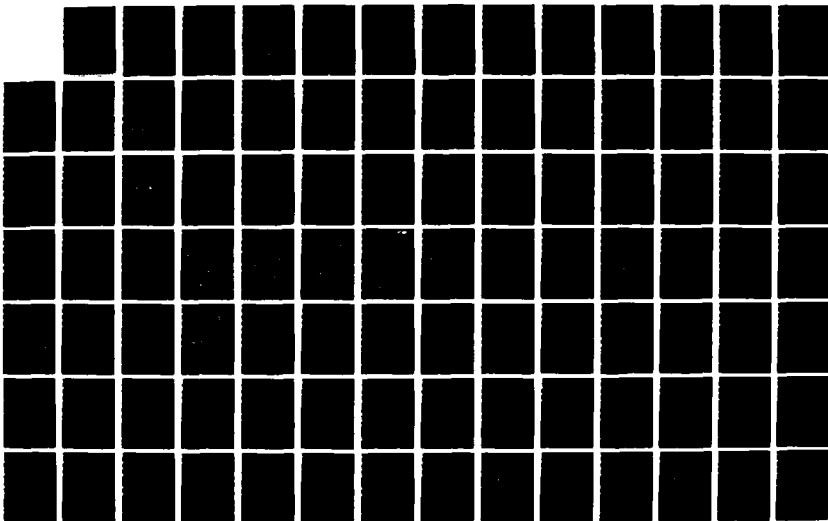
UNITED STATES - JAPAN SEMINAR ON QUANTUM MECHANICAL
ASPECTS OF QUANTUM EL (U) MASSACHUSETTS INST OF TECH
CAMBRIDGE RESEARCH LAB OF ELECTRON

4/7

UNCLASSIFIED

J H SHAPIRO ET AL OCT 87 N00014-87-G-0198 F/G 20/3

NL





1.0



1.1



1.25

5.0
4.5
4.0
3.5
3.15
2.8

2.8

3.15

3.5

4.0

4.5

2.5

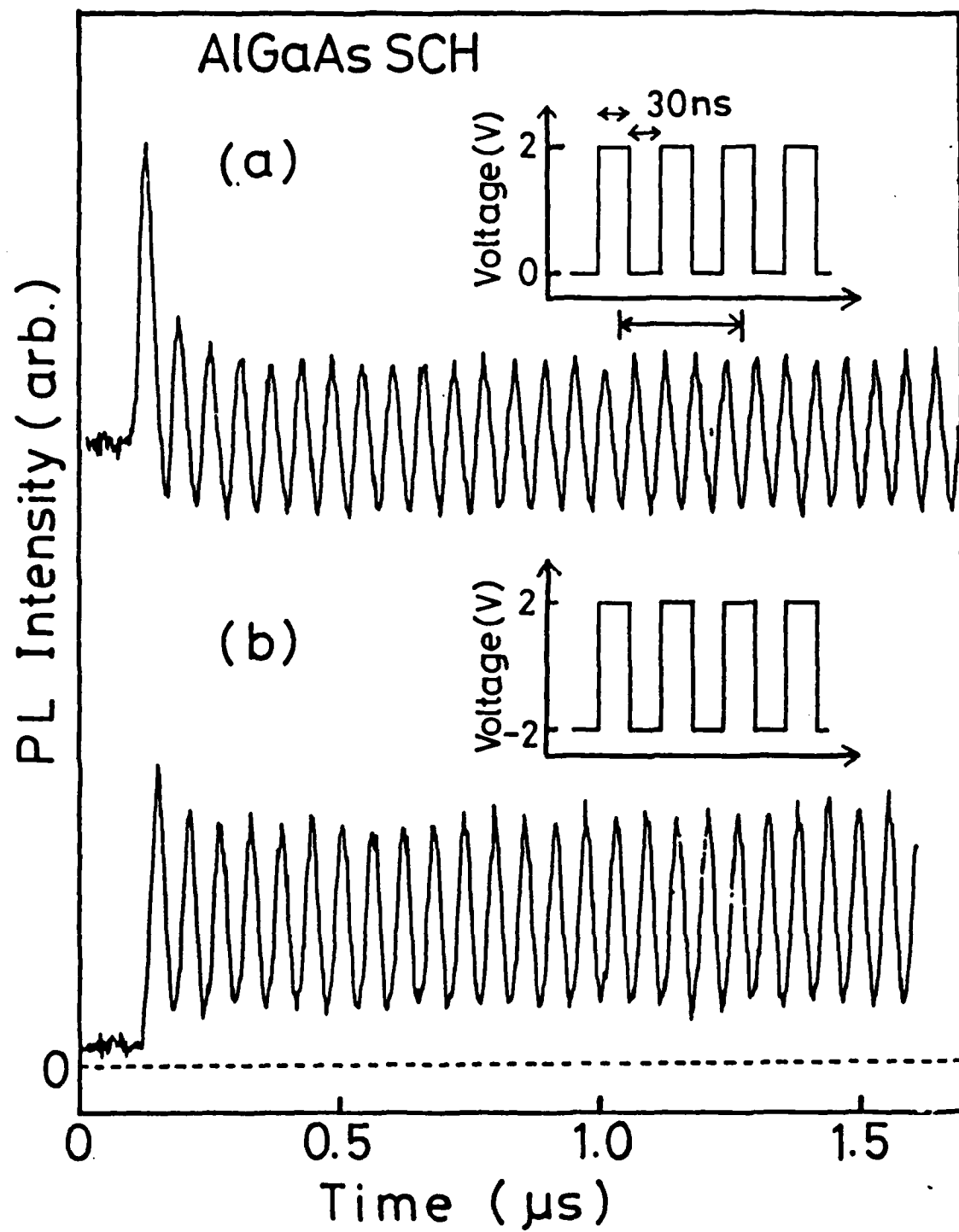
2.2

2.0

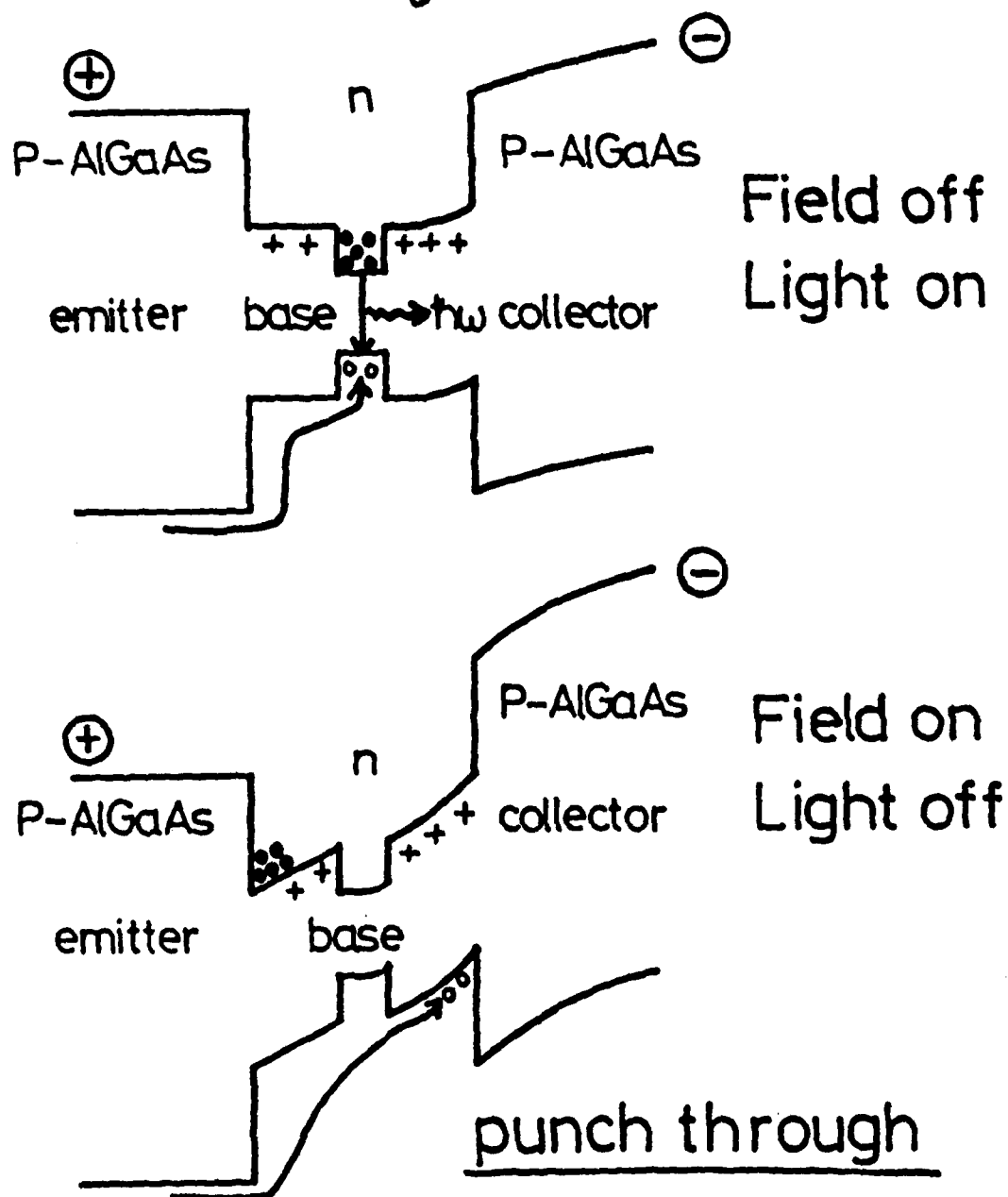
1.8

1.4

1.6

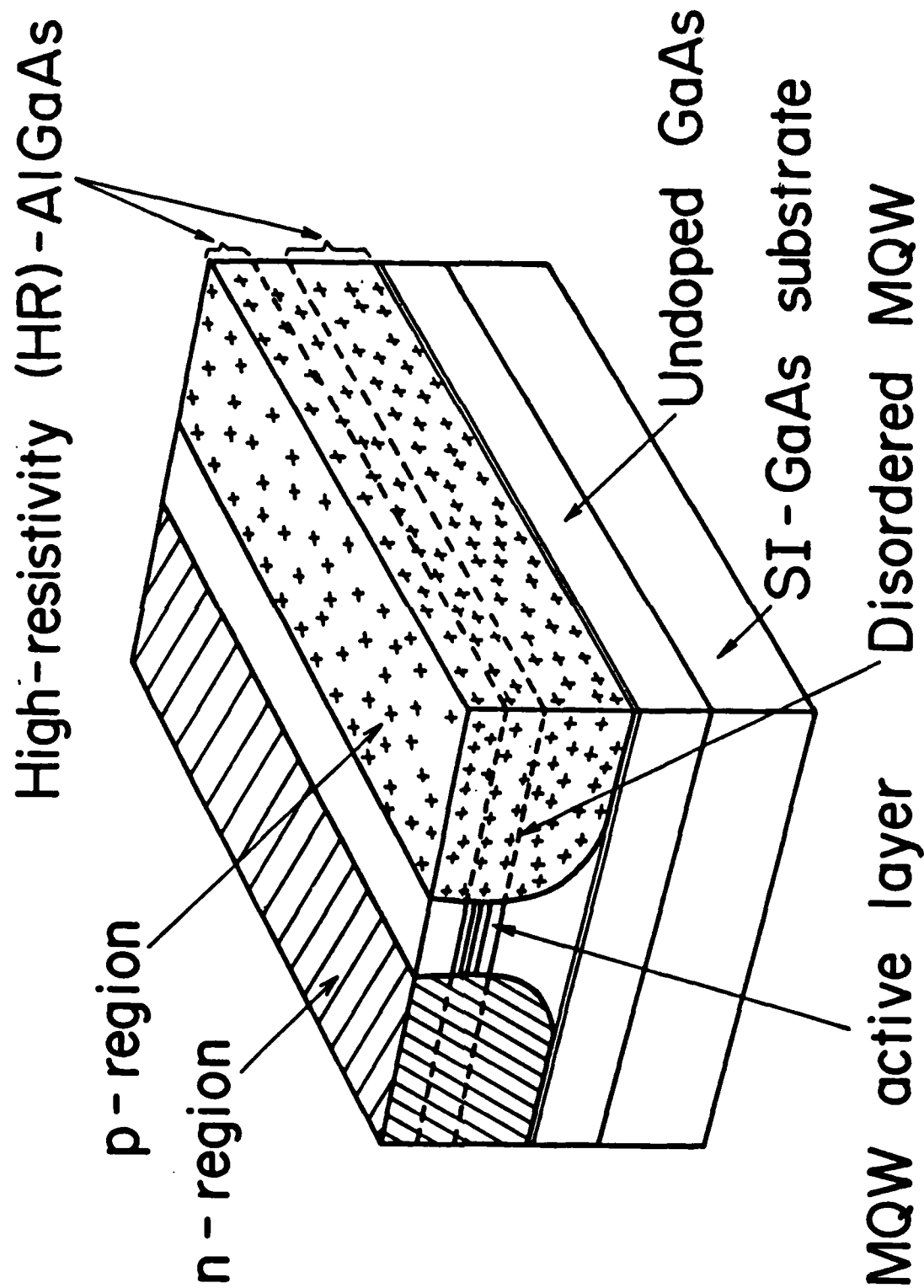


Possible device structure of field controlled light emitter



Hetero Bipolar Transistor

M. Yamashita et al.



Makiuchi et al.
Fujitsu Labs

LCI MQW laser

Summary

1) Demonstration of field control of PL from AlGaAs QWs

- life time free switching of PL by field induced polarization of carriers. combined with carrier escapings
- response time of PL. $\sim 300 \text{ psec}$
 $\sim C \cdot R.$

2) Proposed field controlled light emitters; quite possible

Ultrafast Optical Nonlinearity in Quantum Well Structures Biased by DC Electric Fields

M. Yamanishi
(Hiroshima University)

- Proposal of a new mechanism on
ultrafast optical nonlinearity

switching time \sim 100 femtosec.

Virtual Charge-induced
Optical Nonlinearity: VCON

- A. Mysyrowicz, D. Hulin et al.
A. Von Lehmen et al. (1986)
discovery of AC Stark effects
in AlGaAs QWs
- S. Schmidt-Rink and D. S. Chemla,
Theory of nonlinear optical
properties
Virtual carriers behave
as if real ones
- Proposal of virtual charge induced
optical nonlinearity in DC biased
QWs
M. Yamashita: presented at IECE,
Japan. tech. meeting (Jan. 1987)
and at spring meeting of JSAP
(March, 1987)
D. S. Chemla et al: presented at
'87 IBEC, post deadline paper
(April, 1987).

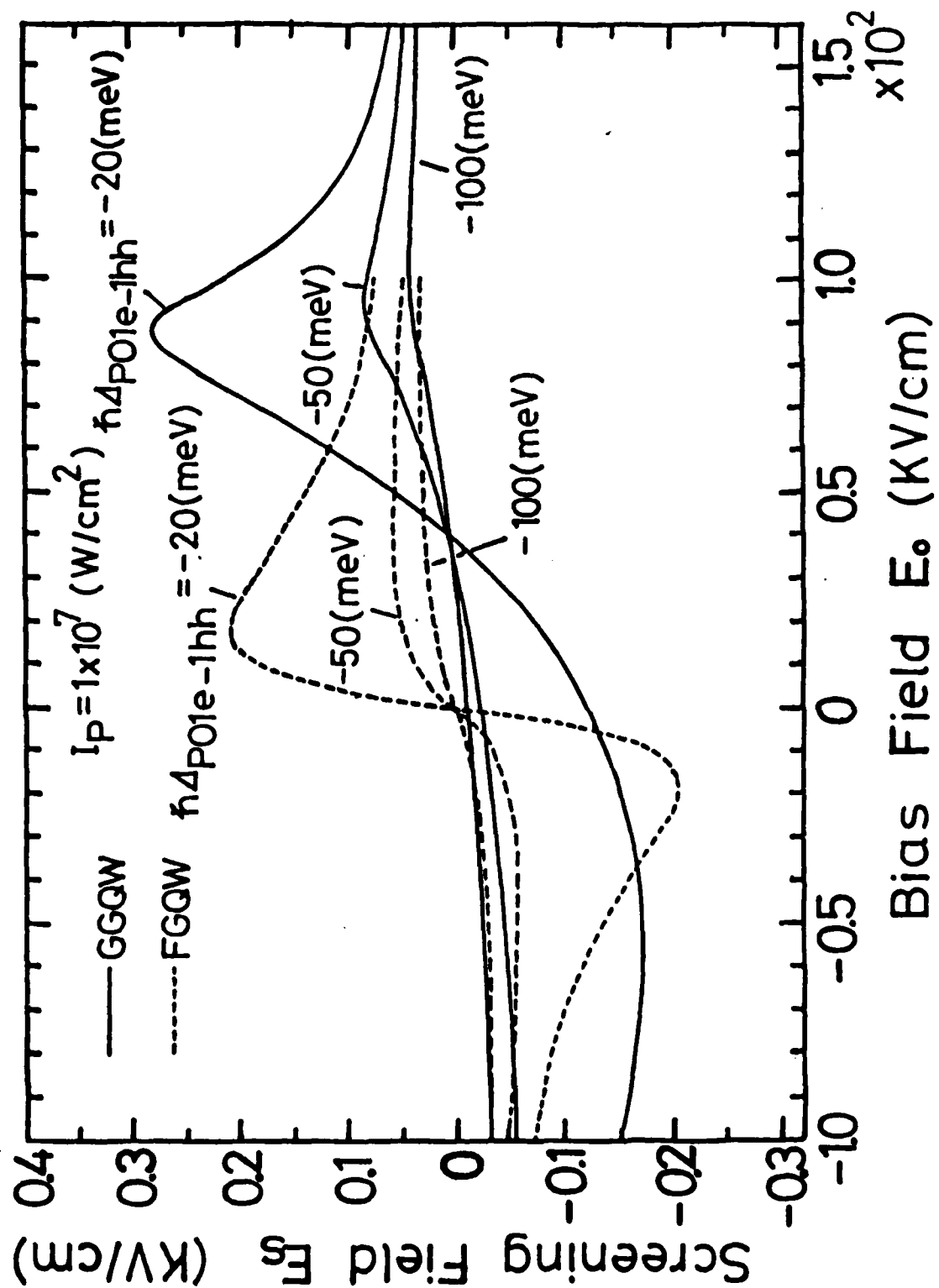
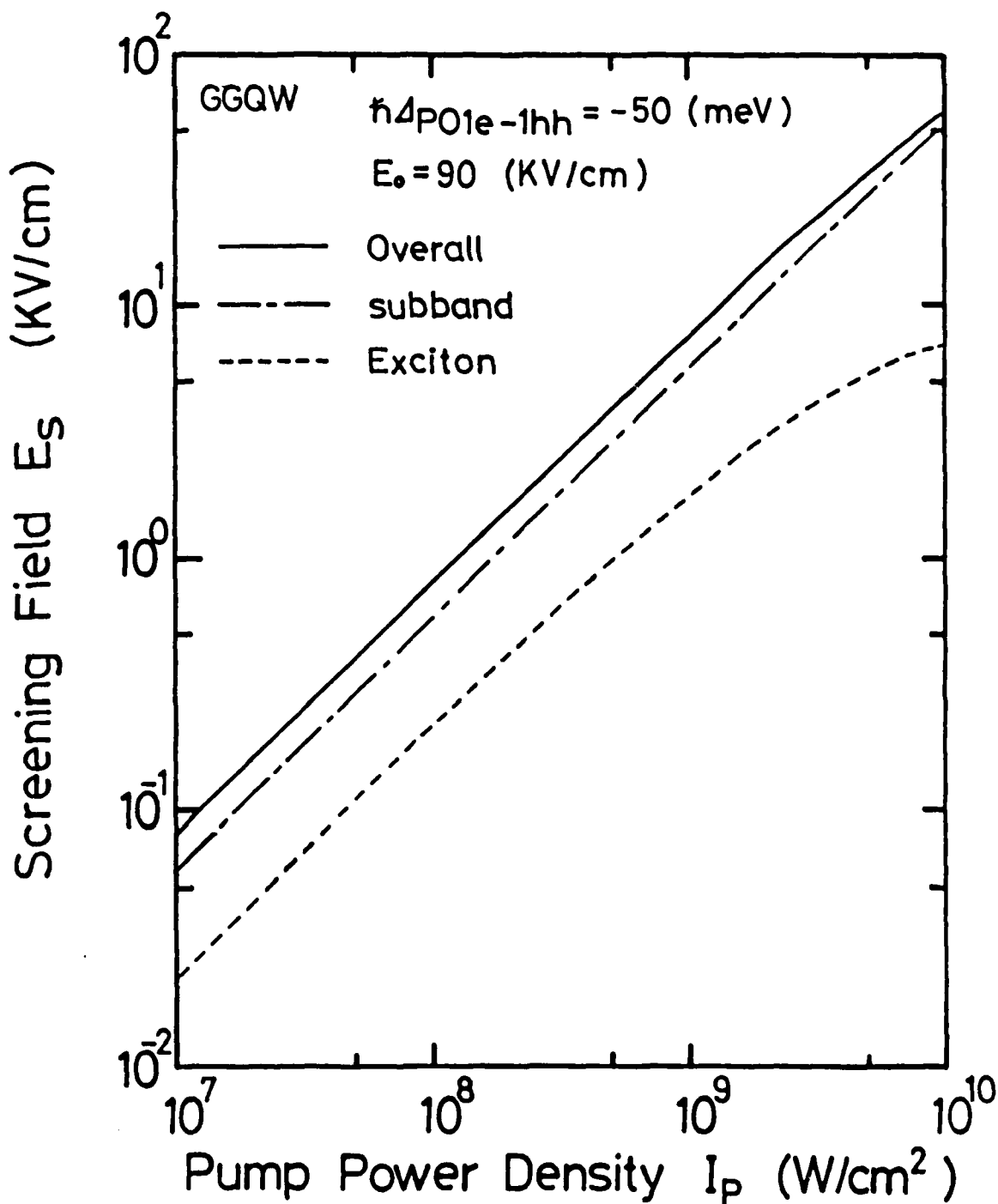


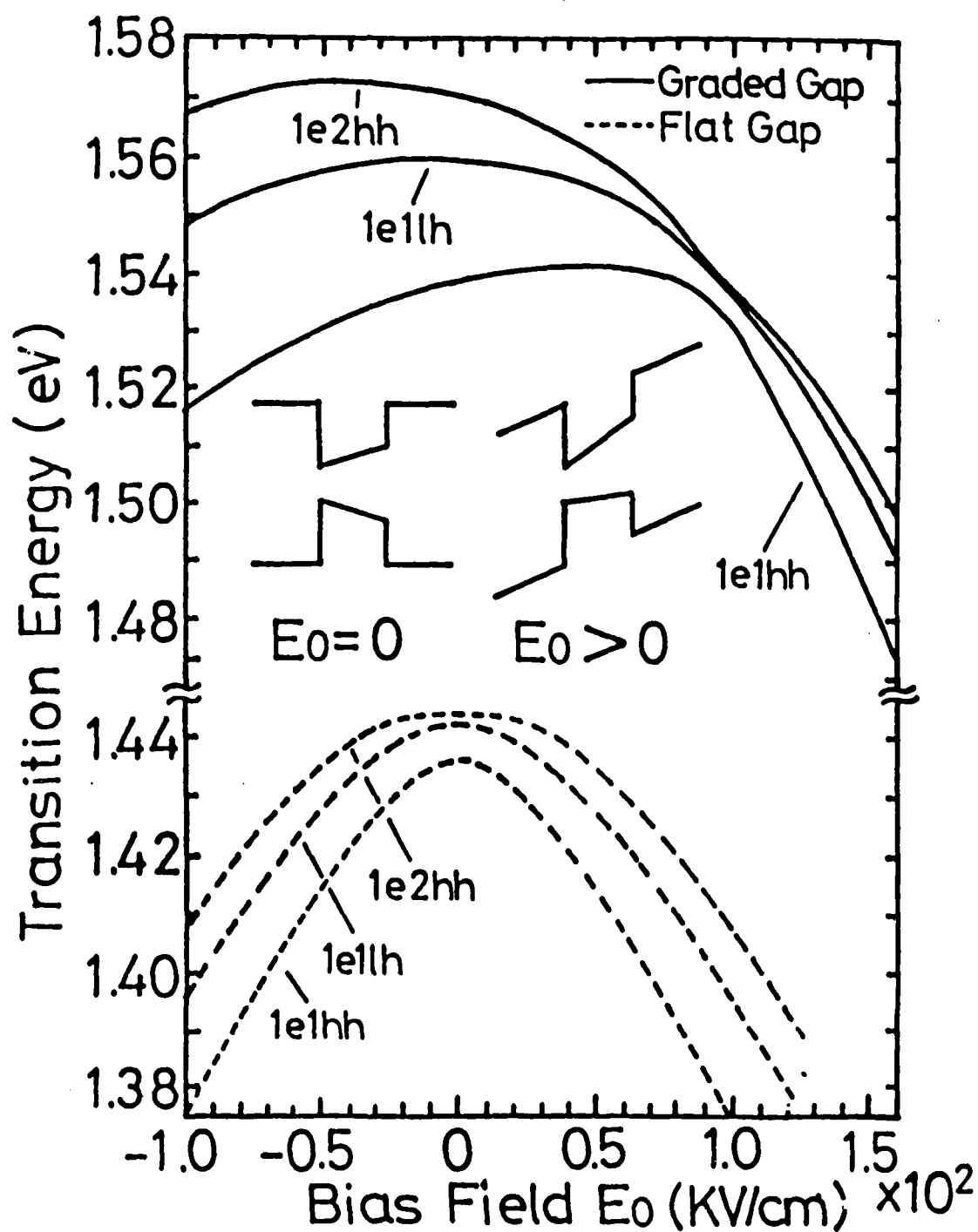
Fig. 2 M.Y.

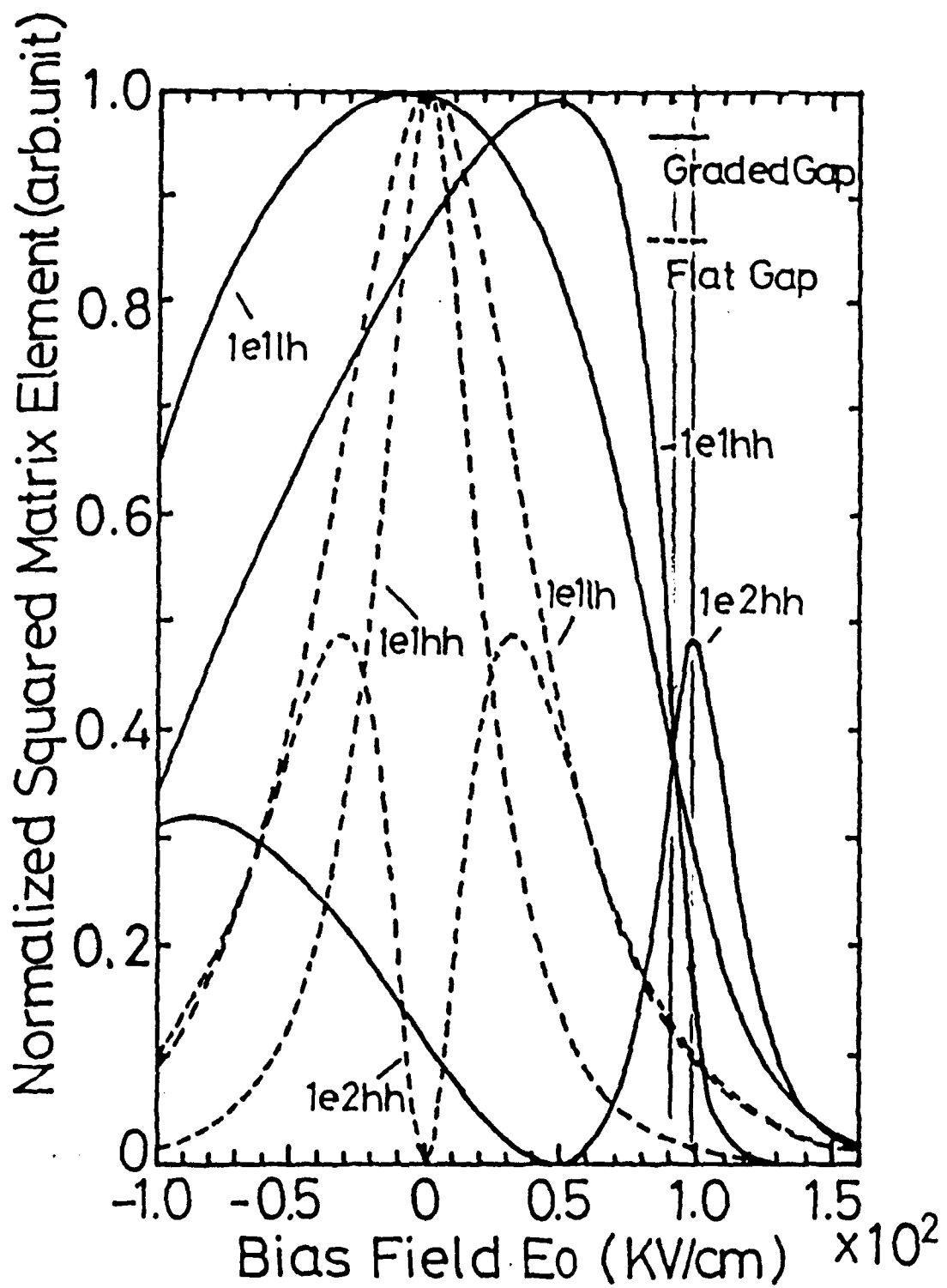


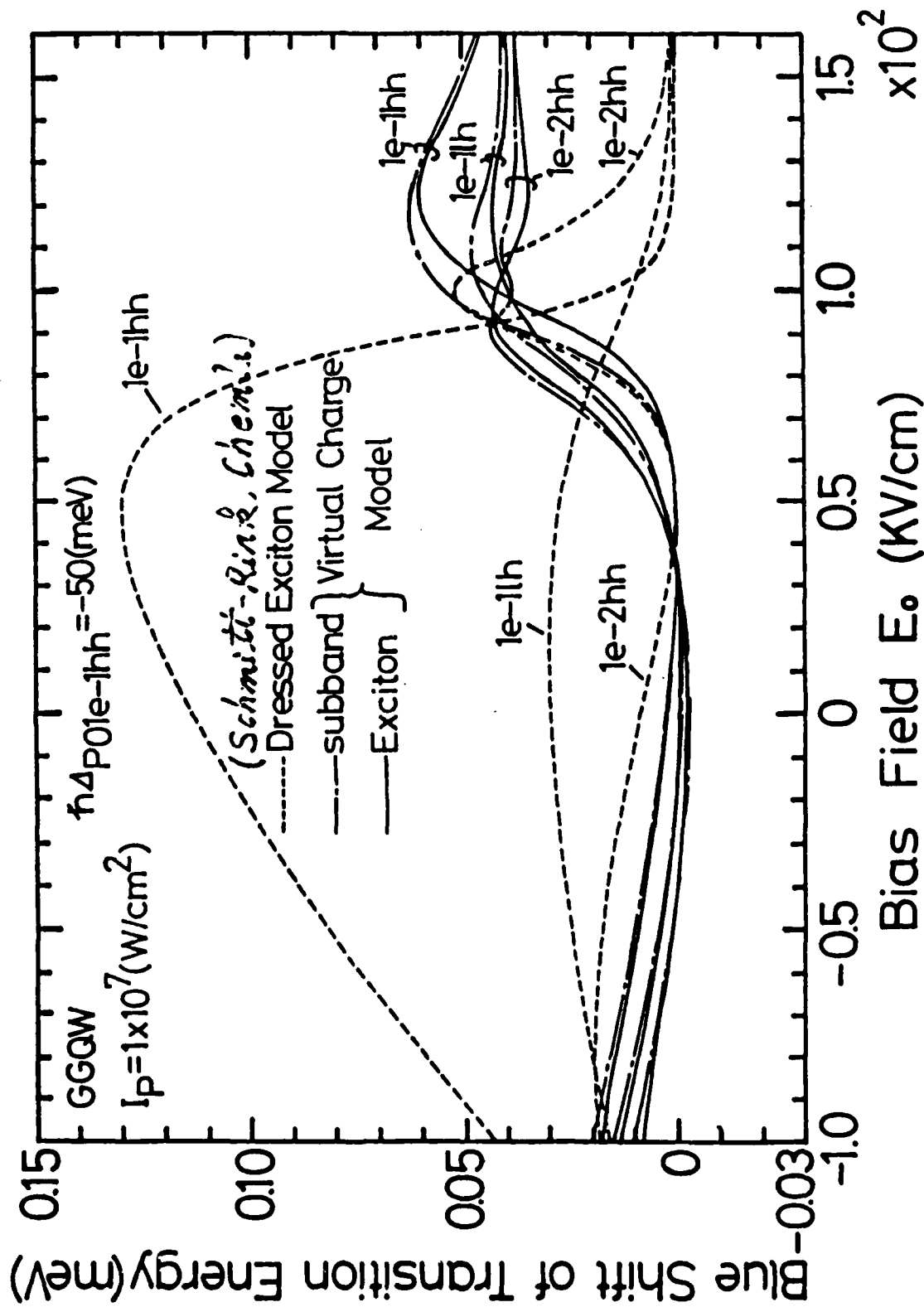
$$E_s = 8 \text{ KV/cm for } I_p = 10^9 \text{ W/cm}^2$$

$\Rightarrow V \sim 0.4V$ in a 25 period MQW
 (Virtual pair density $\sim 5 \times 10^{16} \text{ cm}^{-3}$)

$\text{GaAs/AlAs FGQW } L_z = 200 \text{ \AA}$
 $\text{Ga}_{1-x}\text{Al}_x\text{As/AlAs GGQW } L_z = 200 \text{ \AA}$
 $(x = 0 \rightarrow 0.3)$







Virtual PSF: $4\Omega_{pij}^2 / (\Delta_{poi}^2 + 4\Omega_{pij}^2)$

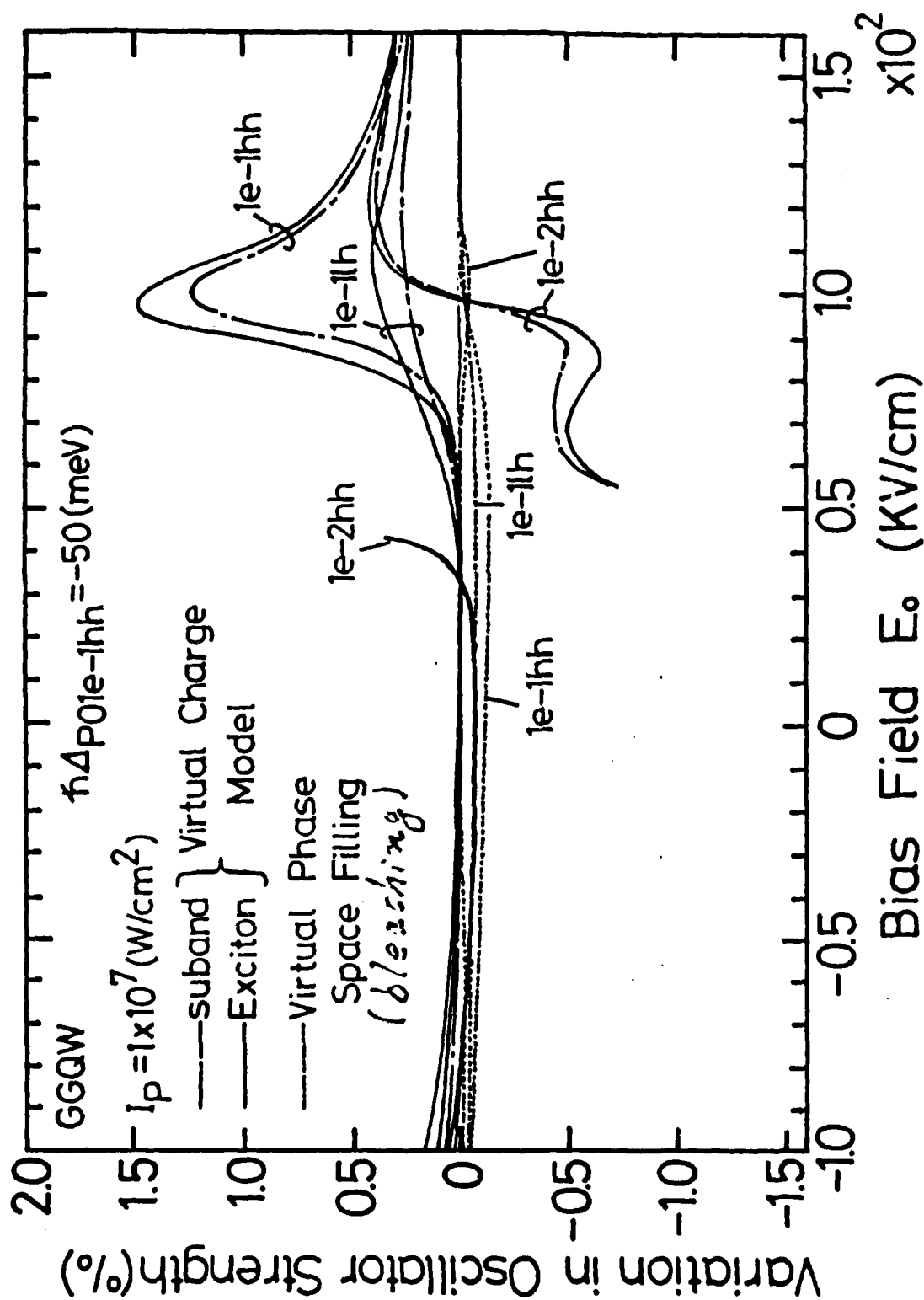


Fig. 6(b) M. Yamashita +

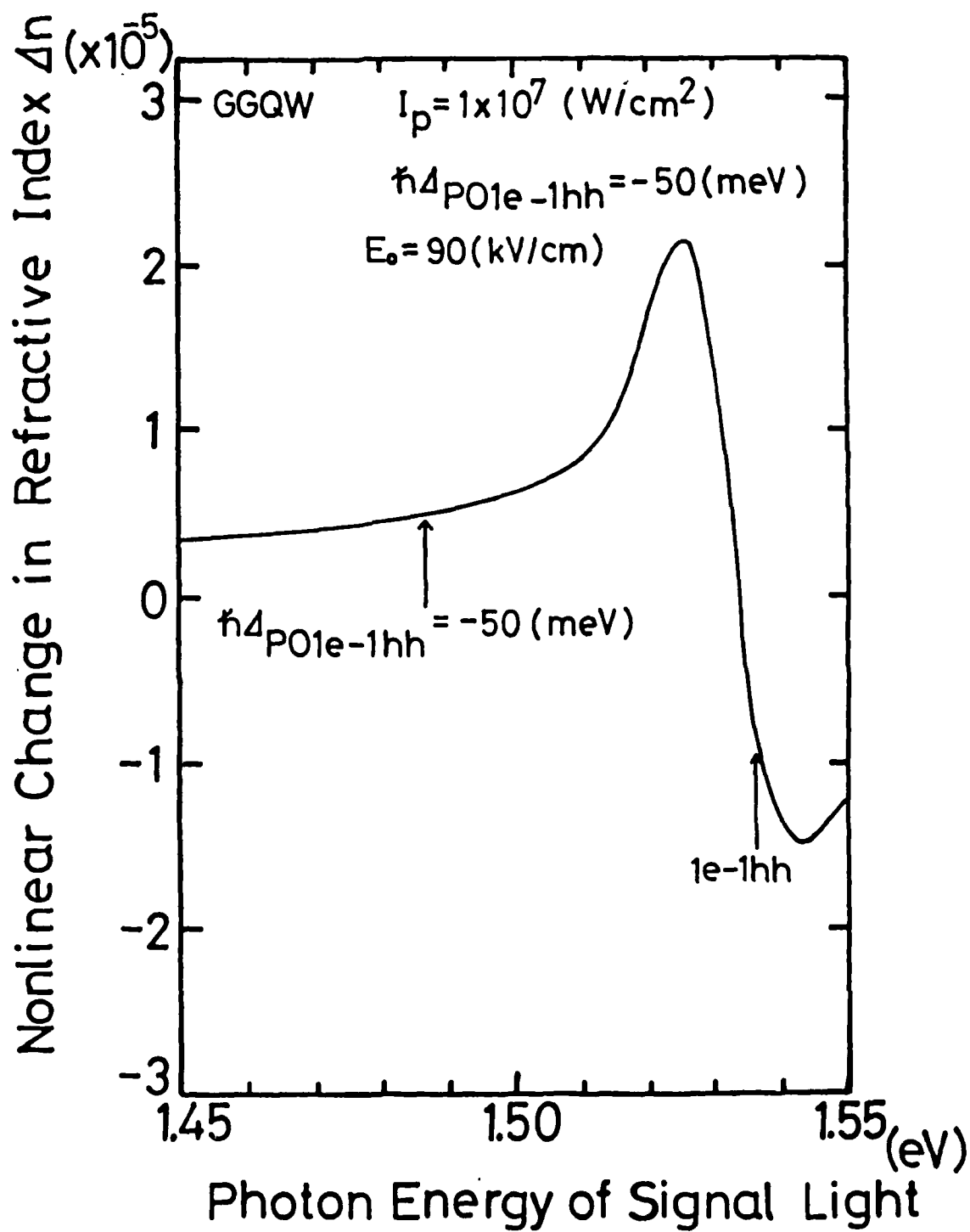


Fig. 7(h) M. Yamashita et al.

Table 1 Estimated nonlinear refraction coefficient n_2 and effective degenerate four-wave $\chi^{(3)}$ s. The FGQW and GGQW were assumed to be biased by electric fields of 20KV/cm and 90KV/cm, respectively. The $\chi^{(3)}$ s are the values for MQW samples with equal well and barrier thickness.

$$n = n_1 + n_2 I_p$$

$$\chi^{(3)}(-\omega_p, \omega_p, -\omega_p, \omega_p) = (1/3)(n_1^2 c_0 \epsilon_0) n_2 \times (1/2)$$

QW ($L_z = 200\text{\AA}$)	Detuning energy $\hbar\Delta_{p01e1hh}$	n_2 [cm^2/W]	$\chi^{(3)}$ [esu]
FGQW	-50 meV	8×10^{-14}	3.2×10^{-11}
GGQW	-50 meV	4.8×10^{-13}	1.9×10^{-10}
	-35 meV	2.6×10^{-12}	<u>1.0×10^{-9}</u>

cf. QW ($L_z = 100\text{\AA}$) $\hbar\Delta_p = 42\text{ meV}$, $E_0 = 100\text{KV/cm}$
 $\chi^{(3)} \sim 7 \times 10^{-11}$ [esu] by D. S. Chemla et al.

$\chi^{(3)} \sim 10^{-12}$ [esu] CS_2 Kerr effect
 $\sim 10^{-14}$ [esu] Silica Fiber

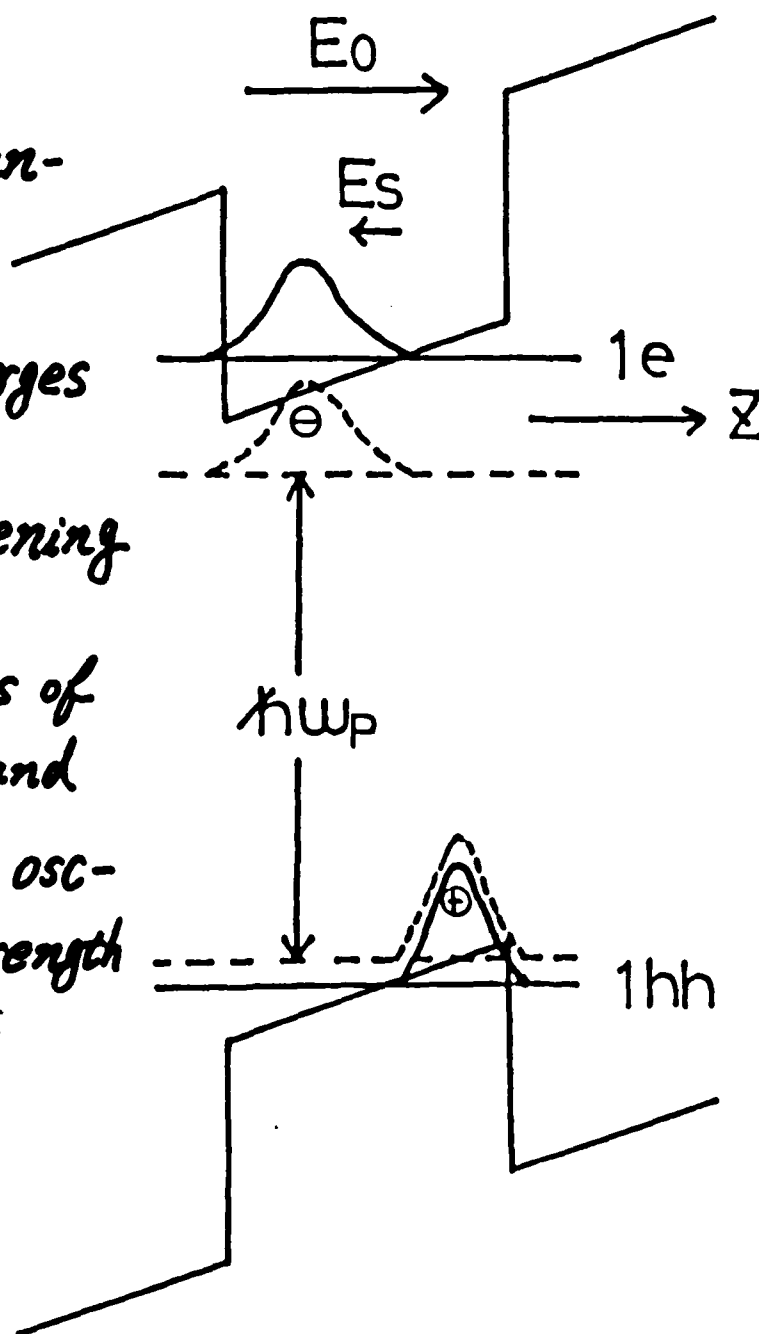
1) Off-resonant
pump light

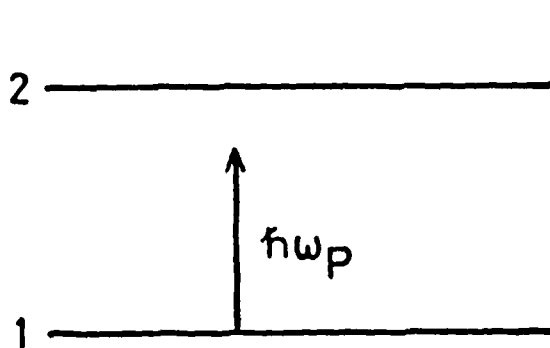
2) Virtual tran-
sitions

3) Virtual charges
 $< 100 \text{ f.s.}$

4) Field screening
 $\leq 10 \text{ f.s.}$

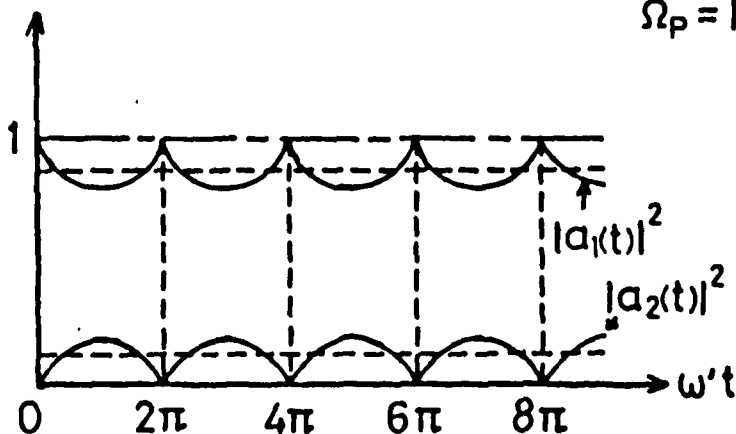
5) Blue shifts of
band gap and
changes in osc-
illator strength
 $\sim 100 \text{ f.s.}$





$E_p \cos(\omega_p t)$: pump light

$$\psi(\vec{r}, t) = a_1(t)\phi_1(\vec{r})e^{-i\omega_1 t} + a_2(t)\phi_2(\vec{r})e^{-i\omega_2 t}$$



$$(\omega')^2 = \Delta_p^2 + 4\Omega_p^2$$

Detuning frequency

$$\Delta_p = \omega_p - (\omega_2 - \omega_1)$$

$$\Omega_p = \mu E_p / 2\hbar$$

Rabi frequency

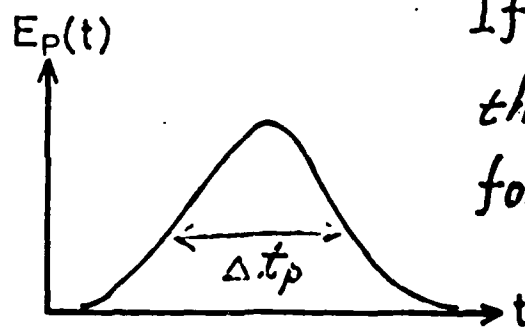
Polarization

$$P_{DC} = \langle \psi | -ez | \psi \rangle_{DC}$$

$$= \{1 - |\overline{a_1(t)}|^2\} \langle \phi_1 | +ez | \phi_1 \rangle + |\overline{a_2(t)}|^2 \langle \phi_2 | -ez | \phi_2 \rangle$$

virtual hole

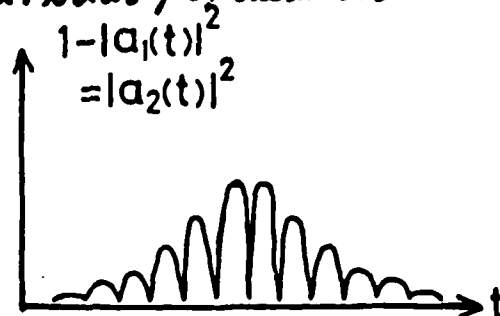
virtual electron



If $1/|\Delta_p| \ll \Delta t_p$,
the virtual charges can
follow up the pump pulse.

$$|\hbar\Delta_p| = 60 \text{ meV} \Rightarrow |1/\Delta_p| = 10 \text{ fs}$$

virtual population



$$\begin{aligned} 1 - |a_1(t)|^2 &= |a_2(t)|^2 = \left(\frac{2\Omega_p}{\omega'}\right)^2 \sin^2(\omega't/2) \\ &= \left(\frac{2\Omega_p}{\omega'}\right)^2 \sin^2(\Omega_p t) \end{aligned}$$

spatial polarization

$$\begin{aligned} \langle P_{DC} \rangle_{QW} &= \sum_{i=1hh, 2hh, \dots} \sum_{j=1e, 2e, \dots} \int (ez) (|\psi_i(z)|^2 - |\psi_j(z)|^2) dz \\ &\times \left[\left(\frac{2\Omega_{pij}^2}{\Delta_{pij}^2 \epsilon_x + 4\Omega_{pij}^2 \alpha} \right) \frac{2|\phi_{exij}(0)|^2}{L_z} \text{ exciton} \right. \\ &\left. + \int_0^\infty \left(\frac{2\Omega_{pij}^2}{\Delta_{pij}^2 + 4\Omega_{pij}^2} \right) \left(\frac{m_{rij}^*}{\pi \hbar^2 L_z} \right) dE \right] \quad (4) \end{aligned}$$

where $\Omega_{pij} = (\int \psi_i^*(z) \psi_j(z) dz) \langle u_1 | er | u_2 \rangle_c \cdot E_p / 2\hbar$,

$$\Delta_{pijex} = \omega_p - \omega_{exij}$$

$$\Delta_{pij} = \omega_p - (\omega_j - \omega_i) - E/\hbar, \quad \alpha = 2|\phi_{exij}(0)|^2 / N_s^{psF} = \frac{32}{7}$$

$$1e, \dots, 4e,$$

$$1hh, \dots, 8hh,$$

$$1eh, \dots, 16eh, \\ 4$$

$$E_s = \langle P_{DC} \rangle_{QW} / \epsilon_0 \epsilon_s$$

Summary

1) Proposal of Ultrafast Optical
Nonlinearity in DC Biased QWs: TCON
over all switching time $\sim 100 \text{ fs}$
(ON. OFF)

2) For a GGQW ($L_z = 200 \text{ \AA}$)
Blue shift of $E_g \sim 0.05 \text{ meV}$
Percentage change in
 $|e-hh|$ oscillator strength, $\sim 1.5\%$
for $I_p = 1 \times 10^7 \text{ W/cm}^2$, $\hbar \Delta_{p0 | e-hh} = -50 \text{ meV}$
and $E_0 = 90 \text{ KV/cm}$.

Effective degenerate four-wave
mixing $\chi^{(3)}(-\omega_p, \omega_p, -\omega_p, \omega_p)$,
 $1 \times 10^{-9} [\text{esu}]$

3) Virtual charge polarization:
a key process in the nonlinearity
a new opportunity in OE devices -303

WHY LOSE SLEEP OVER II-VI COMPOUND SEMICONDUCTOR SUPERLATTICES ? : SELECTED EXAMPLES

S. Chang, Q. Fu, D. Lee, A. Mysyrowicz, A. Nurmikko (Brown)
J.-W. Wu (Indiana)
R. Gunshor, L. Kolodziejski (Purdue)

Outline

- * Bandoffsets, Excitons, and Some Phonons in $\text{CdTe}/(\text{Cd,Mn})\text{Te}$ Quantum Wells
- * Interfaces and the Magnetic Polaron Problem
- * Excitonic Molecules in ZnSe Quantum Wells
- * Dynamics of Nonequilibrium Carriers
- * Magnetic Properties in Lower Dimensions \sim monolayer MnSe
(MSS III)

New: II-VI Superlattices: (strained layer)

1985-

~~CdTe/(Cd,Mn)Te~~ CdTe/ZnTe

~~ZnSe/(Zn,Mn)Se~~ ZnSe/ZnTe

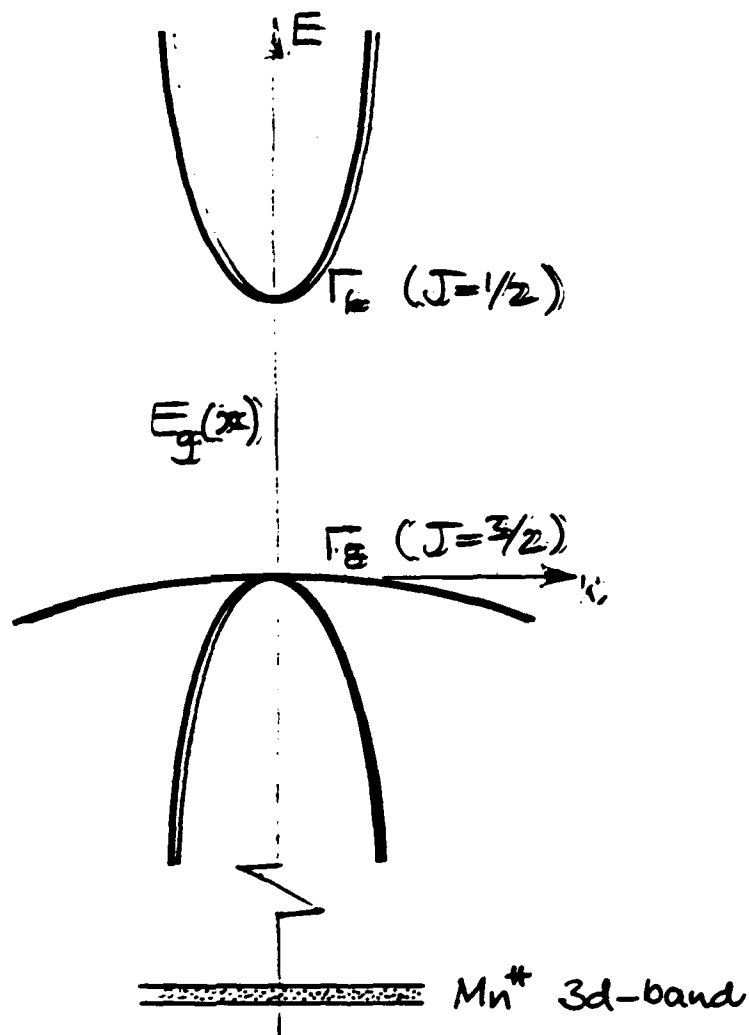
ZnSe/Zn(S,Se) ZnS/ZnTe

- ** optical devices in blue wavelength region (ZnSe)
- ** strong exciton effects in optical spectra (quasi 2D ?)
- ** bandoffset questions (common anion vs. cation, polarity)
- ** magnetic properties in lower dimensions : 3D \rightarrow 2D
- * large electron-phonon coupling

\rightarrow doping still a problem

'Semimagnetic' (Diluted Magnetic) Semiconductors:

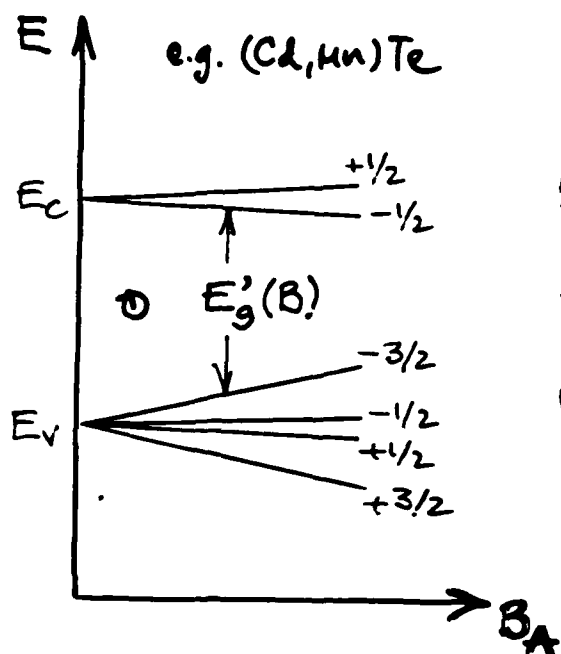
eg.



exchange interaction of s- and p-band electrons with Mn-ion d-electron states: short range (a_0)

$$H_{\text{exch}} \sim \sum_j J(\vec{r}_e - \vec{R}_j) \vec{s}_e \cdot \vec{S}_j$$

e.g. external magnetic field (bulk material)



MFA:

$$E'_g = E_g^0 - N_0 x (\alpha - \beta) \cdot S_z(B_A)$$

where

$$S_z = S_0 B_{S/2} (g \mu_B B_A / k T_L)$$

$\sim S/2$

(paramagnetic limit)

\nearrow low x

\rightarrow 'giant' Zeeman effect (low T)

$$\Delta E_g \approx g_{\text{eff}} \mu_B B_A, \quad g_{\text{eff}} \gtrsim 100-200$$

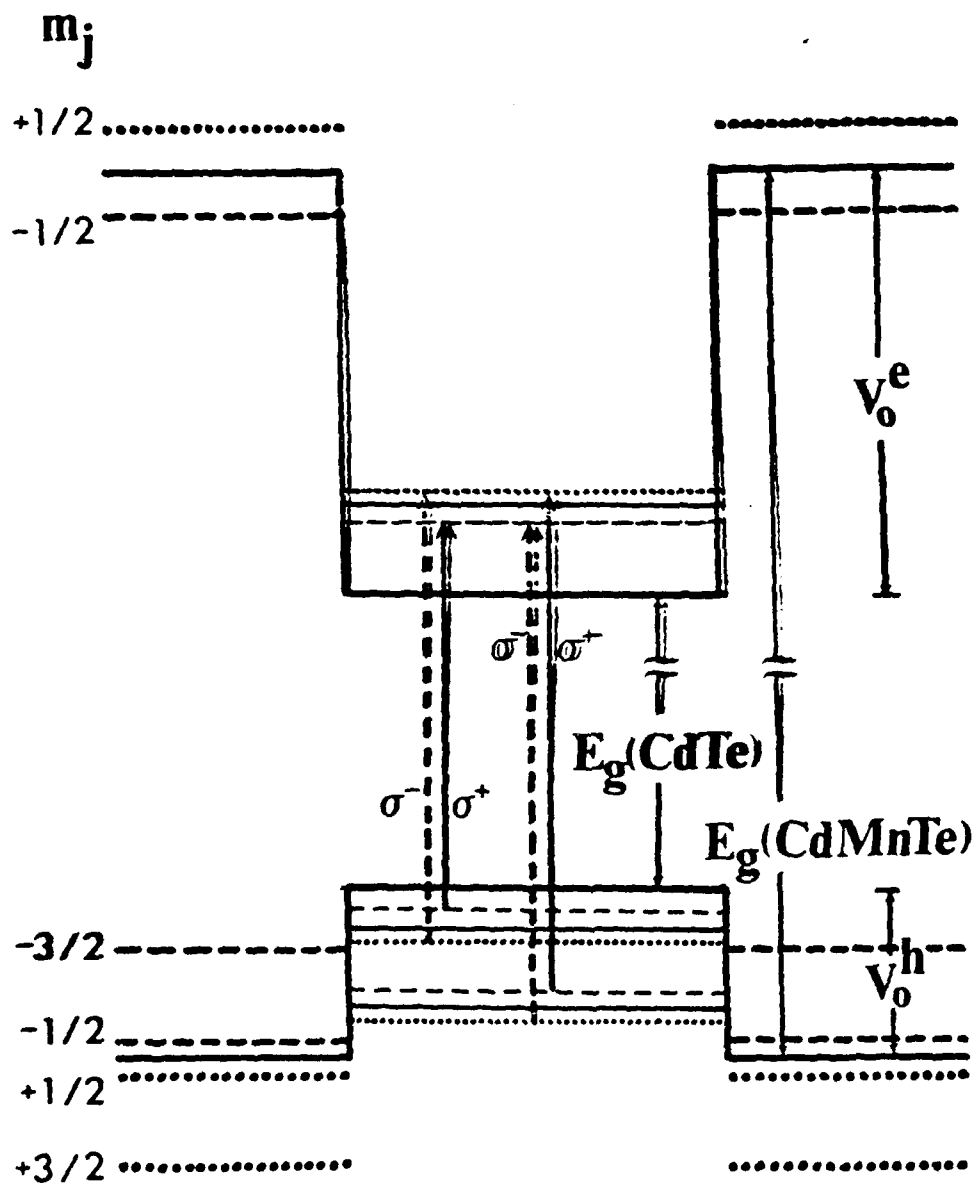


THE NEW YORK HILTON
At Rockefeller Center

Bandoffset Question in Wide-Gap II-VI Heterostructures

- * sparse experimental information to date \leftrightarrow theory
- * early indicators that ΔE_v is small for CdTe/(Cd,Mn)Te (also for CdTe/ZnTe)
- * exciton effects strong e.g. for CdTe, ZnSe, ZnTe etc.
- * exploit the magnetic "tunability" in a DMS quantum well

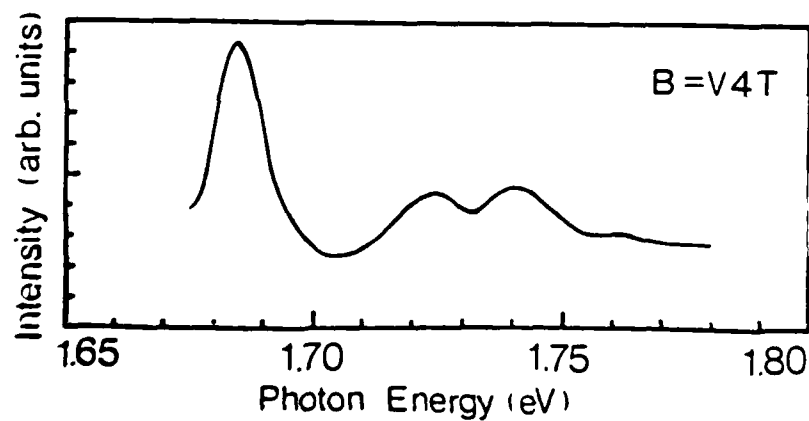
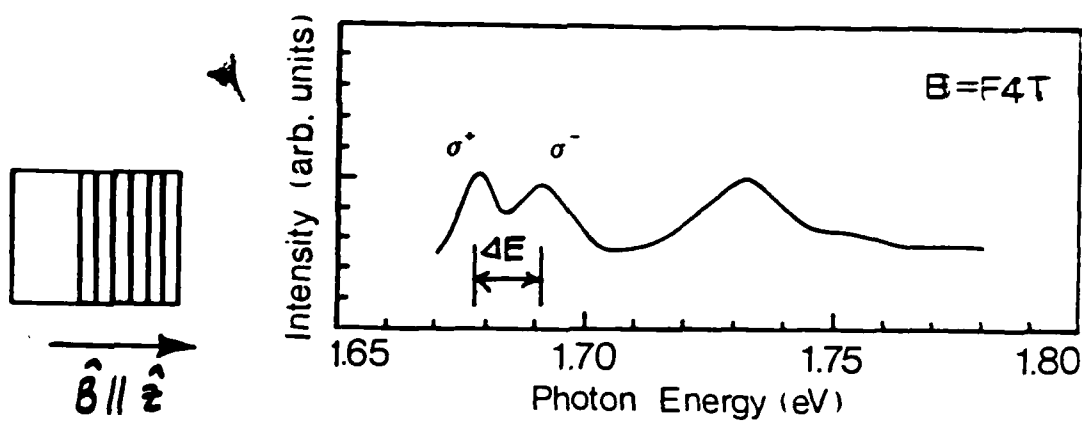
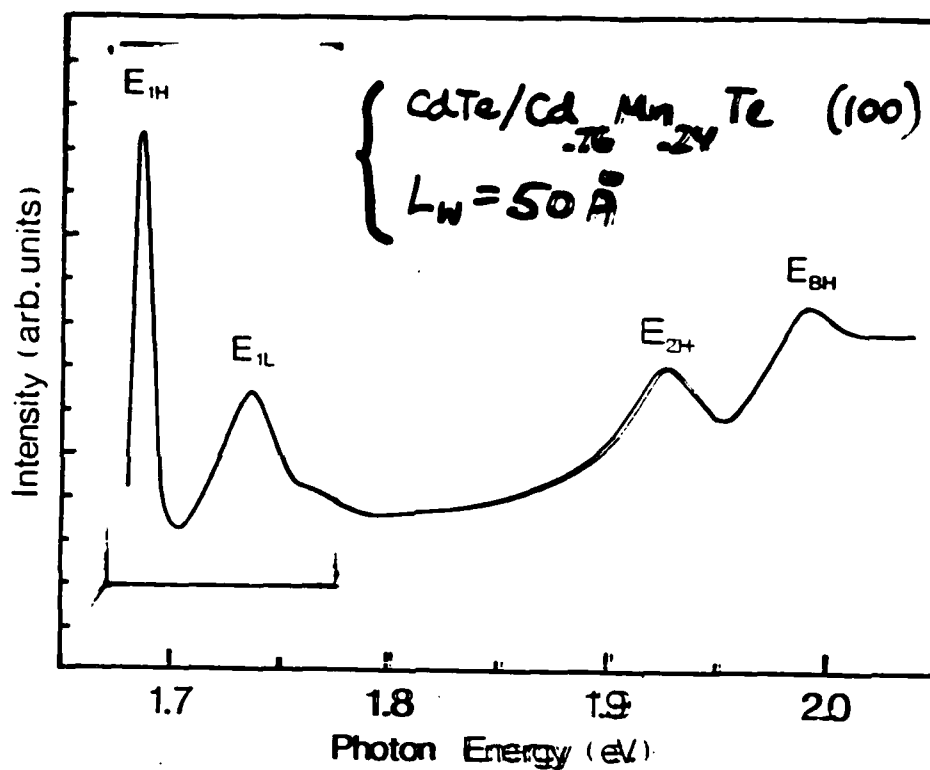
'Giant' Zeeman Effect : Bandoffset and Exciton Effects



- e-h pair vs. exciton

- Faraday vs. Voigt

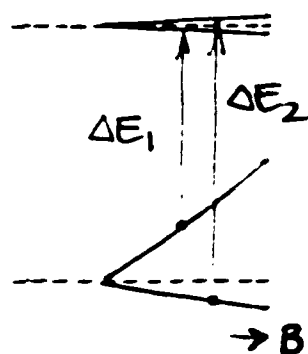
→ anisotropy in exchange interaction



$\left\{ \begin{array}{l} \text{CdTe/Cd}_{.76}\text{Mn}_{.24}\text{Te MQW, } L_w = 50 \text{ \AA} \quad (100) \\ \text{Zeeman splittings in } B_z = 4 \text{ Tesla} \quad (T = 2 \text{ K}): \end{array} \right.$

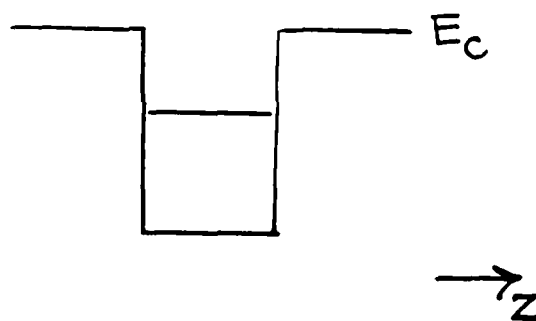
	$n=1 \text{ HH}$	$n=2 \text{ HH}$	$n=1 \text{ LH}$	barrier _{HH}
ΔE	14 meV	44 meV	$\leq 3 \text{ meV}$	80 meV
	$\leq 4 \text{ meV}$		17 meV	

- Single particle calculation predicts large asymmetry in $\Delta E = \Delta E_1 + \Delta E_2$

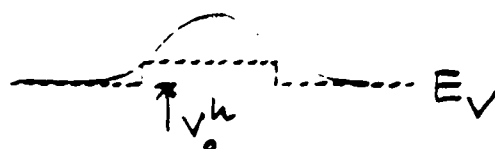


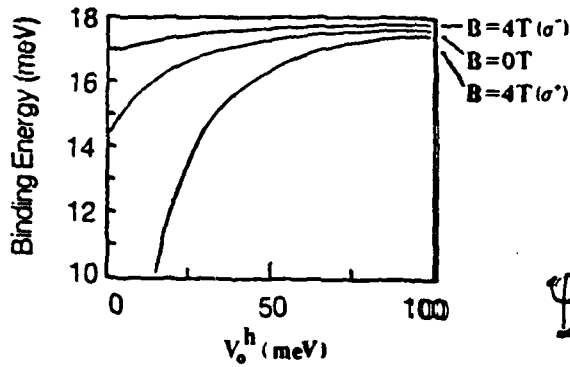
- with exciton contribution $\Delta E_1 \approx \Delta E_2$ as observed

- Coulomb attraction adds 'extra depth' for hole potential



$$V_{\circ}^{hx} > V_{\circ}^h$$



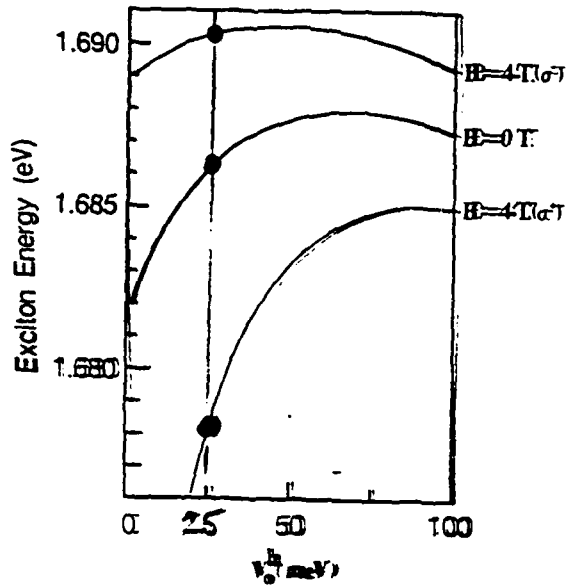


$$\Psi = \psi(z_e) \psi(z_h) \phi(r_{\perp}, z_e - z_h)$$

$$\phi(r_{\perp}) = \frac{\sqrt{2}}{\pi} \lambda^{-1} e^{-r_{\perp}/\lambda}$$

Coulomb interaction:

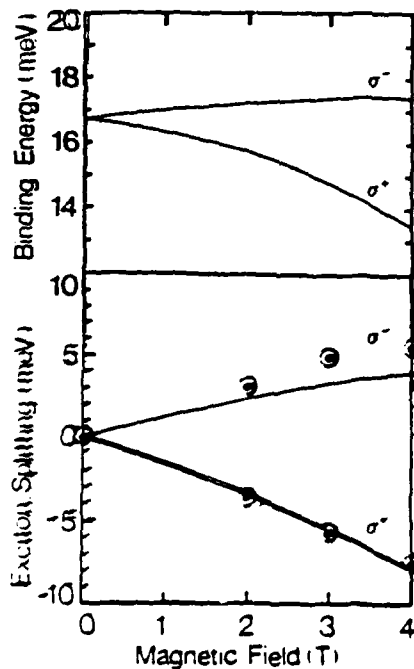
$\psi(z_e)$ and $\psi(z_h)$
no longer simple solutions
in z -directions of
the Hamiltonian.



$$V_o^h = 25 \text{ meV}$$

$$V_o^e \approx 360 \text{ meV}$$

Subtract strain
 $V_o^h \approx 0 \text{ meV}$



$$E_B^{\text{FW}} \rightarrow 20 \text{ meV}$$

$$(E_B^{\text{CITE}} \sim 9 \text{ meV})$$

Summary: CdTe/(Cd,Mn)Te MQW

- * Excitation spectroscopy in external magnetic fields at exciton transitions of the QW and barrier layers: 'tuning' of offsets
- * Theory to account for the strong Coulomb effects in the case of a 2D-electron and a quasi 3D-hole
- * Determination of conduction to valence band offset of 14:1 for a particular QW; when corrected for strain, the valence band offset is zero within 10 meV for the heavy hole

→ at variance with
theory by Tersoff
(interface dipoles)

→ devices (APD & vertical
transport)

Recombining vs. Absorbing Exciton:

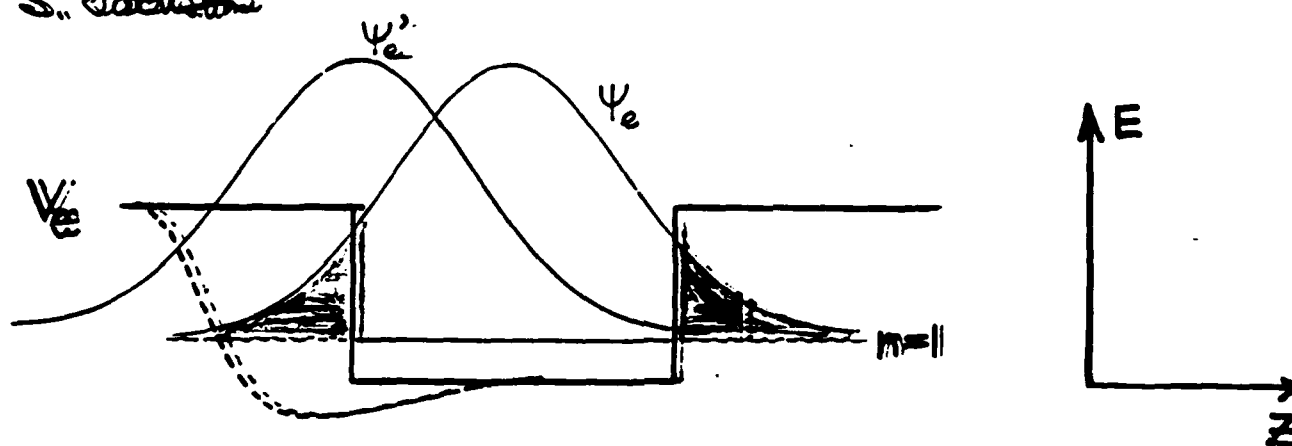
"Magnetic Relaxation" at an interface of a CdTe/(Cd,Mn)Te QW
(Magnetic Polaron)

Concavalves dia. Silvae

J. Inl. W. et. al.

S. Jochims

bulk = Benoit et. al.
Spont. + Dietl
Wolff et. al



$$H \sim p_e^2 / 2m_e^* + \theta(z - L/2) \cdot \left[V_0^e - V_m^e B_{5/2} (g\mu_B \vec{B}_{\text{eff}}(\vec{r}) / \hbar) \right]$$

(MFA) $\hookrightarrow \alpha \text{ or } \beta$

- magnetically induced interface localization (spontaneous magnetization)
- MP effect enhanced for small bandoffset

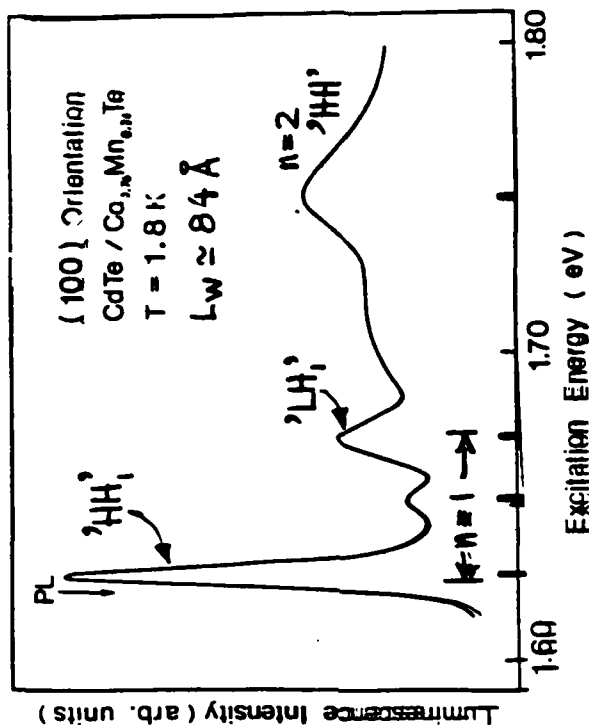
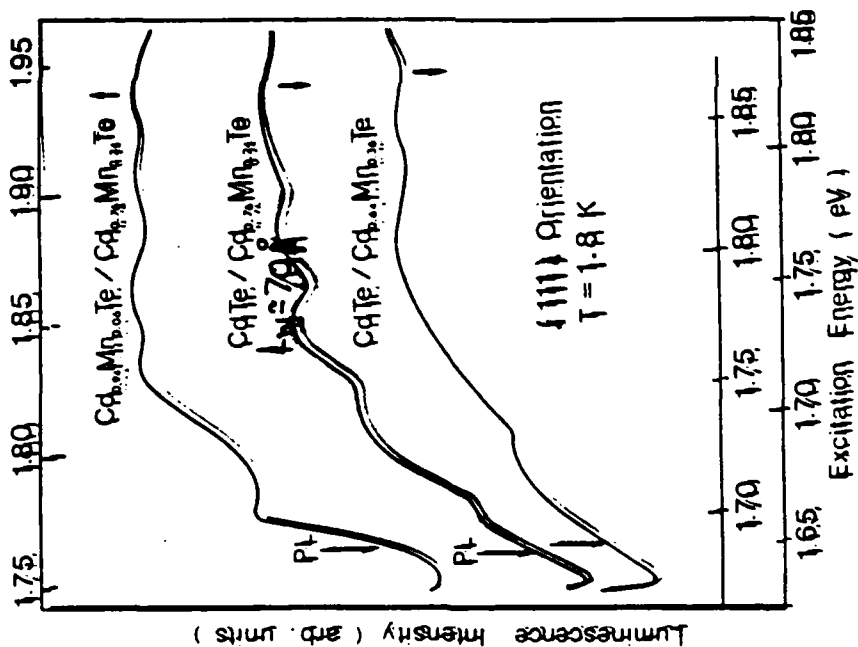
\hookrightarrow CdTe/Cd_{1-x}Mn_xTe

$$V_m^h \ll V_0^e ; \beta > \alpha$$

valence band
→ valence band empty

Differences between (111) and (100) CdTe/(Cd,Mn)Te photoluminescence excitation spectra

S-K. Chang et al.



$$\overline{\Delta E}_v \sim 30 \text{ meV} \approx 0.1 \Delta E_c ?$$

but, a DMS quantum well !

- strain fluctuations } exciton broadening
- microfield screening (Smith, Hainriot)

Q. Fu, Don Lee, Andre Mysyrowicz

Excitonic Molecules in ZnSe Quantum Wells

bulb
2D
H₂

* well established in bulk (e.g. CuCl)



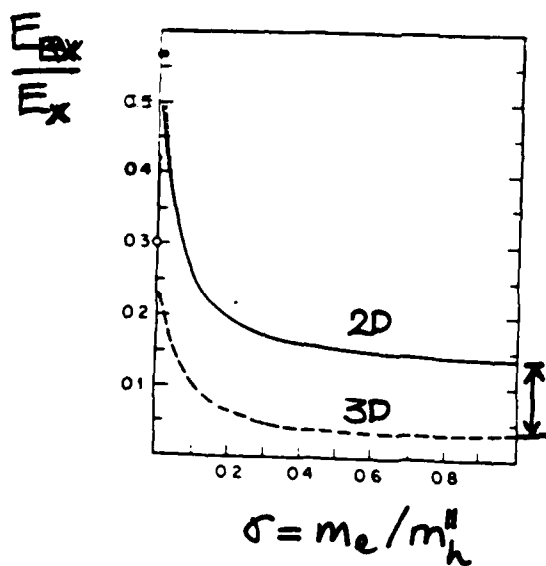
Chad
Peggy

* quasi-2D enhancement for (i) exciton binding and
(ii) molecular binding energy

→ overall $\geq 10\times$ over 3D case

* II-VI vs. III-V heterostructures

→ GaAs/(Ga,Al)As, R. Miller et al.
→ bulk ZnSe $E_{ex} \sim 2-3$ meV

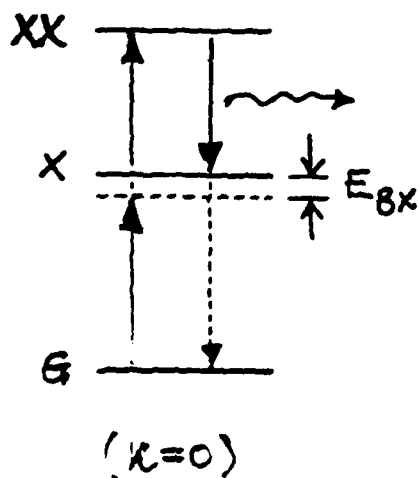
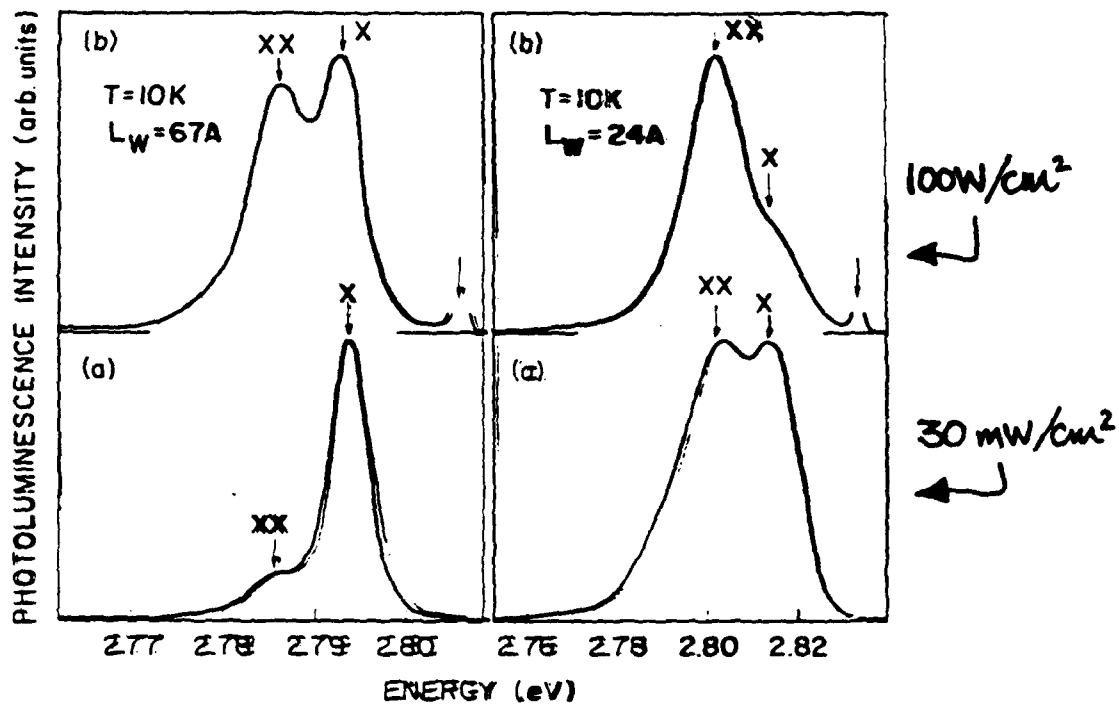


D.A. Kleinman
(1983)

Biese
Exc.
mol.

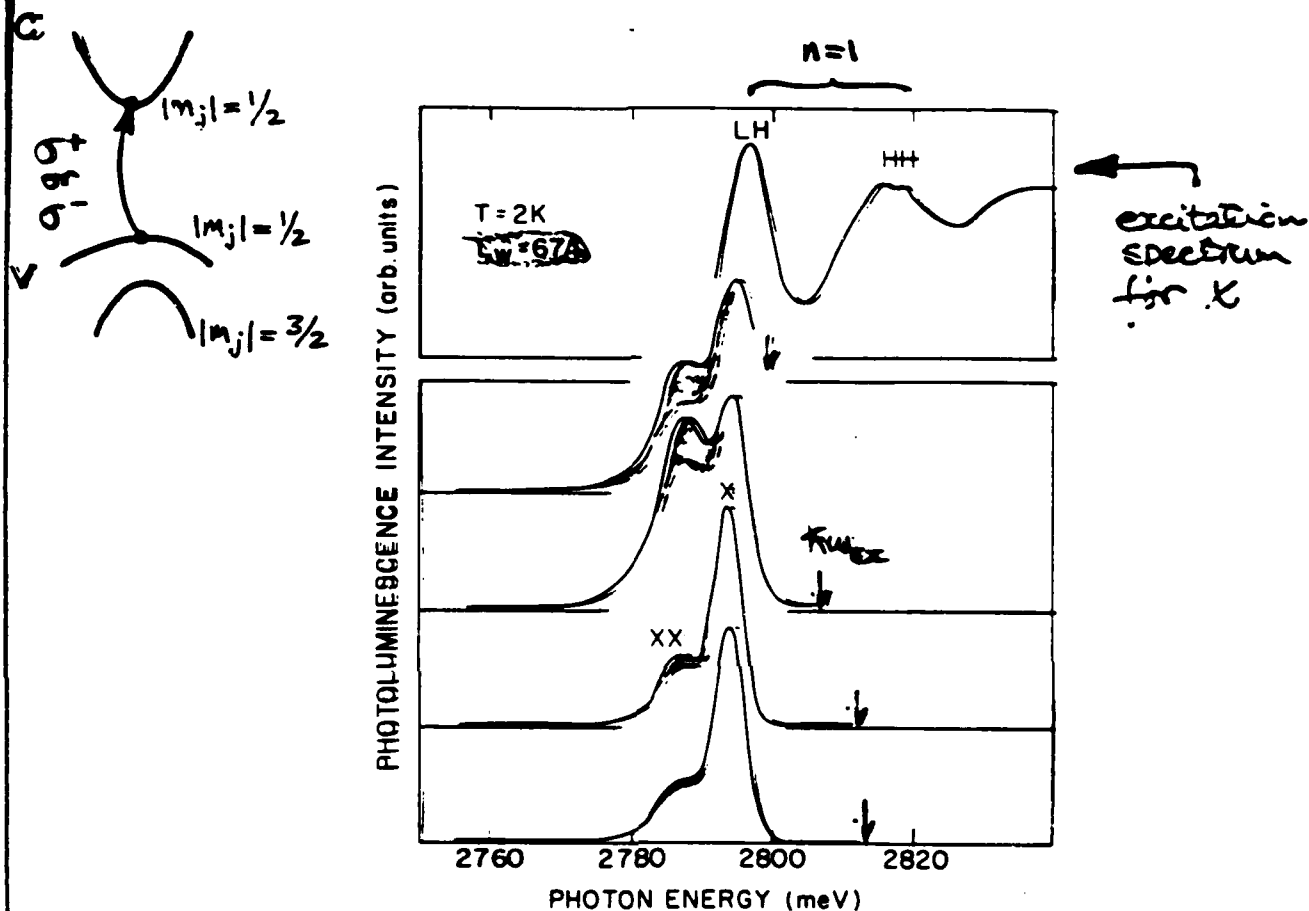
Carl
Linder

$\text{ZnSe}/\text{Zn}_{.72}\text{Mn}_{.28}\text{Se}$ MQW



- 'XX' gains over X with increasing excitation
- Kinetics complicated & difficult to quantify
- 'XX' prominent at low excitation levels

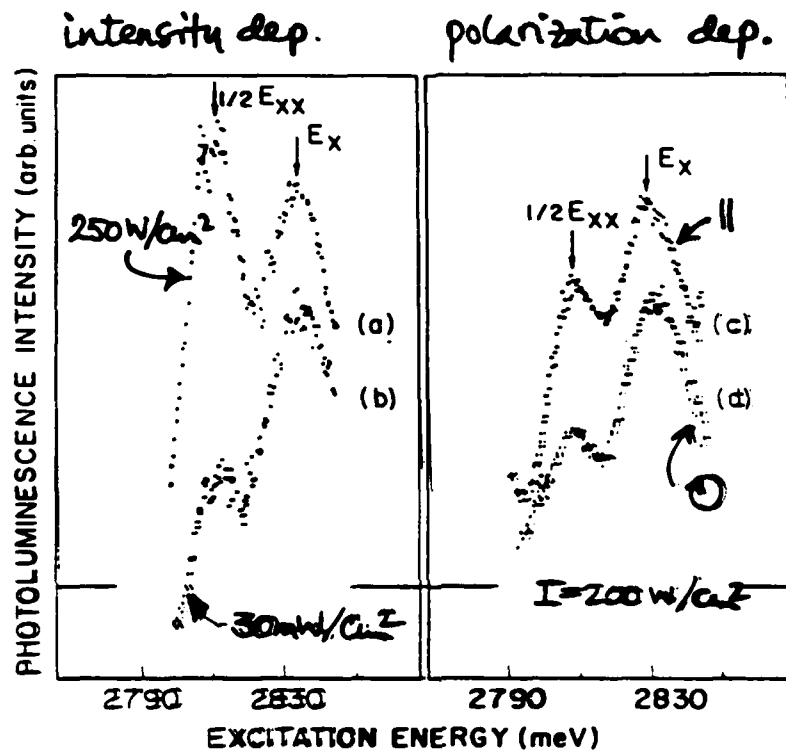
Excitation by circular vs. linear polarization:



- large polarization contrast for XX and X (molecule in singlet state)
- spin relaxing collisions for $\hbar\omega_x \gg E_x$

Giant Two-Photon Absorption

→ excitation spectrum of line 'XX'



$\text{ZnSe/Zn}_{0.72}\text{Mn}_{0.28}\text{Se}$

$L_W = 24 \text{ \AA}$

$T = 2 \text{ K}$

- ($k=0$) $E_{BX}/2 = E_X - \hbar\omega$ at TPA resonance

→ $E_{BX} \sim 40 \text{ meV}$ for $L_W = 24 \text{ \AA}$

from PL $E_{BX} \sim 33 \text{ meV}$

$E_{BX} \sim 11 \text{ meV}$ $L_W = 67 \text{ \AA}$

- note low intensities

Summary

- * evidence for excitonic molecule in ZnSe/(Zn,Mn)Se quantum wells from luminescence, nonlinear absorption, polarization selection rules, and temperature dependence.
- * scaling of E_{Bx} with well thickness roughly as predicted
- * surprisingly stable molecular state $E_x^{30}(ZnSe) \sim 20 \text{ meV}$
- * microscopic details not yet known
 - QW profile
 - band offsets

Enhanced Excitonic Optical Nonlinearity and Exciton Dynamics in
Semiconductor Microstructures

T. Takagahara

NTT Electrical Communications Laboratories, Musashino-shi,
Tokyo 180, Japan

The mechanisms of enhanced excitonic optical nonlinearity in semiconductor microstructures are clarified to be the easily attainable state filling of discretized levels due to the quantum size effect and the enhanced oscillator strength. The calculated third-order nonlinear susceptibility explains successfully the recent experimental results. A comprehensive interpretation of the exciton dynamics in semiconductor microcrystallites is presented to explain the fast and slow decay components in phase conjugation and luminescence measurements.

Recently the excitonic states in semiconductor microstructures have attracted much attention due to the enhanced excitonic optical nonlinearity and fast response time [1-7]. In semiconductor microstructures of lower dimensionality, the energy levels of carriers are discretized due to the quantum size effect. The oscillator strength becomes concentrated on the sharp transitions of the lower energy and the mechanism of excitonic optical nonlinearity is simply the state filling of these sharp excitonic transitions in contrast to the band filling of continuum states in the bulk material. As a consequence, the excitonic optical nonlinearity is enhanced while the saturation power is reduced, relative to the bulk semiconductor. The response time of the optical nonlinearity is determined by the build-up time and recombination lifetime of photo-generated carriers. The dynamics of photo-generated carriers in semiconductor-doped glasses have been studied extensively by the transient grating method [1,3-7] and photo-luminescence [3-5,8,9]. Some controversies

exist about the origins of the fast and slow components of the electron-hole recombination [1,3-9] .

First of all, the excitonic states in semiconductor quantum dots are discussed. The energy of the excitonic state measured from the bulk band gap energy consists of the kinetic energy of the electron and hole(E_k), the Coulomb energy between them(E_c) and the surface polarization energy(E_s) [10] . These are shown in Fig.1 as a function of the quantum dot radius normalized by the exciton Bohr radius a_B in bulk crystals. The exciton binding energy in a semiconductor quantum dot is obtained from the energy difference between the exciton state and a free electron-hole pair state. Figure 2 shows the dependence of the exciton binding energy on the normalized quantum dot radius. It is important to note that the rather small exciton binding energy implies the ionization of excitonic states at room temperature. In fact, for semiconductor(CdS) quantum dots with radii in the range shown in Fig.2, the excitonic state may be ionized to the free electron-hole pair state at room temperature.

The radiative recombination lifetime τ_R of excitons in a quantum dot can be estimated from the oscillator strength of the excitonic transition [11] . For a free electron-hole pair in a semiconductor(CdS) quantum dot, the oscillator strength f_0 is estimated to be 8.14 using the relevant parameters [12] and the corresponding radiative lifetime τ_R is 440 ps. These values are independent of quantum dot size. When the excitonic effect, namely the electron-hole correlation, is included, the oscillator strength f is enhanced since it is proportional to the probability of finding an electron and a hole at the same position. This enhancement factor and the corresponding radiative recombination lifetime are given in Fig.3 as a function of the normalized radius of the quantum dot. For a 100Å radius CdS quantum dot, the radiative recombination time is estimated to be 20 ps. This value is of the same order as the so-far-reported time constants of the fast decay component in transient grating measurements [3-7] .

The excitonic optical nonlinearity in semiconductor quantum dots can be enhanced due to the large oscillator strength of the exciton and the energy level discretization which leads to an easily attainable state filling. The calculated frequency dispersions of the linear susceptibility $\chi^{(1)}$ and the third-order nonlinear susceptibility $\chi^{(3)}$ for the degenerate case, i.e., $\omega_1 = \omega_2$, are shown in Fig.4. The out-of-phase behavior between $\chi^{(3)}$ and $\chi^{(1)}$ for both real and imaginary parts explains the experimental results [2] very well. The absolute value of $\chi^{(3)}$ for CdS quantum dots is estimated to be about 3.8×10^{-8} esu for a number density N of 10^{14} cm^{-3} and for the Lifshitz-Slezov [13] distribution of quantum dot radius with an average of 100 \AA . This value is also in good agreement with the experimental value at room temperature [1]. In this calculation, the oscillator strength of the free electron-hole pair is employed in consideration of the aforementioned possibility that the excitonic state is ionized at room temperature. At low temperatures, the excitonic state is stable and its large oscillator strength is available to enhance the optical nonlinearity. In fact the excitonic optical nonlinearity at low temperatures is calculated to be as large as 10^{-4} esu.

Our comprehensive interpretation of the controversial exciton dynamics in semiconductor quantum dots is presented with respect to the exposure time dependence of the decay characteristics [5,7] and the darkening of the glass [5]. The slow decay component can be attributed to the radiative recombination of an electron and a hole trapped by a donor-acceptor pair, whose rate is dependent on the distance between the donor and the acceptor and which gives rise to a broad luminescence spectrum. This assignment is corroborated by the recent measurement of the donor-acceptor pair recombination rate in bulk CdS [14]. In the course of this recombination process, the emitted phonons induce some kind of structural change around the donor-acceptor pair and efficient non-radiative recombination centers will be formed. The temperature rise due to laser irradiation regarded as uniform in semiconductor microcrystallites is estimated to be rather small. This suggests the importance of local phonon

modes in inducing the structural change. After repeated exposure to laser irradiation, these non-radiative recombination centers are accumulated and the photo-generated carriers lose their energy via these centers. Thus the radiative recombination via a donor-acceptor pair becomes quenched leading to the disappearance of the broad luminescence spectrum [5] and also of the slow decay component in the transient grating measurements [5,7]. This accumulated structural change may be a cause of the permanent holographic grating and the darkening of the glass. This kind of photo-induced structural change is seen extensively in amorphous materials, such as a-Si [15], chalcogenide glasses [16] and Eu-doped glasses [17]. On the other hand, the fast decay component can be considered as arising from the radiative recombination of free excitons as calculated above. This interpretation is consistent with the experimental result [5] that the narrow luminescence line attributed to the excitonic recombination shows a very rapid decay. However, we have to keep in mind the possibility that the fast decay component arises from the nonradiative recombination of an electron-hole pair via defect states or surface states. Thus it is crucial to examine the size dependence of the decay time constant in identifying the origin of the fast decay component.

References:

- [1] R.K. Jain and R.C. Lind, J. Opt. Soc. Am. 73, 647(1983).
- [2] G.R. Olbright and N. Peyghambarian, Appl. Phys. Lett. 48, 1184(1986).
- [3] S.S. Yao, C. Karaguleff, A. Gabel, R. Fortenberry, C.T. Seaton, and G.I. Stegeman, Appl. Phys. Lett. 46, 801(1985).
- [4] P. Roussignol, D. Ricard, K.C. Rustagi, and C. Flytzanis, Opt. Commun. 55, 1431(1985).
- [5] P. Roussignol, D. Ricard, J. Lukasik, and C. Flytzanis, J. Opt. Soc. Am. B4, 5(1987).
- [6] D. Cotter, Technical Digest of XIV International Quantum Electronics Conference, San Francisco, June 1986, PD19.
- [7] H. Shinojima, M. Mitsunaga, and K. Kubodera, presented at the Spring

Meeting of the Physical Society of Japan, March 1987(in Japanese).

- [8] J. Warnock and D.D. Ayschalom, Phys. Rev. B32, 5529(1985).
- [9] M. Chestnoy, T.D. Harris, R. Hull, and L.E. Brus, J. Phys. Chem. 90, 3393 (1986).
- [10] L.E. Brus, J. Chem. Phys. 80, 4403(1984).
- [11] C.H. Henry and K. Nassau, Phys. Rev. B1, 1628(1970).
- [12] C. Welsbuch and R.G. Ulbrich, in Light Scattering in Solids III, ed. M. Cardona and G. Guntherodt(Springer, Berlin 1982), p.218.
- [13] I.M. Lifshitz and V.V. Slezov, J. Exptl. Theoret. Phys.(U.S.S.R) 35, 479 (1958) [Sov. Phys. J.E.T.P. 35, 331(1959)] .
- [14] R.T. Cox and J.J. Davies, Phys. Rev. B34, 8591(1986).
- [15] R.A. Street, Adv. Phys. 30, 593(1981).
- [16] K. Tanaka, In Fundamental Physics of Amorphous Semiconductors, ed. F. Yonezawa(Springer, Berlin 1981), p.104.
- [17] F.M. Durville, E.G. Behrens, and R.C. Powell, Phys. Rev. B35, 4109(1987).

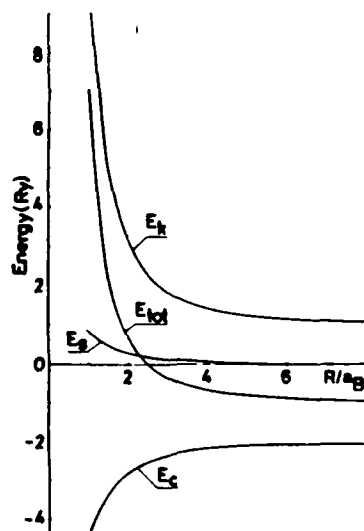


Fig.1: Exciton energy (E_{tot}) versus radius of spherical semiconductor particles (quantum dots). E_k denotes the kinetic energy, E_c , the Coulomb energy and E_g is the surface polarization energy, respectively. a_B is the exciton Bohr radius in bulk semiconductors.

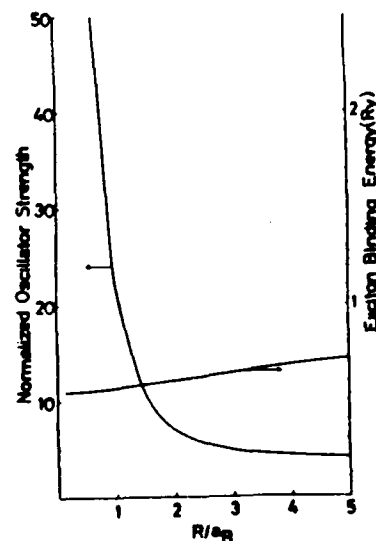


Fig.2: Exciton binding energy in units of Rydberg (Ry) and normalized oscillator strength in spherical semiconductor particles plotted as a function of particle radius.

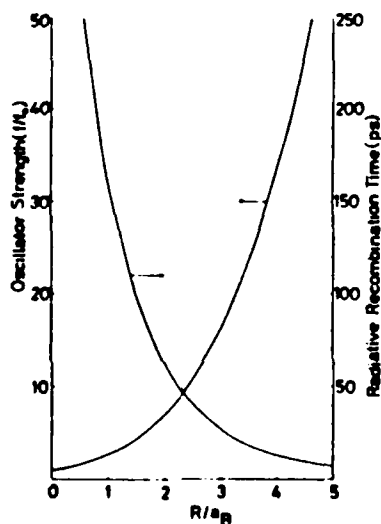


Fig.3: Enhancement factor of the oscillator strength of exciton relative to that of free (uncorrelated) electron-hole pair and the radiative recombination time in spherical semiconductor particles plotted as a function of particle radius.

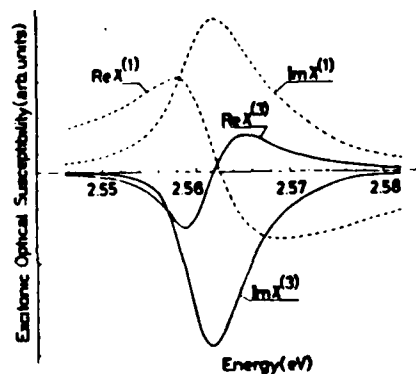


Fig.4: Frequency dispersion of $\chi(1)$ and $\chi(3)$ of spherical semiconductor (CdS) particles. Particle size distribution is taken into account by the Lifshitz-Slezov distribution function for an average radius of 100 Å.

FREE CARRIER NONLINEAR OPTICS

P. A. WOLFF

Francis Bitter National Magnet Laboratory
MIT, Cambridge, MA 02139

Free carriers in semiconductors cause optical nonlinearity in two ways. In some cases it arises from the inherent nonlinearity of electron dynamics in crystals; in others it is caused by scattering. Such processes are interesting because they can be used to study carrier dynamics and kinetics in semiconductors. In particular, the large frequency dispersion of these nonlinearities determines carrier relaxation times. These times, which are generally in the picosecond range, also characterize the speed of the nonlinearity.

Until lately, all known free-carrier-induced optical nonlinearities were weak. We have recently investigated two crystals, HgTe and HgCdSe:Fe, in which large, fast, free-carrier-induced $\chi^{(3)}$'s may be attainable. These materials will be used as examples to illustrate the mechanisms and features of free-carrier-induced optical nonlinearity.

Large, room temperature, third order nonlinear optic susceptibilities are observed in HgTe and HgMnTe at 10.6μ . These materials have the largest known third order optical nonlinearities with response times in the picosecond range. In HgTe, $\chi^{(3)} = 1.6 \times 10^{-4}$ esu at 300K; this value is twenty times the previous record.

The nonlinear susceptibilities were measured by four wave mixing experiments performed with a pair of Q-switched CO₂ lasers. The nonlinear signal varied as $P_3 \sim P_1 P_2$ to the highest laser intensities, $P_1 = P_2 = 500\text{ kW/cm}^2$, used in these experiments. The absence of saturation is striking. We attribute the optical nonlinearity to interband population modulation between the heavy mass Γ_8 valence band and the light mass Γ_8 conduction band. A plasma density modulation exceeding 10^{17} electron-hole pairs/cc is required to produce the observed effect. Calculations suggest that this oscillating plasma could also radiate efficiently in the far infrared.

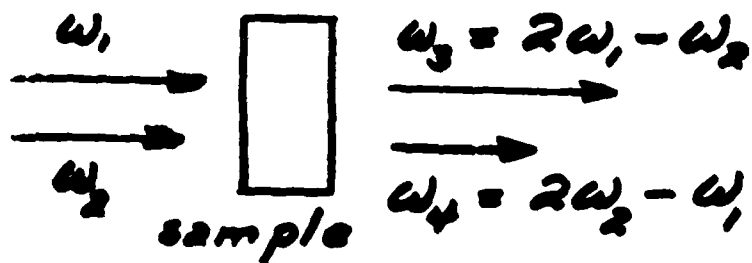
The figure of merit, $\chi^{(3)}/\alpha T$, for HgTe is comparable to that of other semiconductors. However, the product $\chi^{(3)} P_{\text{sat}}$ for HgTe far exceeds that of other semiconductors. Further enhancement of the HgTe nonlinearity is anticipated with appropriate doping or alloying.

We have observed a novel free carrier nonlinear optical effect due to scattering by the resonant $\text{Fe}^{2+}(3d^6)$ donor states in HgCdSe:Fe . The effect is only seen if the Fe states are located inside the conduction band. For a HgCdSe sample with energy bandgap of 303 meV and free electron concentration of $1.7 \times 10^{18} \text{ cm}^{-3}$ at 80K, a third order optical susceptibility of 1×10^{-6} esu was measured by four wave mixing experiments with CO_2 lasers. This value is twenty times larger than that induced by the energy band nonparabolicity, and can be explained by a theory taking into account the strong energy dependence of the scattering rate due to the presence of the resonant scattering level. The theory assumes that the pump lasers modulate the electronic temperature via free carrier absorption, which in turn modulates the dielectric constant through the energy dependent scattering mechanism, leading to large optical nonlinearity. The nonlinear optical effect can be further increased if the resonant scattering level is located closer to the Fermi energy. The theory can also be used to infer the Fe level width from the optical data; in our sample $\Delta = 20$ meV.

1. OPTICAL NONLINEARITIES OF SEMICONDUCTORS

1.

Four Wave Mixing:



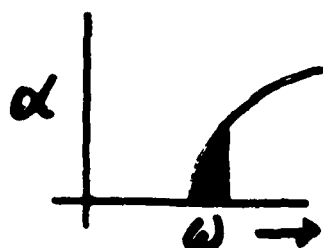
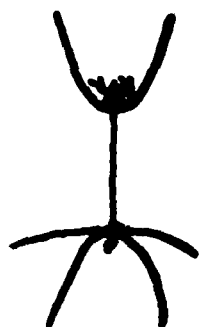
$$P_3 \sim |\chi^{(3)}|^2 P_1^2 P_2$$

$\epsilon(\omega)$ modulated at $\Delta\omega = \omega_1 - \omega_2$.
Beams acquire sidebands at
 $\omega_1 + \Delta\omega = 2\omega_1 - \omega_2$; $\omega_2 - \Delta\omega = 2\omega_2 - \omega_1$,

Here

$$\epsilon(\omega) = \epsilon_0(\omega) - \frac{4\pi n e^2}{m^* \omega(\omega + i/\tau)}$$

for a doped, single-valley semiconductor.




modulate:

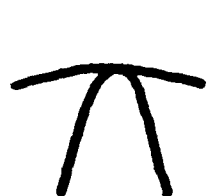
- i) m^*
- ii) τ
- iii) n (in multi-valley crystals)

2. FREE CARRIER NONLINEARITIES

Nonparabolicity (e.g. n -InSb)

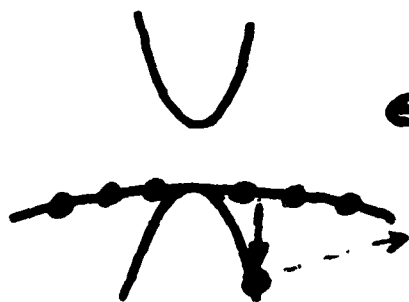


$$\frac{1}{m^*(E)} = \frac{1}{m^*} \left(1 - \frac{2E}{E_G} \right)$$



$$P = |E_1|^2 + |E_2|^2 + 2E_1 \cdot E_2^* + 2E_1^* \cdot E_2$$

Intervalence Band (e.g. p -GaAs)



$$\epsilon = \epsilon_0 - \frac{4\pi n_1 e^2}{m_1^* \omega^2} - \frac{4\pi n_2 e^2}{m_2^* \omega^2}$$

Valley Transfer (e.g. n -GaAs)



$$\epsilon = \epsilon_0 - \frac{4\pi n_L e^2}{m_L^* \omega^2} - \frac{4\pi n_T e^2}{m_T^* \omega^2}$$



(requires $T \approx 800K$)

3. FEATURES OF FREE CARRIER NONLINEARITIES

1.) Broadband.

2.) Fast - response is usually in picosecond range.

3.) Dispersive - $\chi^{(3)}$ varies rapidly with $\Delta\omega$. Why? Consider nonparabolicity:

$$\frac{dT_e}{dt} + \frac{T_e - T_L}{\tau_{th}} = \frac{c\sqrt{\epsilon} \alpha(E; E_2^*)}{8\pi C_V} e^{-i\omega t}$$

$$\Delta T_e = \frac{c\sqrt{\epsilon} \alpha(E; E_2^*)}{8\pi C_V [1 - i(\Delta\omega)\tau_{th}]} e^{-i\Delta\omega t}$$

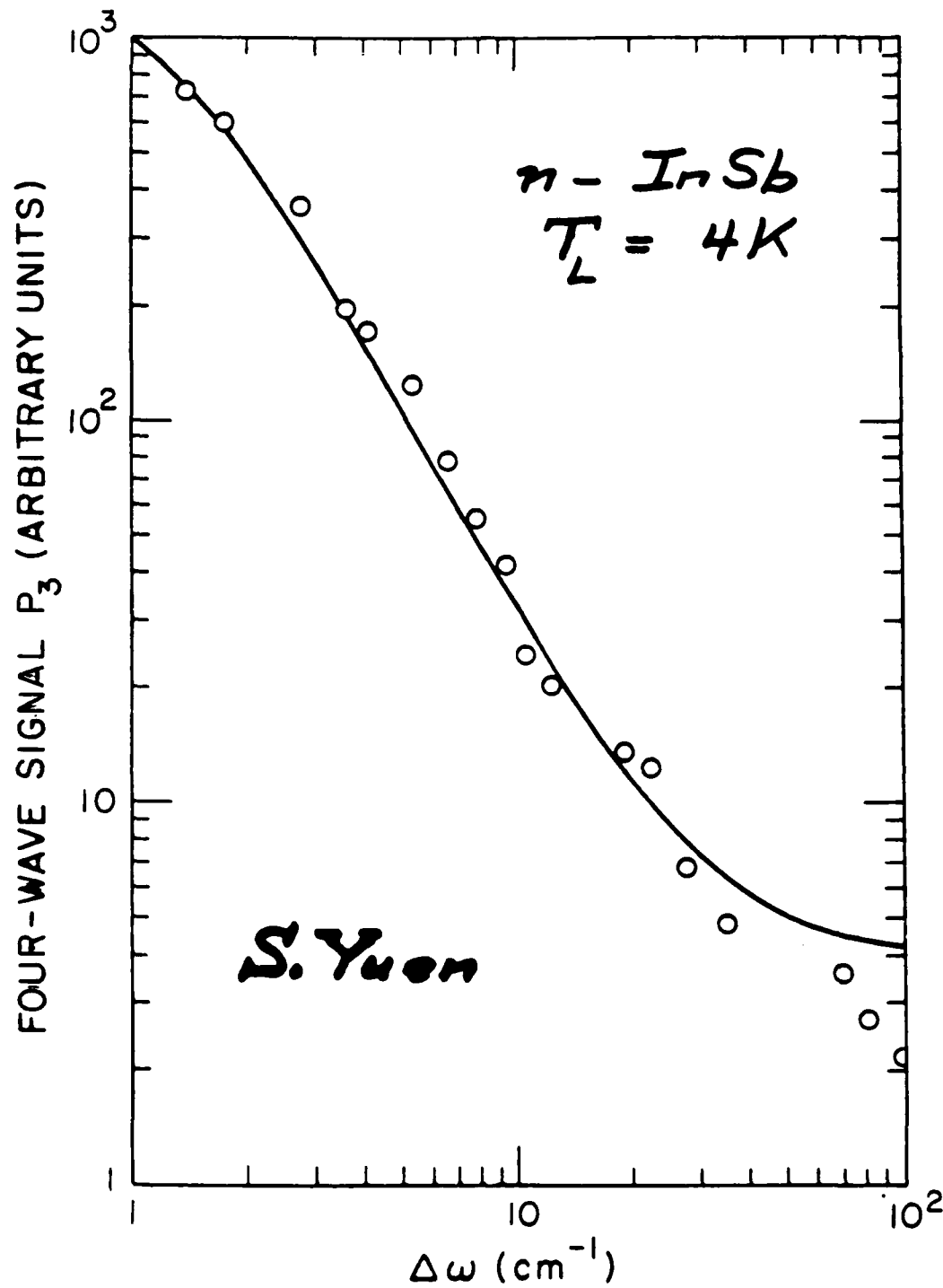
4.) Strong frequency variation

$$\chi^{(3)} \approx \frac{ne^4}{(m^*)^2 \epsilon_c \omega^4} \left(\frac{2\tau_{th}}{\tau_m} \right)$$

5.) Relatively weak:

$\chi^{(3)} \approx 10^{-8}$ esu in n -InSb
with $n = 10^{16}$ electrons/cc.

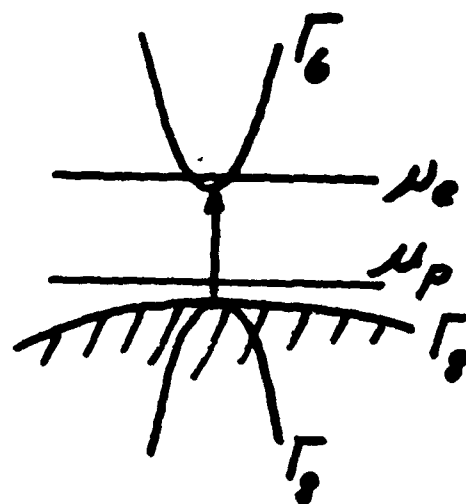
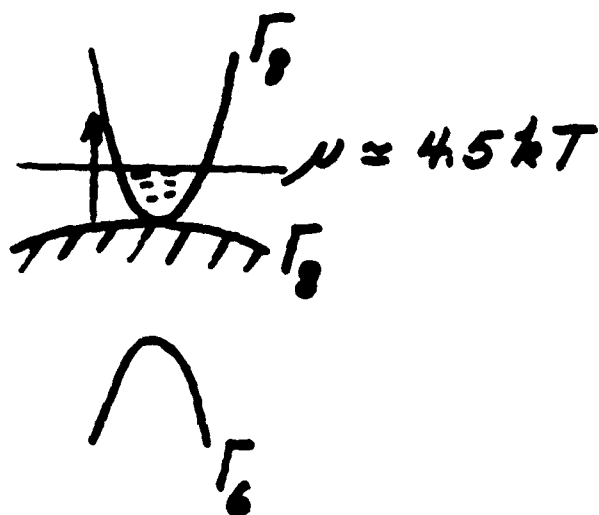
4.



$$\Delta\omega \equiv (\omega_1, -\omega_2)$$

④

5. HgTe EPILAYERS VS HgCdTe



HgTe

$$\chi^{(3)} \approx 2 \times 10^{-4} \text{ esu}$$

$\tau = 5 \text{ psec.}$
(thermal relaxation)

$\tau_r = 0.1 \text{ psec.}$
D'yakonov et al

$$\alpha = 3400 \text{ cm}^{-1}$$

$$\frac{\chi^{(3)}}{\alpha \tau} \approx 10^4$$

$$\mu_e \approx \mu_p \approx \mu$$

HgCdTe

$$\chi^{(3)} \approx 5 \times 10^{-2} \text{ esu}$$

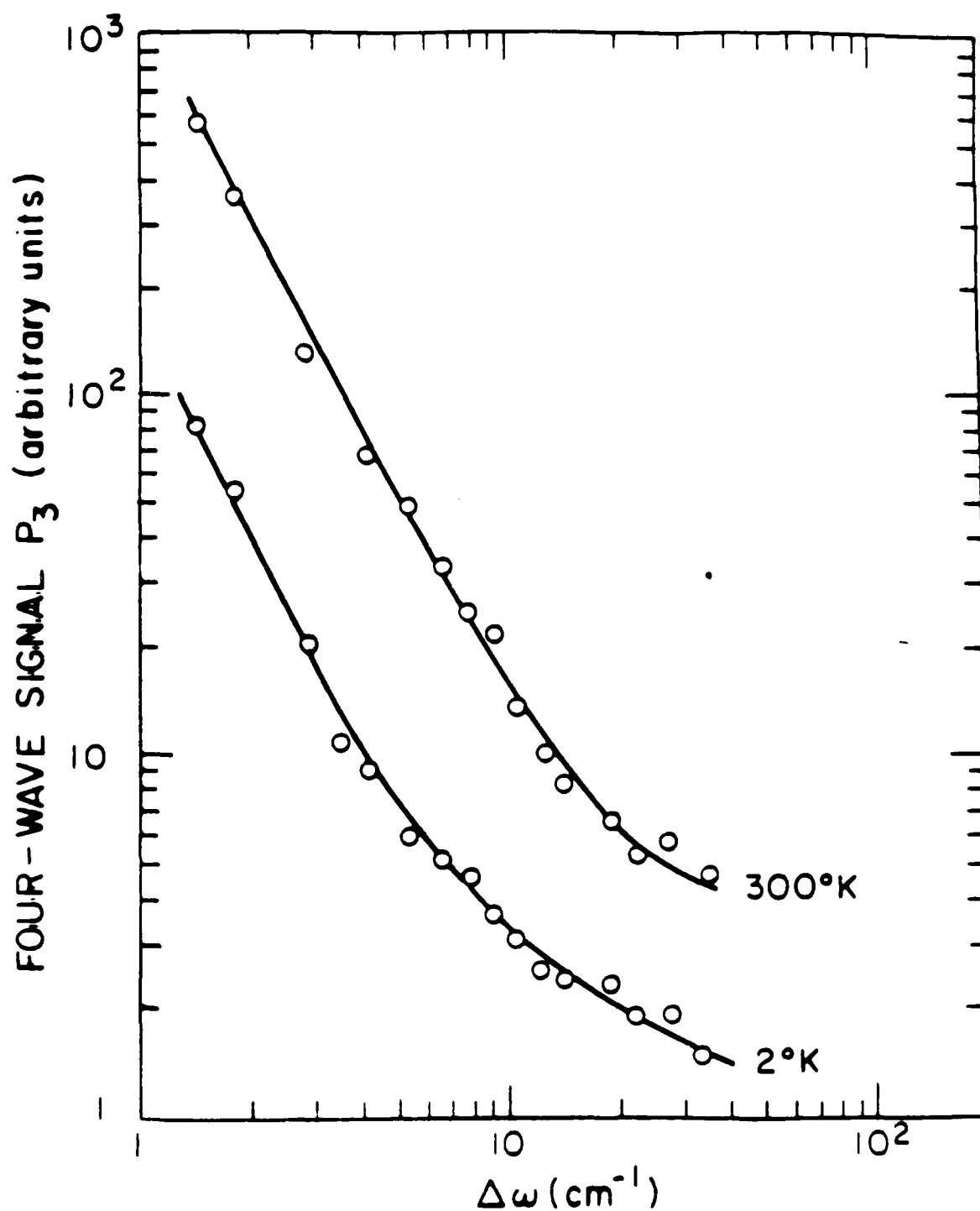
$$\tau_r = 30 \text{ nsec.}$$

$$\alpha = 8 \text{ cm}^{-1}$$

$$\frac{\chi^{(3)}}{\alpha \tau} \approx 2 \times 10^5$$

$$\mu_e \neq \mu_p$$

6.



Holff, Yuen, Harris, Cook,
and Schetzina

7. MODEL FOR HgTe NONLINEARITY

1) τ_r for HgTe ~ 0.1 psec.

2) Electrons and holes in thermal equilibrium $\rightarrow \mu_e \approx \mu_p \approx \mu$. But $T_e > T_L$

3) Carrier density strongly dependent on T_e .

4) For undoped samples $n = p \sim T_e^{3/2}$

These assumptions imply:

$$\chi^{(3)} = \frac{f}{160\pi \left(\frac{e^2}{m_e^* \omega^2} \right)} \frac{c\sqrt{\epsilon} \propto \tau_{th}}{kT_e (1 + i\Delta\omega \tau_{th})}$$

where

$$f = \frac{E_G + \mu/2}{E_G + \mu/2 - \hbar\omega}$$

HgTe: $T_L = 300K$, $E_G \approx 150$ meV

$$\chi_{exp}^{(3)} = 1.6 \times 10^{-4} \text{ esu} ; \chi_{th}^{(3)} = 2.1 \times 10^{-4} \text{ esu}$$

8. HgIe NONLINEARITY

1.) High saturation power. $\chi^{(3)} P_{\text{sat}}$ exceeds that of other fast optical nonlinearities.

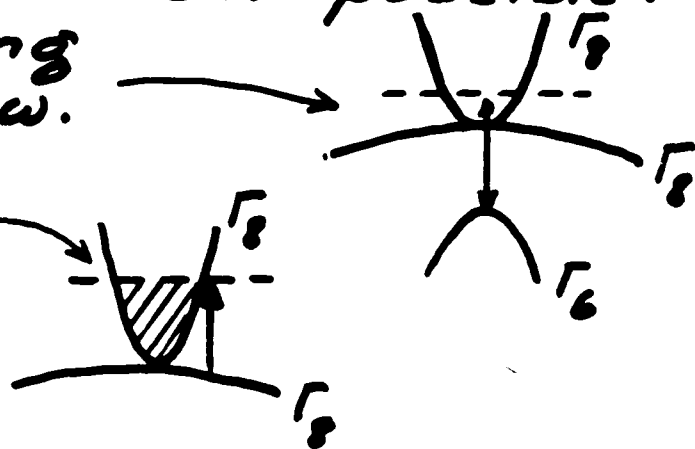
2.) Large, oscillating plasma density. $n \approx 10^{18}$ electron-holes/cc.; $\Delta E \approx 10\% E_g$

3.) Further enhancement possible:

i) By matching $E_g + \mu/2 \approx \hbar\omega$.

ii) By doping $E_F \approx \hbar\omega$

(Genkin et al)



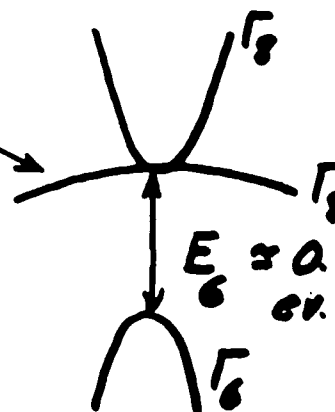
4.) Weak frequency dependence. For a forbidden optical transition $\alpha(\omega) \sim \omega^{3/2} \rightarrow \chi^{(3)} \sim \omega^{-1/2}$.

5.) Tailor semimetal band structure to give large $\chi^{(3)}$ at 3ν ?

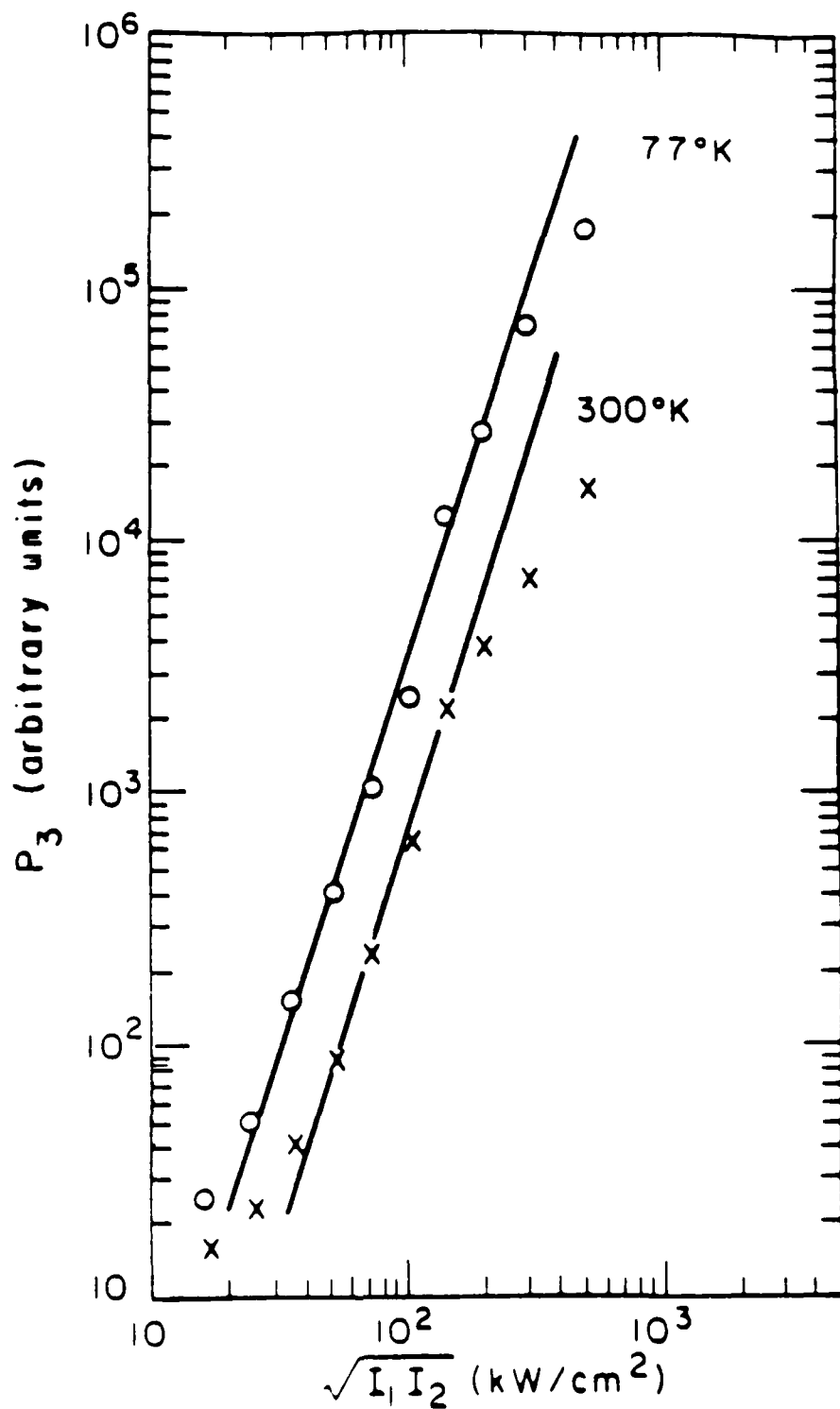
i) Semimetals with larger E_g ?

ii) Pump above E_g ?

6.) Why is τ_{th} so long?



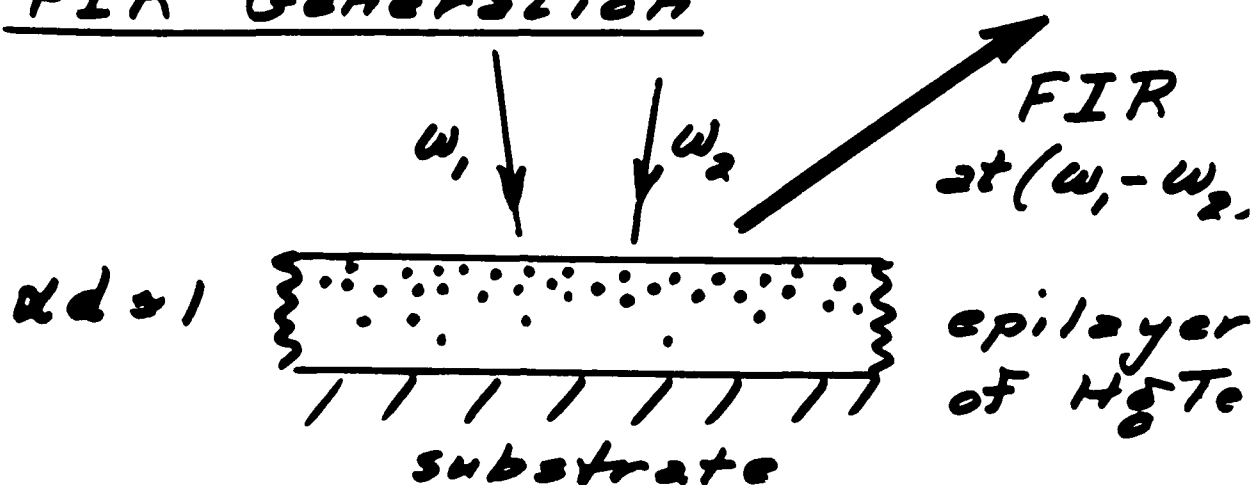
9.



Wolff, Yuen, Harris, Cook,
and Schatzgins

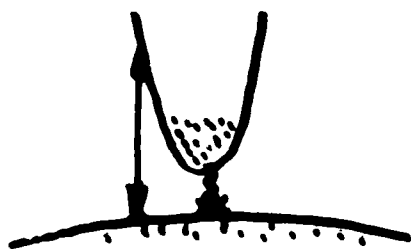
10. WHAT TO DO WITH HgTe OPTICAL NONLINEARITY ?

FIR Generation



Ambipolar diffusion requires charge separation, coupling to plasma modes, radiation.

Stimulated Plasmon Emission



Field induced gap
 $E_c \approx 10 - 20 \text{ meV}$

When pumped hard get

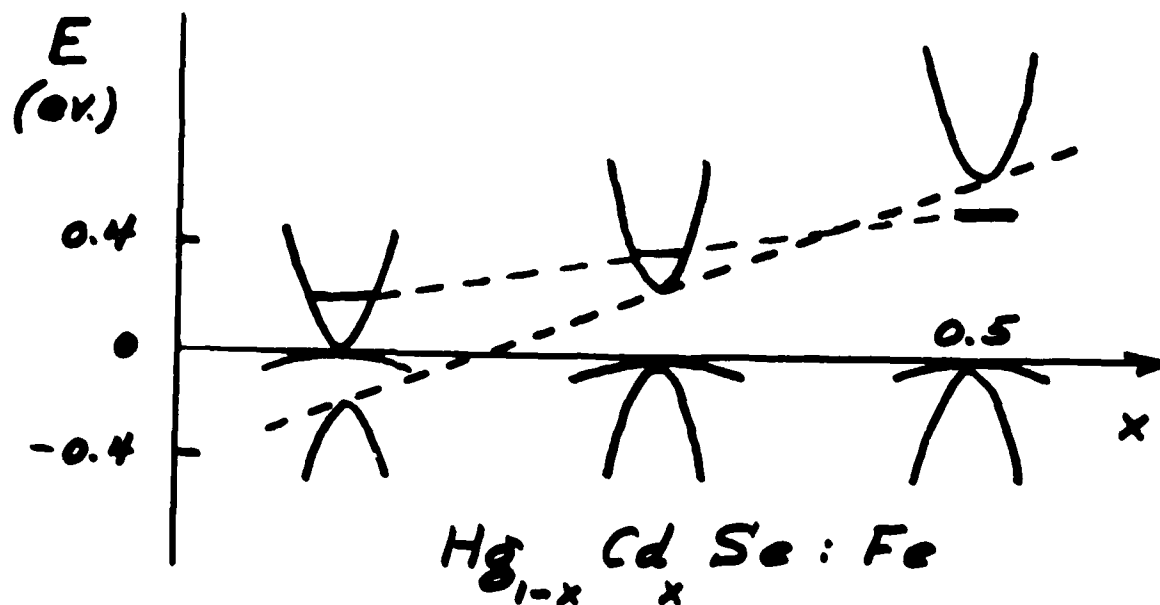
$$n = p \approx 10^{17} \text{ carriers/cm}^3$$



Calculations predict stimulated plasmon recombination -338-

11. OPTICAL NONLINEARITY DUE TO RESONANT DONOR LEVELS

Fe^{2+} level in $Hg_{1-x}Cd_xSe : Fe$
(Mycielski et al)



$Hg_{1-x}Cd_xSe : Fe$ Samples

$T = 80K$ $n = 1-2 \times 10^{18}/cc.$

E_g	E_{Fe}	$\chi_{exp}^{(3)}$	$\chi_{nonp}^{(3)}$	$\chi_{Fe}^{(3)}$
670	420	5×10^{-8}	3×10^{-8}	
330	380	1×10^{-6}	6×10^{-8}	7×10^{-7}

12. MODEL OF TIGLAS-DE HONDE

Laser beams modulate electron temperature, promoting carriers

$$\chi^{(3)} \approx \frac{d\chi^{(1)}}{dT_e} \frac{(\delta T_e)_{NL}}{E, E_2^*}$$

$$\chi^{(3)} \approx -i \left(\frac{d\sigma_1}{dT_e} \right) \frac{c\sqrt{\epsilon_0} \alpha \tau_{th}}{8\pi\omega\epsilon_v [1 + i(\Delta\omega)\tau_{th}]}$$

Here, from the Anderson model:

$$\sigma_1(\omega) = \frac{2\pi e^2 N_i |V|^2}{3m^* \hbar^2 \omega^3} \int \left\{ \rho(E) \rho(E + \hbar\omega) + \right.$$

$$\left. \left[f(E) - f(E + \hbar\omega) \right] \left[\frac{E}{|\mathcal{D}(E + \hbar\omega)|^2} + \frac{(E + \hbar\omega)}{|\mathcal{D}(E)|^2} \right] \right\}$$

$$\text{with } |\mathcal{D}(E)|^2 = [(E - E_0)^2 + \Delta^2]$$

Fit to experiment gives:

$$\alpha = 90 \text{ cm}^{-1}; \quad \chi^{(3)} \approx 10^{-6} \text{ esu}$$

with

$$\Delta = 20 \text{ meV.}$$

NONLINEAR MECHANISM	MEDIUM	$\chi^{(3)}$ (esu)	τ (sec)	α (cm ⁻¹)	$\chi^{(3)}/\alpha\tau$ (esu-cm/s)
band filling	HgCdTe	5×10^{-2}	3×10^{-8}	8	2×10^5
interband	HgTe	2×10^{-4}	5×10^{-12}	3400	9×10^3
inter-valence	p-HgCdTe	8×10^{-6}	2×10^{-13}	48	8×10^5
resonant-scattering	HgCdSe:Fe	1×10^{-6}	5×10^{-12}	100	2×10^3
impurity	Si:P	3×10^{-7}	1×10^{-12}	700	430
nonparabolicity	InSb	2×10^{-7}	4×10^{-12}	2	3×10^4
intervalley	Gasb	1×10^{-7}	2×10^{-12}	30	2×10^3
free exciton	GaAs/GaAlAs	4×10^{-2}	2×10^{-8}	12000	170

RELAXATION MECHANISMS	MEDIUM	$N \text{ (cm}^{-3}\text{)}$	$T \text{ (K)}$	$\tau_{\text{exp}} \text{ (ps)}$	$\tau_{\text{th}} \text{ (ps)}$
$LN \rightarrow HH$ Optical phonon emission	p-GaAs	4×10^{16}	300	0.09	0.13
	p-GaAs	4×10^{16}	80	0.23	0.20
	p-GaAs	2×10^{19}	300	0.46	0.52
	p-Ge	3×10^{16}	300	0.70	1.7
$T \leftrightarrow L$	n-GaSb	4×10^{17}	300	2	
	n-InSb	2×10^{16}	2	3	
thermalization	n-Si:P	2×10^{18}	300	1	
	n-GaAs	3×10^{17}	300	0.7	
	n-HgCdSe:Fe	2×10^{18}	300	0.7	

15. DIRECTIONS FOR FUTURE

1.) Free carrier induced optical nonlinearities can be fast and large:

i) Optimize $\chi^{(3)}$ of HgCdTe via alloying and doping. Expect $\chi^{(3)} = 10^{-3} - 10^{-2}$ esu; $\tau \sim 5$ ps.

ii) Study $\chi^{(3)}$ vs. ω in HgTe.

iii) Tailor band parameters in HgTe/CdTe superlattices.

2.) Enhanced optical nonlinearity at the threshold of electrical instabilities. Optical triggering of electrically bistable structures?

Berry's Phase in Fiber Optics

(A talk by R. Y. Chiao at the U. S. - Japan Seminar on Quantum Mechanical Aspects of Quantum Electronics at Monterey, July 21-24, 1987)

Abstract: Berry discovered in quantum mechanics a topological phase factor similar to the Aharonov-Bohm phase factor. This phase is acquired by a system when it is adiabatically transported around a closed circuit in the parameter space of the Hamiltonian. Several experiments have now confirmed the existence of this phase. I shall report on an optical experiment which observed a manifestation of Berry's phase as a topological optical activity in a helical optical fiber. The wavelength-independence of this new optical activity has also been verified. Recently, this phase has been generalized to nonadiabatic evolutions by Aharonov and Anandan. I shall report on another optical experiment to observe this nonadiabatic phase. Possible applications, e.g., to gyroscopes, will be discussed.

U.S. - Japan Seminar
July 21-24, 1987

Berry's Phase in Fiber Optics

Collaborators:

Y. S. Wu (Theory)

A. Tomita (Experiment)

Recent work:

A. Antaramian, K. Ganga, H. Jiao,

A. Landsberg (students at Berkeley)

Dr. H. Nathel (LLNL)

Outline

I. What is Berry's phase?

- A. A Classical Analog: Hannay's angle
- B. QM adiabatic theorem derivation
- C. Relationship to Sagnac effect and Aharonov-Bohm effect: the twin paradoxes
- D. Relationship to Dirac monopole

II. The Optical Fiber Experiment

- A. Theory
- B. Schematic of experiment
- C. Data showing topological invariance
- D. " " wavelength independence

III. The Three-Mirror Experiment.

- A. Kitano-Yabuzaki-Ogawa Periscope
- B. Aharonov-Anandan Phase
- C. Interferometry

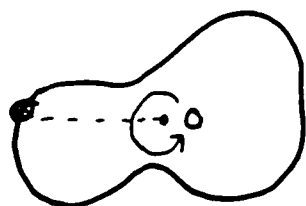
IV. Applications to gyroscopes

Hannay's Angle

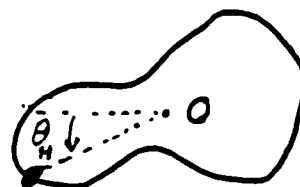
J. H. Hannay, J. Phys. A18, 221 (1985)
M. V. Berry, J. Phys. A18, 15 (1985)

1. Frictionless bead on a hoop:

Stroboscopic
views →



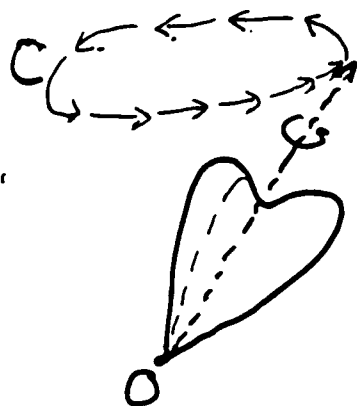
Rotate
 $\xrightarrow{360^\circ}$
around O



$$\theta_H \propto \frac{\text{Area}}{(\text{Perimeter})^2} \quad \leftarrow \text{SHIFT IN ANG. POSITION}$$

2. Symmetric top forced around circuit

Stroboscopic
views



after
 $\xrightarrow{\text{circuit}}$



$$\theta_H \propto \text{Solid angle subtended by } C \text{ w.r.t. } O$$

$$\theta_H = \frac{d\gamma_n}{dn} \text{ as } n \rightarrow \infty$$

Berry's phase

M.V. Berry, Proc. Roy. Soc.
A392, 45 (1984)

$$S.E. \quad i\hbar \frac{d}{dt} |\psi(t)\rangle = H(\underline{R}(t)) |\psi(t)\rangle$$

Adiabatic theorem

$$H(\underline{R}) |n(\underline{R})\rangle = E_n(\underline{R}) |n(\underline{R})\rangle$$

Berry's Ansatz

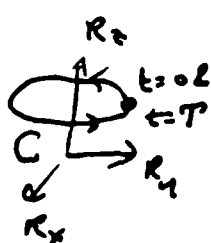
$$|\psi(t)\rangle = e^{-\frac{i}{\hbar} \int_0^t dt' E_n} e^{i\gamma_n(t)} |n(\underline{R}(t))\rangle$$

$$\begin{aligned} i\hbar \frac{d}{dt} |\psi(t)\rangle &= i\hbar \left(-\frac{i}{\hbar} E_n \right) |\psi(t)\rangle \\ &\quad - \hbar \dot{\gamma}_n e^{-\frac{i}{\hbar} \int_0^t dt' E_n} e^{i\gamma_n(t)} |n(\underline{R}(t))\rangle \\ &\quad + e^{-\frac{i}{\hbar} \int_0^t dt' E_n} e^{i\gamma_n(t)} i\hbar \frac{d}{dt} |n(\underline{R}(t))\rangle \\ &= H |\psi(t)\rangle = E_n |\psi(t)\rangle \end{aligned}$$

$$\therefore \dot{\gamma}_n = i \langle n(\underline{R}(t)) | \frac{d}{dt} |n(\underline{R}(t))\rangle$$

$$= i \langle n(\underline{R}(t)) | \nabla_{\underline{R}} |n(\underline{R}(t))\rangle \cdot \dot{\underline{R}}(t)$$

Now let $t = T$ be cycle time, i.e. $\underline{R}(T) = \underline{R}(0)$

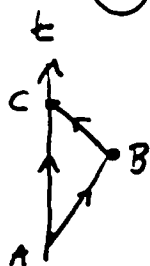


$$\gamma_n(C) = i \oint_C \underbrace{\langle n(\underline{R}) | \nabla_{\underline{R}} |n(\underline{R})\rangle}_{\vec{A}} \cdot d\underline{R}$$

t drops out. cf. Aharonov-Bohm Phase.

Four Types of Twin Paradoxes (from Chiao's seminar at M.I.T., Oct 28, 1986)

① Special relativistic twin paradox.



$$\Delta t = \underbrace{\oint \frac{ds}{c}}_{\text{proper time}} = \oint \sqrt{1 - \frac{v^2(t)}{c^2}} dt$$

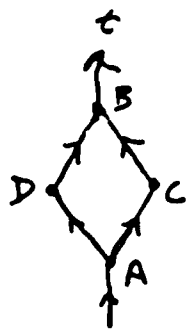
checked
by
Hafele &
Keating,
Science,
177, 166 (1972)

② Sagnac-effect twin paradox.

$$\Delta t = \frac{1}{c^2} \oint \vec{v}_a \cdot d\vec{l} = -\frac{1}{c} \oint \frac{g_{0i} dx^i}{g_{00}} \quad (i=1,2,3)$$

Interferometers best way to measure Δt :

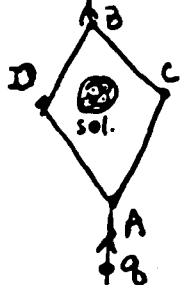
$$\Delta \phi = \omega \Delta t = \frac{\omega}{c^2} \oint \vec{v}_a \cdot d\vec{l} = \frac{\omega}{c^2} \vec{S} \cdot \vec{\omega}$$



For neutrons, $\omega = \frac{mc^2}{\hbar}$ (Werner et al, PRL 42, 1103 (1979))

For photons, $\omega = \text{freq. of light} \Rightarrow \text{LASER GYRO}$

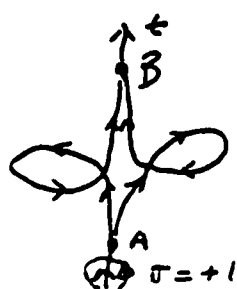
③ Aharonov-Bohm twin paradox



$$\Delta \phi = \frac{q}{\hbar c} \oint \vec{A} \cdot d\vec{l} \quad \text{NO FORCES!}$$

(Tonomura et al, PRL 56, 792, (1986))

④ Berry's phase: Generalization of A-B effect



$$\Delta \phi \equiv \gamma(C) = \frac{q}{\hbar c} \oint_C \vec{A} \cdot d\vec{l}$$

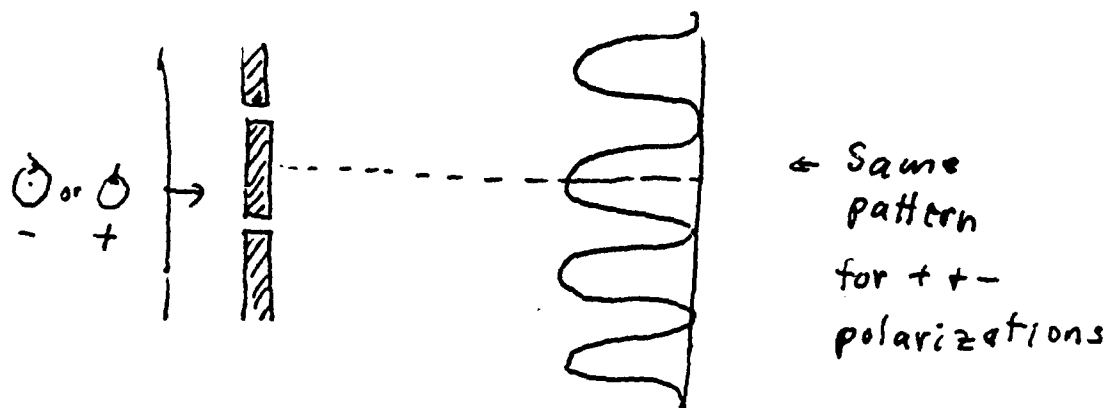
$d\vec{l}$ = line element in parameter space

\vec{A} = effective vector potential $\equiv \langle n | \frac{d}{d\vec{l}} | n \rangle$

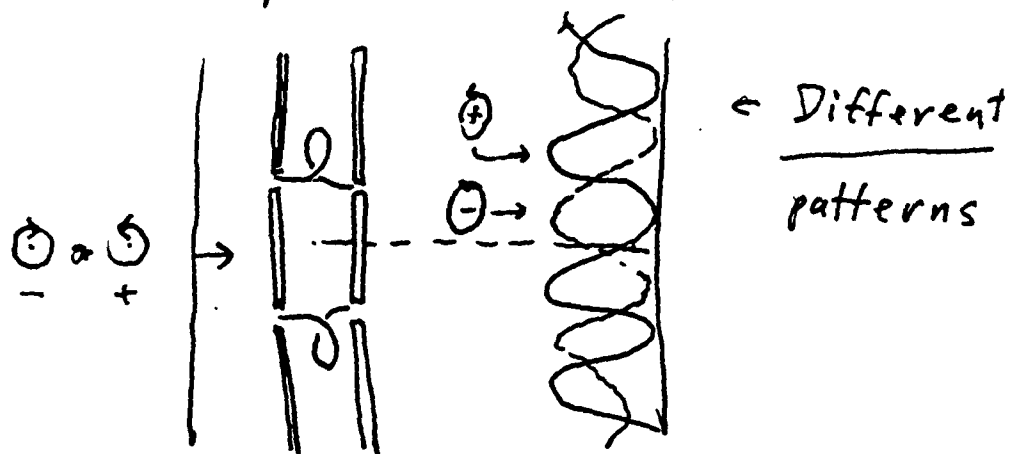
γ = topological charge = σ , for example

(Chiao & Wu, PRL 57, 933 (1986); Tomita & Chiao, PRL 57, 937 (1986)).

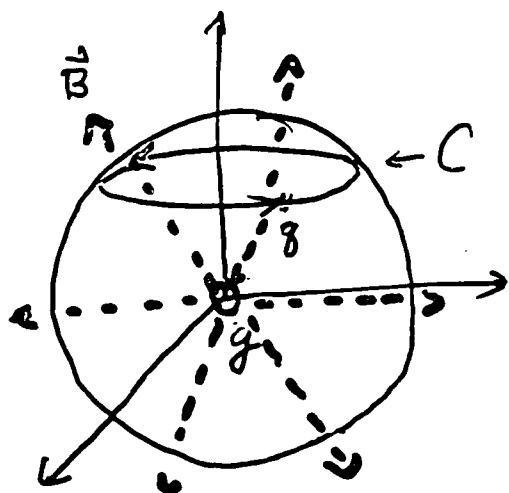
Young's two-slit interference



Now replace two slits by two fibers



Dirac Monopole + charge on sphere



A - B phase shift
around circle C

$$\Delta\phi = \frac{eg\Phi}{\hbar}$$

$$\Phi = \frac{\Omega(C)}{4\pi} \cdot 4\pi g$$

$$(\oint \vec{B} \cdot d\vec{S} = 4\pi g \text{ Gauss's law})$$

$$\therefore \Delta\phi = \frac{eg\Omega(C)}{\hbar}$$

Quantization of charge

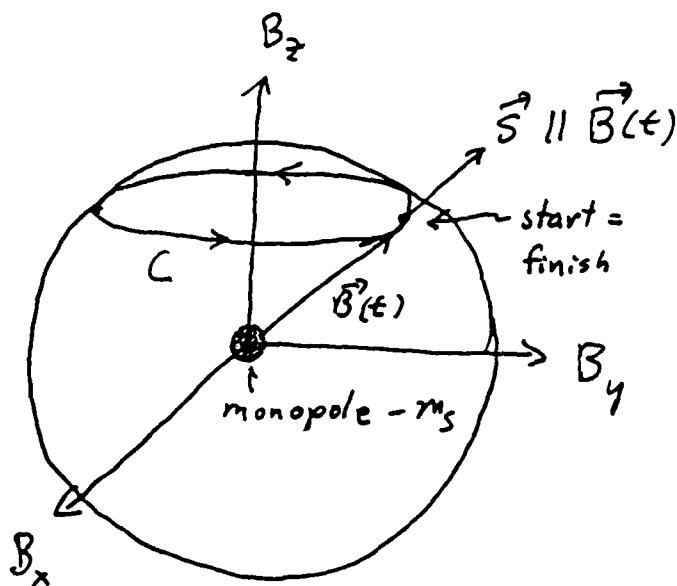
$$\Delta\phi = \frac{eg\Omega}{\hbar} = -\frac{eg(4\pi - \Omega)}{\hbar} \pm 2\pi n \quad \text{--- WITTEN}$$

$$\therefore eg \frac{4\pi}{\hbar} = \pm 2\pi n$$

$$\boxed{eg = \pm n \frac{\hbar}{2}}$$

Topological result (can deform S & C)
global

SPIN \vec{S} IN ADIABATIC $\vec{B}(t)$



$$\gamma(C) =$$

$$-m_s \Omega(C)$$

or

$$\gamma(C) = \frac{g}{\hbar} \oint \vec{A} \cdot d\vec{Q}$$

$$= \frac{g}{\hbar} \int \vec{\nabla} \times \vec{A} \cdot d\vec{S}$$

$$= \frac{g}{\hbar} \int \vec{B} \cdot d\vec{S}$$

$$= \frac{1}{\hbar} \cdot 4\pi g \cdot \frac{\Omega}{4\pi} = g \frac{\Omega}{\hbar}$$

PHOTON SPIN \vec{S} IN HELICAL WAVEGUIDE $\vec{k}(\tau)$

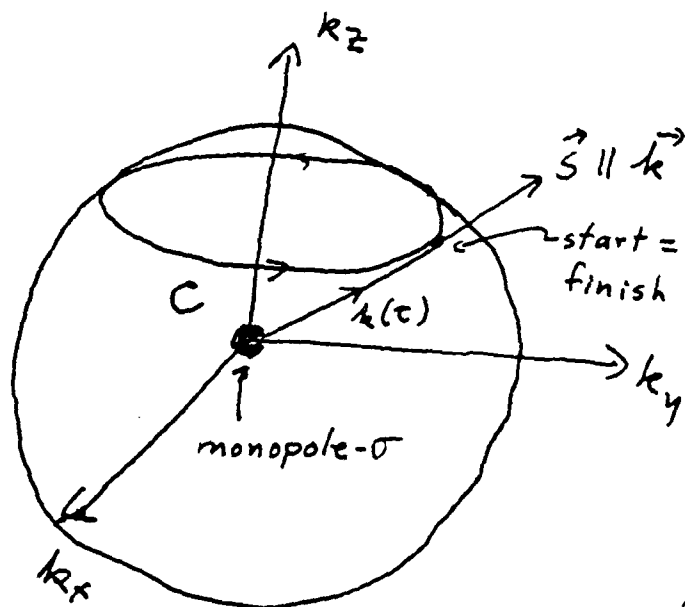


HELICITY $\vec{S} \cdot \vec{k}(\tau)$ IS ADIABATIC

$$\text{INVARIANT: } \vec{S} \cdot \vec{k}(\tau) |\vec{k}(\tau), \sigma\rangle = \sigma |\vec{k}(\tau), \sigma\rangle$$

σ = HELICITY IS EITHER +1 OR -1

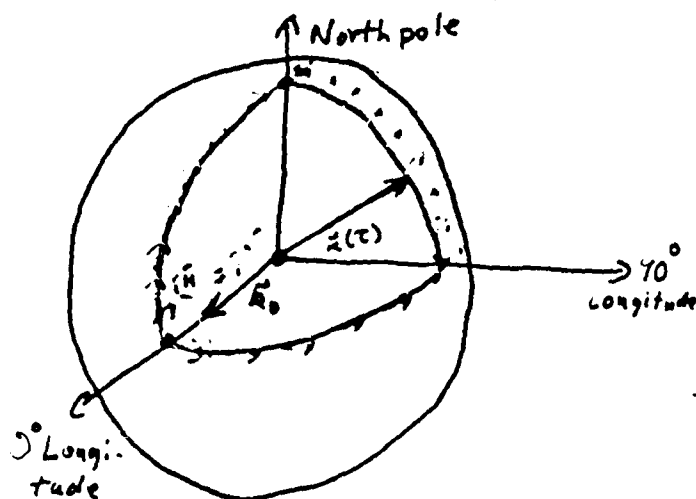
PHOTON IN \vec{k} -SPACE



$$\gamma(C) = -\sigma \Omega(C)$$

\Rightarrow
Dirac
monopole of
topological charge $-\sigma$

FOR LINEAR POLARIZATION, AND
STANDARD EXAMPLE:



Our theory predicts
 $-\gamma_+ = \textcircled{+} = \text{angle of rotation of linear polarization}$

$$\Omega = \frac{1}{8} \times 4\pi = \frac{\pi}{2}$$

one octant

$$\therefore \textcircled{+} = \frac{\pi}{2} = 90^\circ$$

Ordinary Optical Activity:

$$\Delta\phi = 2\pi(n_+ - n_-)L/\lambda$$

$$\Theta = \Delta\phi/2$$

Topological Optical Activity:

$$|x\rangle = (|+\rangle + |-\rangle)/\sqrt{2}$$

$$|x'\rangle = (e^{i\vartheta}|+\rangle + e^{-i\vartheta}|-\rangle)/\sqrt{2}$$

$\vartheta = -\Omega$ is Berry's phase for $|+\rangle$

$$\langle x | x' \rangle = \cos\vartheta$$

$$|\langle x | x' \rangle|^2 = \cos^2\vartheta \text{ is Malus's law}$$

Therefore, $\Theta = \pm\Omega$.

The sign of effect is determined by interference with ordinary optical activity.

Answer: a left-handed helix is dextrorotatory.

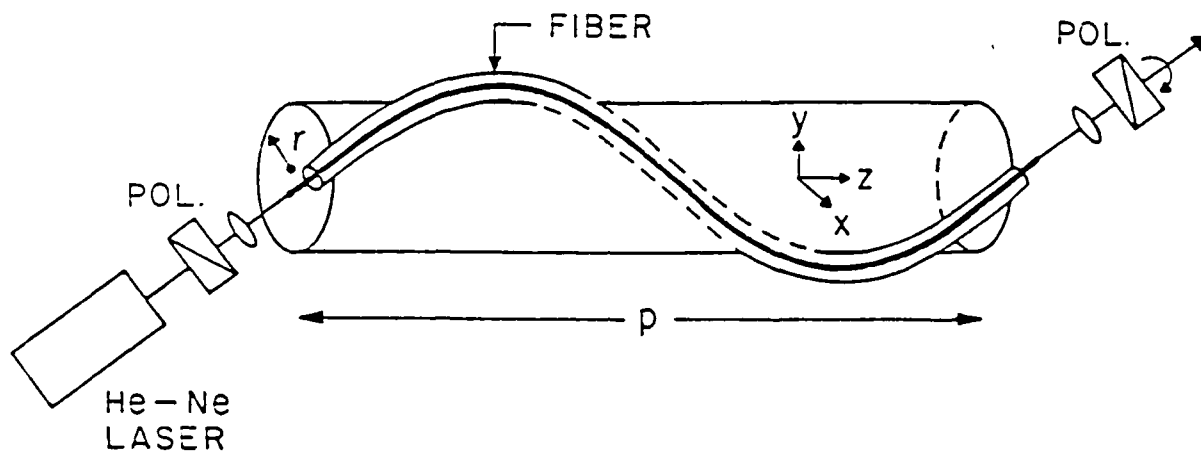
Comparing

$$\Theta = \pi(n_+ - n_-)L/\lambda$$

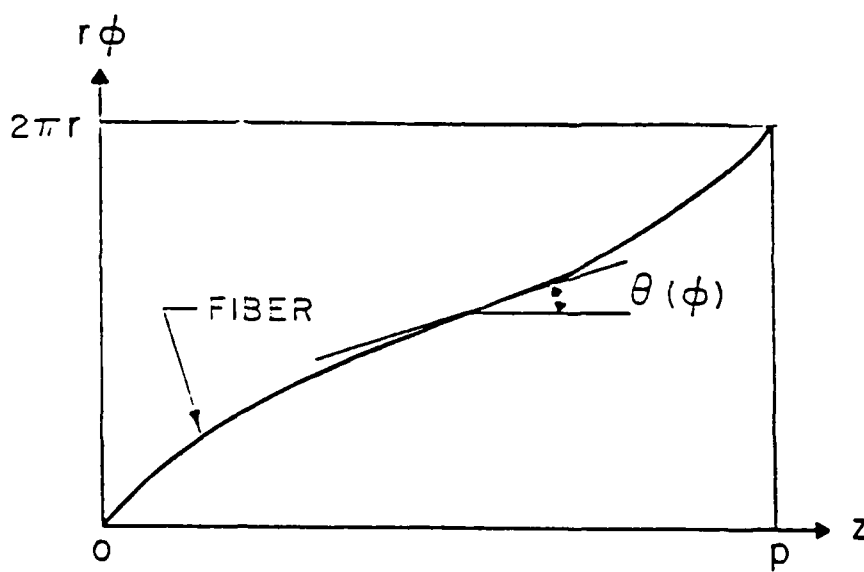
and

$$\Theta = \Omega$$

we see that the topological optical activity is wavelength independent.



(a)



(b)

Fig. 1

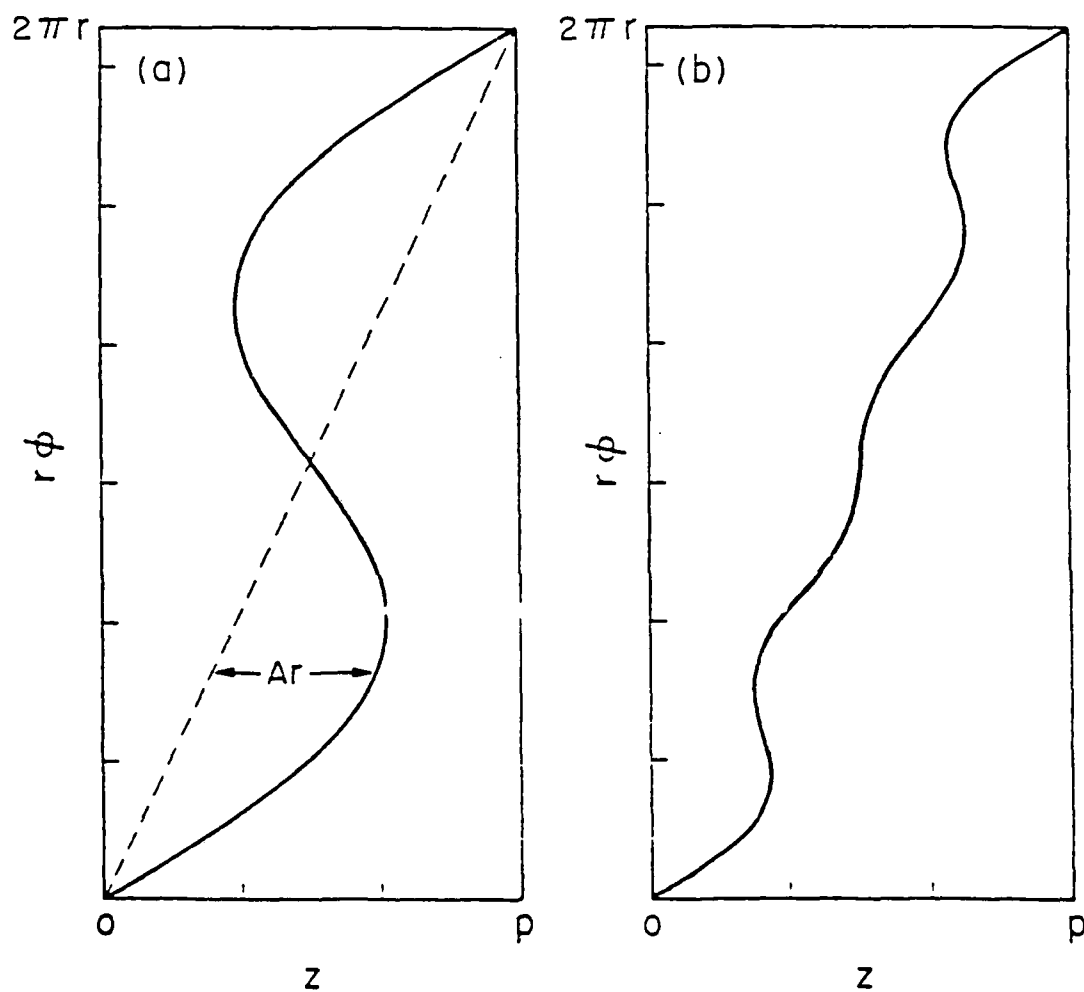
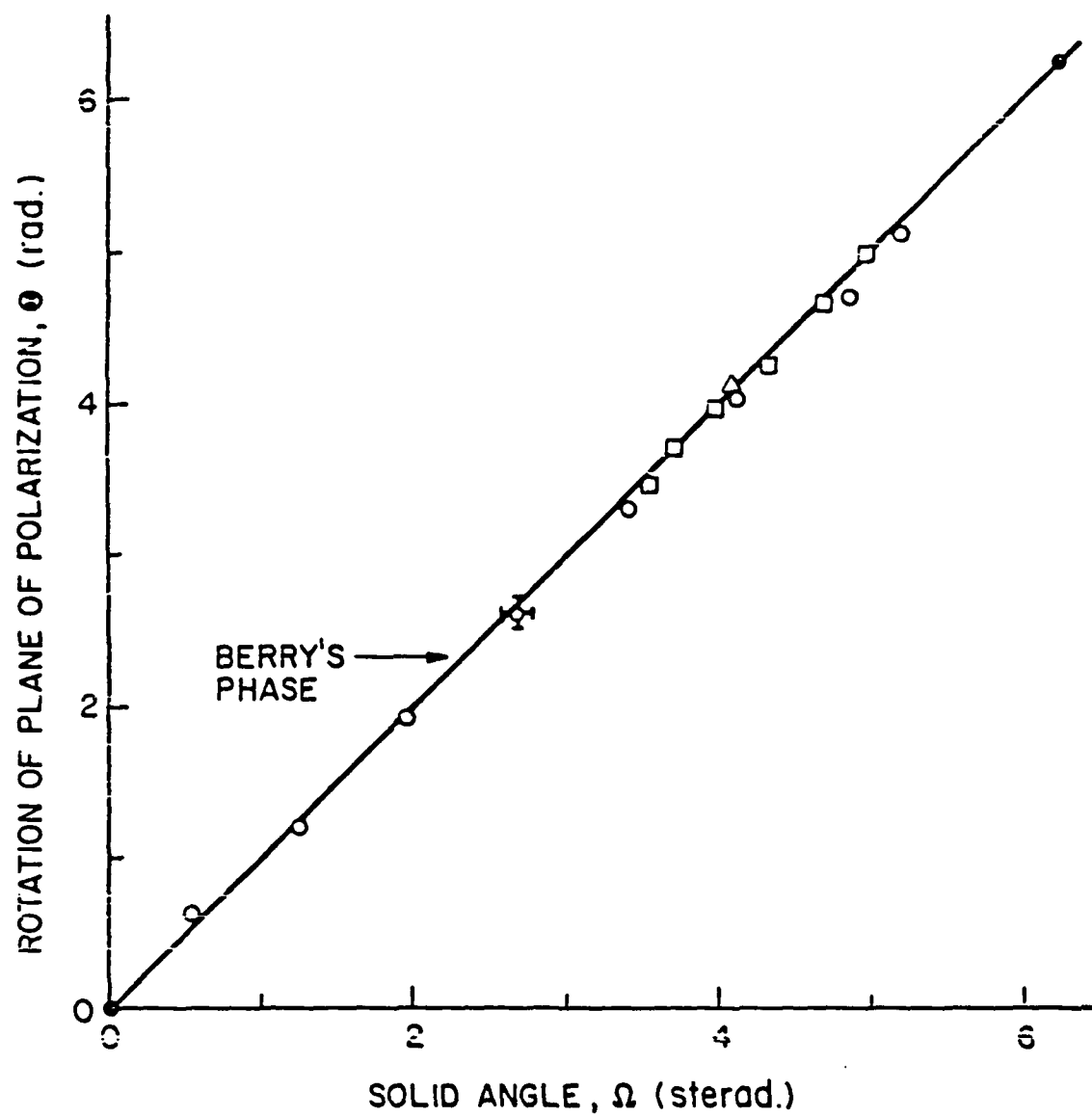
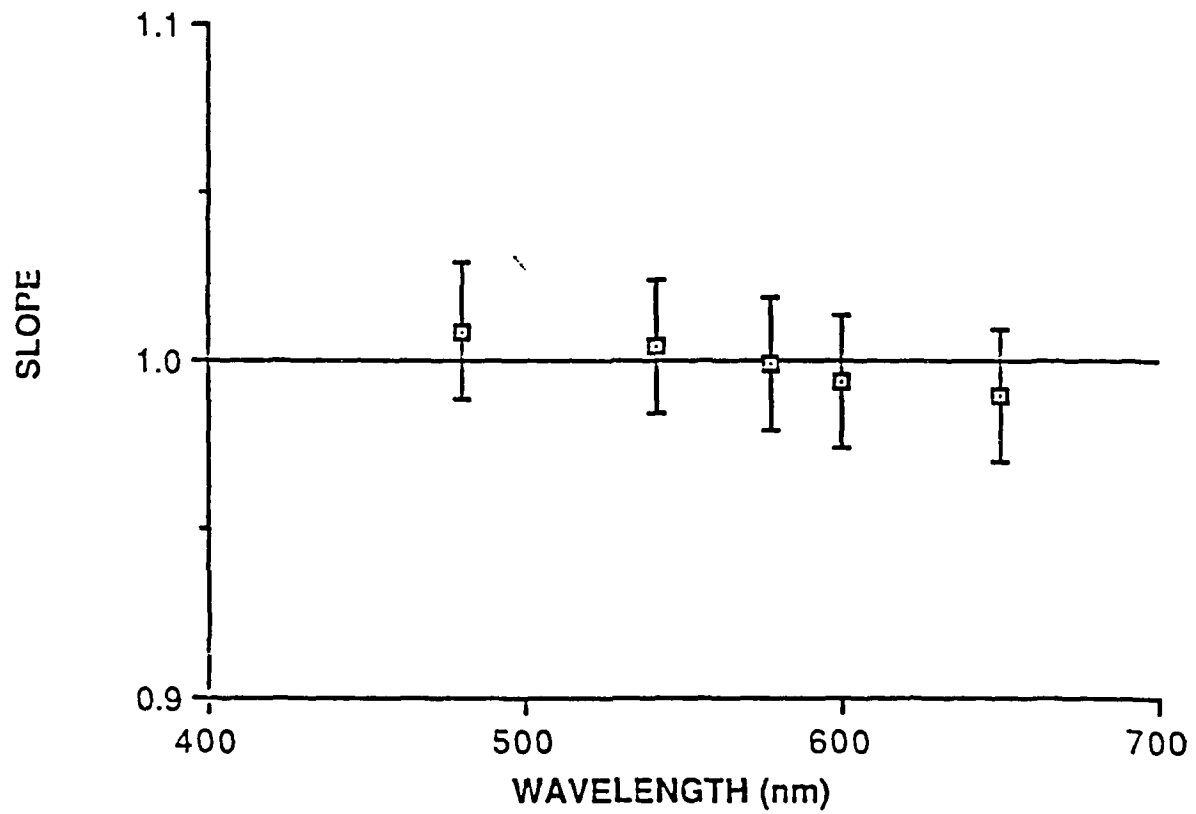
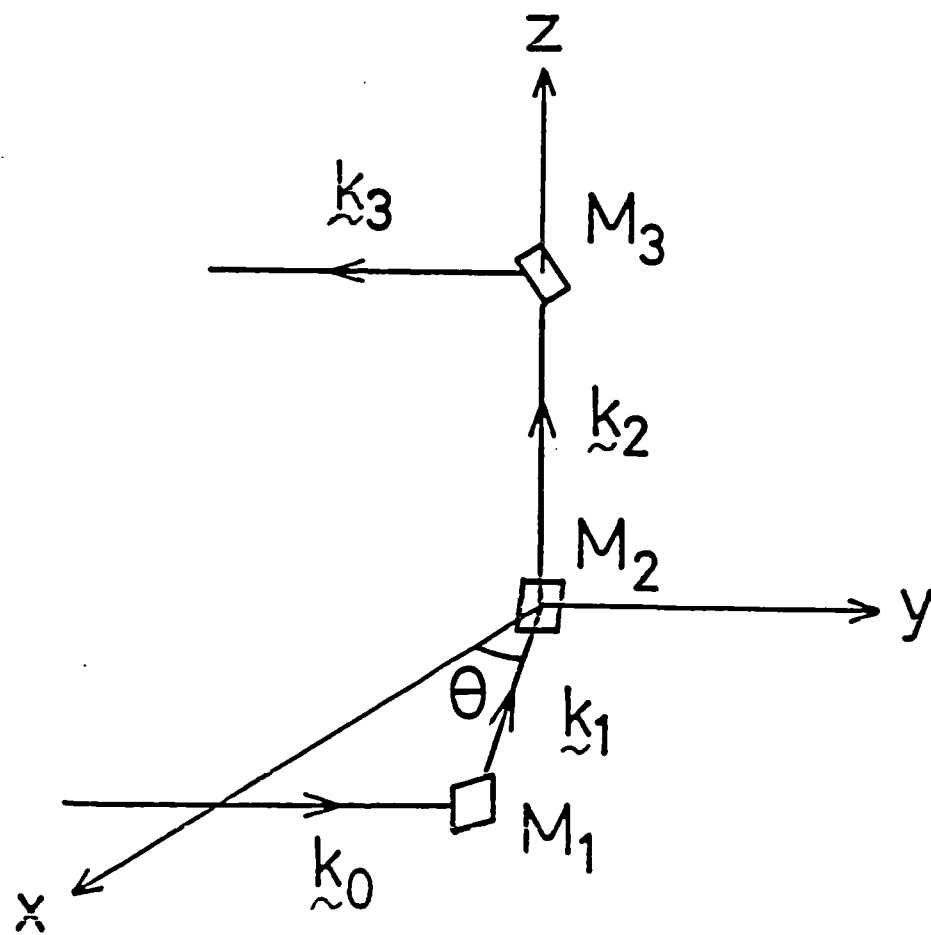


Fig. 3



SLOPE VERSUS WAVELENGTH





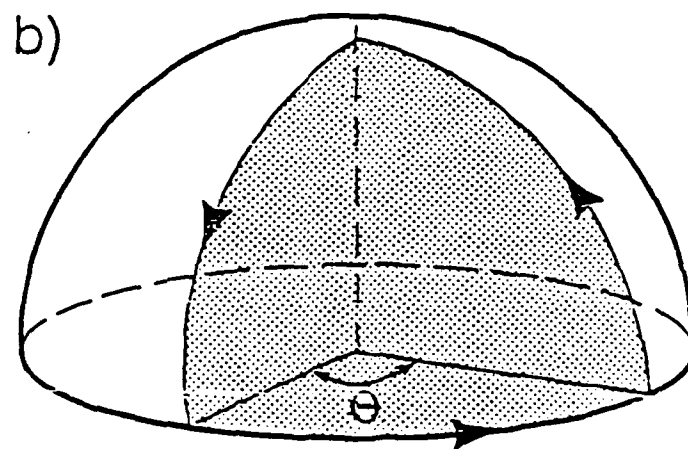
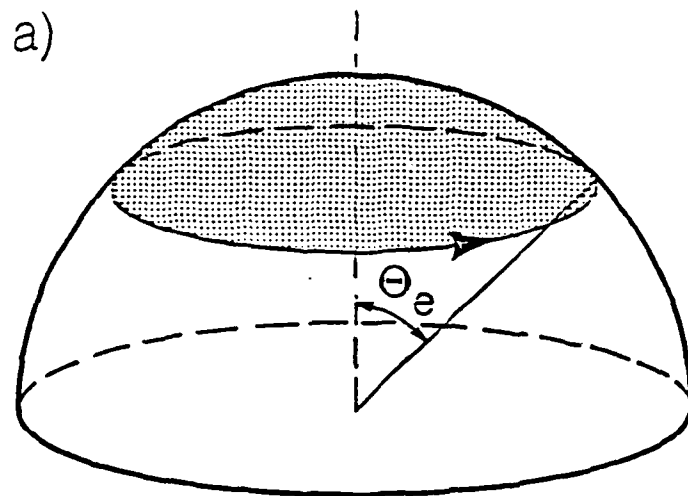
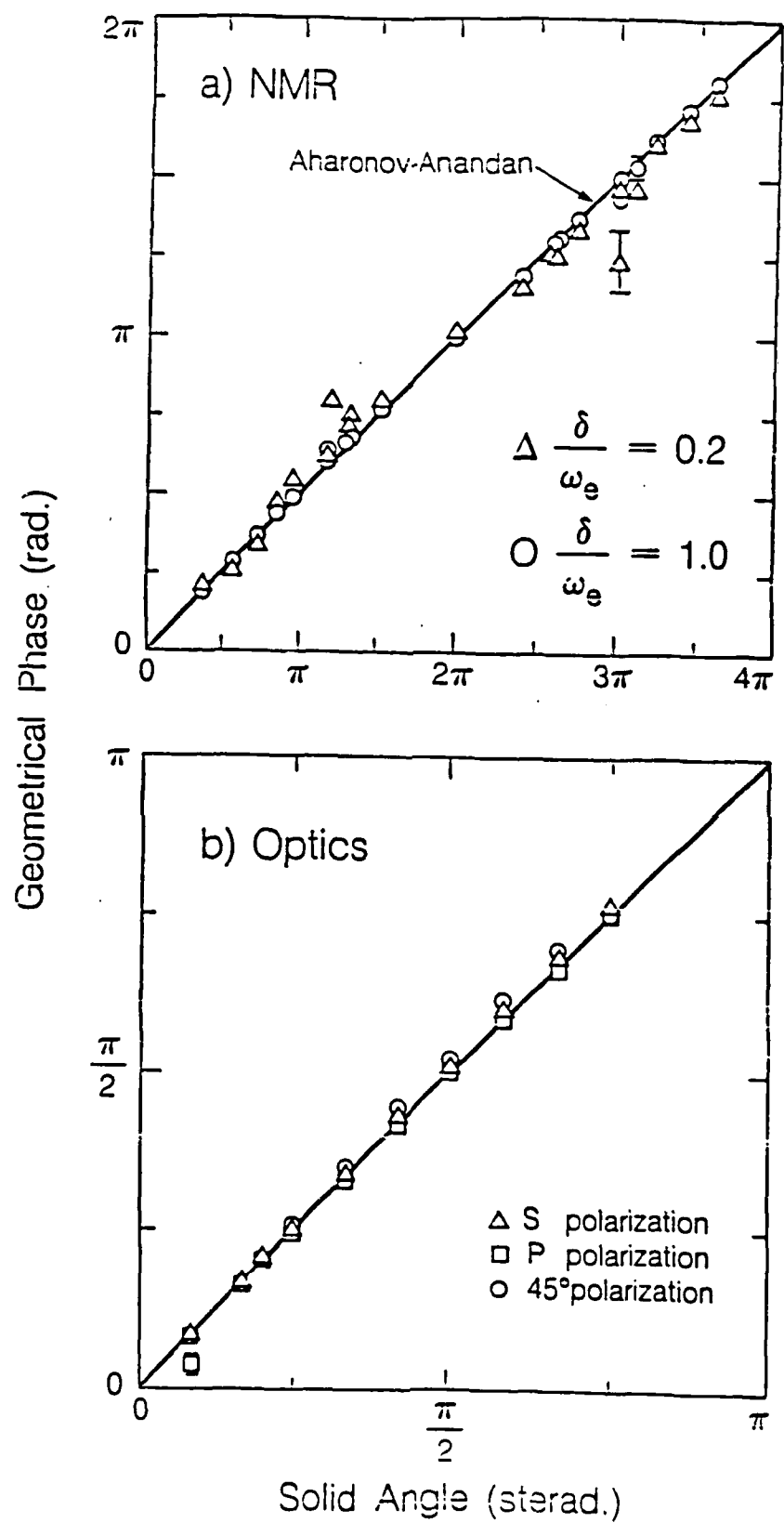
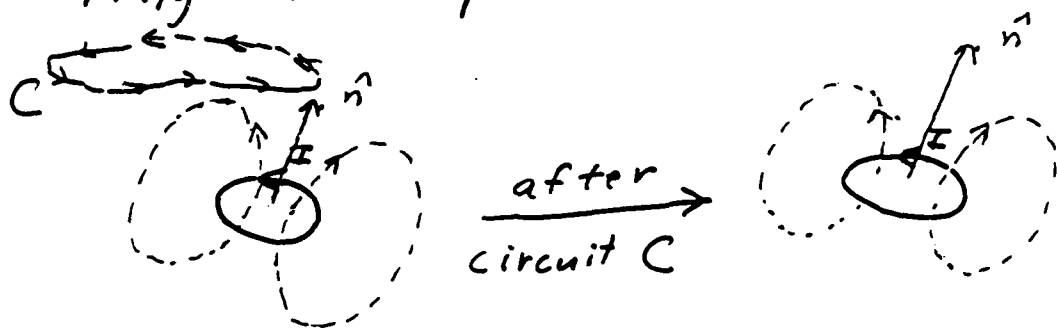


Figure 2



Application to gyroscopes

Let us replace spin by persistent current ring in a superconductor

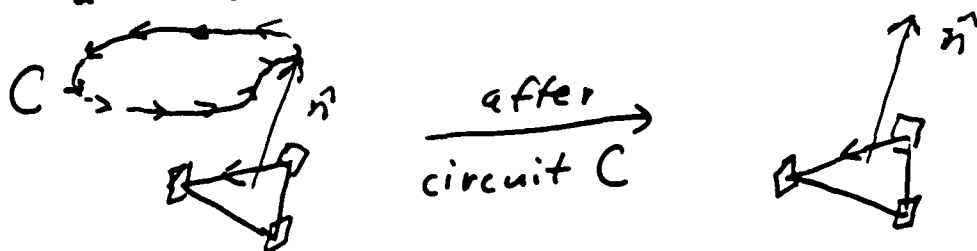


$$\psi \longrightarrow \psi \cdot e^{i\gamma(C)}$$

where $\gamma(C) = -n \Omega(C)$ ← detect with J.J

where n = flux quantum number

Alternatively, use unidirectional ring laser gyro



$$E \longrightarrow E \cdot e^{i\gamma(C)}$$

$\gamma = -n\Omega$, n = mode number (NOT SAGNAC EFFECT)

HIGH DENSITY FEMTOSECOND EXCITATION OF NONTHERMAL CARRIER DISTRIBUTIONS IN INTRINSIC AND MODULATION DOPED GaAs QUANTUM WELLS

Wayne H. Knox, Daniel S. Chemla and Gabriela Livescu
AT&T Bell Laboratories
Holmdel, N.J. 07733

We investigate the dynamics of non-thermal carrier distributions in undoped and modulation doped GaAs Quantum Well Structures (layer thickness $\approx 100 \text{ \AA}$) with near bandgap-resonant intense femtosecond light pulses. We are able to study selectively the carrier-carrier scattering process up to very high densities and we carry out the first optical investigation of non-thermal carrier generation in the presence of a thermalized Fermi-sea of electrons. In undoped quantum wells we find a reduction of the thermalization time from about 100 fs to about 30fs as the photocarrier density increases from $N_{eh} \approx 2 \times 10^{10} \text{ cm}^{-2}$ to $\approx 10^{12} \text{ cm}^{-2}$. The thermalization time is found to be sensitive to background doping with excess electrons in modulation doped samples.

Following absorption of light by a semiconductor, electrons and holes are placed into states of energy which are defined by the power spectrum of the exciting light and the band structure of the material. The very first relaxation process which the electrons and holes undergo is a scattering interaction, mediated by the Coulomb force between the particles. This process is only one of the many elementary interactions which may occur in semiconductors such as phonon absorption and emission, intervalley scattering, plasmon emission and radiative recombination.

We have designed experiments in which the carrier-carrier scattering process can be effectively isolated and studied under diverse conditions in order to learn more about this basic interaction mechanism which has been to date elusive by virtue of both its short time constants (10-100 fs) and its admixture with other processes. In particular, it is interesting to consider the separate roles of electron-electron scattering, electron-hole scattering and hole-hole scattering and to understand their various contributions in optical experiments. Of course, optical experiments in intrinsic semiconductors give little information about the distinction of these effects since equal numbers of electrons and holes are simultaneously created. We have begun investigations in modulation-doped samples which are designed to help us understand more clearly the effects of the electron and hole relaxations in the presence of both excess electrons and excess holes.

The first evidence of rapid thermalization of carriers in GaAs with high excess energy excitation was obtained by Tang and Erskine (1983) in single-wavelength experiments with femtosecond optical pulses at 625 nm. Oudar and coworkers (1985) later studied spectral hole burning in bulk GaAs with 500 fs pulses near the bandgap. Knox and coworkers (1986) then reported experiments in GaAs Multiple Quantum Well Structures (MQWS) wherein pulses of 80 fs duration near the bandgap were used to

probe the dynamics of thermalization of an initially non-thermal distribution. In this experiment, the excitation pulsewidth was less than the thermalization time, so the actual thermalization process was spectrally and temporally resolved. Excitation at 1.50 eV insured that the electrons and holes were excited only in the gamma valley and had insufficient energy to emit optical phonons. Under these conditions, carrier-carrier scattering is the dominant operable relaxation mechanism. The maximum excitation density in this experiment was about $N_{eh} \approx 2 \times 10^{10} \text{ cm}^{-2}$, limited by optical pulse energy due to the weak infrared continuum which is available from a system which operates in the visible spectral range, since the continuum intensity decays exponentially with energy on both sides of the center wavelength. In the present experiments, we use a new laser system which has recently been developed which makes available for the first time intense femtosecond continuum pulses with a center wavelength in the near infrared at 805 nm at 6 kilohertz repetition rate (Knox 1987). This system now allows us to continue the study of non-thermal distributions to much higher densities than previously possible. In fact, we have been able to achieve carrier densities near the maximum theoretical carrier density, beyond which the sample has no optical absorption at the pump wavelength. The laser system has been discussed in detail (Knox 1987), and only the essential features will be mentioned here. Optical pulses of 100 fs duration are generated at 805 nm wavelength in a two-jet synchronously pumped dispersion-compensated dye laser and amplified to 1 microjoule energies at 6 kilohertz repetition rate in a six-pass jet amplifier (Knox and colleagues 1984). These pulses are focused into a 1 mm jet of ethylene glycol and generate a white continuum pulse which is centered at 805 nm. The continuum distribution on the infrared side 810-900 nm is used for the present set of measurements. A probe continuum is split off with a 4% reflection and the rest of the continuum beam is used as a continuously tunable intense pump pulse. An interference filter at 825 nm (1.50 eV) is selected for the pump pulse filter. The probe pulse passes through a 0.1 μm resolution stepper motor for time delay adjustments, and is focused to a 20 μm diameter spot on the sample. The pump beam is focused to a diameter of 55 μm at the same point on the sample. The sample and interference filter are the same ones which were used in our previous hole-burning experiment (Knox and coworkers 1986). The system time response as determined by replacing the sample with a 1 mm LiIO_3 crystal is 150 fs FWHM, corresponding to 100 fs continuum and selected continuum pulsewidths.

It has been shown experimentally (Knox and coworkers 1986) and theoretically (Schmitt-Rink, Chemla and Miller 1985) that in MQWS the effects of the Pauli exclusion principle (phase-space filling and exchange) are much more efficient than the direct screening of the Coulomb interaction in bleaching the excitonic as well as the continuum absorption. Consequently when an electron hole (e-h) plasma is photogenerated in the continuum above the exciton resonances of the $n_s = 1$ subband transition, it produces first a spectral-hole in the absorption spectrum, that reproduces the electron, $n_e(k)$, and hole, $n_h(k)$, distributions. In the leading order in the perturbation the absorption coefficient in the continuum can be written;

$$\alpha_c \approx [1 - n_e(k) - n_h(k)] \alpha_c^{(0)} \quad (1)$$

In addition the carriers can induce a strong bleaching of the excitonic resonances by occupying states that form the basis for the exciton wavefunction in k -space which describes the correlated e-h pair relative motion $\Phi(k)$. These states are located within one exciton binding energy ($E_b \approx 10 \text{ meV}$) of the bottom of the band (Schmitt-Rink, Chemla and Miller 1985). Therefore, measurement of the evolution of the changes in absorption both at the energy where the photocarriers are generated and at the exciton resonance yields two internal probes of the dynamics of the carriers. The line shape and the evolution of the spectral-hole gives information about the scattering of the carriers out of the state in which they were generated. The evolution of the exciton peak gives information on the time they take to reach the bottom of the band and the internal details of the relative importance of Pauli exclusion, screening and exchange contributions (Schmitt-Rink, Chemla and Miller 1985).

We discuss first high density excitations in undoped quantum wells. Fig. (1) shows the absorption spectrum of an undoped sample before excitation and at a time delay which corresponds to the best time overlap of the pump and probe pulses (which we refer to as the " $t = 0$ " point) and at a delay $\Delta t = 132 \text{ fs}$. The excitation distribution as determined by the pump beam interference filter is also shown. A deep spectral hole burning is observed, where the absorption dips nearly to zero. Also shown in Fig. 1 is the approximate absorption saturation which was obtained in the previous experiment at about $2 \times 10^{10} \text{ cm}^{-2}$ carrier density, for comparison. At high densities, we find that this distribution is well-centered at the pump energy, and very rapidly relaxes. This is shown in Fig. (2) where a set of differential spectra at various delays between $\Delta t = -270 \text{ fs}$ and $+270 \text{ fs}$ are presented. They show very clearly the effect of the photocarriers on the continuum and excitonic absorption as they are generated and during their thermalization. It is difficult to determine accurately the carrier density in these type of experiments, and particularly so at high densities, since the absorption of the pump pulse is both weak and time-varying over a significant range during the excitation pulse. We estimate that in the case of Fig. (2): $N_{eh} \approx 10^{12} \text{ cm}^{-2}$ within a 50% accuracy.

In order to determine the dynamics of the thermalization, we show in Fig. (3) the value of the absorption bleaching at the peak of the spectral hole and at the $n_s = 1$ heavy hole (hh) exciton. Two excitation intensities are shown: Fig. (3a) $N_{eh} \approx 2 \times 10^{11} \text{ cm}^{-2}$, Fig. (3b) $N_{eh} \approx 1 \times 10^{12} \text{ cm}^{-2}$. The insets show the spectral shape of the pump and non-thermal signals at $t = 0$ for the respective cases.

It is clear from this study that the relaxation of the non-thermal peak becomes faster at higher densities. The time courses in Fig. 3 indicate this point in several ways. The recovery of the absorption at the hole is time resolved for the medium excitation case of Fig. 3a, as indicated by the asymmetry in the time course compared to the measured system time response. For this case, the measured hole burning signal has about the same magnitude as the excitonic differential signal. For the high density case, the time asymmetry disappears, indicating that the thermalization time is significantly less than the system response, and the height of the measured hole-

burning decreases relative to the excitonic differential signal. Two processes are responsible for this behavior. First, we determine that the thermalization time is density-dependent. Second, the excitonic differential signal saturates at a lower carrier density than the non-thermal distribution signal. Figure 1 shows that the exciton absorption is completely bleached at the high density, and it is replaced by renormalized continuum absorption. Therefore, we explain these results as follows: at low densities, thermalization times are longer than the system response, but since the density is much below the saturation density, the excitonic signal is about 10 times larger than the hole signal (Knox and coworkers 1986). At these new higher densities, the resulting hole burning signal increases with density until the thermalization time becomes comparable to the system time response, beyond which point it decreases. Dynamically, the bleaching at the exciton peak increases steadily and reaches its maximum value in a shorter time as the excitation density is increased. This shows that the carriers fill up the bottom of the band more rapidly at high densities. We note that the width of the spectral hole also increases as the carrier density is increased, as can be seen in the insets of Fig. 3. This result is related to the strong saturation of the $n = 1$ continuum. In Fig. 1 it is clearly seen that a density-dependent broadening is expected since there is less absorption near the peak of the pump spectrum than there is at the wings.

A complete analysis of these results is extremely complicated, even in our case with only carrier-carrier scattering in the Γ valley with no significant phonon emission. To our knowledge, two groups have performed Monte-Carlo simulations of our experiment in the low density limit: Goodnick and Lugli (1987) and Bailey and coworkers (1987), an approach which requires heavy numerical computations but allows for the inclusion of a number of important effects. We have developed a simple model for the thermalization of the photocarriers, involving a single relaxation time τ_r , in which we assume that no energy is exchanged with the lattice in the time scale of the experiment, and there is no loss of carriers to intervalley scattering or recombination. The absorption saturation is obtained according to Eq.(1) and we assume a local equilibrium relaxation toward the Fermi distribution corresponding to the instantaneous number of carriers present in the sample. This simple model thus incorporates the major ingredients of the experiment and summarizes the results in a single parameter τ_r . This model will be discussed in more detail elsewhere. We find that the measured spectral-hole and exciton bleaching evolution of Fig. (3) are nicely reproduced by $\tau_r = 60\text{fs}$ and 30fs respectively. Similar consideration of the data of Knox and coworkers (1986) yields $\tau_r = 100\text{fs}$. Thus when N_{eh} increases by at least a factor of 50, τ_r decreases by approximately a factor of 3, showing that the relaxation is not a very strongly varying function of the density. It is interesting to note that the relaxation time we measure at the highest density is significantly slower than that measured by Lin and coworkers (1987) for densities of a few times 10^{11}cm^{-2} . We attribute this difference to the fact that in our experiment carrier-carrier scattering is the only relaxation channel whereas in the case of large excess photon energy phonon scattering as well as a number of other processes also participate in the relaxation, and the measured relaxation rate is the sum of the individual rates. All these processes may have different scalings with carrier densities, so it is important to isolate each process to determine its density dependence. Nonetheless, the weak dependence

which we find for the density dependence of the carrier-carrier scattering rate in our high density experiments is consistent with the weak dependence which has been found in other experiments. It is interesting to note that the relaxation time for our highest density is only 30 fs (our model indicates that if it were less than 30 fs, such a prominent hole would not be observed) and this is only about a factor of two lower than the maximum theoretically obtainable excitation density for a 96 Å quantum well. By incorporating a properly saturating driving term into our model, we are able to explain our experimental result that the spectral hole becomes broader at high saturation levels. We note that in the previous experiment (Knox and coworkers 1986) the spectral hole width was essentially equal to the excitation bandwidth, whereas in the data of Fig. 2 at high density, the differential spectrum is about twice as broad as the pump spectrum. We note that the small energy offset between the pump and spectral hole in the previous experiment (Knox and coworkers 1986) is not reproduced in these experiments. We determine that the spectral hole center is within 1 meV from the center of the excitation pulse in the present experiments.

As mentioned in the introduction, by performing identical experiments in samples in which a distribution of excess charged particles already exists before excitation, we may learn more about the carrier-carrier scattering process and about the various components it involves. In particular, experiments on ballistic transistors are performed in such a way that nearly monoenergetic electrons are injected into a gate region in which a sea of carriers are already thermalized to the lattice (Levi and coworkers 1985) and Heiblum and coworkers (1985). Under these conditions, it has been possible to calculate scattering rates as a function of excess energy and density (Levi and coworkers 1985). In optical experiments in undoped samples, the non-thermal distribution at time t thermalizes by interactions with itself and not another already thermalized distribution. In order to investigate these effects we have repeated the experiment with modulation doped (MD) samples. Here we report preliminary results on a n-type sample which consists of 50 periods of 120 Å GaAs QW sandwiched between 350 Å AlGaAs barriers whose central 113 Å contain $3 \times 10^{17} \text{ cm}^{-3}$ Si dopant. The density of electrons in the QW, $N_e = 3.5 \times 10^{11} \text{ cm}^{-2}$ was determined by Hall measurements. Figure (4) shows the absorption spectrum of a room temperature MD-MQWS before excitation and the $\Delta t = 0$ absorption spectrum of the sample excited to $N_{eh} \approx 1 \times 10^{12} \text{ cm}^{-2}$ by a pump centered at 840 nm. It is clear that the relaxation is very different from that of the undoped sample, since there is no hole-burning. The line shape of the unexcited sample absorption spectrum deserves some comments. The peak seen at 1.45 eV is not an exciton, but corresponds to the electron-hole correlation singularity recently investigated theoretically (Ruckenstein and Schmitt-Rink 1987), and experimentally (Livescu and coworkers 1987). This resonance is due to the motion of the Fermi-sea of electrons in reaction to the sudden appearance of the hole upon absorption of a photon. This screening of the Coulomb potential of the hole correlates this latter to the whole Fermi-sea thus forming a collective "many-body" analog of the hydrogenic exciton of the undoped samples. In Fig. (5) the complete time delay scans are shown. A thermalized distribution is observed instantaneously in this experiment. Apparently, the effect of a moderate background density of excess electrons which are thermalized to the lattice

is to greatly increase the scattering rate. We estimate by comparison with our model that the relaxation time is less than 10 fs for these conditions. One possible explanation of this is that electron-electron scattering rates are enhanced by carrier occupation near $k = 0$. Before the non-thermal distribution thermalizes, there is no $k=0$ occupation, as has been shown experimentally (Knox and coworkers 1986) and theoretically (Schmitt-Rink, Chemla and Miller 1985). This striking result is consistent with recent Monte-Carlo simulations in which a variable background density was included (Bailey and coworkers 1987). These calculations indicated that the non-thermal component vanishes when the background density is increased. This can be interpreted as a very rapid thermalization which is faster than the laser pulses which are used to make the measurements.

To our knowledge, these results represent the first optical investigations of non-thermal carrier generation in doped structures, and we envision further extensions to p-doped structures in which we may obtain information on the separate roles of electron and hole contributions in optical experiments.

SUMMARY

We have investigated non-thermal carrier generation in GaAs MQWS at high excitation densities by making use of a new laser system which generates intense 100 fs white light continuum pulses centered at 805 nm at 6 kilohertz repetition rate. We find that carrier-carrier scattering alone yields thermalization rates only as fast as 30 fs at densities close to the theoretical maximum for $n=1$ in-band excitation. We find that as the density is varied over approximately 50-100 times, the scattering rate varies by only a factor of 3 or so. We find that the width of the non-thermal distribution depends on carrier density. A simple dynamic relaxation-time approximation with a self-consistent renormalized Fermi local-equilibrium distribution function reproduces our dynamic results quite well, and agrees qualitatively with Monte-Carlo simulations. Experiments in modulation-doped samples show significant sensitivity to background electron doping, and relaxation times of less than 10 fs are found for doping densities of $3.5 \times 10^{11} \text{ cm}^{-3}$.

ACKNOWLEDGEMENTS

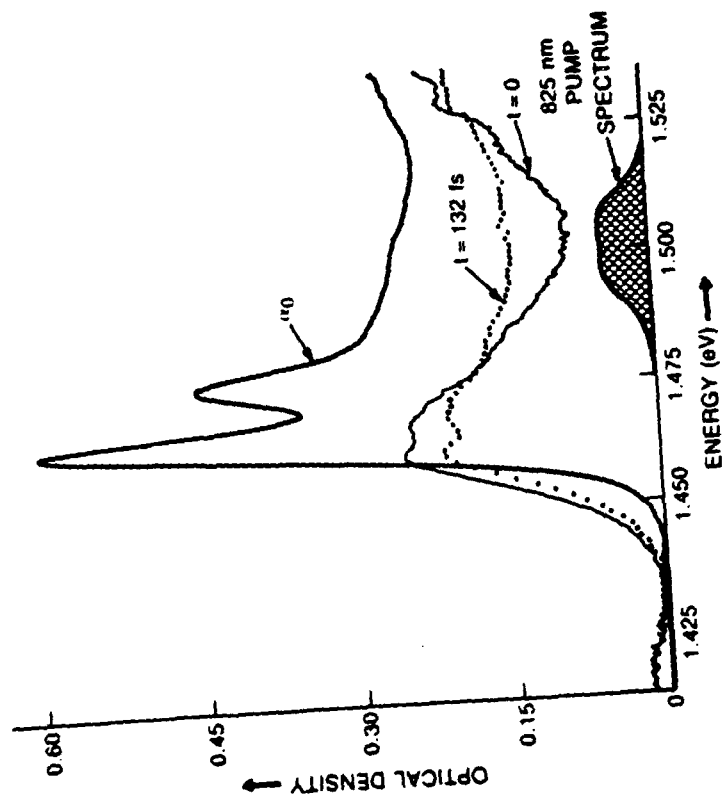
We wish to thank A. VonLehmen, and D.A.B. Miller for stimulating discussions and J.E. Henry and D. Burrows for expert technical assistance.

REFERENCES

- [1] Bailey, D.W., Artaki, M.A., Stanton, C.J. and Hess, K. (1987). Private communication.
- [2] Goodnick, S.M. and Lugli, P. (1987). Private communication.
- [3] Heiblum, M., Nathan, M.I., Thomas, D.C. and Knoedler, C.M. (1985). Phys. Rev. Lett. 55,2200.
- [4] Knox, W.H., Downer, M.C., Fork, R.L. and Shank, C.V. (1984). Opt. Lett. 9, 552.
- [5] Knox, W.H., Hirlimann, Miller, D.A.B., Shah, J., Chemla, D.S. and Shank, C.V. (1986). Phys. Rev. Lett. 56, 1191.
- [6] Knox, W.H. (1987, October). Journal of the Optical Society of America B.
- [7] Levi, A.F.J., Hayes, J.R., Platzmann, P.M. and Wiegmann, W. (1985). Phys. Rev. Lett. 55, 2071.
- [8] Lin, W.Z., Fujimoto, J.G., Ippen, E.P. and Logan, R.A. (1987). Appl. Phys. Lett., 50, 124.
- [9] Livescu, G., Miller, D.A.B., Chemla, D.S., Gossard, A.C., English, J.H.,submitted to Phys. Rev. Lett.
- [10] Oudar, J.L, Migus, A., Hulin, D., Grillon, G., Etchepare, Antonetti, A. (1984). Phys. Rev. Lett. 53, 384.
- [11] Ruckenstein, A.E. and Schmitt-Rink, S. (1987). Phys. Rev. B35, 7551.
- [12] Schmitt-Rink, S., Chemla, D.S. and Miller, D.A.B. (1985). Phys. Rev. B32, 6601.
- [13] Tang, C.L. and Erskine, D.J. (1983). Phys. Rev. Lett. 51, 840.

FIGURE CAPTIONS

- Figure 1 - Optical absorption spectra of 96 Å GaAs MQWS at 300 K, before excitation, at $t = 0$ when non-thermal distribution is at a peak, and at 132 fs after $t = 0$, and the excitation pulse spectrum.
- Figure 2 - Differential transmission spectra at 66 fs delay intervals for undoped 96 Å MQWS.
- Figure 3 - Time courses at exciton and at the nonthermal peak for (a) medium density : $2 \times 10^{11} \text{ cm}^{-2}$, and (b) high density : $1 \times 10^{12} \text{ cm}^{-2}$. Insets show the shape of the spectral hole burning signals at $t = 0$.
- Figure 4 - Modulation doped n-type sample spectra. Absorption spectrum before $t = 0$, at $t = 0$ and pump pulse spectrum, and pump spectrum at 845 nm. showing no evidence for non-thermal distribution. This result implies a thermalization time of less than 10 fs.
- Figure 5 - Differential transmission scans for n-type doped sample at 33 fs intervals. Doping density is $3.5 \times 10^{11} \text{ cm}^{-2}$, as determined from Hall measurements.



4700-33-11-0001-7

FIGURE 1

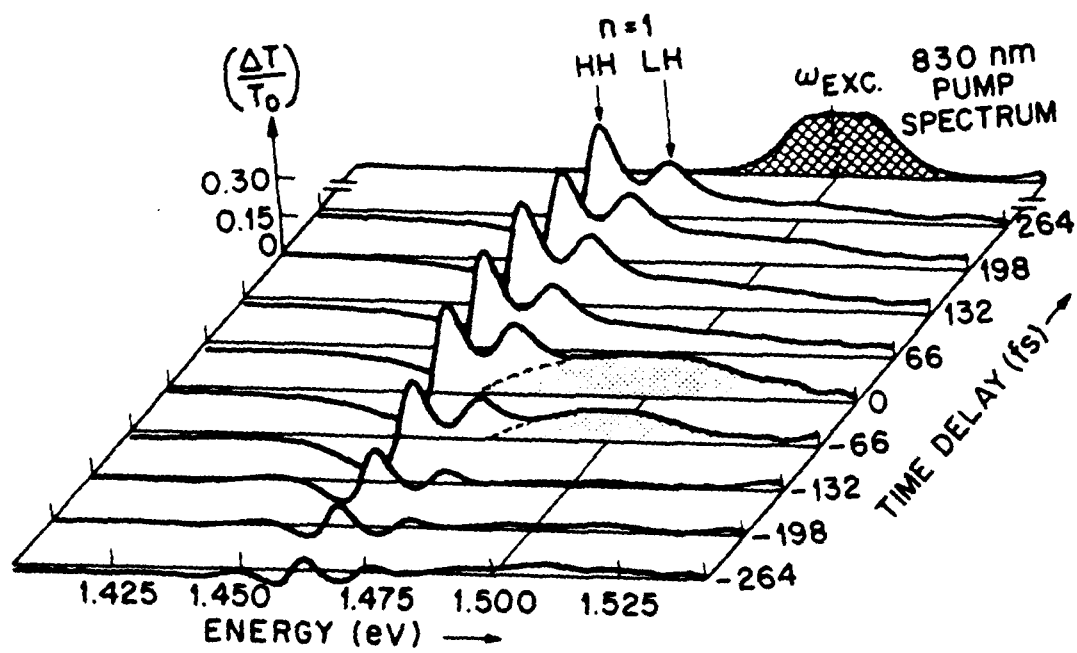


FIGURE 2

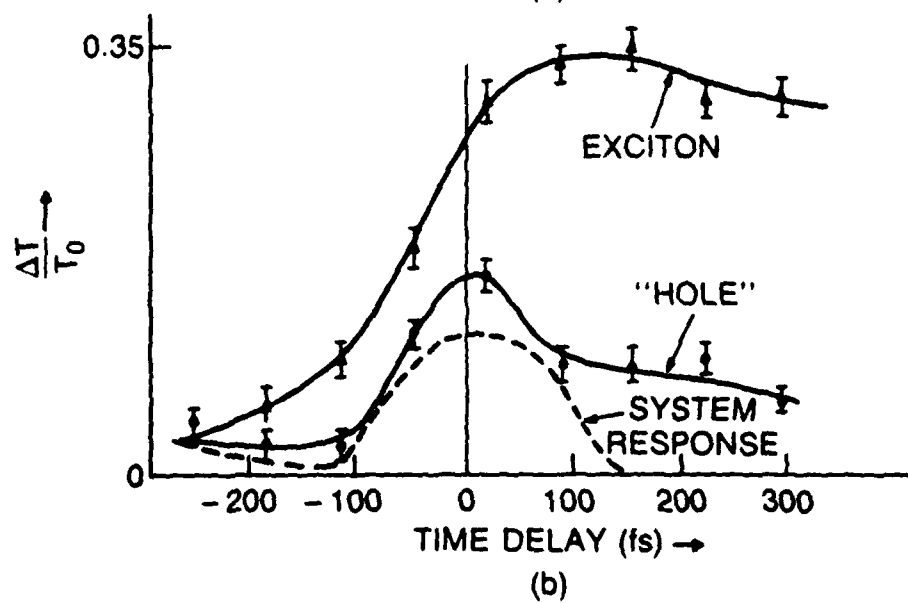
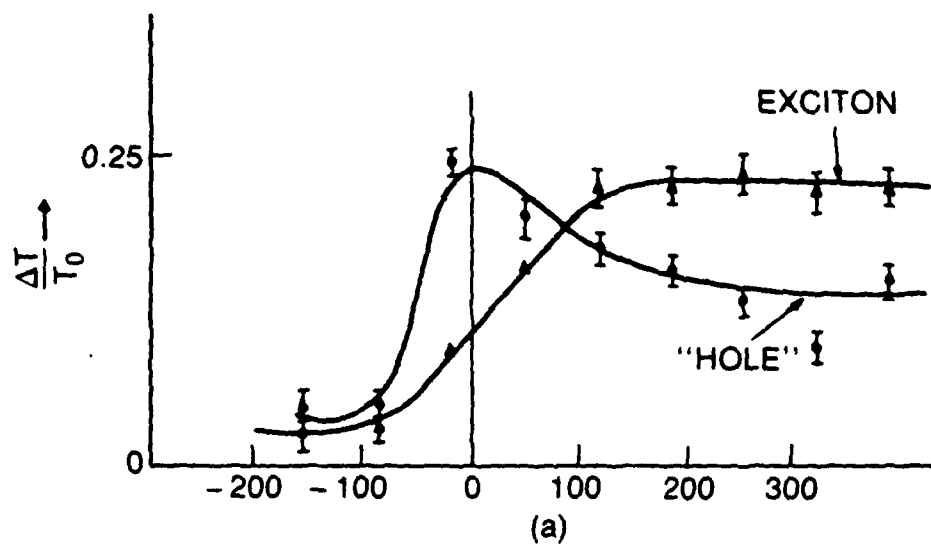


FIGURE 3

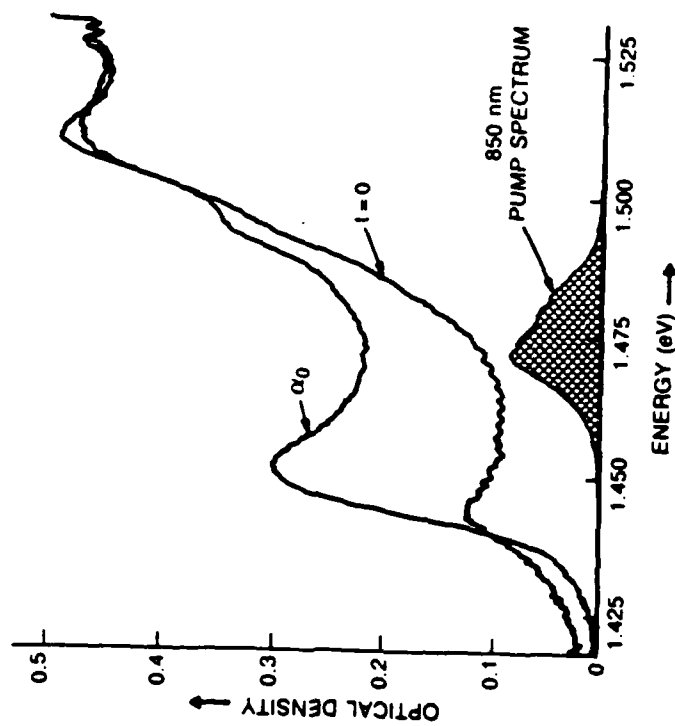


FIGURE 4

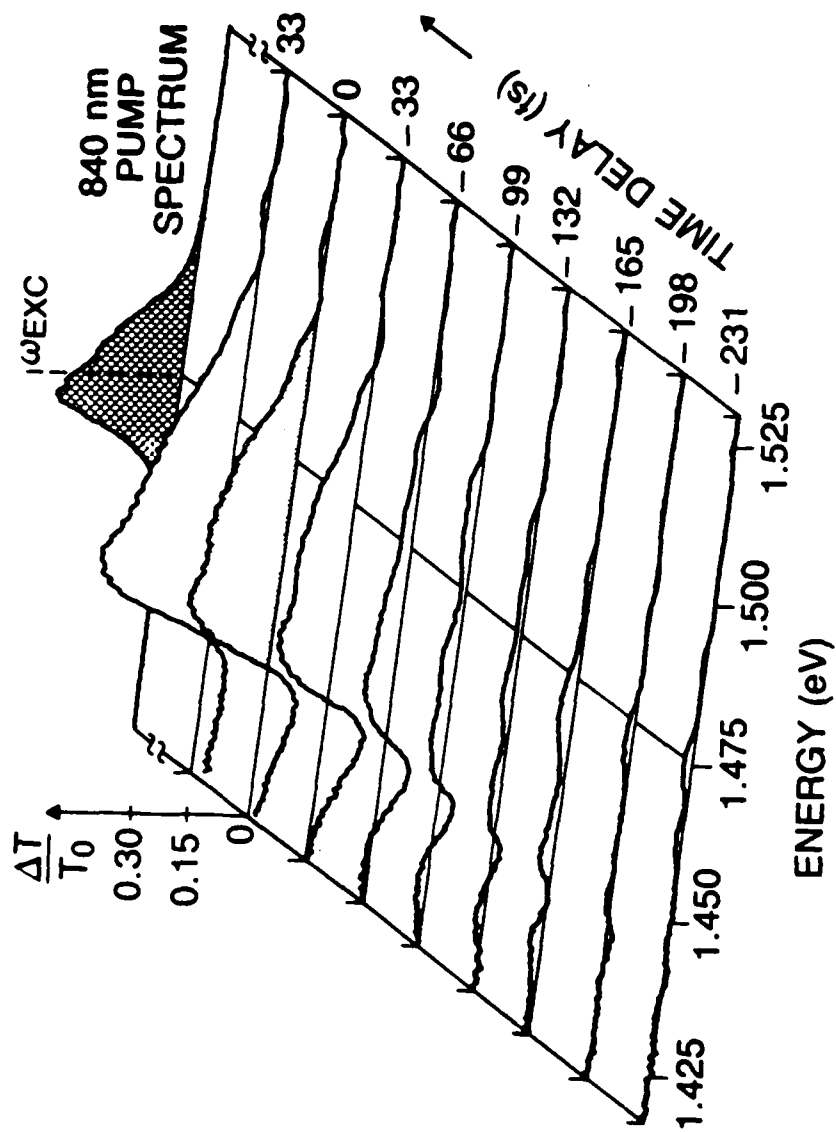


FIGURE 5

Dynamical Aspects of Carrier Tunneling
in Semiconductor Superlattices

Yasuaki Masumoto

Institute of Physics, University of Tsukuba,
Sakura-mura, Niihari-gun, Ibaraki 305, Japan

Abstract

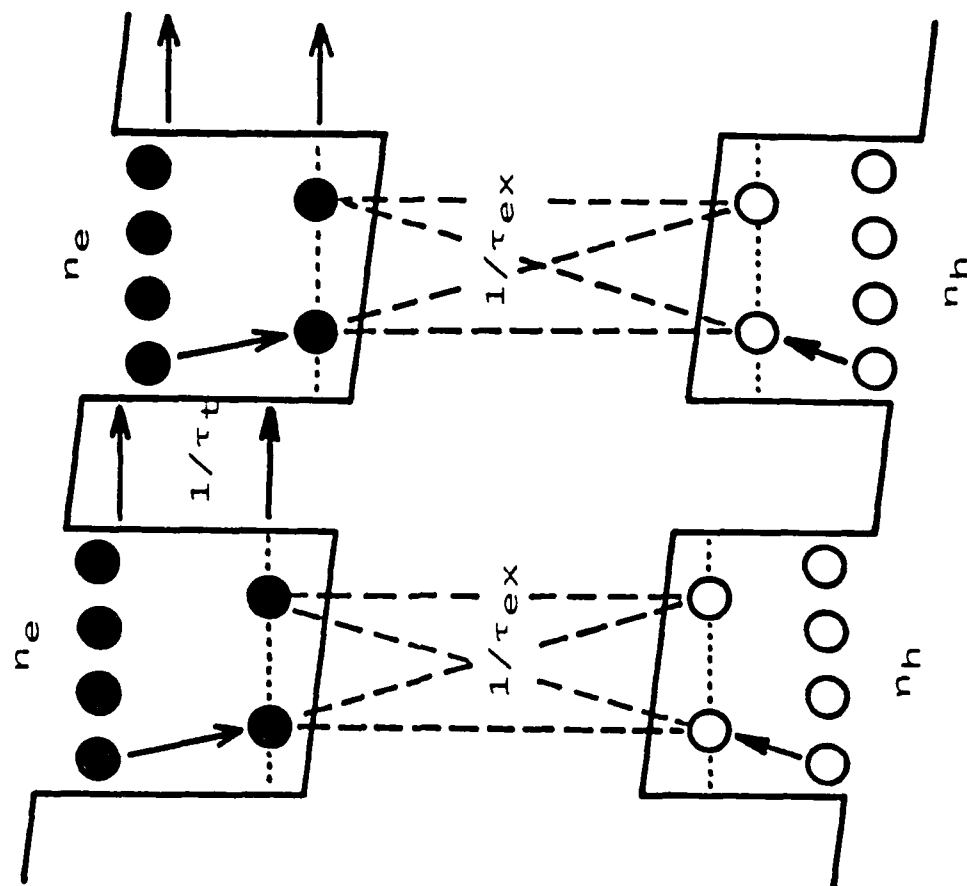
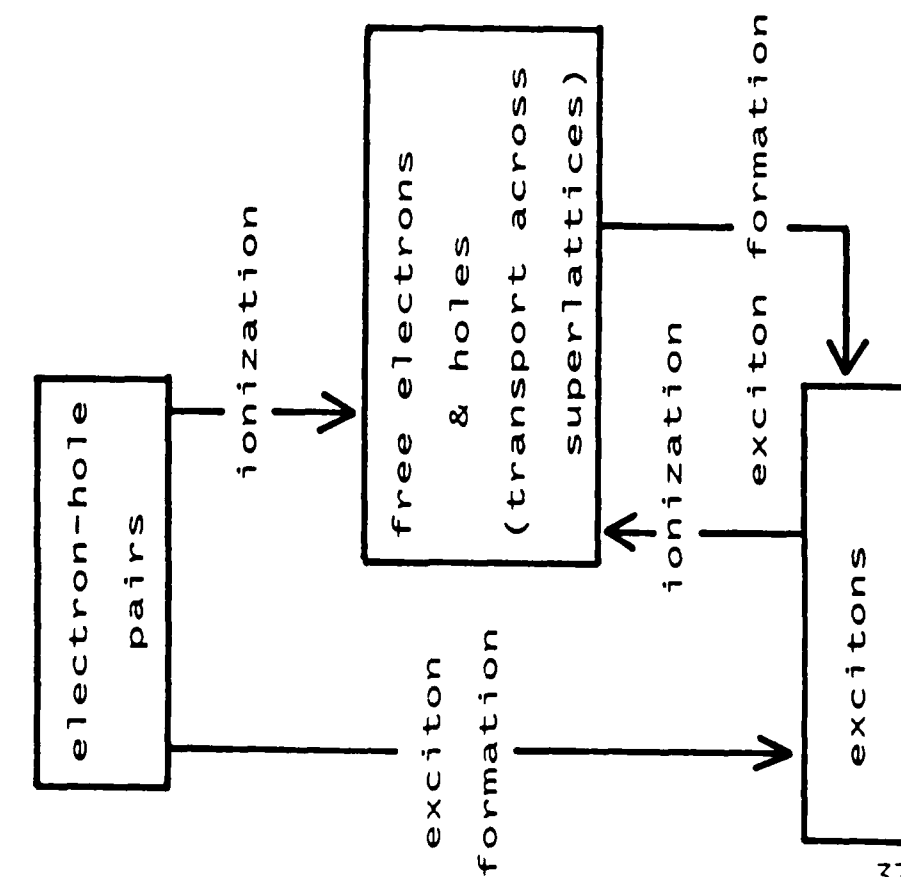
Dynamical carrier processes in GaAs-AlGaAs superlattices are studied by means of picosecond spectroscopy and population mixing technique under the electric field along the superlattice direction. Two prominent structures are found in the curves of exciton luminescence and photocurrent vs. the electric field. They are ascribed to the onset of exciton dissociation followed by electron tunneling through AlGaAs barriers and resonant electron sequential tunneling. The electron tunneling rate is determined to be $1/(430\text{ps})$ and is compared with calculations. In addition, competitive nature of ultrafast processes of photo-excited electron-hole pairs, exciton formation and pair ionization followed by tunneling through barriers, are clarified under the various electric field.

**Dynamical Aspects of Carrier Tunneling
in Semiconductor Superlattices**

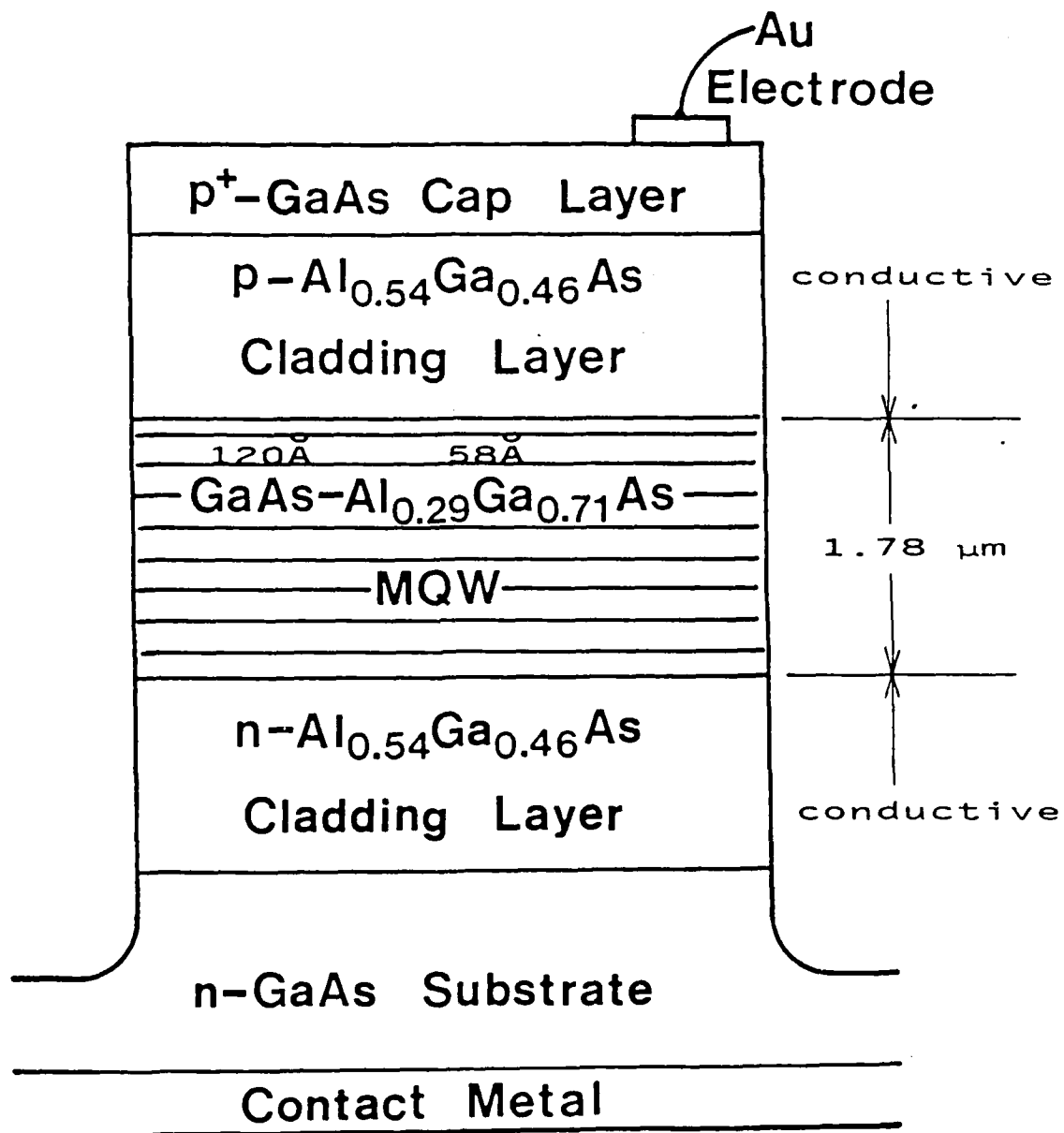
Yasuaki Masumoto

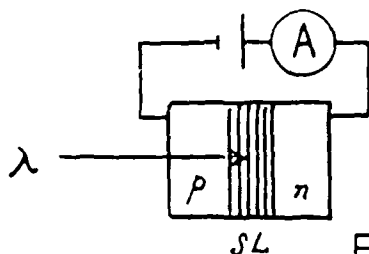
**Institute of Physics, University of Tsukuba,
Sakura-mura, Niihari-gun, Ibaraki 305, Japan**

Ultrafast processes of carriers in semiconductor superlattices under the perpendicular electric field



PIN DIODE STRUCTURE

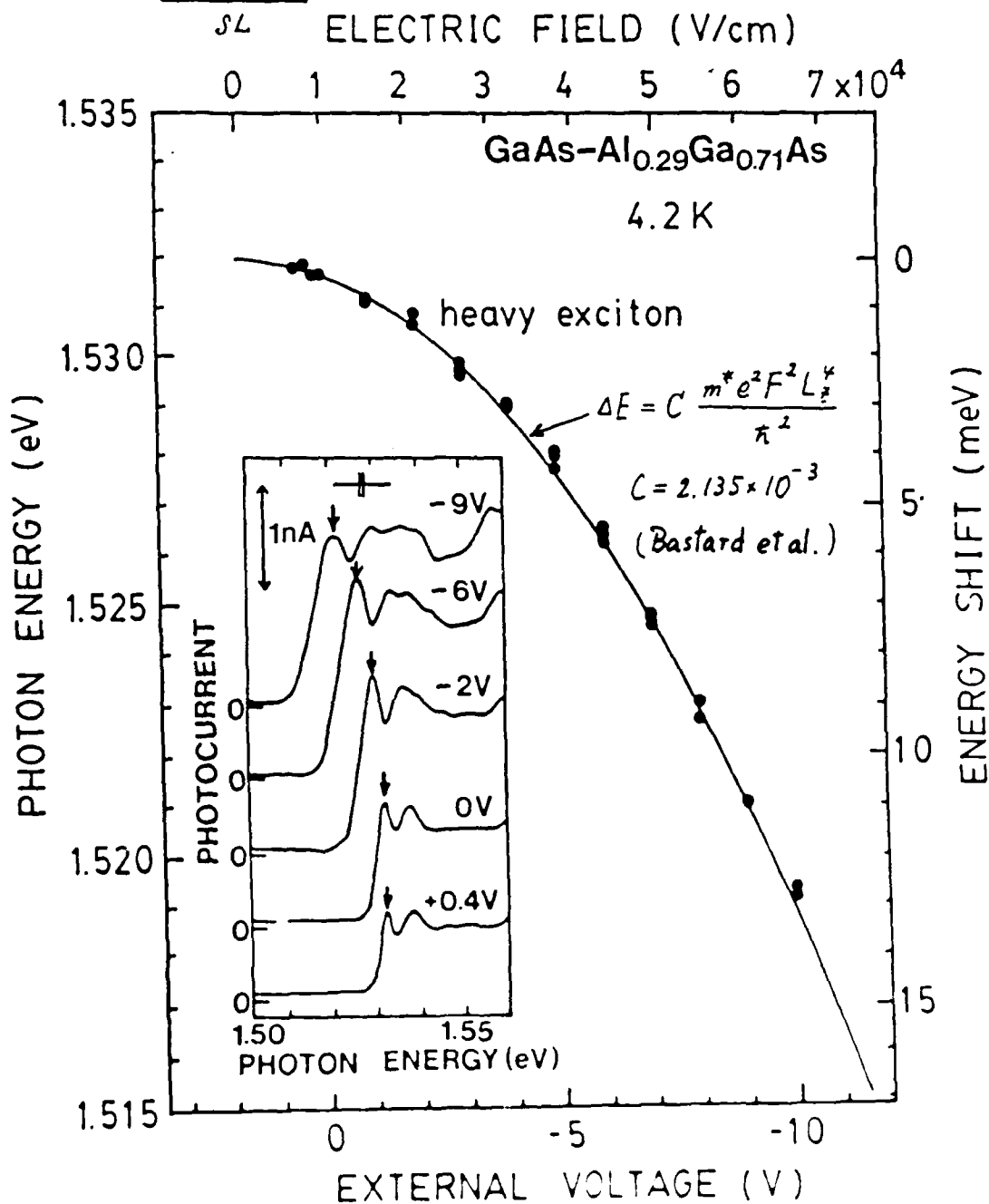




$$F = \frac{V_{ext} - V_{bi}}{d}$$

$$V_{bi} = +1.8 \text{ V}$$

$$d = 1.78 \mu\text{m}$$



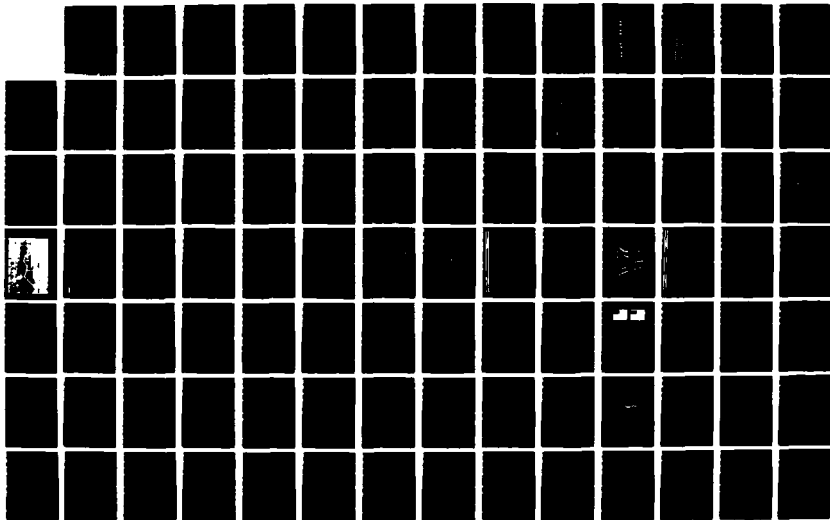
NO-A186 938

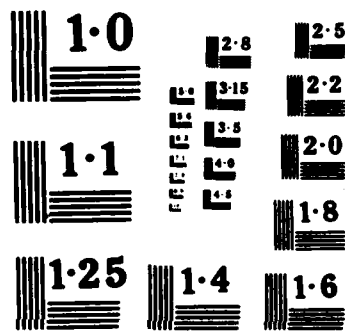
UNITED STATES - JAPAN SEMINAR ON QUANTUM MECHANICAL
ASPECTS OF QUANTUM EL (U) MASSACHUSETTS INST OF TECH
CAMBRIDGE RESEARCH LAB OF ELECTRON
J H SHAPIRO ET AL OCT 87 N00014-87-G-0198 F/G 20/3

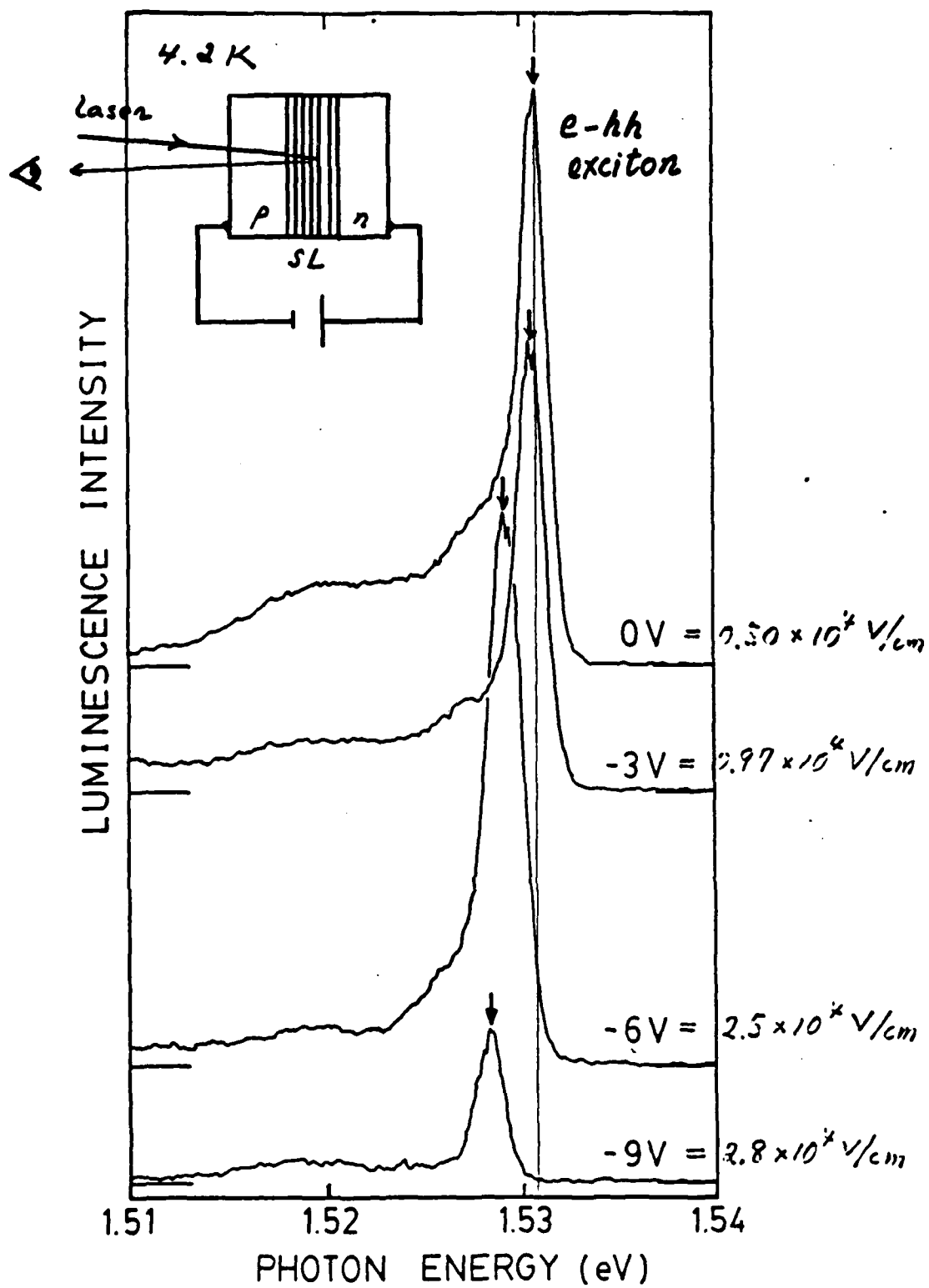
5/7

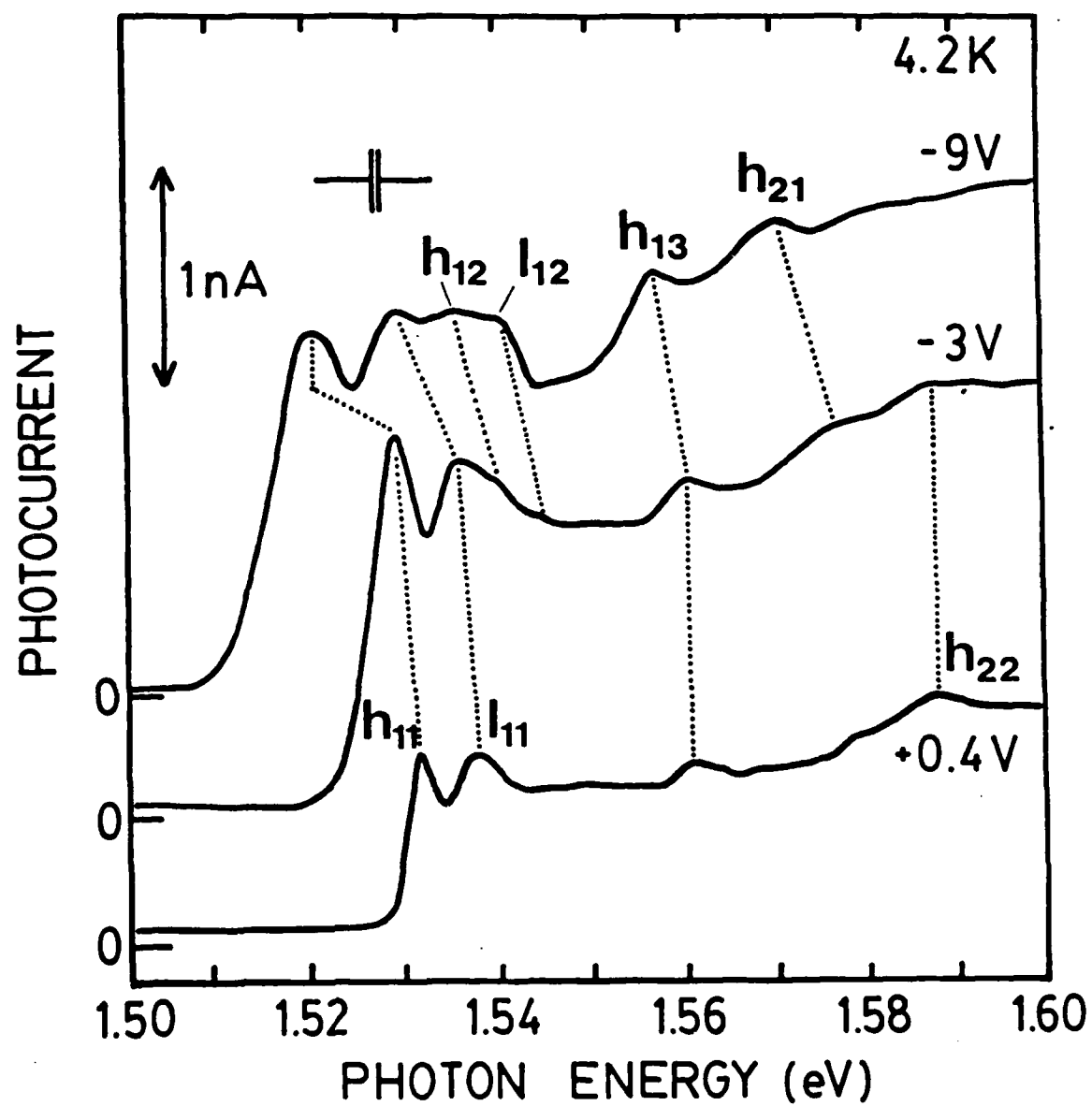
UNCLASSIFIED

NL









Subband Energy Splits (meV)		
$2e - 1e$	$(h_{21} - h_{11})$	49
$3hh - 1hh$	$(h_{13} - h_{11})$	30
$2hh - 1hh$	$(h_{12} - h_{11})$	10
$2lh - 1lh$	$(l_{12} - l_{11})$	9
$1lh - 1hh$	$(l_{11} - h_{11})$	6

Table I. The estimated subband gaps for electrons and holes in 120Å GaAs wells. $ne(hh, lh)$ denotes the n -th electron (heavy hole, light hole) subband. In the parentheses, exciton transition pairs used for the estimation are shown.

178\AA
 $\frac{1}{eFd}$
 Field Gain
 (1 Period)

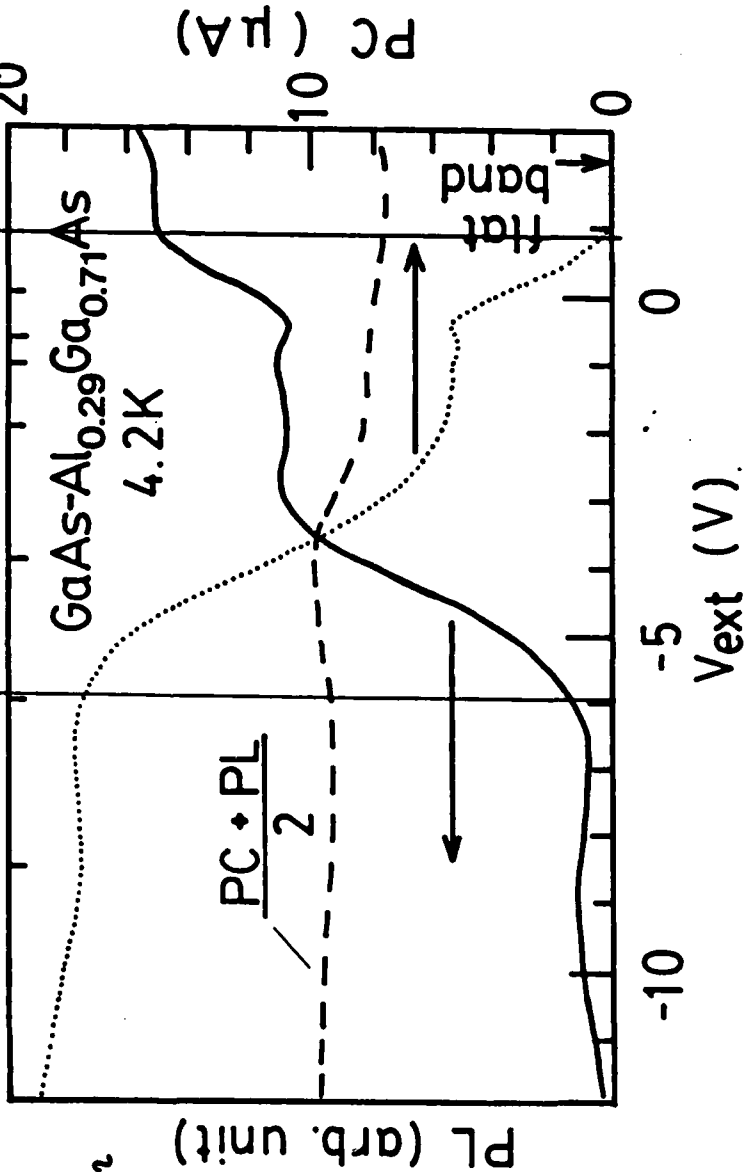
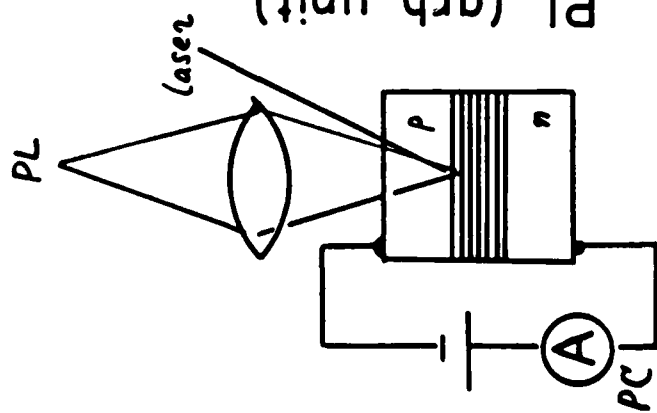
$ex \rightarrow e + h$

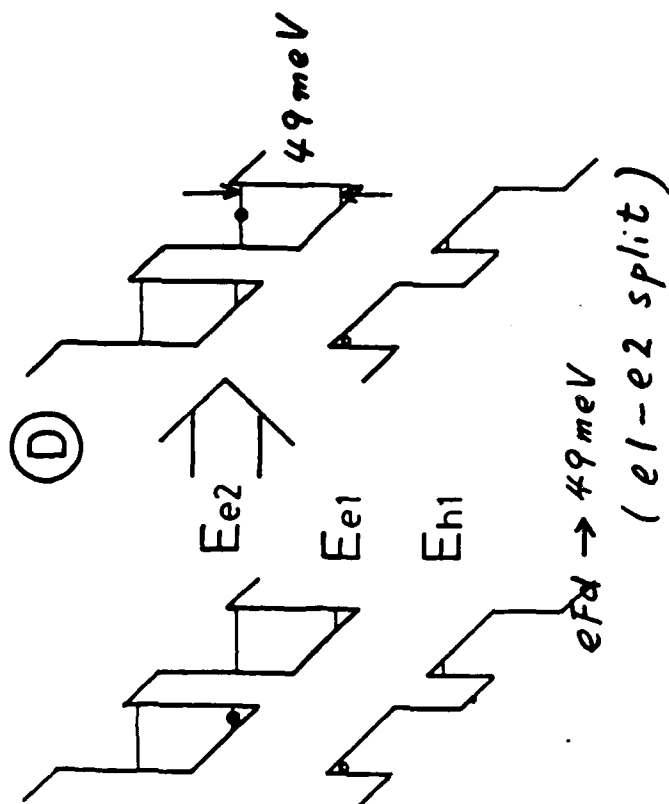
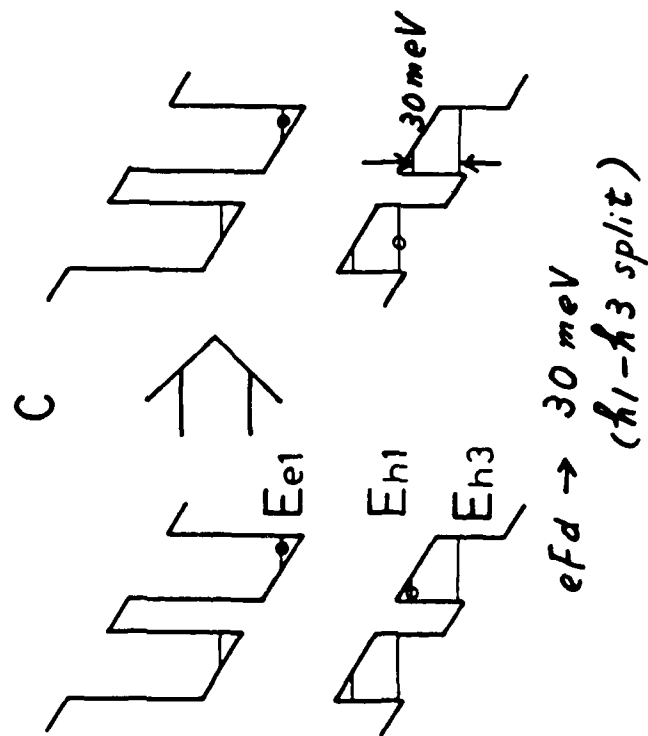
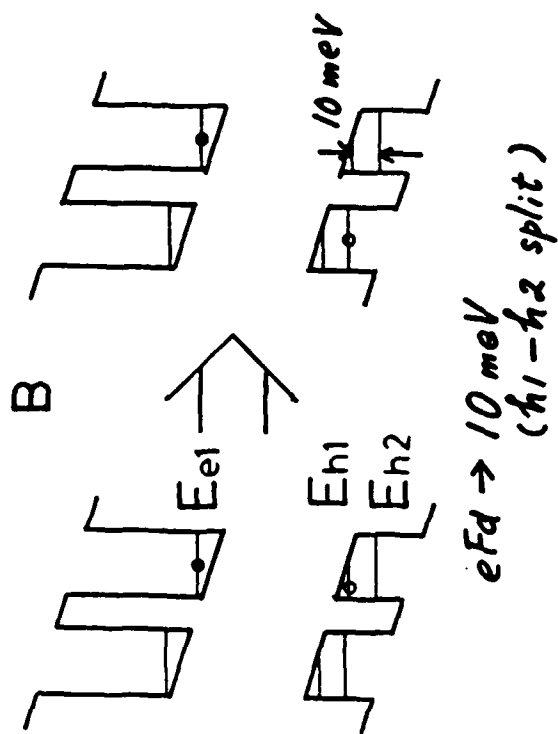
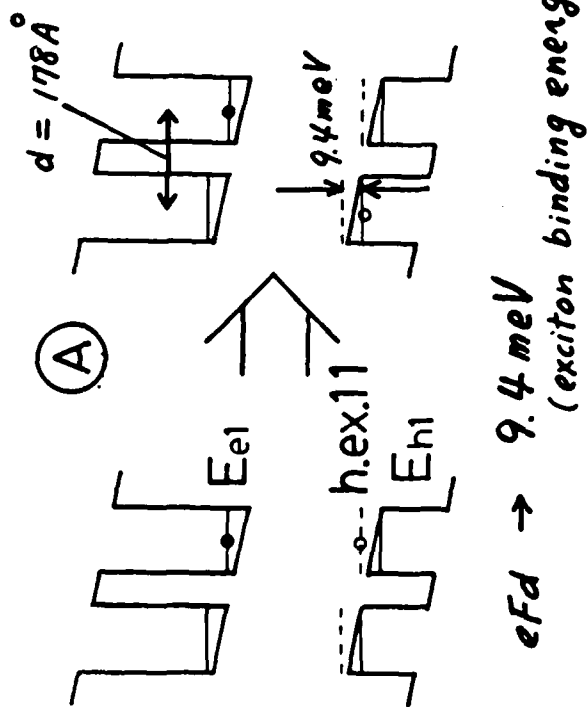
$1/e \rightarrow 2e$

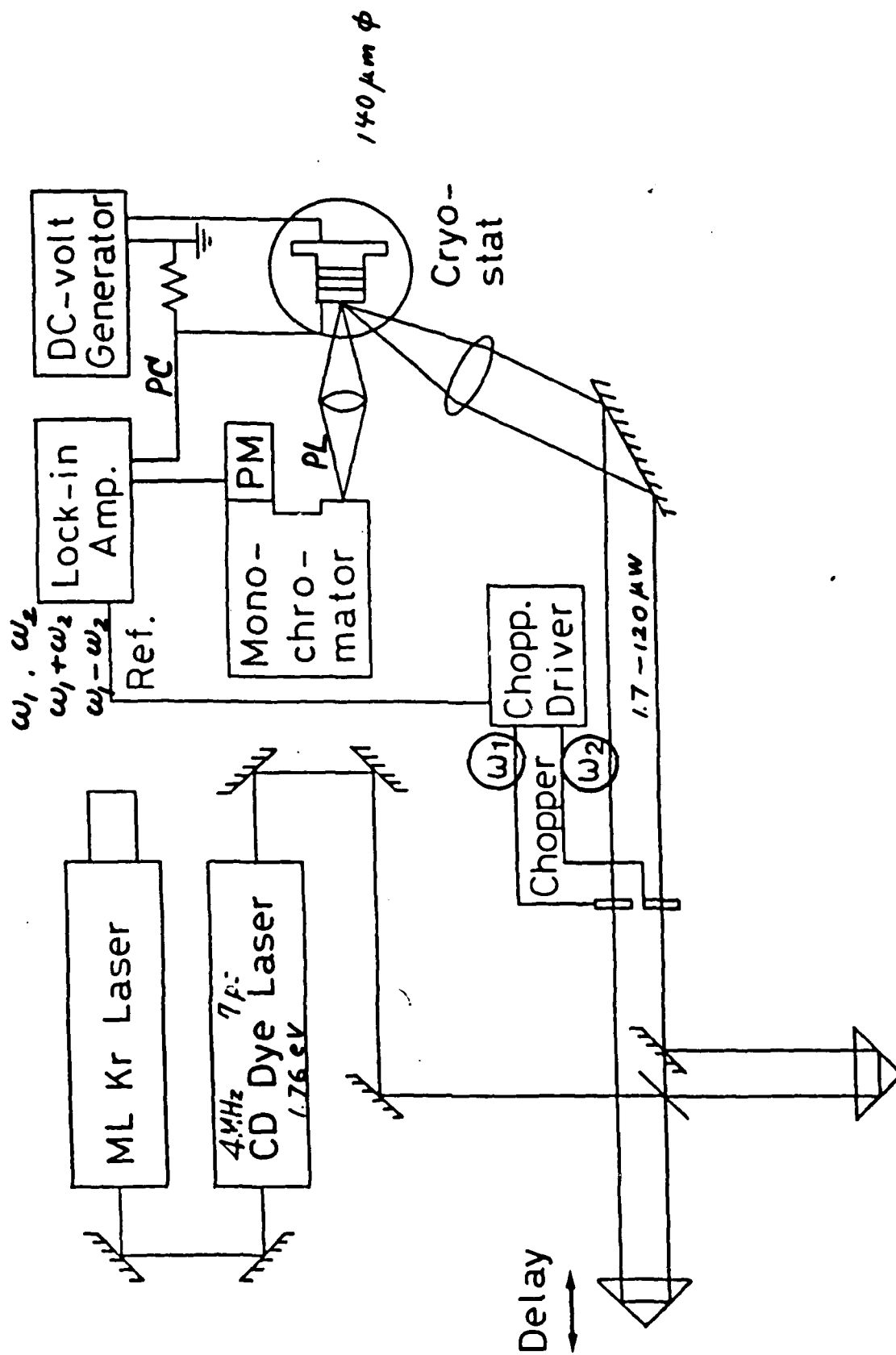
$(Kr^+ \rightarrow LD700 \text{ Dye})$
 4.2 K
 1.75 eV

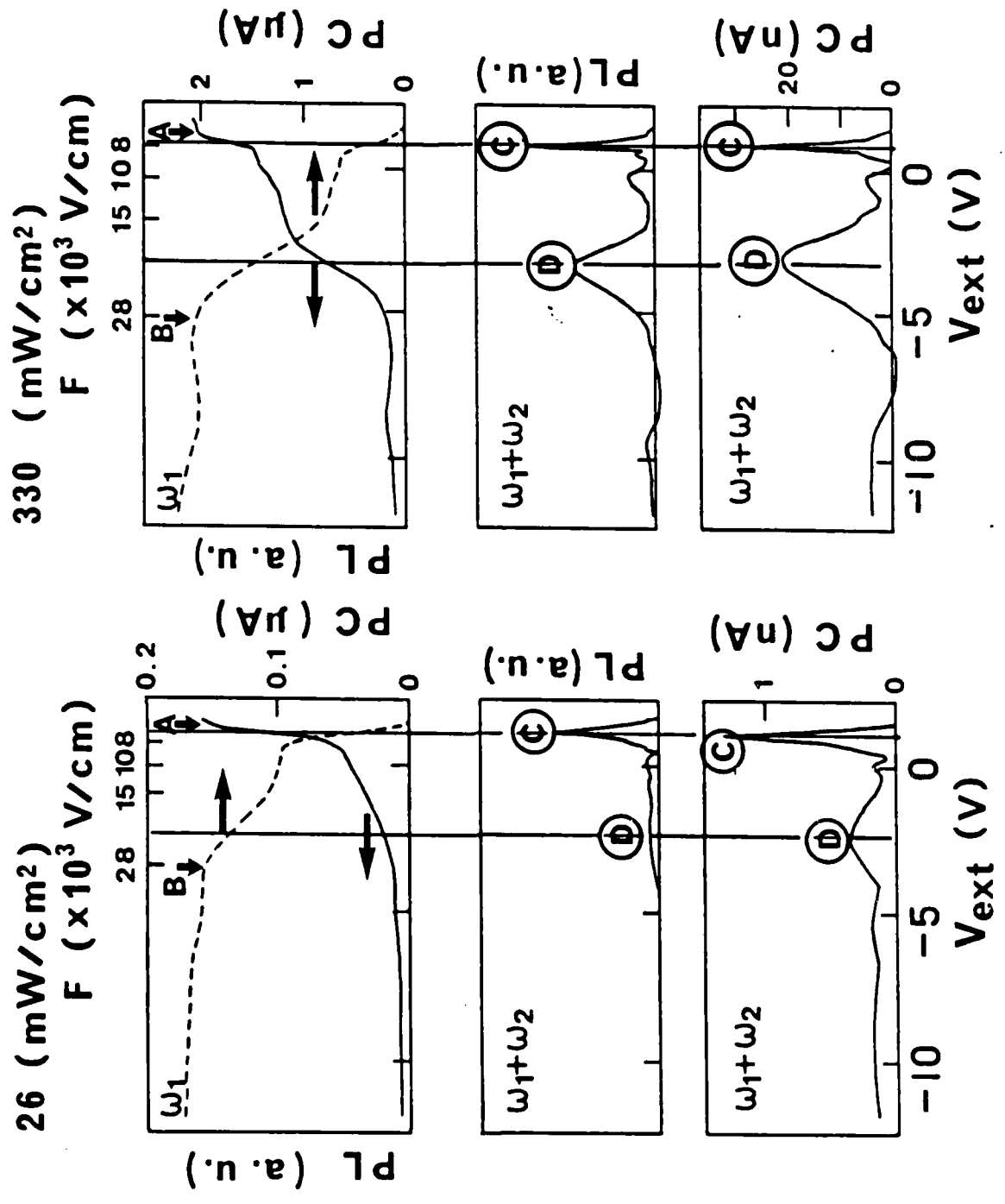
27
 15
 10
 9 (meV)

$F \text{ (} \times 10^3 \text{ V/cm)}$
 42
 28
 22
 15
 10
 9

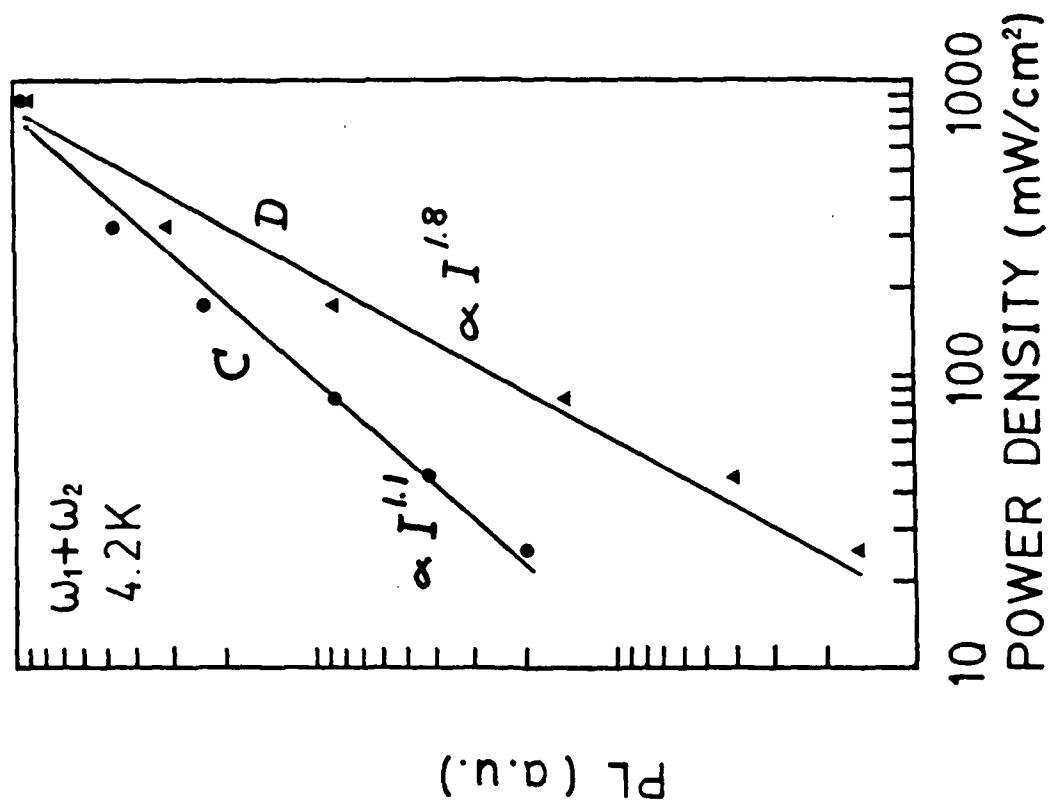


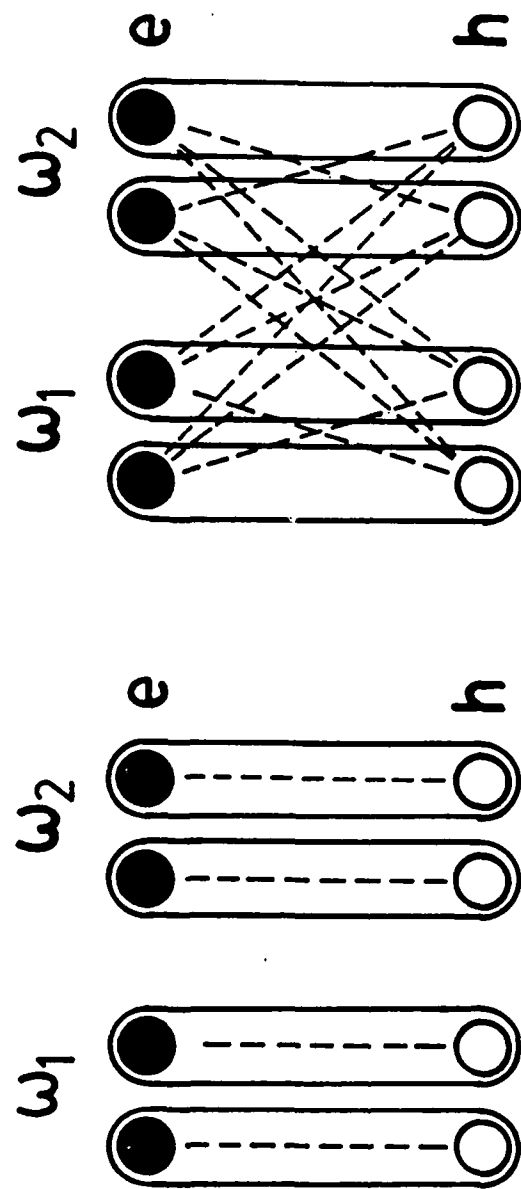






4.2 K





geminate exciton non-geminate exciton

$$2\omega_1, 2\omega_2$$

$$\omega_1 + \omega_2, \omega_1 - \omega_2$$

electron tunneling rate

$$1/\tau_t$$

non-geminate exciton
formation rate

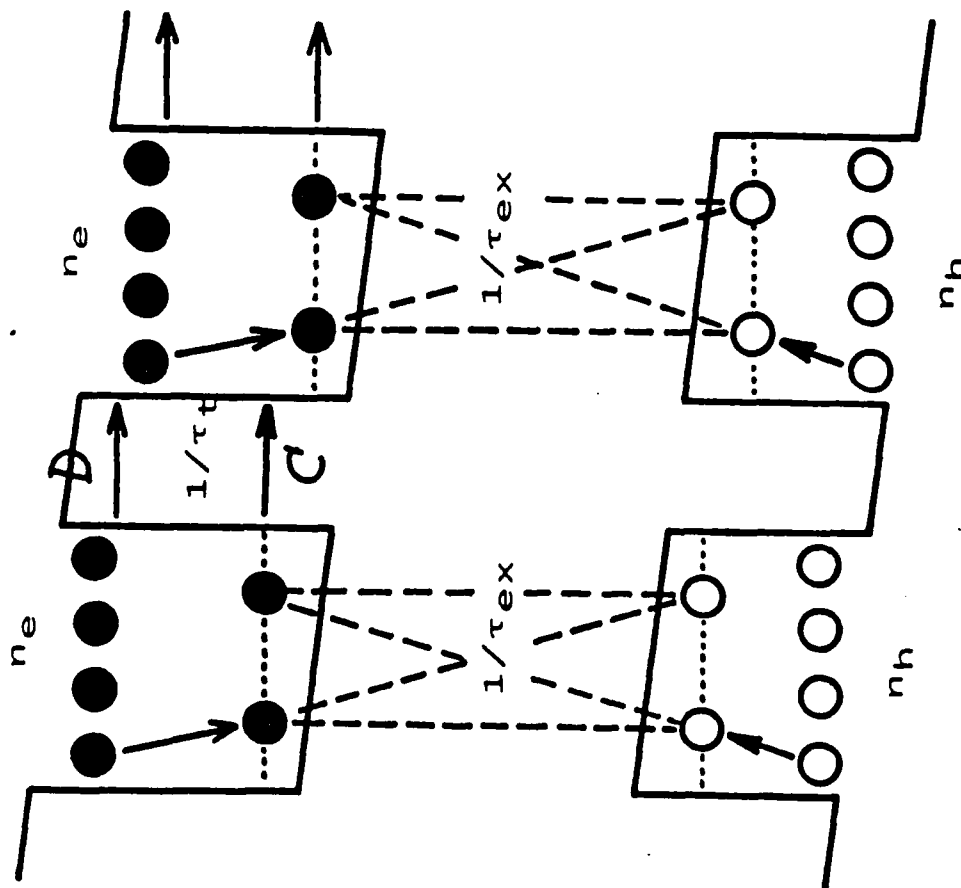
$$1/\tau_{ex} \propto n_e n_h$$

$$(1) \quad 1/\tau_t \gg 1/\tau_{ex}$$

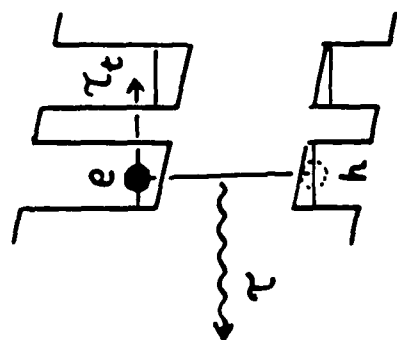
$$PL(\omega_1 + \omega_2) \propto I^2$$

$$(2) \quad 1/\tau_t \ll 1/\tau_{ex}$$

$$PL(\omega_1 + \omega_2) \propto I$$

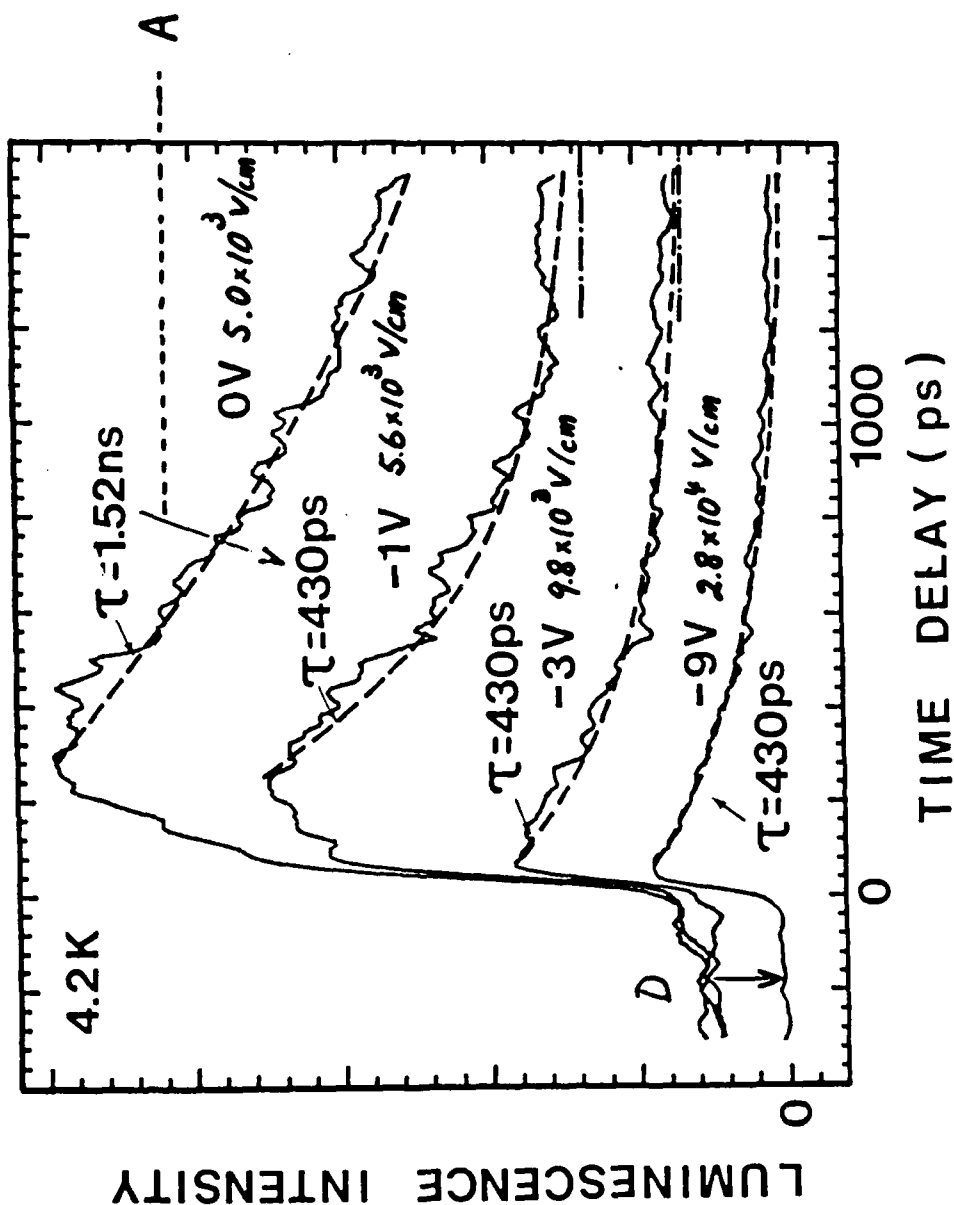


picosecond dye laser + synchroscan streak camera

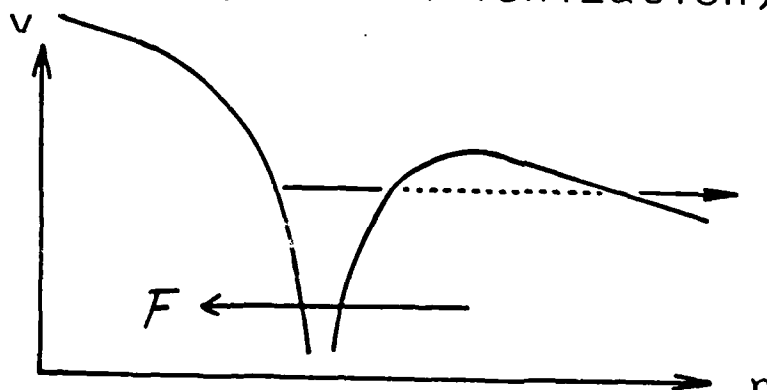


Heavy Exciton

τ_e dominates τ
when $F > 5 \times 10^3 \text{ V/cm}$



(1) Tunneling of Coulomb barrier
(Exciton ionization)



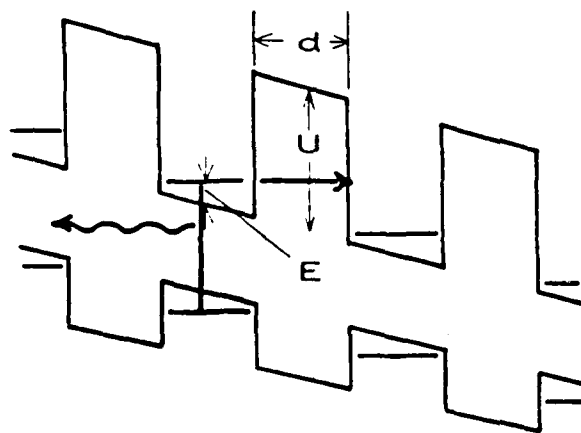
ionization rate

$$w = \frac{16R_y^2}{eFa_B\hbar} \exp\left(-\frac{4R_y}{3eFa_B}\right) \sim 2.8 \times 10^{13} \text{ s}^{-1}$$

$$(\tau \sim 36 \text{ fs})$$

$$\text{at } F = 5 \times 10^3 \text{ V/cm}$$

(2) Tunneling of potential barrier



$$U \sim 206 \text{ meV}$$

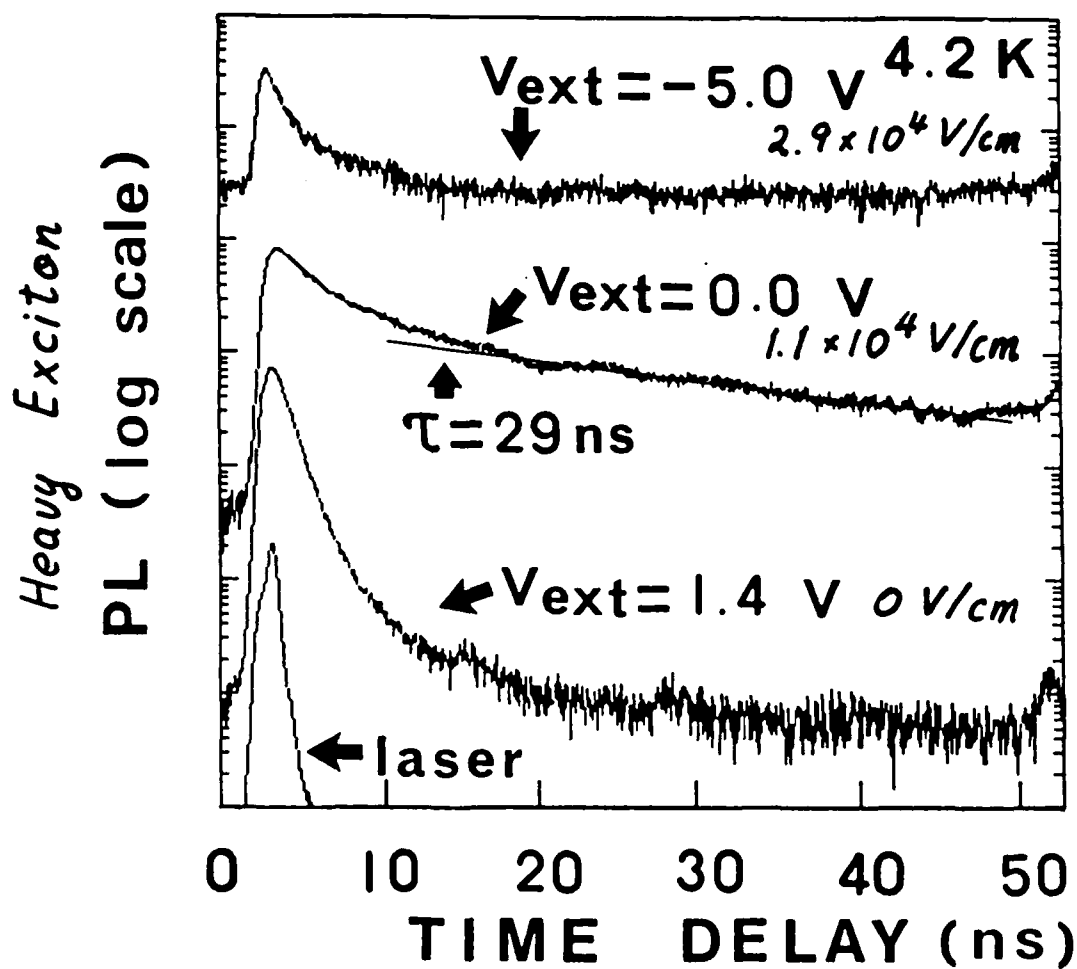
electron tunneling rate

$$w = \frac{\pi \hbar}{2m_e L_z^2} \exp\left\{-\frac{2}{\hbar} \sqrt{2m_e(U-E)}d\right\} \sim 1.8 \times 10^{10} \text{ s}^{-1}$$

$$(\tau \sim 55 \text{ ps})^{\dagger}$$

Electron tunneling rate little depends on F , if $eFd \ll U-E$ holds.

cavity dumped picosecond dye laser
+
single photon counting



Summary

- Exciton dissociation followed by electron tunneling through AlGaAs barriers and resonant electron sequential tunneling are observed in GaAs-AlGaAs superlattices.
- Excitons dissociate when the field gain can compensate for the exciton binding energy.
- The tunneling rate of the electrons is determined to be $1/(430\text{ps})$, slower than the simple calculation.
- Competitive nature of ultrafast processes of photo-excited electron-hole pairs, exciton formation and pair ionization followed by tunneling through barriers, are clarified under the various electric field.

SUMMARY

EXPERIMENTAL AND THEORETICAL STUDIES OF COHERENT AND NONTHERMAL PROCESSES IN SEMICONDUCTORS PROBED BY FEMTOSECOND LASER TECHNIQUES

N. Peyghambarian and S. W. Koch
Optical Sciences Center
University of Arizona
Tucson, AZ 85721

The coherent interaction of femtosecond laser pulses and a thin CdSe sample is investigated both experimentally and theoretically. Observation of coherent phenomena in semiconductors is very rare because the incoherent processes occur in the femtosecond time domain in these materials. One example of such a phenomena is the so called optical Stark effect of exciton where a blue shift of the exciton resonance occurs as a result of pumping below the bandgap (in the transparency region). Here, we report on our investigations of coherent effects involving band-to-band and also exciton transitions. Using femtosecond transmission measurements we observe clear evidence for coherent interference effects of the light field and the driven material polarization. These interferences manifest themselves as oscillatory structures in the differential transmission spectra. The structures are observed either in the spectral vicinity of the exciton pulse for resonant interband excitation, or around the exciton resonance. Experiments were performed in a pump-probe geometry with the pulses having ≈ 80 fs durations. The transmission of the probe pulse in the presence and absence of the pump pulse is detected and the normalized difference (DTS) is plotted against probe wavelength at various time delays between the two pulses. DTS show oscillatory behavior at early times where the probe precedes the pump on the sample (negative time delays).

These oscillatory features are explained by comparison with a semiclassical theory. We assume a weak, short probe pulse interacting with the time-dependent medium polarization

which is driven by the strong pump field. We consider the case, where the peak of the probe pulse precedes the maximum of the pump pulse. The different electron-hole-pair states of the semiconductor are modelled as mutually uncoupled transitions, each of which is described by a density matrix. The dissipative scattering processes among the elementary excitations are included through phenomenological decay rates in the equation of motion for the density matrix. The theory has been evaluated for the cases of resonant interband pumping where the transmission is probed around the frequency of the pump, and for the case of nonresonant pumping where the transmission changes are measured at the exciton.

Examples of the computed results are presented for different time delays between probe and pump. Similar to the experimental results, the spectra show clear oscillatory structures when the probe precedes the pump. The physical explanation of the observed oscillatory structures, which are reminiscent of Ramsey fringes in atomic physics, is a transient population grating originating from the pump and probe inside the crystal. The grating is generated essentially during the temporal overlap of the pulses and the oscillations in the spectra are caused by the interference between the probe pulse and that part of the pump pulse which is scattered from the grating into the direction of the probe beam. The oscillation frequency is determined by the time delay between pump and probe. An increase of the temporal overlap between the pulses reduces the number and the amplitude of the oscillations with respect to the central peak. A detailed analysis of the relative importance of the different damping processes shows that the shape of the oscillatory structures is rather insensitive to the value of the dipole damping rate. However, the oscillatory features depend very strongly on the population decay rate. Increasing the population decay decreases the amplitude of the oscillations with respect to the central peak until only a broadened peak, the spectral hole, is left.

To analyze the situation where the transmission spectra are measured in the vicinity of the exciton frequency, we modelled the exciton as a single homogeneously broadened transition. The oscillations in the differential transmission spectra now occur around the exciton frequency. Assuming non-resonant excitation spectrally below the exciton, we obtain asymmetric

structures due to the detuning of the pump laser from the exciton resonance. When the delay time approaches zero, the oscillations gradually disappear and the transmission changes assume the dispersive shape characteristic for the optical Stark shift. Hence, the oscillatory structures should be viewed as the early stages of the optical Stark effect in short-pulse pump-probe spectroscopy. For large time delays, only a Lorentzian remains representing the exciton saturation caused by the pump pulse. For the case of resonant interband excitation, one can observe the oscillatory structures not only around the central pump frequency, but also around the exciton resonance. These experimental observations are in qualitative agreement with the theoretical results which predict large oscillation amplitudes around the exciton transition even for large detunings partly due to the greater exciton oscillator strength.

EXPERIMENTAL AND THEORETICAL
STUDIES OF COHERENT AND
NONTHERMAL PROCESSES IN
SEMICONDUCTORS PROBED BY
FEMTOSECOND LASER TECHNIQUES

N. Peyghambarian and S. W. Koch

Collaborators:

Experiment: B. Fluegel

Theory: M. Lindberg

Support:

NSF
NATO
OCC

OUTLINE

- Introduction
- Observation of Coherent Optical Phenomena Around the Pump Frequency and Exciton in CdSe
- Theoretical Simulations
- Conclusion

Dynamics of Laser-Excited Electron-Hole Pairs

1. Coherent Regime or Collision-Free Regime

Rabi flopping of electrons between band states.

2. Nonthermal Distribution Regime

Collisions destroy phase coherence
Spectral hole burning

3. Quasi-Thermal Regime

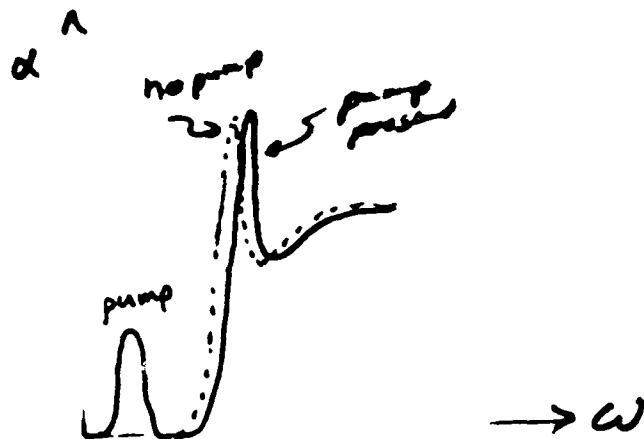
Optical Nonlinearities
Coulomb Screening
Bandgap Renormalization
State Blocking

Optical Stark Effect

Non-resonant Excitation

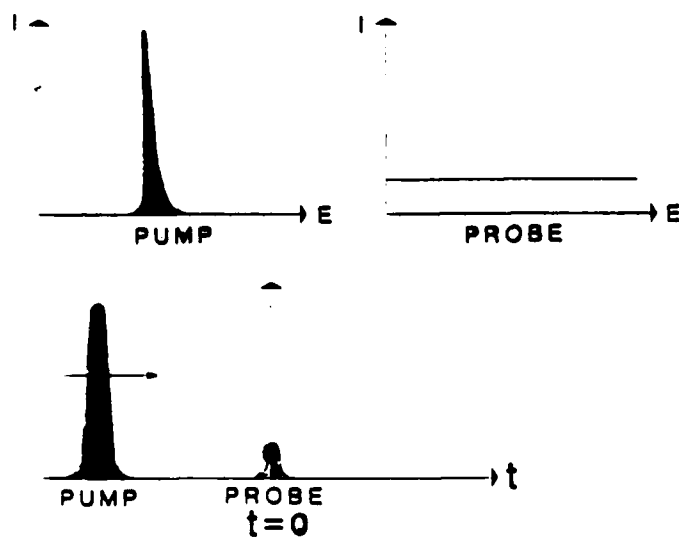
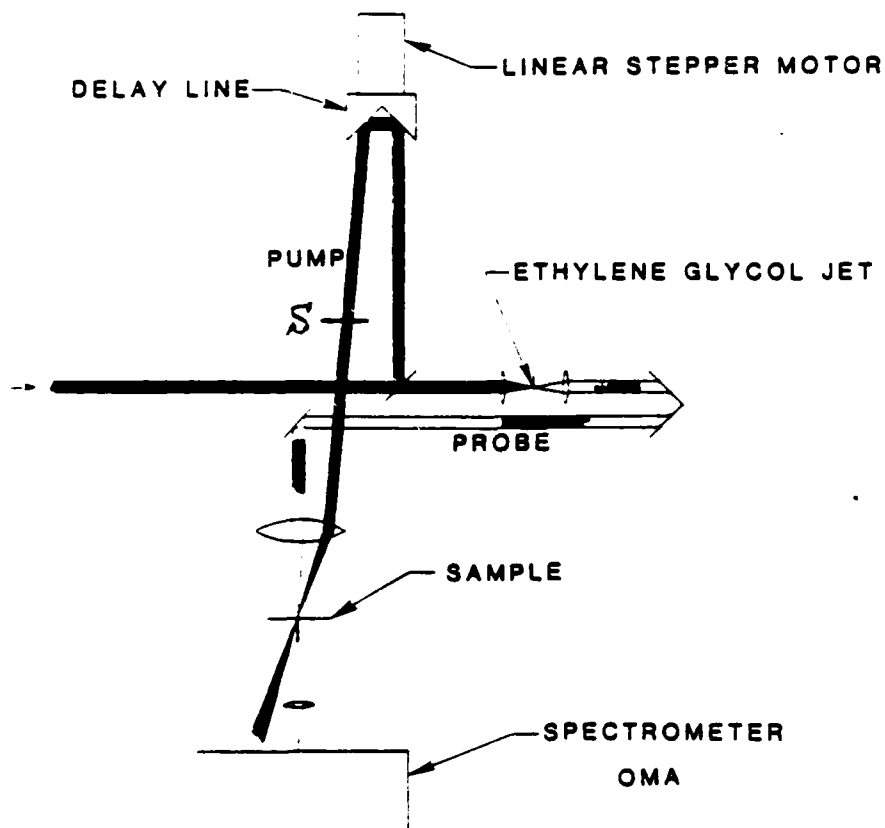
- Mysyrowicz et al.

- Von Lehman et al.

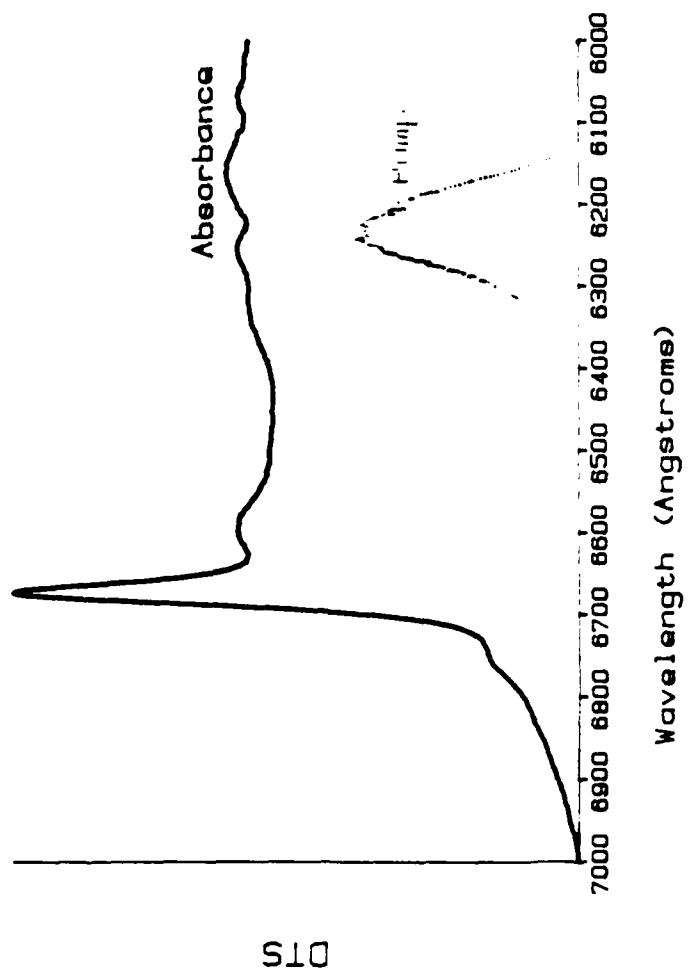


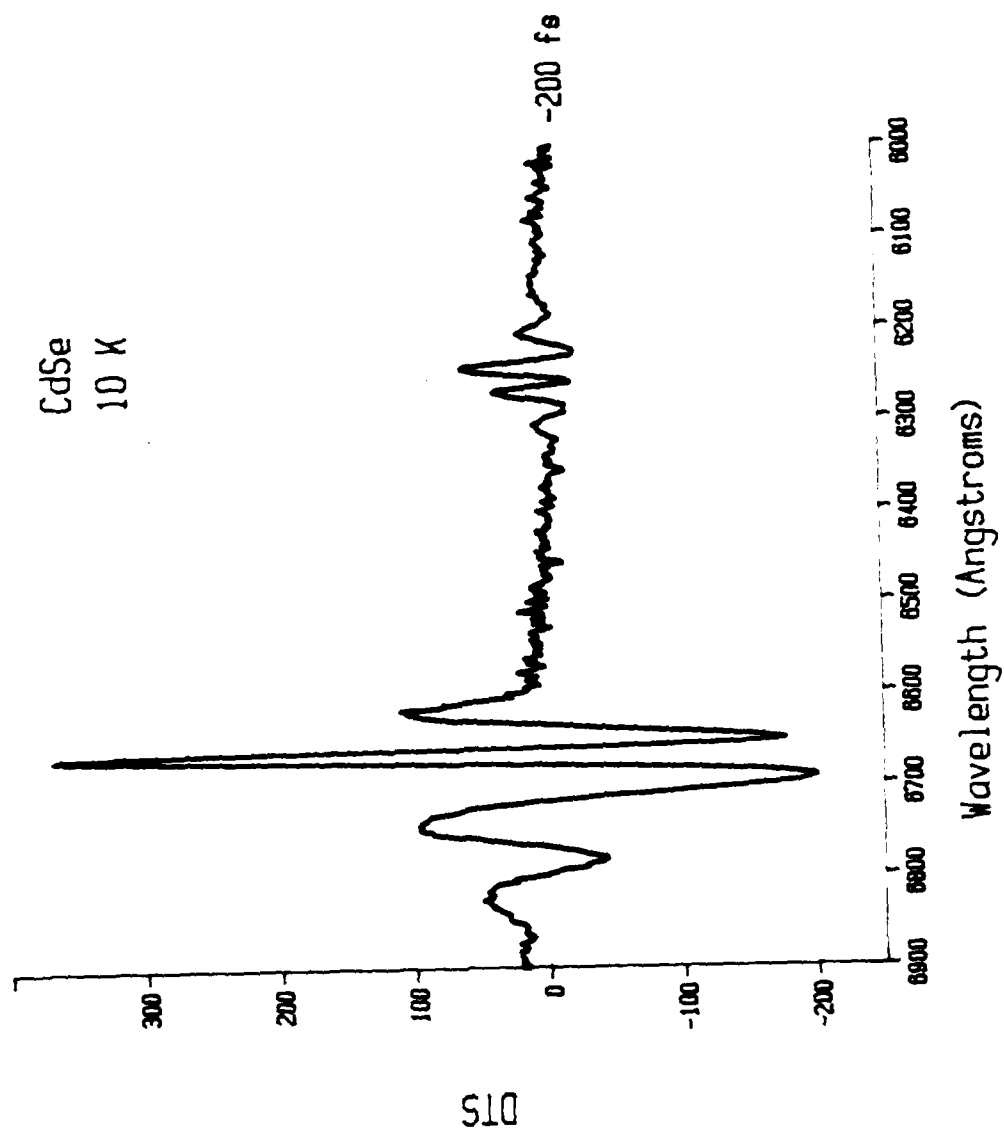
Exciton shift $\propto \mu \cdot E \propto$ Rabi Freq.

PUMP PROBE SPECTROSCOPY

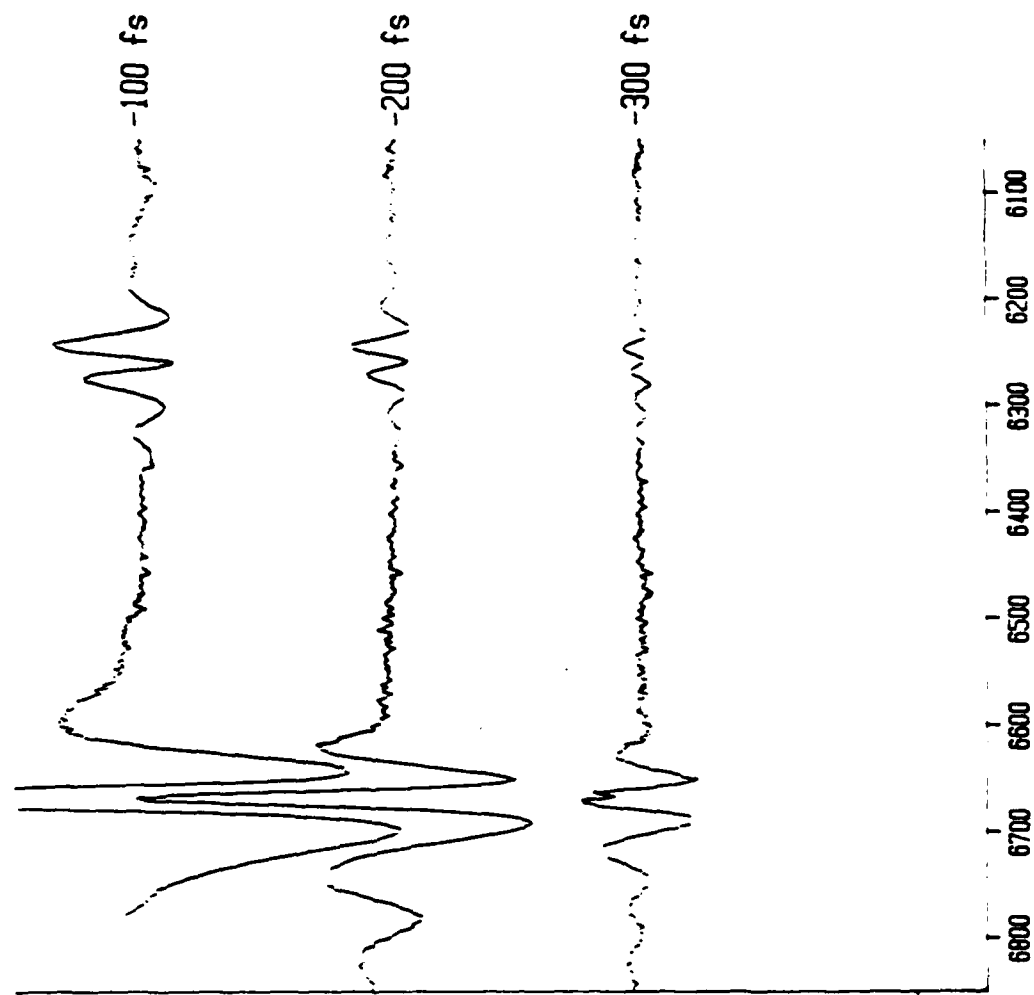


CdSe
10 K





CdSe 10 K



DT

Wavelength (Angstroms)

SEMICLASSICAL THEORY

- Treat Fields Classically and Material Response q.m.

$$E(t) = \underbrace{E_L(t) e^{i(\vec{k}_L \cdot \vec{r} - \omega_L t)}}_{\text{pump}} + \underbrace{E_p(t) e^{i(\vec{k}_p \cdot \vec{r} - \omega_p t)}}_{\text{probe}}$$

$$\frac{\partial}{\partial x} E_p + \frac{1}{c} \frac{\partial}{\partial t} E_p = \frac{i \omega_p}{2 \epsilon_0 c} \underbrace{P_p}_{\text{Induced Medium polarization}}$$

$$P_p(t) = \int_{-\infty}^t dt' X(t, t') E_p(t') \quad \text{Linear Response}$$

$$\text{where } X(t, t') = \underbrace{X_0(t-t')}_{\text{Unperturbed susceptibility}} + \underbrace{\delta X(t, t')}_{\text{perturbation caused by pump pulse}}$$

$$\delta T(\omega) = \text{DTS} = \frac{|E_p(\omega)|_{\text{pump on}}^2 - |E_p(\omega)|_{\text{pump off}}^2}{|E_p(\omega)|_{\text{pump off}}^2}$$

$$\delta T(\omega) \propto -\text{Im} \left[\int_0^\infty dt e^{i(\omega - \omega_L)t} \delta X(t+t_p, t_p) \right]$$

$t_p = \text{delay time}$

Model Semiconductor: collection of mutually independent k -states. Include Coulomb & phonon scattering phenomenologically by damping & pumping rates for each k -state.

Density Matrix Formalism, ρ for each k state

$$\frac{\partial}{\partial t} \rho_{22} = i\mu [E(t)\rho_{12} - E^*(t)\rho_{21}] - \Gamma \rho_{22}$$

$$\frac{\partial}{\partial t} \rho_{11} = i\mu [E^*(t)\rho_{21} - E(t)\rho_{12}] - \Gamma \rho_{11} + \Lambda$$

$$\frac{\partial}{\partial t} \rho_{21} = -[ie(k) + \gamma] \rho_{21} - i\mu E(t)(\rho_{22} - \rho_{11})$$

Extra- and scatt. $\left\{ \begin{array}{l} \Gamma = \text{Decay rate for diagonal element, population decay (not recombination)} \\ \gamma = \text{" " " non-diagonal " , dipole damping} \end{array} \right.$

$$P_k = \text{induced polarization} = \mu (\rho_{12} + \rho_{21})$$

for a single k state

get

2 = conduction band

μ = dipole matrix element

1 = valence band

For Band-Band Region

Resonant pumping: pump
resonantly excites b-b transition

Continuum of k -states

Sum over the response of all individual contributions

$$P = \sum_k P_k$$

For Exciton Region

Non-resonant excitation
of exciton. pump is
detuned from exciton

An isolated transition

Contribution of band states are neglected

Band-Band Region:

$$\delta T(\omega) = T_0 \operatorname{Re} \left\{ \int_0^\infty dt e^{i(\omega - \Omega_L)t} \left(e^{-2\gamma t} \times \right. \right. \\ \left. \int_0^\infty dt' e^{-\Gamma t'} E_L(t_p - t') E_L^*(t_p - t' - t) + e^{-\Gamma t} \times \right. \\ \left. \left. \int_0^t dt' e^{-(2\gamma - \Gamma)t'} E_L(t + t_p - t') E_L^*(t_p - t') \right) \right\}$$

Exciton Region:

For large detuning

$$\delta T(\omega) \propto \frac{1}{\Omega_L - \omega_x} \operatorname{Im} \left[\frac{1}{\nu - i\Delta} \int_0^\infty dt |E_L(t + t_p)|^2 e^{i\Delta t} \right] \\ + O[(\omega_x - \Omega_L)^2]$$

Ω_L = pump central frequency

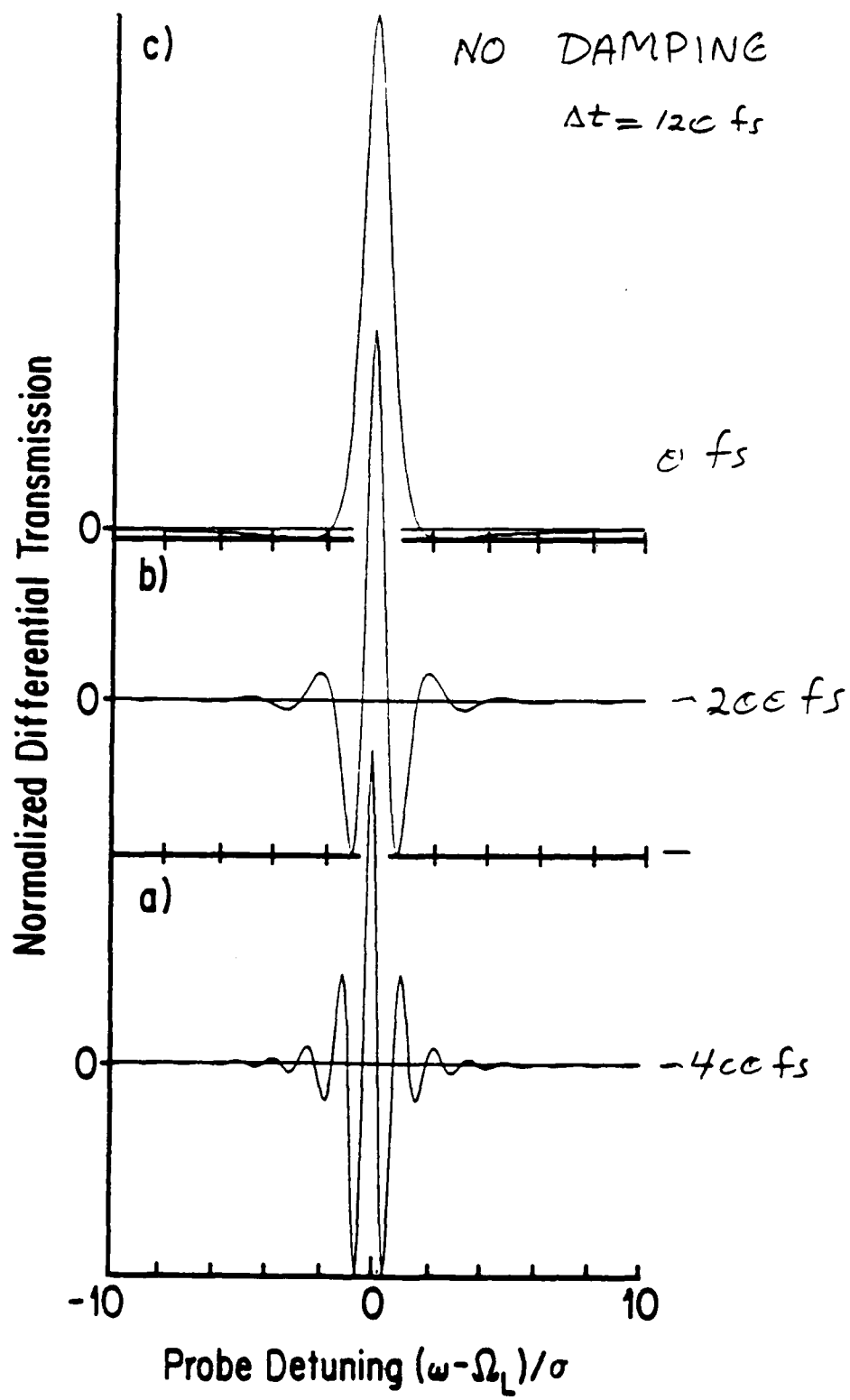
ν = exciton linewidth

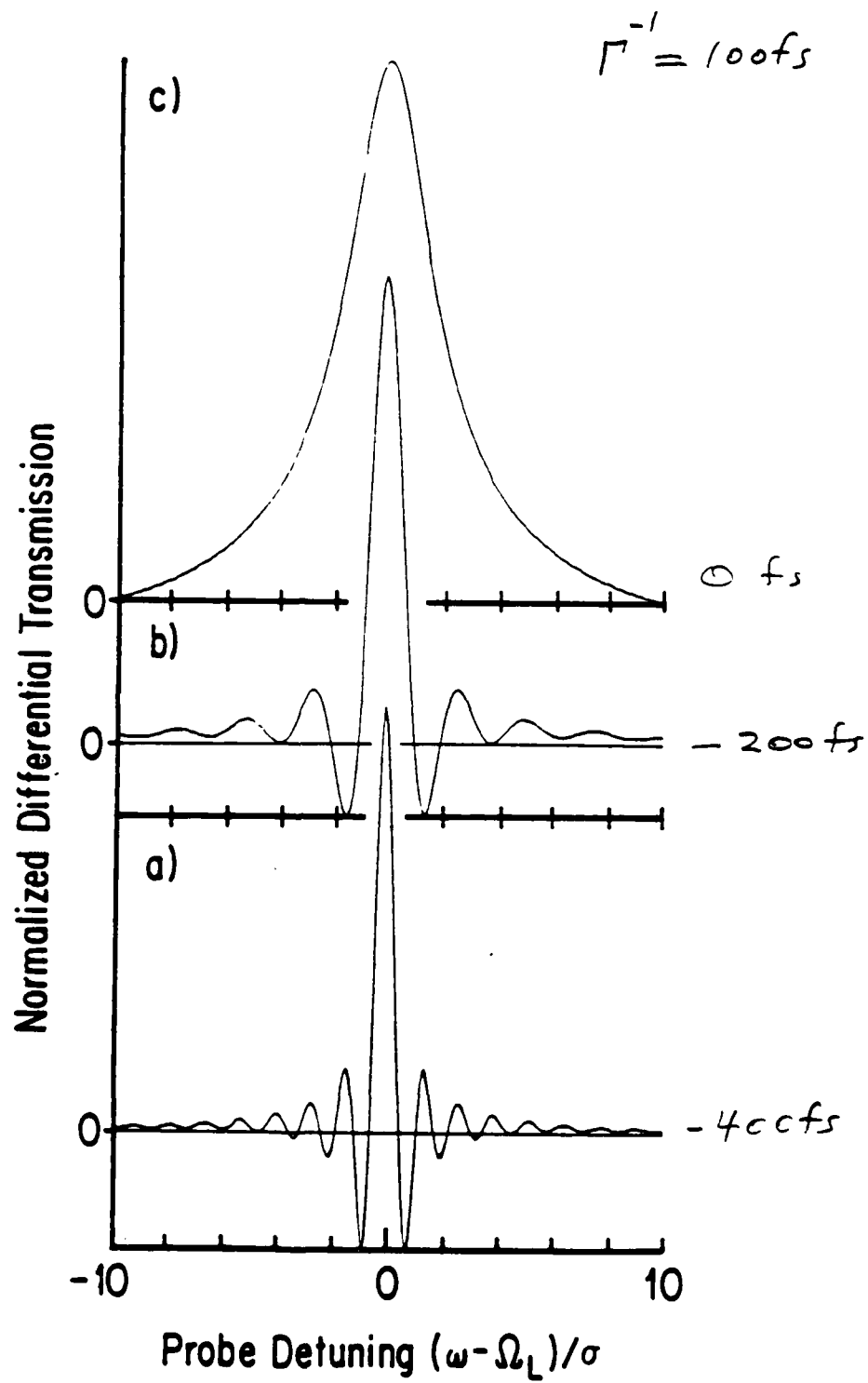
$\Delta = \omega - \omega_x$ detuning from exciton

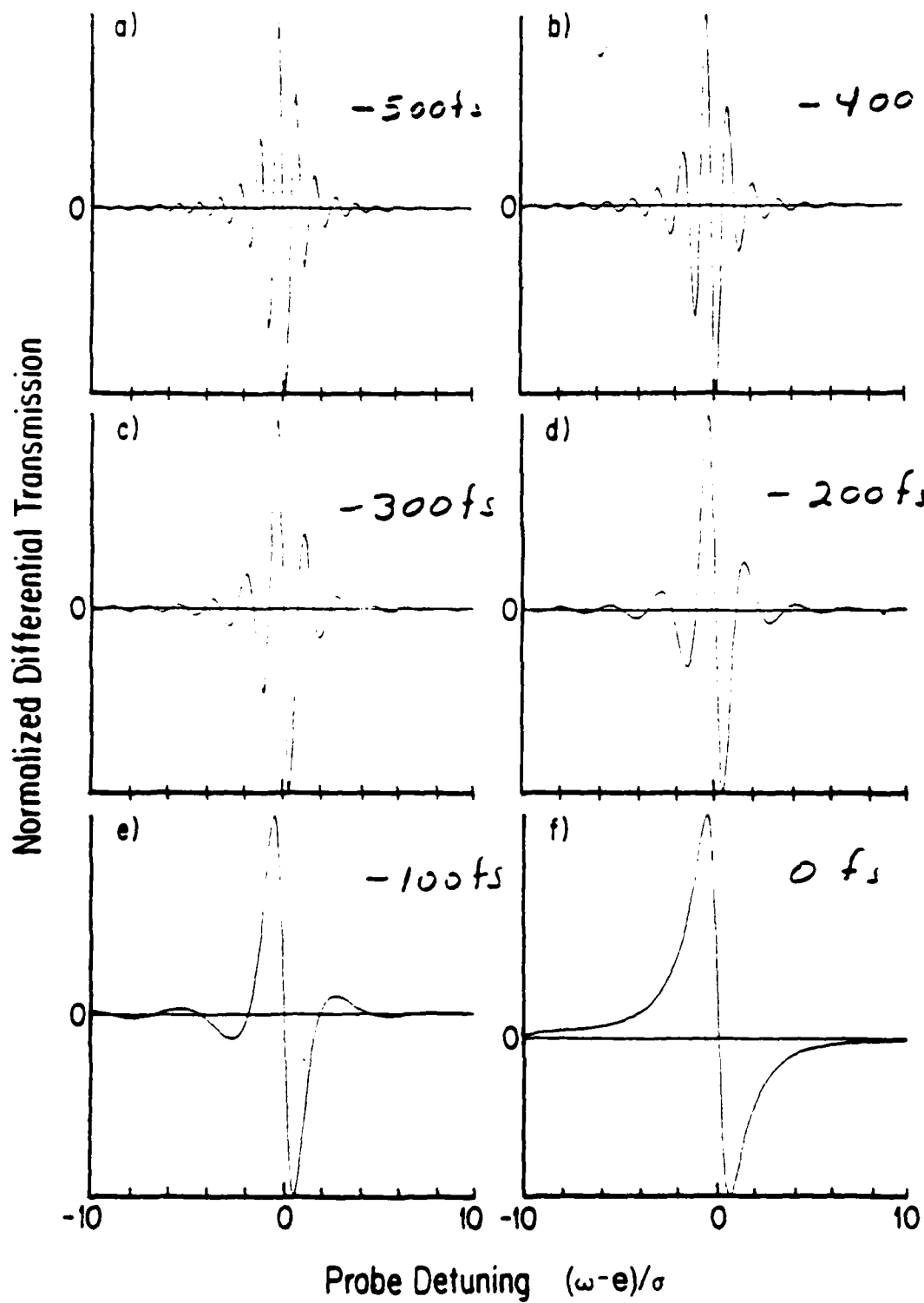
$$\left| \frac{\Delta T_x}{\Delta T_b} \right| = \frac{\alpha_x}{\alpha_b} \left| \frac{\gamma_b + 2\gamma}{(\omega_x - \Omega_L)(5 - 6\gamma_b t_p)} \right| e^{-2\gamma_b t_p}$$

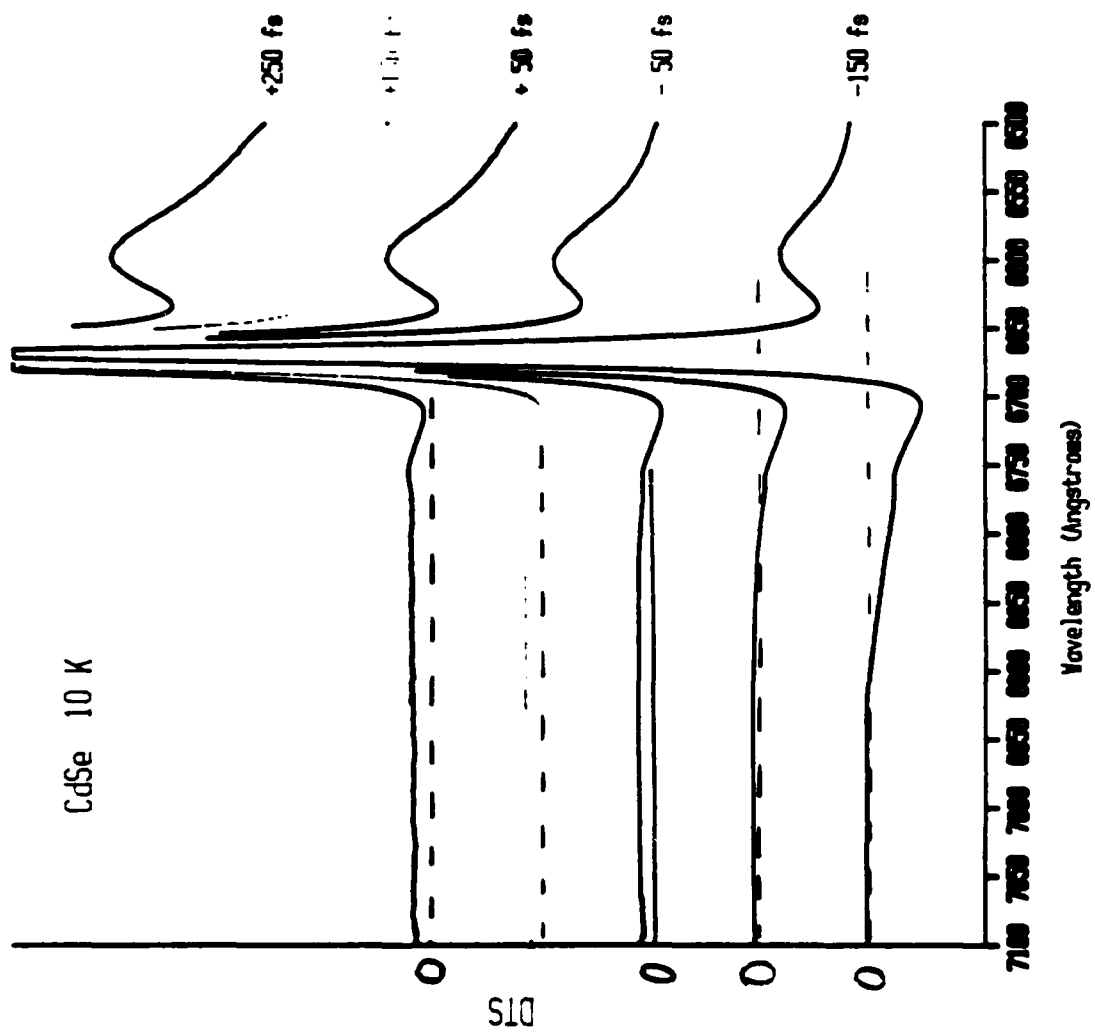
$$\gamma_b = \frac{2 \ln 2}{\Delta t}$$

Δt = FWHM of pump pulse









U.S.-Japan Workshop
Monterey, 1987

Femtosecond Studies of Hot Carrier
Relaxation in GaAs and AlGaAs

E. P. Ippen and J. G. Fujimoto

Department of Electrical Engineering and
Computer Science and the Research Laboratory
of Electronics
Massachusetts Institute of Technology
Cambridge, MA 02139

ABSTRACT

Femtosecond carrier dynamics in GaAs and AlGaAs thin films have been studied by femtosecond pump-probe absorption saturation spectroscopy. Identical pulse measurements monitor the rapid scattering of the carriers out of their initial, optically excited states. Multi-wavelength continuum probe investigations confirm the presence of the initial non-thermal carrier distribution as well as the appearance of state-filling throughout the band on a timescale of tens of femtoseconds.

SUMMARY

We describe a series of experiments which use femtosecond optical pulses to excite carriers in thin films of GaAs and AlGaAs semiconductors. Other, time-delayed femtosecond pulses are then used to probe the induced, and time-varying, changes in optical absorption that follow the excitation. Using pump and probe pulses of the same wavelength, we have investigated how long it takes highly excited carriers to scatter out of their

initial, excited energy distribution. These experiments were performed as a function of excitation density, pulse duration, and sample composition. For an excitation photon energy of 1.98 eV, the largest changes in behavior were found to occur with changes in Al concentration. In a second set of investigations, we have used probe pulses of various wavelengths, derived from a femtosecond continuum, to determine where the carriers go when they leave their initial excited states and how their distribution develops subsequently. In these experiments, the initial excitations can be observed directly as absorption saturation holes. Electrons are then observed to redistribute rapidly, in tens of femtoseconds, throughout the conduction band and to cool to the lattice on a slower, picosecond timescale.

The laser source for the identical-pulse experiments was a CPM ring dye laser incorporating internal prisms for control of dispersion. In addition, a pair of prisms was used external to the laser cavity to permit independent adjustment of pulse duration and chirp. Thus, we were able to produce either bandwidth-limited pulses of variable duration (35 - 150 fs) or pulses of variable chirp. Variations of both parameters were used to verify the speed and energy shifts of the carrier relaxation dynamics being observed. Pump-probe traces revealed dynamic behavior that could be separated into two different temporal regimes: a partial rapid recovery of absorption corresponding to the carriers leaving their initial excited states; and a slower, picosecond decay that can be attributed to the cooling of the distribution to the lattice via LO phonon

emission. The latter, picosecond contribution had approximately the same time constant in all samples studied. The early rapid response, however, varied in time constant from less than 30 fs for GaAs to 130 fs for AlGaAs with 0.3 mole fraction Al. This variation is due to changes in a number of factors including the initial excess energy of the carriers, simultaneous excitation of carriers from different valence bands, and the probability of intervalley scattering.

For the continuum probe experiments the output of the CPM laser was amplified with the help of a high-repetition-rate pulsed copper vapor laser. A fraction of the amplified output was split off for use as a pump beam. The remainder was focussed into a thin jet of ethylene glycol to generate a broadband continuum probe pulse. Results obtained using this system were consistent with the results described above; and they revealed, for the first time, transient absorption holes due to excitation from the split-off valence band as well as that from the light and heavy hole band. The continuum probe also confirmed that state filling throughout the band becomes evident within tens of femtoseconds of excitation.

This work was supported in part by the Air Force Office of Scientific Research Grant 85-0213. JGF acknowledges support from the National Science Foundation Presidential Young Investigator Program Grant ECS-8552701.

REFERENCES

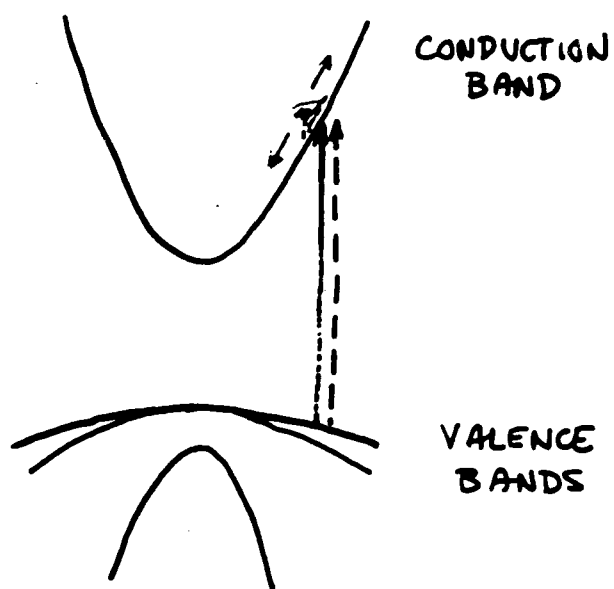
W. Z. Lin, J. G. Fujimoto, E. P. Ippen and R. A. Logan, Proc. Internat. Conf. LASERS '86 (1986)

W. Z. Lin, J. G. Fujimoto, E. P. Ippen and R. A. Logan, Appl. Phys. Lett. vol.50, p.124 (1987)

W. Z. Lin, J. G. Fujimoto, E. P. Ippen and R. A. Logan, Appl. Phys. Lett. vol.51, p.161 (1987)

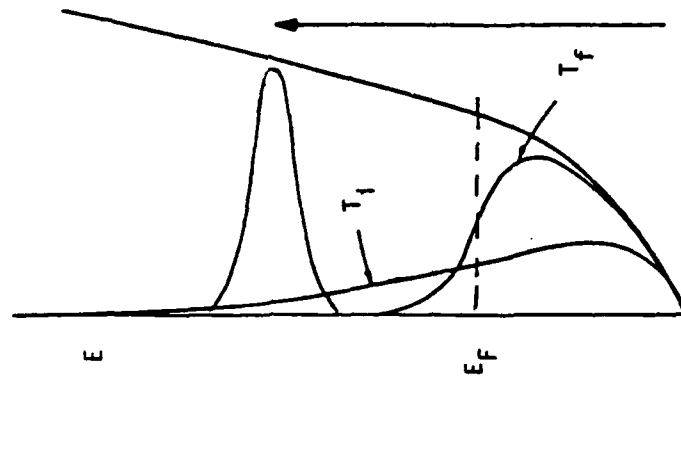
R. W. Schoenlein, W. Z. Lin, E. P. Ippen and J. G. Fujimoto, Appl. Phys. Lett. in press

HOT CARRIER RELAXATION IN SEMICONDUCTORS

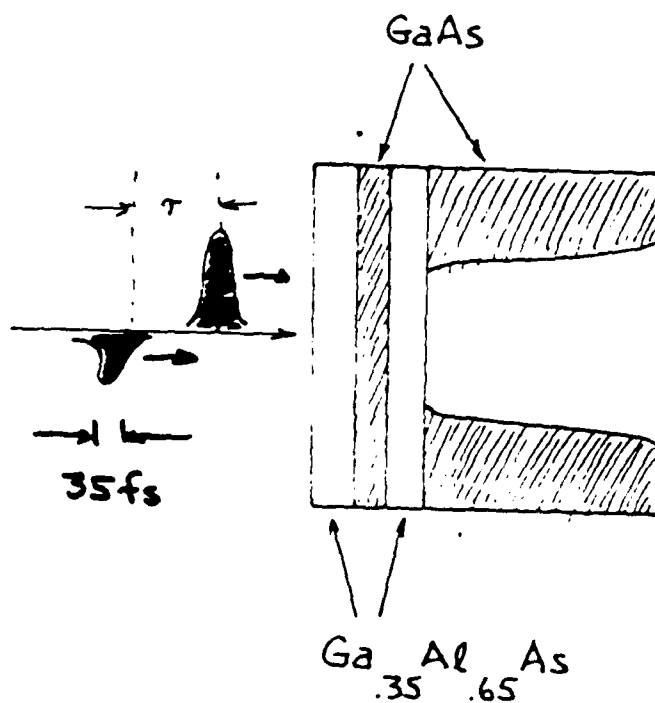


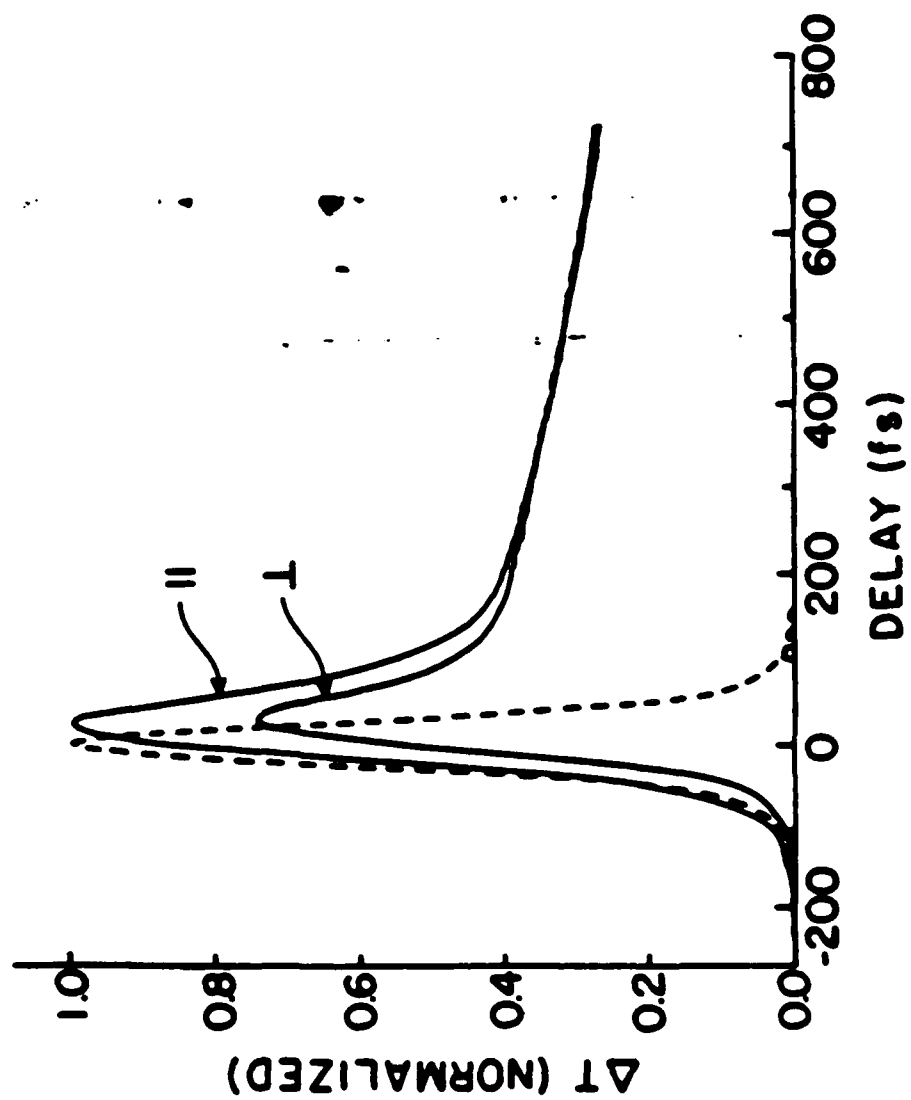
FEMTOSECOND PROCESSES IN SEMICONDUCTORS

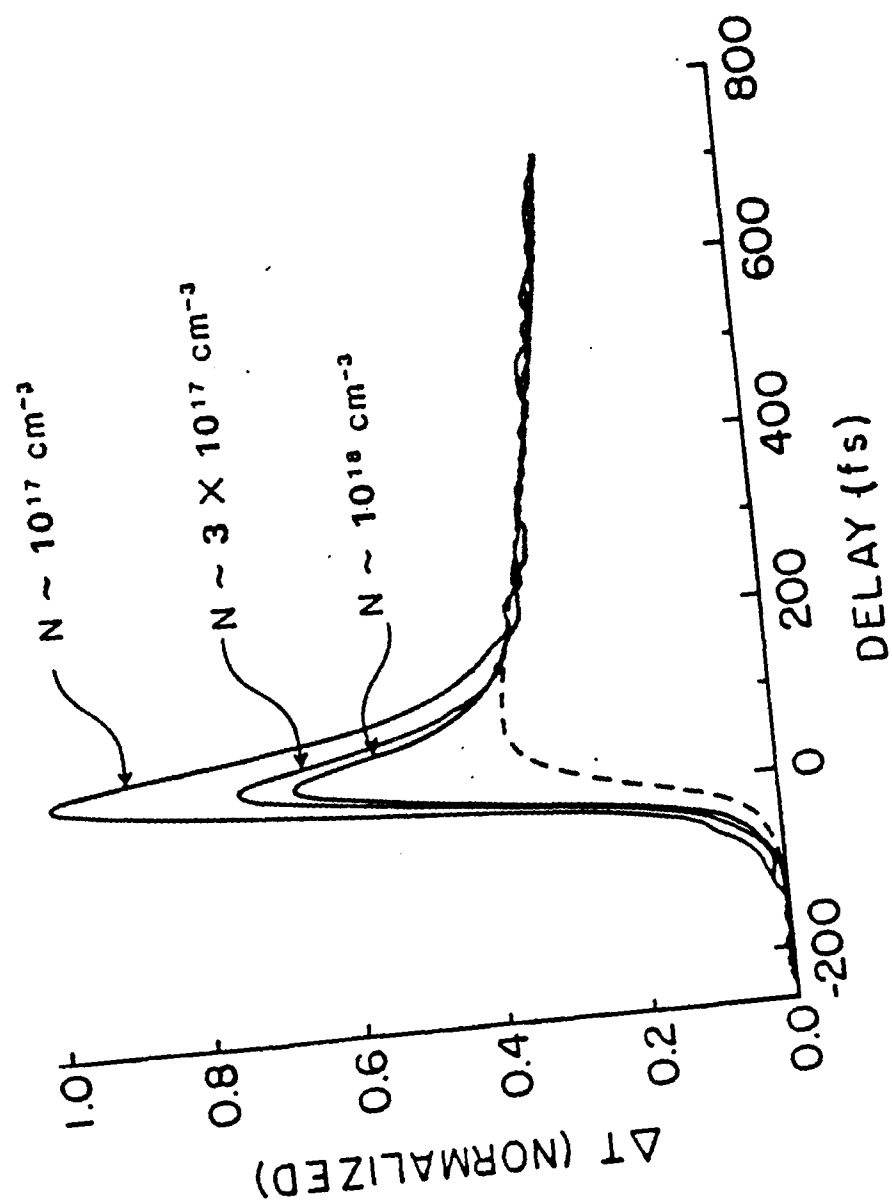
- INTERBAND ABSORPTION
e - h PAIRS
- CARRIER-CARRIER SCATTERING
THERMAL DISTRIBUTION
- CARRIER-PHONON SCATTERING
EQUILIBRATION WITH
LATTICE
- INTERVALLEY TRANSFER

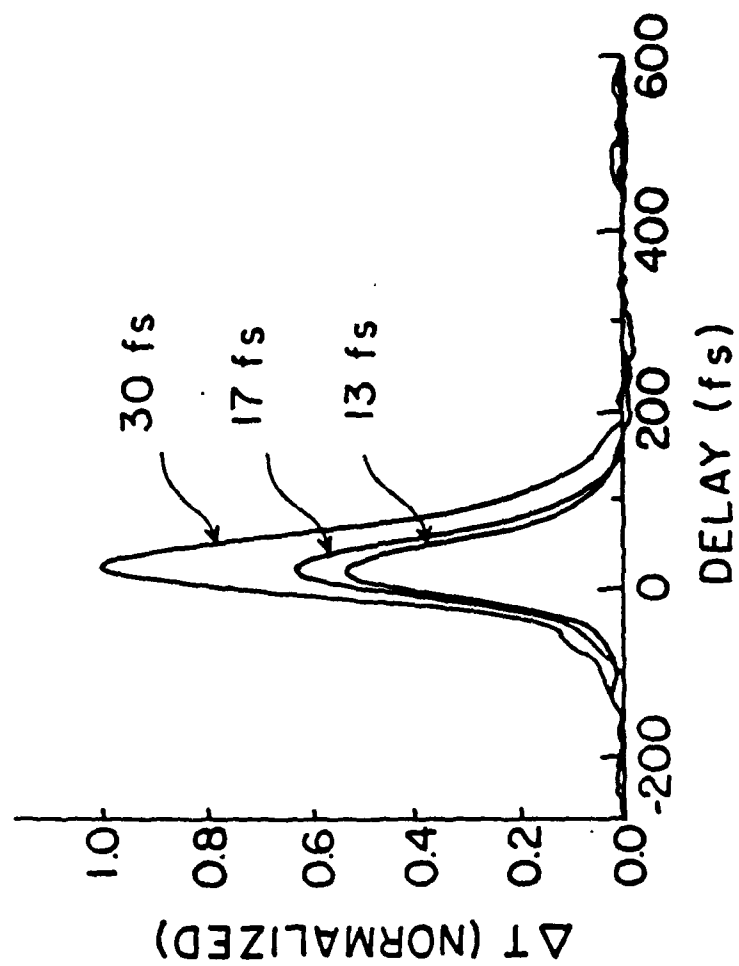


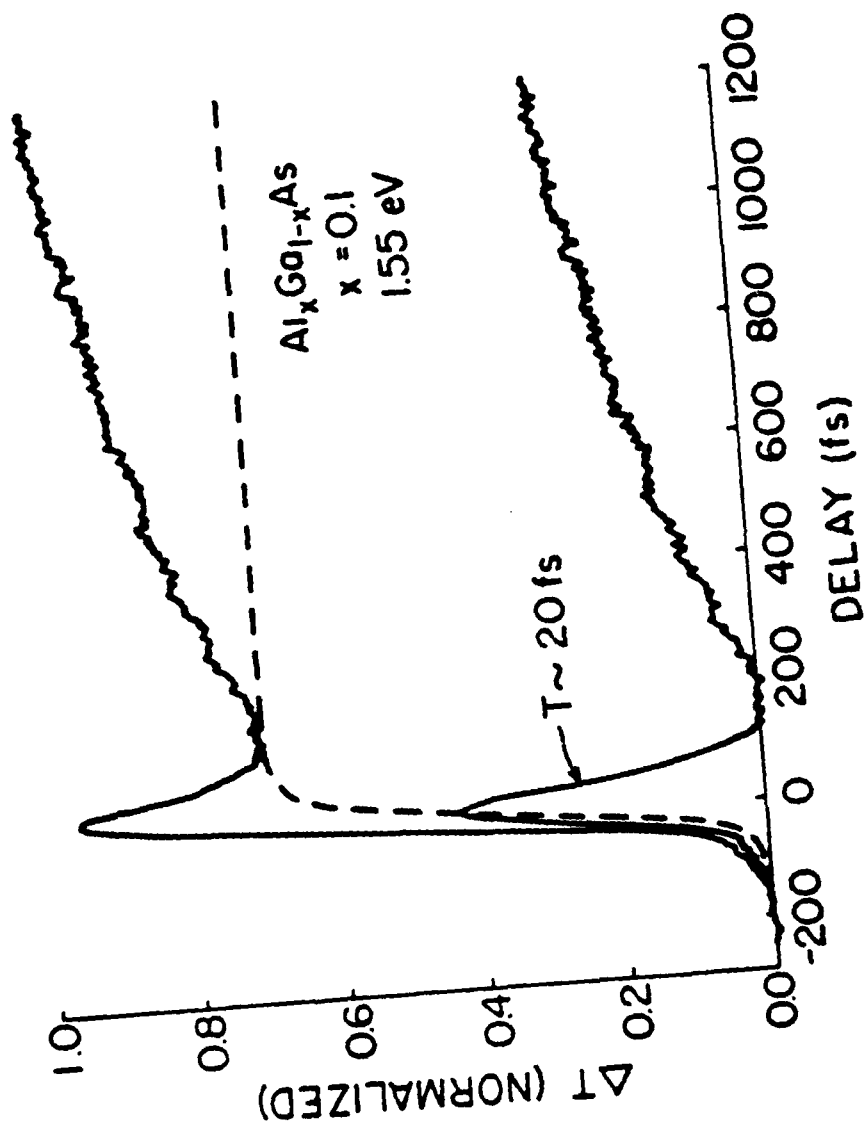
THIN FILM GaAs SAMPLES

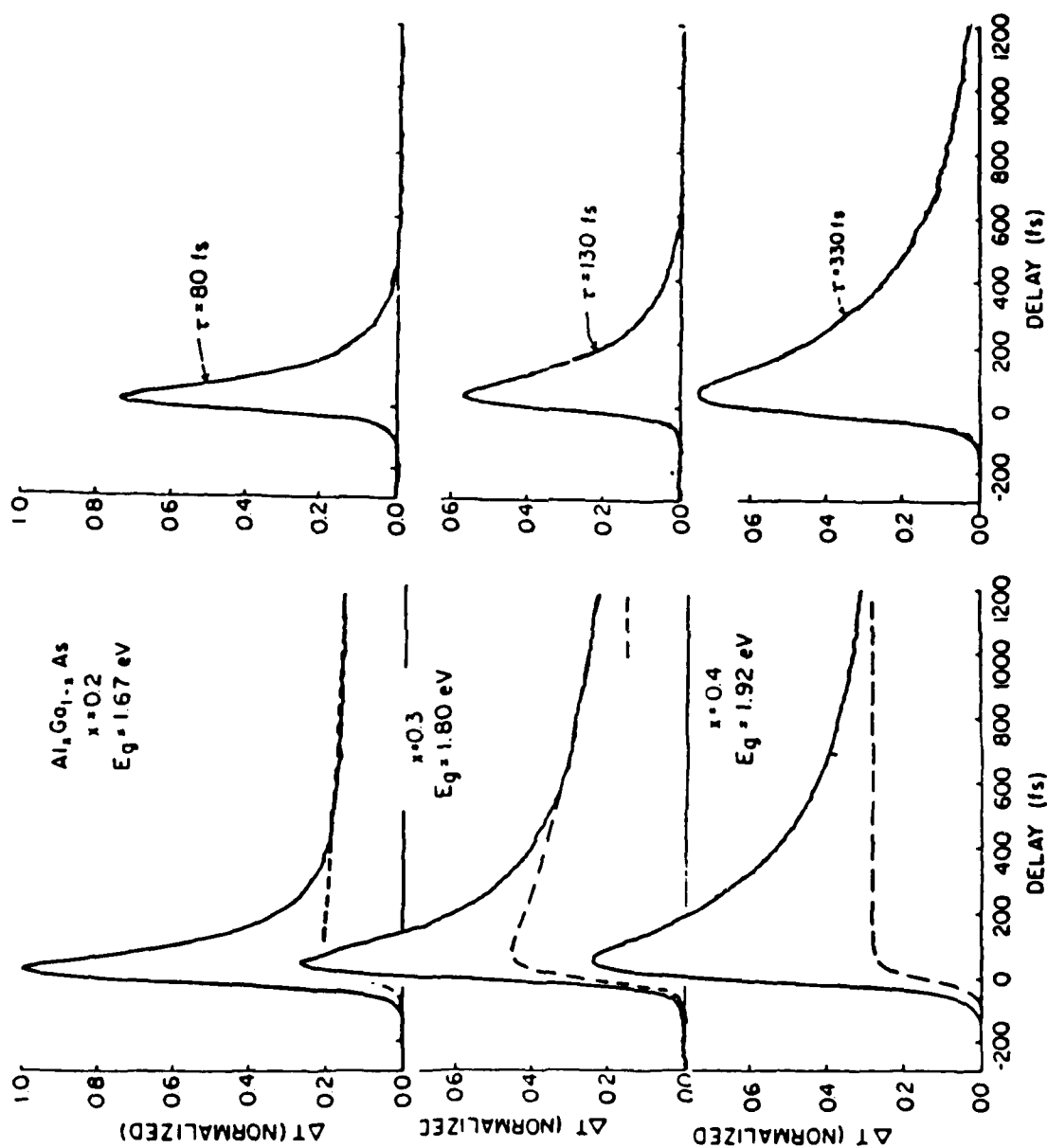


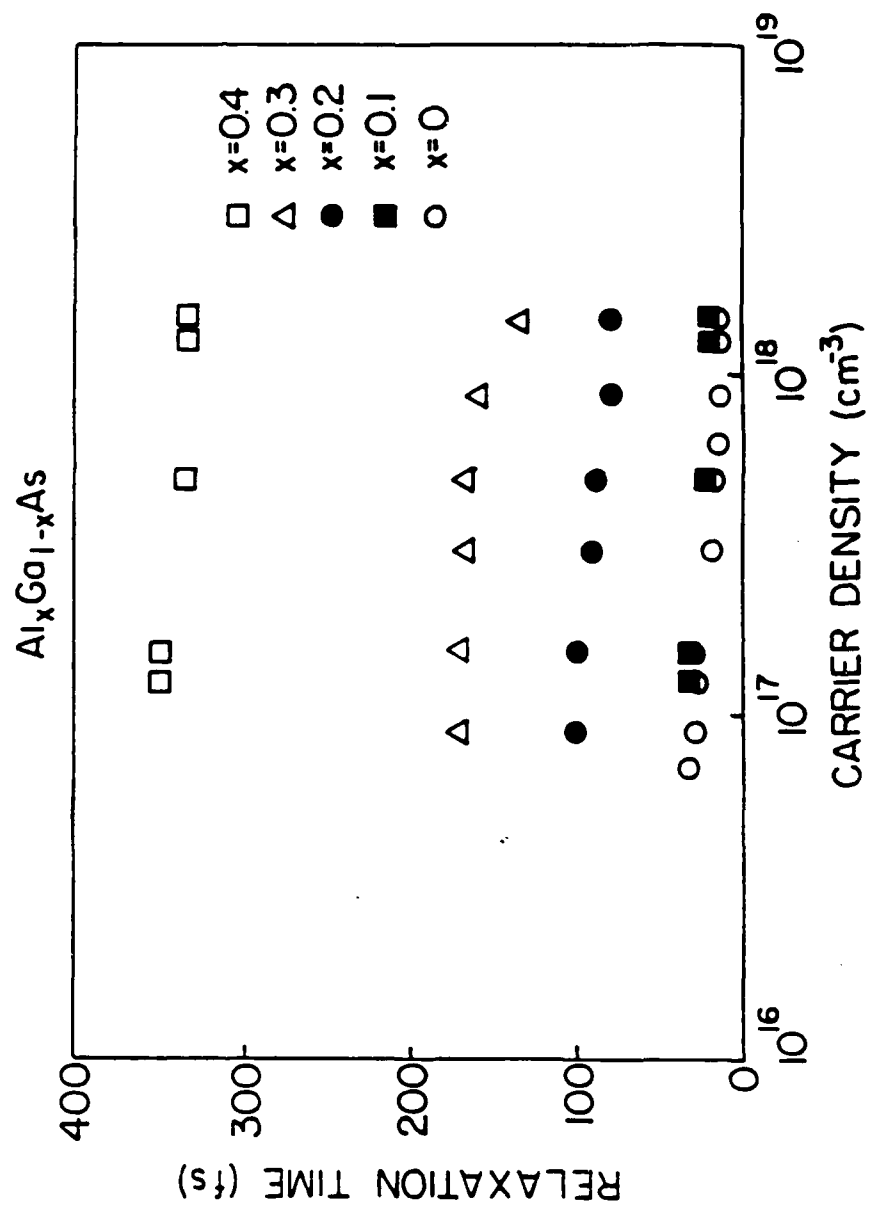






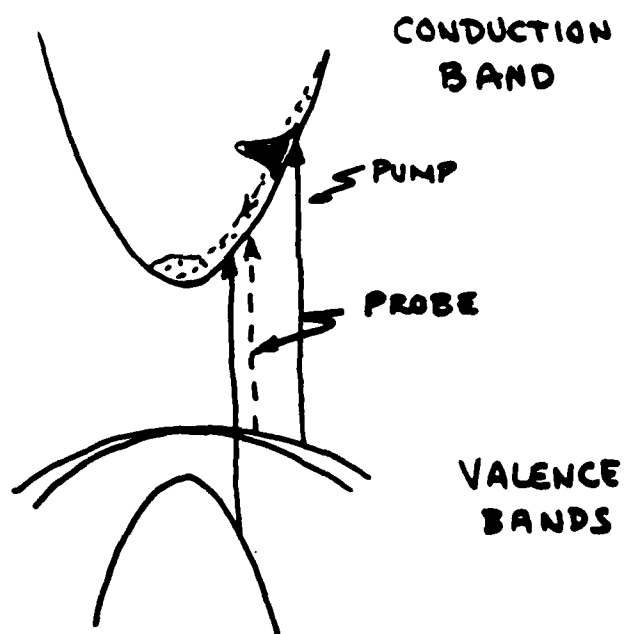




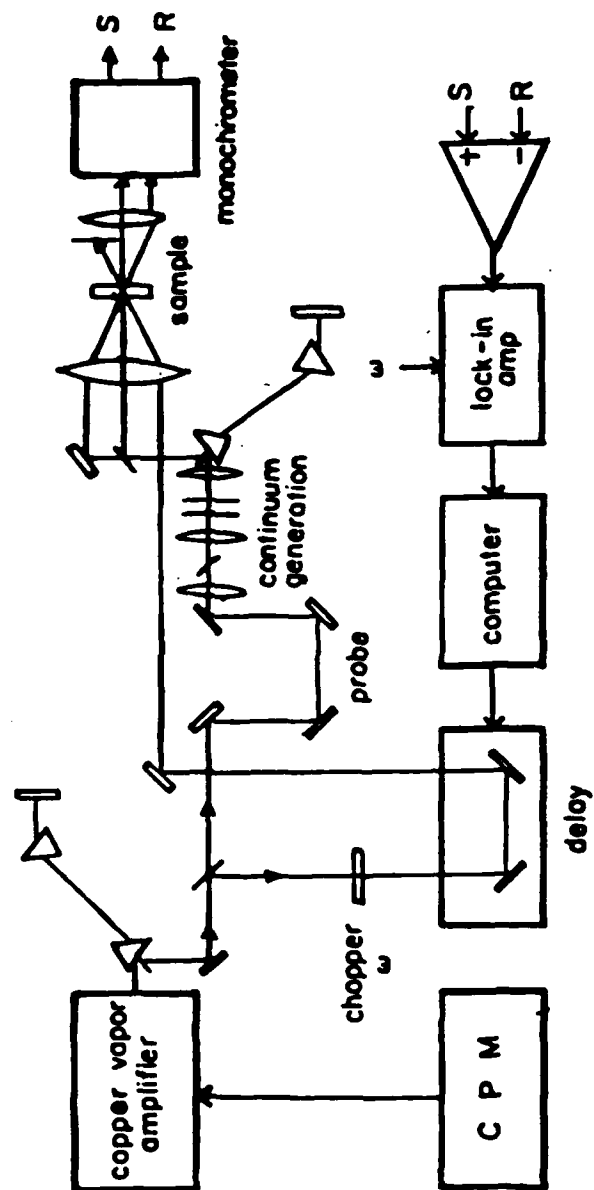


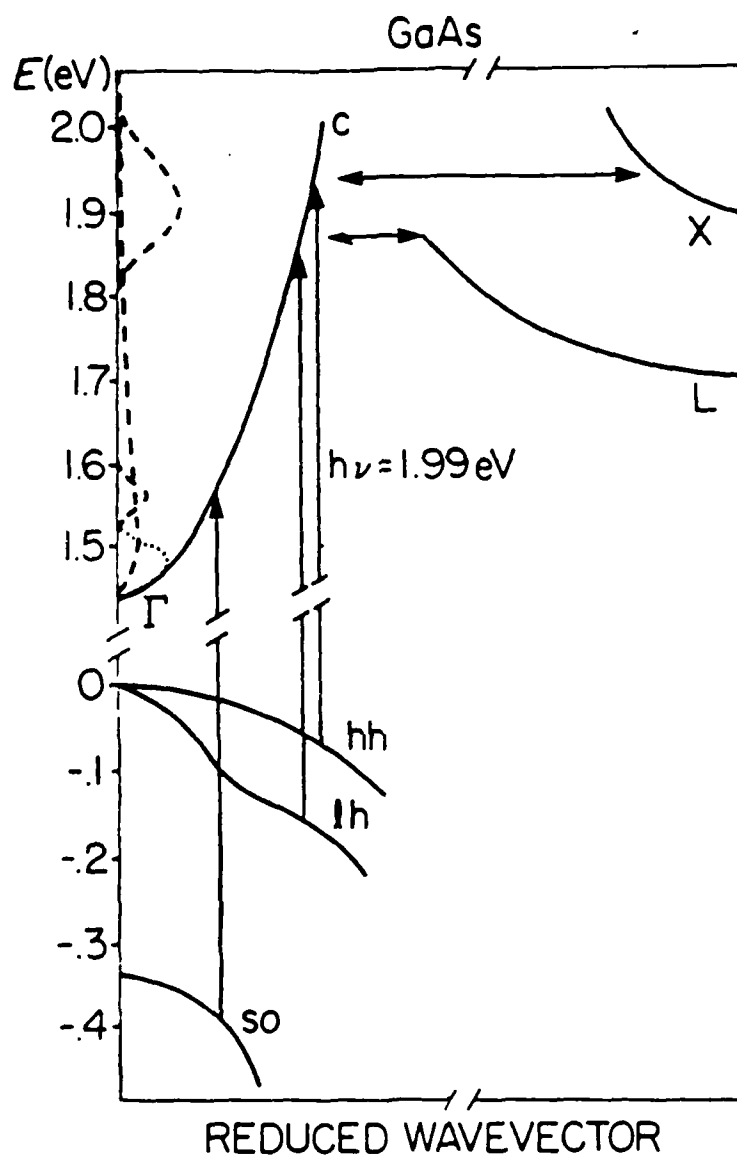
CARRIER DYNAMICS

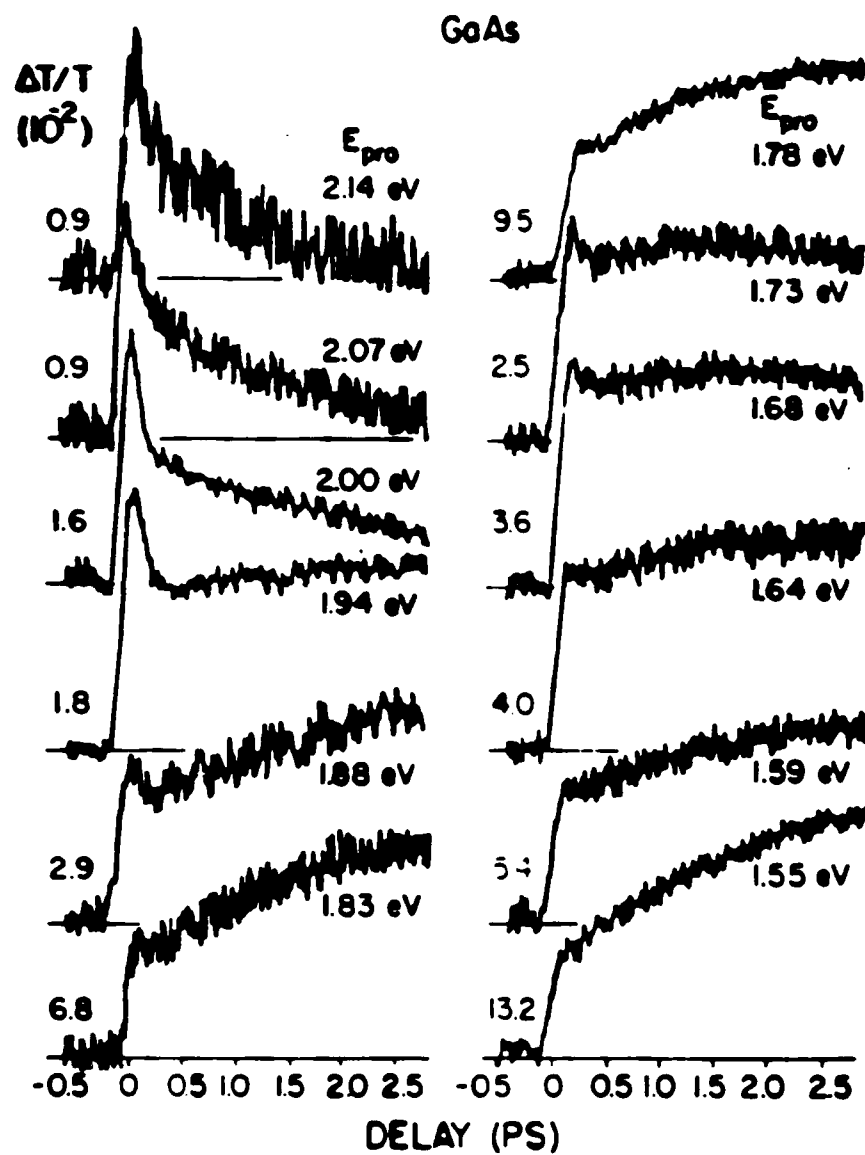
- TUNABLE PROBE



EXPERIMENTAL SCHEMATIC







SUMMARY

FEMTOSECOND CARRIER ENERGY RELAXATION DYNAMICS

- TRANSIENT NONTHERMAL CARRIER DISTRIBUTION
 - ABSORPTION SATURATION HOLES
 - TIME SCALE \leq PULSE DURATION
- CARRIER-CARRIER SCATTERING
 - RAPID SCATTERING TO RANGE OF ENERGIES
 - $N \sim 10^{18}$
- CARRIER-PHONON SCATTERING
 - ELECTRON COOLING
 - INTERVALLEY SCATTERING?
 - TIME SCALE ~ 2 ps

Exciton Relaxation Phenomena in a Disordered System

Masaki Aihara

Department of Physics, Faculty of Liberal Arts
Yamaguchi University

Exciton relaxation phenomena in a disordered system are theoretically investigated by transient resonant light scattering and the transient optical parametric effect.

For transient resonant scattering, following observation are made. In the case of weak disorder, the fast scattering-like and the slow luminescence-like components distinctively arise in the time-resolved spectrum of resonantly scattered radiation, as shown in Fig. 1. In figures, Δ is the disorder strength, C_A is the atomic concentration of a binary mixed crystal, γ_A is the inverse of the exciton lifetime, Ω_i and Ω_s are mean photon energies for incident and scattered radiation, and δ is the spectral width of incident radiation.

In the case of strong disorder, the scattering-like rapid component and the luminescence-like slow components are amalgamated as shown in Fig. 2, which reflect the diffusive motion of excitons caused by the higher-order multiple scattering of excitons due to strong disorder.

In the case of very strong disorder with the split spectrum, the quantum beat effect inherent in the excitons in mixed crystals arises as shown in Fig. 3.

For the transient optical parametric effect, a significant deviation from the exponential decay is found even in the case of relatively weak disorder, as shown in Figs. 4 and 5. This is a kind of the non-Markovian relaxation, where the memory effect associated with the exciton dephasing takes part in the problem.

In the case of strong disorder, there arises a transient response similar to the photon-echo phenomenon, as shown in Fig. 6. This is the reflection of the fact that excitons are not coherently extended in crystals, but are momentarily localized due to disorder.

Fig. 1

$$C_R=0.5 \quad \Delta=0.1 \quad r=0.01 \quad \Omega_i=-0.7 \quad \delta=0.1$$

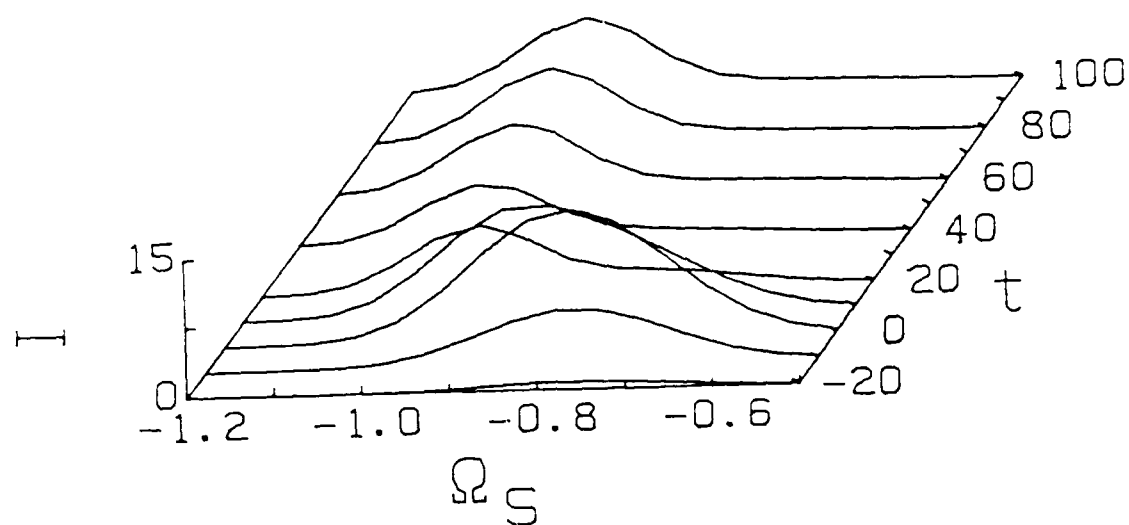


Fig. 2

$$C_R=0.5 \quad \Delta=1 \quad r=0.01 \quad \Omega_i=-0.988 \quad \delta=0.1$$

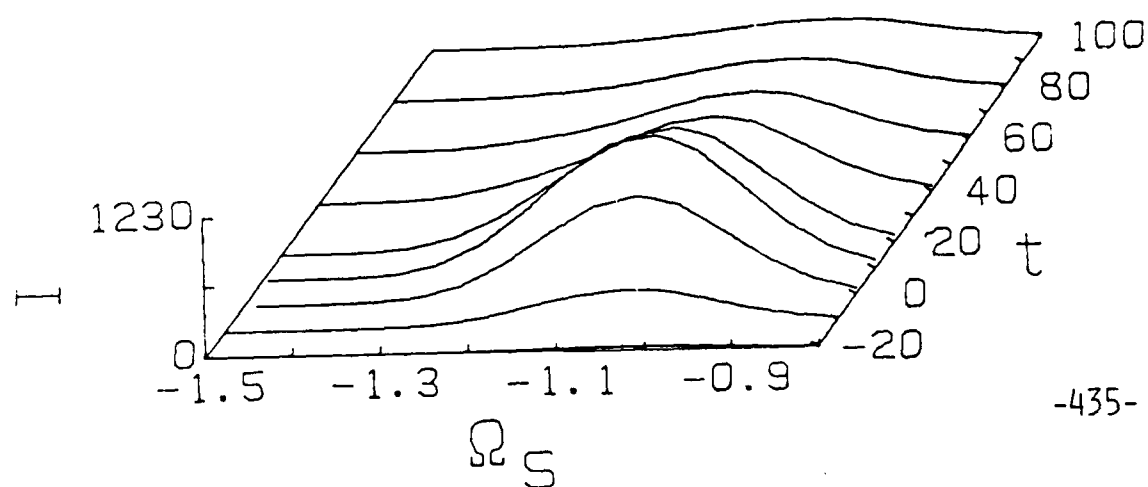


Fig. 3

$$C_A=0.5 \quad \Delta=1.6 \quad r=0.2 \quad \Omega_i=0 \quad \delta=1$$

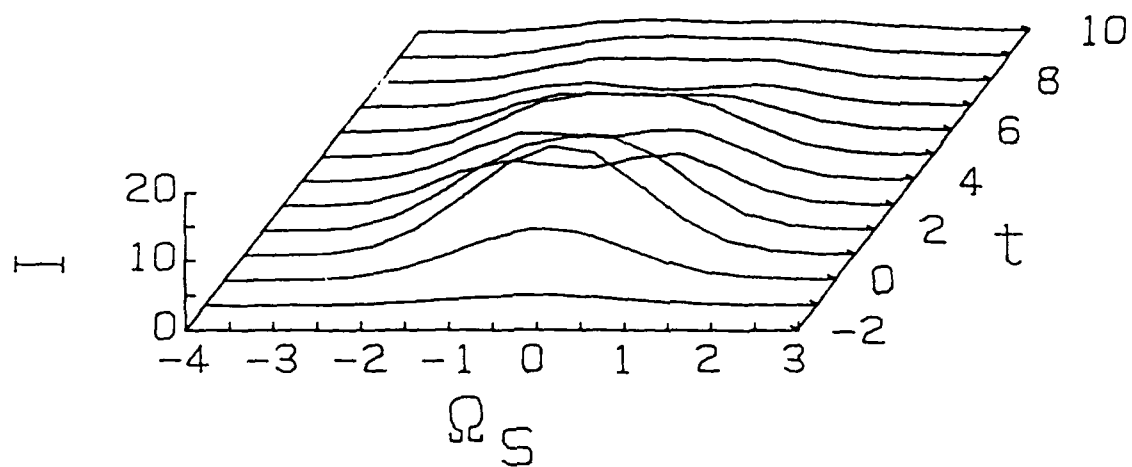


Fig. 4

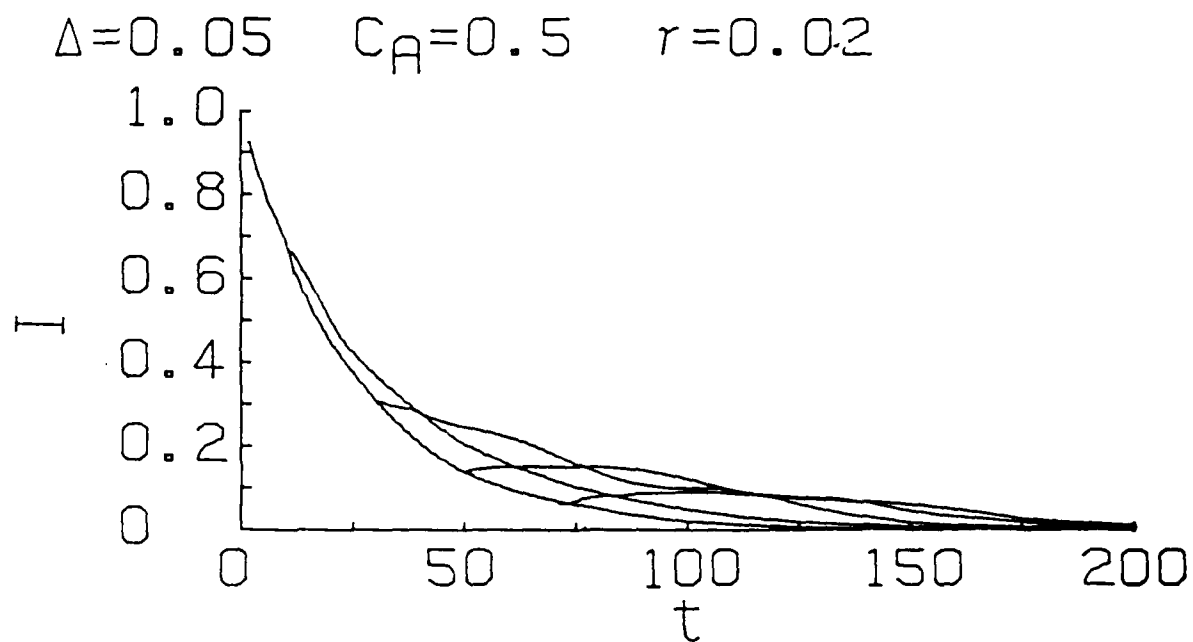
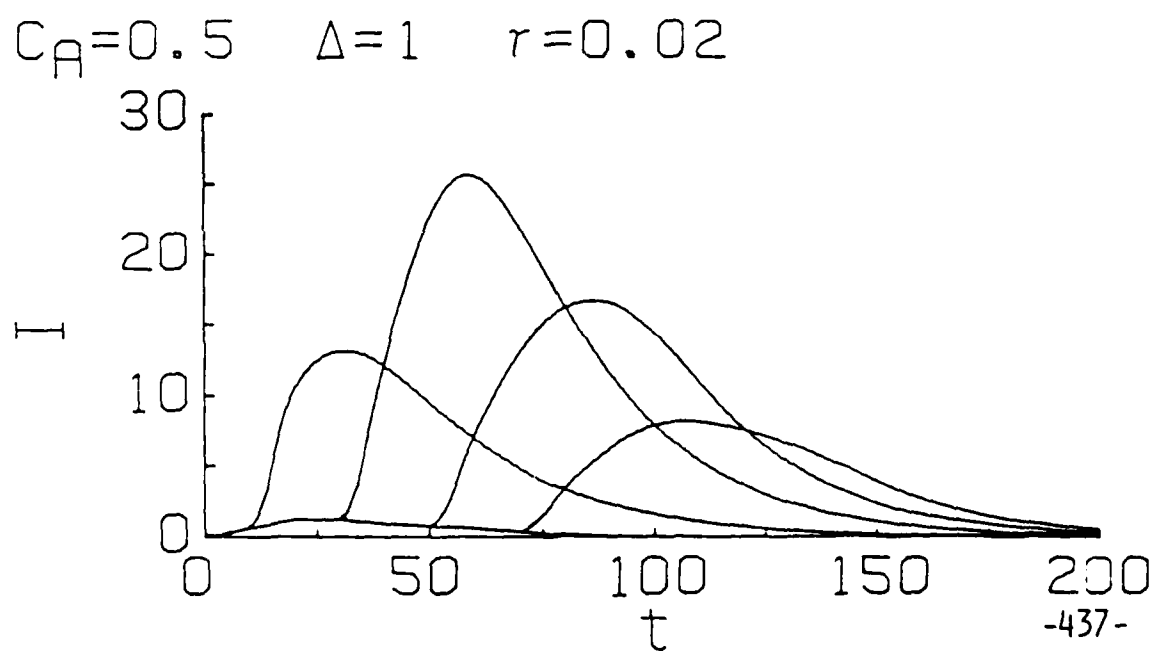


Fig. 5



Generation of number-phase minimum uncertainty states

Y. Yamamoto, S. Machida, N. Imoto, M. Kitagawa and G. Björk

NTT Basic Research Laboratory

Musashinoshi, Tokyo 180, Japan

The difference between the two nonclassical lights, i.e. the squeezed state and number-phase minimum uncertainty state (NUS) is discussed. The four different generation principles for NUS are described. They are

- 1) unitary evolution using self-phase modulation¹⁾,
- 2) nonunitary state reduction by the first kind measurement²⁾,
- 3) controlled state reduction by quantum correlation measurement-feedback³⁾⁻⁵⁾, and
- 4) highly saturated laser oscillator with suppressed-pump-noise⁶⁾⁻⁸⁾.

The constant current-driven semiconductor laser based on the last principle generated the NUS with photon number noise reduced below the standard quantum limit by 40% in the entire frequency region from dc to 1.1GHz. Several applications of NUS including quantum communication⁹⁾, quantum mechanical computers¹⁰⁾ and interferometric gravitational detection are discussed briefly.

- 1) M. Kitagawa and Y. Yamamoto, Phys. Rev. A34, 3974 (1986)
- 2) M. Kitagawa, N. Imoto and Y. Yamamoto, Phys. Rev. A35, 5270 (1987)
- 3) Y. Yamamoto, N. Imoto and S. Machida, Phys. Rev. A33, 3243 (1986)

- 4) H. A. Haus and Y. Yamamoto, Phys. Rev. A34, 270 (1986)
- 5) G. Björk and Y. Yamamoto, to be published
- 6) Y. Yamamoto, S. Machida and O. Nilsson, Phys. Rev. A34, 4025 (1986)
- 7) Y. Yamamoto and S. Machida, Phys. Rev. A35, 5114 (1987)
- 8) S. Machida, Y. Yamamoto and Y. Itaya, Phys. Rev. Lett. 58, 1000 (1987)
- 9) Y. Yamamoto and H. A. Haus, Rev. Mod. Phys. 56, 1001 (1986)
- 10) K. Igeta and Y. Yamamoto, to be published

Generation of Number-Phase Minimum Uncertainty States

Y. Yamamoto, S. Machida, N. Imoto, M. Kitagawa and G. Björk
NTT Basic Research Laboratory

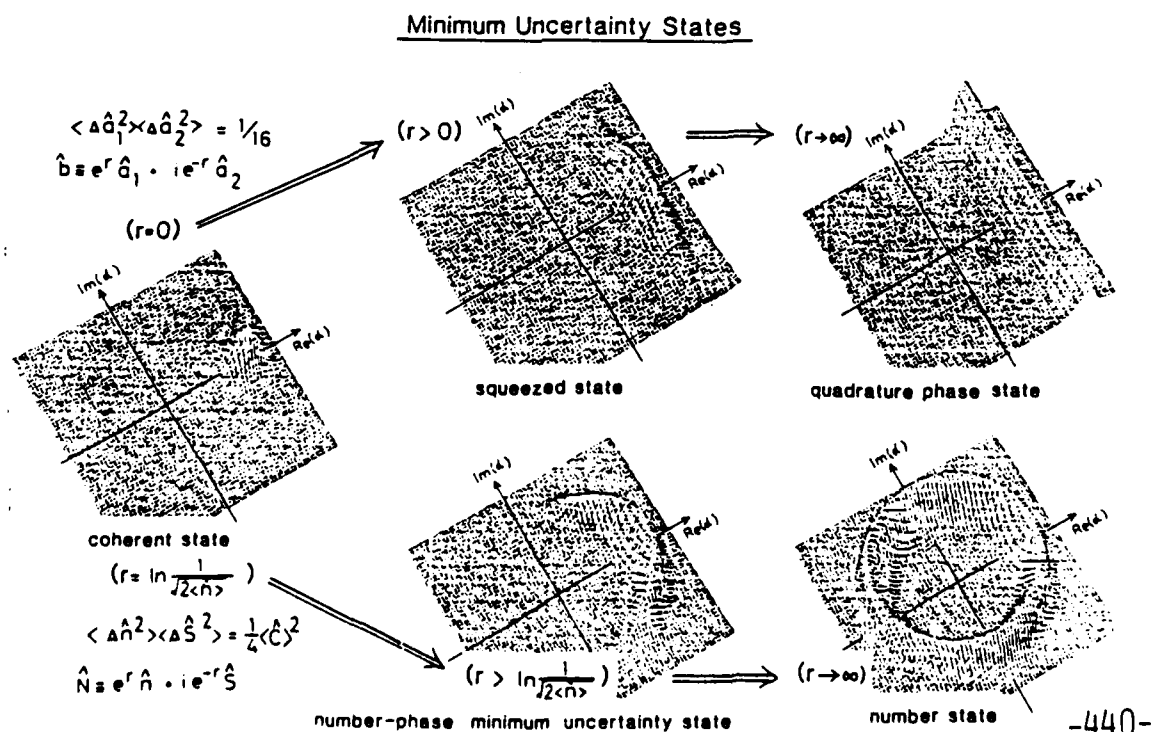
1. Squeezed state (SS) vs. Number-phase minimum uncertainty state(NUS)

2. Four generation schemes of NUS

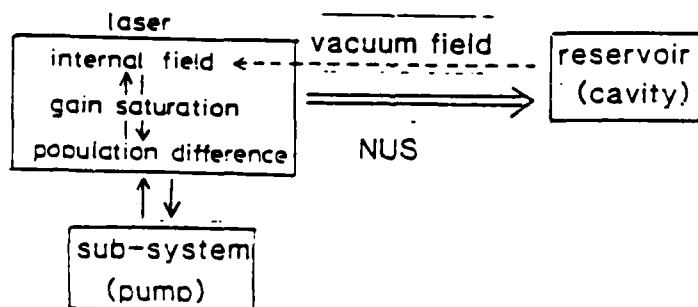
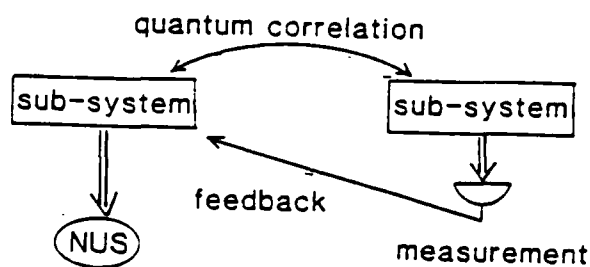
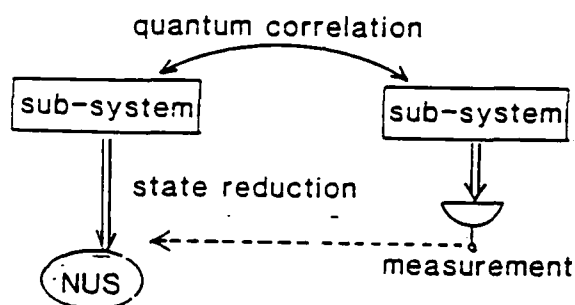
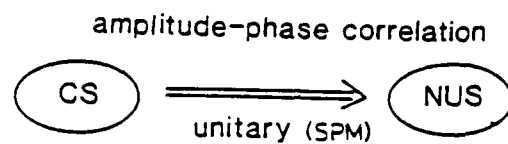
- unitary evolution
- nonunitary state reduction
- measurement- feedback
- saturated oscillator

40% below SQL from dc to 1.1 GHz

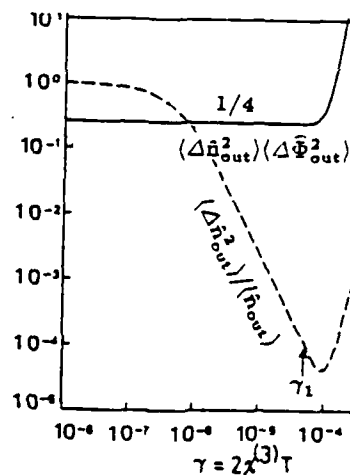
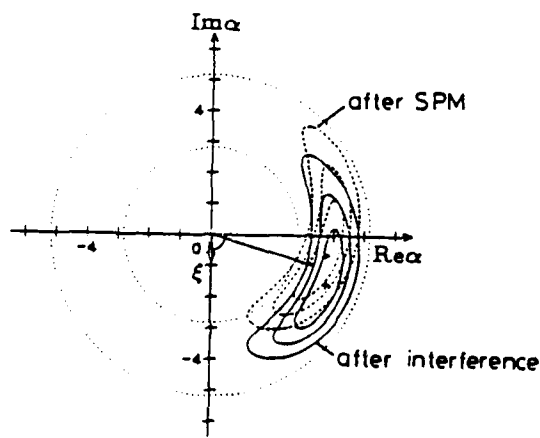
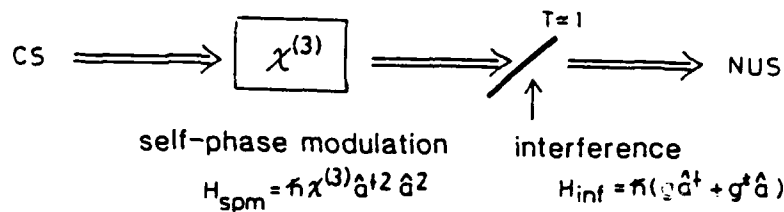
3. Applications

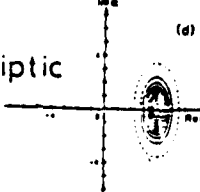
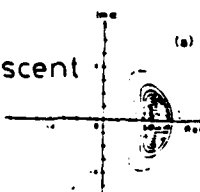


Four different generation schemes of NUS



Unitary Evolution for NUS Generation

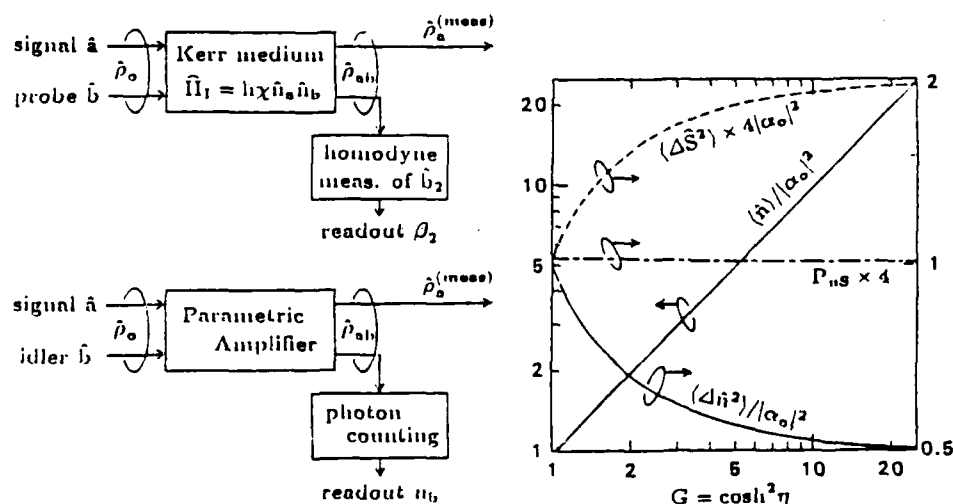


	Squeezed state	Number-phase minimum uncertainty state
Configuration	spatially nondegenerate four wave mixing	spatially degenerate four wave mixing
Interaction Hamiltonian	$H_I = \frac{\hbar}{2}(\chi \hat{a}^{\dagger 2} + \chi^* \hat{a}^2)$	$H_I = \hbar \chi \hat{a}^{\dagger 2} \hat{a}^2$
Interaction type	Active (amp./deamp.)	Passive (SPM)
QPD	elliptic 	crescent 
$\langle \Delta \hat{n}^2 \rangle_{\text{min}}$	$\sim \langle \hat{n} \rangle^{2/3}$	$\sim \langle \hat{n} \rangle^{1/3}$

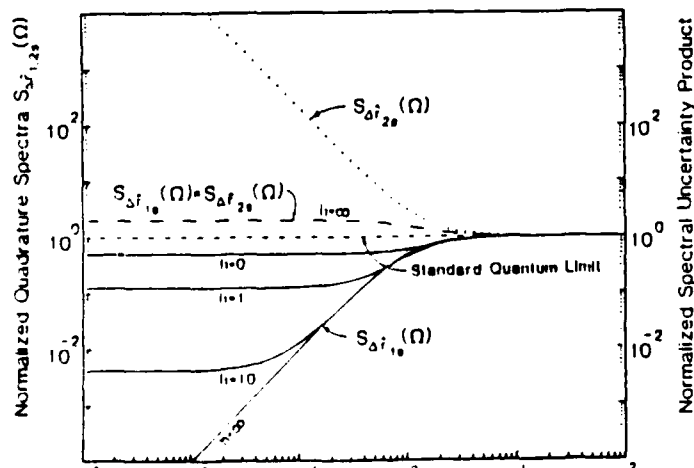
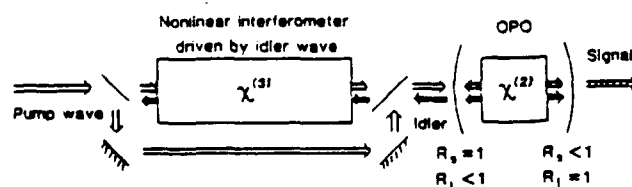
Nonunitary State Reduction by 1st kind Measurement

$$\hat{\rho}_0 = |\alpha\rangle_{aa}\langle\alpha| \otimes |0\rangle_{bb}\langle 0| \xrightarrow[U=\exp(i\eta\hat{a}^\dagger\hat{b}^\dagger + \hat{a}\hat{b})]{} \hat{\rho}_{ab} = U\hat{\rho}_0U^\dagger$$

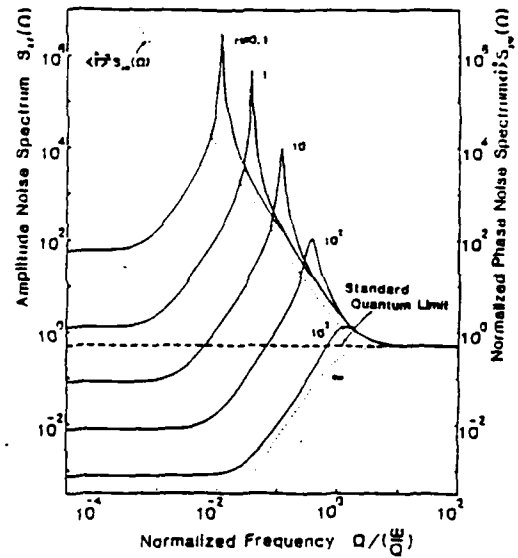
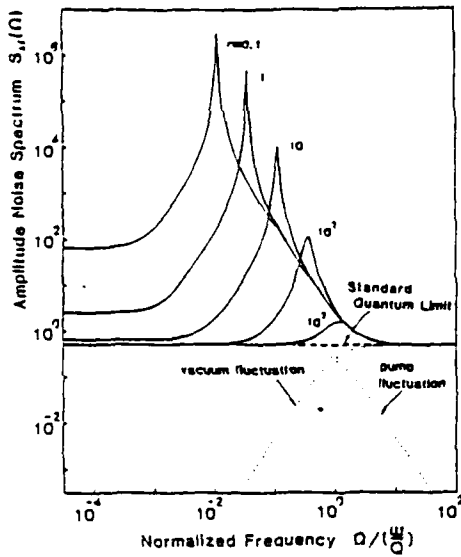
$$\hat{\rho}_a^{(meas)} \xrightarrow[\text{projection postulate}]{} \text{Tr}_b(|n\rangle_{bb}\langle n| \hat{\rho}_{ab})$$



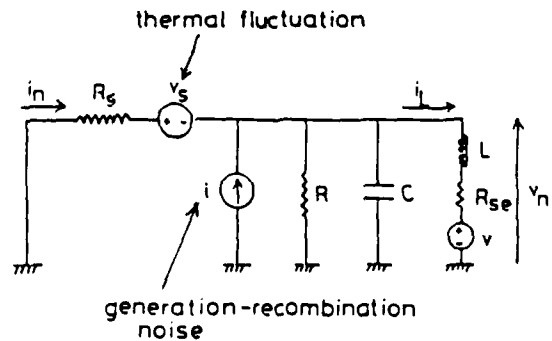
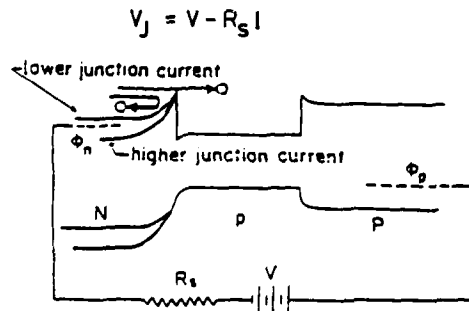
Optical Parametric Oscillator with measurement-feedback



Pump-Noise-Suppressed Laser Oscillator



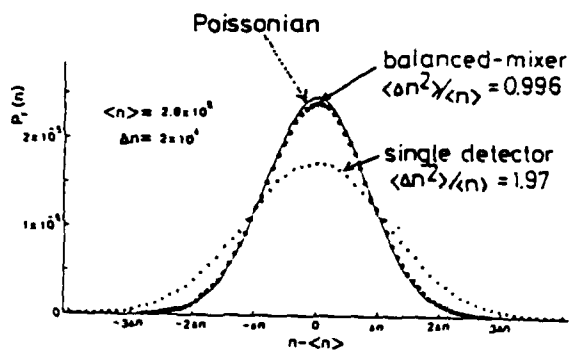
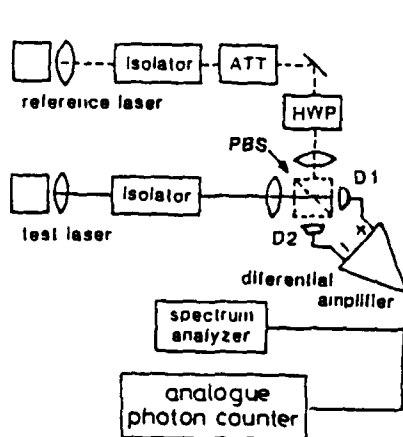
High Impedance Suppression of Pump Current Noise



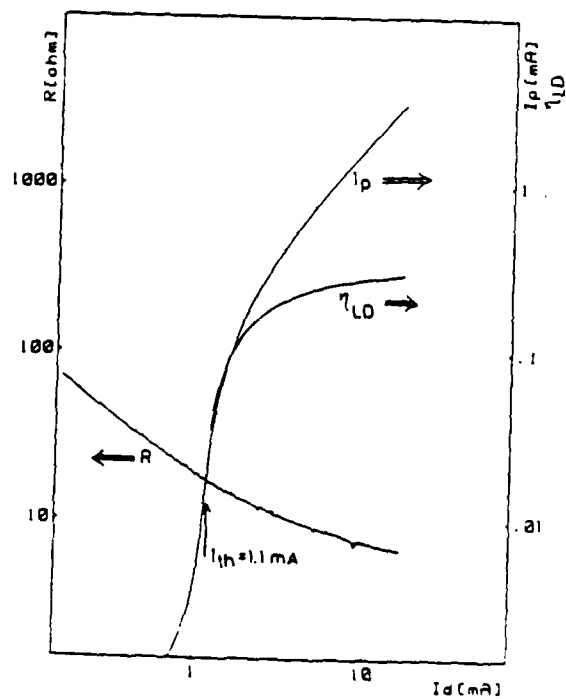
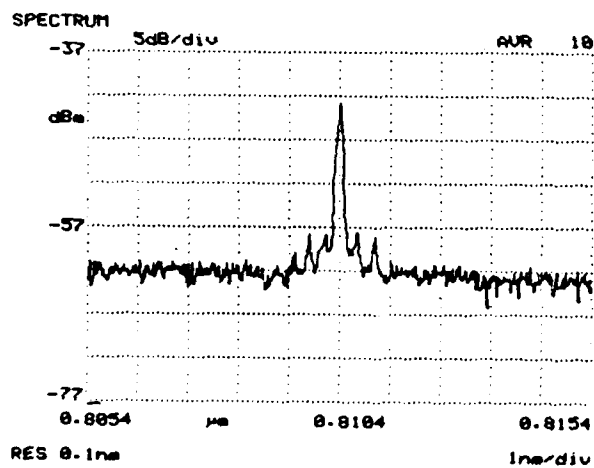
$$R_s \ll 2R \implies S_{v_n}(\Omega) \rightarrow 0 \quad (\text{constant voltage operation})$$

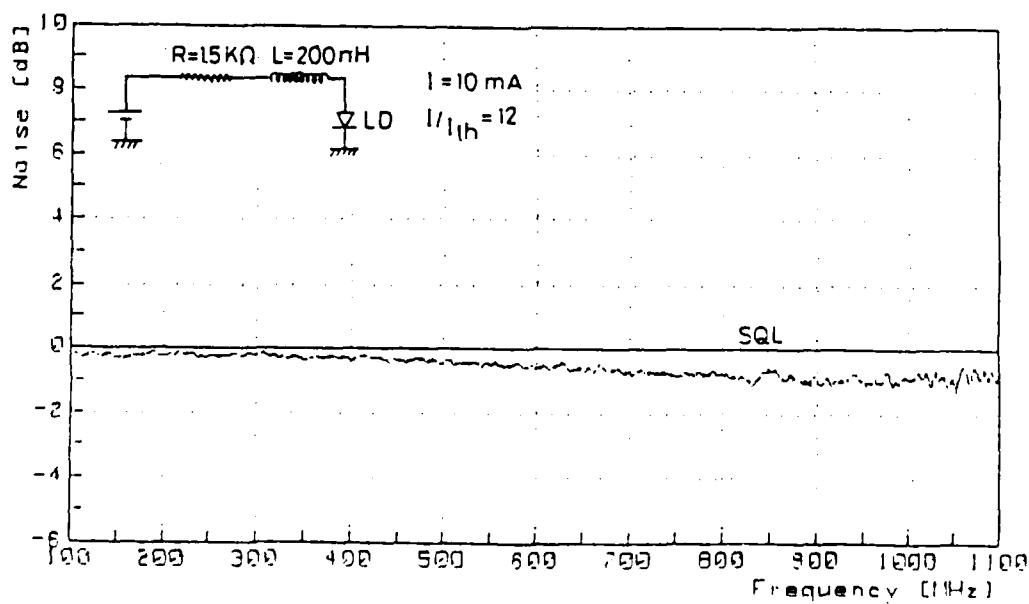
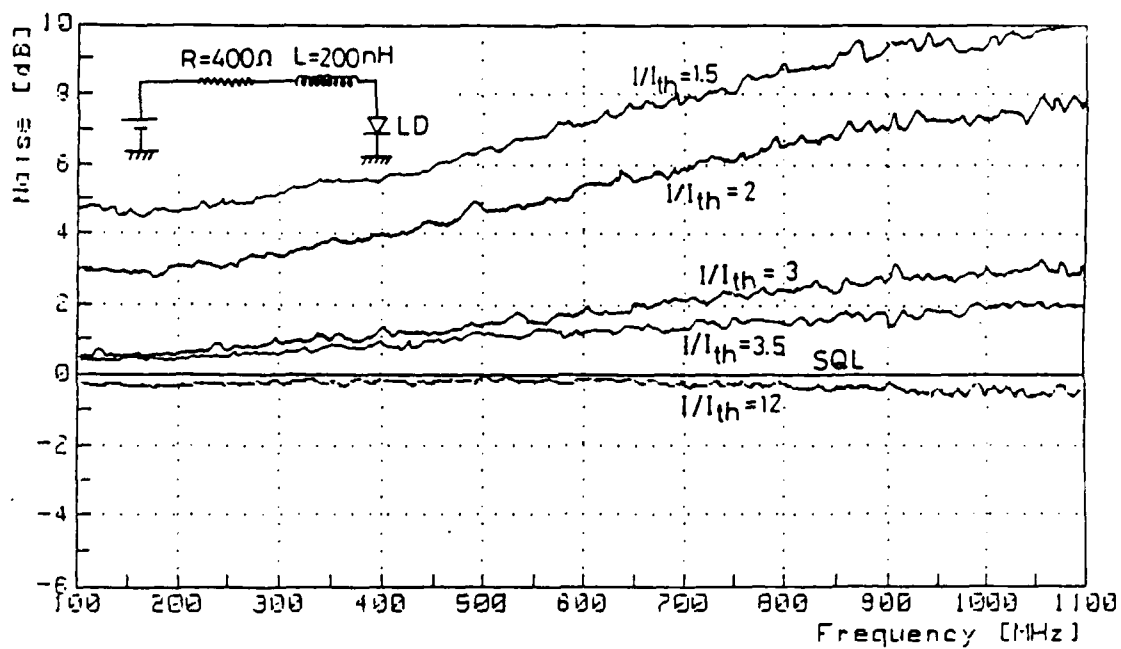
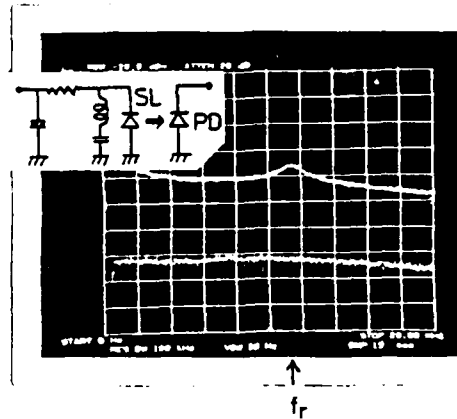
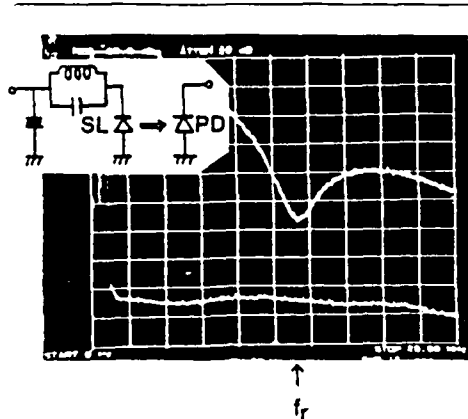
$$R_s \gg 2R \implies S_{i_n}(\Omega) \rightarrow 0 \quad (\text{constant current operation})$$

Calibration of Standard Quantum Limit

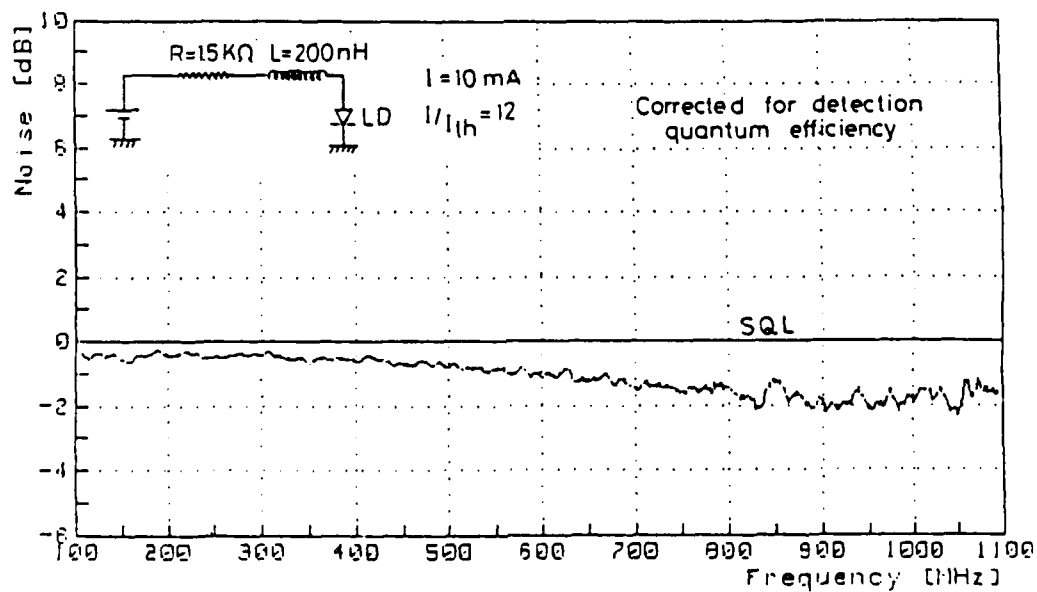
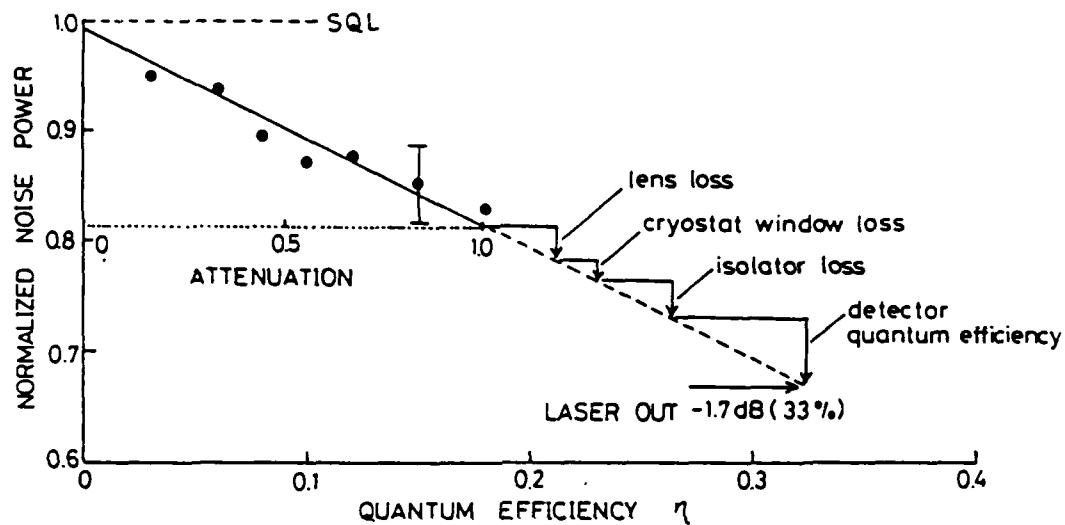


0.8 μm GaAs Transverse Junction Stripe Laser

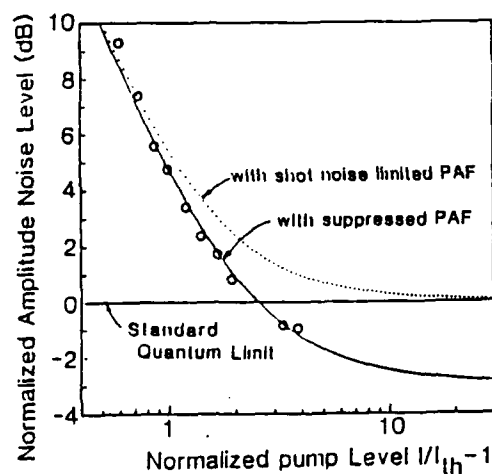




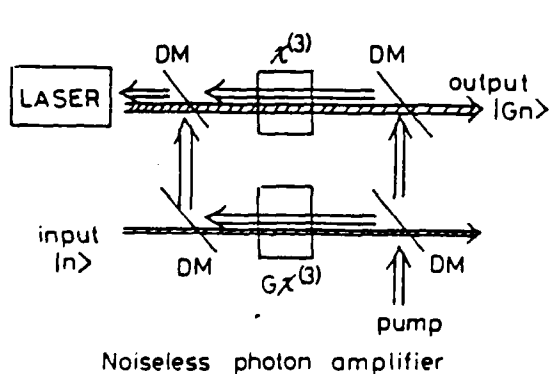
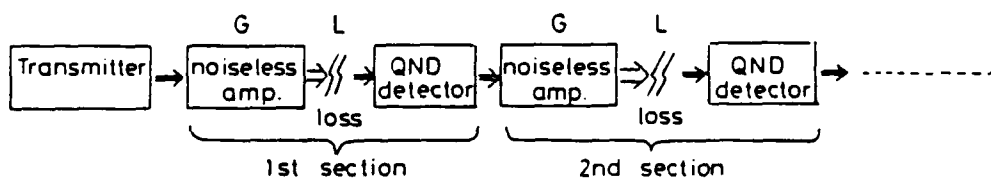
AMPLITUDE SQUEEZING vs. OPTICAL LOSS



1.5 μ m InGaAsP Distributed Feedback Laser



Application I — Quantum Communication —

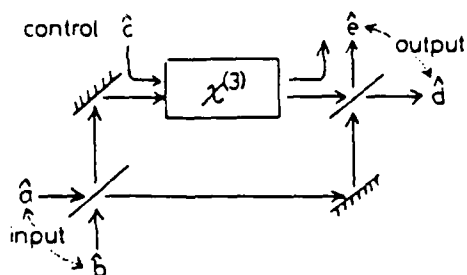


$$S/N = \begin{cases} \frac{\langle \hat{n}_s^2 \rangle}{\langle \Delta \hat{n}_s^2 \rangle + \frac{1-L}{L} \langle \hat{n}_s \rangle} \xrightarrow{\text{no gain}} \frac{\langle \hat{n}_s \rangle}{L} \text{ (SQL)} \\ \frac{\langle \hat{n}_s^2 \rangle}{\langle \Delta \hat{n}_s^2 \rangle + m(1-L) \langle \hat{n}_s \rangle} \xrightarrow{(GL=1)} \frac{\langle \hat{n}_s \rangle}{m} \\ \frac{\langle \hat{n}_s^2 \rangle}{\langle \Delta \hat{n}_s^2 \rangle + \frac{1-L}{GL-1} \langle \hat{n}_s \rangle} \xrightarrow{(GL>1)} \frac{\langle \hat{n}_s^2 \rangle}{\langle \Delta \hat{n}_s^2 \rangle} \end{cases}$$

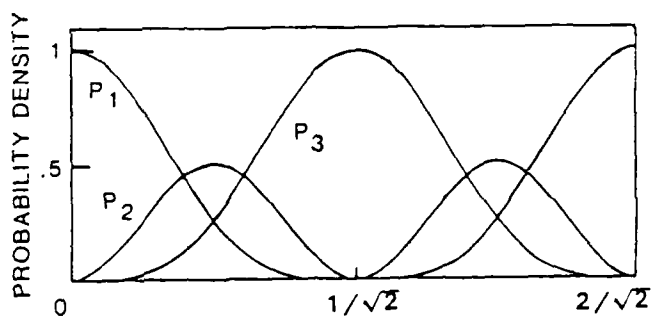
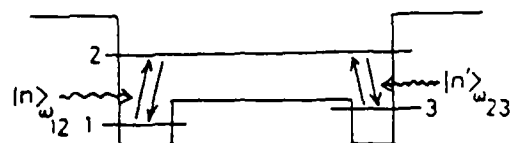
Application II—Quantum Mechanical Computer —

Reversible logic (Fredkin gate)

Microscopic memory (QND readout)



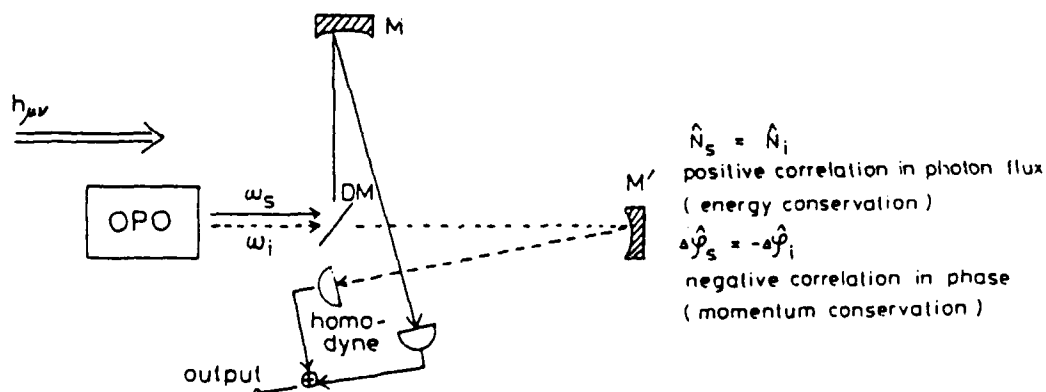
	NOT & FAN OUT	OR	AND
CONT- ROL	INPUT	INPUT1	INPUT1
input a	PRESET 1	INPUT2	INPUT2
b	0 PRESET	1 PRESET	0 PRESET
output c	NOT	OR	GARBAGE
d	FAN OUT	GARBAGE	AND



INTERACTION TIME t/T

$$\tau = \pi/g\sqrt{n} = \pi/g'\sqrt{n'}$$

Application III—Gravitational Wave Detection —



Suppression of detection noise

$$\Delta \phi_s^{(FM)} \cdot \Delta \phi_i^{(FM)} < \text{SQL}$$

negative correlation

Suppression of radiation pressure noise

$$\Delta \phi_s^{(rp)}(N_s) - \Delta \phi_i^{(rp)}(N_i) < \text{SQL}$$

positive correlation

Conclusion

1. Four different generation schemes of NUS
2. Constant current-driven semiconductor laser
 - large squeezing quantum efficiency limited
 - broadband from dc to several (ten) GHz
 - wavelength tunability from 0.6 μm to 10 μm
3. Applications
 - Quantum communication / Quantum computer / Interferometry

Acknowledgement

Hermann A. Haus (M.I.T.)
Olle Nilsson (Royal Institute of Technology)
Horace P. Yuen (Northwestern)

**SQUEEZING VIA TRAVELLING-WAVE FORWARD FOUR-WAVE MIXING
IN ATOMIC VAPORS: COMPARISON WITH NONDEGENERATE THEORY**

Prem Kumar

Northwestern University

In this paper, I show that our recent observation of 4% squeezing via travelling-wave forward four-wave mixing in sodium vapor¹ is in good agreement with our quantum theory of nondegenerate multiwave mixing.² Squeezing spectra for the parameter values employed in the Maeda et al.¹ experiment are presented. It is shown that for the available dye-laser power, as much as a factor of four squeezing should be achievable from about 50 to 700 MHz in the sodium vapor experiment. However, Doppler broadening, optical pumping, and self-focussing effects may limit the observable squeezing.

1. M. W. Maeda, P. Kumar, and J. H. Shapiro, Opt. Lett. 12, 161 (1987).
2. S.-T. Ho, P. Kumar, and J. H. Shapiro, Phys. Rev. A 35, 3982 (1987).

Squeezing via Travelling-Wave
Forward Four-Wave Mixing in Atomic
Vapors : Comparison with Nondegenerate Theory

PREM KUMAR
Northwestern University

July 23, 1987

U.S.-Japan Seminar on
Quantum Mechanical Aspects of Quantum Electronics

COLLABORATORS

MIT - Jeffrey H. Shapiro

Mari W. Maeda

Seng-Tiong Ho

N.U. - Manjusha Madabushi

Outline

- i) Observation of squeezing in forward four-wave mixing
- ii) Quantum theory of nondegenerate multiwave mixing
- iii) Calculation of squeezing spectrum
- iv) Comparison with Maeda et al. experiment
- v) Prognosis

SQUEEZED STATES

(3)

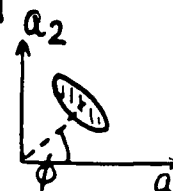
SINGLE MODE

$$\hat{E}^{(+)} = \sqrt{\frac{\hbar \omega_0}{AT}} \hat{a} e^{-i\omega_0 t}$$

$$\hat{a}_\phi \equiv \frac{1}{2} [\hat{a} e^{-i\phi} + \text{H.c.}]$$

- vacuum state $| \rangle_0$: $\langle \Delta \hat{a}_\phi^2 \rangle_0 = 1/4$

- squeezed state $| \rangle_s$: $\langle \Delta \hat{a}_\phi^2 \rangle_s < 1/4$ for some ϕ



TWO MODE : Nondegenerate ; $a_{\pm} : \omega_0 \pm \Omega$

$$\hat{E}^{(+)} = \sqrt{\frac{\hbar \omega_0}{AT}} [\hat{a}_+ e^{-i\Omega t} + \hat{a}_- e^{i\Omega t}] e^{-i\omega_0 t}$$

$$\hat{a}_{\phi, \Phi}(\Omega) \equiv \left[\frac{1}{2} (\hat{a}_+ e^{-i\phi} + \hat{a}_-^\dagger e^{i\phi}) e^{-i\Phi} + \text{H.c.} \right]$$

- vacuum state $| \rangle_0 = | \rangle_+ | \rangle_-$: $\langle \Delta \hat{a}_{\phi, \Phi}^2(\Omega) \rangle_0 = 1/4$

- squeezed state $| \rangle_s = \hat{Q}(| \rangle_+ | \rangle_-)$:

Independent of $\Phi \rightarrow \langle \Delta \hat{a}_{\phi}^2(\Omega) \rangle_s < 1/4$ for some ϕ, Ω
for 2-mode squeezing

HOMODYNE DETECTION

$$S_{ii}(\Omega) \propto \langle \Delta \hat{a}_{\phi}^2(\Omega) \rangle_s$$

Ideal Forward Four-wave Mixing

$$\hat{E}_{\text{OUT}}^{\text{p,c}}(t) = \left(\frac{\hbar\omega_0}{AT}\right)^{\frac{1}{2}} \left[\hat{a}_{\text{IN}}^{\text{p,c}}(+\Omega) e^{-i(\omega_0+\Omega)t} + \hat{a}_{\text{IN}}^{\text{p,c}}(-\Omega) e^{-i(\omega_0-\Omega)t} \right]$$

$\hat{a}_{\text{IN}}^{\text{p,c}}(-\Omega) \quad \hat{a}_{\text{IN}}^{\text{p,c}}(+\Omega)$

$\omega_0 - \Omega \quad \omega_0 \quad \omega_0 + \Omega \rightarrow \omega$

FFWM

$$\hat{a}_{\text{OUT}}^{\text{p,c}}(\pm\Omega) = \mu \hat{a}_{\text{IN}}^{\text{p,c}}(\pm\Omega) + i\nu \hat{a}_{\text{IN}}^{\text{c,p}\dagger}(\mp\Omega)$$

$$\mu = \cosh(|K|L), \quad \nu = e^{-i\theta} \sinh(|K|L)$$

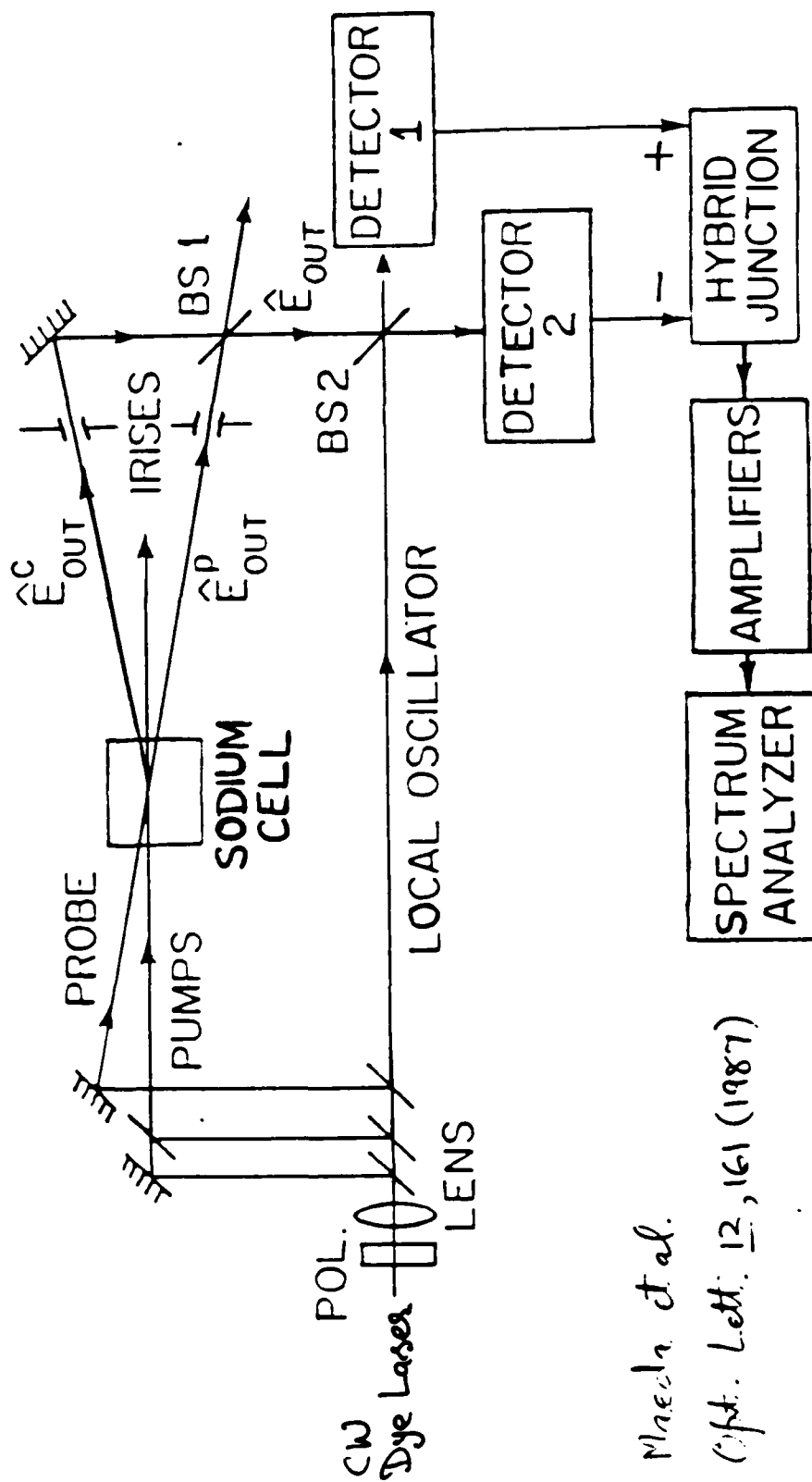
Squeezing

$$\begin{aligned} \hat{E}_{\text{OUT}}^{\text{p}}(t) &= [\hat{E}_{\text{IN}}^{\text{p}}(t) + \hat{E}_{\text{IN}}^{\text{c}}(t) e^{ih\Delta L}] / \sqrt{2} \\ &\equiv \left(\frac{2\hbar\omega_0}{AT}\right)^{\frac{1}{2}} \left[\hat{a}_{+}^{\text{IN}}(\Omega) \cos(\Omega t) + \hat{a}_{-}^{\text{IN}}(\Omega) \sin(\Omega t) \right] e^{-i\omega_0 t} \end{aligned}$$

$$\hat{a}_{\pm}^{\text{OUT}}(\Omega) = \mu \hat{a}_{\pm}^{\text{IN}}(\Omega) + i\nu e^{ih\Delta L} \hat{a}_{\pm}^{\text{IN}}(\Omega) \quad \text{Yuen 1976}$$

Homodyne Detection of $\hat{E}_{\text{OUT}}(t)$

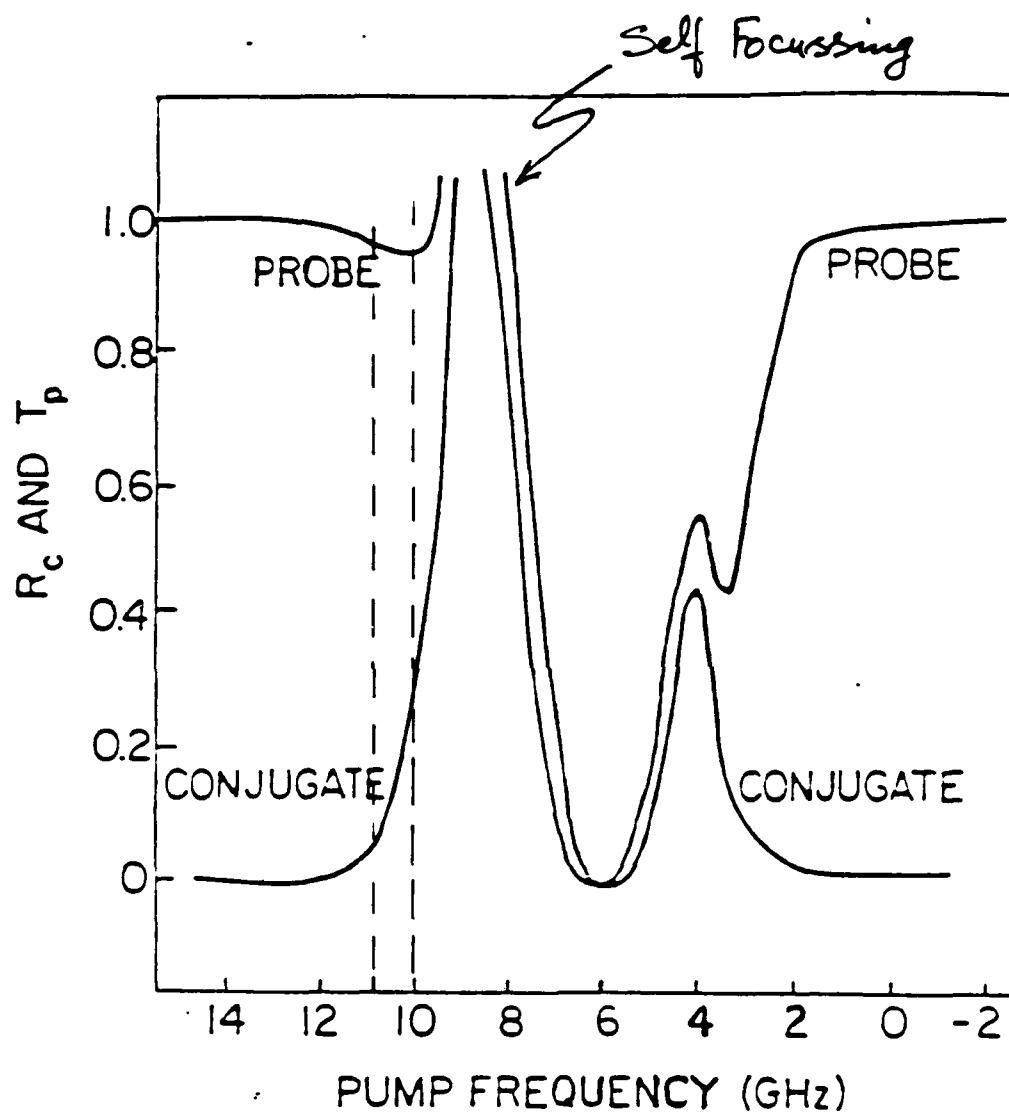
$$\begin{aligned} V_{\phi}^2(\Omega) &= 4e^2 \frac{P_{L0}}{\hbar\omega_0} B R^2 G \left[\eta \left\{ [\text{Re}(\hat{a}_{+}^{\text{OUT}}(\Omega) e^{-i\phi})]^2 + [\text{Re}(\hat{a}_{-}^{\text{OUT}}(\Omega) e^{-i\phi})]^2 \right\} + \frac{1-\eta}{2} \right] \\ &= V_{\phi}^2(\text{vac}) \left[\eta |\mu - i\nu^* e^{-i(h\Delta L - 2\phi)}|^2 + 1 - \eta \right]_{-456-} \end{aligned}$$



Maele et al.

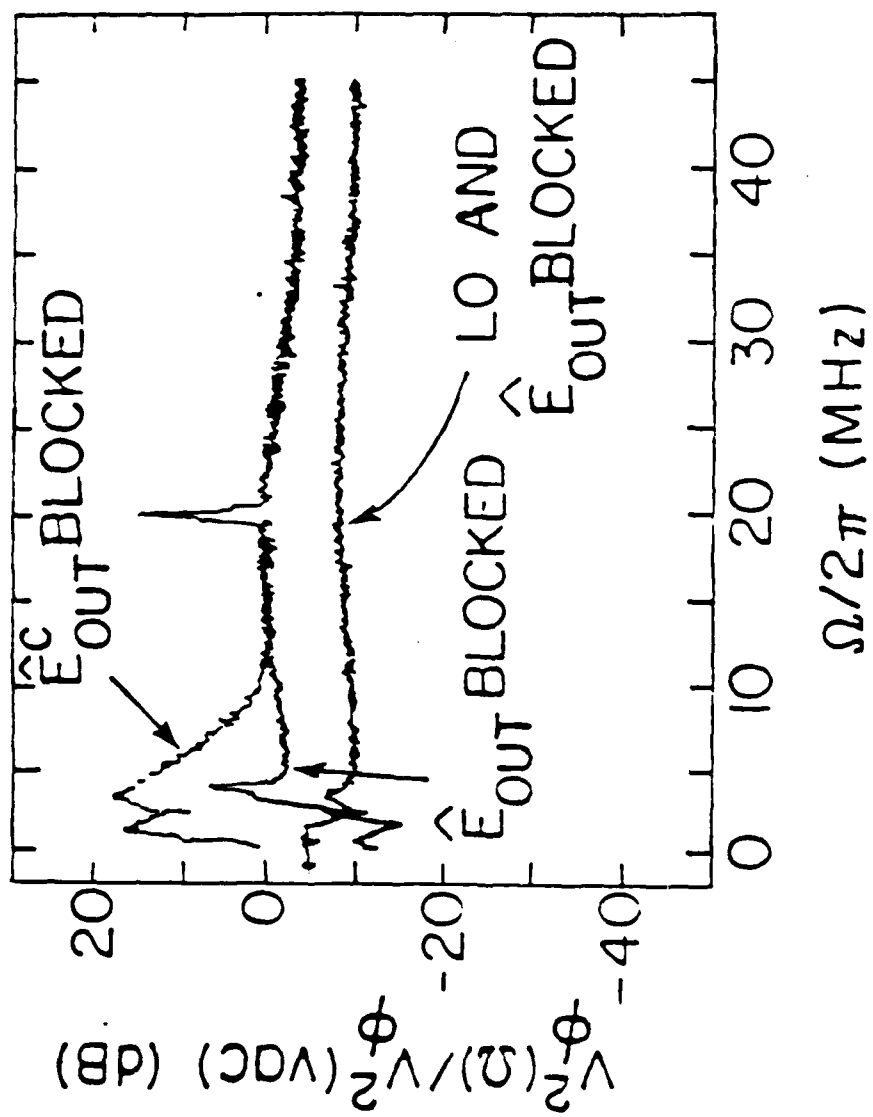
Opt. Lett. 12, 161 (1987)

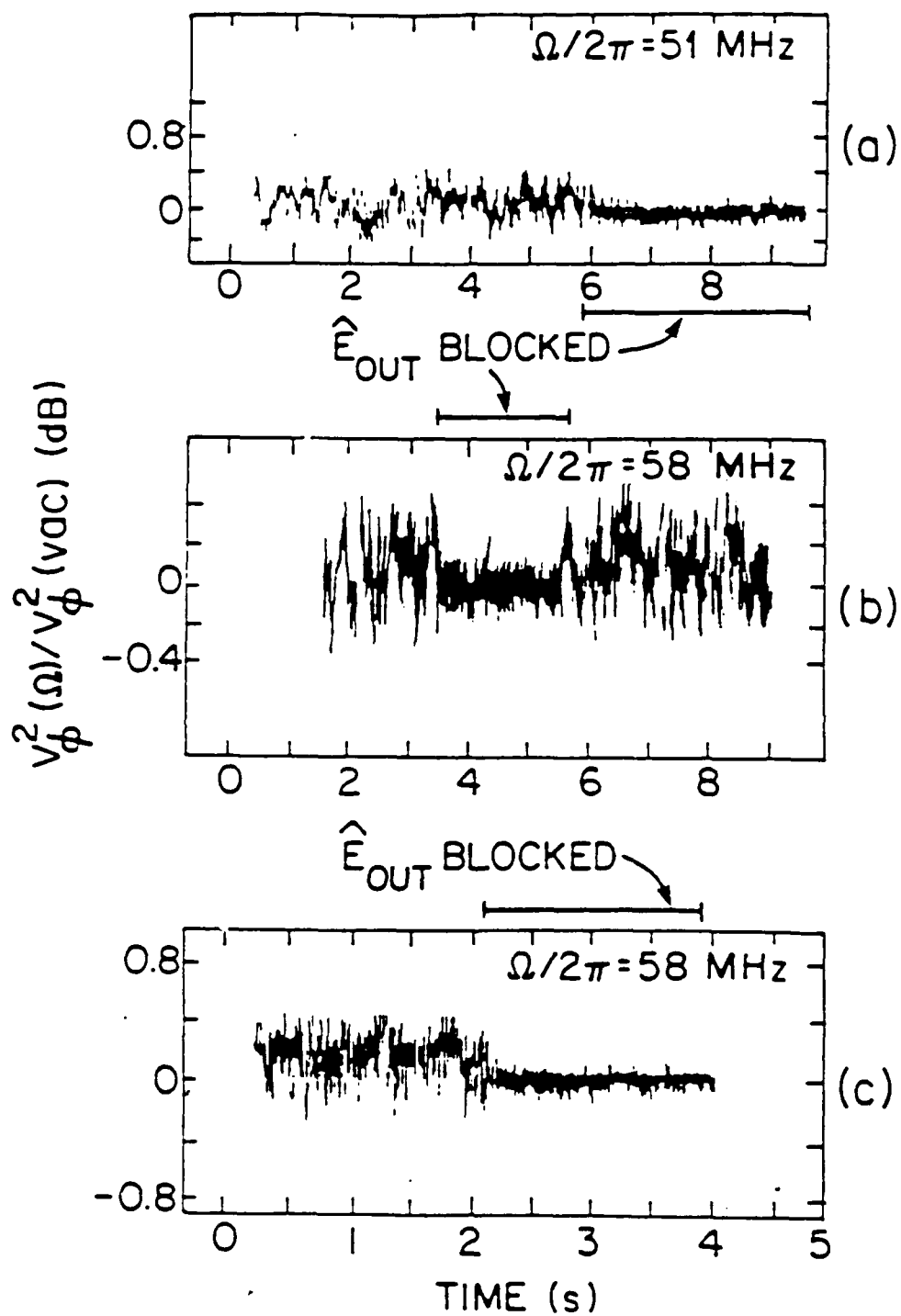
(6)



Detuning $\approx 4-5$ GHz ; $I_p \approx 20-50$ mW/0.5 mm dia.
 $\alpha_0 L \approx 5 \times 10^4$

(2)





Theories of Nondegenerate Four-Wave Mixing

- Reid and Walls (1985, 86)
- Holm and Sargent (1986, 87)

Apply to cavity configurations

Replace $z \rightarrow ct$

(not valid in an optically thick medium
with dispersion and nonlinear mixing)

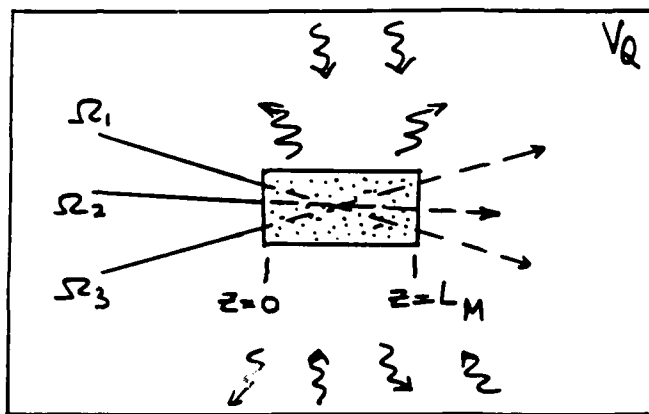
Quantum Theory of Nondegenerate Multiwave Mixing

He et al. (1987)

System Hamiltonian

N two-level atoms
 q field modes

Rest of the modes constitute a common thermal-field reservoir. In addition each atom is coupled to a separate phase-damping reservoir.



$$\hat{H} = \hat{H}_0 + \hat{H}_I + \hat{H}_R + \hat{H}_C$$

$$\hat{H}_0 = \sum_{j=1}^q \hbar \omega_j \hat{a}_j^\dagger \hat{a}_j + \frac{\hbar \omega_a}{2} \sum_{i=1}^N \hat{n}_{di}$$

$$\begin{aligned} \hat{n}_i &= |e\rangle_i \langle e| \\ \hat{n}_{gi} &= |g\rangle_i \langle g| \\ \hat{n}_{di} &= (|e\rangle_i \langle e| - |g\rangle_i \langle g|) \end{aligned}$$

$$\hat{H}_I = \sum_{j=1}^q \sum_{i=1}^N \left\{ i \hbar C_j(\vec{k}_i) \hat{a}_j \hat{V}_i^\dagger + \text{H.c.} \right\} \quad \hat{V}_i = |g\rangle_i \langle e|$$

Rotating Wave & Dipole

$$\hat{H}_R = \sum_{s=q+1}^{\infty} \hbar \omega_s \hat{a}_s^\dagger \hat{a}_s + \sum_{s=q+1}^{\infty} \sum_{i=1}^N \left\{ i \hbar C_s(\vec{k}_i) \hat{a}_s \hat{V}_i^\dagger + \text{H.c.} \right\}$$

$$\hat{H}_C = \sum_{i=1}^N \hat{\Gamma}_i \hat{n}_{di} \quad \text{Coulomb gauge} \quad \begin{cases} C_j(\vec{k}_i) = g_j \mu_j e^{i \vec{k}_j \cdot \vec{r}_i} \\ \mu_j = \langle e | e^{i \vec{k}_i \cdot \vec{r}} | g \rangle_i \cdot \vec{e}_j \\ g_j = \left(\omega_a^2 / 2 \pi \epsilon_0 \omega_j V_Q \right)^{\frac{1}{2}} \end{cases}$$

-462-

C-Number Langevin Equations Haken: Laser Theory
Drummond and Walls: Bistability

$$\frac{\partial V_i}{\partial t} = -i\omega_a V_i - \sum_{j=1}^q C_j(\bar{\kappa}_i) a_j (n_{gi} - n_i) - \gamma_{\perp} V_i + f_{V_i}$$

$$- \underbrace{\sum_{i' \neq i} \gamma_{ii'} (\bar{\kappa}_i - \bar{\kappa}_{i'}) [n_{gi} - n_i] V_{i'}}_{\text{Superradiance terms}}$$

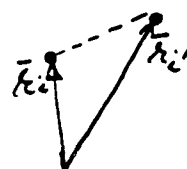
$$\frac{\partial n_i}{\partial t} = - \sum_{j=1}^q [C_j^*(\bar{\kappa}_i) a_j^{\dagger} V_i + C_j(\bar{\kappa}_i) a_j V_i^{\dagger}] - \gamma_{\parallel} n_i + f_{n_i}$$

$$- \underbrace{\sum_{i' \neq i} \gamma_{ii'} (\bar{\kappa}_i - \bar{\kappa}_{i'}) [V_i^{\dagger} V_{i'} + V_{i'}^{\dagger} V_i]}_{\text{Superradiance terms}}$$

$$n_{gi} + n_i = 1$$

Superradiance terms

Agree with Bonifacio
et al. (1971)



$$\frac{\partial a_j}{\partial t} = -i\omega_j a_j + \sum_{i=1}^N C_j^*(\bar{\kappa}_i) V_i$$

$$\gamma_{\perp} = \gamma_p + \gamma_{\parallel}/2 \equiv \frac{\gamma_{\parallel}}{2F} ; \quad 0 \leq F \leq 1$$

Superradiance terms are negligible : a) # of atoms in a diffraction volume is small

b) atoms pumped far off-resonance

Noise Correlations

We neglect superradiance $\langle f_{V_i^{\dagger}}(t) f_{V_{i'}}(t') \rangle = 2\gamma_p n_i \delta_{ii'} \delta(t-t')$

$$\langle f_{V_i}(t) f_{V_{i'}}(t') \rangle = \left[\sum_{j=1}^q C_j(\bar{\kappa}_i) a_j V_i \right] \delta_{ii'} \delta(t-t')$$

$$\langle f_{n_i}(t) f_{n_{i'}}(t') \rangle = \langle f_{n_{gi}}(t) f_{n_{gi'}}(t') \rangle = - \langle f_{n_i}(t) f_{n_{gi'}}(t') \rangle$$

$$= \left[- \sum_{j=1}^q (C_j^*(\bar{\kappa}_i) a_j^{\dagger} V_i + C_j(\bar{\kappa}_i) a_j V_i^{\dagger}) + \gamma_{\parallel} n_i \right] \delta_{ii'} \delta(t-t')$$

Delta correlated in space and time

Solution Technique For Atomic Polarization

• Fourier Decomposition

$$a_{\bar{k}_i}(t) \equiv \sum_{j=1}^q C_j(\bar{k}_i) a_j(t) = \sum_{m=1}^{\infty} A_m(\bar{k}) e^{-i\nu_m t}$$

$$X(\omega) \equiv \int_{-\infty}^{\infty} \frac{dt}{2\pi} X(t) e^{i\omega t}; \quad X \in \{V, V^+, n, \{V, \{V^+, \{n\}\}$$

Iterative solution developed which converges when all strong modes are frequency-degenerate and remaining nondegenerate modes are weak.

$$V_i(t) = \sum_{m=1}^{\infty} \gamma(\nu_m, \bar{k}_i, t) A_m(\bar{k}_i) e^{-i\nu_m t} + \Gamma_{V_i}(t)$$

Slowly-Varying Amplitude Approximation Frequency Domain Method

$$a_{\bar{k}_i}(t) = \sum_{j=1}^q C_j(\bar{k}_i) a_j(t) = \sum_{j=1}^q C_j(\bar{k}_i) \alpha_j(t) e^{-i(\omega_j - \Delta\omega_j)t}$$

$$\alpha_j(t-t') \approx \alpha_j(t) - t' \frac{\partial \alpha_j(t)}{\partial t}$$

$$V_i(t) = \sum_{j=1}^q C_j(\bar{k}_i) e^{-i\omega_j^\delta t} \hat{D}_j(t) \gamma(\omega_j^\delta, \bar{k}_i, t) + \Gamma_{V_i}(t)$$

$$\hat{D}_j(t) \equiv \left[\alpha_j(t) + i \frac{\partial \alpha_j(t)}{\partial t} \frac{\partial}{\partial \omega_j^\delta} \right]$$

$$\omega_j^\delta \equiv \omega_j - \Delta\omega_j$$

↑ Dispersion is built in

γ is recursive and contains the operator $\hat{D}_j(t)$.

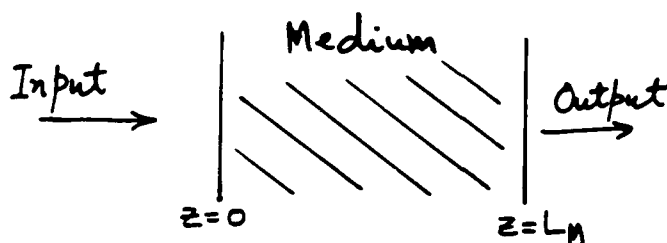
Temporal Coupled-Mode Equations

$$\frac{\partial \alpha_m(t)}{\partial t} = -i \Delta \omega_m \alpha_m(t) + \int_{V_M} d\bar{r} \rho_a C_m^*(\bar{r}) V_{\bar{r}}(t) e^{i(\omega_m - \Delta \omega_m)}$$

$$V_{\bar{r}}(t) = \rho_a \sum_{i=1}^{N_0} \frac{V_{\bar{r}_i}(t)}{N_0}$$

volume integral leads to mode coupling

Spatial Propagation



a) Quantum Method

$$E(x, y, z=0, t) = \sum_j C_j(x, y, z=0) \alpha_j(t)$$

$$\alpha_j(t) \xrightarrow{\substack{\uparrow \\ \text{paraxial treatment}}} E_j(x, y, z, t) = \sum_m C_m(\bar{r}) \alpha_m(t) e^{i K_m z}$$

coupled \uparrow mode equations

$$\text{Finally, } E(\bar{r}, t) = \sum_j C_j(x, y, z=0) E_j(\bar{r}, t)$$

b) Slowly-Varying-Envelope-Method

$$\hat{E}(z, t) = \sum_{l=1}^m \hat{\alpha}_l(z, t) e^{-i(\Omega_l t - K'_l z)} + \text{H.c.}$$

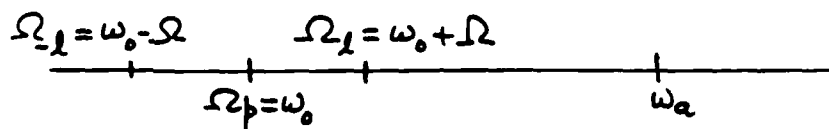
$$\hat{P}(z, t) = \sum_{l=1}^m \hat{P}_l(z, t) e^{-i(\Omega_l t - K'_l z)} + \text{H.c.}$$

$$\frac{\partial \hat{\alpha}_l}{\partial z} + \frac{1}{c} \frac{\partial \hat{\alpha}_l}{\partial t} = i \frac{K'_l}{2\epsilon_0} \hat{P}_l$$

$$P(z, t) = \mu P_a V_{\vec{k}_i}(t)$$

Wave-equation gives spatial-coupled-mode equations for $\alpha_l(z, t)$. Both methods agree.

Four-wave Mixing



$$(\Omega_l - \Omega_p) = (\Omega_p - \Omega_l) \quad \text{frequency-matching}$$

$$2\bar{K}'_p = \bar{K}'_l + \bar{K}'_{-l} \quad \text{phase-matching}$$

Spatial Coupled-Mode Equations

$$\frac{\partial \alpha_l}{\partial z} = -i \tilde{\gamma}_l \alpha_l + \tilde{\chi}_l e^{i\delta K'_l z} \alpha_{-l}^+ + \tilde{\Gamma}_l$$

$$\frac{\partial \alpha_{-l}}{\partial z} = i \tilde{\gamma}_{-l}^* \alpha_{-l}^+ + \tilde{\chi}_{-l}^* e^{-i\delta K'_{-l} z} \alpha_l + \tilde{\Gamma}_{-l}^+$$

$\{\tilde{\gamma}_l, \tilde{\gamma}_{-l}\}$	dispersion coefficients	} agree with: Fu & Sargent (1979) Boyd et al. (1981)
$\{\tilde{\chi}_l, \tilde{\chi}_{-l}\}$	nonlinear mixing coefficients	
$\{\tilde{\Gamma}_l, \tilde{\Gamma}_{-l}\}$	noise terms	

give correct resonance fluorescence spectrum, Mollow (1969)

$$\delta K'_l = (\bar{K}'_l + \bar{K}'_{-l} - 2\bar{K}'_p) \cdot \bar{e}_z$$

Squeezing spectra

$$\Delta_p \equiv \frac{\omega_a - \Omega_p}{\gamma_1} = \frac{\omega_a - \omega_0}{\gamma_1}$$

$$\delta_m = \frac{\Omega_m - \Omega_p}{\gamma_1} = \frac{\Omega}{\gamma_1}$$

$$\beta = \frac{\Omega_R}{\gamma_1} = \sqrt{I_p/I_a^0} = \sqrt{S_0}$$

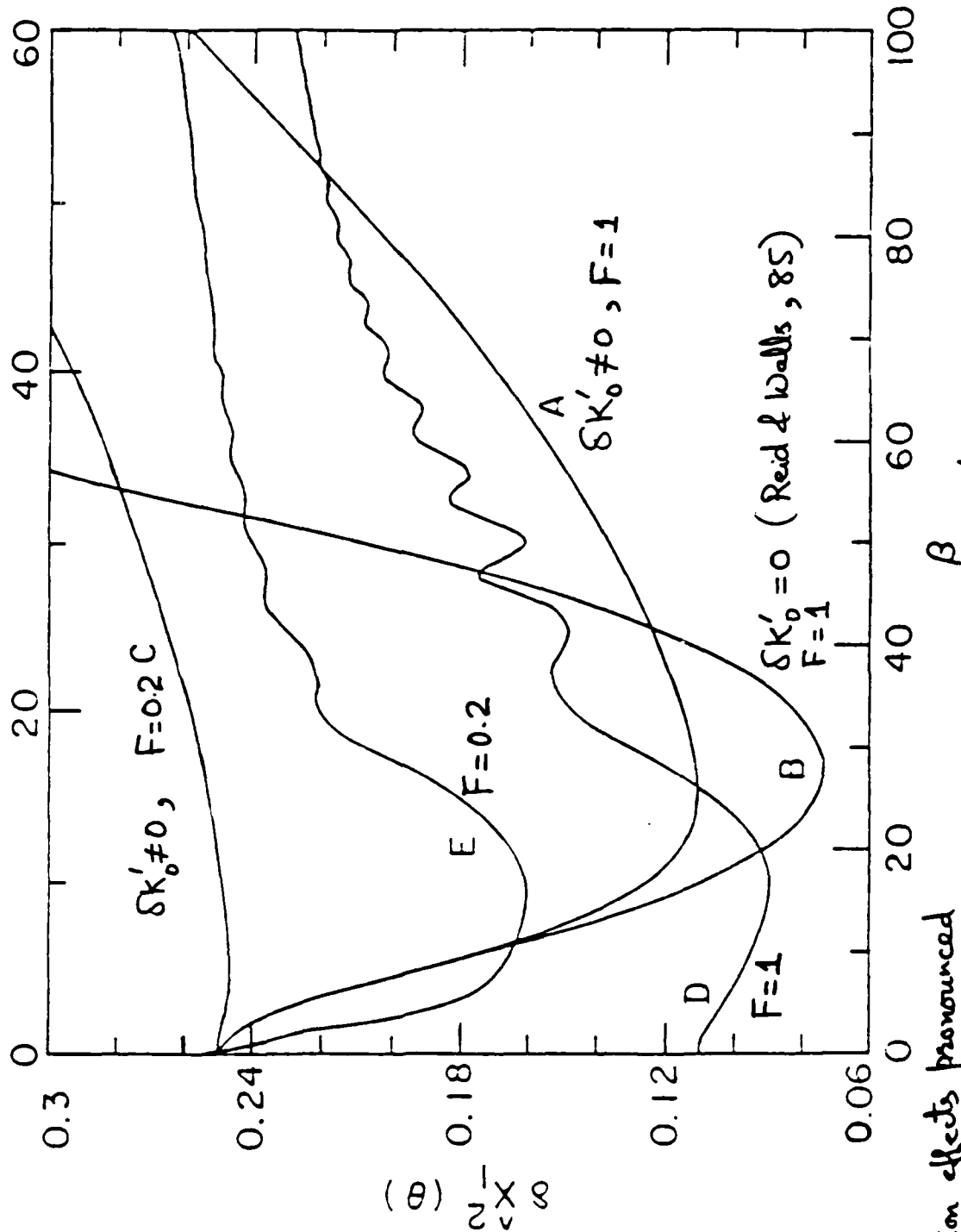
$$\delta \hat{X}_1^2(\theta) = \langle (\hat{X}_1(\theta) - \langle \hat{X}_1(\theta) \rangle)^2 \rangle ;$$

$$\hat{X}_1(\theta, \Omega) \equiv \frac{1}{2} (\alpha(\Omega, L_M) e^{-i\theta} + \alpha^\dagger(-\Omega, L_M) e^{i\theta}) + c.c.$$

• Pick θ for minimum $\delta \hat{X}_1^2(\theta)$

$\Delta p = 100, \alpha_0 L_M = 10^4$
 $\beta = 26$

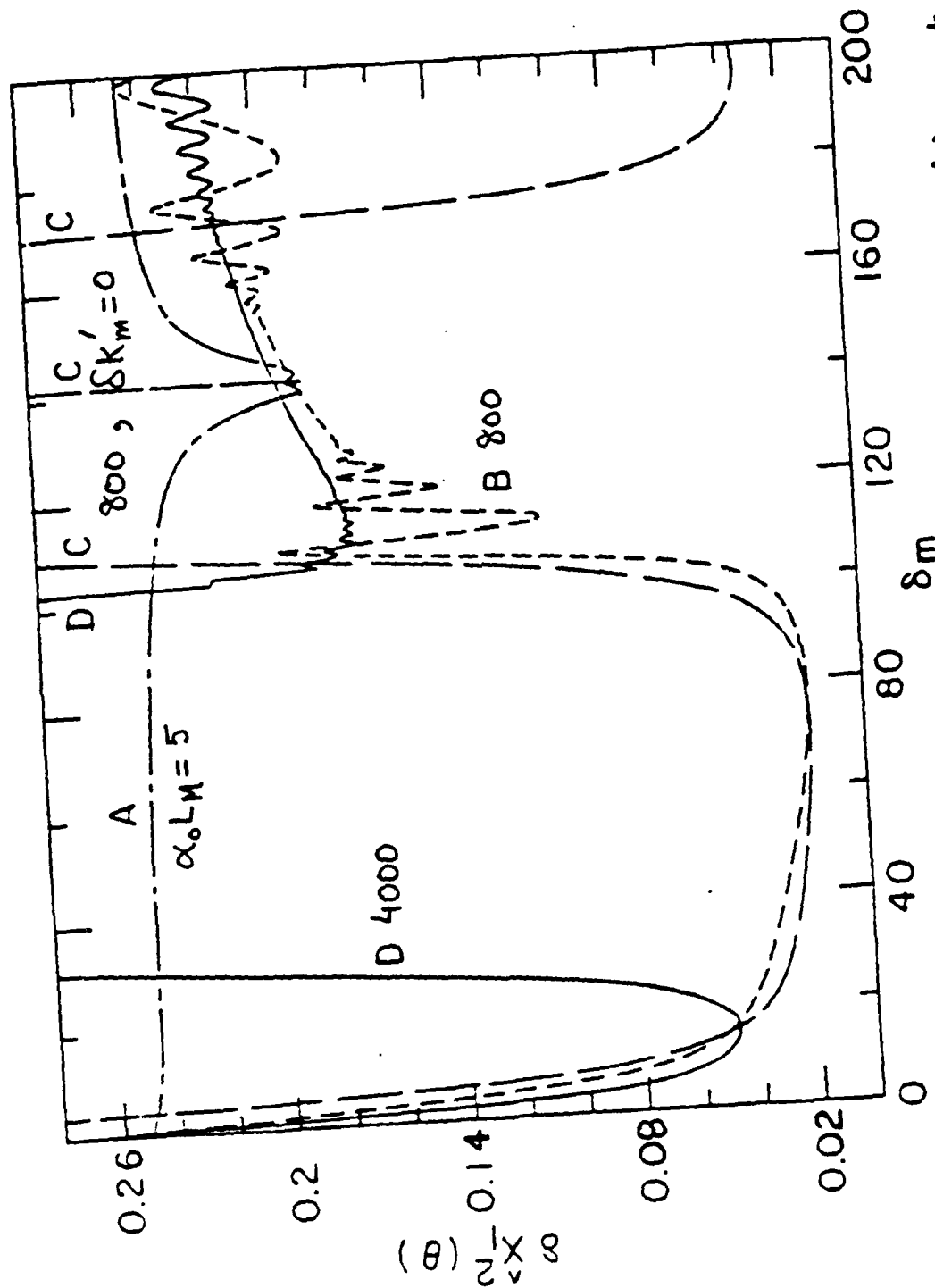
Nondegenerate
 δ_m



• Collision effects pronounced
 only at degenerate frequencies.

Squeezing Spectra

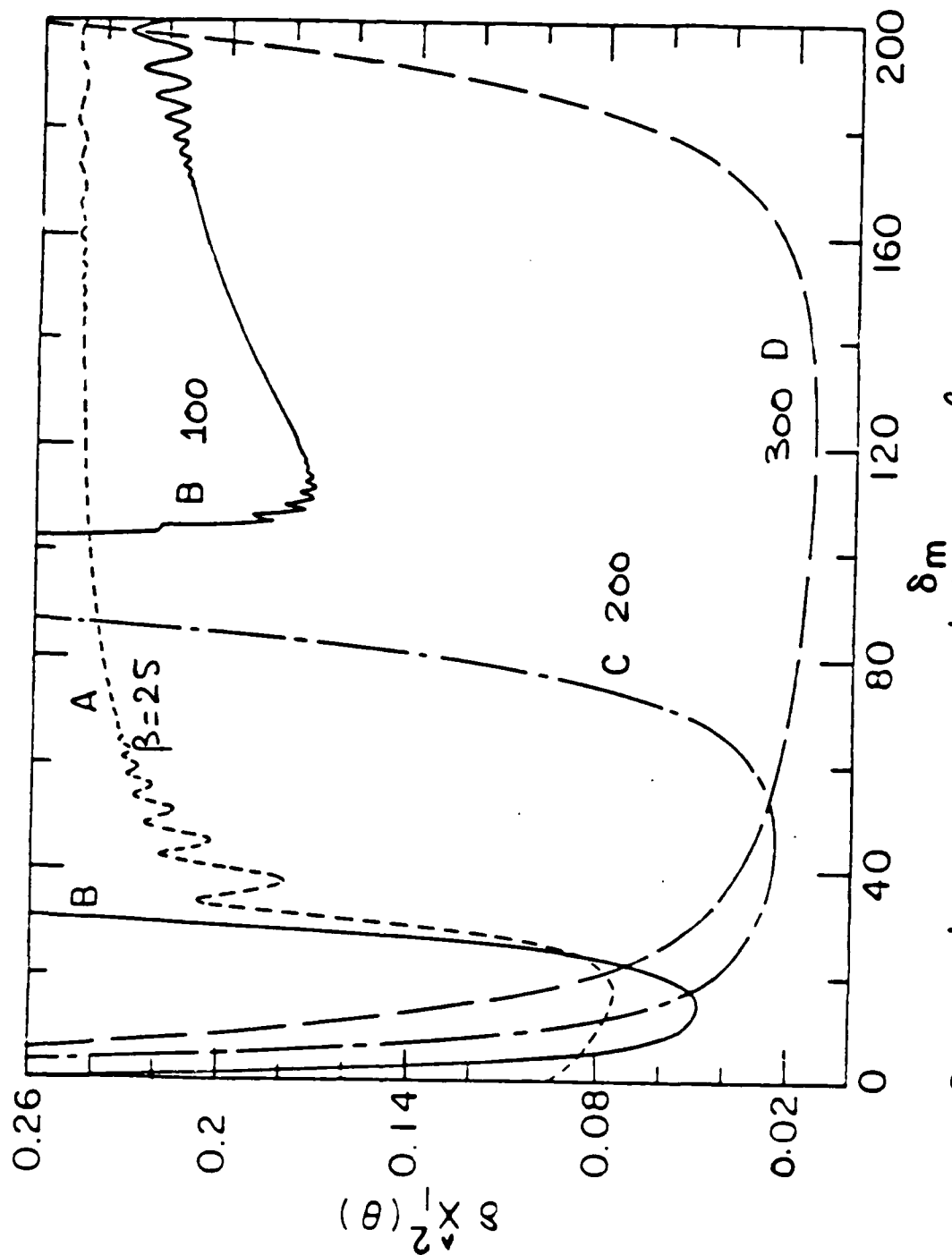
$$\Delta_p = 100, \beta = 100, F = 1$$



• Wiggles are due to phase-mismatch effects.

(17)

$\Delta\beta = 100, \alpha_0 L_M = 4000, F=1$
Squeezing Spectra



• Degenerate Squeezing at low β only

Maeda et al. Experiment

- Observed squeezing 4% (0.2 dB)
- Inferred squeezing 12% (0.6 dB)

$$\alpha_0 L_M = 5 \times 10^4$$

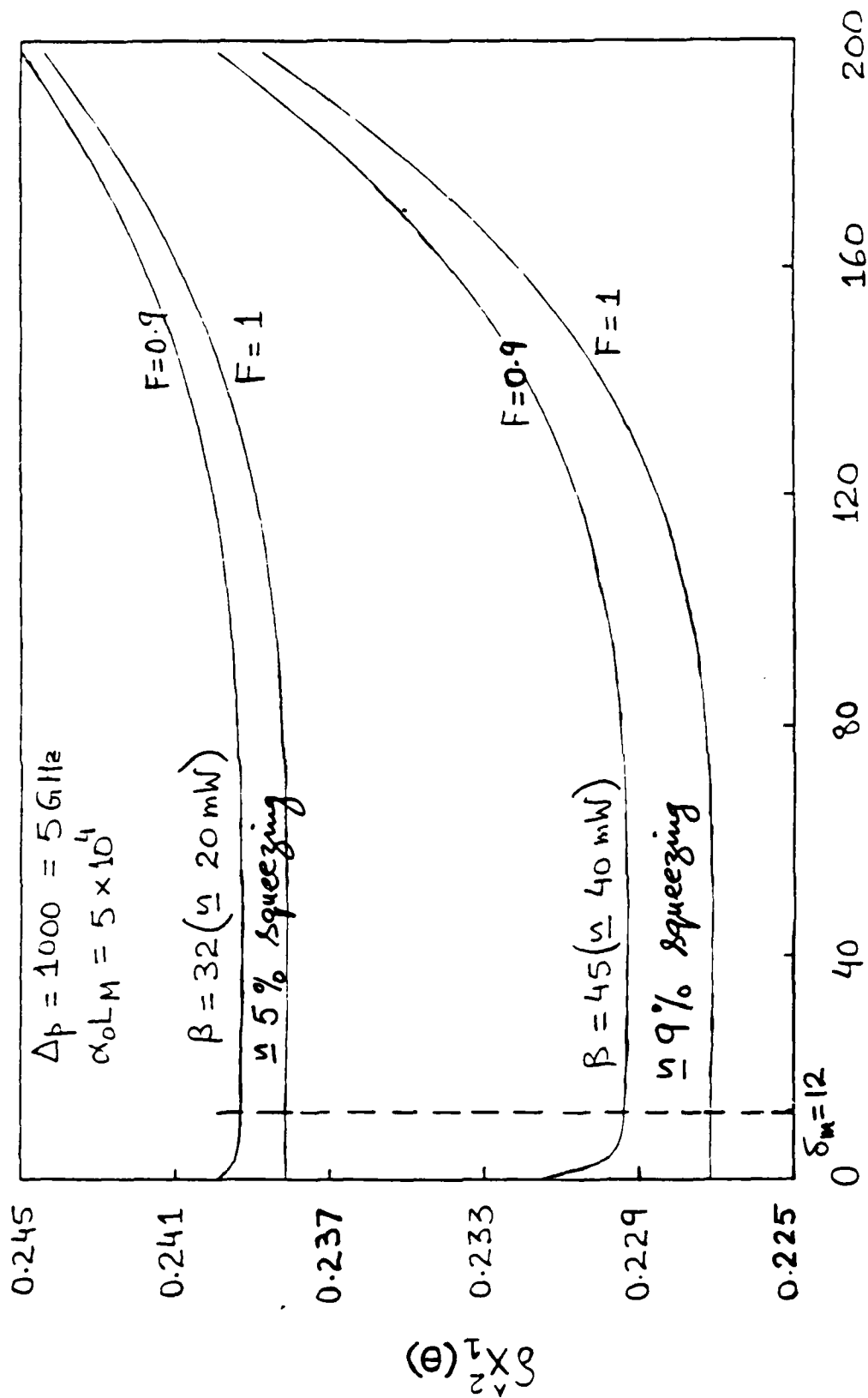
$$\beta = \sqrt{I/I_0} = \sqrt{1000} \approx 32 \quad [20 \text{ mW focussed to } 0.5 \text{ mm dia.}]$$

$$\delta_m = \frac{58 \text{ MHz}}{\gamma_1} \approx 12$$

$$\text{For sodium } \gamma_1 \approx 5 \text{ MHz}$$

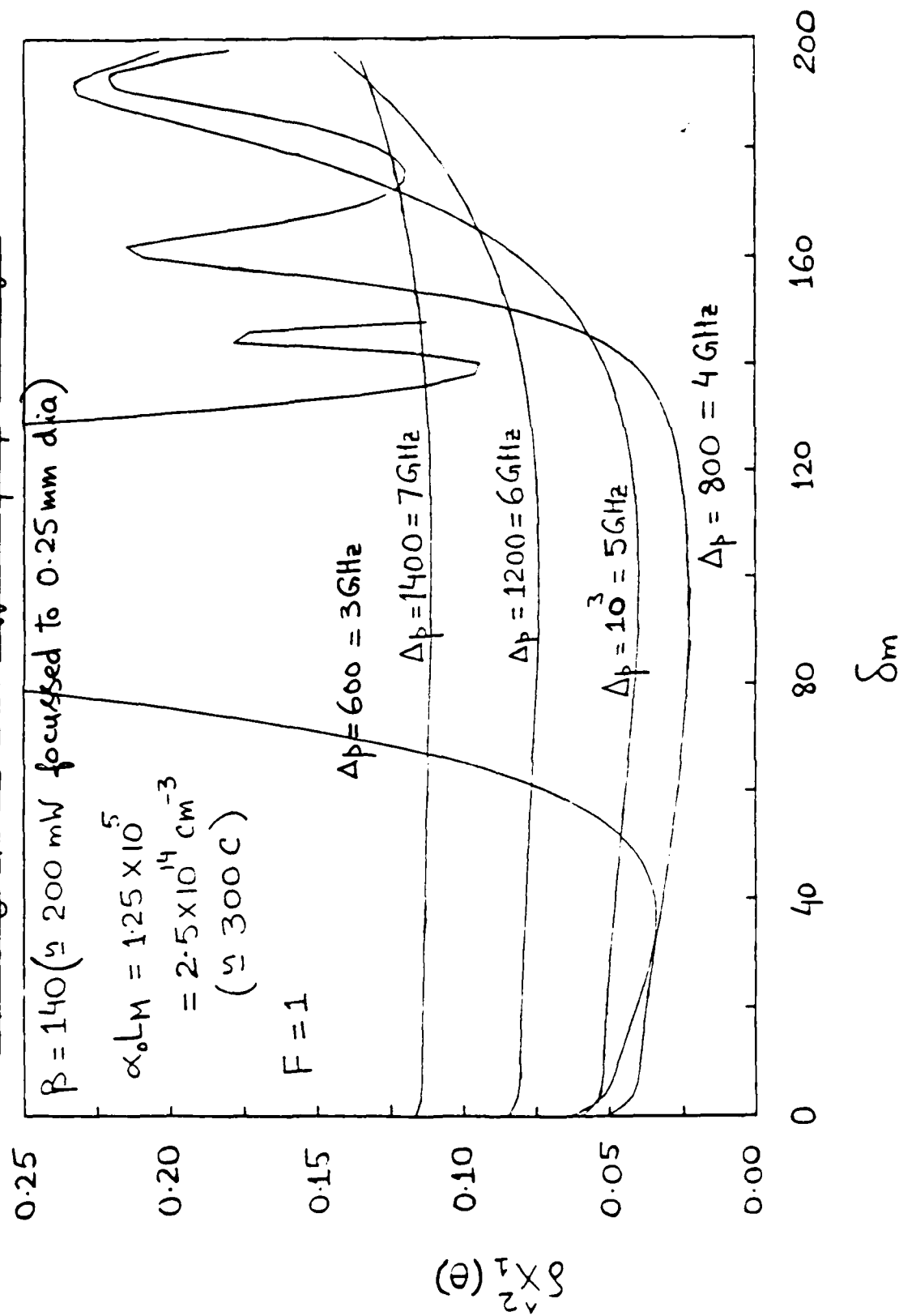
$$\Delta p = \frac{5 \text{ GHz}}{\gamma_1} \approx 1000$$

Squeezing spectra under conditions of Maeda et al. experiment



• Due to self-focussing, intensity may be higher.

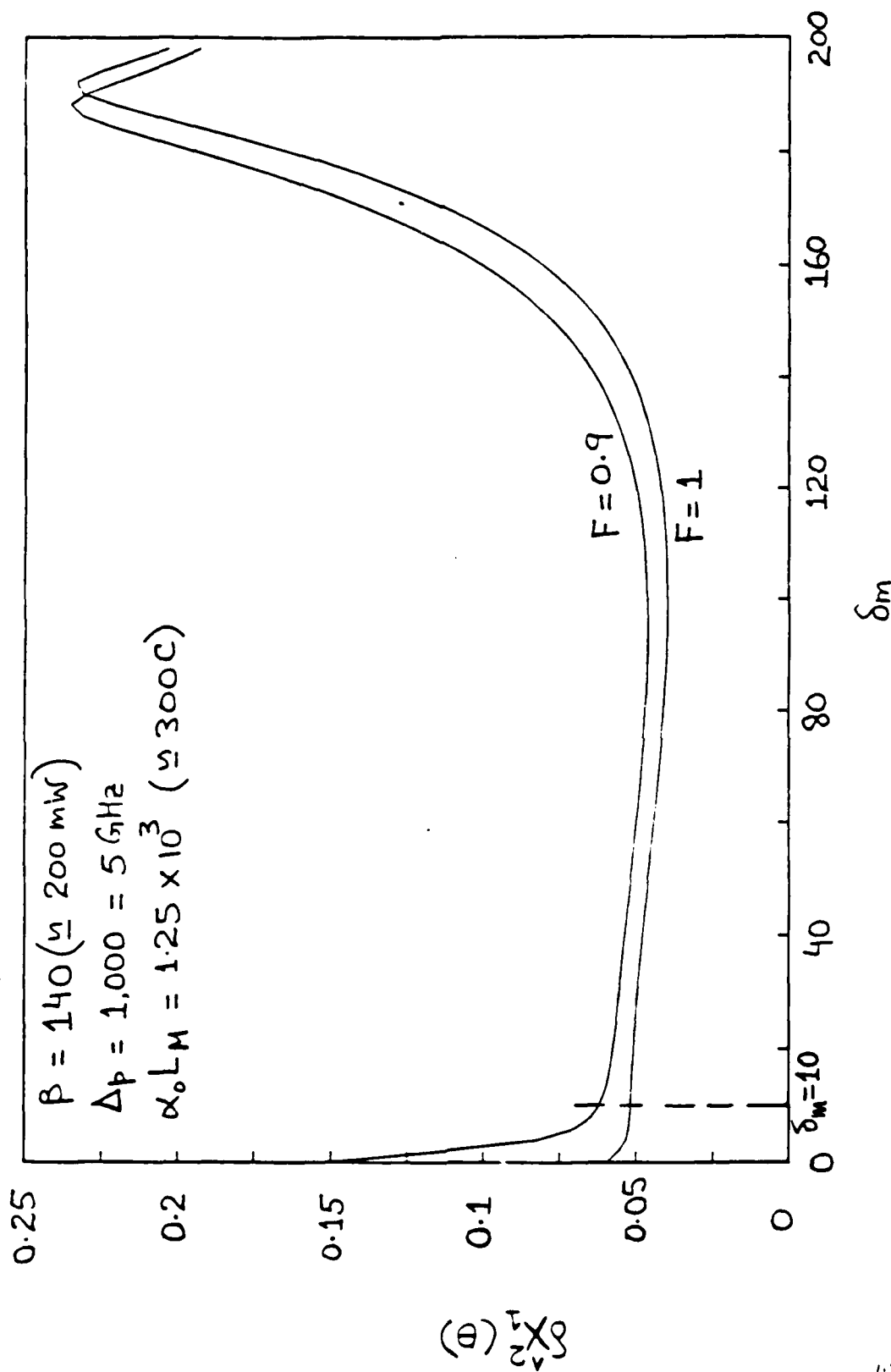
Squeezing spectra for different pump detunings



• Above conditions are achievable in the lab.

(2)

Effect of collisions on the sodium experiment



• At least a factor of 4 squeezing between 50 to 700 MHz

Conclusions

- Maeda et al. experiment is in good agreement with theory.
- Atleast a factor of four squeezing should be achievable with available dye laser power.
- Doppler broadening, optical pumping, and self-focussing effects may limit observable squeezing.

References

1. M.W. Maeda, P. Kumar, and J.H. Shapiro, Opt. Lett. 12, 161 (1987).
2. S.-T. Ho, P. Kumar, and J.H. Shapiro, Phys. Rev. A 35, 3982 (1987).

GENERATING SQUEEZED MICROWAVE RADIATION
WITH A JOSEPHSON PARAMETRIC AMPLIFIER

B. Yurke
AT&T Bell Laboratories
Murray Hill, New Jersey 07974

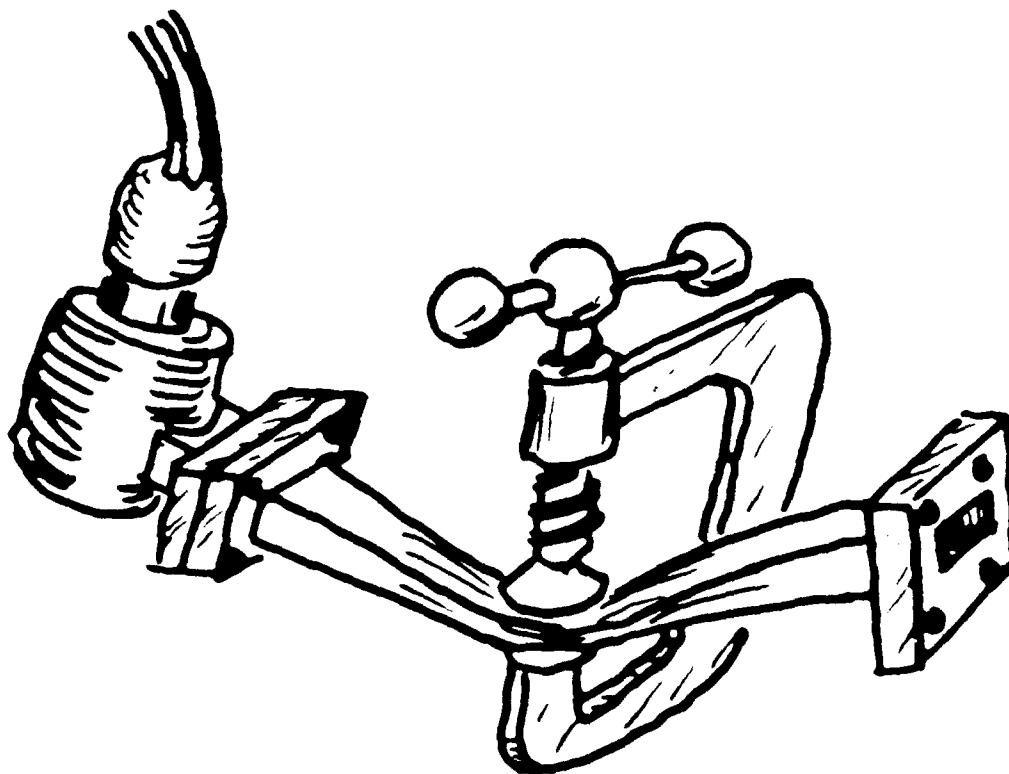
In an effort to generate squeezed microwave radiation at 20 GHz via a Josephson parametric amplifier, we have recently demonstrated a factor of 2 squeezing of 4.2K thermal noise. A room temperature mixer with a 660K noise temperature was employed for homodyne detection. The overall detector system noise temperature (including waveguide losses) was 2100K. In order to rule out detector saturation effects, a probe signal was injected into the mixer to monitor the detector system gain. Since at 4.2K one is only an order of magnitude from the quantum noise floor, we are hopeful of observing quantum noise squeezing when the device is cooled well below .5K.

Generating Squeezed Microwave Radiation with a Josephson Parametric Amplifier

B. Yurke, P.G. Kaminsky, R.E. Miller;
AT&T Bell Laboratories

E.A. Whittaker; Stevens Institute

A.D. Smith, A.H. Silver, R.W. Simon;
TRW Space & Technology Group.



DO NOT AFFIX OVERLAYS ALONG THIS SURFACE

UNITED STATES - JAPAN SEMINAR ON QUANTUM MECHANICAL
ASPECTS OF QUANTUM EL (U) MASSACHUSETTS INST OF TECH
CAMBRIDGE RESEARCH LAB OF ELECTRON
J H SHAPIRO ET AL OCT 87 N00014-87-G-0198 F/G 20/3

67

AD-A186 938

UNCLASSIFIED

J H SHAPIRO ET AL

OCT 87

N00014-87-G-0198

F/G 28/3

NL

1·0

1·1

1·25

EEEEEE

1·4

2·8

3·15

3·5

4·0

4·5

2·5

2·2

2·0

1·8

1·6

SQUEEZED STATE GENERATION AT 20 GHz

Motivation:

- (1) One wants squeezed state sources at as many frequencies as possible.
- (2) Study Rydberg atoms interacting with squeezed radiation
 - (a) level shifts.
 - (b) fluorescence spectrum line narrowing.
- (3) Study quantum behavior of Josephson circuits.

Why 20 GHz:

- (1) $h\nu = kT$
for $T = 1K$ and $\nu = 21$ GHz.
- (2) K-band waveguide is of a convenient size to fit in a cryostat.
- (3) Josephson technology works well here.

TOP
DO NOT AFFIX OVERLAYS ALONG THIS SURFACE

Optics News

JUNE 1987 ■ VOLUME 13, NUMBER 6

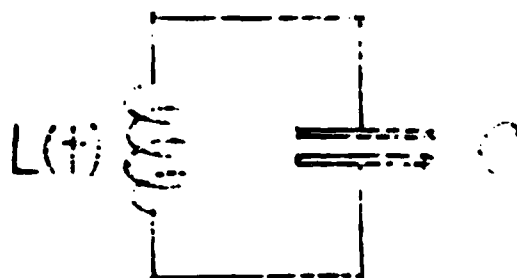
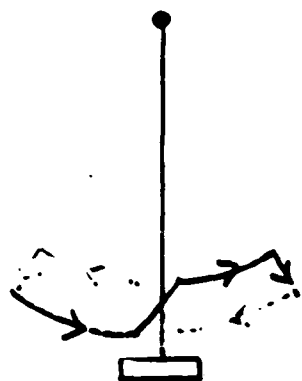


-479-

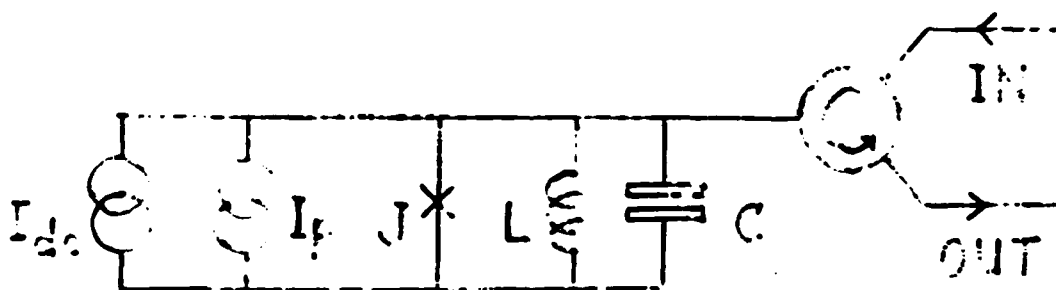
Squeezed light and
the parametric swing

JOSEPHSON PARAMETRIC AMPLIFIER

TOP
DO NOT AFFIX OVERLAYS ALONG THIS SURFACE

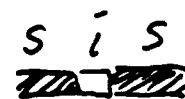


$$\frac{d}{dt} \left(I(t) \frac{d\phi}{dt} \right) + K\phi = 0 \quad \frac{d}{dt} \left(L(t) \frac{dQ}{dt} \right) + \frac{Q}{C} = 0$$

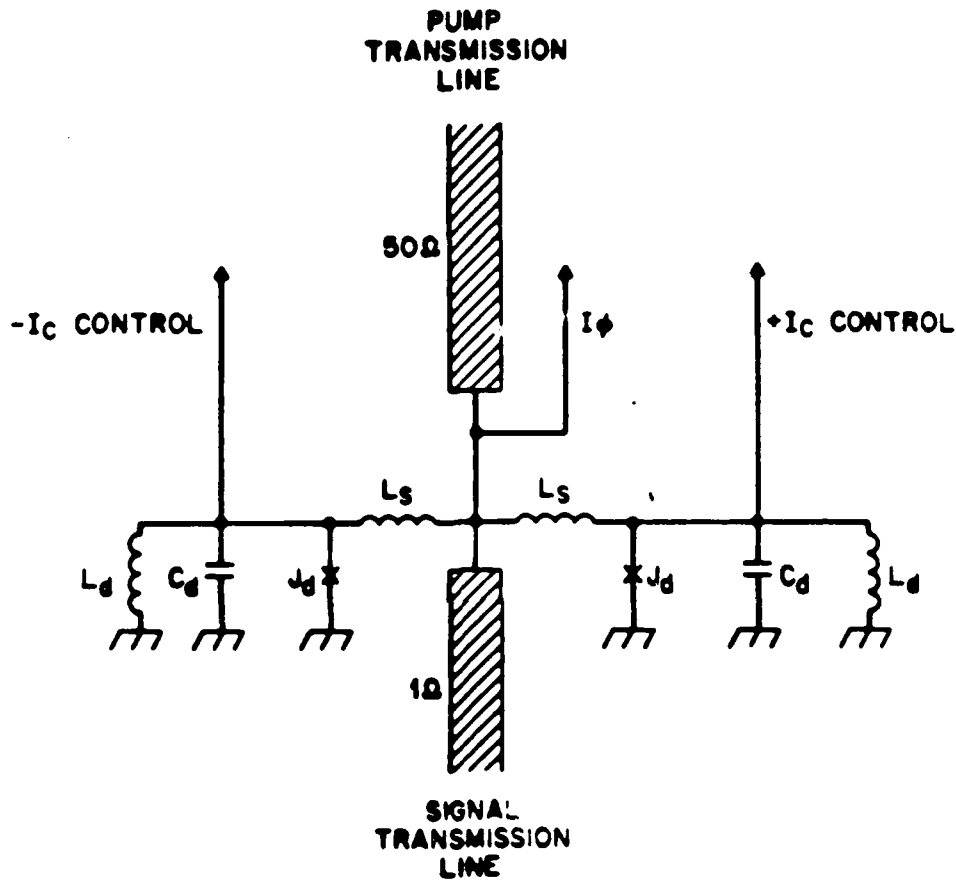


Josephson inductance

$$L_J(I) = \frac{\hbar}{2eI_c} \left[\frac{\sin^{-1}(I/I_c)}{I/I_c} \right]$$



THE JOSEPHSON PARAMETRIC AMPLIFIER



DO NOT AFFIX OVERLAYS ALONG THIS SURFACE

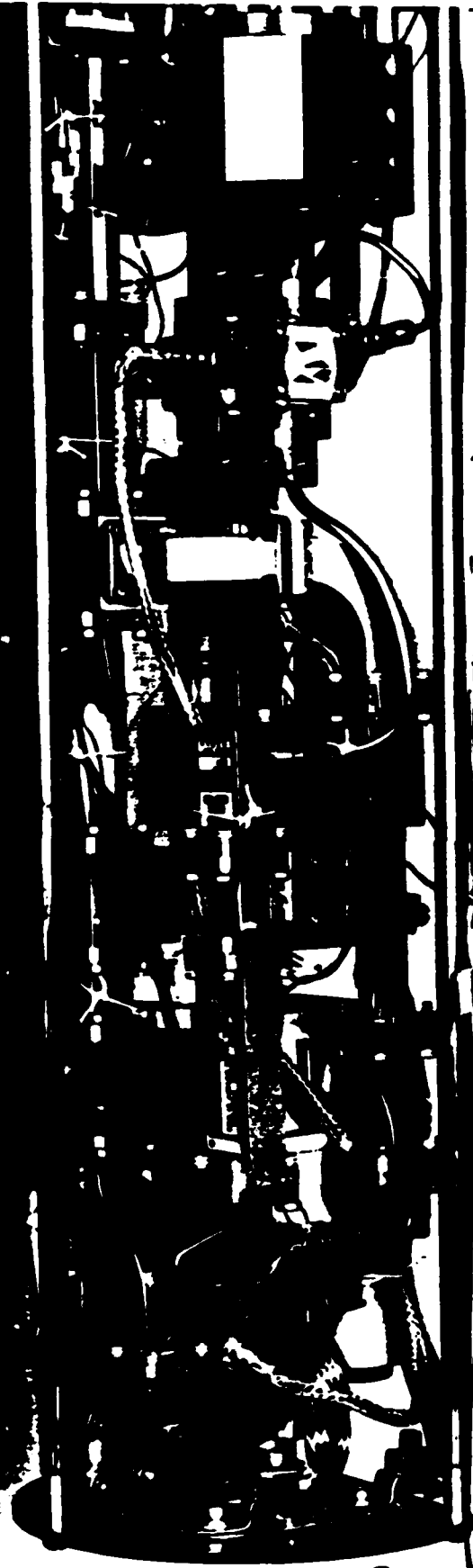
Junction technology Nb-AIO-Nb

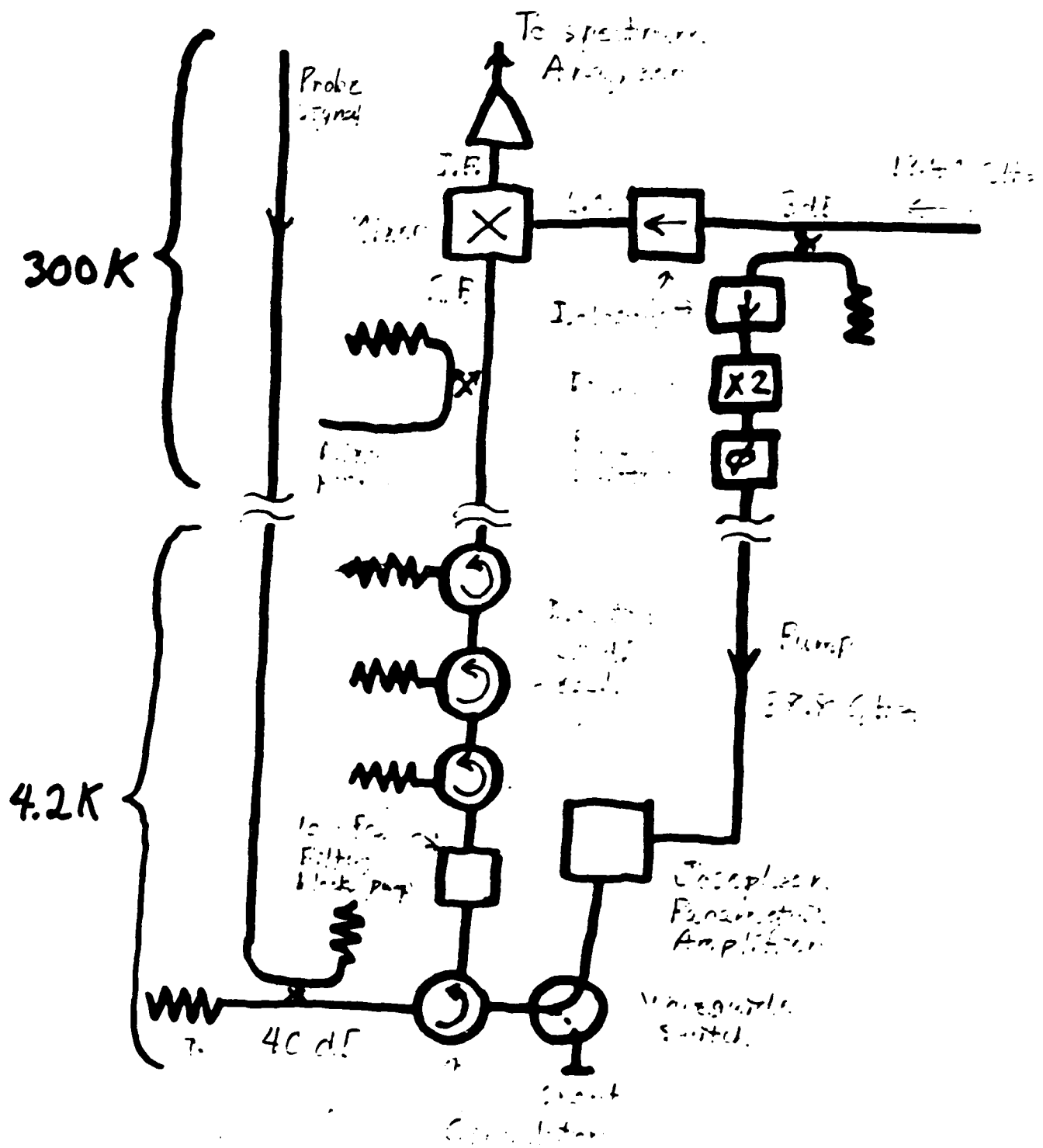
$$f_s = 20 \text{ GHz}$$

Novel Features:

- (1) Two junctions employed to tune critical current via I_c^- , I_c^+ control lines.
- (2) Four-Stage Impedance Transformer (1 GHz passband).





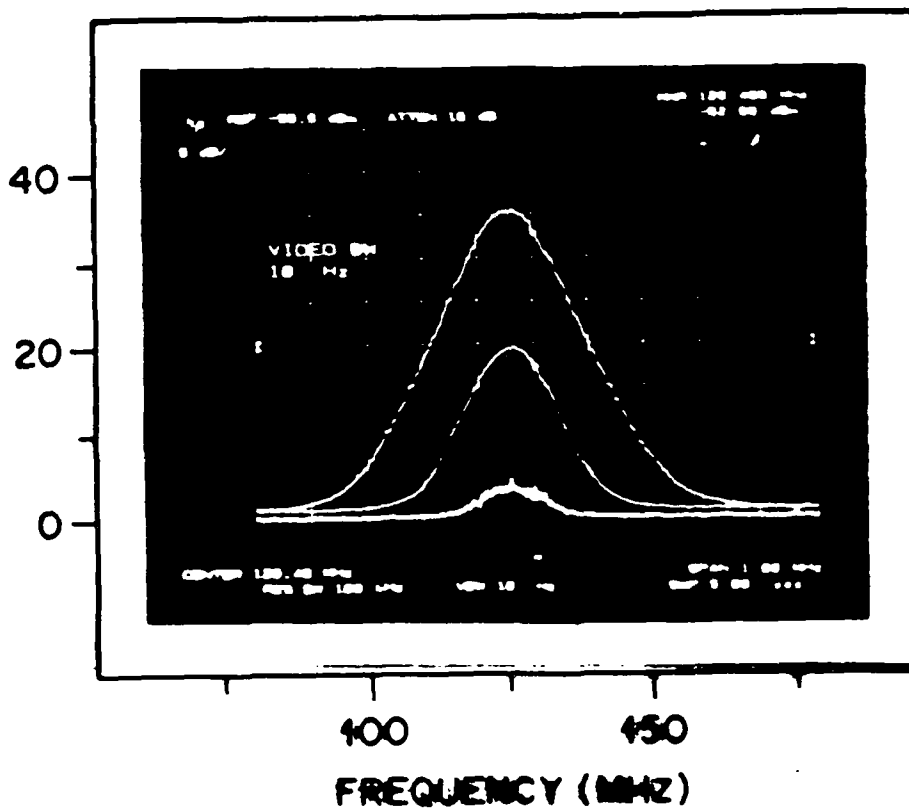


Sold body, source of 4.2K thermal noise when in the 40 dB attenuator.

VG. NO. _____

TOP
DO NOT AFFIX OVERLAYS ALONG THIS SURFACE

RELATIVE SIGNAL POWER (dB)



17 dB CLASSICAL SQUEEZING

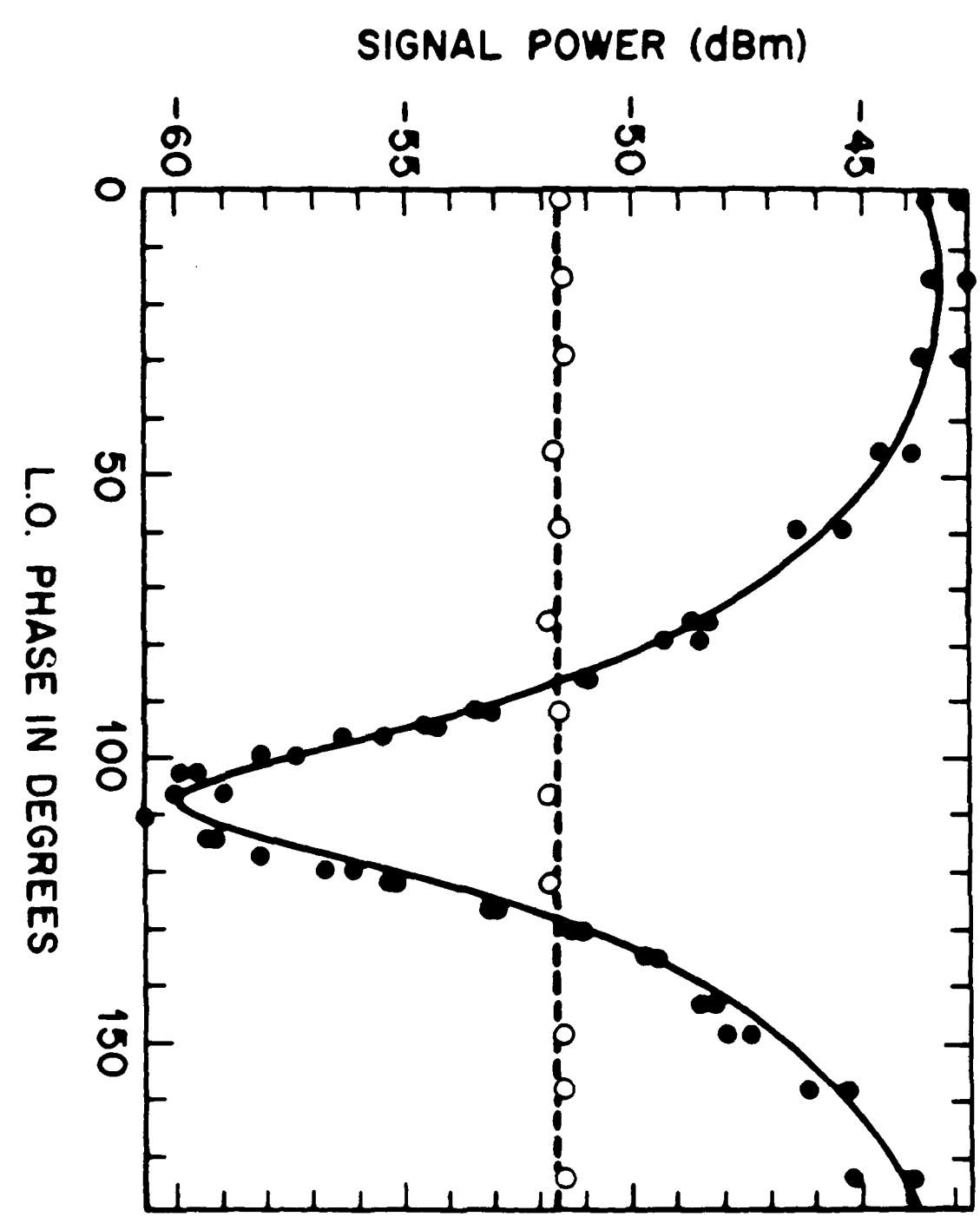
Red - Amplified Component

White - Pump Off

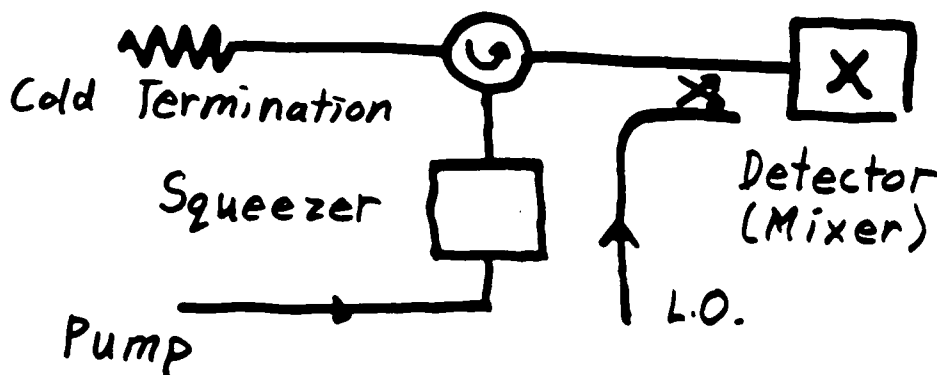
Green - Squeezed Component

F-9148 (6-85)

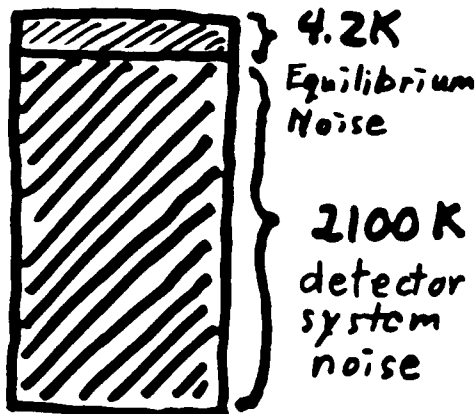
CHARACTERISTICS OF THE SURFACE



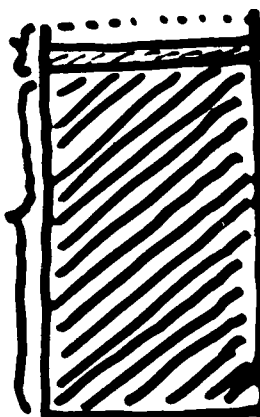
Detecting Squeezing with Noisy Detectors



Pump off



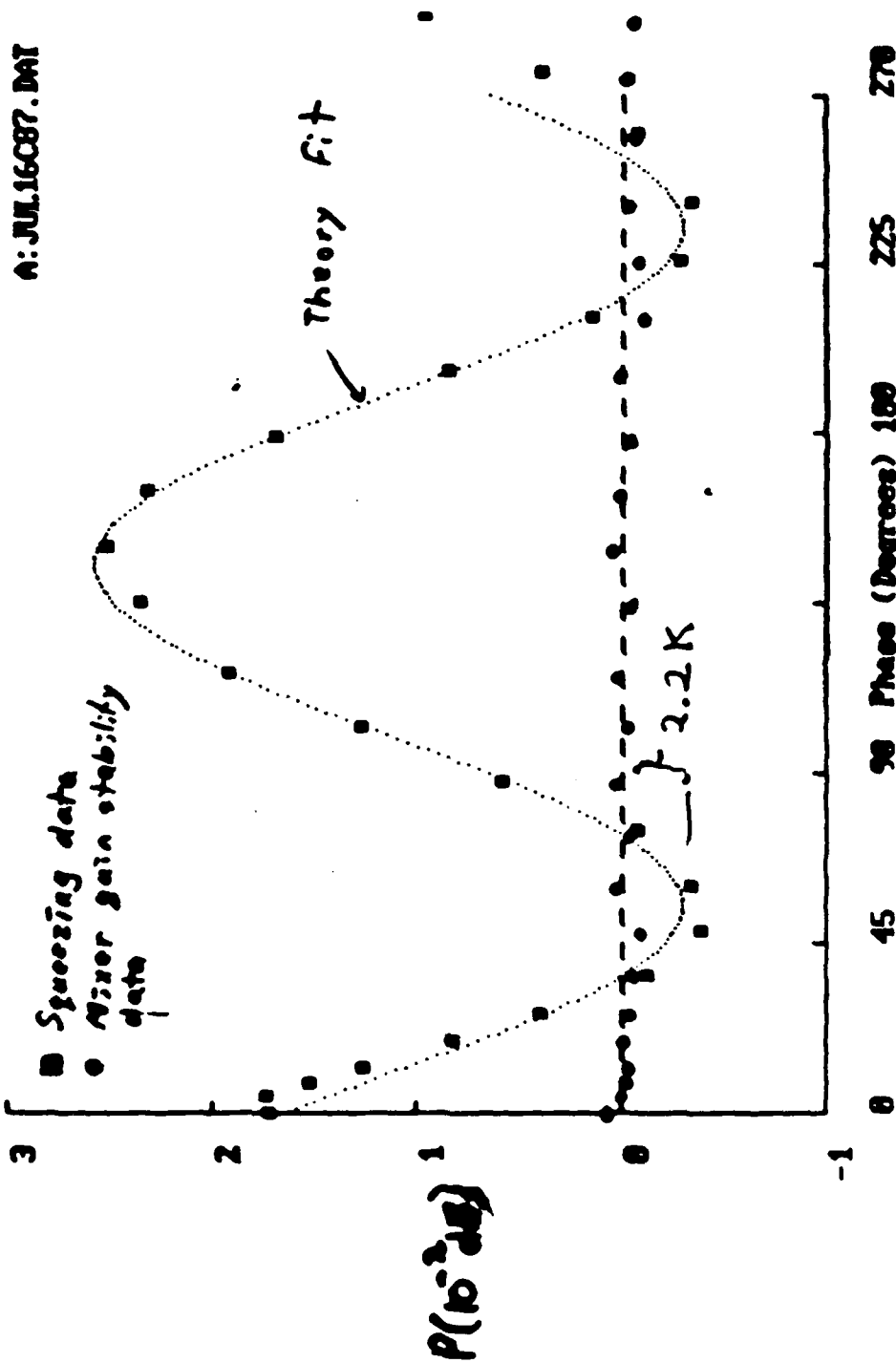
Pump on



We are looking for changes in the noise floor of 2 parts in 10^{-4} or changes of the order of 10^{-3} dB

SEQUENCE NO. _____

A: JUL16C87. DAT



-488-

DO NOT AFFIX OVERLAYS ALONG THIS SURFACE

TOP

12

Detecting Squeezed States by Cross-Correlation*

Z.Y. Ou, C.K. Hong and L. Mandel

Department of Physics and Astronomy
University of Rochester
Rochester, New York 14627

Abstract

It is shown that squeezed states can be detected by cross-correlation measurements of the outputs of two detectors in a homodyne experiment, and that squeezing shows up as a positive correlation. The technique offers some of the same advantages as the balanced homodyne technique of Yuen and Chan, without the need to balance the detectors.

* This work was supported by the National Science Foundation and by the Office of Naval Research. A paper on this work is to appear in The Physical Review A.

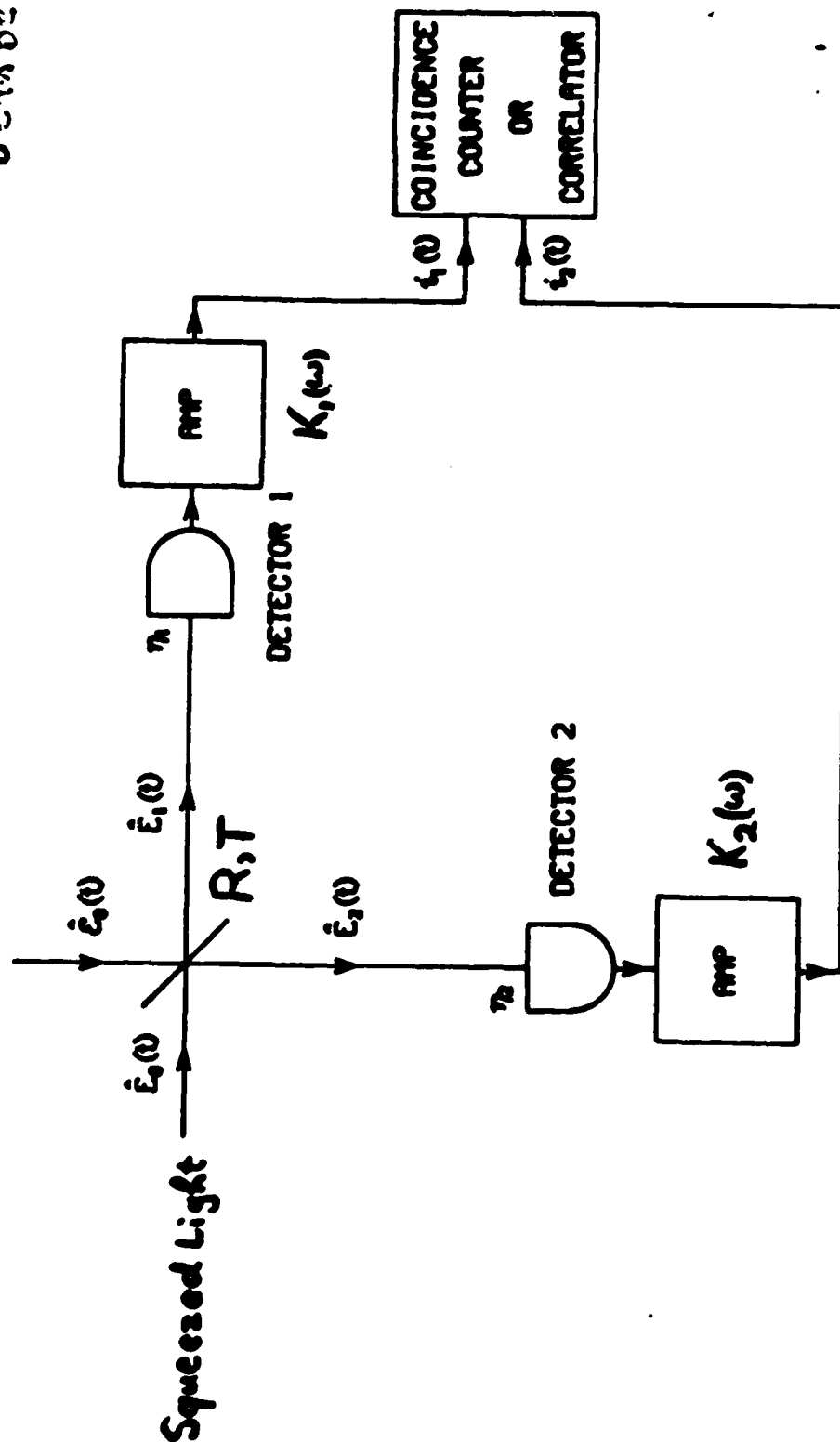
Advantages of the Cross-Correlation Technique

- (a) the method is insensitive to detector after-pulsing
- (b) squeezing in the full sense can be measured by photon coincidence counting, with few photons
- (c) no balancing of the two detectors is required
- (d) the method has some of the virtues of the balanced homodyne method for cancelling local oscillator fluctuations.

Coherent Field from
Local Oscillator

$$E_0(t) = |E_0| e^{-i(\omega_0 t - \theta)}$$

θ can be varied



Homodyne Experiment

Beam Splitter Fields

Outputs from Beam Splitter



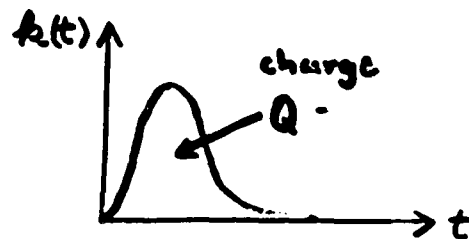
$$\left. \begin{aligned} \hat{E}_1^{(+)}(t) &= \sqrt{T} \hat{E}_0^{(+)}(t) + i\sqrt{R} \hat{E}_0^{(+)}(t) \\ \hat{E}_2^{(+)}(t) &= i\sqrt{R} \hat{E}_0^{(+)}(t) + \sqrt{T} \hat{E}_0^{(+)}(t) \end{aligned} \right\} (1)$$

\hat{E}_1 & \hat{E}_2 obey same commutation relations as \hat{E}_0 and \hat{E}_0 when $R+T=1$.

The local oscillator field is in a coherent state, with eigenvalue

$$E_0(t) = |E_0| e^{-i(\omega_0 t - \theta)}$$

Photocurrents & their Moments



Currents

$$i_j(t) = \sum_{\ell} k_j(t-t_{\ell}) \quad (j=1,2)$$

Mean Current

$$\langle i_j \rangle = \underset{\substack{\uparrow \\ \text{detector}}}{\eta_j} Q_j \langle \hat{E}_j^{(-)}(t) \hat{E}_j^{(+)}(t) \rangle = \eta_j Q_j \langle \hat{I}_j \rangle \quad (j=1,2) \quad (2)$$

Cross-Correlation

$$\langle i_1(t) i_2(t) \rangle = \iint_{-\infty}^{\infty} k_1(t-t_{\ell}) k_2(t-t_m) P_{12}(t_{\ell}, t_m) dt_{\ell} dt_m \quad (3)$$

with

$$P_{12}(t_{\ell}, t_m) = \eta_1 \eta_2 \langle T : \hat{I}_1(t_{\ell}) \hat{I}_2(t_m) : \rangle \quad (4)$$

Mean Intensities & Intensity Correlations

From Eq(1) for the beam splitter

$$\langle \hat{I}_1(t) \rangle = R|\mathcal{E}_0|^2 + i|\mathcal{E}_0|\sqrt{RT}\langle \hat{E}_0^{(1)}(t) \rangle e^{-i(\omega_1 t - \theta)} + c.c. + \dots$$

$$\langle \hat{I}_2(t) \rangle = T|\mathcal{E}_0|^2 - i|\mathcal{E}_0|\sqrt{RT}\langle \hat{E}_0^{(1)}(t) \rangle e^{-i(\omega_1 t - \theta)} + c.c. + \dots \quad (5)$$

and to $O(|\mathcal{E}_0|^2)$

$$\langle T: \Delta \hat{I}_1(t) \Delta \hat{I}_2(t+\tau) : \rangle = -RT|\mathcal{E}_0|^2 T_{11}(\tau, \theta + \pi/2) \quad (6)$$

\nearrow
 autocorrelation of
 one quadrature

Definition of $T_{11}(\tau, \beta)$:

Resolve $\hat{E}_0(t)$ into two quadratures

$$\hat{E}_0(t) = \hat{E}_0^{(1)}(t) \cos(\omega_1 t - \beta) + \hat{E}_0^{(2)}(t) \sin(\omega_1 t - \beta)$$

then

$$T_{11}(\tau, \beta) \equiv \langle T: \Delta \hat{E}_0^{(1)}(t) \Delta \hat{E}_0^{(1)}(t+\tau) : \rangle$$

If $\hat{E}_0^{(1)}$ is squeezed, $T_{11}(0, \beta) < 0$

Photoelectric Cross-Correlations

By combining eqs. (3), (4) & (6) we obtain

$$\langle \Delta i_1(t) \Delta i_2(t) \rangle = -\eta_1 \eta_2 R T |\mathcal{E}_0|^2 \iint_{-\infty}^{\infty} k_1(t') k_2(t'') \Gamma_{11}(t'-t'', \theta + \frac{\pi}{2}) dt' dt'' \quad (7)$$

$$= -\eta_1 \eta_2 R T |\mathcal{E}_0|^2 \frac{1}{2\pi} \int_{-\infty}^{\infty} K_1(\omega) K_2(\omega) \Phi_{11}(\omega, \theta + \frac{\pi}{2}) d\omega \quad (8)$$

where

$$k_j(t) = \frac{1}{2\pi} \int_{-\infty}^{\infty} K_j(\omega) e^{-i\omega t} d\omega \quad (j=1,2)$$

$$\Gamma_{11}(\tau, \theta) = \frac{1}{2\pi} \int_{-\infty}^{\infty} \Phi_{11}(\omega, \theta) e^{-i\omega \tau} d\omega$$

For fast response detectors (7) is more appropriate

For sharply tuned detectors (8) is more appropriate

Fast Response Detectors : Coincidences

If the response $k_j(t)$ of detector j is very short compared with range of $T_{11}(\tau, \theta)$, then eq.(7) reduces to

$$\langle \Delta i_1(t) \Delta i_2(t) \rangle = -\eta_1 \eta_2 R T |E_0|^2 Q_1 Q_2 T_{11}(0, \theta + \frac{\pi}{2}) \quad (9)$$

This is positive if $\hat{E}_0^{(1)}$ is squeezed in the full sense, in which case $T_{11}(0, \theta + \frac{\pi}{2}) < 0$.

If $\langle \hat{E}_0 \rangle = 0$, and separate measurements are made with squeezed field turned off, the effects of local oscillator fluctuations cancel by subtraction.

Effects of Local Oscillator Fluctuations

If there are fluctuations of the local oscillator
then in eq(9)

$$|E_0|^2 \rightarrow \langle |E_0|^2 \rangle$$

and, in addition, there are extra terms in

$$\langle (\Delta |E_0|^2)^2 \rangle \text{ and}$$

$$\langle \Delta |E_0|^2 \Delta E_0 \rangle, \langle (\Delta |E_0|)^2 \rangle, \langle (\Delta E_0)^2 \rangle, \text{ and c.c.}$$

The effect of the first can be cancelled by
making separate measurements with squeezed
light turned off and subtracting.

The effects of the other terms vanish if

$$\langle \hat{E}_0^{(+)}(t) \rangle = 0$$

Offers some of the same benefits as balanced homodyne scheme
of Yuen & Chan

Spectral Analysis

If the detector amplifiers are sharply tuned to frequency ω_F within $\delta\omega$, with

$\delta\omega \ll$ bandwidth of $\Phi_{11}(\omega, \theta)$, then eq. (8) reduces to

$$\langle \Delta i_1(t) \Delta i_2(t) \rangle = -\gamma_1 \gamma_2 RT |E_0|^2 \Phi_{11}(\omega_F, \theta, \frac{\pi}{2}) \frac{1}{\pi} \int_{\omega_F - \delta\omega}^{\omega_F + \delta\omega} |K_1(\omega) K_2(\omega)| d\omega \quad (10)$$

This is positive if there is squeezing at frequency ω_F ,

$$\Phi_{11}(\omega_F, \alpha) < 0.$$

In all cases squeezing is manifest in the presence of positive cross-correlations

Different Categories of Squeezing

Quadratures $\hat{E}_0^{(1)}(t)$ and $\hat{E}_0^{(2)}(t)$.

$$\hat{E}_0(t) = \hat{E}_0^{(1)}(t) \cos(\omega_1 t - \beta) + \hat{E}_0^{(2)}(t) \sin(\omega_1 t - \beta)$$

(1) If

$$\langle : (\Delta \hat{E}_0^{(1)})^2 : \rangle = T_{11}(0, \beta) < 0,$$

then $\hat{E}_0^{(1)}(t)$ is squeezed in the full sense.

(2) Let

$$\Phi_{11}(\omega, \beta) = \int_{-\infty}^{\infty} T_{11}(\tau, \beta) e^{i\omega\tau} d\tau$$

If

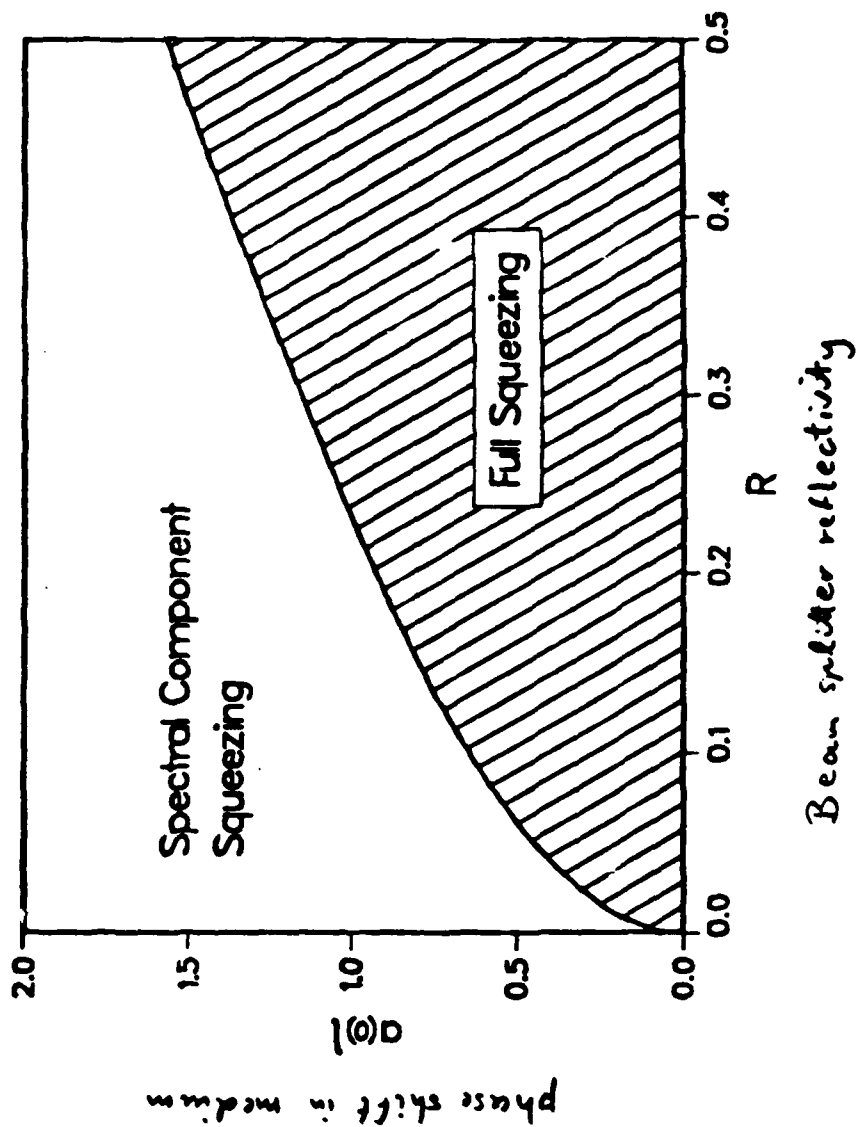
$$\Phi_{11}(\omega, \beta) < 0,$$

then the field is squeezed at frequency ω .

(3) If $\hat{E}_0^{(1)}$ is squeezed in the full sense, but $\Phi_{11}(\omega) > 0$ at some frequencies, the squeezing is inhomogeneous.

(4) If $\hat{E}_0^{(1)}$ is not squeezed in the full sense, but $\Phi_{11}(\omega) < 0$ for some ω , then we have spectral component squeezing

Squeezing in 4-wave Mixing



Degree of Squeezing

If $\hat{E}_1^{(w)}$ is squeezed at frequency w ,

$$q(w) \equiv \left(\frac{\eta_1 \eta_2}{\alpha_1 \alpha_2} \right)^{1/2} \Phi_{\eta}(w)$$

$q(w)$ is independent
of detector
efficiency

$-1 \leq q(w) \leq 0$ can be obtained from cross-correlation,
together with auto-correlation with squeezed light
blocked, when detectors collect all the light;

$$q(w) = -(\alpha_1 \alpha_2 R T)^{-1/2} \frac{\langle \Delta i_1 \Delta i_2 \rangle}{[\langle (\Delta i_1)^2 \rangle \times \langle (\Delta i_2)^2 \rangle]_{\text{blocked}}^{1/2}}$$

(11)

quantum efficiencies

Conclusions

1. Squeezing in the full sense and spectral component squeezing result in positive cross-correlations in a homodyne experiment.
2. Squeezing in the full sense can be identified by photon coincidence counting.
3. The correlation technique is largely independent of detector after-pulsing.
4. The technique has some of the virtues of the balanced homodyne method for cancelling out local oscillator fluctuations.
5. No balancing of the two detector signals is required.

WHAT HAS BEEN DONE AND WHAT WILL BE DONE
BY SUBNATURAL LINEWIDTH SPECTROSCOPY

Hiroshi Takuma, Kazuko Shimizu

Institute for Laser Science and Department of Engineering Physics
University of Electro-Communications, 1-5-1 Chofugaoka, Chofu-shi Tokyo 182 Japan
and Fujio Shimizu

Department of Applied Physics, Faculty of Engineering
University of Tokyo, Hongo, Bunkyo-ku, Tokyo 113 Japan

1. INTRODUCTION

Reduction of linewidth is an essential approach in high resolution spectroscopy. Several methods to remove or reduce inhomogeneous linewidth have been developed resulting in a drastic improvement in the high resolution capability of laser spectroscopy. On the other hand, application of lasers has not been very effective in reducing homogeneous linewidth.

Main causes of the homogeneous line broadening in gaseous media are pressure broadening, saturation broadening, limited interaction time (transit time in the atomic/molecular beam spectroscopy), and natural width. Among those, the first and the second ones are easily removed or reduced. The third one can be reduced by the use of recently developed laser cooling techniques. Thus the present discussion will be concentrated in the last one: reduction of the natural linewidth.

2. BASIC PRINCIPLE

As is well known, the natural width is caused by the uncertainty principle: when the natural life time of an excited state is τ , observation of the fluorescence from the excited state gives the time at which the atom is in the excited state with an accuracy of τ . Thus uncertainty principle requires that the limit in the accuracy of measuring the energy of the excited state is given by $h/(2\pi\tau)$, thus the fluorescence spectrum should have a linewidth (uncertainty in the frequency) of $1/(2\pi\tau)$.

The same phenomenon can be described by classical picture as follows: if an ensemble of atoms is excited instantly to the excited state. The fluorescence intensity should be described as $I=I_0 \exp(-t/\tau)$, where I_0 is a constant. Then the amplitude of the electric field should be $E=E_0 \exp(-t/2\tau)$, and corresponding Fourier transform, that is the frequency domain representation of the fluorescence as a response to an impulse excitation, should have a FWHM of $1/(2\pi\tau)$.

It is in principle easy to reduce a natural width: that is, to deal with only such atoms which happen to remain in the excited state longer than T , which is a time much longer than the life time τ . Because the number of such atoms is proportional to $\exp(-T/\tau)$, where T is the time much longer than τ , we must sacrifice the fluorescence intensity in order to reduce the linewidth.

However, one cannot expect any reduction of linewidth by simply carrying out delayed fluorescence measurement. Reduction of the linewidth can be expected if we could detect the response of each atom independently. It is needed to carry out the delayed measurement of a quantity which reflects the amplitude of the fluorescence including the phase. A typical example is seen in various types of coherent interactions of atoms and the electromagnetic field.

3. POSSIBLE SCHEMES AND EXPERIMENTAL RESULTS

[1] DELAYED OBSERVATION OF SINGLE EVENT

In order to certify that a photon is emitted in a time interval longer than T , we must know when the atom made a transition to the excited state. It can be easily done in γ -ray spectroscopy using Mossbauer effect. The 14.4 keV γ -ray is emitted by the spontaneous emission by a nuclear excited state of ^{57}Fe having a life time of 10^{-7} sec. This metastable nuclear state is occupied by 122 keV γ -ray of a higher excited state. Thus detection of 122 keV γ -ray tells us when a nucleus makes transition to the 14.4 keV excited state. If we observe only such a photon which is emitted more than T sec after the emission of a 122 keV photon, we will be able to obtain a sharp linewidth characterized by T [1].

[2] DOUBLE RESONANCE

In many spectroscopic applications, direct purpose of high resolution spectroscopy is to observe the hyperfine structure of the upper or the lower state. Double resonance is a convenient method to observe the hyperfine structure of the upper state, and the linewidth of the radiofrequency spectrum can be much shorter than that of the optical spectrum[2]. Although this is not a direct observation of the subnatural linewidth and does not contribute in improving the accuracy of the optical spectrum, it is an excellent method to determine the hyperfine structure accurately.

[3] RAMSEY RESONANCE

The most straightforward scheme of subnatural linewidth spectroscopy should be that of Ramsey resonance: if an atom is excited to the resonant state in the first field and keeps coherence until it is interacted by the second radiation field, signal takes a "Ramsey pattern." Apparently coherence of the atom is conserved only when it stays in the excited state, and the number of such atoms should decrease by a factor $\exp(-T/\tau)$.

For resonant transitions in the visible region, the natural lifetime is too short to practice conventional Ramsey resonance experiment. In such a case, acceleration of atoms (ionization — acceleration — neutralization) is a reasonable solution, though technically tedious to accelerate neutral atoms [3].

[4] LEVEL CROSSING

Level crossing signal is a result of mixing of two quantum states, and interference of the probability amplitudes is directly detected. Thus we have a possibility of narrowing the line by delayed observation. This method has been applied by several groups in early 70's on Ca and Ba [4], and also on Na [5,6] successfully observing narrowed linewidth.

[5] QUANTUM BEAT

When a couple of nearby states of the same symmetry are excited at the same time by a pulsed light, we can observe a quantum beat signal, which is essentially the interference of the probability amplitudes of the two states. Thus the observation of the quantum beat allows us to narrow the linewidth by carrying out the delayed observation. Theoretical treatment on this scheme was discussed in detail [7,8].

[6] COHERENT TRANSIENT

Coherent transient phenomena generally includes all the effects in which interaction of coherent light and coherent quantum states of matter give rise to a signal as the beat note of the coherent incident light and the radiation emitted by the induced dipole of the matter. Thus there are many possible arrangements by which we can expect narrowing by delayed observation.

However, an experimental success has been obtained only on our phase switching method [9,10]. In this method, one observes the effect of phase switching in the nutation signal of the atoms. Recently, hyperfine components in the D₂ line of lithium which are overlapping in the natural linewidth limited spectroscopy have been successfully separated by this method [11]. This may be the first experimental demonstration that SNWS is practically useful if it allows to separate hyperfine structures hidden within the natural width, as shown in a computer simulation [12].

4. FUTURE TRENDS

Importance of SNWS has been increased by recent technical improvements on laser cooling and trapping of atoms and ions. Ultimate linewidth limit in SNWS is atomic/molecular transit time in the optical field and signal-to-noise ratio. The former can be very much extended by cooling the atoms under observation and can be even infinite by trapping the atoms. The former can be eliminated simply extending the total accumulation time, if we have sufficient absolute frequency stability of lasers, and the SNWS scheme guarantees the center frequency of the spectrum to be investigated. This last point is especially important in choosing the SNWS scheme.

REFERENCES

1. W. Neuwirth, Z. Phys. 197, 473 (1966).
2. I.J. Ma, G. zuPutlitz and G. Schutte, Z. Phys. 208, 276 & 352 (1968).
3. K.A. Safinya, K.K. Chan, S.R. Lundeen and F.M. Pipkin, Phys. Rev. Lett., 45, 1934 (1980).
4. P. Schenck, R.C. Hilborn and H. Metcalf, Phys. Rev. Lett., 31, 189 (1973).
5. H. Figger and H. Walther, Z. Phys. 267, 1 (1974).
6. J.S. Deech, P. Hannaford and G.W. Series, J. Phys. B, 7, 1131 (1974).
7. P. Meystre, M.O. Scully and H. Walther, Opt. Communicat., 33, 153 (1980).
8. H.W. Lee, P. Meystre and M.O. Scully, Phys. Rev. A, 24, 1914 (1981).
9. F. Shimizu, K. Umezu and H. Takuma, Phys. Rev. Lett., 47, 825 (1981).
10. F. Shimizu, K. Shimizu and H. Takuma, Phys. Rev. A, 28, 2248 (1983).
11. F. Shimizu, K. Shimizu and H. Takuma, Phys. Rev. A, 35, 3149 (1987).
12. H. Metcalf and W. Phillips, Opt. Lett., 5, 540 (1980).

SUBNATURAL LINEWIDTH SPECTROSCOPY

WHAT IS NATURAL LINEWIDTH?

(1) QUANTUM MECHANICAL

NATURAL LINEWIDTH:

UNCERTAINTY

$$\Delta E = h / 2\pi \tau$$

(τ : RAD. LIFETIME)

$$\rightarrow \Delta \nu = 1 / 2\pi \tau$$

(2) CLASSICAL

FOURIER TRANSFORM OF

DECAYING EMISSION

$$I(t) = I_0 \exp(-t/\tau) \quad (\text{INTENSITY})$$

$$\rightarrow E(t) = E_0 \exp(-t/2\tau) \quad (\text{AMPLITUDE})$$

↓ F.T.

$$I(\omega) = I_p / [(\omega - \omega_0)^2 + (1/2\pi\tau)^2]$$

NATURAL LINEWIDTH CANNOT BE
REDUCED BY A SIMPLE
DELAYED OBSERVATION OF INTENSITY

$$\text{Re}\{E(\omega)\} = \{E_0 e^{-\gamma T} / [(\Delta\omega)^2 + \gamma^2]\} \\ \times [\gamma \cos(\Delta\omega T) - \Delta\omega \sin(\Delta\omega T)],$$

$$\text{Im}\{E(\omega)\} = \{E_0 e^{-\gamma T} / [(\Delta\omega)^2 + \gamma^2]\} \\ \times [\gamma \sin(\Delta\omega T) + \Delta\omega \cos(\Delta\omega T)].$$

However,

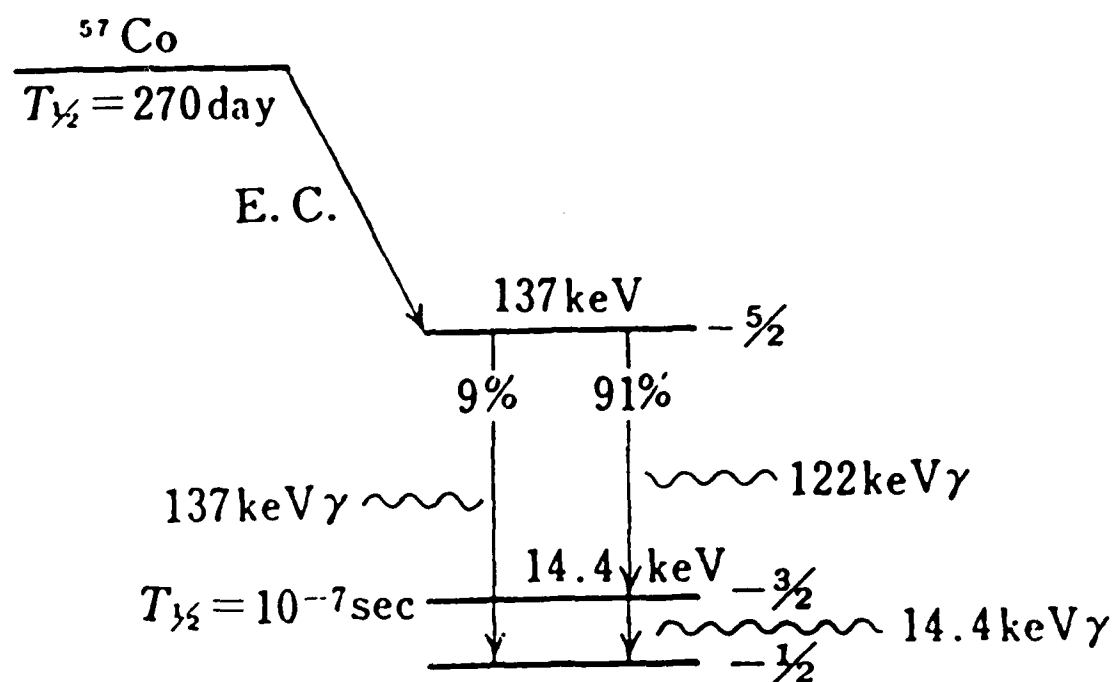
$$I = \text{Re}\{E(\omega)\}^2 + \text{Im}\{E(\omega)\}^2 = E_0^2 e^{-2\gamma T} / [(\Delta\omega)^2 + \gamma^2]$$

NEEDED TO PICK UP
A COHERENT INTERACTION

SUCH AS:

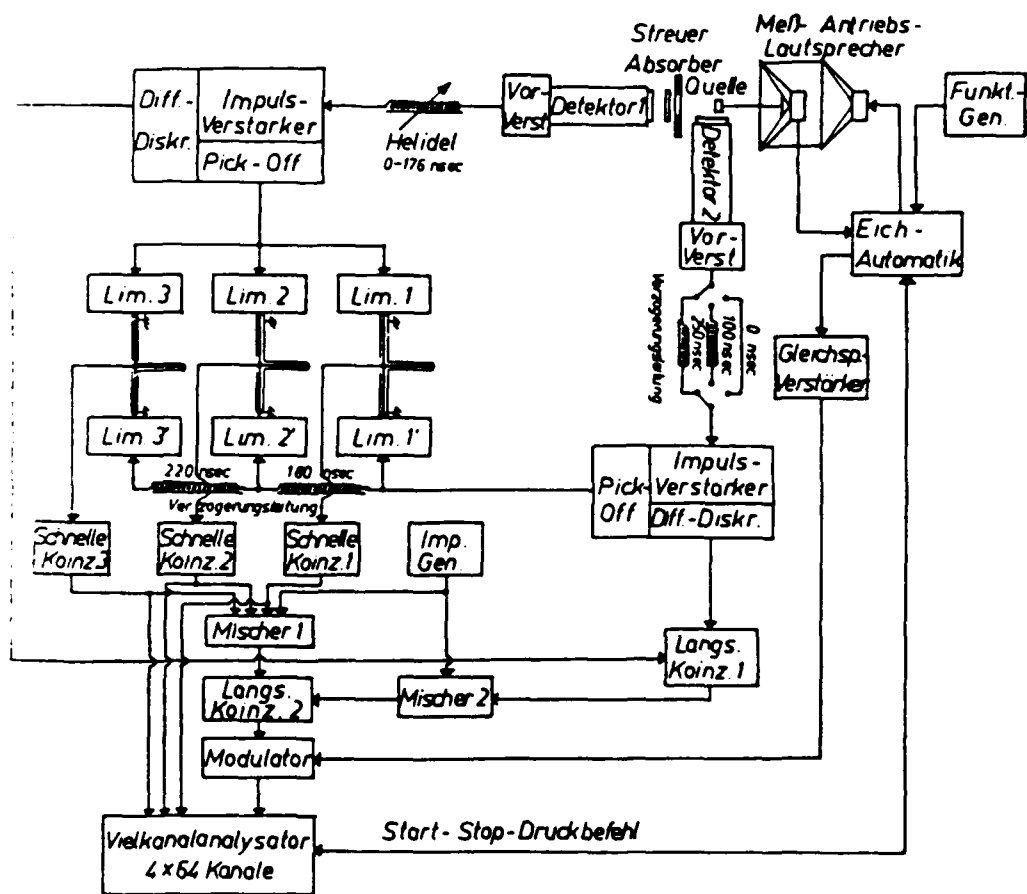
- [1] SINGLE ATOM PHENOMENUM
- [2] DOUBLE-RESONANCE
- [3] RAMSEY RESONANCE
- [4] LEVEL CROSSING BEAT
- [5] QUANTUM BEAT
- [6] COHERENT TRANSIENTS

[1] SINGLE ATOM EMISSION
 γ - RAY SPECTROSCOPY (1)



γ - RAY SPECTROSCOPY (2)

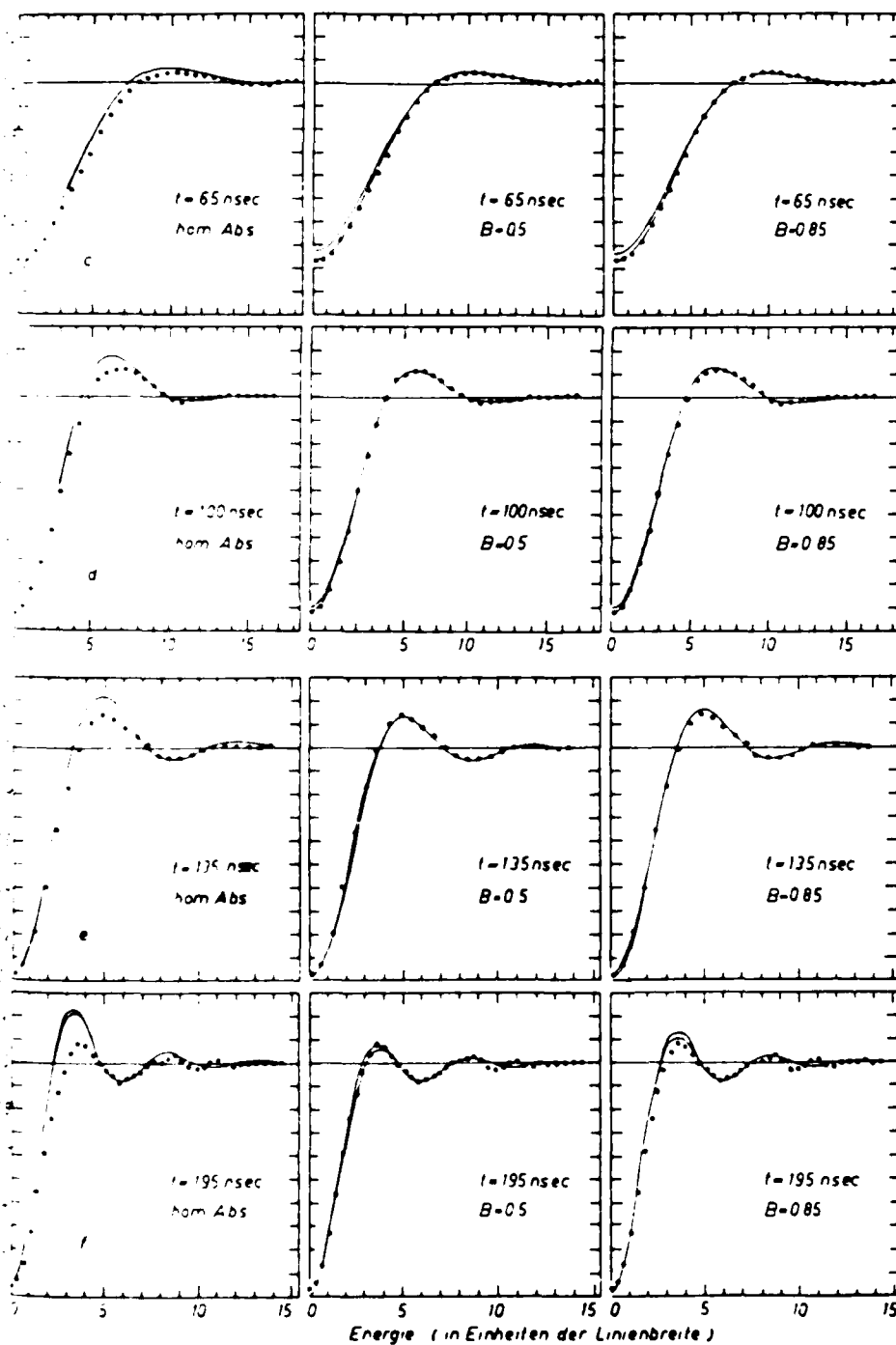
ex.) W. NEUWIRTH, 1966
SCHEMATIC EXPERIMENTAL SETUP



γ - RAY SPECTROSCOPY (3)

ex.) W. NEUWIRTH, 1966

EXPERIMENTAL RESULT

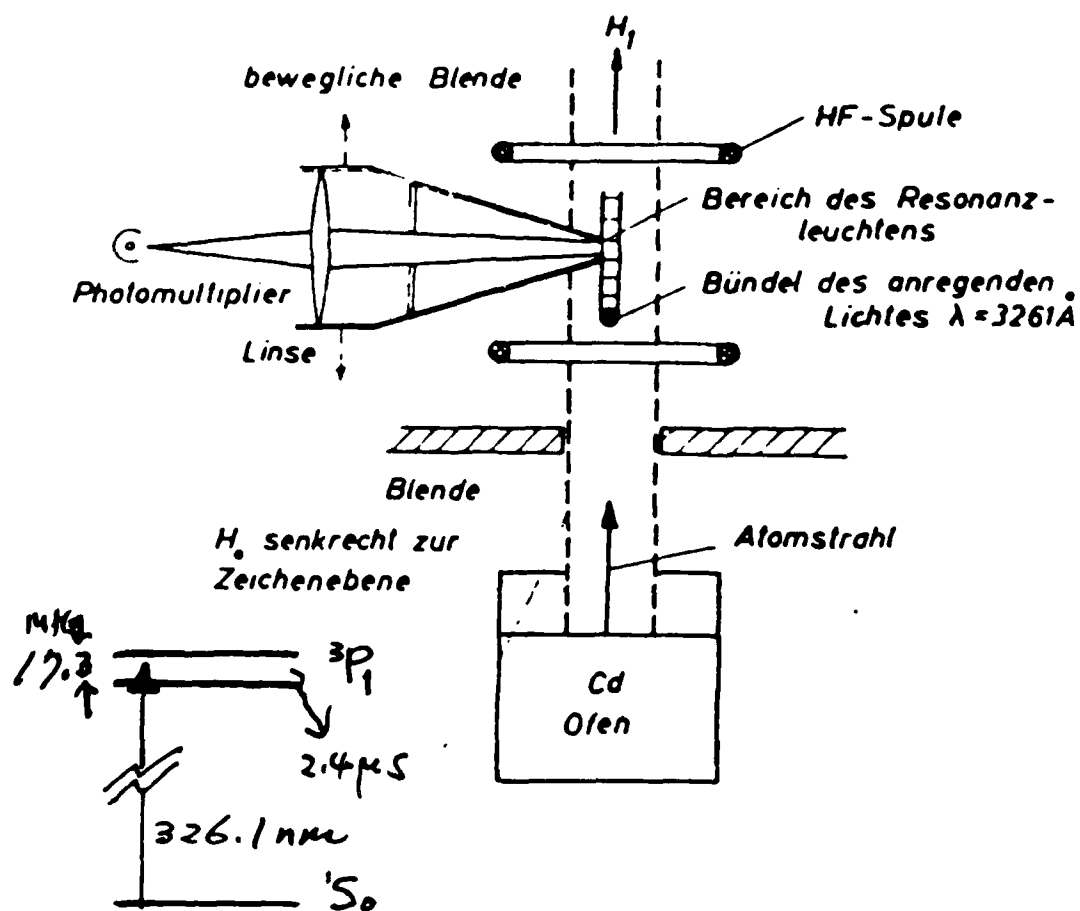


[2] DOUBLE RESONANCE (1)

ex.) I. J. MA et al., 1968

Cd & Sr

SCHEMATIC EXPERIMENTAL SETUP

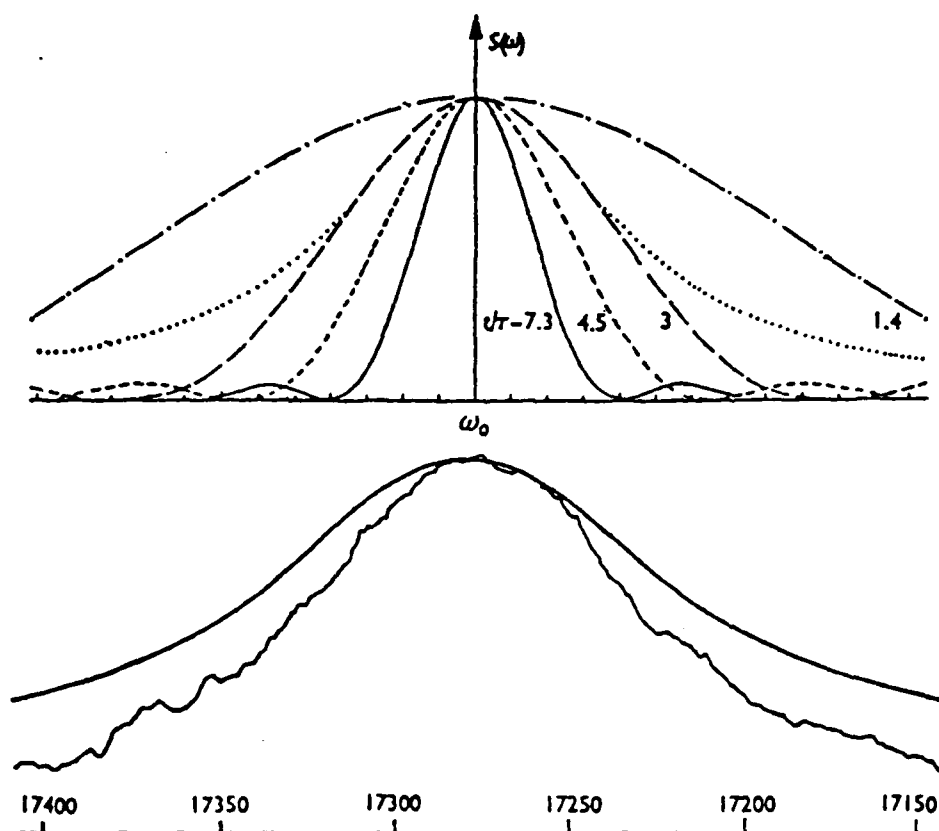


[2] DOUBLE RESONANCE (2)

ex.) I. J. MA et al., 1968

Cd & Sr

EXPERIMENTAL RESULT



[4] LEVEL CROSSING (1) ENERGY LEVELS

J S Deech et al

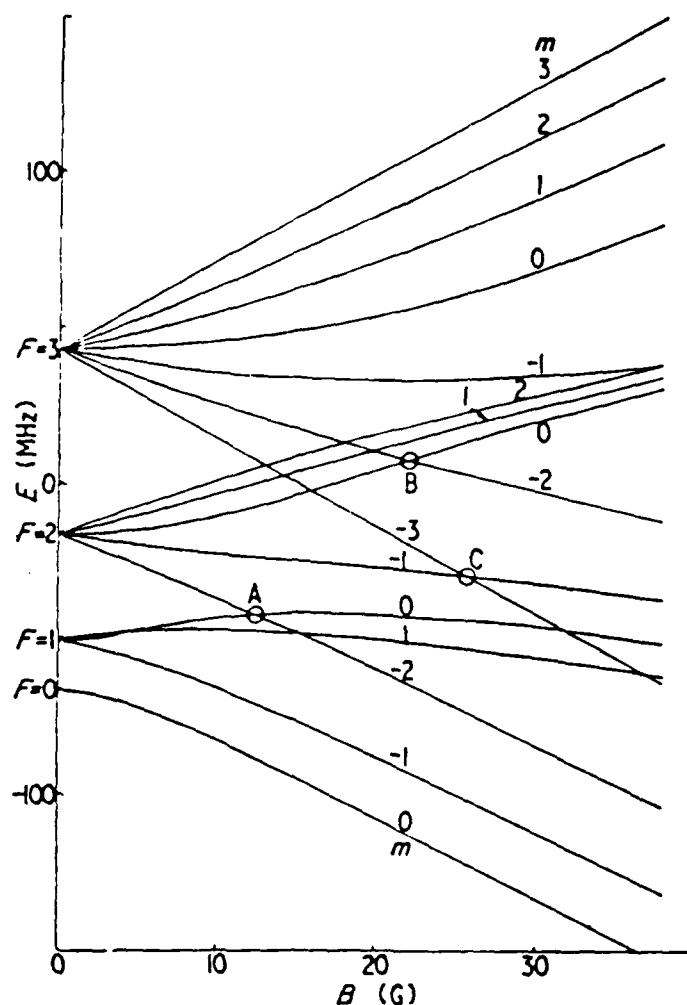


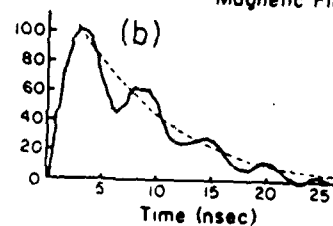
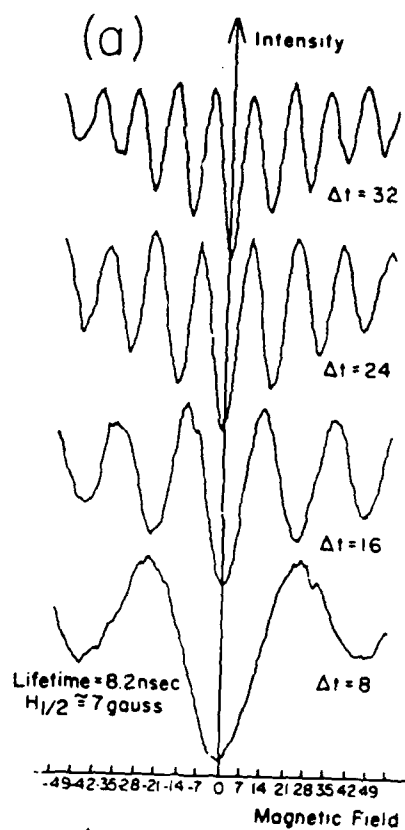
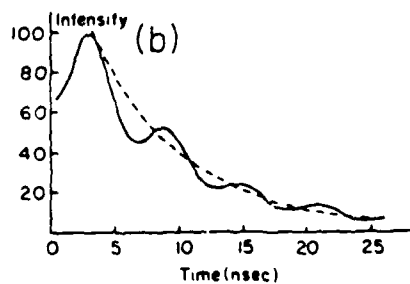
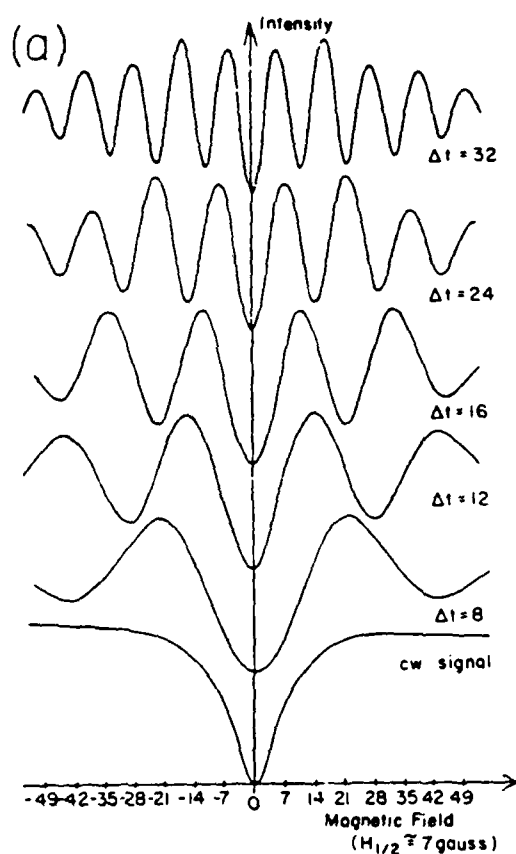
Figure 3. Energy eigenvalues for $l = \frac{1}{2}$, $J = \frac{1}{2}$, plotted against magnetic field, with $a = 18$ MHz, $b = 3.0$ MHz

[4] LEVEL CROSSING (2)
EXPERIMENTAL RESULTS

ex.) P. SCHENK et al., 1973 Ba

THEORY

EXPERIMENT



[4] LEVEL CROSSING (3)
 EXPERIMENTAL RESULTS
 ex.) H. WALTHER et al., 1974 Na

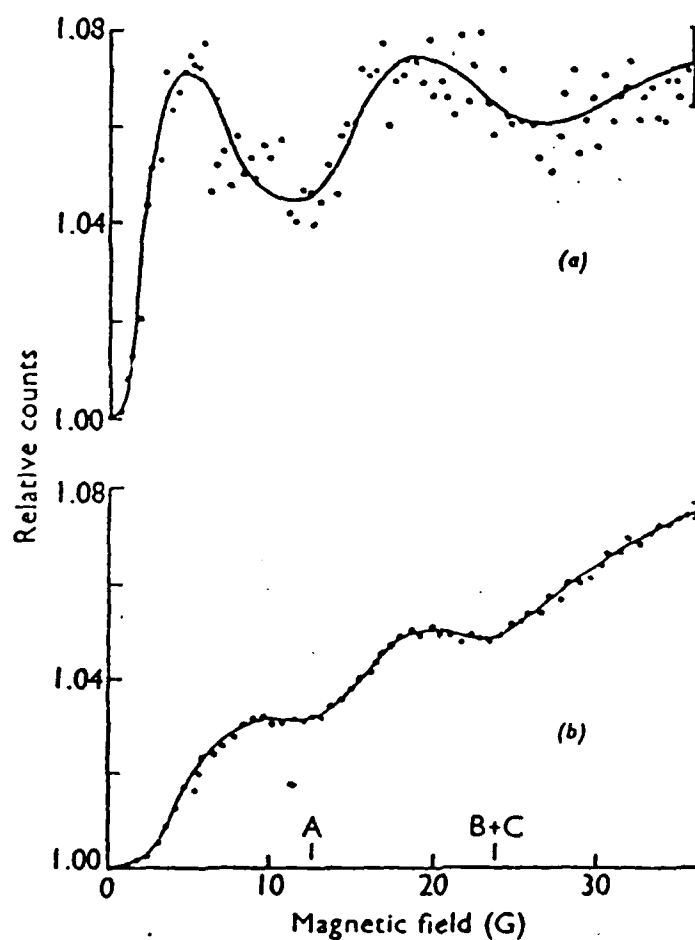


FIG. 3. Hanle effect and level-crossing curves in the $3^2P_{1/2}$ state of Na^{22} with (a) and without (b) narrowing. Delay time 40 nsec (Ref. 10).

[3] RAMSEY RESONANCE (1)

ex.) K.A. SAFINYA et al. 1980

SCHEMATIC EXPERIMENTAL SETUP

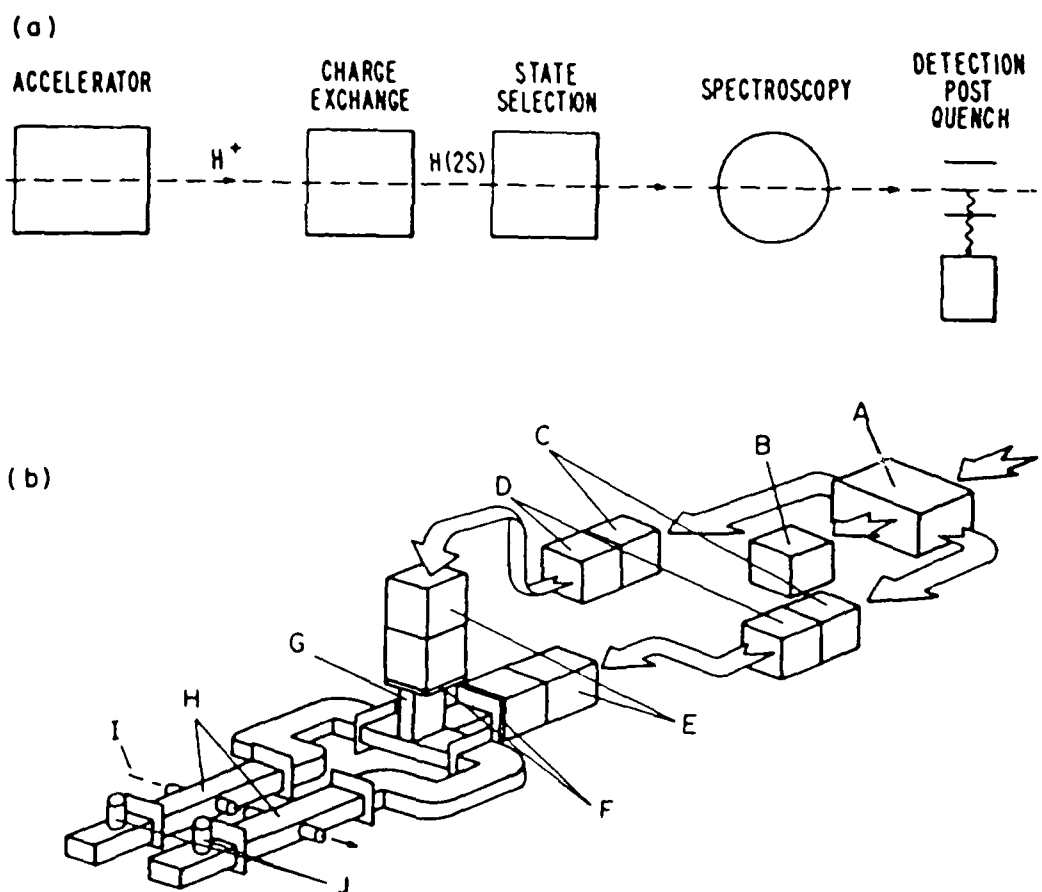


FIG. 1. (a) A schematic drawing of the apparatus. (b) A schematic drawing of the microwave plumbing in the spectroscopy region. *A*, three-pole switch; *B*, matched load; *C*, low-pass filters; *D*, precision variable attenuators; *E*, 50-dB circulators; *F*, vacuum windows; *G*, magic tee; *H*, interaction waveguides; *I*, beam; *J*, detector diodes.

-517-

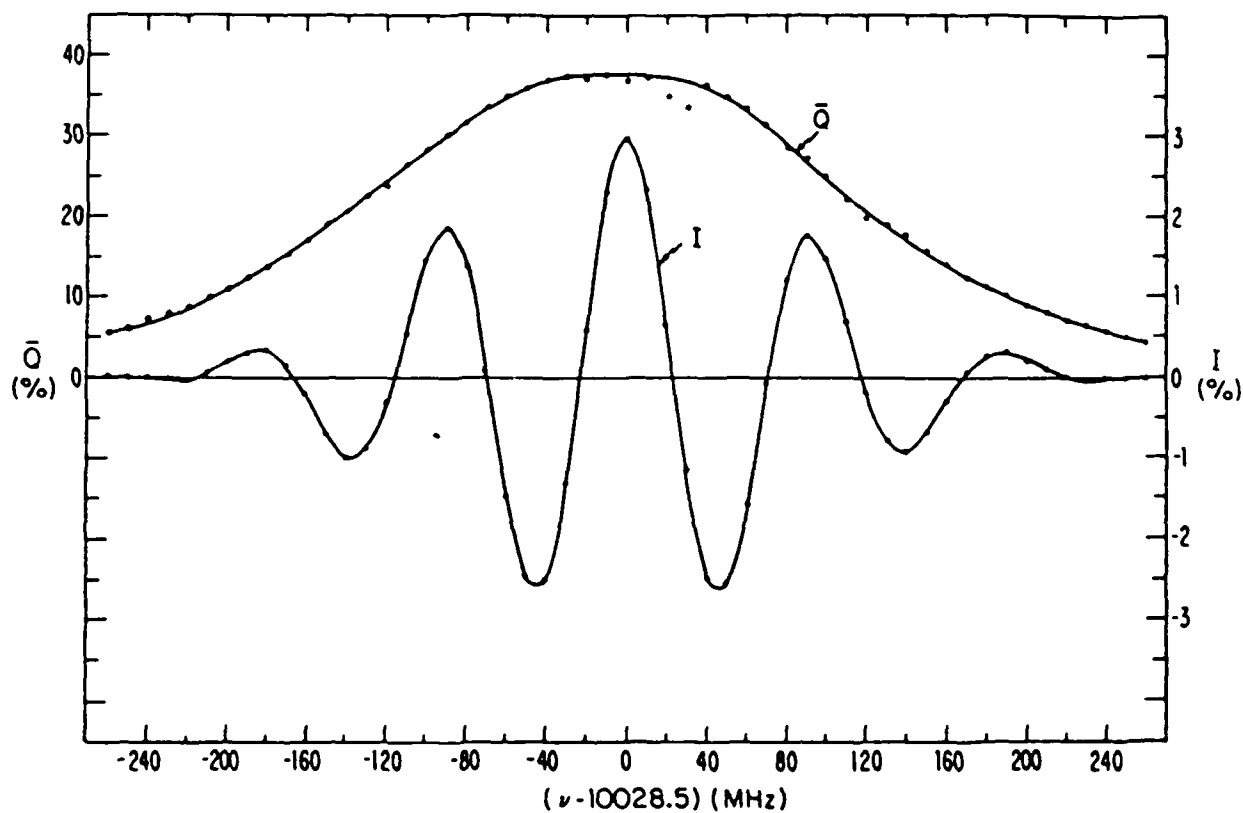
[3] RAMSEY RESONANCE(2)

ex.) K.A.SAFUNYA et al., 1980

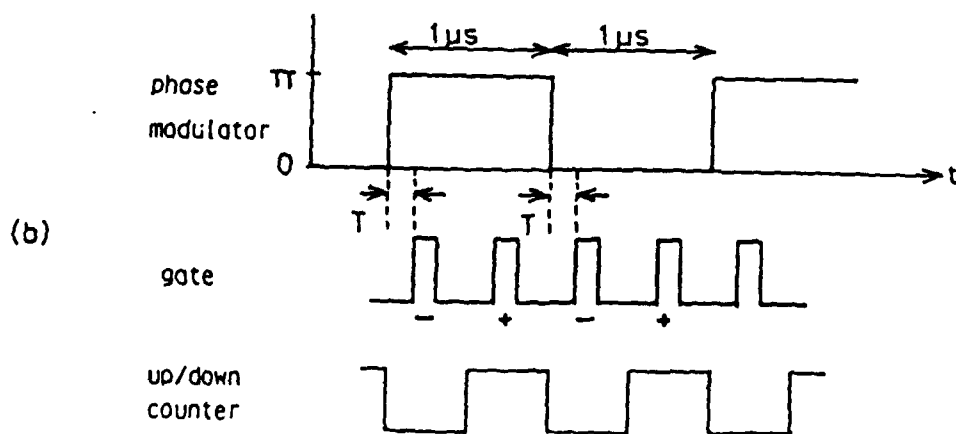
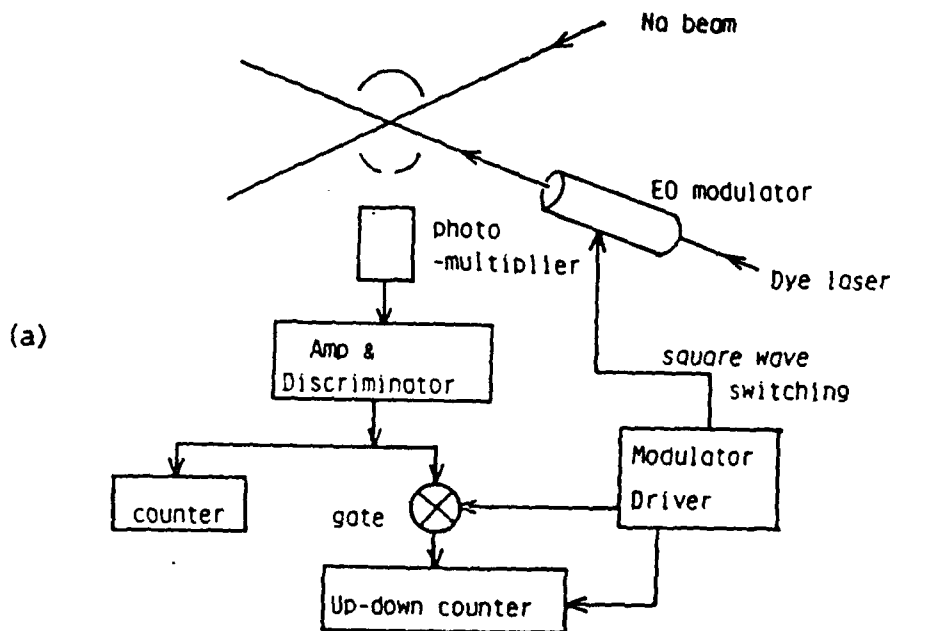
EXPERIMENTAL RESULT

$2^2P_{3/2} \rightarrow 2^2S_{1/2}$ OF H

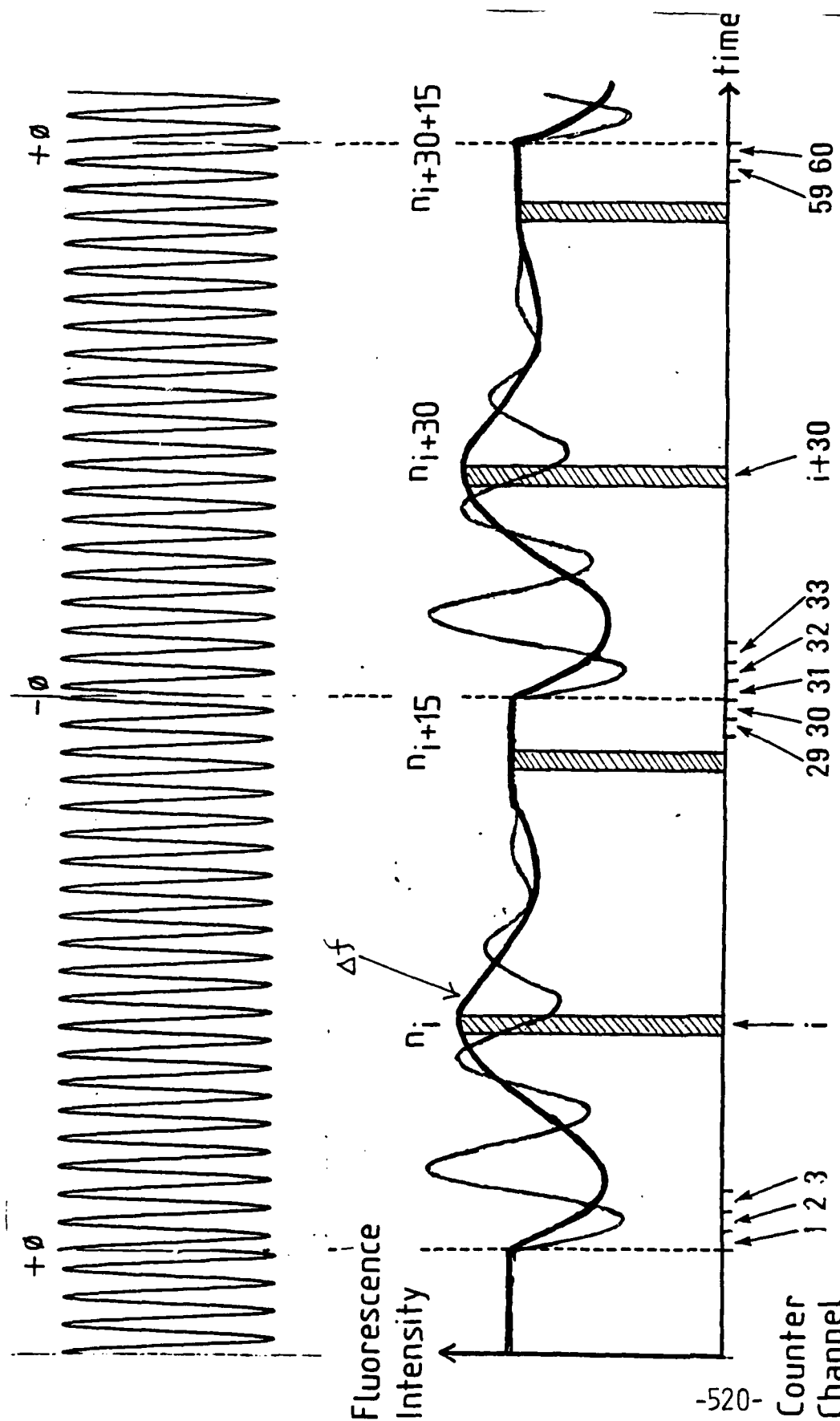
9911.117(41) MHz



[6] COHERENT TRANSIENT
 ex.) PHASE SWITCHED NUTATION
 BY F. SHIMIZU et al. 1981 Na



Laser



DENSITY MATRIX FORMULATION

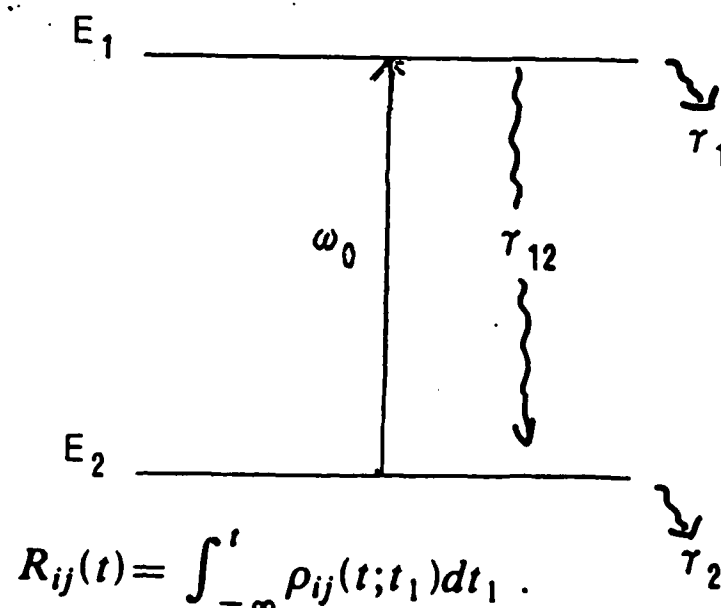
$$d\rho_{11}/dt = -i\Omega(\rho_{12}-\rho_{21}) - \tau_{11}\rho_{11}$$

$$d\rho_{22}/dt = i\Omega(\rho_{12}-\rho_{21}) - \tau_{22}\rho_{22}$$

$$d\rho_{12}/dt = (i\omega_0 - \tau_{12})\rho_{12} - i\Omega(\rho_{11}-\rho_{22})$$

$$\rho_{21} = \rho_{12}^*, \quad \Omega = \mu E / \hbar$$

$$E = \begin{cases} E_0 \exp(-i\psi - i\omega t) + c. c. & (t < 0) \\ E_n \exp(-i\omega t) + c. c. & (t > 0) \end{cases}$$



$$R_{ij}(t) = \int_{-\infty}^t \rho_{ij}(t; t_1) dt_1$$

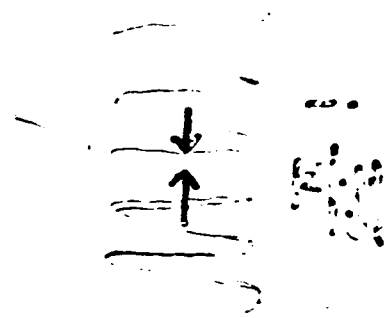
For fluorescence

Steady state signal
↓
Incoherent transient

$$R_{11}(t) = \frac{\mu^2}{\hbar^2} \frac{1}{\gamma_1 \gamma_2 - i\Delta\omega + \gamma_{12}} \frac{1}{[|E_n|^2 + (|E_0|^2 - |E_n|^2)e^{-\gamma_1 t}]}$$

decay rate is that of spontaneous emission

$$+ \frac{\mu^2}{\hbar^2} \frac{1}{\gamma_2 - i\Delta\omega + \gamma_{12}} \frac{1}{i\Delta\omega - \gamma_{12} + \gamma_1} (E_n^* E_0 e^{-i\varphi} - |E_n|^2)$$



$$\times (e^{(i\Delta\omega - \gamma_{12})t} - e^{-\gamma_1 t}) + c.c.$$

Coherent transient

$$\Delta R_{11} \equiv R_{11}(\varphi, t) + R_{11}(-\varphi, t) - 2R_{11}(0, t)$$

$$= 4 \frac{\mu^2}{\hbar^2} \frac{1}{\gamma_2 (\Delta\omega)^2 + \gamma_{12}^2} \frac{1}{(\Delta\omega)^2 + (\gamma_1 - \gamma_{12})^2} |E|^2 (\cos\varphi - 1)$$

$$\times \{ [(\Delta\omega)^2 - \gamma_{12}^2 + \gamma_1 \gamma_{12}] \underbrace{[e^{-\gamma_{12}t} \cos(\Delta\omega t) - e^{-\gamma_1 t}]}_{\text{}} \}$$

$$- \Delta\omega(\gamma_1 - 2\gamma_{12}) e^{-\gamma_{12}t} \underbrace{\sin(\Delta\omega t)}_{\text{}} \} ,$$

$$\gamma_{12} = \frac{1}{2} (\gamma_1 + \gamma_2)$$

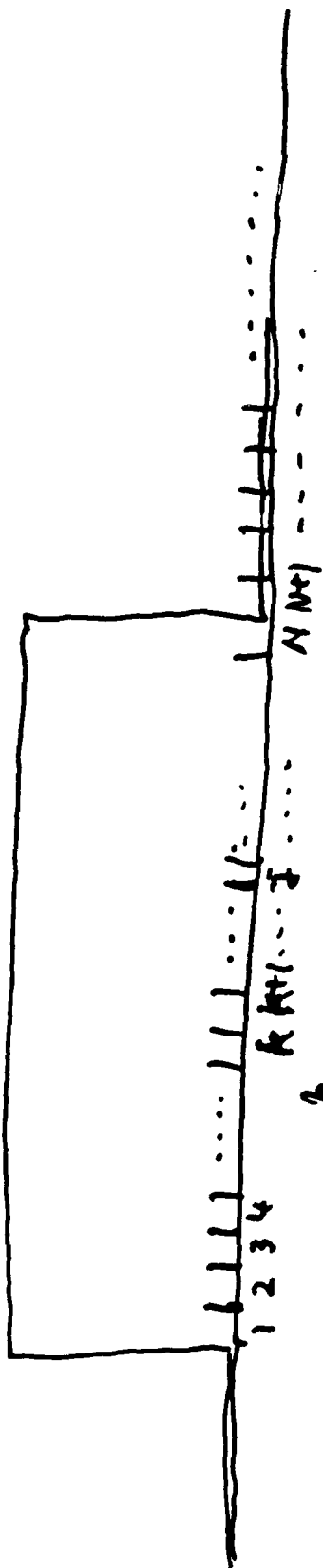
If $\gamma_2 > \gamma_1$, observe ΔR_{22}

$$\text{For } \gamma_1 = 2\gamma_{12}$$

$$\Delta R_{11} = 4 \frac{\mu^2}{\hbar^2} |E|^2 (\cos \varphi - 1) \frac{1}{\gamma_2 (\Delta \omega)^2 + \gamma_{12}^2}$$

$$\times [e^{-\gamma_{12} t} \cos(\Delta \omega t) - e^{-2\gamma_{12} t}].$$

$$\Delta \bar{R}_{11} = \gamma \int_{t_1}^{t_2} [R_{11}(\varphi, t) + R_{11}(-\varphi, t) - 2R_{11}(0, t)] e^{\gamma t} dt$$

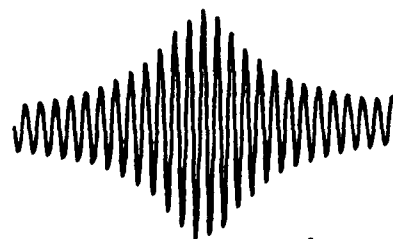
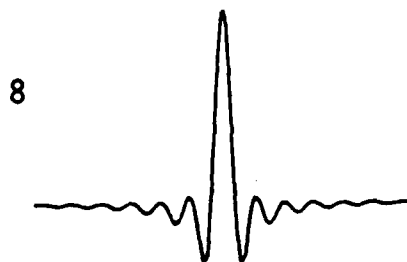
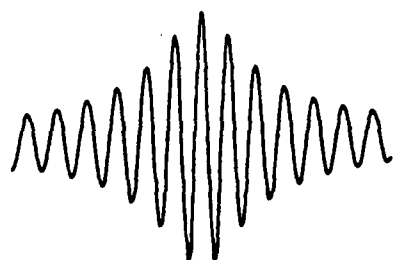
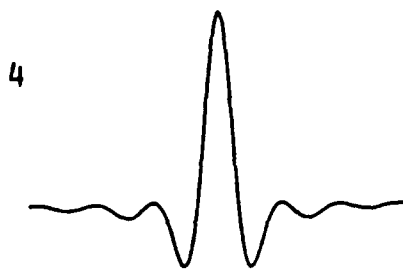
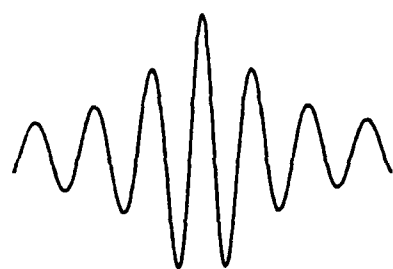
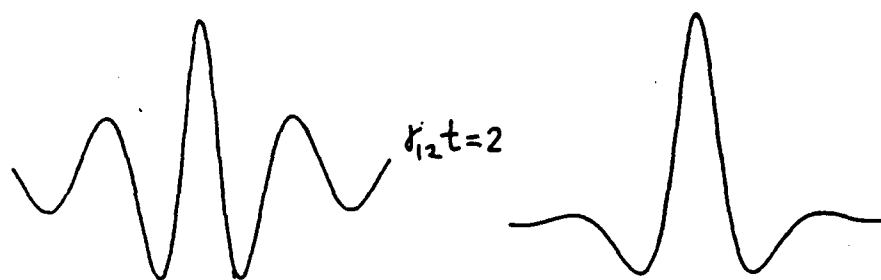


$$I_d = \sum_{i=1}^k (I_i + I_{i+N} - I_{i+j+N} - I_{i+j}) \exp(i-k\pi\tau/c\tau N)$$

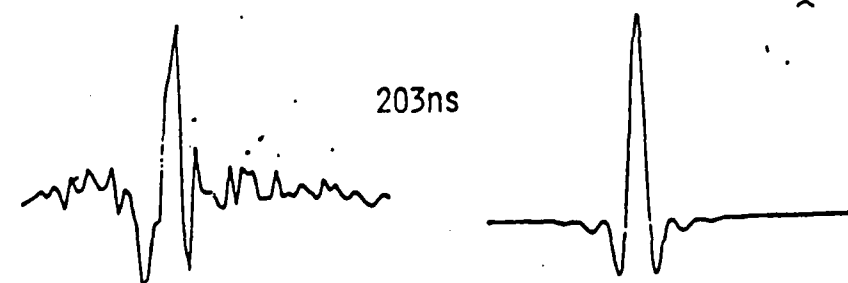
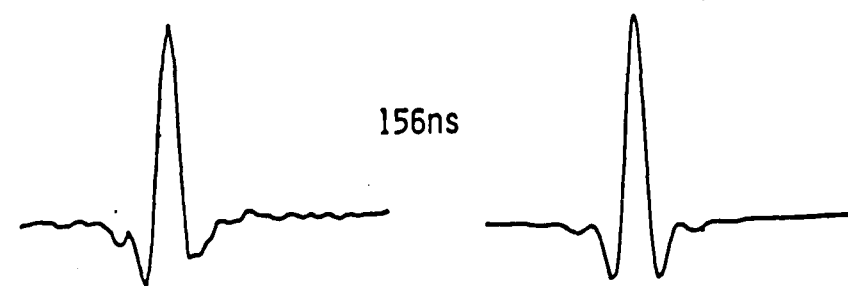
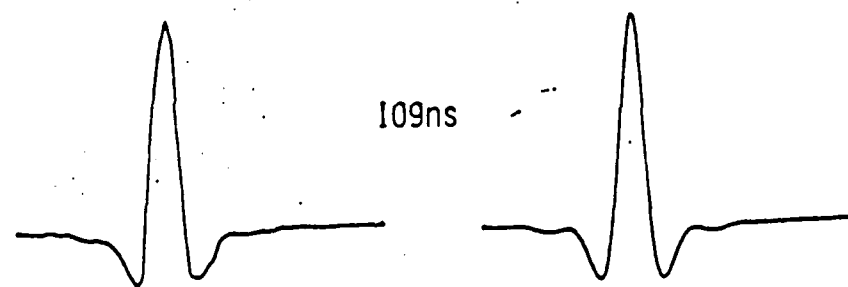
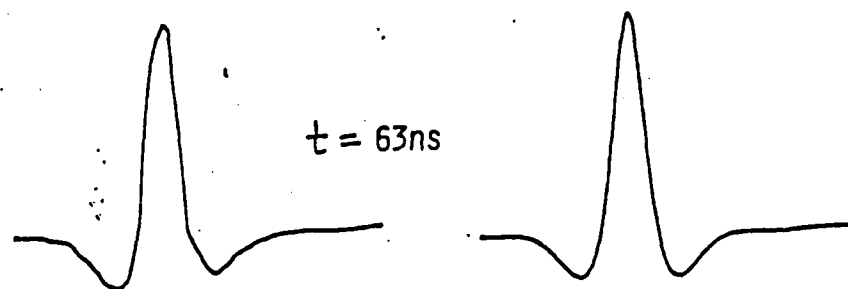
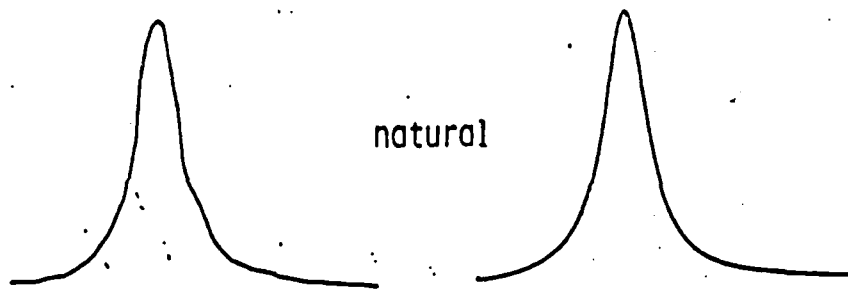
$$I(\Delta\omega) = I_0 \frac{\gamma^2}{\Delta\omega^2 + \gamma^2} \left[\frac{\sin(\Delta\omega T)}{\Delta\omega T} + \frac{1 - \exp(-\gamma T)}{\gamma T} \right]$$

$$\gamma = \frac{1}{T} \gamma'$$

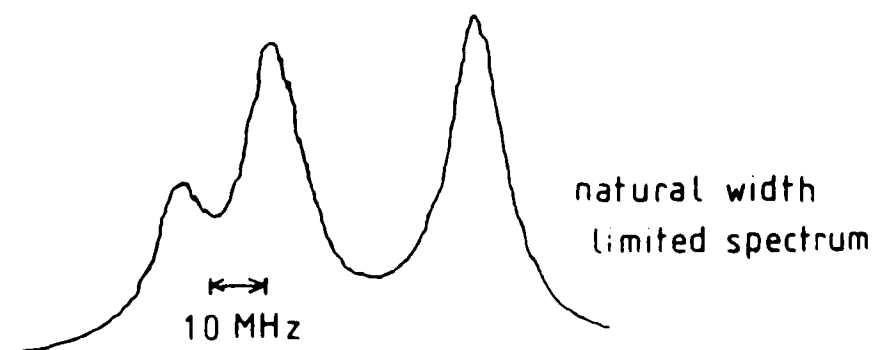
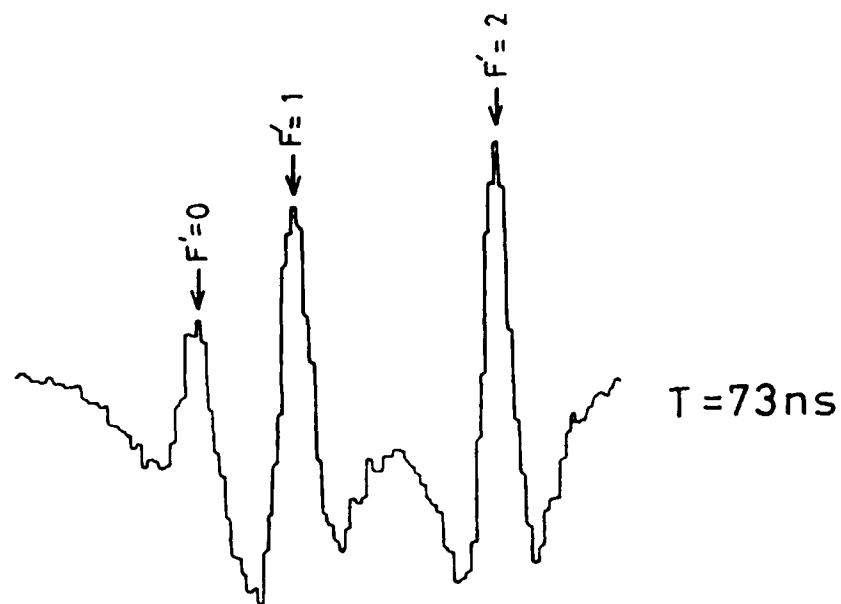
Theoretical curves, absorption.



$$r_c = r_{12}$$

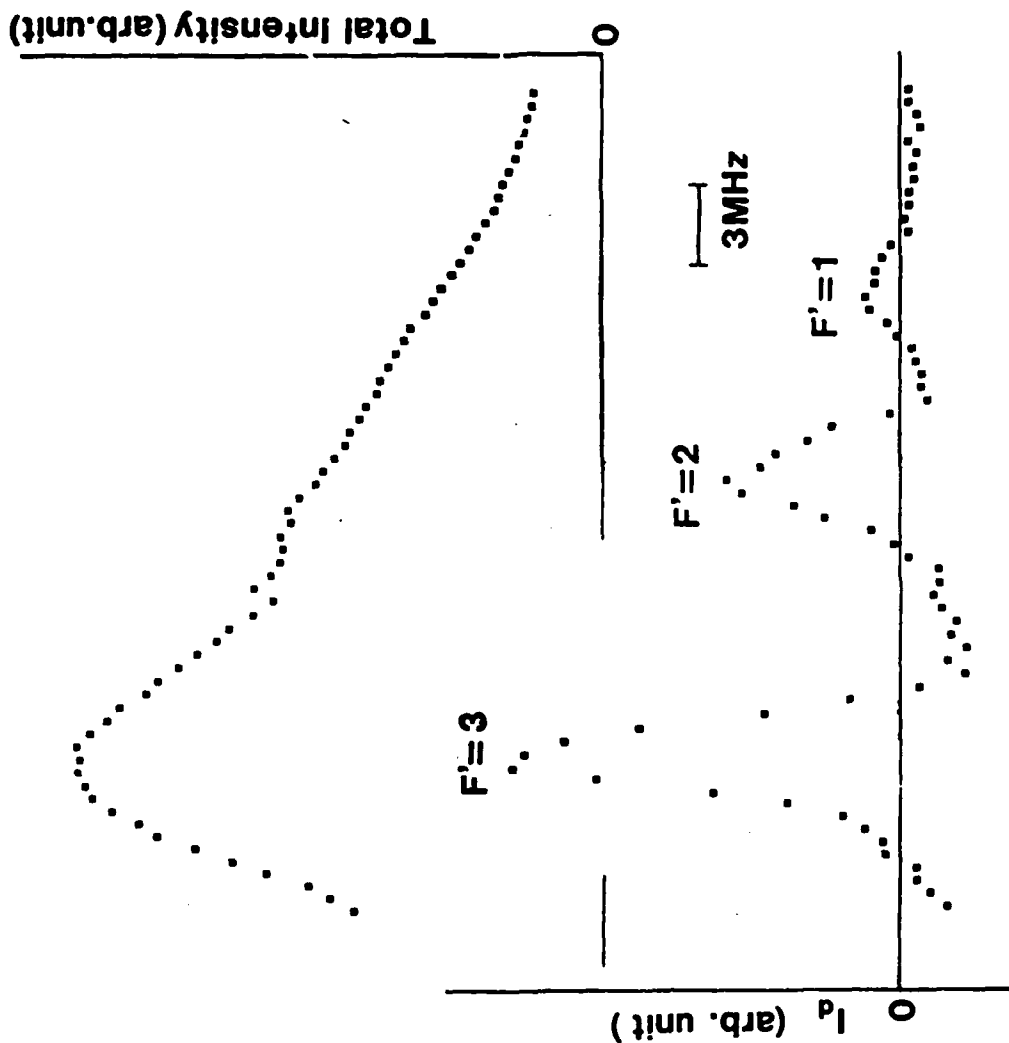
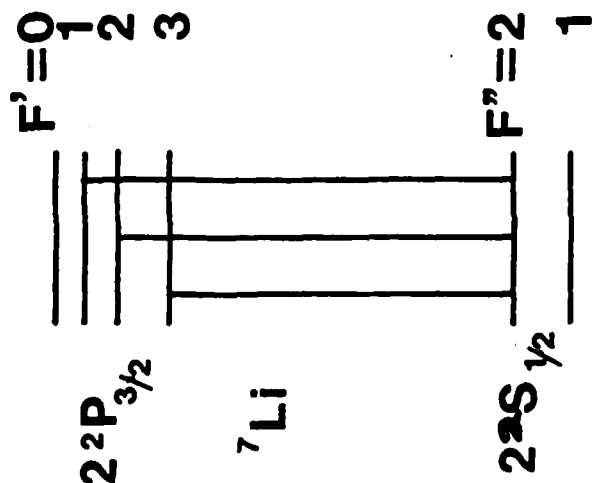


Lineshape with exp. average.



Subnatural Linewidth Spectroscopy by Phase Switching

H. Shimizu et al.
(1987)



CONCLUDING REMARKS

- ① Natural Width of Optical Spectral Lines can be narrowed by delayed observation of Coherent transient effects.
- ② Phas switching method has been demonstrated to be practical in SNWS.
- ③ SNWS is meaningful in spite of a drastic loss in Intensity
- ④ New techniques (laser cooling & trapping) increases the Importance of SNWS.

Comprehensive Model for Laser Instability in a CO_2 Laser
with Gaseous Saturable Absorber

Tadao Shimizu, Maki Tachikawa, and Kazuhito Tani

Department of Physics, Faculty of Science, University of Tokyo,
7-3-1 Hongo, Bunkyo-ku, Tokyo 113, Japan

Summary: A periodic self-pulsation well known as passive Q-switching (PQS) is observed in a CO_2 laser containing a gaseous saturable absorber inside its cavity. PQS was developed at first as a high power pulse source to pump far-infrared lasers. In response to the recent interest in laser instability, it is now being reinvestigated extensively. Dynamic properties of the relating molecular systems are sensitively reflected in the transient pulse structure, and various features of PQS pulsation are realized, depending on lasing conditions and characteristics of the absorbing molecules. The most familiar PQS pulse is that with a single peak as is shown in Fig.1(a). Several new types of PQS have recently been reported.^{1,2} The laser output is modulated sinusoidally when saturable absorbers such as CH_3I or CH_3OH is used (Fig.1(b)). An undamped undulation appears over the quasi-cw tail of PQS pulse with HCOOH absorber (Fig.1(c)). The undulation appears only in the ending part of the pulse tail in the case of SF_6 absorber (Fig.1(d)).

So far, in spite of extensive efforts to analyze the PQS

behavior. there has been no good model which reproduces the observed pulse structure with fidelity. We have tried a semiclassical rate-equation analysis introducing the vibrational relaxation of the lower laser level. It is found that this rate-equation approximation is very effective to describe the PQS phenomenon in the gas laser system. It seems that all the essential physical processes are included in this model to describe a transient behavior in the quantum mechanical system with strong nonlinearity. Through the numerical integration of the rate equations we have succeeded in systematic reproduction of all the PQS pulses, especially the PQS pulse with the undamped undulation for the first time (see Fig.1(a')-(d')). The undulation was revealed as a relaxation oscillation induced by the relaxation of the lower laser level. The model also describes optical bistability observed in the present laser system well.

The computer calculation based on the present model shows that chaotic pulsation is realized led by the period-doubling route. This is the first demonstration of chaos in a laser containing a saturable absorber. (In other words this is the first aperiodic passive Q-switching.) The chaos appears in a very limited parameter region where the undulation period is close to the pulse interval. The presence of the two close time constants may be a key to the production of chaos. The present analysis suggests that it is possible by introducing saturable absorbers inside the cavity to observe chaos even in small-gain lasers such as CO_2 and N_2O lasers far from the bad-cavity condition.

References

1. E.Arimondo, P.Bootz, P.Glorieux, and E.Menchi: J.Opt.Soc.Am.B 2, 193-201 (1985).
2. M.Tachikawa, K.Tanii, M.Kajita, and T.Shimizu: Appl.Phys. B39, 83-90 (1986).

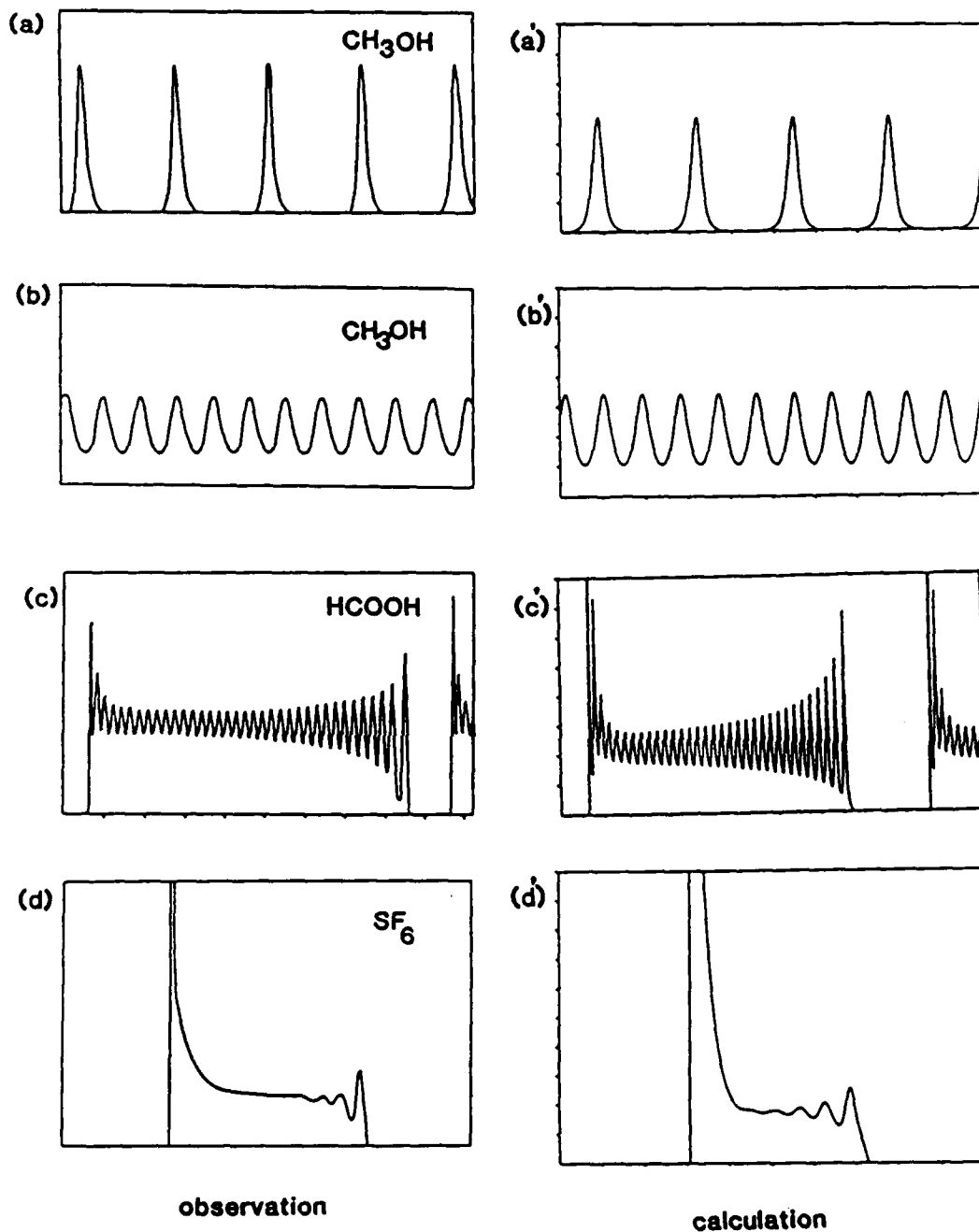


Fig.1 observed ((a)-(d)) and calculated ((a')-(d')) PQS pulse shapes. Full scale is 500 μs for (c) and (c'), and 200 μs for others.

U.S. Jap. Seminar

Comprehensive Model for Laser Instability
in a CO₂ Laser with Gaseous Saturable
Absorber

T. Shimizu

M. Tachikawa

K. Tani

Dept. of Physics, Univ. of Tokyo

1. Comprehensive model

for { PQS time-dependent
behavior
optical bistability

Is semiclassical rate-equation
analysis effective?

its limitation?

2. Possibility of chaos in a laser system with a saturable absorber

What is the mechanism of chaos?

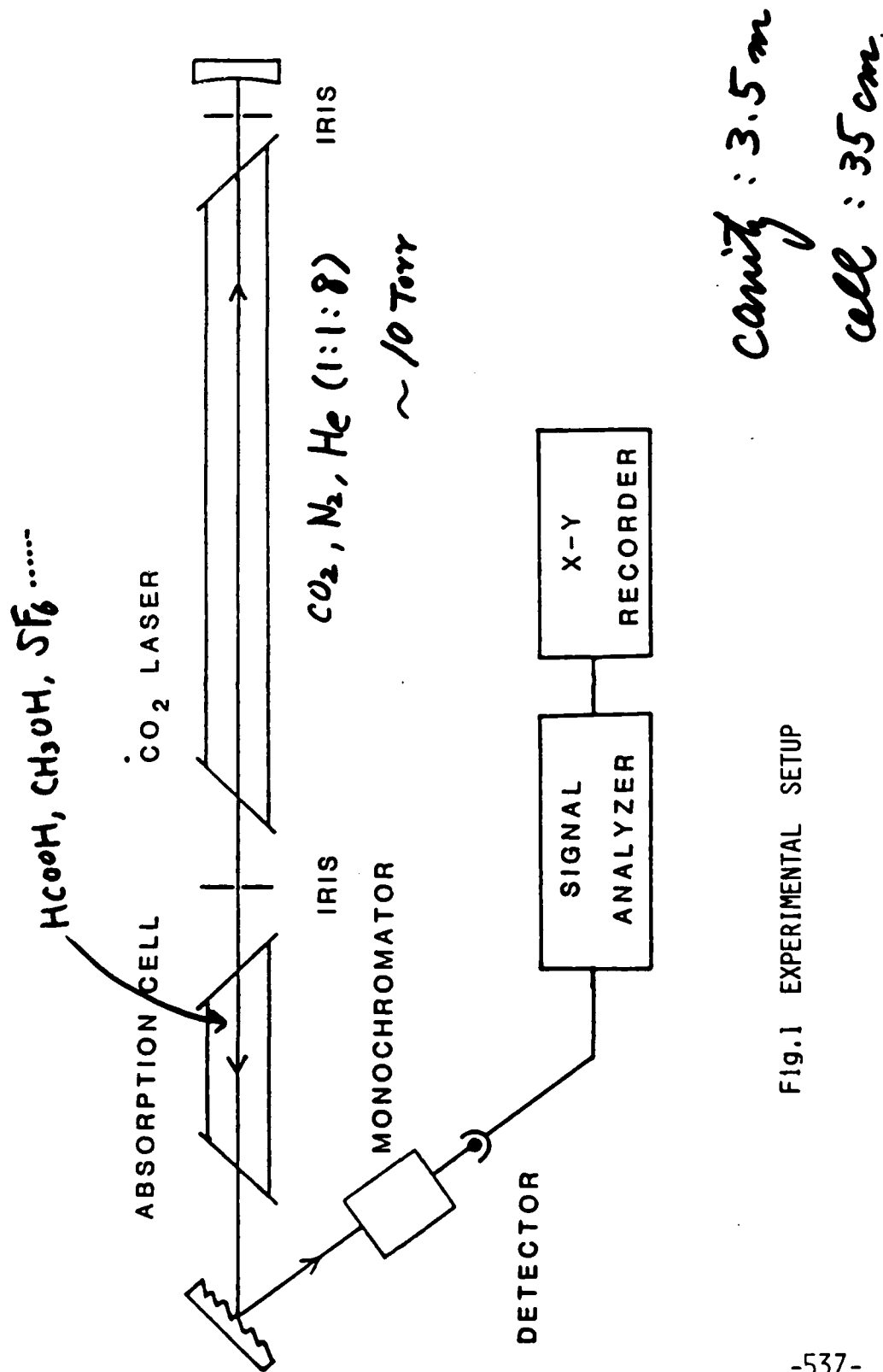
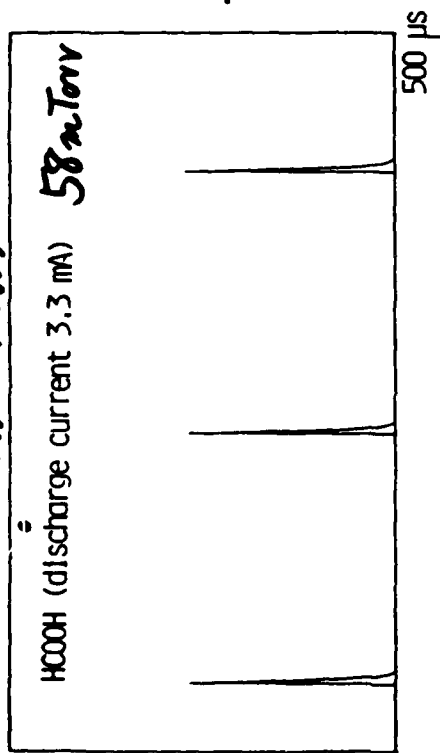
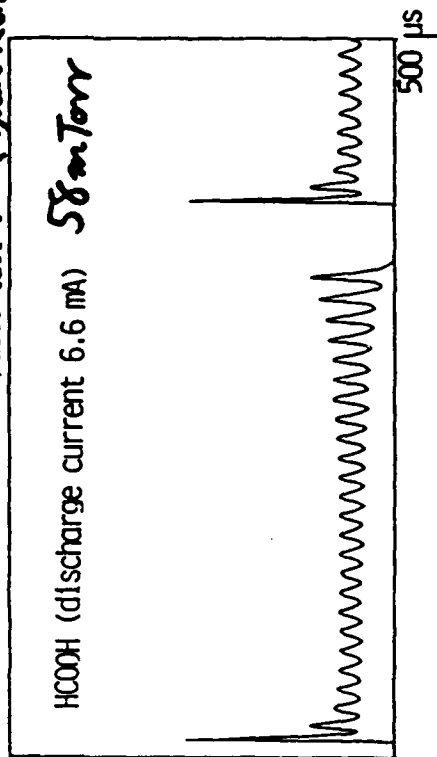


Fig.1 EXPERIMENTAL SETUP

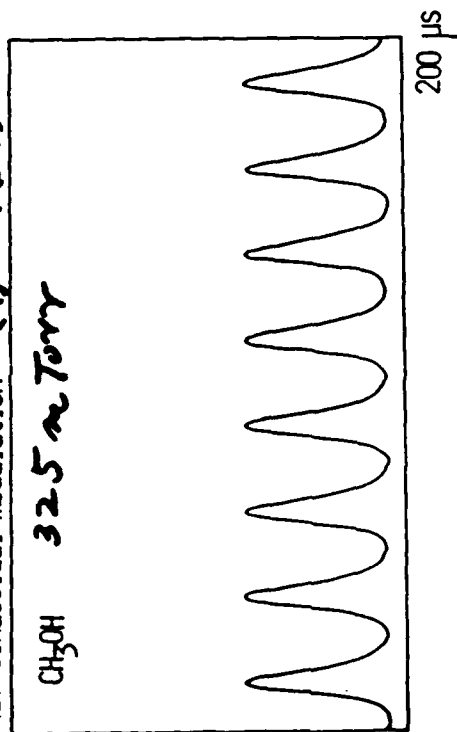
(a) single spike (9 μ m R08))



(c) undamped undulation on pulse tail I (9 μ m R08))



(b) sinusoidal modulation (9 μ m P32))



(d) undamped undulation on pulse tail II (10 μ m P20))

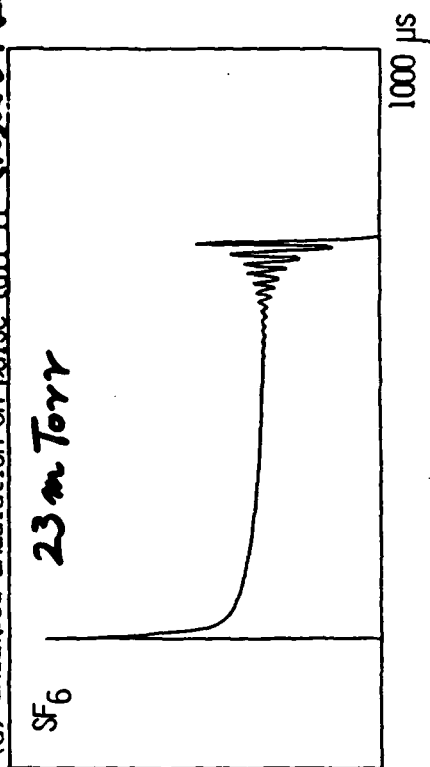


FIG.2 OBSERVED PQS PULSE SHAPES

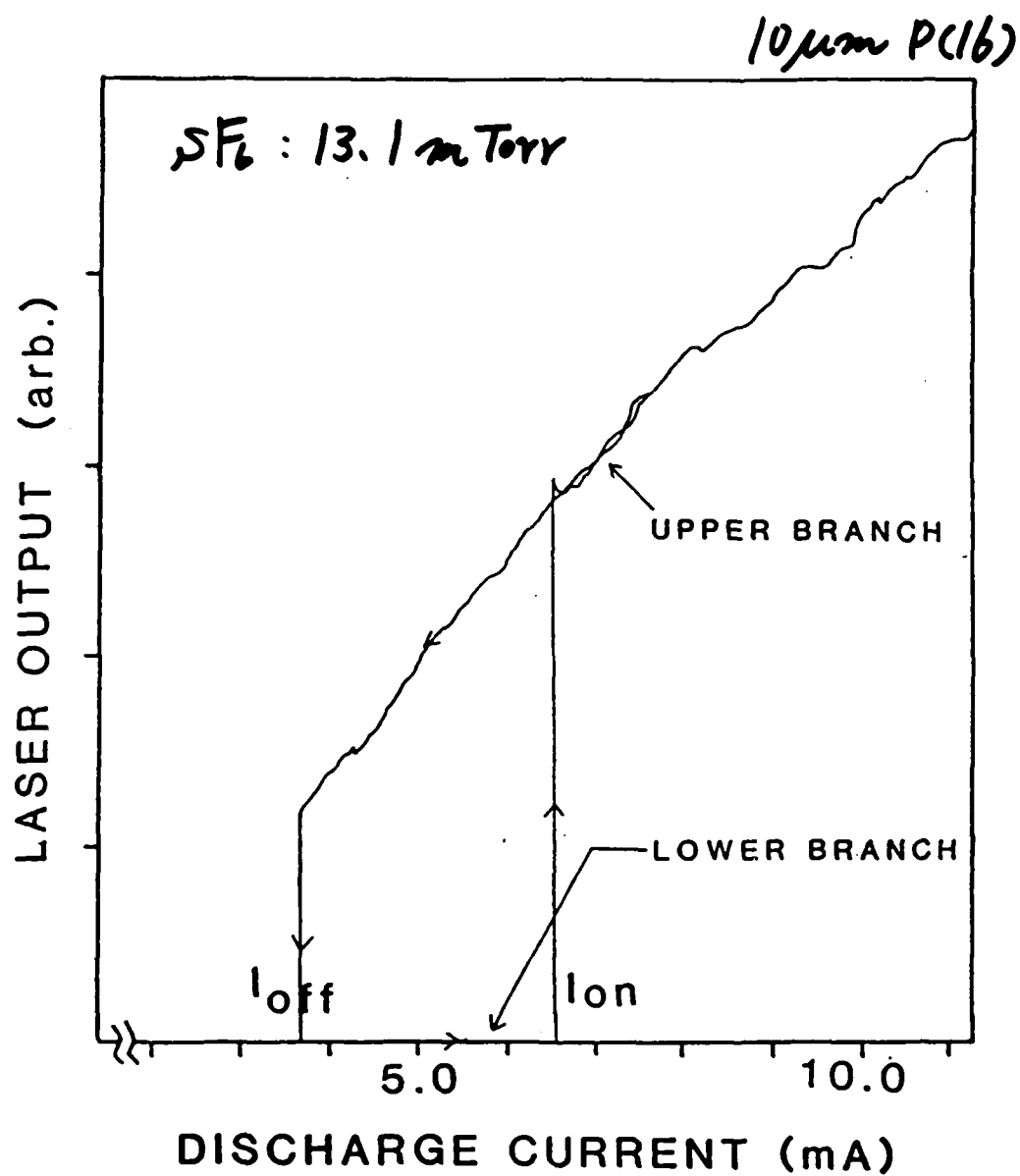


FIG.3 OBSERVED HYSTERESIS CURVE OF THE LASER OUTPUT
AS A FUNCTION OF THE DISCHARGE CURRENT

Rate Equations

$$\frac{dn}{dt} = B_g f_g(J) n (M_1 - M_2) \frac{l_g}{L} - B_a n N \frac{l_a}{L} - \kappa n + A M_1$$

$$\frac{dM_1}{dt} = -B_g f_g(J) n (M_1 - M_2) + P M - (P + R_{10} + R_{12}) M_1 - P M_2$$

$$\frac{dM_2}{dt} = B_g f_g(J) n (M_1 - M_2) + R_{12} M_1 - R_{20} M_2$$

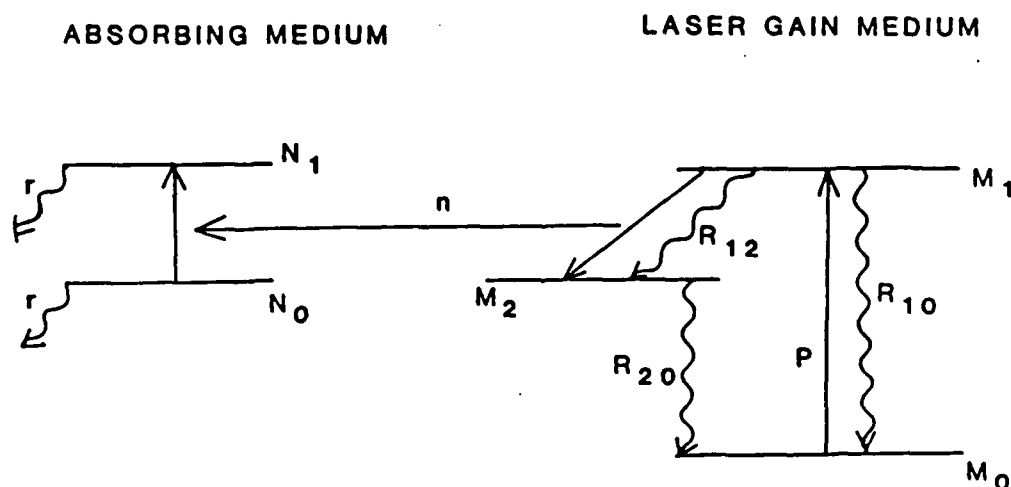
$$\frac{dN}{dt} = -2 B_a n N - r (N - N^*)$$

n : photon density

M_1 : population density on the upper laser level

M_2 : population density on the lower laser level

N : difference of population density between the absorption levels



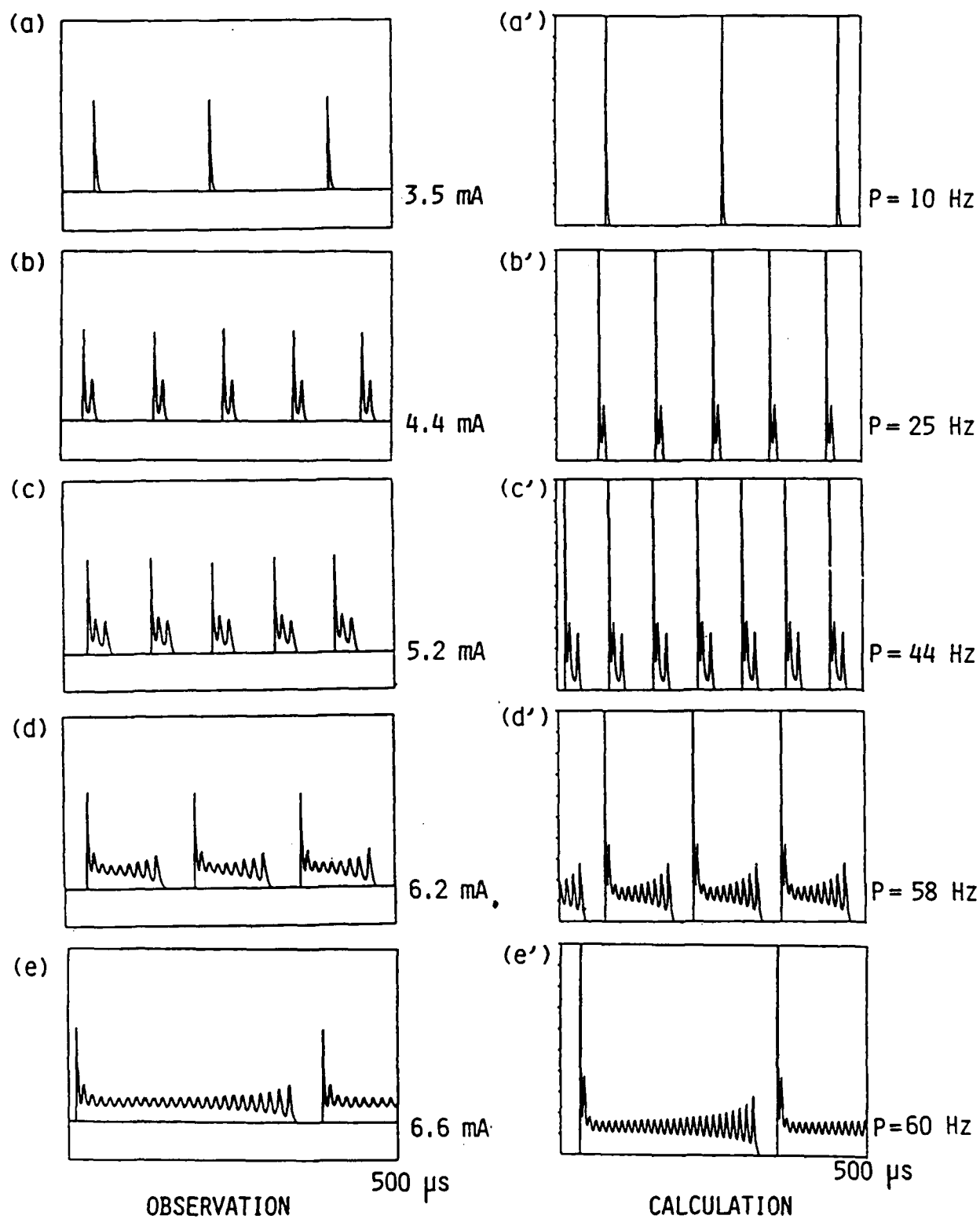


FIG.6 DEPENDENCE OF PQS PULSES ON THE DISCHARGE CURRENT
IN THE HCOOH CASE

(HCOOH: 58 mTorr)

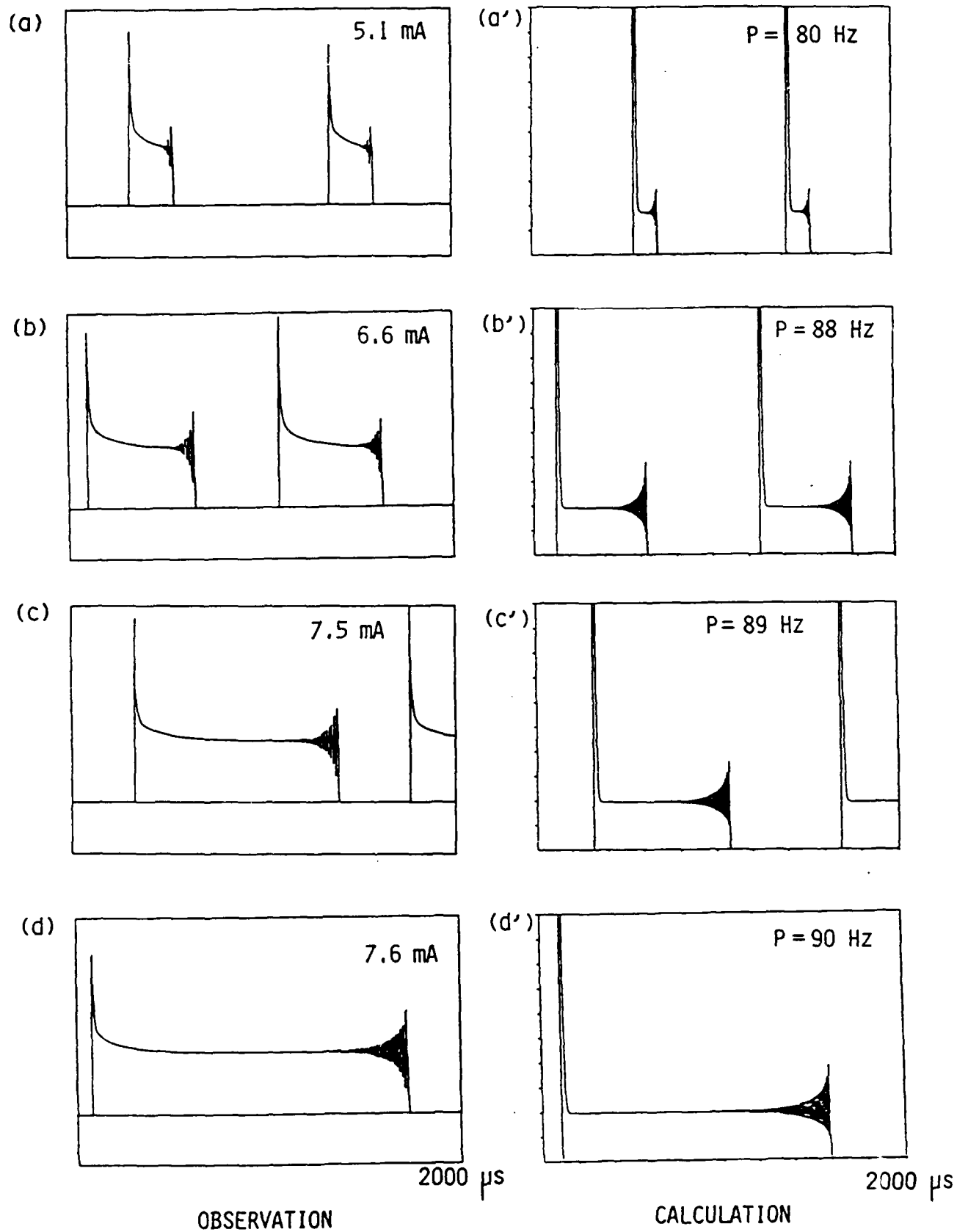


FIG.7 DEPENDENCE OF PQS PULSES ON THE DISCHARGE CURRENT
IN THE SF_6 CASE ($\text{SF}_6 : 23 \text{ Torr}$)

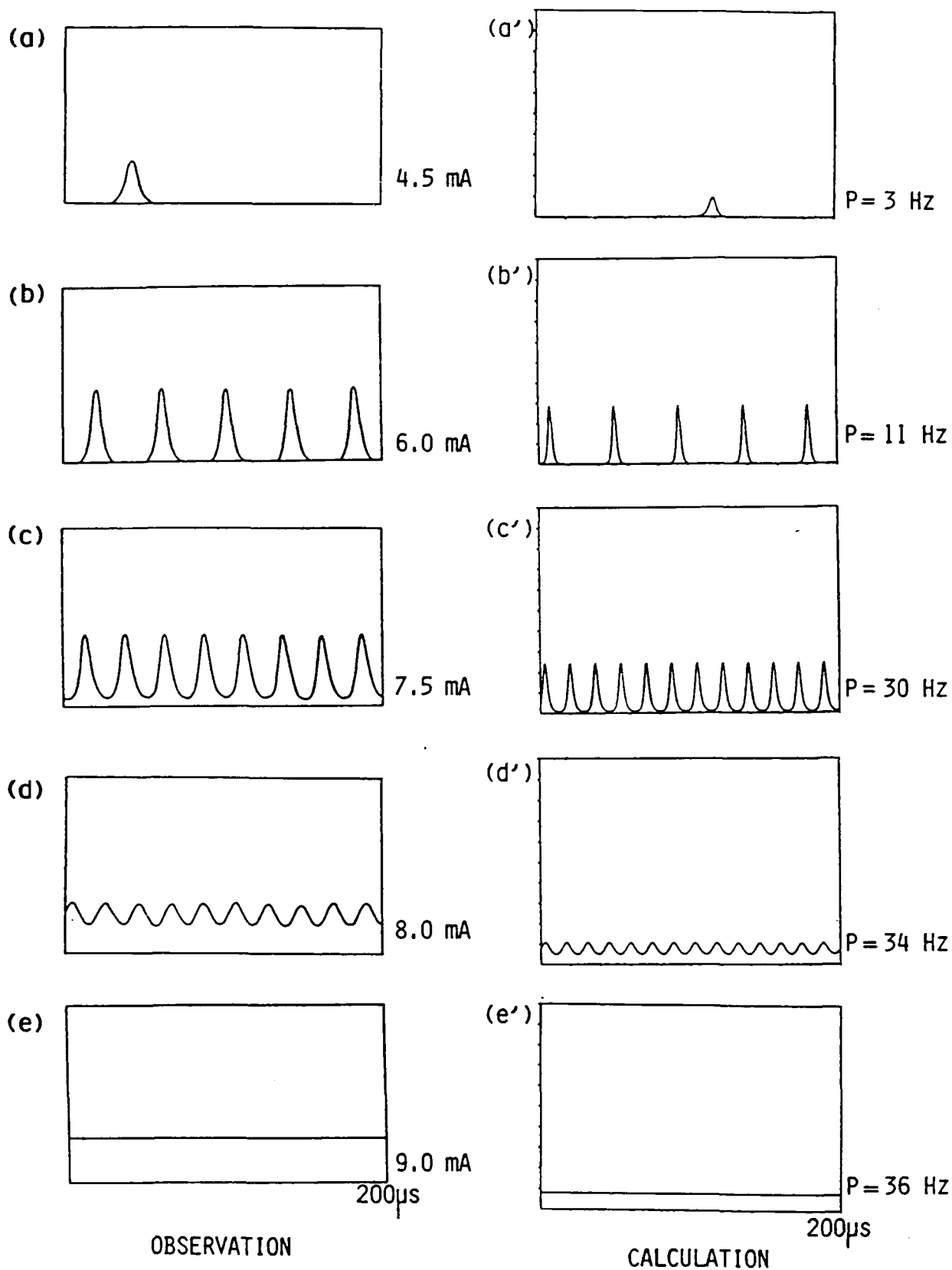
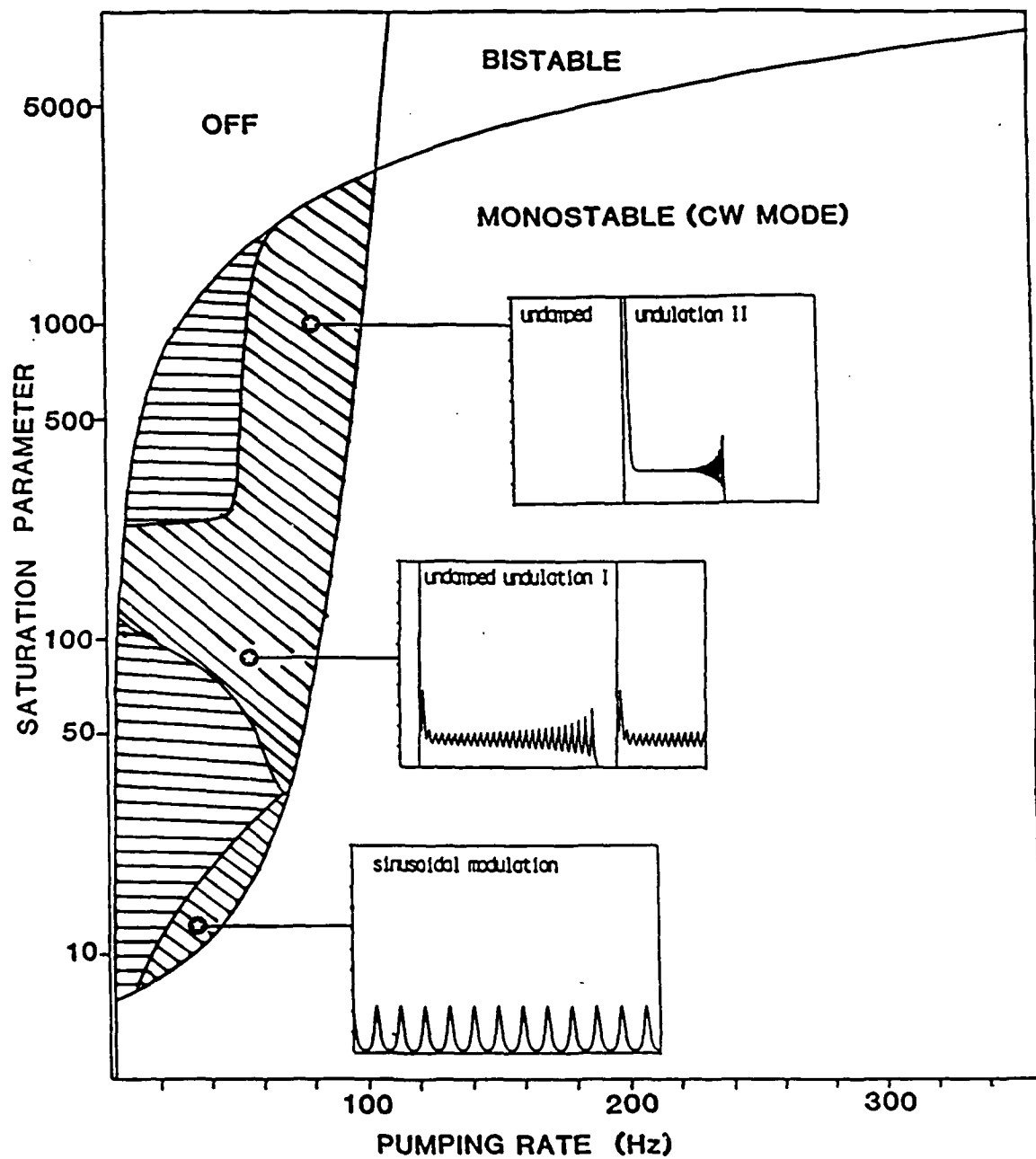


FIG.5 DEPENDENCE OF PQS PULSES ON THE DISCHARGE CURRENT
IN THE CH_3OH CASE

($\text{CH}_3\text{OH} : 325\text{ mTorr}$) -543-



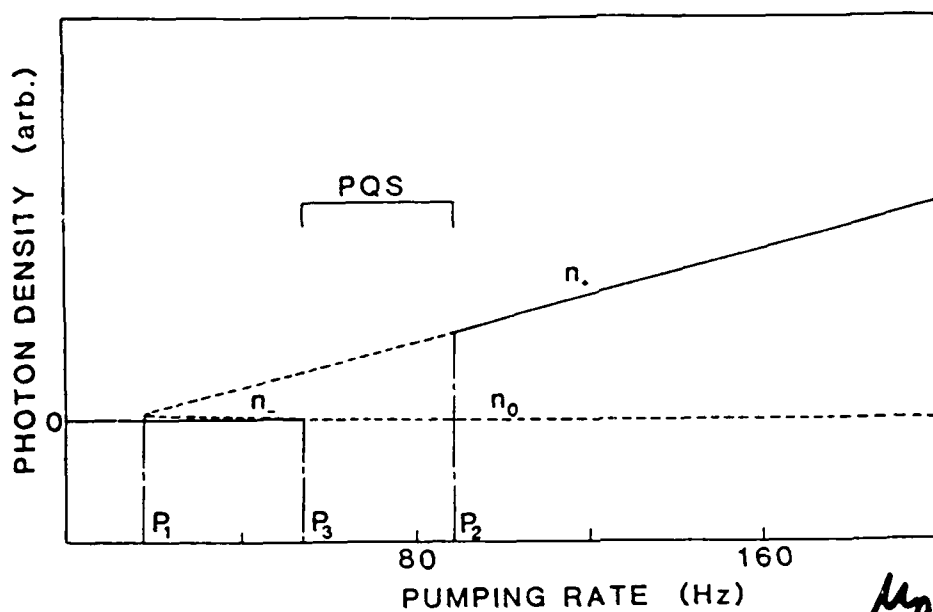
saturation parameter

$$\equiv \frac{Ba}{\gamma} = \frac{1}{\gamma} \frac{2\pi^2 \nu \mu_a^2}{3\epsilon_0 h} \cdot g(\nu - \nu_0)$$

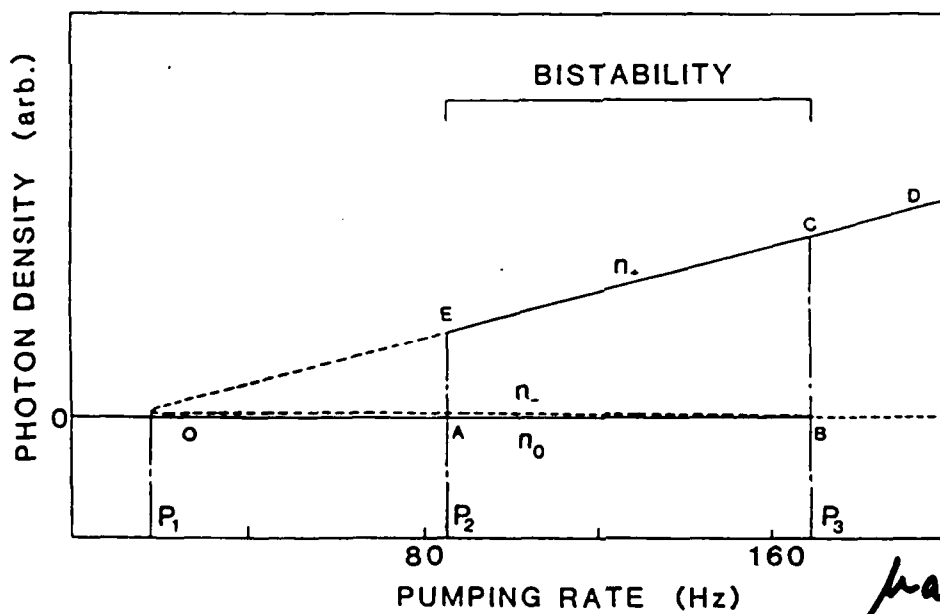
▨ · PQS with undulation

▨ · sinusoidal modulation

▨ · single spike



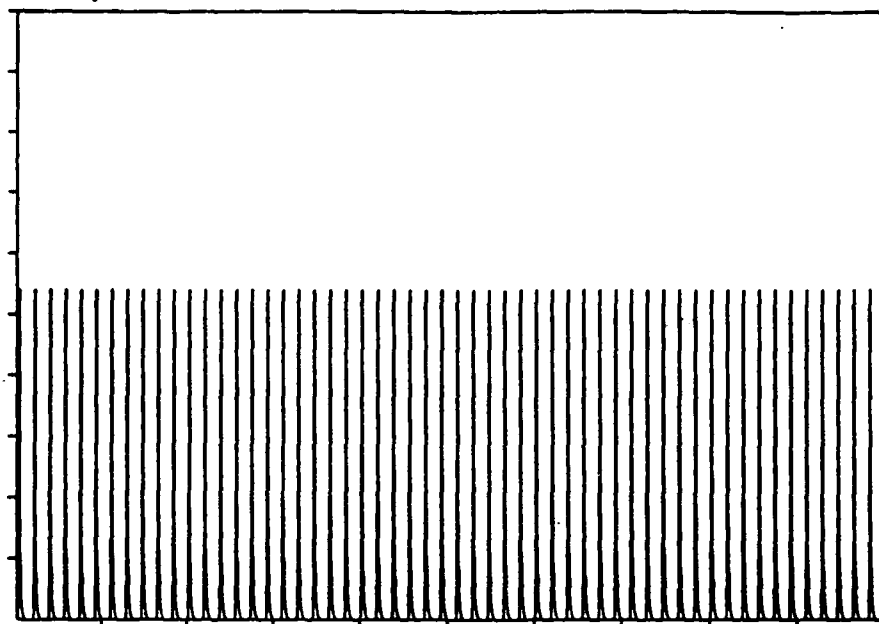
$$\mu_a = 0.20 D$$



$$\mu_a = 0.35 D$$

FIG.9 STATIONARY SOLUTION OF THE PHOTON DENSITY
AS A FUNCTION OF THE PUMPING RATE

(1) period - 1

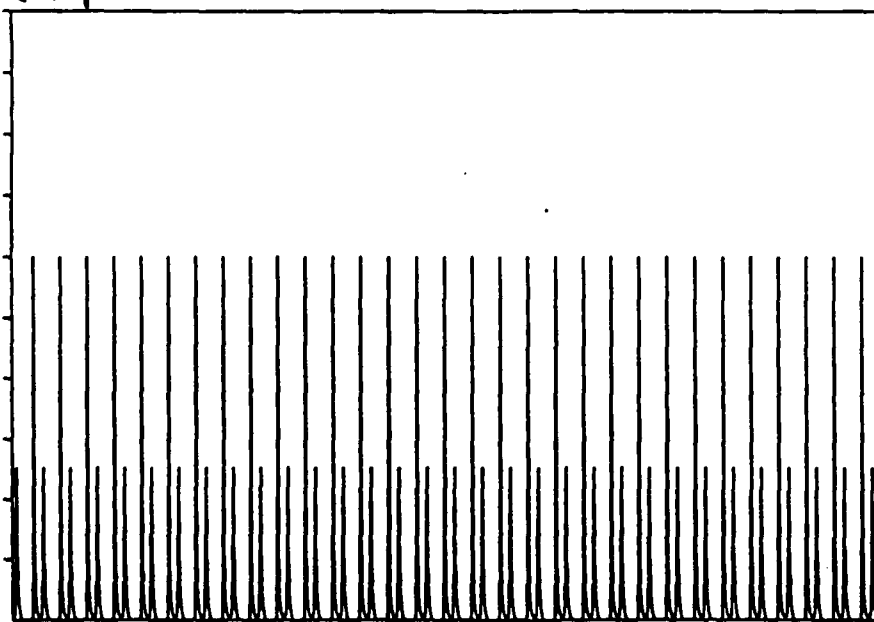


pumping rate

$$P = 61 \text{ Hz}$$

1000 μs

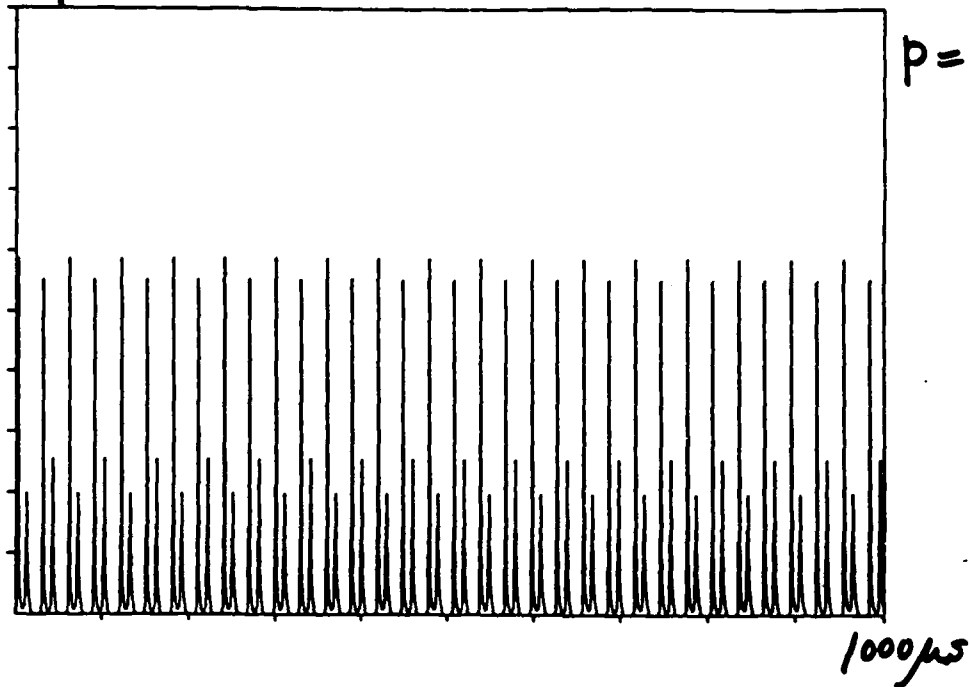
(2) period - 2



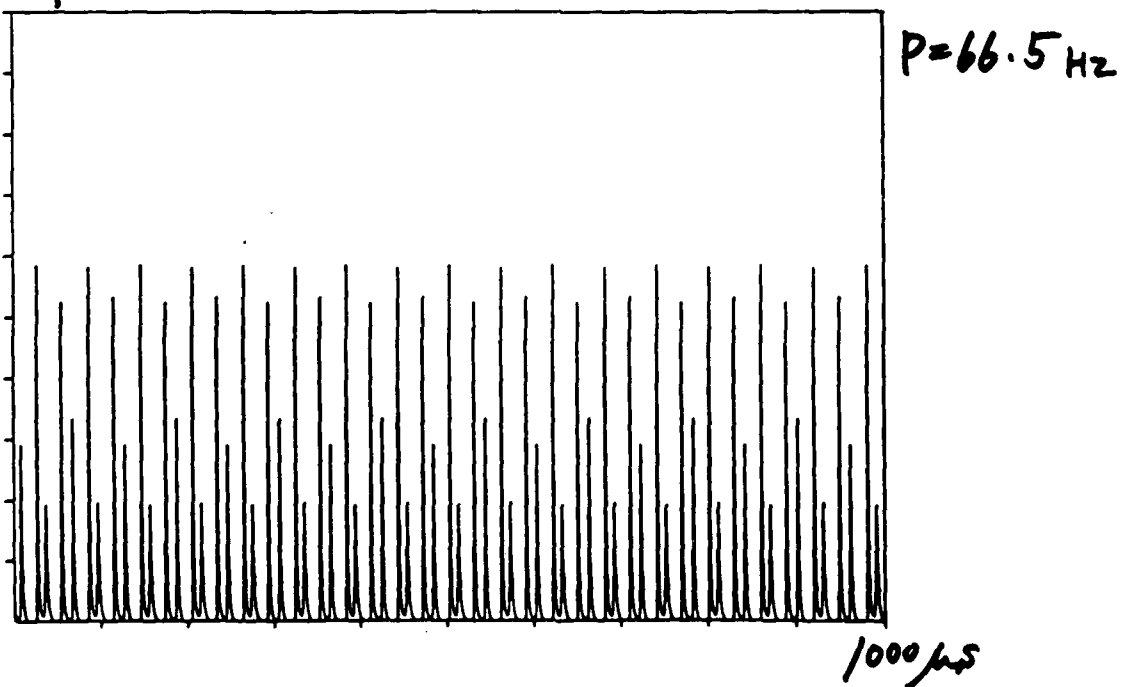
$$P = 63 \text{ Hz}$$

1000 μs

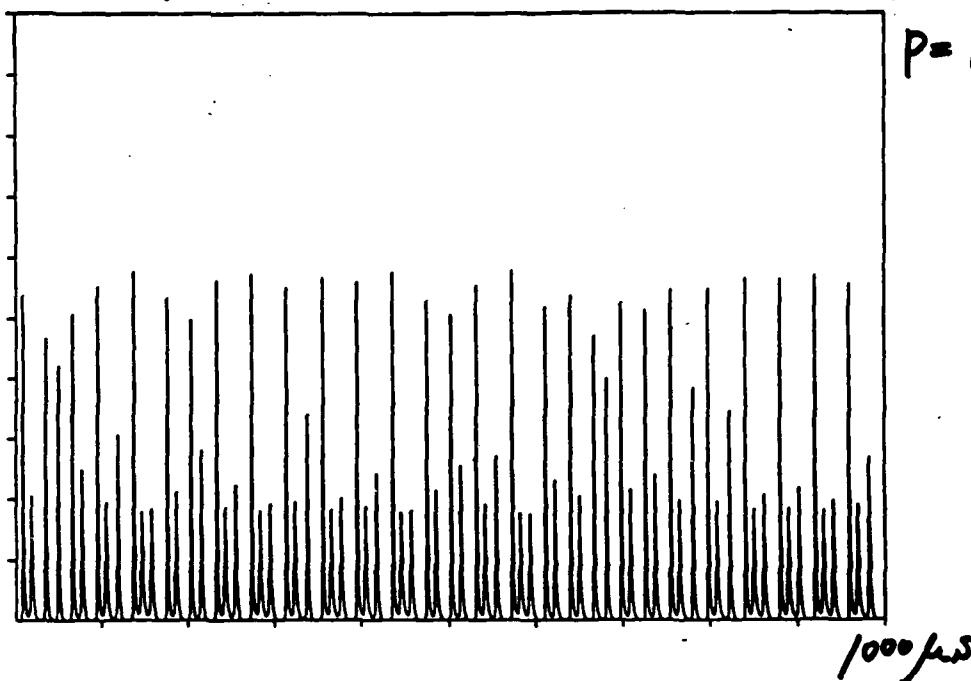
(3) period - 4



(4) period - 8

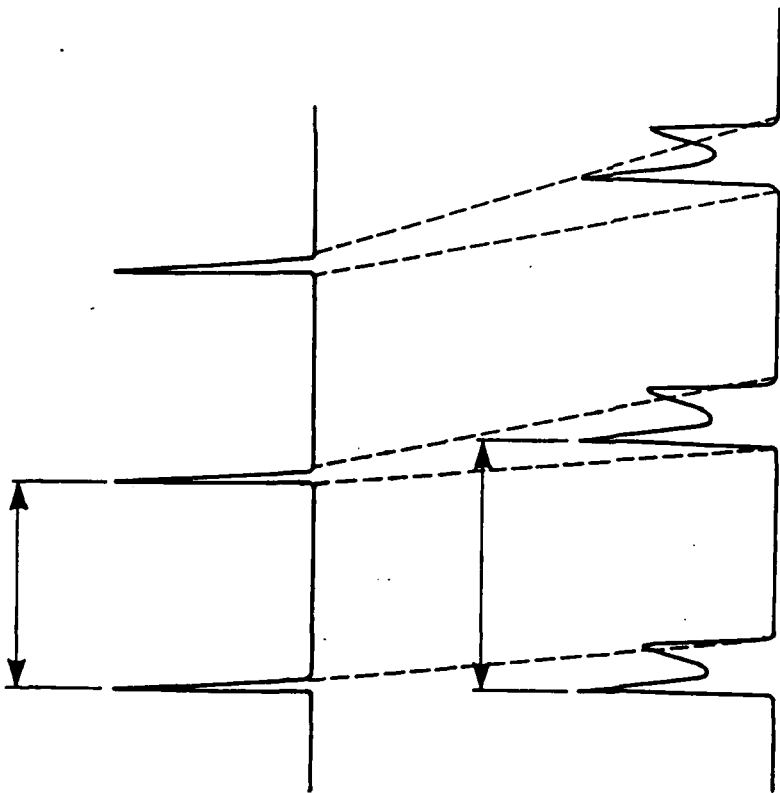


(5) chaos

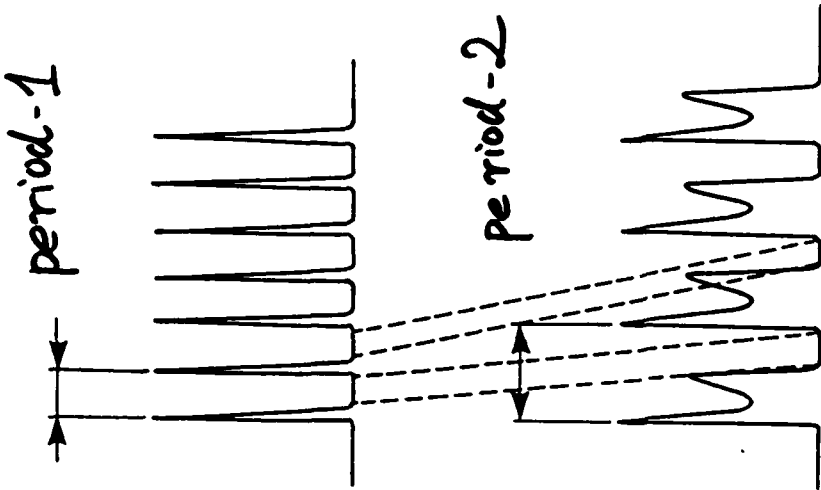


* first chaos in a laser system containing a saturable absorber inside its cavity
(first aperiodic passive Q-switching)

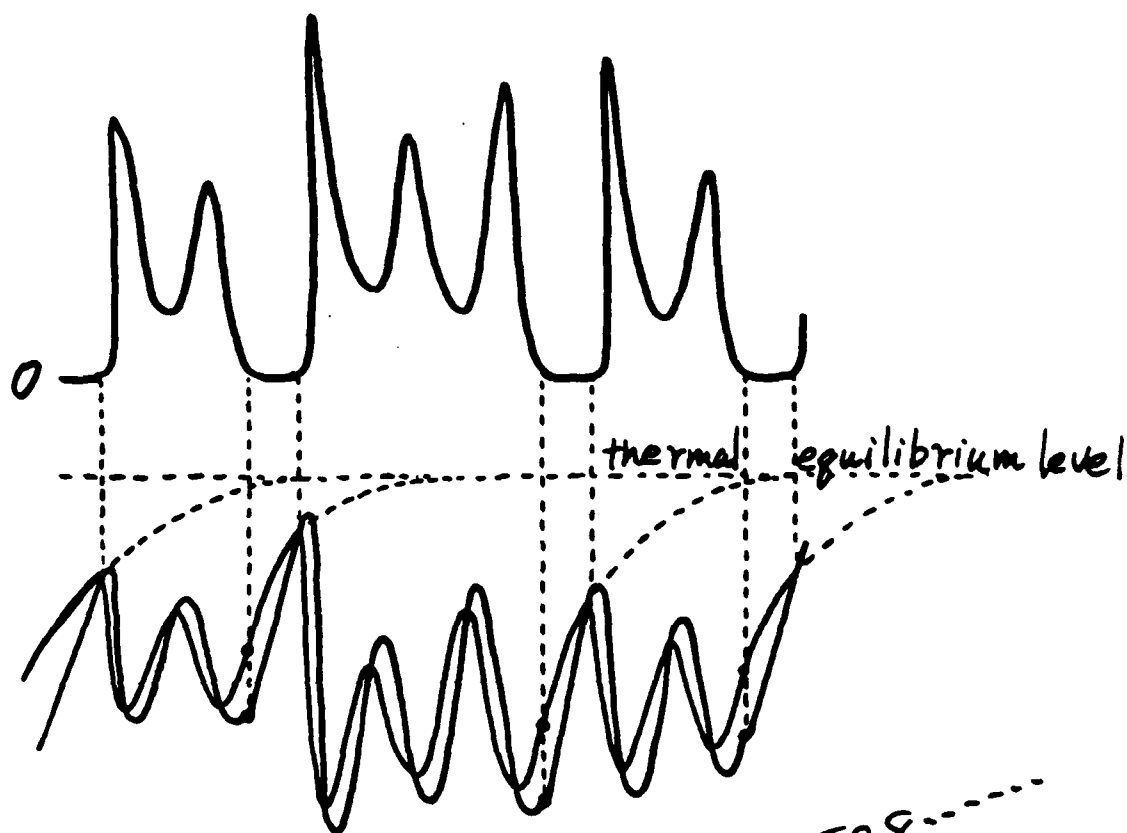
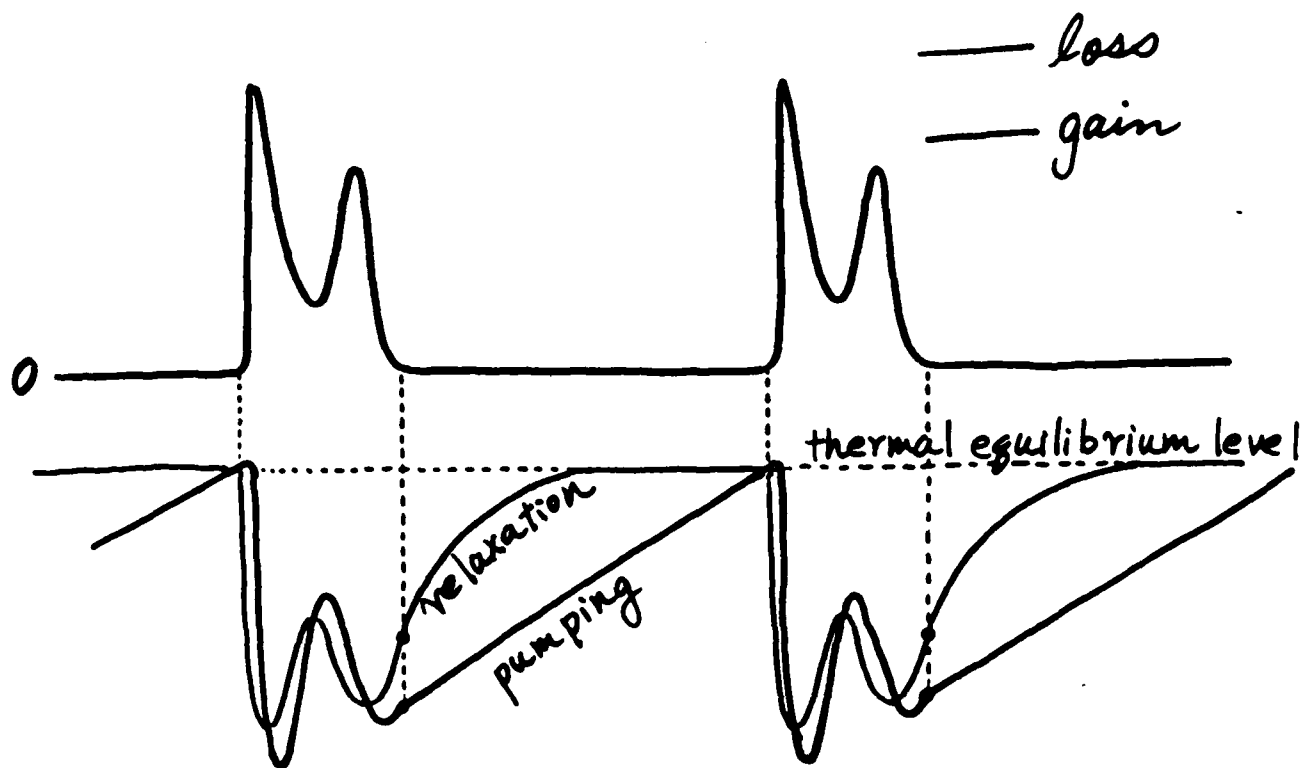
→ even in a laser with small gain
(such as CO_2 , N_2O lasers)



periodic PDS pulses with many peaks
 ⇓



⇓
 period-doubling route
 to chaos



π 3.141528...
 ???
 -550-

Summary

1. The rate-equation approximation is very effective to describe the PDS in a CO_2 laser with gaseous saturable absorbers, and all the pulse shapes are reproduced in the computer simulation based on the rate-equation model.

Simultaneous presence of PDS and bistability can not be derived from the present model. \longrightarrow Maxwell-Bloch equations may be desirable.

2. Chaos was demonstrated for the first time in a laser system with saturable absorber.

The presence of two close time-constants may be essential to produce chaos in this case.

RECENT PROGRESS IN OPTICAL BISTABILITY AND TRISTABILITY

T. Yabuzaki and M. Kitano *,

Department of Physics, Kyoto University, Kyoto 606, Japan, and

* Radio Atmospheric Science Center, Kyoto University, Uji, Kyoto
611, Japan

Summary

In recent years we have been studying theoretically and experimentally on the new type of optical bistability and tristability, and on the related phenomena such as self-pulsing, chaos, and transient chaos. I would like to focus my present talk on the optical bistability in the first place, which is caused by the spin polarization in the presence of optical feedback. This bistability is considerably different from the ordinary one, because it has no hysteresis cycle, while it does have a pitchfork bifurcation, i.e. symmetry-breaking. Secondly I would like to talk about the self-switching of the light polarization by spin-precession, which takes place in the same optical system. Finally, I discuss about the multistability observed experimentally, using simplified models with coupling between spatial modes of light.

Recent Progress In Optical Bi- and Tri-Stability

T. Yabuzaki and M. Kitano
Kyoto University

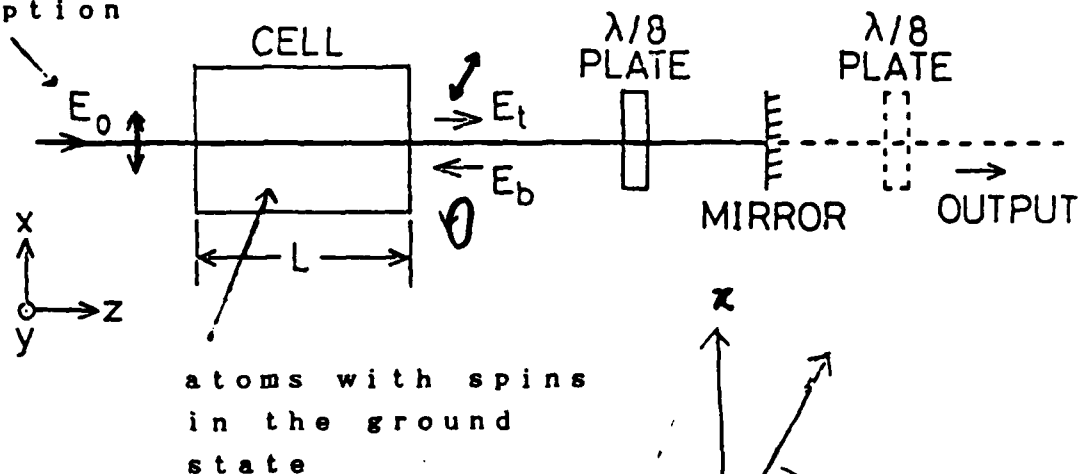
Bistability and tristability with
symmetry-breaking caused by the spin-
polarization through optical pumping
in the presence of optical feedback

Focused Phenomena

- o (1) Self-pulsing, or self-sustained
spin-precession associated with
the optical bistability with
symmetry-breaking
- o (2) Optical multistability in the same
system
- (2) Chaos and transient chaos in the
optically tristable system

Optical Bistability with Symmetry Breaking

near-resonant
to absorption
line

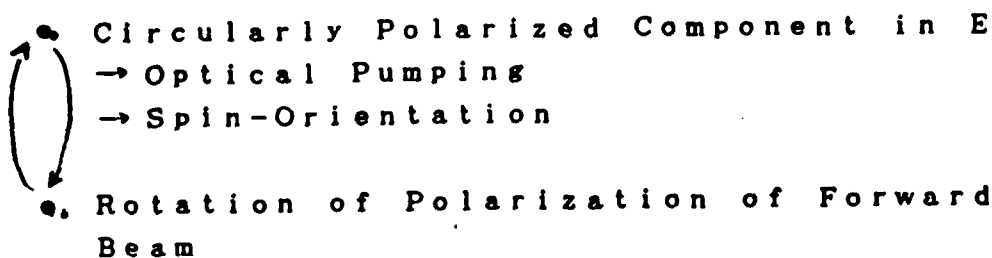


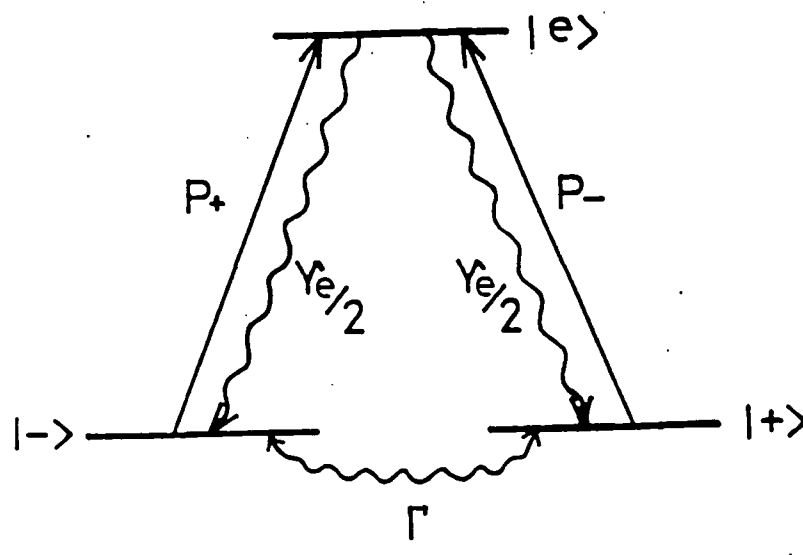
Positive Feedback Loop

for rotation of polarization of
forward beam

or

spin orientation





steady state population

$$I_{\pm} = I_0 \left\{ 1 \pm \frac{1}{2} \sin 2(\theta + \theta_0) \right\}$$

$$N_{\pm} = \frac{I_{\pm} + 1}{I_{+} + I_{-} + 2} N_0$$

wavenumber & absorption coeff.

$$k_{\pm} = k_0 + (\sigma/2) (\Delta\omega/\gamma_e) N_{\mp}$$

$$d_{\pm} = (\sigma/2) N_{\mp}$$

$$\Delta\omega = \omega - \omega_0$$

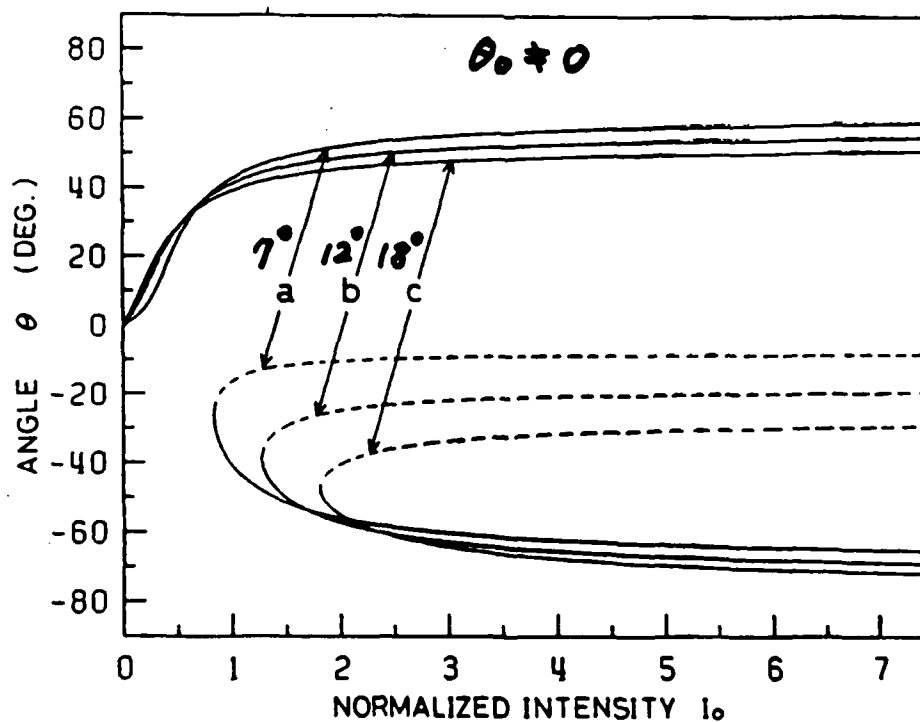
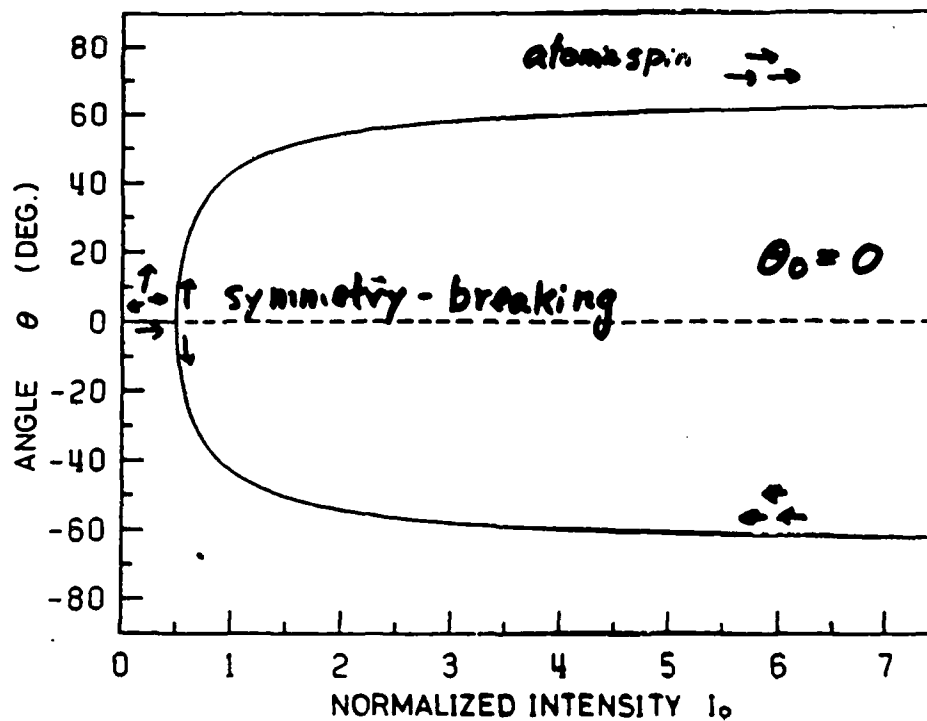
$$\theta = (L/2) (k_{+} - k_{-})$$

rotation angle θ

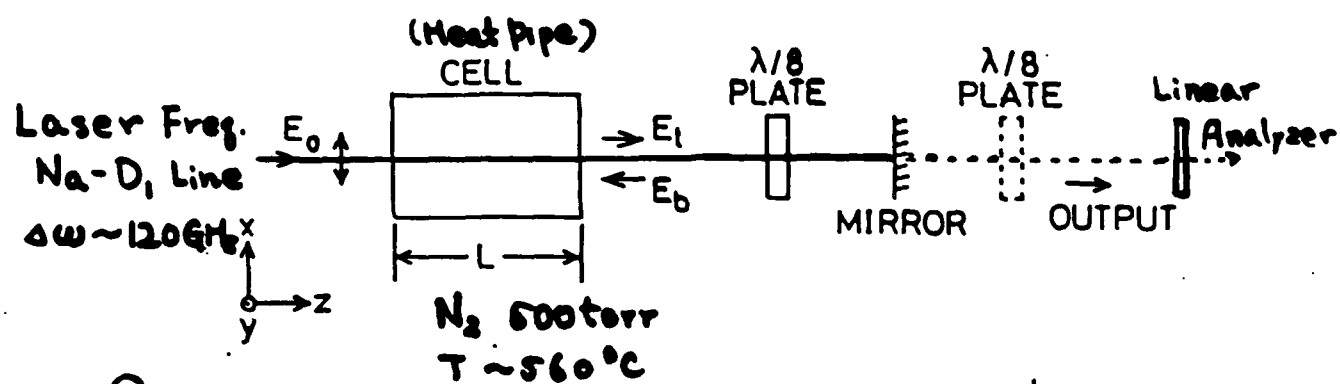
$$\theta = \frac{kL}{2} \frac{I_0 \sin 2(\theta + \theta_0)}{I_0 + 1}$$

I_0 : incident light intensity -555-

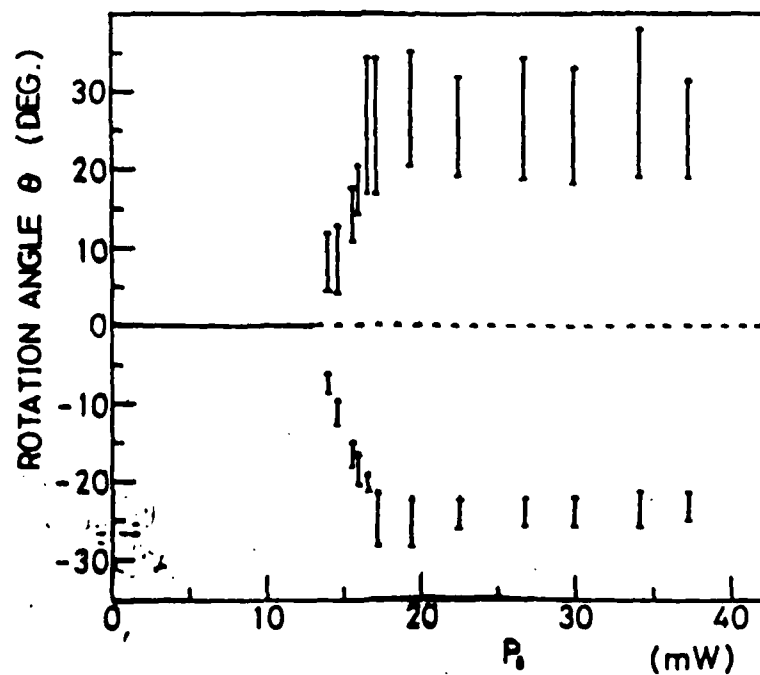
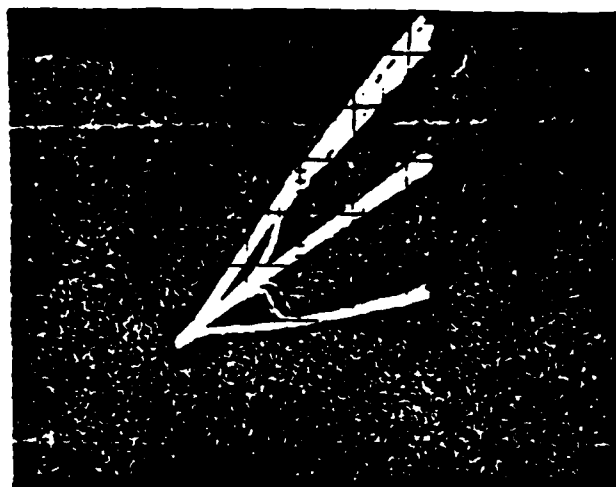
θ_0 : offset angle of $\lambda/8$ plate



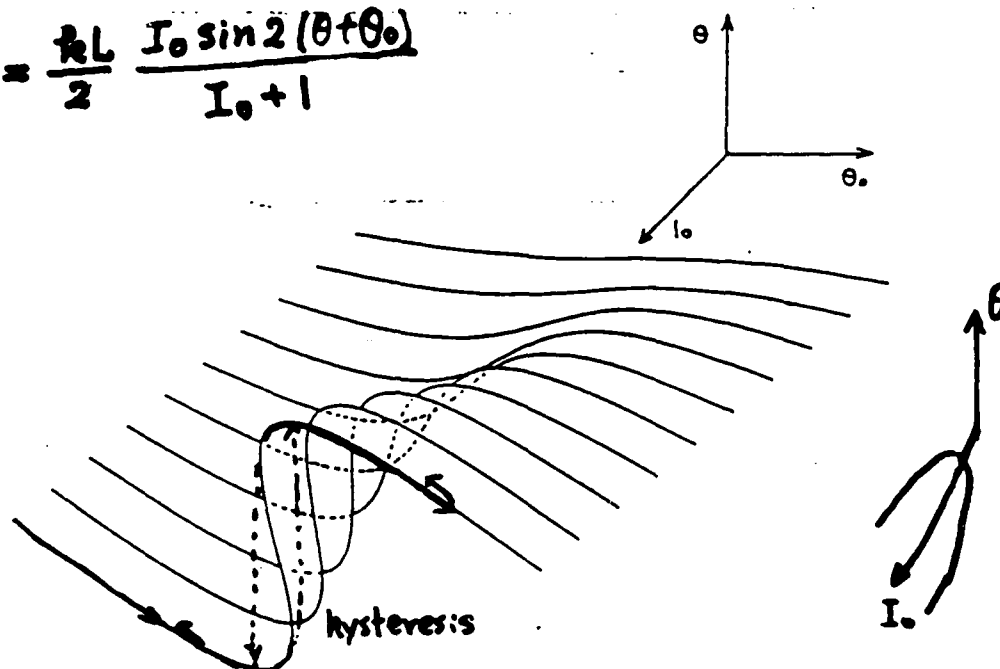
Experiment



$$I_1 \propto I_0 \cos^2(\theta + 45^\circ)$$



$$\theta = \frac{kL}{2} \frac{I_0 \sin 2(\theta + \theta_0)}{I_0 + 1}$$



Cusp Catastrophe

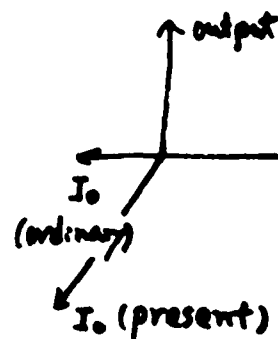
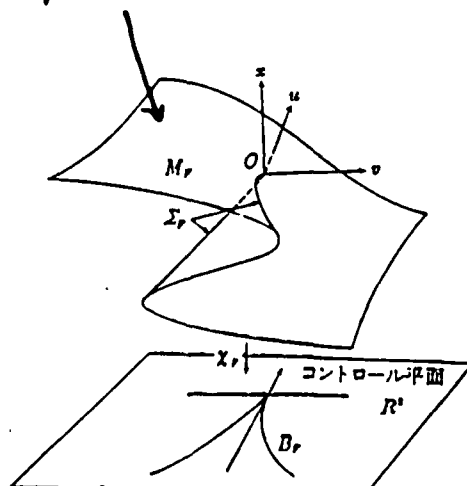
system potential

$$V(x) = \frac{1}{4} x^4 + \frac{1}{2} u x^2 + v x$$

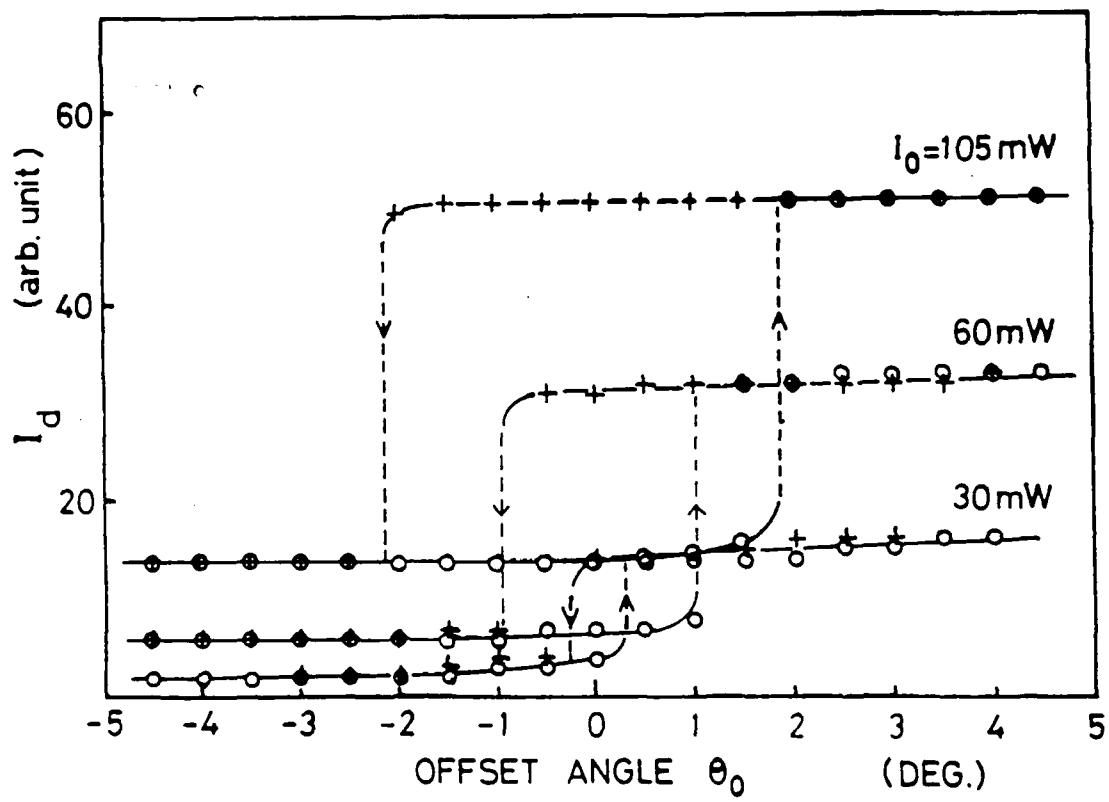
x : behavior variable

u, v : control parameter

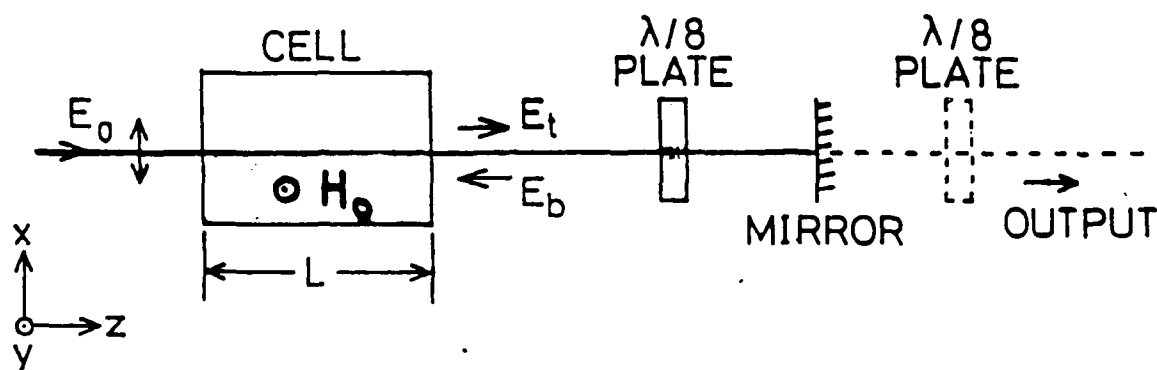
steady state surface $\partial V(x)/\partial x = 0$



(B) (Aの図を向こう側($u < 0$ の側)よりみた図)



Self-Pulsing by Spin Precession



Bloch eq. for $\theta_0 = 0$

$$\frac{dm_x}{dt} = -\Omega_0 m_z - \Gamma(1 + I_0) m_x$$

$$\frac{dm_z}{dt} = -\Omega_0 m_x - \Gamma(1 + I_0) m_z + \frac{\Gamma I_0}{2} \sin 2kL m_z$$

$$(\Omega_0 = \gamma H_0)$$



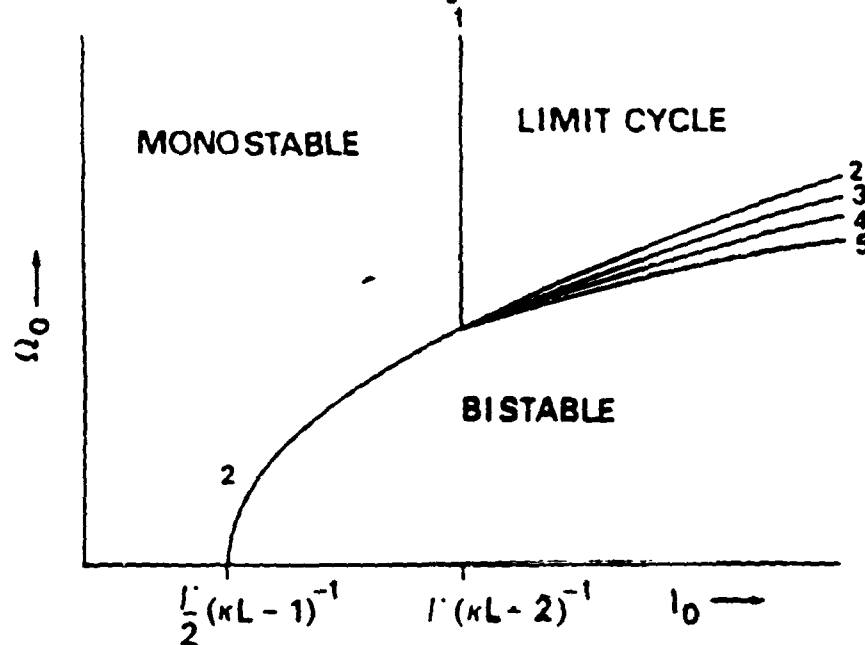
van der Pol equation

Steady-state solutions

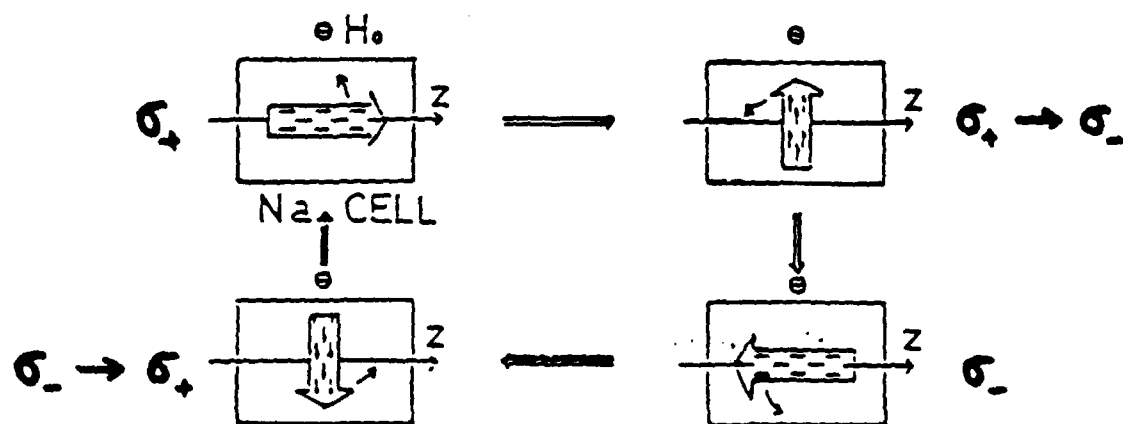
- o monostable solution $(m_x, m_z) = (0, 0)$
- o bistable solutions $(m_{x0}, m_{z0}), (-m_{x0}, -m_{z0})$
- o rotation along a limit cycle

-560-

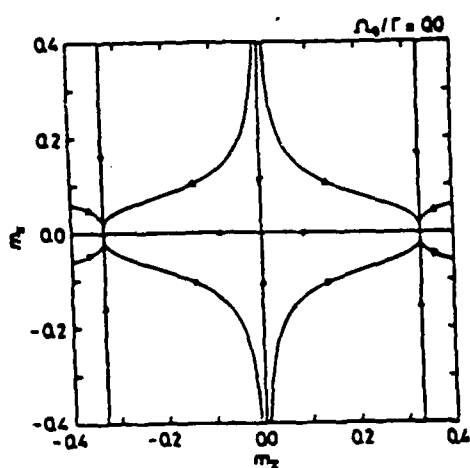
Phase Diagram



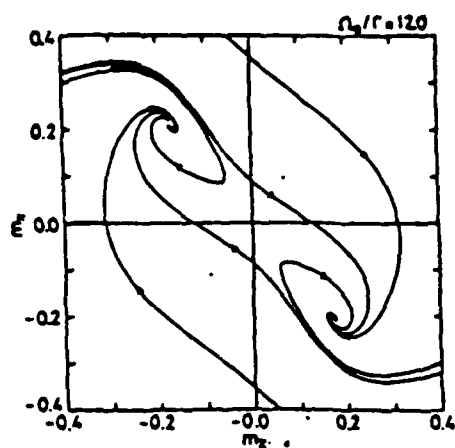
Spin-precession by synchronous Switching of Polarization



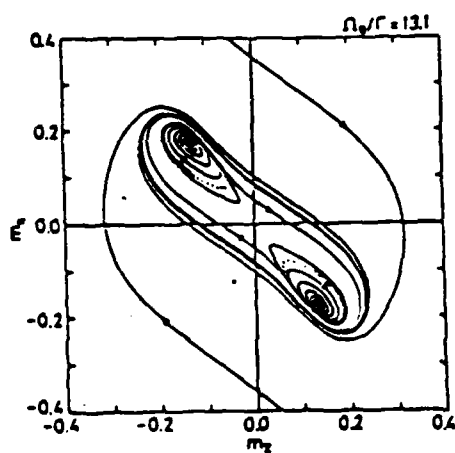
$I_0 = 9$
 $KL = 3.5$



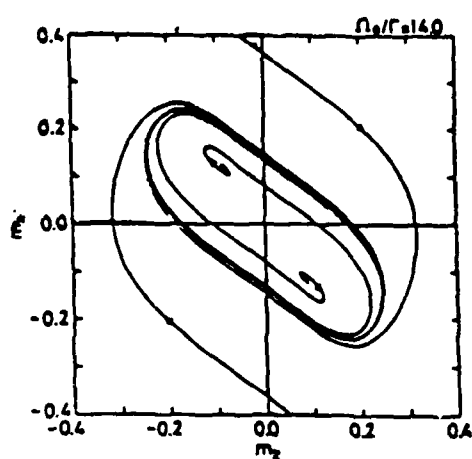
(a)



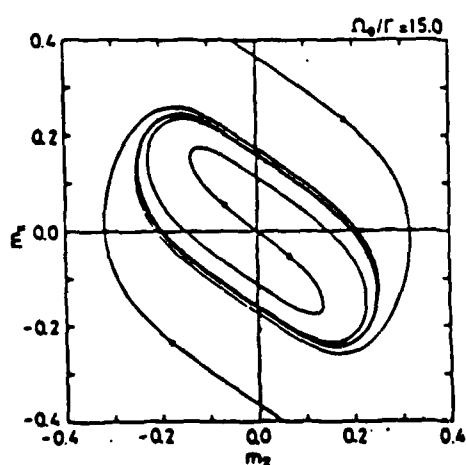
(b)



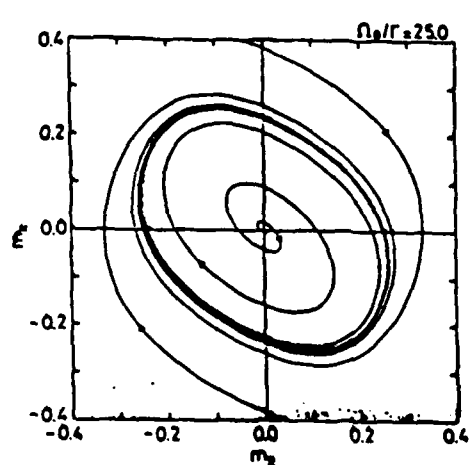
(c)



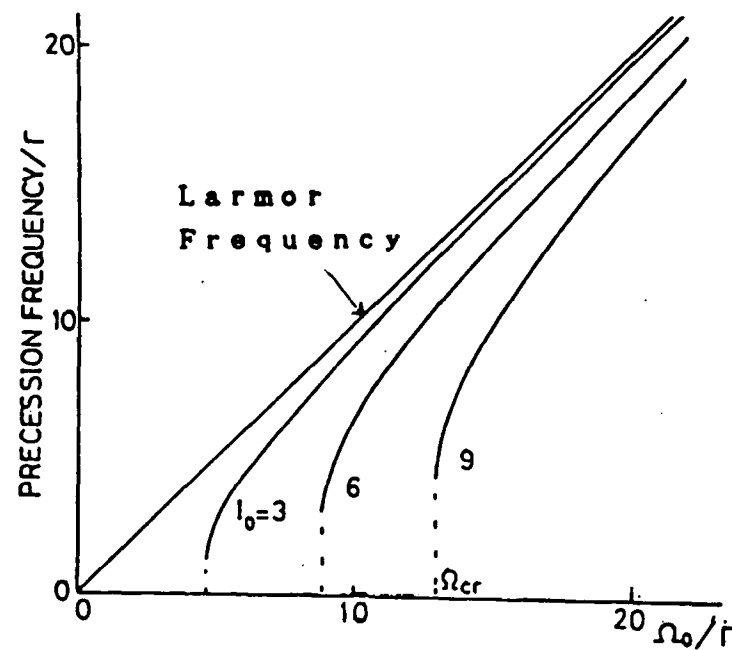
(d)



(e)



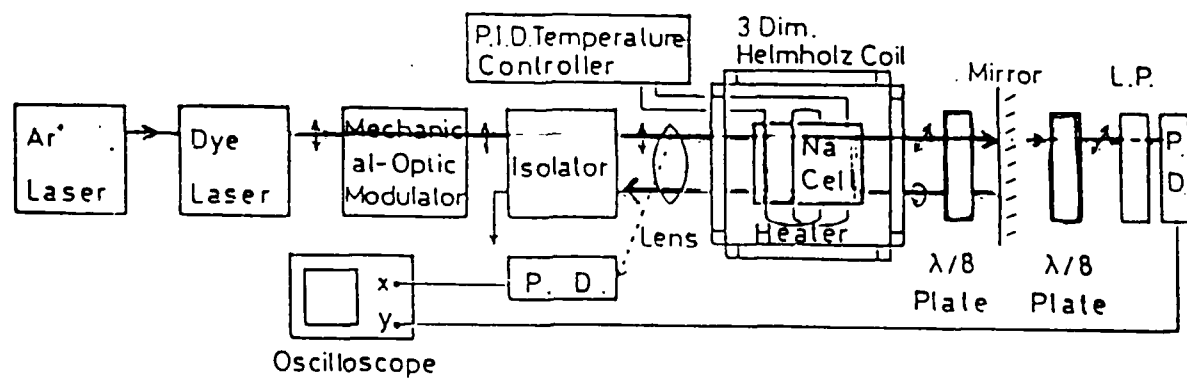
(f)

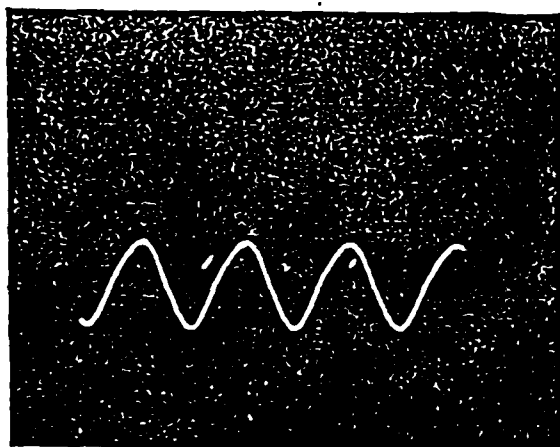


Upper limit of precession Frequency

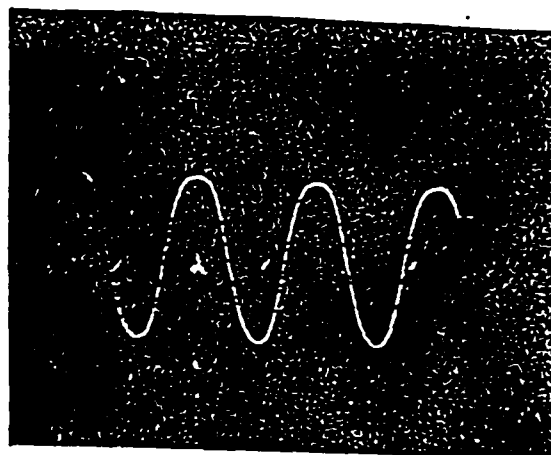
~ width of the absorption line.

(In the present experiment,
pressure broadening of the D_2 line
at He pressure ~500 torr is about
10 GHz.)

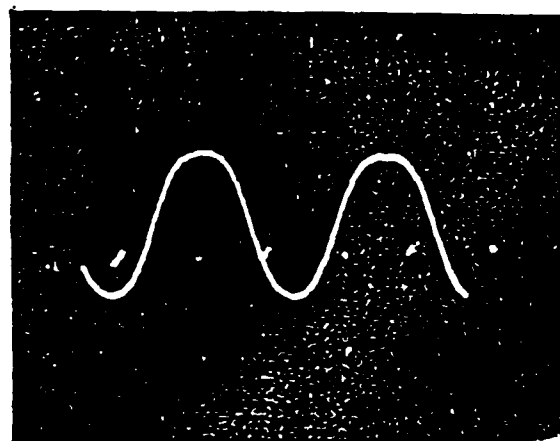




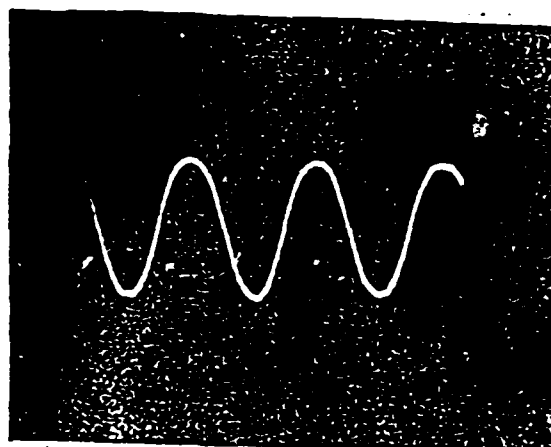
(a) $H_y = 0.158$ (Gauss)



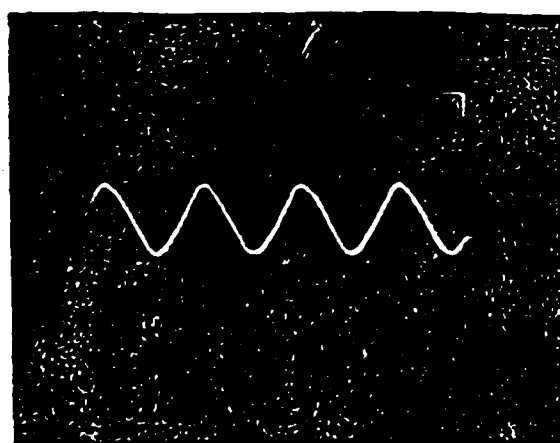
(b) $H_y = 0.455$ (Gauss)



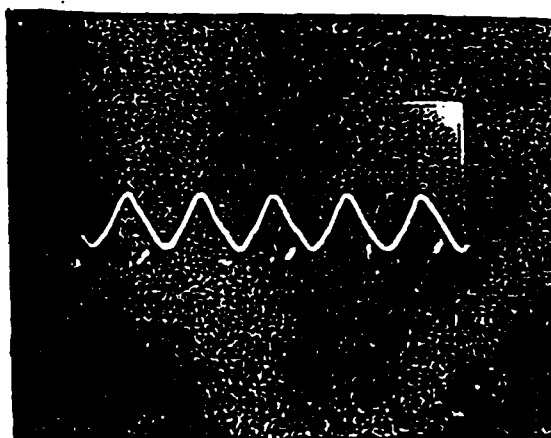
(c) $H_y = 1.364$ (Gauss)



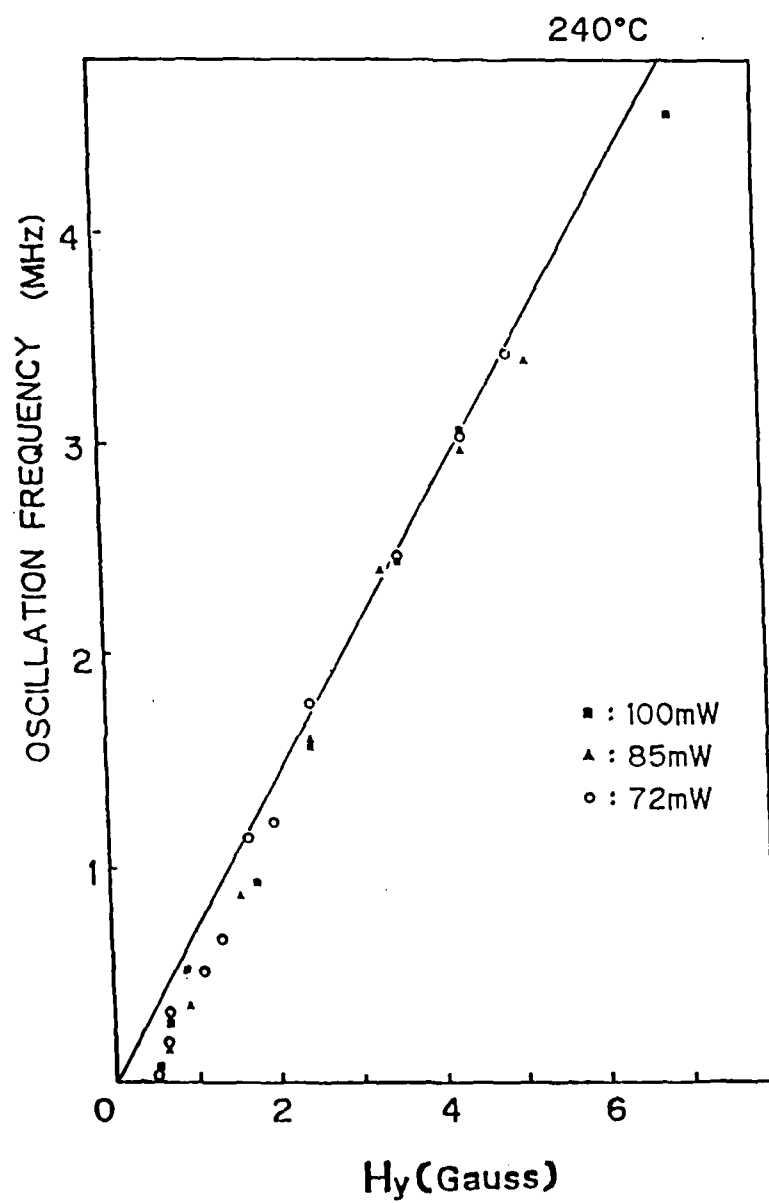
(d) $H_y = 2.948$ (Gauss)

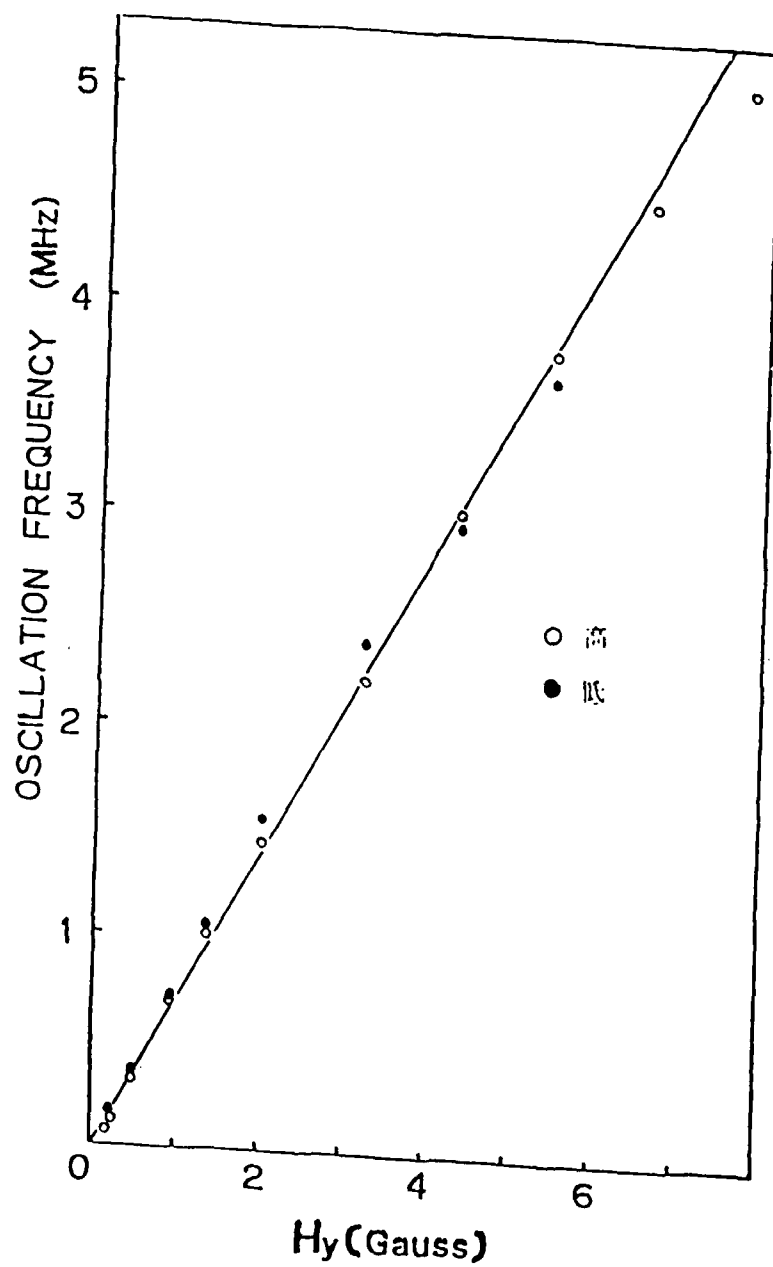


(e) $H_y = 5.464$ (Gauss)

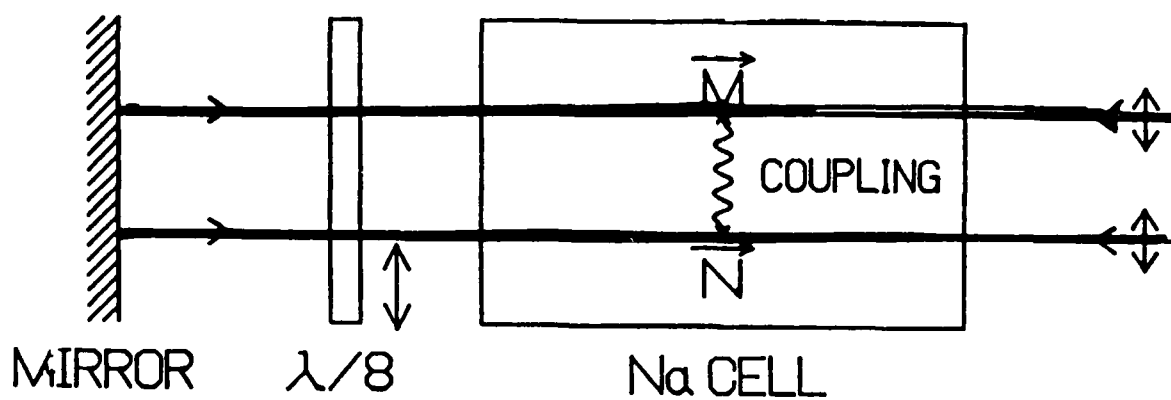


(f) $H_y = 7.741$ (Gauss)



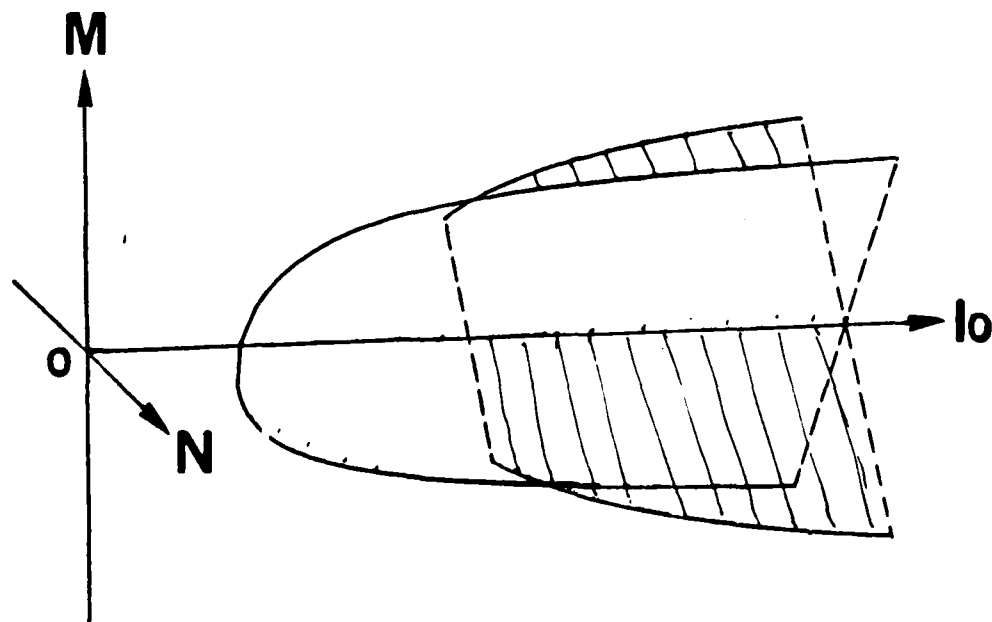


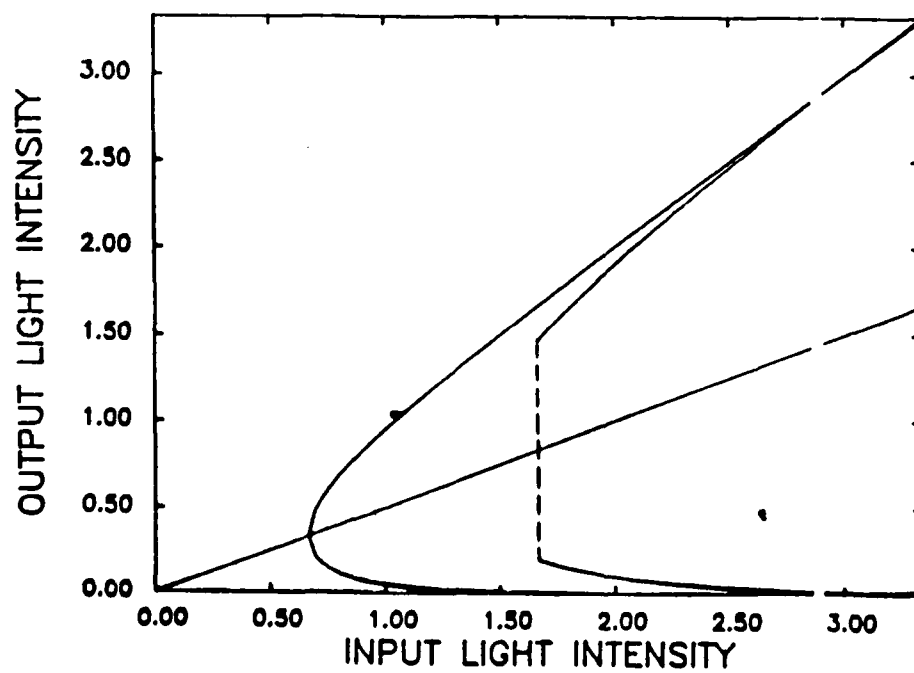
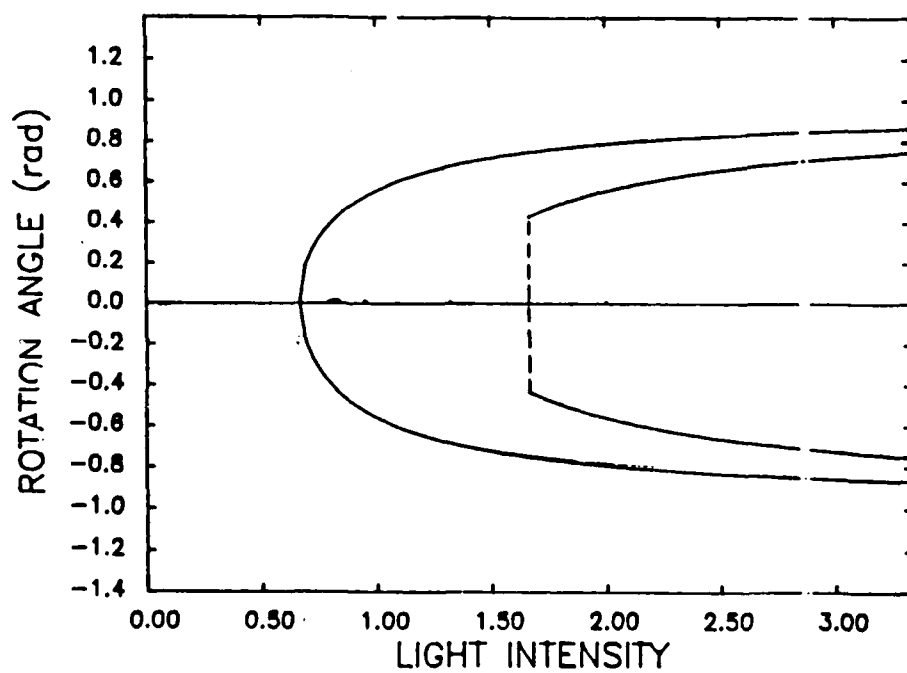
1



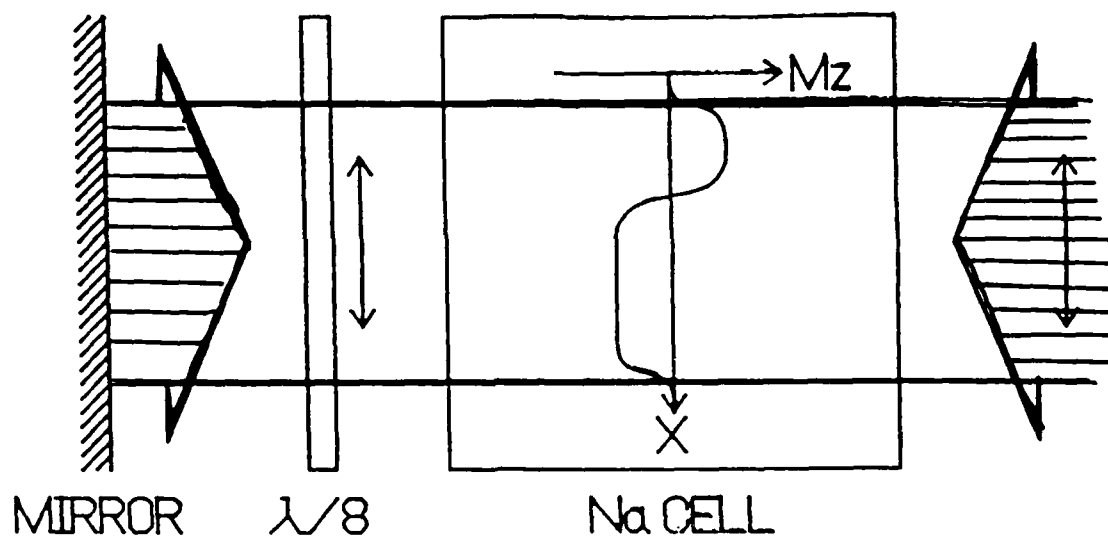
$$\begin{cases} \frac{dM}{dt} = -\gamma M + \mu M (1 - a M^2) + c (N - M) \\ \frac{dN}{dt} = -\gamma N + \mu N (1 - a N^2) + c (M - N) \end{cases}$$

coupling coeff.
 c : 結合係数





2

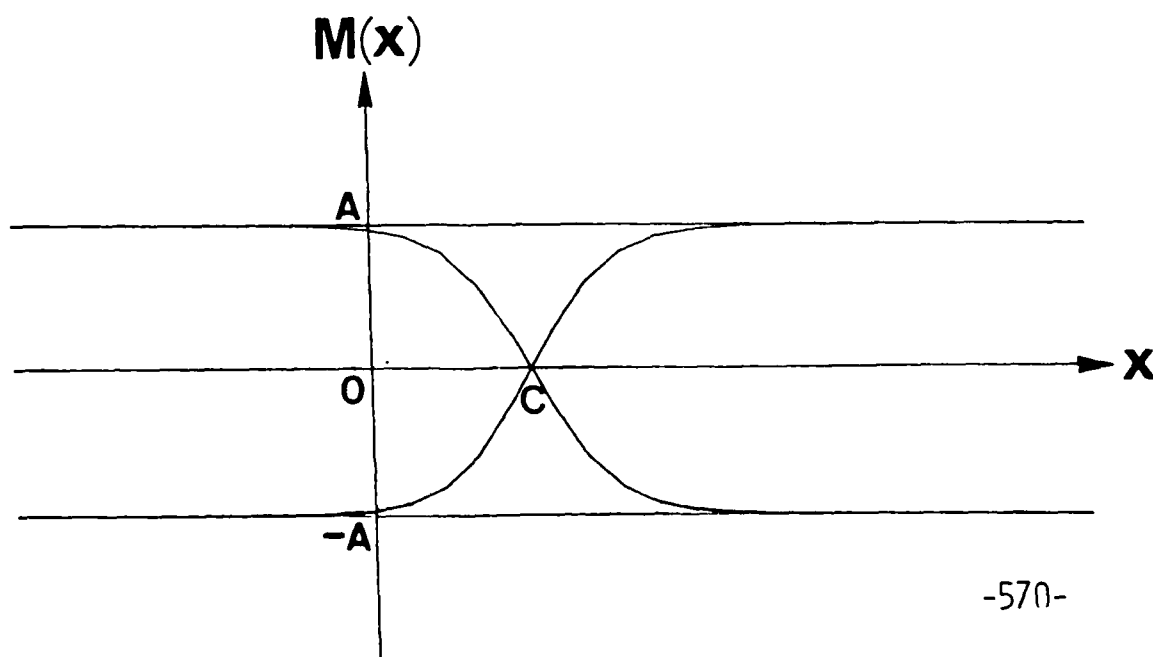


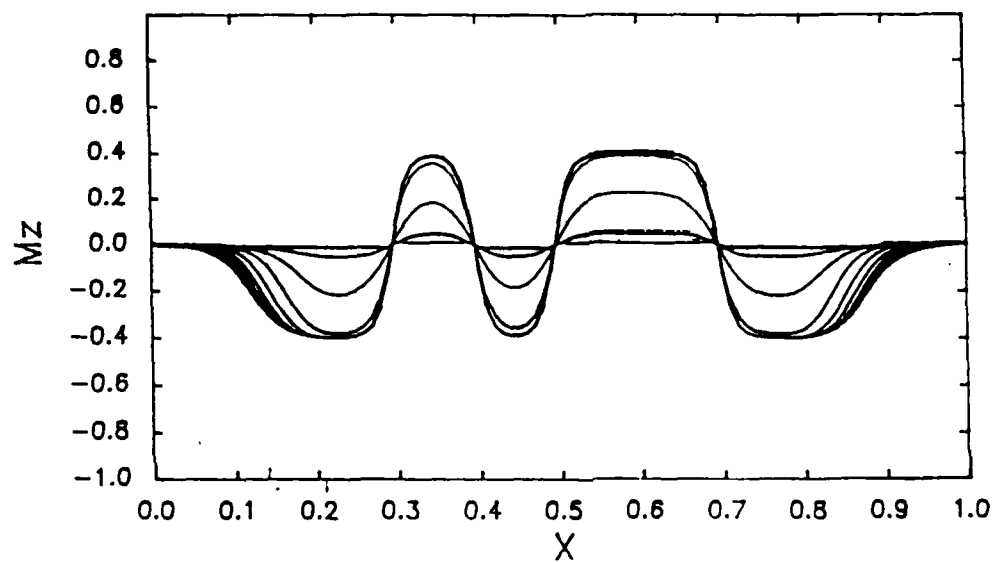
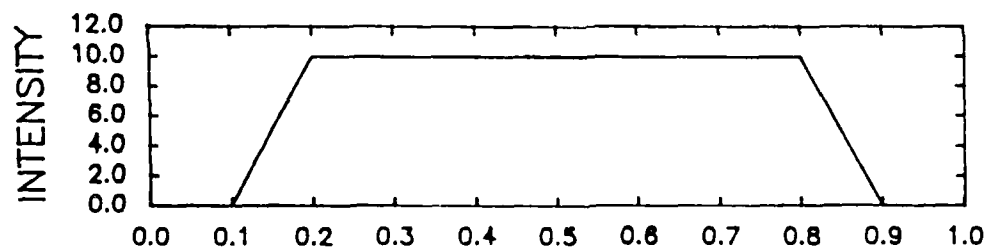
$$\partial M / \partial t = D \partial^2 M / \partial x^2 - \gamma M + \mu M (1 - a M^2)$$

$$M(x) = A \tanh(\pm Bx - C), \pm A$$

$$A = \sqrt{(1 - \gamma / \mu) / a}$$

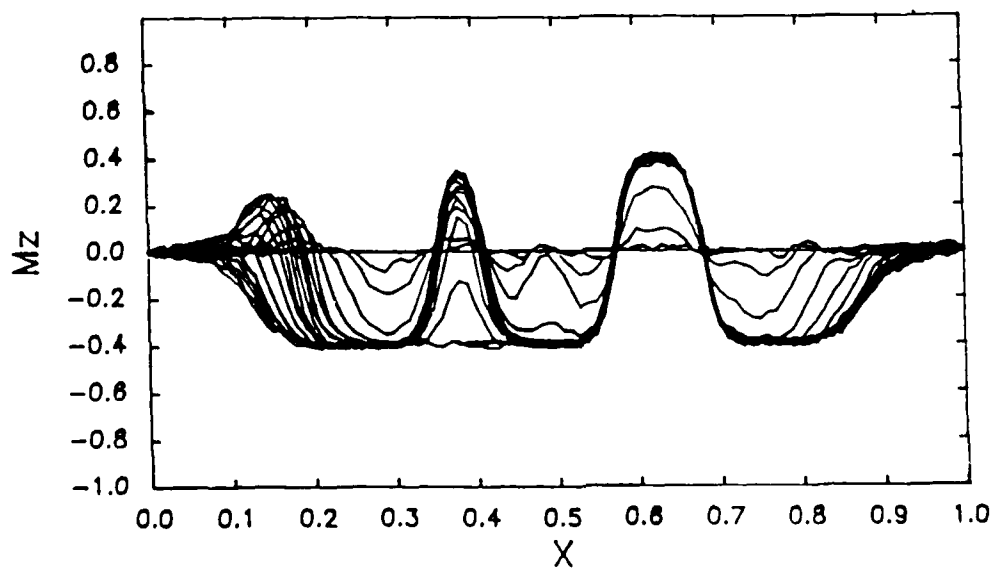
$$B = \sqrt{(\mu - \gamma) / 2D}$$





$k_L = 2.0$

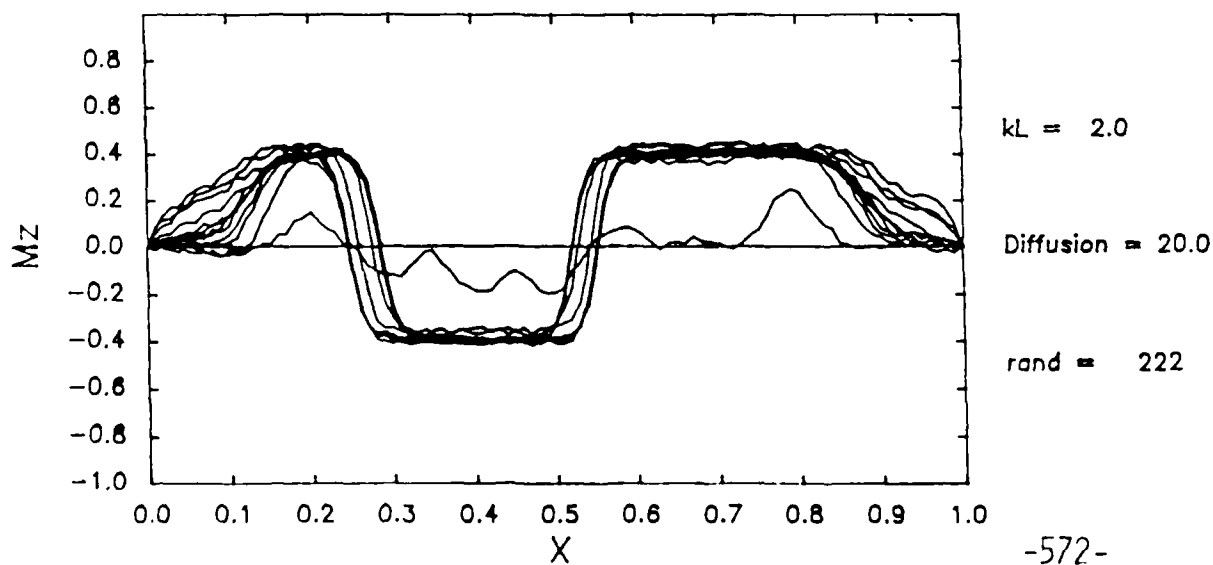
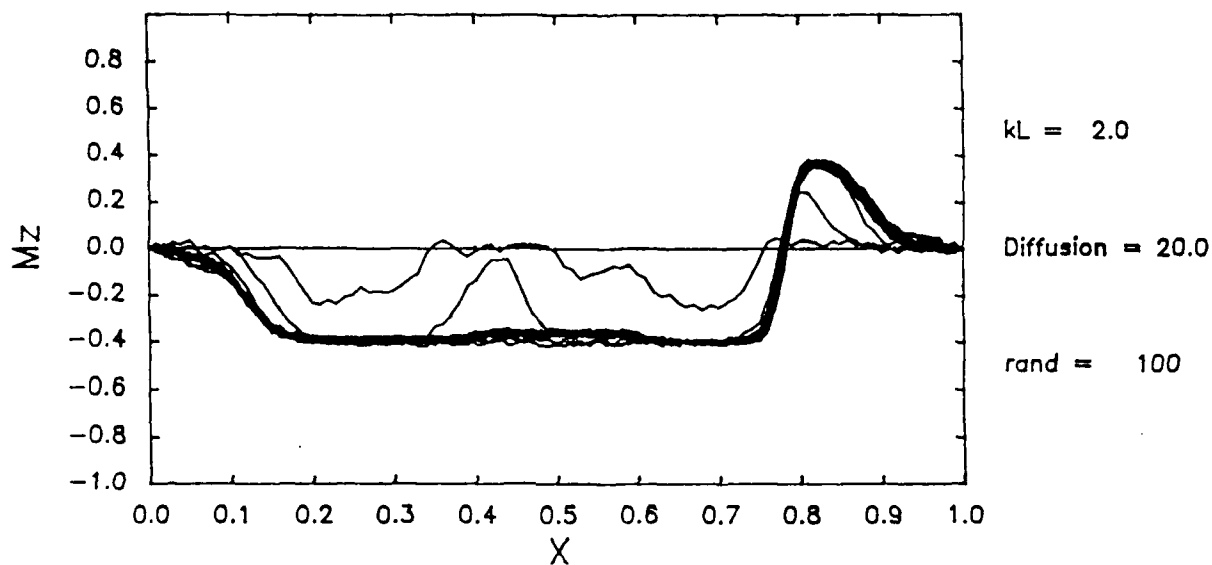
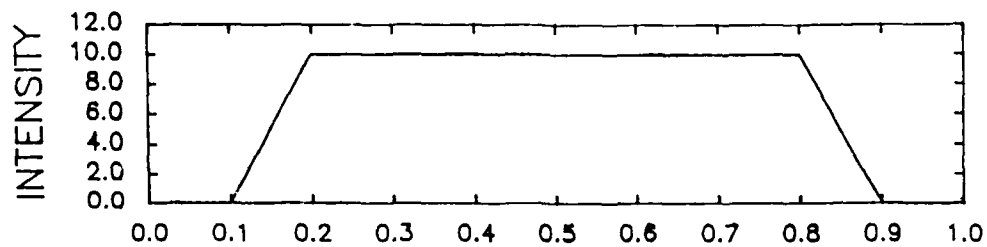
Diffusion = 20.0



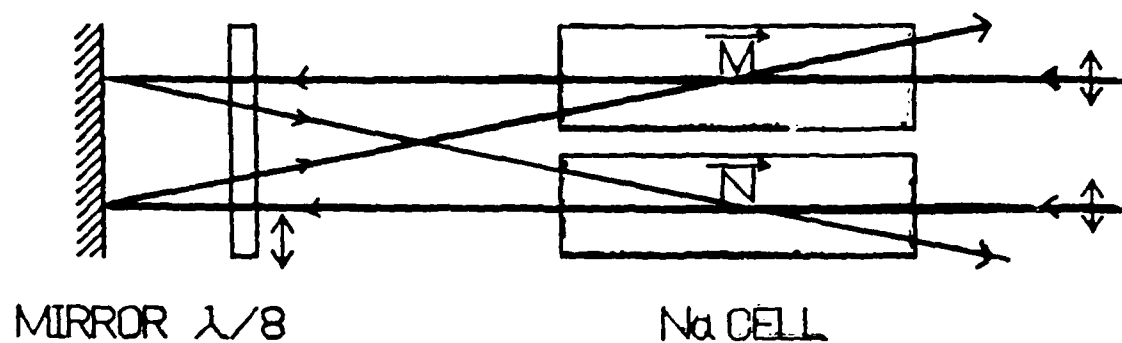
$k_L = 2.0$

Diffusion = 20.0

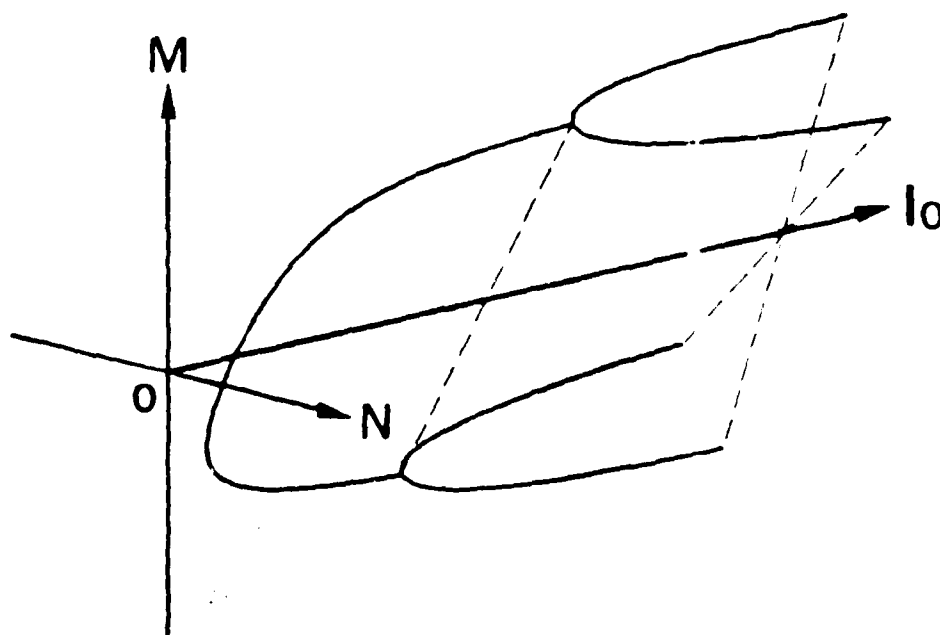
rand = 963



3



$$\begin{cases} \frac{dM}{dt} = -\gamma M + \mu N (1 - a N^2) \\ \frac{dN}{dt} = -\gamma N + \mu M (1 - a M^2) \end{cases}$$



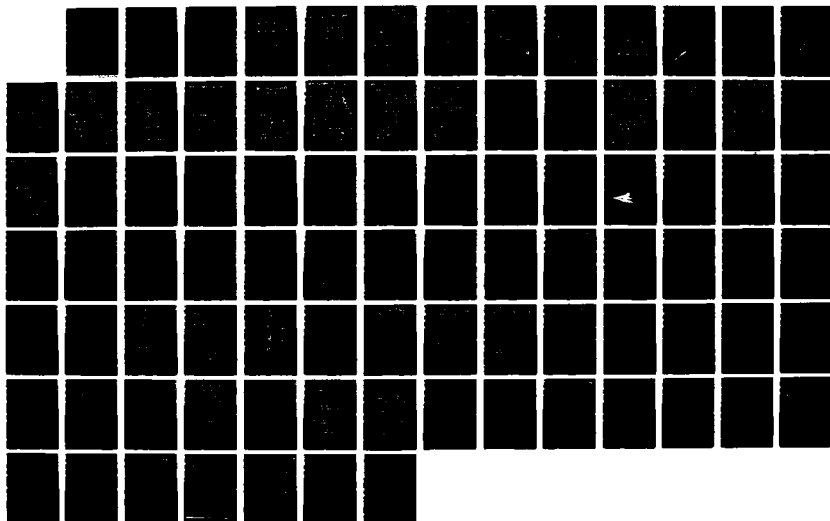
0-A186 938

UNITED STATES - JAPAN SEMINAR ON QUANTUM MECHANICAL
ASPECTS OF QUANTUM EL (U) MASSACHUSETTS INST OF TECH
CAMBRIDGE RESEARCH LAB OF ELECTRON
J H SHAPIRO ET AL OCT 87 N00014-87-G-0198 F/G 20/3

777

UNCLASSIFIED

NL



1·0

1·1

1·25

2·8
3·15
3·5
4·0
4·5

1·4

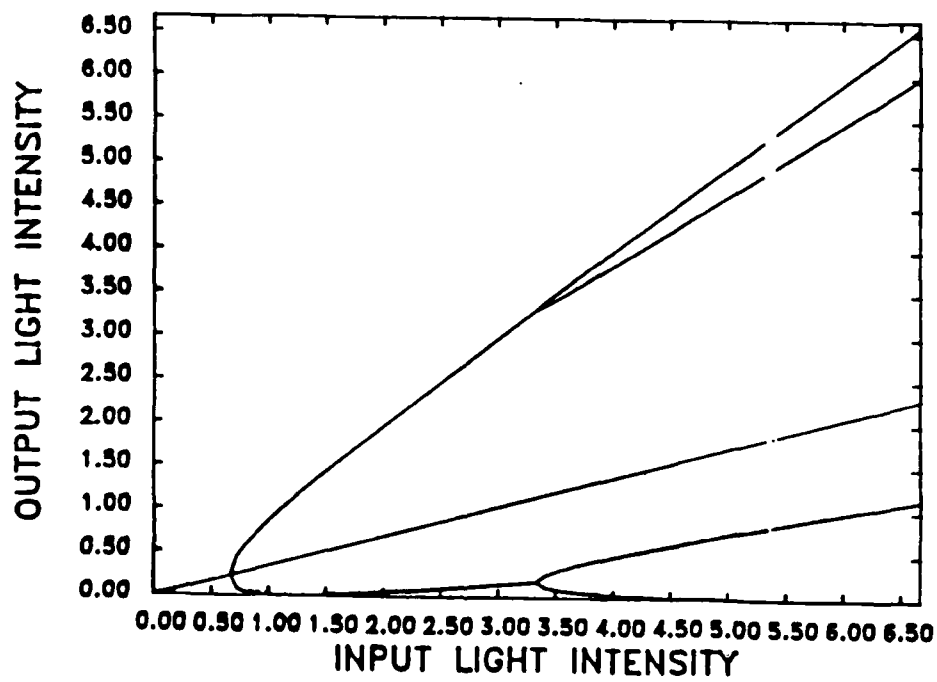
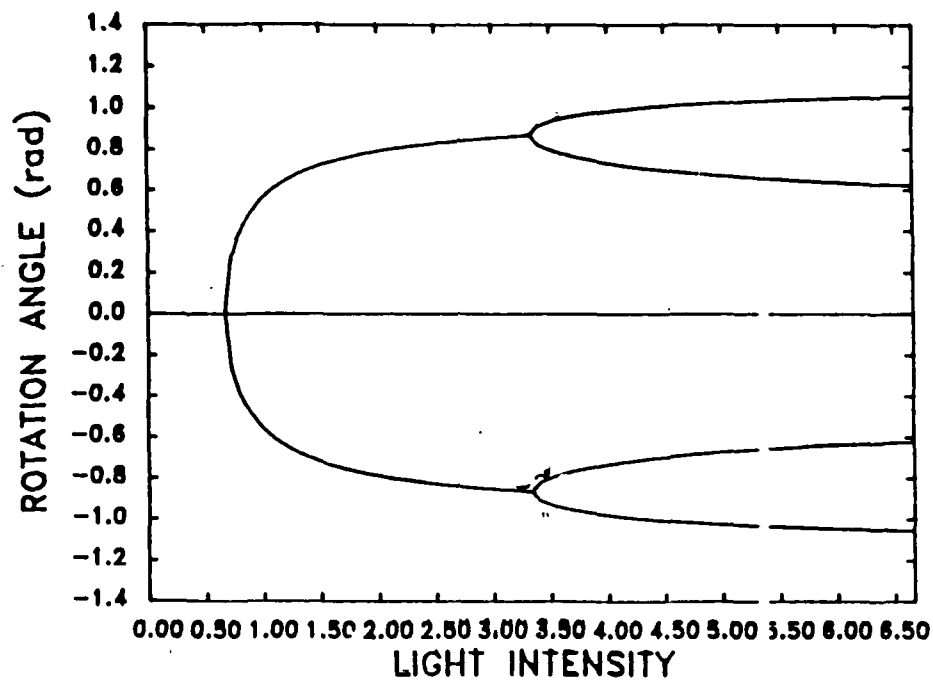
2·5

2·2

2·0

1·8

1·6



NONCLASSICAL LIGHTS

Horace P. Yuen
Department of Electrical Engineering and Computer Science
Northwestern University
Evanston, Illinois 60208

SUMMARY

The differences between "nonclassical" lights and coherent-state lights are reviewed. Some general observations are made concerning the generation, propagation, and detection of squeezed-state and near number-state lights. The role of phase-sensitive linear amplifiers and photon-number amplifiers is emphasized. Certain possible applications of nonclassical lights to communications are described, including optic local area networks.

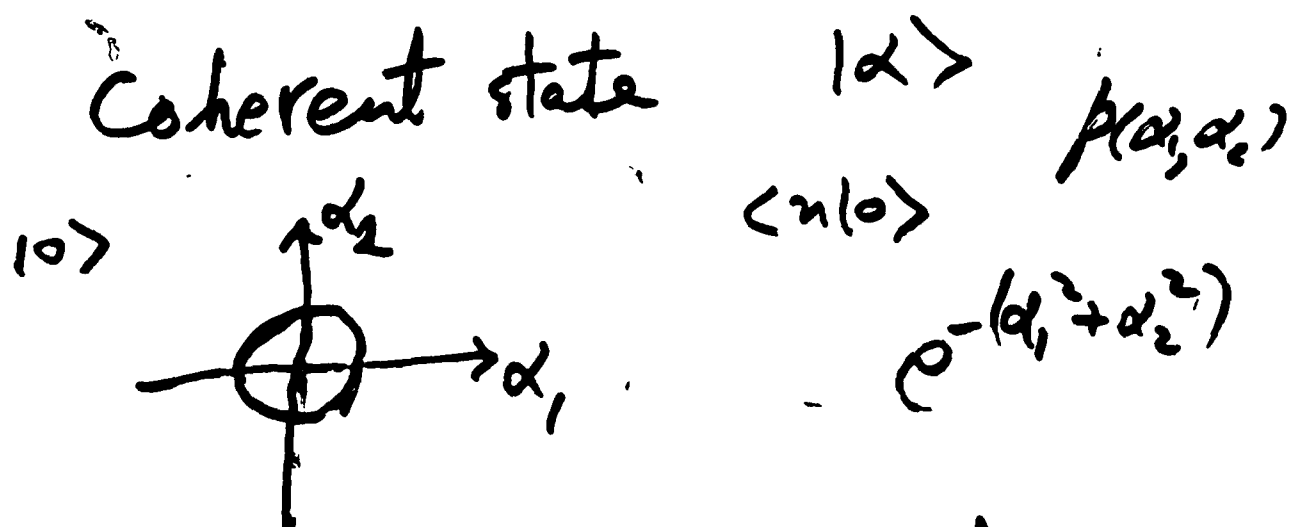
NONCLASSICAL NONSTANDARD LIGHTS

beating standard quantum limits
from standard sources (amplifiers)

ALL LIGHTS ARE QUANTUM

Single measurement
—— one conventional
probabilistic description

Two incompatible measurements
—— quantum



no single probabilistic description

RICHARD P. FEYNMAN (82 quote)

I think it is fair to say that no one understands quantum mechanics. Do not keep saying to yourself, if you can possibly avoid it, "But how can it be like that because you will go "down the drain" into a blind alley from which nobody has yet escaped. Nobody knows how it can be like that.

R.P. FEYNMAN in "Simulating Physics with Computers", Intern. J. Theoret. Phys. 82

... We always have had (secret, secret, close the doors!) we always have had a great deal of difficulty in understanding the world view quantum mechanics represents. I cannot define the real problem, therefore I suspect there is no real problem, but I am not sure there is no real problem. So that is why I like to investigate things.

how can we simulate the quantum mechanical phenomena
the challenge of explaining quantum mechanical phenomena

"vacuum" em field

ground state $|0\rangle$

↓
a coherent state

Single mode
quadrature components

$$\begin{array}{c} q \quad p \\ \downarrow \quad \downarrow \\ a = a_1 + i a_2 \end{array}$$

Coherent states

$$a|\alpha\rangle = \alpha|\alpha\rangle$$

uncertainty principle

$$\langle \Delta a_1^2 \rangle \langle \Delta a_2^2 \rangle \geq \frac{1}{16}$$

⇓

Minimum sum
fluctuation energy

$$\langle \Delta a_1^2 \rangle + \langle \Delta a_2^2 \rangle \geq \frac{1}{2}$$

= for coherent states

(classical or) standard light: _____

(a random superposition of) coherent states

Properties of Coherent State Light

$|\alpha\rangle$: $\langle\alpha|a|\alpha\rangle = \alpha = \alpha_1 + i\alpha_2$ mean field
 $\langle\alpha|a^\dagger a|\alpha\rangle = |\alpha|^2$

photoncount statistics
 (direct detection) $|\langle\alpha|n\rangle|^2 = e^{-|\alpha|^2} \frac{|\alpha|^{2n}}{n!}$

Poisson mean = var = $|\alpha|^2$

field amplitude statistics
 (homodyne detection)

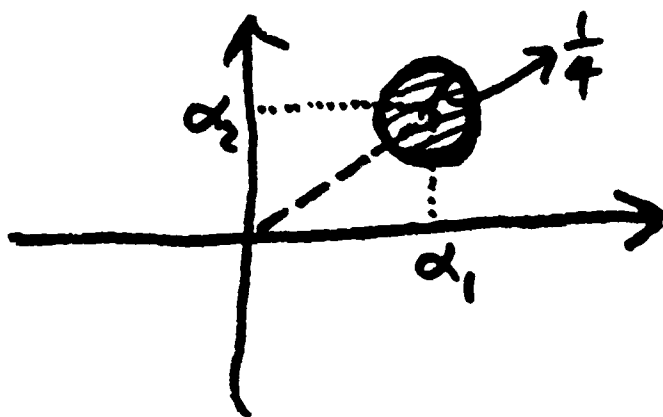
Gaussian

mean α ,
 var $\frac{1}{4}$ ($\hbar\omega$)

Signal & noise representation

$$a_\phi = a_1 \cos \phi - a_2 \sin \phi$$

$$\langle \Delta a_\phi^2 \rangle = \frac{1}{4}$$



NOTE :

- 1/ coherent states are not at all classical.
- 2/ they do not have unique space-time coherence property — any single excited mode
- 3/ they do not necessarily obtain in an ideal ordinary laser
- 4/ they are special because the "vacuum state" is a coherent state

terminology —

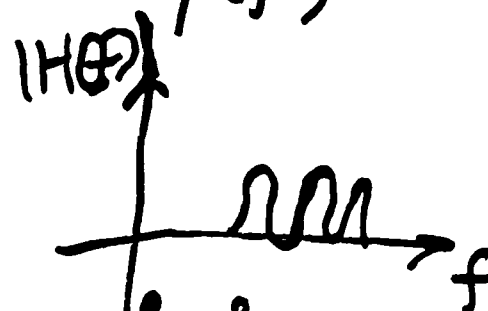
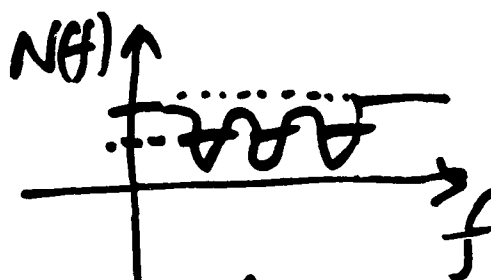
nonclassical light
? nonstandard light
? ...

QUANTUM FIELD MODES

$$\Psi(\bar{x}, t) \rightarrow \psi(\bar{r}) \phi(t) \text{ determ. mode function}$$

$$E = \sum_n a_n \bar{\Psi}$$

$$\phi(f)$$



Single mode \neq single freq.
more power in pulsed mode
Space-time Coherence

$$\propto \frac{\bar{\Psi}(\bar{x}, t)}{a}$$

Coherent number state field

$$E = a \bar{\Psi}(\bar{r}, t) + \text{vacuum}$$

\uparrow
 $|n\rangle$

TWO-PHOTON COHERENT STATE LIGHT (TCS, squeezed state light)

$$|\mu\nu\alpha\rangle: \quad |\mu|^2 - |\nu|^2 = 1 \quad \text{normalized}$$

$$\langle |a| \rangle = \alpha_1 + i\alpha_2$$

$$\langle |a|^2 \rangle = |\alpha|^2 + |\nu|^2$$

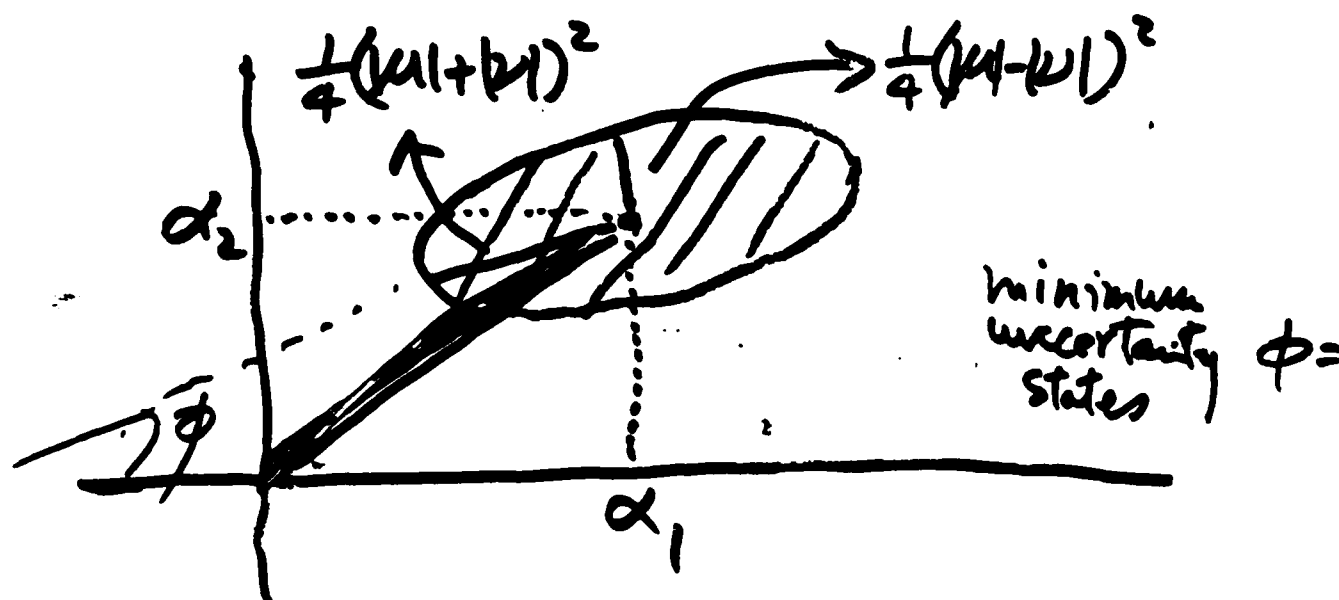
photoncount statistics $\dots H_n(\dots) \dots$

can be sub-Poissonian ($\text{var} < \text{mean}$)

$\langle \mu\nu 0 | n \rangle \neq 0$ only for even n

field amplitude statistics

Gaussian with unsymmetric noi



SQUEEZING

$$\langle \Delta a_\phi^2 \rangle < \frac{1}{4} \text{ for some } \phi$$

$$\langle \Delta a_\phi^2 \rangle \langle \Delta a_{\phi+\pi/2}^2 \rangle \geq \frac{1}{16}$$

Squeezed state — any quantum state that exhibits squeezing

TCS — above rotated minimum uncertainty states

For a given level of squeezing, not a "classical state"
TCS has the smallest total energy

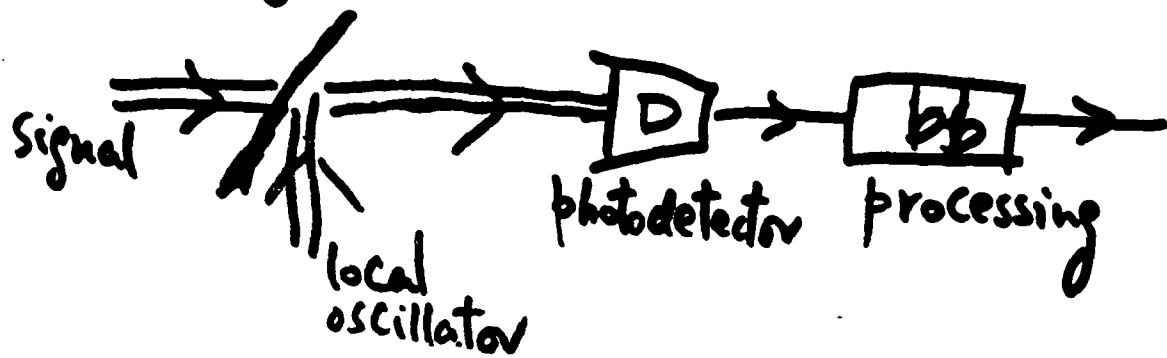
For a fixed energy, TCS yields the best homodyne signal-to-noise ratio among all states

$$\left(\frac{S}{N} \right)_{\text{TCS}}^{\text{hom}} \equiv \frac{\langle a_\phi \rangle^2}{\langle \Delta a_\phi^2 \rangle} = 4S(S+1) \quad \text{tr } \rho a^\dagger a \leq S$$

$$\left(\frac{S}{N} \right)_{\text{TCS}}^{\text{hom}} = 4S$$

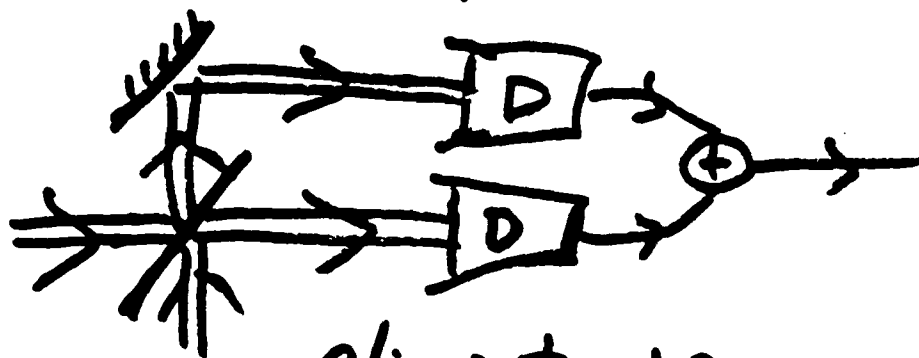
DETECTION OF TCS

homodyning



noise from signal, not local oscillator

balanced homodyning



eliminate LO excess noise

problem of quantum efficiency

— 90% 1 order
99% 2 order improvement limit

EFFECT OF LOSS for all nonstandard lights

$$b = \eta^{\frac{1}{2}} a + (-\eta)^{\frac{1}{2}} \sqrt{\frac{1}{4}}$$

vacuum $|0\rangle$ is a CS

$$\langle \Delta b_{\phi}^2 \rangle = \eta \langle \Delta a_{\phi}^2 \rangle + (-\eta) \frac{1}{4} \geq (-\eta) \frac{1}{4}$$

noise floor in addition
to signal attenuation

General Principle for Overcoming Loss

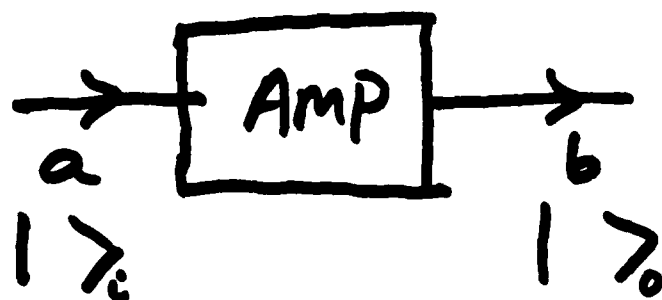
any linear loss
in system



Appropriate (match detection
and/or state)

OPTICAL PRE-AMPLIFICATION

heterodyne (CS)	— PEA	phase insens ^t linear ampli.
homodyne (TCS)	— PSA	phase sensit ^t linear ampli.
direct (NNS)	— PNA	photon-num -587- amplifier



PIA

$$b = G^{1/2} a + (G-1)^{1/2} v$$

$$SNR_b = SNR_a \text{ --- any } P_a$$

$$SNR_{b\phi} = \frac{1}{2} SNR_{a\phi} > CS \text{ } P_a$$

$$SNR_{N_b} = \frac{1}{2} SNR_{N_a}$$

PSA

$$b_1 = G^{1/2} a_1, \quad b_2 = G^{-1/2} a_2$$

$$SNR_{b\phi} = SNR_{a\phi} \text{ --- any } P_a$$

PNA

$$|n\rangle_i \rightarrow |Gn\rangle_o$$

$$SNR_{N_b} = SNR_{N_a} \text{ --- any } P_a$$

PHOTON NUMBER EIGENSTATES

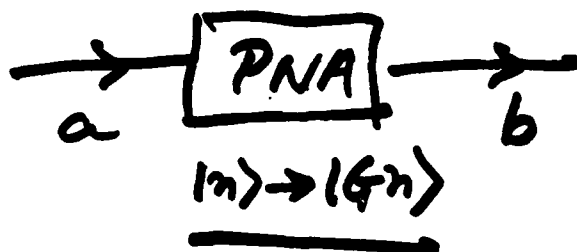
→ NNS

$$N \equiv a^\dagger a \quad N|n\rangle = n|n\rangle$$

measure N — $\langle \Delta N^2 \rangle = 0$, etc.

$$SNR_N \triangleq \frac{\langle N \rangle^2}{\langle \Delta N \rangle^2} \rightarrow \infty \text{ but discrete}$$

PHOTON NUMBER AMPLIFIER

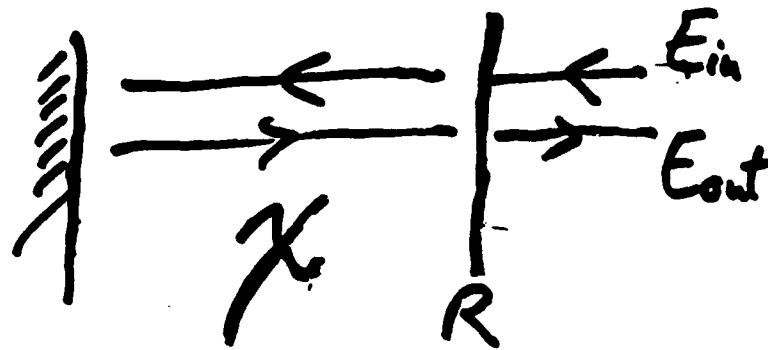


$$SNR_{N_b} = SNR_{N_a} \text{ for any } P_a$$

P_b nonclassical for $P_a = |\alpha\rangle\langle\alpha|$

Comparison with PIA

SQUEEZING GENERATION VIA A CAVITY



Coherent cancellation of noise
for long observation time or
narrow enough bandwidth



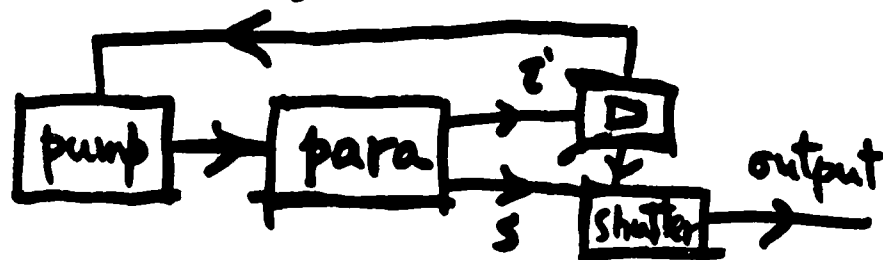
effect of loss

near-perfect narrow-band
parametric amplifier

NEAR NUMBER STATE LIGHT

$|n\rangle$ photon number eigenstate
— or strongly sub-Poissonian

generation



Correlated photon pairs feedforward
feedback

solid state

laser diode with pump fluc. suppress

⋮

propagation

special fibers and/or amplifier

detection

- noiseless photon amplifier
- transfer to another mode & homodyne (QND)

application

similar to TCS
local area network

APPLICATIONS

interferometry

$\frac{S}{N}$ improvement \rightarrow grav. wave to
in gyros (fiber or not)

gravitational wave interferometer

communications

better system performance

— local area fiber network

long distance fiber transmission

near field space communication

precision measurements

interaction of radiation with matter

optical signal processing or computing

optical memory

Performance Advantage

general noise reduction

bandwidth W
power S

Capacity — general & specific
modulation schemes

P_e, R, C tradeoff
 ϵ^2

digital
analog Comm

new capability



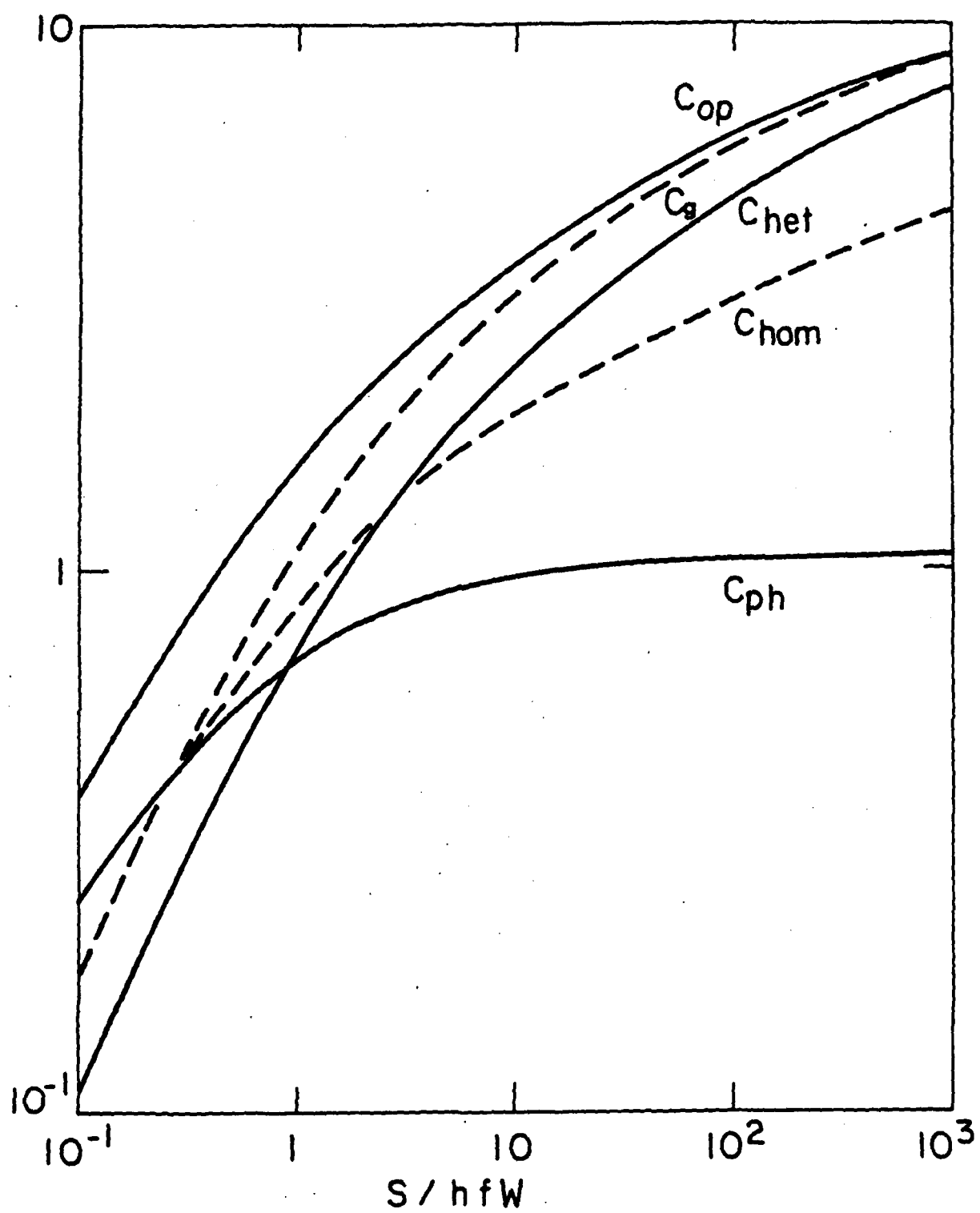
CAPACITY COMPARISON

$$C_g = W \log \left(1 + 2 \frac{S}{hfW} \right)$$

$$C_{het} = W \log \left(1 + \frac{S}{hfW} \right)$$

$$C_{hom} = \frac{W}{2} \log \left(1 + 4 \frac{S}{hfW} \right)$$

$$C_{op} = C_{het} + \frac{S}{hf} \log \left(1 + \frac{hfW}{S} \right)$$



FIBER-OPTIC LAN

PSA — wideband parametric amplifier
fiber & integrated optics

PNA — need practical scheme

LONG-HAUL FIBER TRANSMISSION

Use of distributive - amplifier
compensated fibers, discrete
amplifier stages, etc. for

← CS

— TCS

— NMS

to get
significant
↑

in both cases, no need for nonclassical source;

FIBER-OPTIC QUANTUM COMMUNICATIONS

ordinary optical communication

SOURCES

coherent states
CS

AMPLIFIERS

phase-insensitive
PIA

quantum

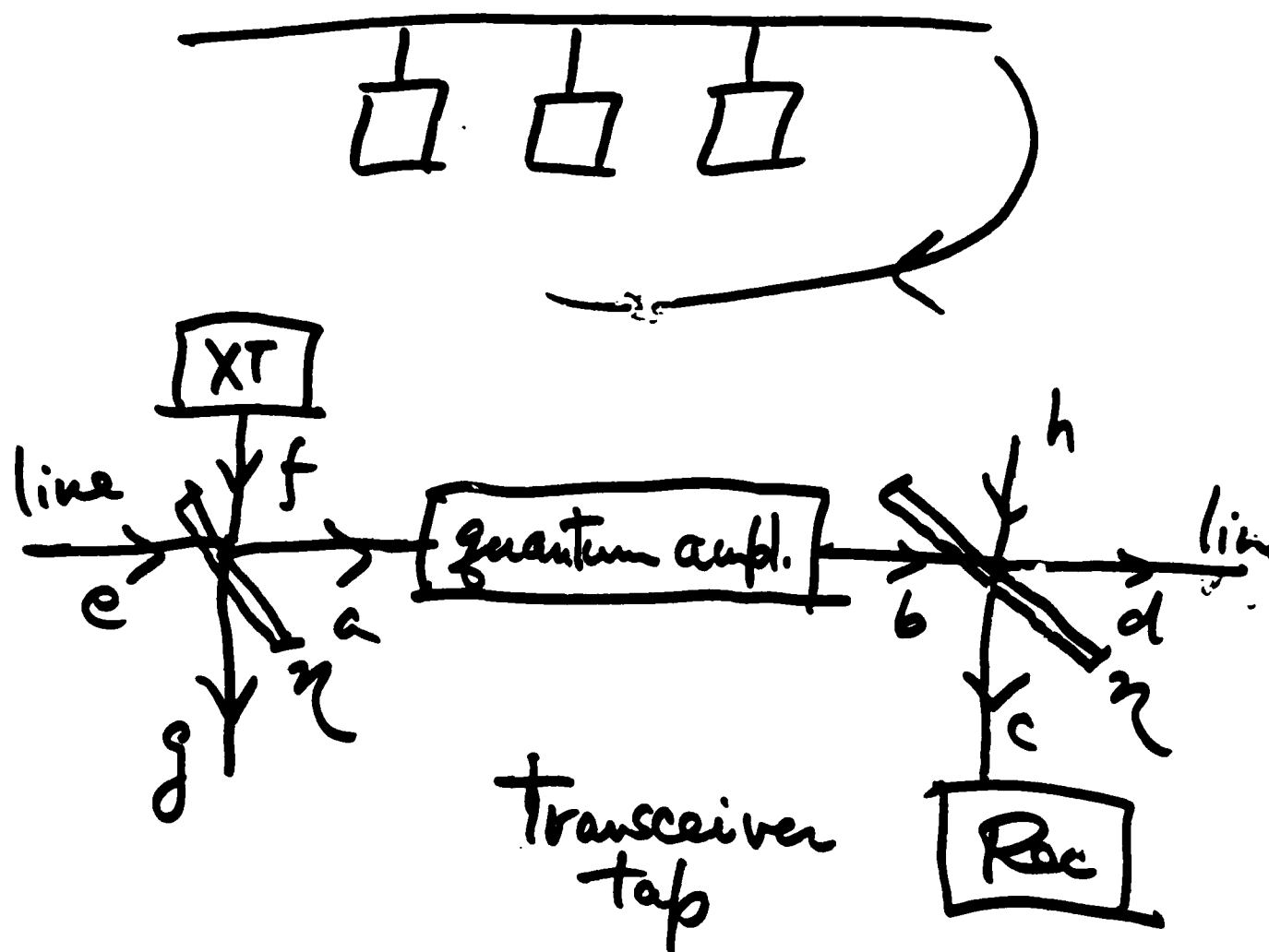
two-photon coherent
states or squeezed
states
TCS

phase-sensitive
PSA

near-number states
NNS

photon-number
PNA

LINEAR BUS IN LOCAL AREA NETWORK



$$\text{amp} = PCA$$

$$SNR_{N_{c,d,c,p,d,b}} \sim \frac{1}{2} SNR_{N_{a,p}}$$

hot main
user

$$AMP = PNA$$

$$SNR_{N_c} = SNR_{N_a} / \left[1 + \frac{\eta}{G(1-\eta)} \frac{\langle N_a \rangle}{\langle N_a^2 \rangle} \right]$$

$$SNR_{N_d} = SNR_{N_a} / \left[1 + \frac{1-\eta}{G\eta} \frac{\langle N_a \rangle}{\langle N_a^2 \rangle} \right]$$

$$SNR_{N_c} \sim SNR_{N_d} \sim SNR_{N_a}$$

ampl Switched on-off line — $\eta = \frac{1}{2}, G \geq 10$

turned on-off but
permanent online

— η small

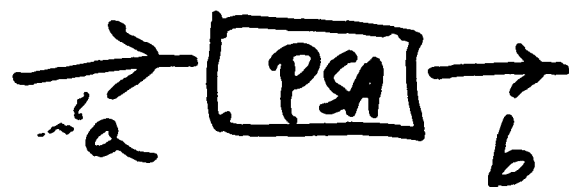
$G(1-\eta)$ large
enough

$$\langle N_d \rangle \sim G \langle N_a \rangle$$

long haul too

amplification good for subsequent detect

$$AMP = PSA$$



$$b_1 = G^{1/2} a_1$$

$$b_2 = G^{-1/2} a_2$$

$$SNR_{b_p} = SNR_{a_p}$$

$$SNR_{c_1} = SNR_{a_1} / \left[1 + \frac{\eta}{G(G-\eta)} \frac{1}{4 \langle \Delta a_1^2 \rangle} \right]$$

$$SNR_{d_1} = SNR_{a_1} / \left[1 + \frac{1-\eta}{G\eta} \frac{1}{4 \langle \Delta a_1^2 \rangle} \right]$$

$$SNR_{c_1} \sim SNR_{d_1} \sim SNR_{a_1}$$

& similar to PNA case

Comparison to Shapiro's tap

h mode in TCS

utilize large squeezing vs here noise
also have amplification ^{insensitive}

Quantum Statistics of Parametric Oscillators Above Threshold

D.F. Walls*, M.J. Collett⁺, A.S. Lane*,
M.D. Reid* and C.M. Savage^Δ

* Physics Department
University of Waikato
Hamilton, New Zealand

⁺ Physics Department
University of Essex
Colchester, Essex, U.K.

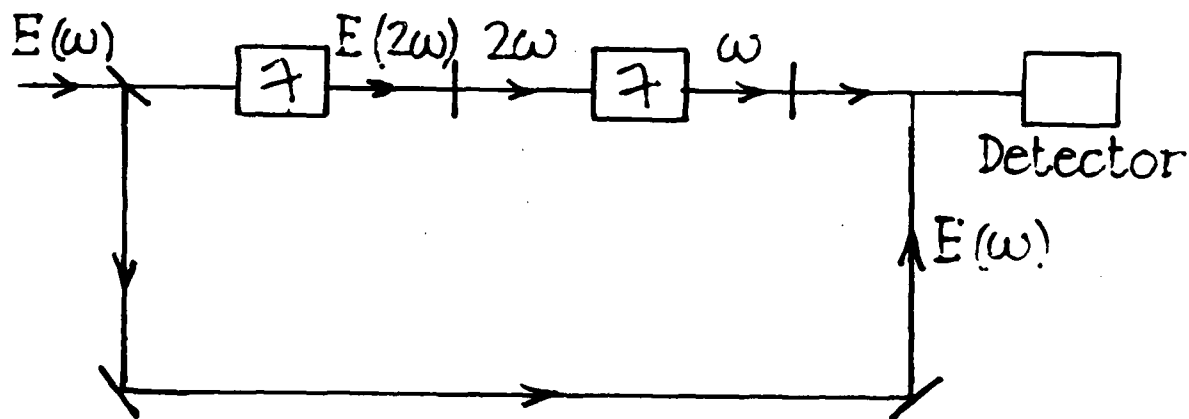
^Δ Optical Sciences Center
University of Arizona
Tucson, AZ, U.S.A.

Summary

The quantum statistics of the degenerate parametric oscillator above threshold are described. The squeezing spectrum is plotted for a range of parameters. The nondegenerate parametric oscillator is studied above threshold where the solutions are known to undergo phase diffusion. The fluctuations in the difference current from the signal and idler modes are calculated for the case where the signal and idler may have different cavity decay rates.

GENERATION PARAMETERS OF OSCILLATOR

Collett



HAMILTONIAN

Non linear coupling

$$\chi a_1^2 a_2^\dagger + \chi a_1^{\dagger 2} a_2$$

Cavity losses

$$a_1 \Gamma_1^\dagger + a_2 \Gamma_2^\dagger + hc$$

Driving fields

$$a_2 E^* + a_2^\dagger E$$

Equations for mode amplitudes:

$$\dot{\alpha}_1 = -\kappa_1 \alpha_1 + \gamma \alpha_1 \alpha_2^\dagger + \sqrt{\gamma \alpha_2} \Gamma_1(t)$$

$$\dot{\alpha}_2 = E - \kappa_2 \alpha_2 - \frac{\gamma}{2} \alpha_1^2$$

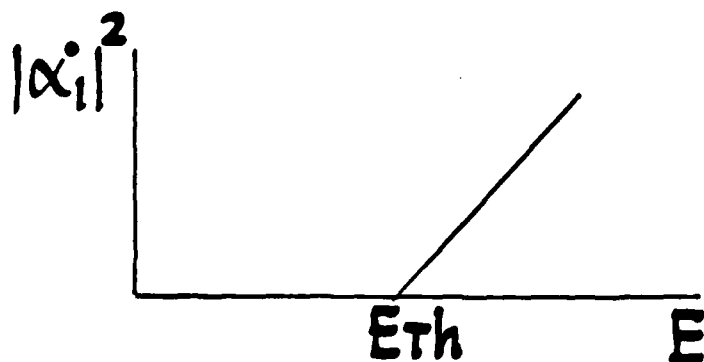
White noise limit:

$$\langle \Gamma_1(t) \Gamma_1(t') \rangle = \delta(t-t')$$

Steady state for all times:

$$|\alpha_i|^2 = 0 \quad E \ll E_{Th}$$

$$|\alpha_i|^2 = \left[\frac{2}{\gamma} (E - E_{Th}) \right] \quad E > E_{Th}$$



Define quadrature

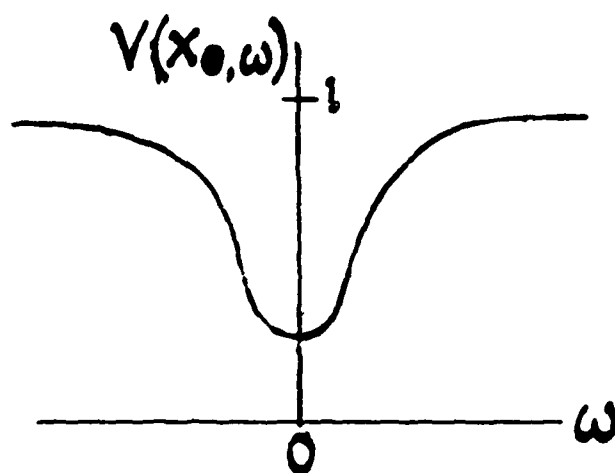
$$x_{\theta} = (ae^{-i\theta} + a^{\dagger}e^{i\theta})$$

Powering spectrum

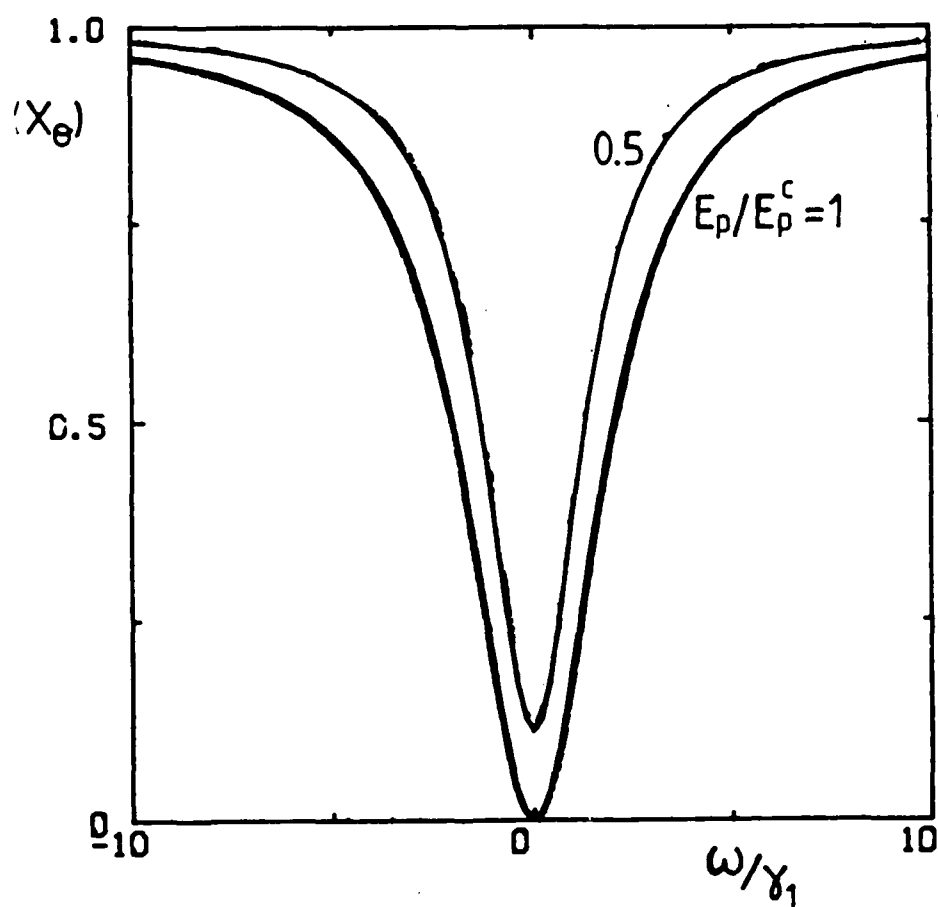
$$V(x_{\theta}, \omega) = \int [\langle x_{\theta}(\tau) x_{\theta}(0) \rangle - \langle x_{\theta}(\tau) \rangle \langle x_{\theta}(0) \rangle] e^{i\omega\tau} d\tau$$

Power spectrum

$$V(x_{\theta}, \omega) = 1 - \frac{4\chi_1 \epsilon}{(\chi_1 + \epsilon)^2 + \omega^2}$$



Squeezing Spectrum for Parametric Oscillator Below Threshold



Above Threshold

Squeezing Spectrum

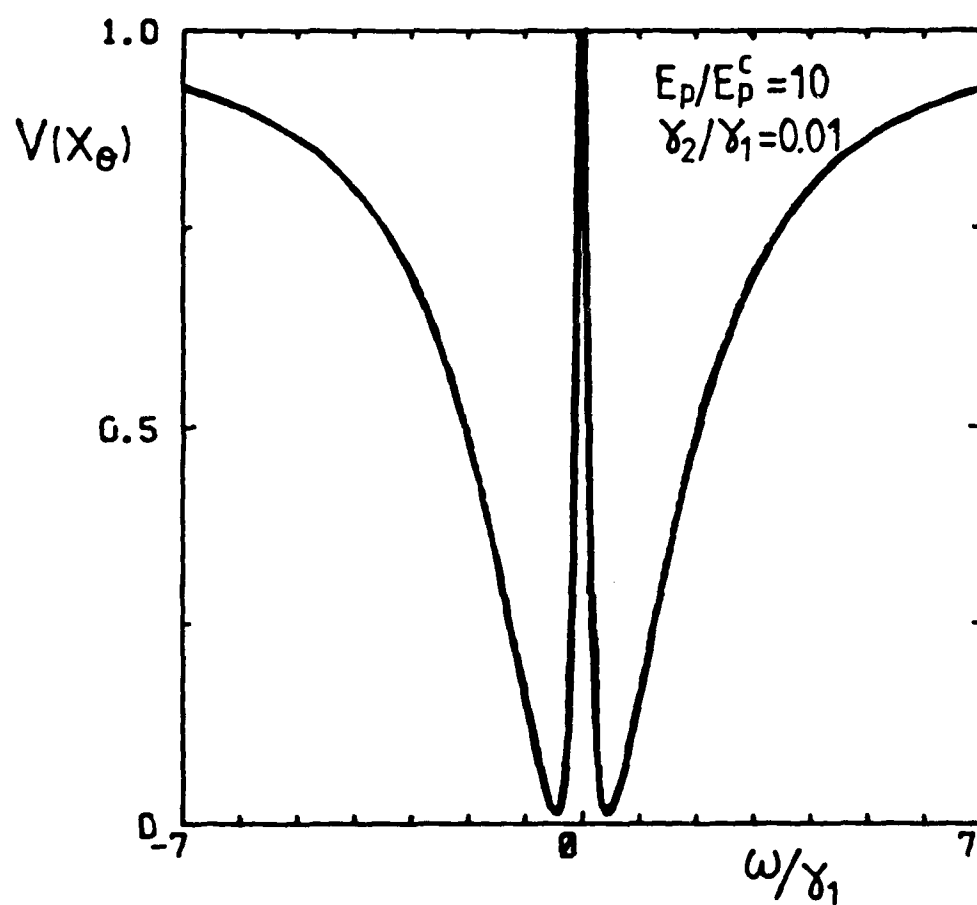
$$V(\chi_0, \omega) = 1 - \frac{4\kappa |\epsilon_2| (\kappa_2^2 + \omega^2)}{[\kappa_2 (\kappa_1 + |\epsilon_2|) + |\epsilon_1|^2 - \omega^2]^2 + \omega^2 (\kappa_1 + |\epsilon_2| + \kappa_2)^2}$$

$$\epsilon_1 = 2\gamma \alpha_1^0$$

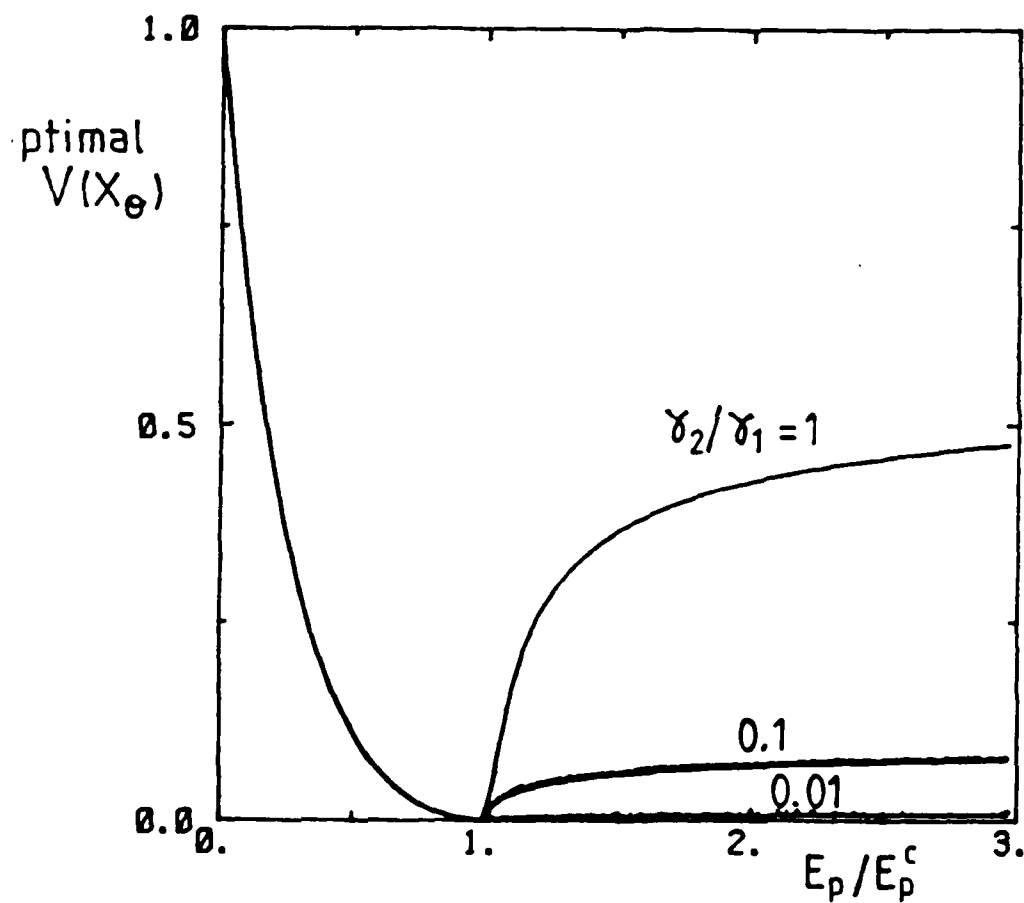
$$\epsilon_2 = 2\gamma \alpha_2^0$$

Collett

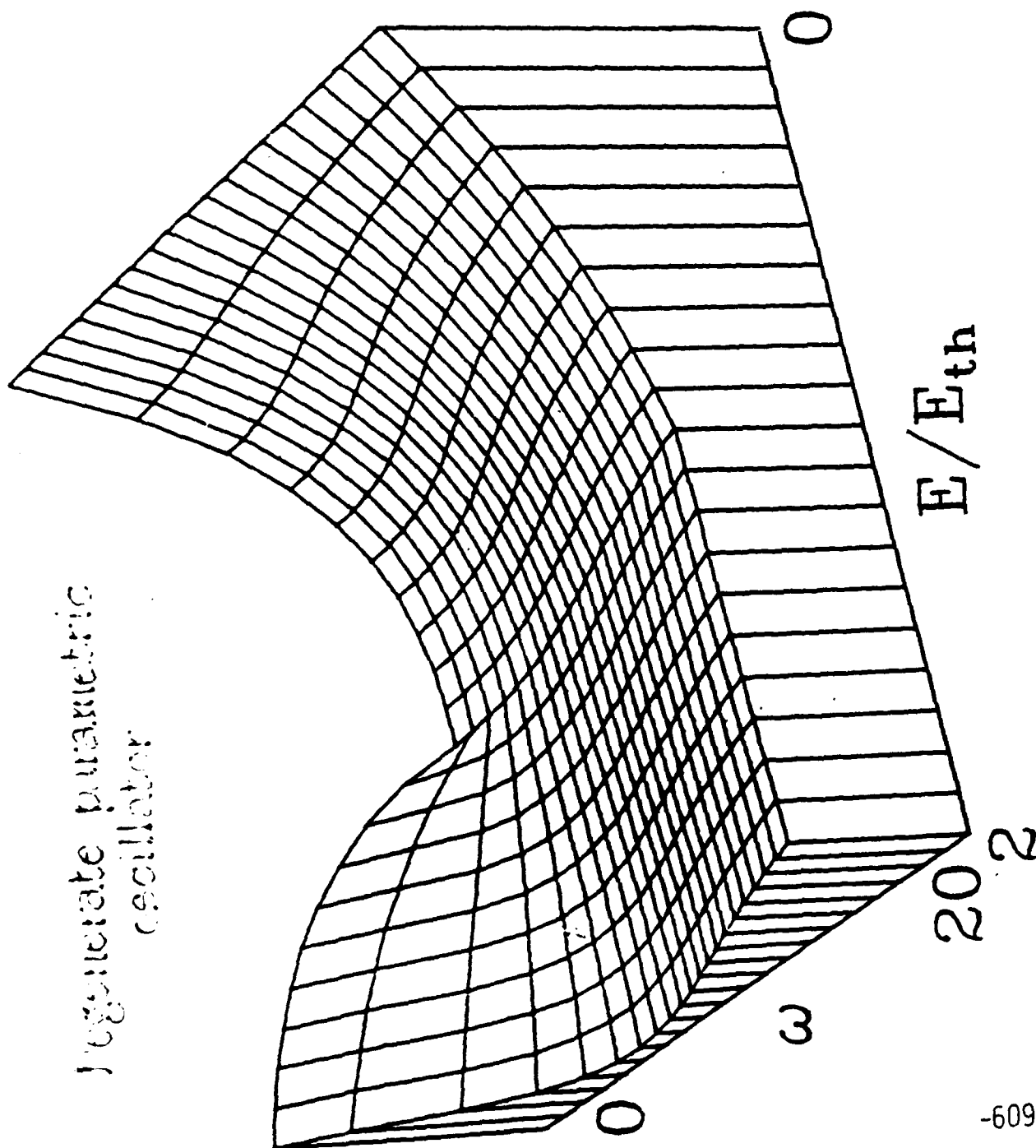
Squeezing Spectrum for Parametric Oscillator above Threshold



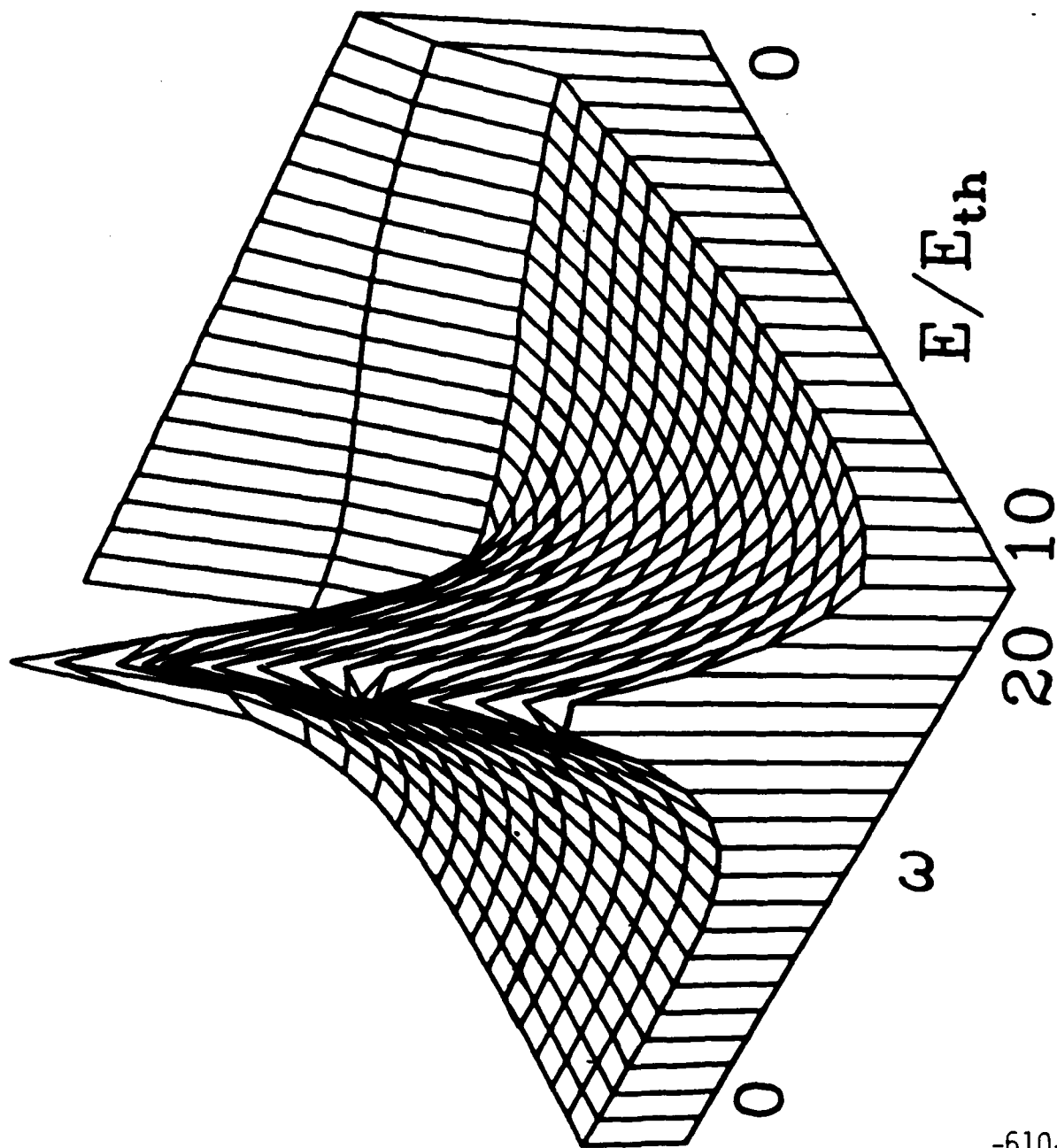
Optimal Squeezing for the Parametric Oscillator as a Function of Pump Amplitude



Regenerate parametric
oscillator

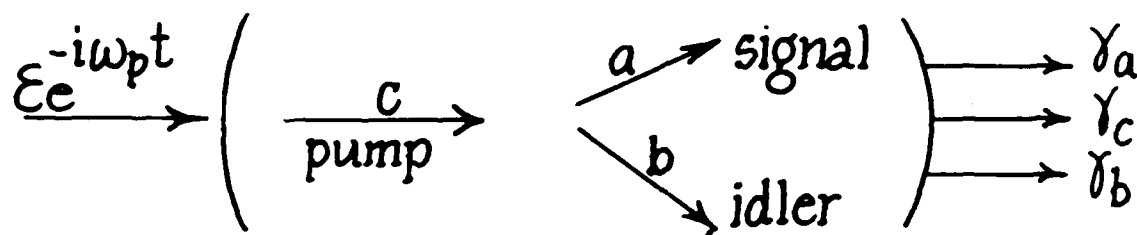


Savag



Non Degenerate Parametric Oscillator

Reid & Lane



Hamiltonian

$$\begin{aligned}
 H = & i\hbar (\mathcal{E} e^{-i\omega_p t} c^\dagger - c \mathcal{E}^* e^{i\omega_p t}) \\
 & + i\hbar k (c a^\dagger b^\dagger - c^\dagger a b) \\
 & + (a \Gamma_a^\dagger + b \Gamma_b^\dagger + c \Gamma_c^\dagger + h.c.)
 \end{aligned}$$

Langevin Equations

$$\begin{aligned}
 \dot{c} &= -\gamma_c c + \mathcal{E} - k \alpha \beta \\
 \dot{\alpha} &= -\gamma_a \alpha + k c \beta^\dagger + F_a \\
 \dot{\beta} &= -\gamma_b \beta + k c \alpha^\dagger + F_b
 \end{aligned}$$

$$\langle F_\alpha(t) F_\beta(t') \rangle = k c \delta(t-t')$$

Steady State Solutions

Threshold $|\epsilon| = \frac{\gamma_c \sqrt{\gamma_a \gamma_b}}{\kappa}$

Below threshold

$$\alpha = \beta = 0$$

$$c = \frac{\epsilon}{\gamma_c}$$

Above threshold

$$|c|^2 = \frac{\gamma_a \gamma_b}{\kappa^2}$$

$$|\alpha|^2 = \frac{|\epsilon|}{\kappa} \sqrt{\frac{\gamma_b}{\gamma_a}} - \frac{\gamma_c \gamma_b}{\kappa^2}$$

$$|\beta|^2 = \frac{|\epsilon|}{\kappa} \sqrt{\frac{\gamma_a}{\gamma_b}} - \frac{\gamma_c \gamma_a}{\kappa^2}$$

Phases

$$\theta_p = \theta_c = \theta_\beta + \theta_\alpha$$

$$\epsilon = |\epsilon| e^{i\theta_p}, \quad c = |c| e^{i\theta_c}$$

$$\alpha = |\alpha| e^{i\theta_\alpha}$$

$$\beta = |\beta| e^{i\theta_\beta}$$

Linearized Stability Analysis

$$\delta \bar{c} = -\gamma_c \delta_c - \kappa \alpha_0 \delta_\beta - \kappa \beta_0 \delta_\alpha$$

$$\delta \bar{\alpha} = -\gamma_a \delta_\alpha + \kappa c_0 \delta_\beta^+ + \kappa \beta_0^+ \delta_c$$

$$\delta \bar{\beta} = -\gamma_b \delta_\beta + \kappa c_0 \delta_\alpha^+ + \kappa \alpha_0^+ \delta_c$$

Below threshold

Eigenvalues $\lambda = -\gamma_c$

$$\lambda = -\left(\frac{\gamma_a + \gamma_b}{2}\right) \pm \frac{1}{2} \left[(\gamma_a + \gamma_b)^2 - 4(\gamma_a \gamma_b - \left(\frac{\kappa \epsilon}{\gamma_c}\right)^2) \right]^{1/2}$$

Stability for $|\epsilon| < \frac{\gamma_c \sqrt{\gamma_a \gamma_b}}{\kappa}$

Above threshold

Find a zero eigenvalue
solutions unstable
undergo phase diffusion

Graham & Haken

Above threshold:

Transform equations to radial
and phase variables

$$c = \sqrt{I_c} e^{-i\phi_c}$$

$$\alpha = \sqrt{I_\alpha} e^{-i\phi_\alpha}$$

$$\beta = \sqrt{I_\beta} e^{-i\phi_\beta}$$

Relative phase $\phi = (\phi_\alpha + \phi_\beta) - \phi_c$

Linearized equations:

$$\delta \dot{I}_C = \left(-2\chi_c - \frac{|\mathcal{E}|}{\sqrt{I_C}} - k \sqrt{\frac{I_A I_B}{I_C}} \right) \delta I_C - k \sqrt{\frac{I_C I_A}{I_B}} \delta I_B - k \sqrt{\frac{I_C I_B}{I_A}} \delta I_A$$

$$\delta \dot{I}_A = \left(-2\chi_a + k \sqrt{\frac{I_C I_B}{I_A}} \right) \delta I_A + k \sqrt{\frac{I_A I_B}{I_C}} \delta I_C + k \sqrt{\frac{I_C I_A}{I_B}} \delta I_B + F_A$$

$$\delta \dot{I}_B = \left(-2\chi_b + k \sqrt{\frac{I_C I_A}{I_B}} \right) \delta I_B + k \sqrt{\frac{I_A I_B}{I_C}} \delta I_C + k \sqrt{\frac{I_C I_B}{I_A}} \delta I_A + F_B$$

$$\delta \dot{\phi}_C = - \frac{|\mathcal{E}|}{\sqrt{I}} \delta \phi_C - k \sqrt{\frac{I_A I_B}{I}} \delta \phi$$

$$\delta \dot{\phi} = \left(-k \sqrt{\frac{I_C I_B}{I_A}} - k \sqrt{\frac{I_C I_A}{I_B}} + k \sqrt{\frac{I_A I_B}{I_C}} \right) \delta \phi + \frac{|\mathcal{E}|}{\sqrt{I_C}} \delta \phi_C + F_\phi$$

Linear correlation functions

$$\langle F_A(t) F_B(t') \rangle = 2k \sqrt{I_A I_B I_C} \delta(t-t')$$

$$\langle F_A(t) F_C(t') \rangle = -k \sqrt{\frac{I_C}{I_A}} \delta(t-t')$$

Phase equations

$$\lambda_{p\pm} = -\left(\frac{2\gamma + \gamma_c}{2}\right) \pm \frac{1}{2} \sqrt{(2\gamma + \gamma_c)^2 - 8k|\epsilon|}$$

stable

Intensity equations ($\gamma_a = \gamma_b$)

$$\delta I_D = \delta I_A - \delta I_B, \quad \delta I_S = \delta I_A + \delta I_B$$

$$\delta \dot{I}_c = -\gamma_c \delta I_c - \gamma \delta I_S$$

$$\delta \dot{I}_S = \frac{2k^2}{\gamma} I_A \delta I_c + F_S$$

$$\delta \dot{I}_D = -2\gamma \delta I_D + F_D$$

$$\lambda = -2\gamma$$

$$\lambda = -\frac{\gamma_c}{2} \pm \frac{1}{2} \sqrt{\gamma_c^2 - 8k^2 I_A}$$

stable

Spectrum of fluctuations in the
difference current

$$\delta I_D(\omega) = \frac{1}{\sqrt{2\pi}} \int e^{i\omega t} \delta I_D(t) dt$$

$$\delta I_D(\omega) = \frac{F_D(\omega)}{(2\gamma - i\omega)}$$

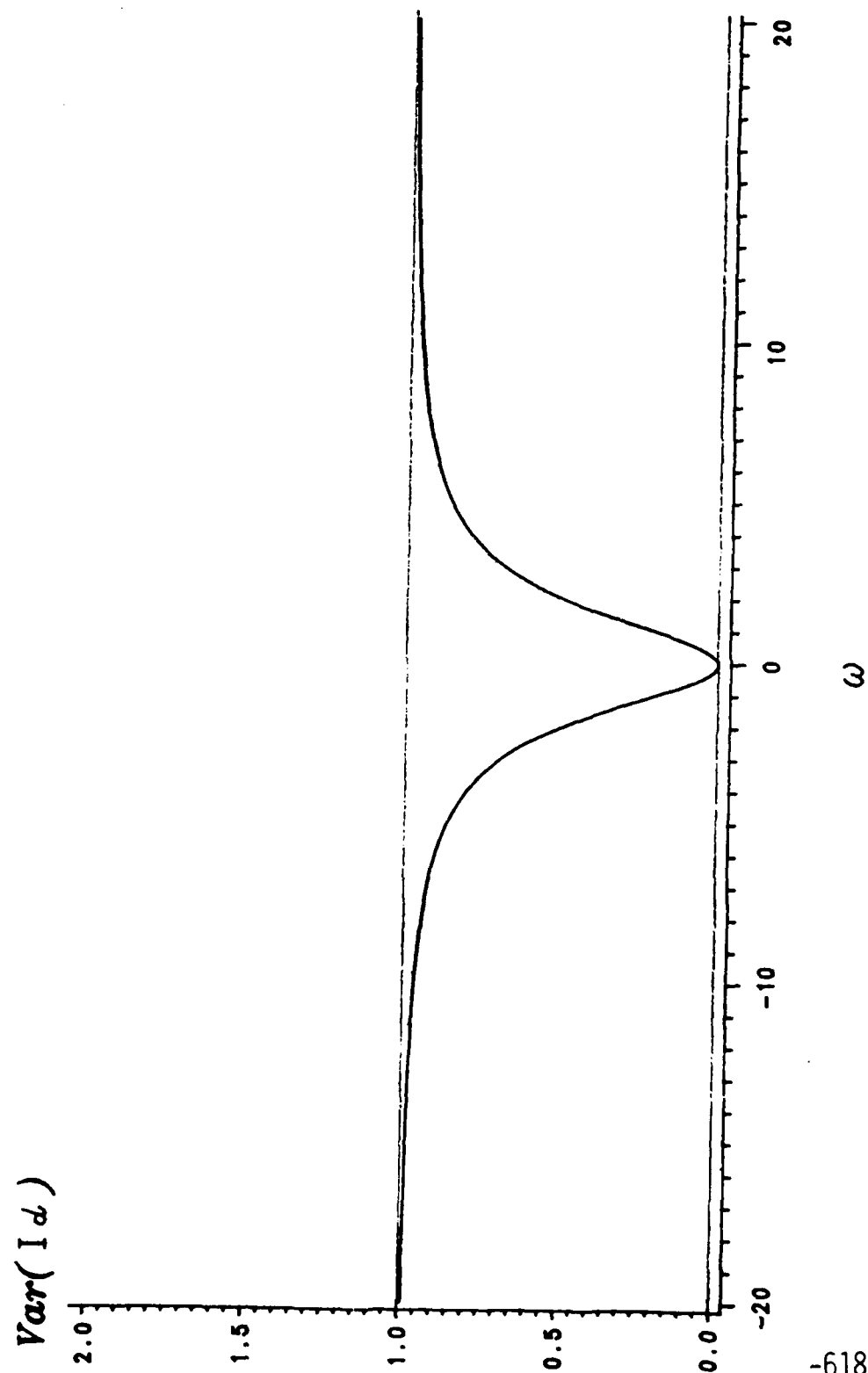
Spectrum

$$\begin{aligned} S_D(\omega) &= 1 + \gamma \langle \delta I_D(\omega), \delta I_D(-\omega) \rangle \\ &= \frac{\omega^2}{4\gamma^2 + \omega^2} I_A \end{aligned}$$

Reynaud, Fabre + Giacobino

Experiment: Giacobino

Param
 $\kappa_0 = 1 \quad \kappa_1 = 1 \quad \kappa_2 = 1$



Unequal Dampings $\Delta = \gamma_A - \gamma_B$

Intensity Equations

$$\dot{\delta I_c} = -\gamma_c \delta I_c - \gamma \delta I_d$$

$$\dot{\delta I_d} = \Delta \delta I_d + \frac{2k^2}{\gamma} I_A \delta I_c + F_s$$

$$\dot{\delta I_d} = -\gamma \delta I_d + \Delta \delta I_c + F_d$$

Spectrum of intensity fluctuations
in difference current

$$S_D(\omega) = I_A \frac{\omega^2 + 4\Delta^2 (1 + 4(\gamma^2 - \Delta^2)\gamma)}{4\gamma^2 + \omega^2}$$

where

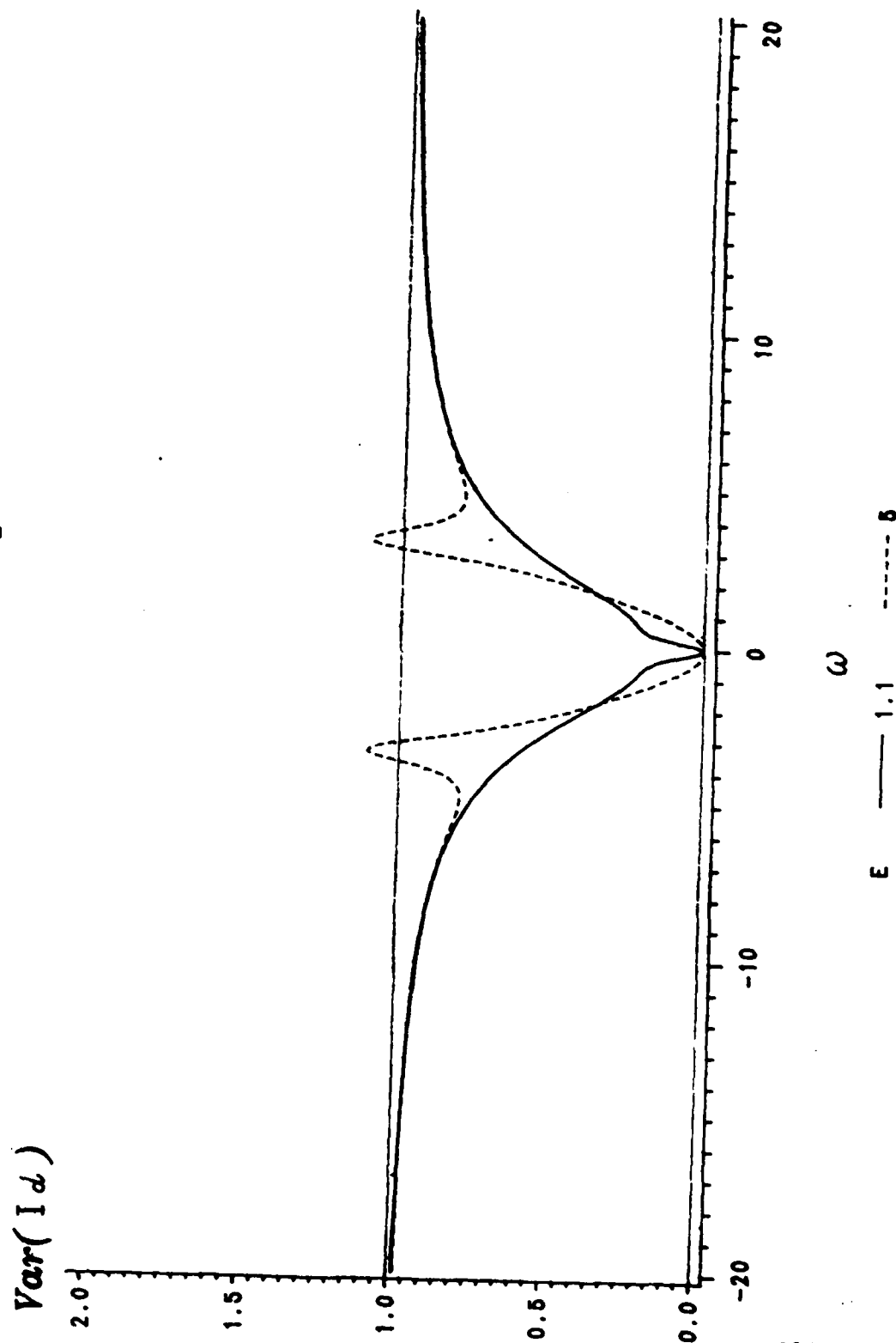
$$\gamma = \frac{\omega^2 + 2\omega \text{Im}(A) + 4(\gamma^2 - \Delta^2) - 4\gamma \text{Re}(A)}{(4\gamma^2 + \omega^2) |A|^2}$$

$$\text{Re}(A) = 2\gamma - \frac{8\Delta^2\gamma}{4\gamma^2 + \omega^2} - \frac{\omega^2}{\gamma_c(E-1)}$$

$$\text{Im}(A) = \omega \left(\frac{4\Delta^2}{4\gamma^2 + \omega^2} + \frac{1}{E-1} \right)$$

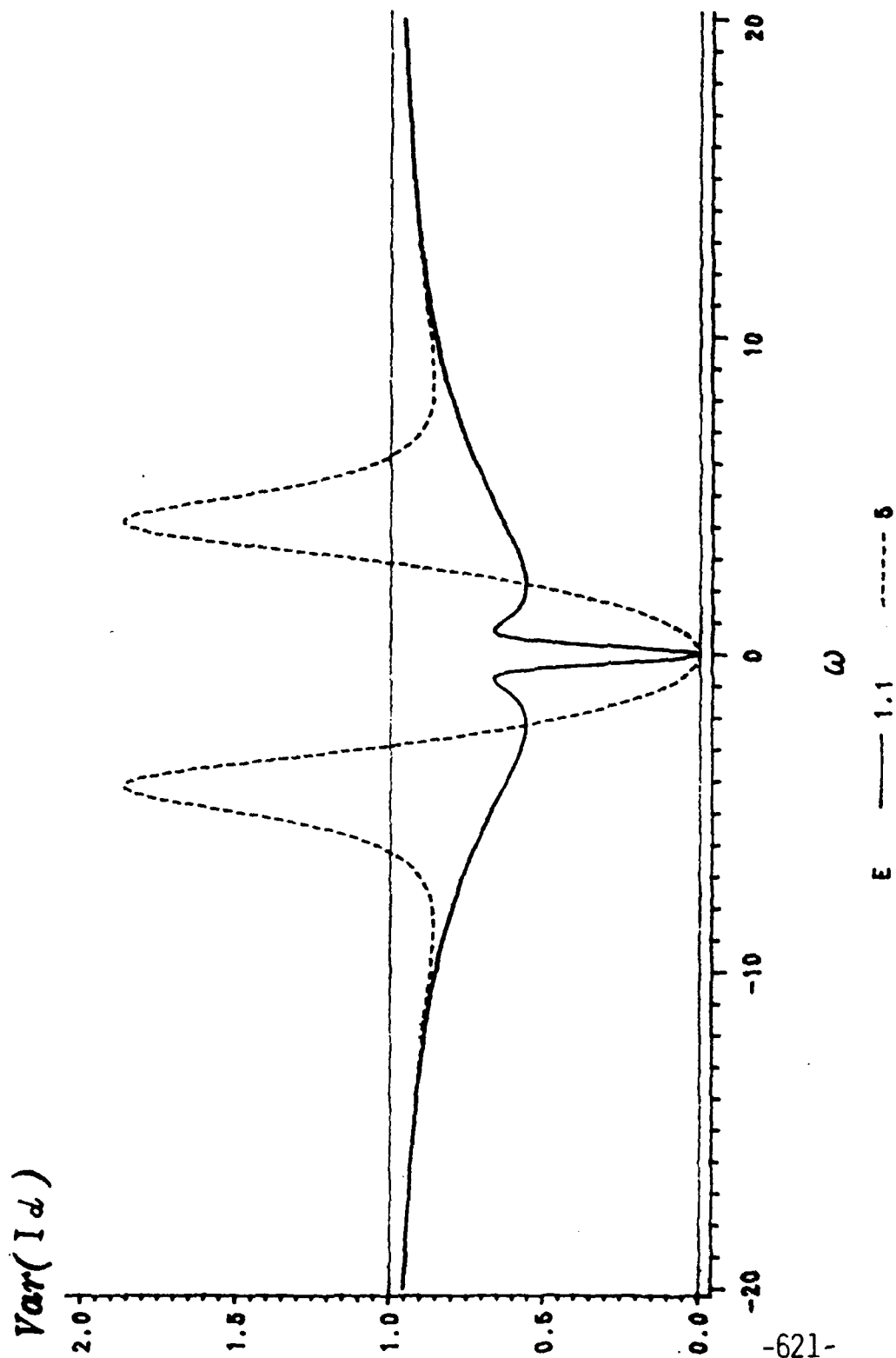
Paramp

$\kappa_0 = 1 \quad \kappa_1 = 1 \quad \kappa_2 = 2$

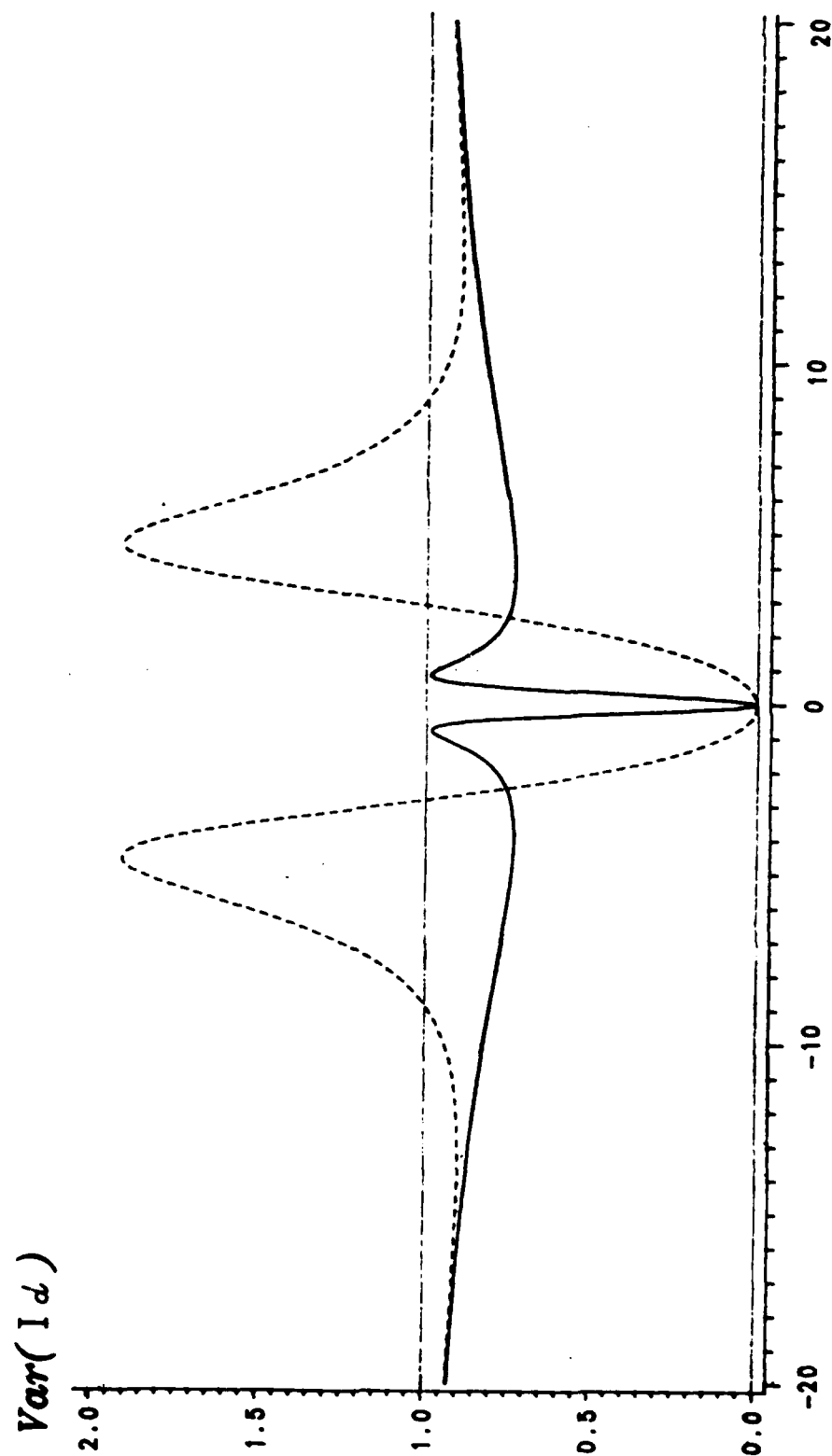


Paramp

$\kappa_0 = 1$ $\kappa_1 = 1$ $\kappa_2 = 5$



Param
 $\kappa_0 = 1 \quad \kappa_1 = 1 \quad \kappa_2 = 10$



ω
 E — 1.1 - - - - 5

High Loss pump $\gamma_c \gg 1$

$$\gamma_+ = \gamma_a + \gamma_b$$

$$\gamma_- = \gamma_a - \gamma_b$$

Eigenvalue

$$\lambda = -\frac{\gamma_+}{2} P \pm \frac{\gamma_+}{2} \left[(P-2)^2 + \frac{\gamma_-^2}{\gamma_+^2} 4(P-1) \right]^{\frac{1}{2}}$$

$P = 1$ threshold power

For $\left(\frac{\gamma_-}{\gamma_+}\right)^2 \ll 1$

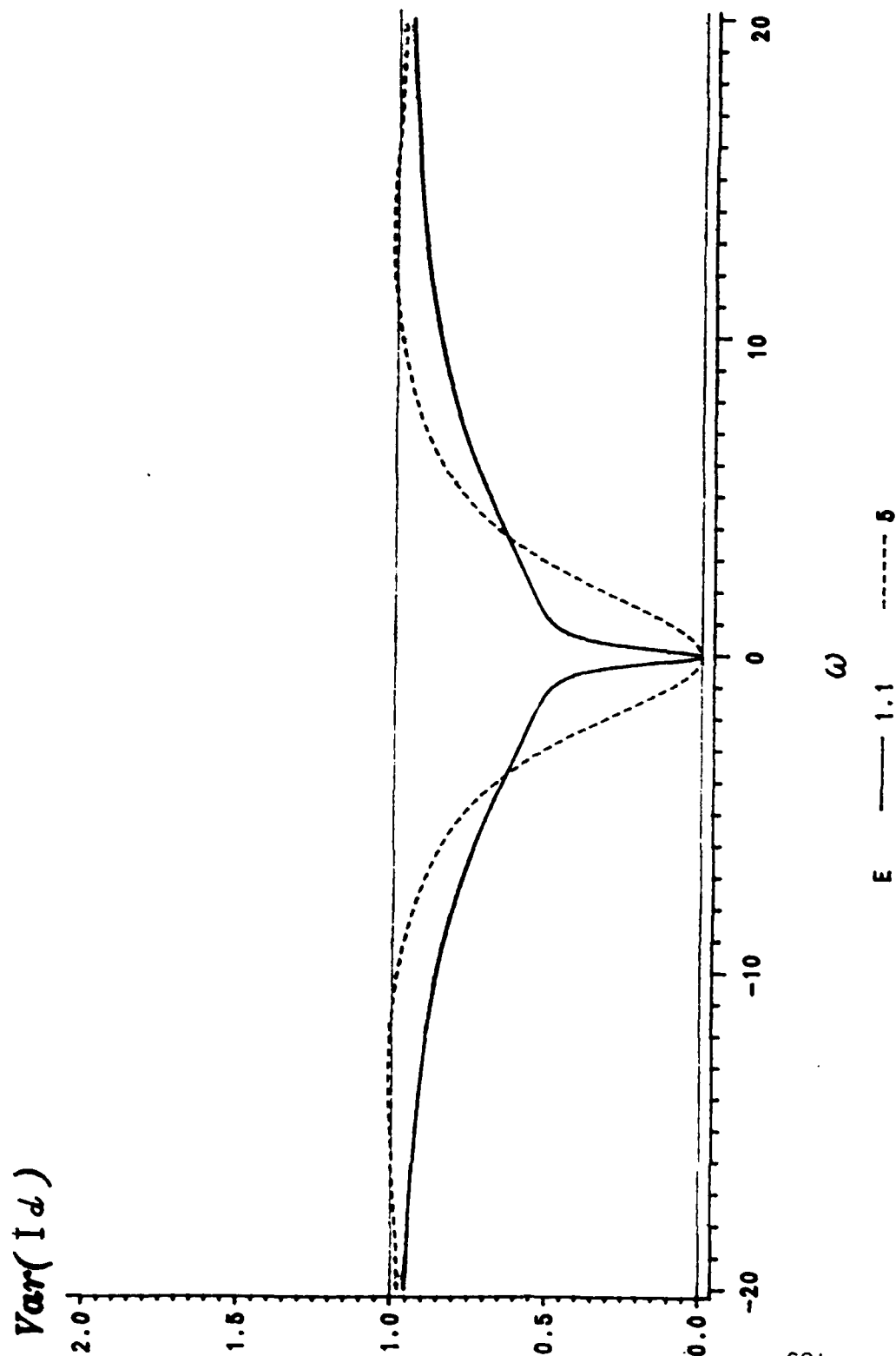
$$\lambda \approx -\gamma_+, -\gamma_+ (P-1)$$

just above threshold

linewidth $\sim \gamma_+ (P-1)$

power broadens to γ_+

Paramp
 $\kappa_0 = 10 \quad \kappa_1 = 1 \quad \kappa_2 = 5$



Low Loss Pump $\gamma_c \ll 1$

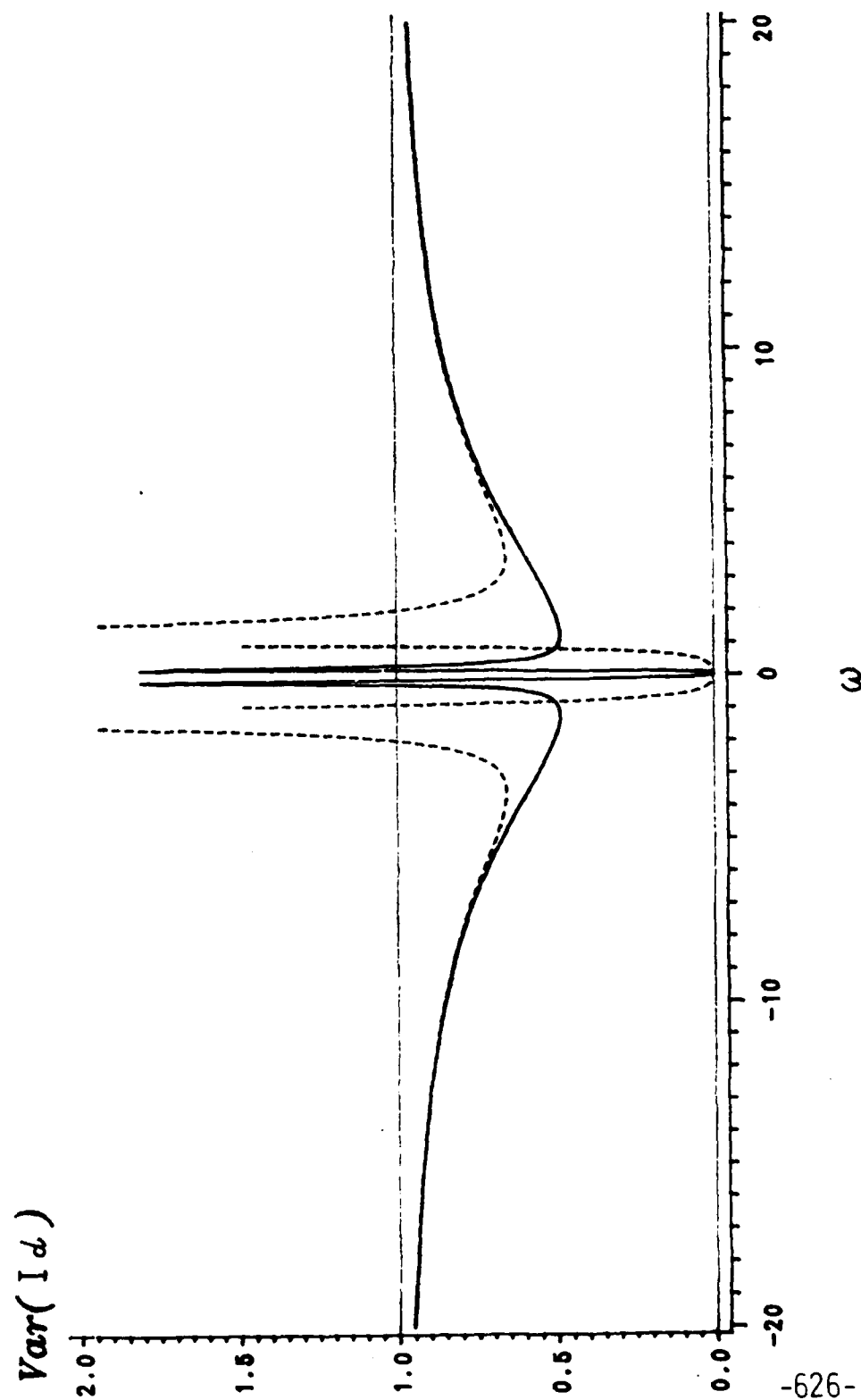
Eigenvalue

$$\lambda = -\frac{\gamma_c}{2} \pm \left[\gamma_c^2 - 4\gamma_c(P-1)\gamma_+ + 4\gamma_c(P-1)\frac{\gamma_-^2}{\gamma_+} \right]^{\frac{1}{2}}$$

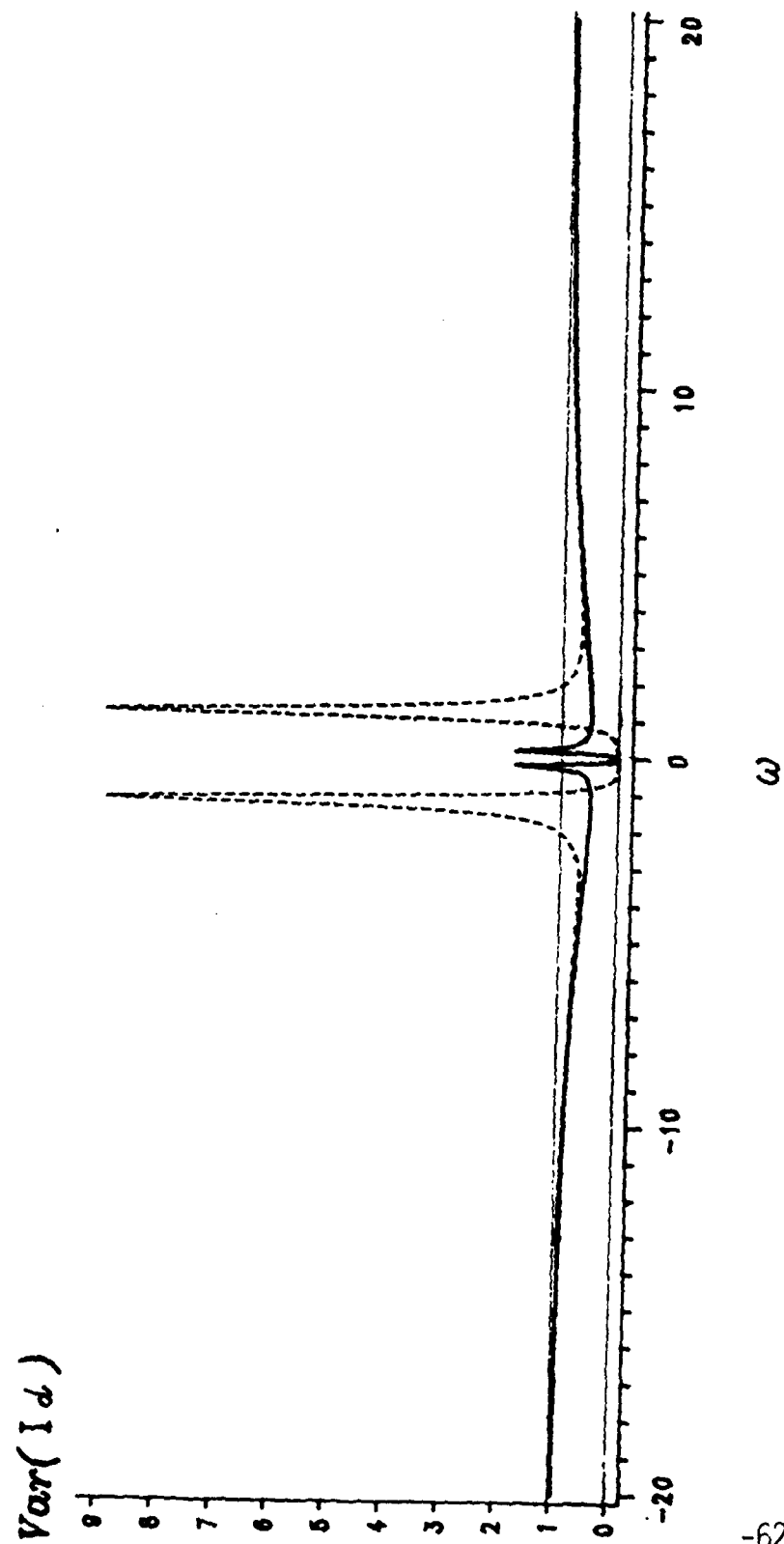
γ_c determines linewidth

sidebands appear for higher
pump powers

Paramp
 $\kappa_0 = 0.1 \quad \kappa_1 = 1 \quad \kappa_2 = 5$



Paramp
 $\kappa_0 = 0.1 \quad \kappa_1 = 1 \quad \kappa_2 = 5$



ϵ ——— 1.1 - - - - - 5

OPEN QUESTIONS IN CLOSED-LOOP PHOTODETECTION

Jeffrey H. Shapiro

Massachusetts Institute of Technology
Department of Electrical Engineering and Computer Science
Cambridge, Massachusetts 02139

The usual open-loop quantum and semiclassical theories of light detection apply to configurations in which there is no feedback from the photodetector to the light beam impinging on that detector [1] - [3]. In these circumstances there are unmistakable signatures of nonclassical light, such as sub-shot-noise spectra and sub-Poisson photocounts. No such unmistakable signatures exist for the case of closed-loop photodetection, i.e., for configurations in which there is a feedback path from the detector to the light source. This talk reviews recent progress [4], [5] in the theory of closed-loop photodetection, and extrapolates therefrom to possible future schemes for quantum-state synthesis and quantum-measurement synthesis.

References

- [1] J.H. Shapiro, H.P. Yuen, and J.A. Machado Mata, IEEE Trans. Inform. Theory IT-25, 179 (1979).
- [2] H.P. Yuen and J.H. Shapiro, IEEE Trans. Inform. Theory IT-26, 78 (1980).
- [3] J.H. Shapiro, IEEE J. Quantum Electron. QE-21, 237 (1985).
- [4] J.H. Shapiro, M.C. Teich, B.E.A. Saleh, P. Kumar, and G. Saplakoglu, Phys. Rev. Lett. 56, 1136 (1986).
- [5] J.H. Shapiro, G. Saplakoglu, S.-T. Ho, P. Kumar, M.C. Teich, and B.E.A. Saleh, J. Opt. Soc. Am. B4, xxxx (1987).

OPEN QUESTIONS IN CLOSED-LOOP PHOTODETECTION

J.H. SHAPIRO

MIT

ACKNOWLEDGEMENTS

H. P. YUEN

P. KUMAR

R. S. BONDURANT

G. SAPLAKOGLU

S.-T. HO

C. M. CAVES

B. YURKE

Y. YAMAMOTO

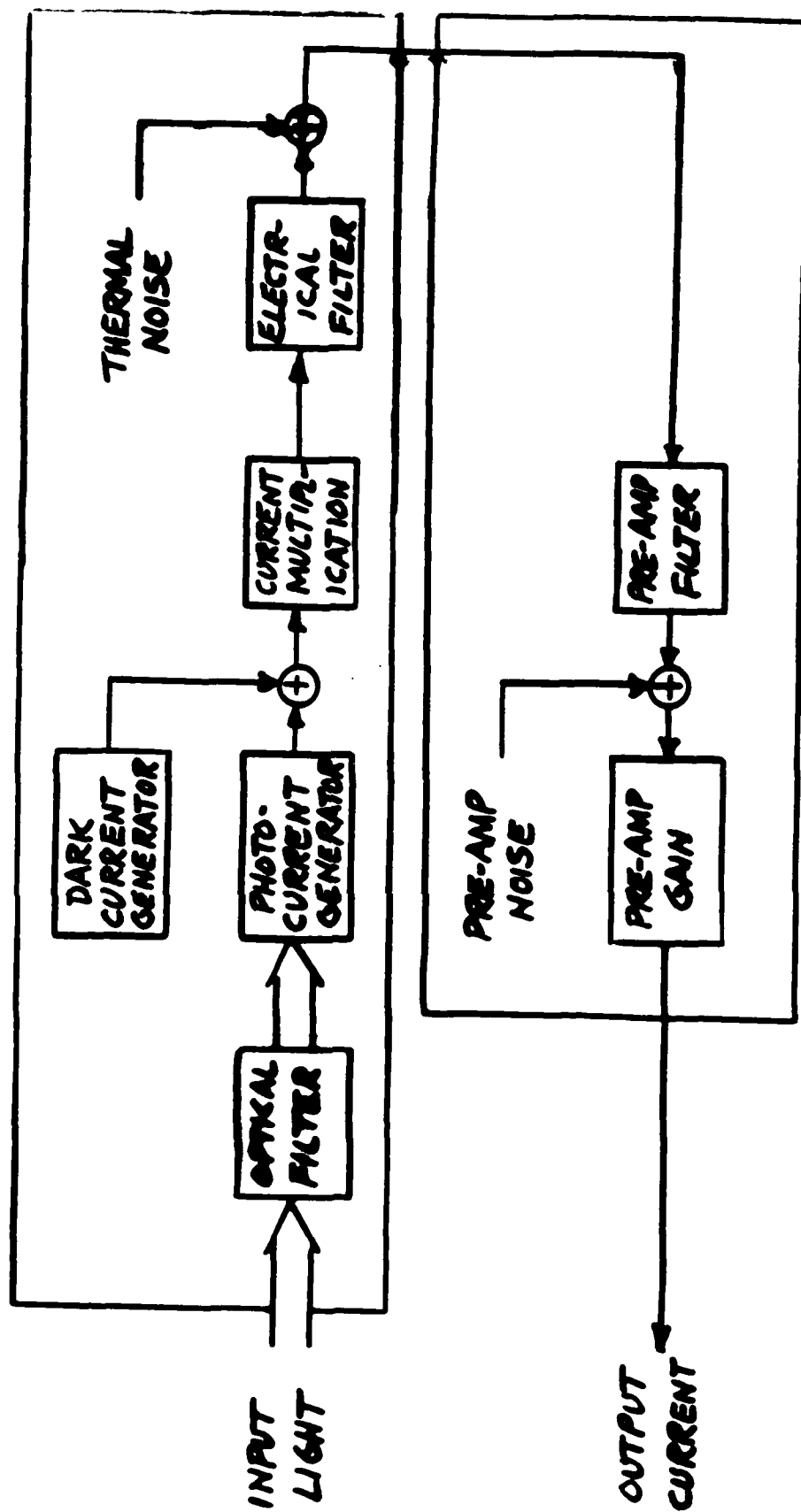
M. C. TEICH

B. E. A. SALEH

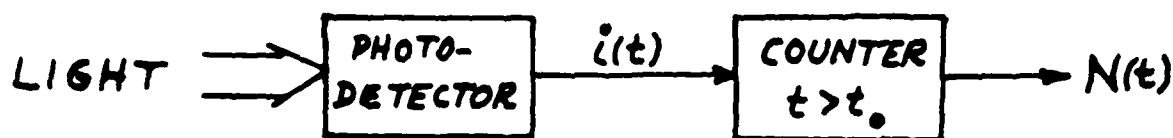
PHOTODETECTION STATISTICS

- **PHOTOCURRENT & PHOTOCOUNTS**
- **SELF-EXCITING PROCESSES**
Semiclassical vs. Quantum
- **CONVENTIONAL SYSTEMS**
Direct Detection
Nonclassical Signatures
- **UNCONVENTIONAL SYSTEMS**
Closed-Loop Photodetection
Quantum-State Synthesis
Quantum-Measurement Synthesis

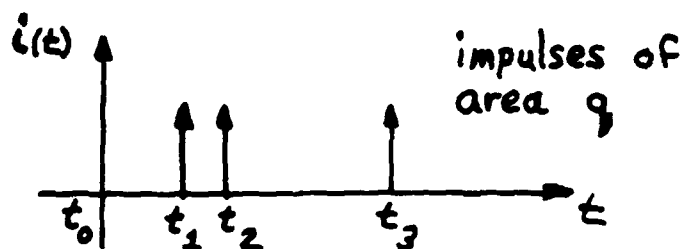
REAL PHOTODETECTION



PHOTOCURRENT & PHOTOCOUNTS



- LIGHT - QUASIMONOCHROMATIC PARAXIAL SCALAR WAVE: $E(\vec{x}, t)$ OR $\hat{E}(\vec{x}, t)$
- PHOTODETECTOR - IDEAL EXCEPT FOR $\eta < 1$
- PHOTOCURRENT



- PHOTOCOUNTS



SELF-EXCITING COUNTING PROCESSES

- $N(t)$ SELF-EXCITING -
EVENTS OCCUR ONE AT A TIME
WITH INCREMENTAL CONDITIONAL
PROBABILITIES

$$Pr[\Delta N_t = n | \underline{t}, N_t] \approx \begin{cases} 1 - \mu(t; \underline{t}, N_t) \Delta t, & n=0 \\ \mu(t; \underline{t}, N_t) \Delta t, & n=1 \\ 0, & n \geq 2 \end{cases}$$

WHERE $\Delta N_t \equiv N(t + \Delta t) - N(t)$

$\underline{t} \equiv (t_1, t_2, \dots, t_{N_t})$

event times up to t

$N_t \equiv N(t)$

events up to t

POISSON COUNTING PROCESSES

- $N(t)$ POISSON -

$$Pr[\Delta N_t = n | \underline{t}, N_t] \approx \begin{cases} 1 - \lambda(t)\Delta t, & n=0 \\ \lambda(t)\Delta t, & n=1 \\ 0, & n \geq 2 \end{cases}$$

WHERE $\lambda(t) \geq 0$ IS DETERMINISTIC

- POISSON PROCESS IS SELF-EXCITING PROCESS WITH

$$\mu(t; \underline{t}, N_t) = \lambda(t)$$

DOUBLY-STOCHASTIC POISSON PROCESSES

- $N(t)$ DOUBLY-STOCHASTIC
POISSON -

$$Pr[\Delta N_t = n | \underline{z}, N_t, \underline{\lambda}_t] \approx \begin{cases} 1 - \lambda(t)\Delta t, & n=0 \\ \lambda(t)\Delta t, & n=1 \\ 0, & n \geq 2 \end{cases}$$

WHERE $\lambda(t) \geq 0$ IS STOCHASTIC,
 $\underline{\lambda}_t \equiv \{ \lambda(\tau) : \tau \leq t \}$

- DOUBLY-STOCHASTIC POISSON
PROCESS IS SELF-EXCITING
PROCESS WITH

$$\mu(t; \underline{z}, N_t) = \langle \lambda(t) | \underline{z}, N_t \rangle$$

MULTICOINCIDENCE RATES

- kth ORDER MCR FOR CLASSICAL COUNTING PROCESS $N(t)$

$$w_k(t_1, t_2, \dots, t_k) = \lim_{\Delta t \rightarrow 0} (\Delta t)^{-k} \Pr \left[\left(\prod_{i=1}^k \Delta N_{t_i} \right) = 1 \right]$$

- $N(t)$ IS COMPLETELY CHARACTERIZED STATISTICALLY BY KNOWLEDGE OF MCRs

$$\{w_k(t_1, t_2, \dots, t_k) : 1 \leq k < \infty\}$$

- FOR EXAMPLE

$$\Pr[N(t) = n] =$$

$$\sum_{m=n}^{\infty} \frac{(-1)^{m-n}}{(m-n)! n!} \int_{t_0}^t dt_1 \dots \int_{t_0}^t dt_m w_m(t_1, t_2, \dots, t_m)$$

MOMENT STATISTICS

• PHOTOCOUNTS

MEAN- $\langle N(t) \rangle = \int_{t_0}^t ds w_1(s)$

VARIANCE-

$$\text{VAR}(N(t)) = \langle N(t) \rangle + \int_{t_0}^t ds \int_{t_0}^t ds' [w_2(s, s') - w_1(s)w_1(s')]$$

• PHOTOCURRENT

ASSUME $w_1(t) = w_1$, $w_2(t, s) = w_2(t-s)$

MEAN -

$$\langle i(t) \rangle = q w_1$$

NOISE SPECTRUM (BILATERAL) -

$$S_{ii}(f) = q \langle i \rangle + q^2 \int_{-\infty}^{\infty} d\tau [w_2(\tau) - w_1^2] e^{-j2\pi f\tau}$$

CLASSICAL FIELDS

- POSITIVE-FREQUENCY ELECTRIC FIELD
 $E^{(+)}(\bar{x}, t)$ volts/m units
 ILLUMINATES DETECTOR

- PHOTON-UNITS POSITIVE-FREQUENCY FIELD

$$E(\bar{x}, t) = \int d\nu \int d\tau (c\epsilon_0/2h\nu)^{1/2} E^{(+)}(\bar{x}, \tau) e^{-j2\pi\nu(t-\tau)}$$

$$\sqrt{\text{photons/m}^2\text{s}} \quad \text{units}$$

- MODAL EXPANSION

$$E(\bar{x}, t) = \sum_n \alpha_n \xi_n(\bar{x}, t), \quad \bar{x} \in \mathcal{A}_d, t \in \mathcal{T}$$

$\{\xi_n\}$ CON MODE SET

$\{\alpha_n\}$ COMPLEX-VALUED RANDOM
VARIABLES

QUANTUM FIELDS

- POSITIVE-FREQUENCY ELECTRIC FIELD OPERATOR $\hat{E}^{(+)}(\vec{r}, t)$ ILLUMINATES DETECTOR

- PHOTON-UNITS FIELD OPERATOR

$$\hat{E}(\vec{r}, t) = \int d\nu \int d\tau (\epsilon_0 / 2h\nu)^{1/2} \hat{E}^{(+)}(\vec{r}, \tau) e^{-j2\pi\nu(t-\tau)}$$

- MODAL EXPANSION

$$\hat{E}(\vec{r}, t) = \sum_{\vec{n}} \hat{a}_{\vec{n}} \xi_{\vec{n}}(\vec{r}, t), \quad \vec{r} \in \mathcal{A}_d, t \in \mathcal{T}$$

$\{\xi_{\vec{n}}\}$ CON MODE SET

$\{\hat{a}_{\vec{n}}\}$ MODAL ANNIHILATION OPERATORS

$\hat{\rho}$ = DENSITY OPERATOR (STATE) OF MODES

PHOTODETECTION MCRs

- SEMICLASSICAL THEORY

$$w_k(t_1, t_2, \dots, t_k) = \eta^k \langle P(t_1) P(t_2) \dots P(t_k) \rangle$$

WHERE

$$P(t) = \int_{A_d} d\vec{x} |E(\vec{x}, t)|^2$$

= CLASSICAL PHOTON FLUX

- QUANTUM THEORY

$$w_k(t_1, t_2, \dots, t_k) =$$

$$\int_{A_d} d\vec{x}_1 \dots \int_{A_d} d\vec{x}_k \langle \left(\prod_{i=1}^k \hat{E}^{\dagger}(\vec{x}_i, t_i) \right) \left(\prod_{i=1}^k \hat{E}'(\vec{x}_i, t_i) \right) \rangle$$

WHERE

$$\hat{E}'(\vec{x}, t) = \eta^{1/2} \hat{E}(\vec{x}, t) + (1-\eta)^{1/2} \hat{E}_{vac}(\vec{x}, t)$$

$\hat{E}_{vac}(\vec{x}, t)$ = FICTITIOUS VACUUM-STATE
FIELD OPERATOR

CONVENTIONAL SYSTEMS

- PHOTODETECTOR RUNS OPEN LOOP, $i(t)$ IS NOT FED BACK TO CONTROL LIGHT BEAM ILLUMINATING THE DETECTOR

- SEMICLASSICAL THEORY

$P(t)$ IS ORDINARY NON-NEGATIVE
RANDOM PROCESS

$$w_1(t) = \eta \langle P(t) \rangle$$

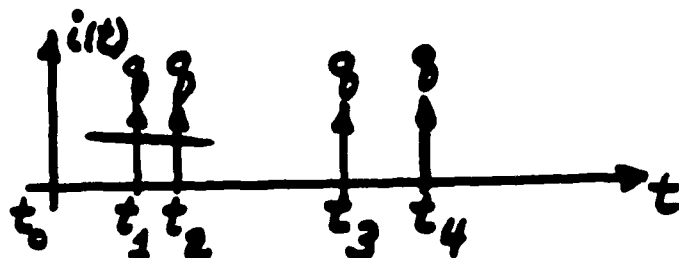
$$w_2(t, s) - w_1(t)w_1(s) = \eta^2 K_{pp}(t, s)$$

- QUANTUM THEORY

$\hat{\rho}$ IS ORDINARY FREE-FIELD
DENSITY OPERATOR

DIRECT DETECTION

- PHOTOCURRENT



- SEMICLASSICAL STATISTICS

(i) CONDITIONALLY POISSON WITH
EMISSION RATE $\eta \int_{A_d} |E(\vec{x}, t)|^2 d\vec{x}$

- QUANTUM STATISTICS

(i) MEASURES $g \int_{A_d} \hat{E}'^\dagger(\vec{x}, t) \hat{E}'(\vec{x}, t) d\vec{x}$

$$\hat{E}'(\vec{x}, t) = \eta^{1/2} \hat{E}(\vec{x}, t) + (1-\eta)^{1/2} \hat{E}_{VAC}(\vec{x}, t)$$

$\hat{E}_{VAC}(\vec{x}, t)$ = FICTITIOUS VACUUM-STATE
FIELD OPERATOR

DIRECT DETECTION

- NOISE IN $i(t)$ IS -
DETECTOR SHOT NOISE IN THE
SEMICLASSICAL MODEL

\hat{E}' QUANTUM NOISE IN THE
QUANTUM MODEL

- SEMICLASSICAL STATISTICS ARE
QUANTITATIVELY CORRECT IF
 $\hat{\rho}$ IS A CLASSICAL STATE,
i.e., IF

$$\hat{\rho} = \int d^2\alpha \, P(\alpha; \alpha^*) |\alpha\rangle \langle \alpha|$$

FOR $|\alpha\rangle =$ MULTIMODE COHERENT STATE

$P(\alpha; \alpha^*) =$ CLASSICAL PROBABILITY
DENSITY

NONCLASSICAL SIGNATURES

- SEMICLASSICAL THEORY

$K_{pp}(t,s)$ POSITIVE SEMIDEFINITE

$$\Rightarrow \text{VAR}(N(t)) \geq \langle N(t) \rangle$$

$$g_{ii}(f) \geq g \langle i(t) \rangle$$

- QUANTUM THEORY

$\text{VAR}(N(t)) < \langle N(t) \rangle$ possible,
SUB-POISSONIAN BEHAVIOR

$g_{ii}(f) < g \langle i(t) \rangle$ possible,
SUB-SHOT NOISE BEHAVIOR

UNCONVENTIONAL SYSTEMS

- PHOTODETECTOR RUNS CLOSED LOOP; $i(t)$ IS FED BACK TO CONTROL LIGHT BEAM ILLUMINATING THE DETECTOR
- SELF-EXCITING PROCESS
CHARACTERIZATION IN TERMS OF MCRs STILL VALID
- SEMICLASSICAL THEORY
 $w_2(t,s) - w_1(t)w_1(s)$ IS NOT A COVARIANCE
 $\text{VAR}(N(t)) < \langle N(t) \rangle$ possible
 $S_{ii}(f) < g \langle i(t) \rangle$ possible

DIRECT DETECTION

- PHOTOCURRENT



- SEMICLASSICAL STATISTICS

$i(t)$ IS SELF-EXCITING WITH
EMISSION RATE $\eta \int_{A_d} |E(\vec{r}, t)|^2 d\vec{r}$

$E(\vec{r}, t)$ DEPENDS EXPLICITLY ON
PAST MEASUREMENTS

- QUANTUM STATISTICS

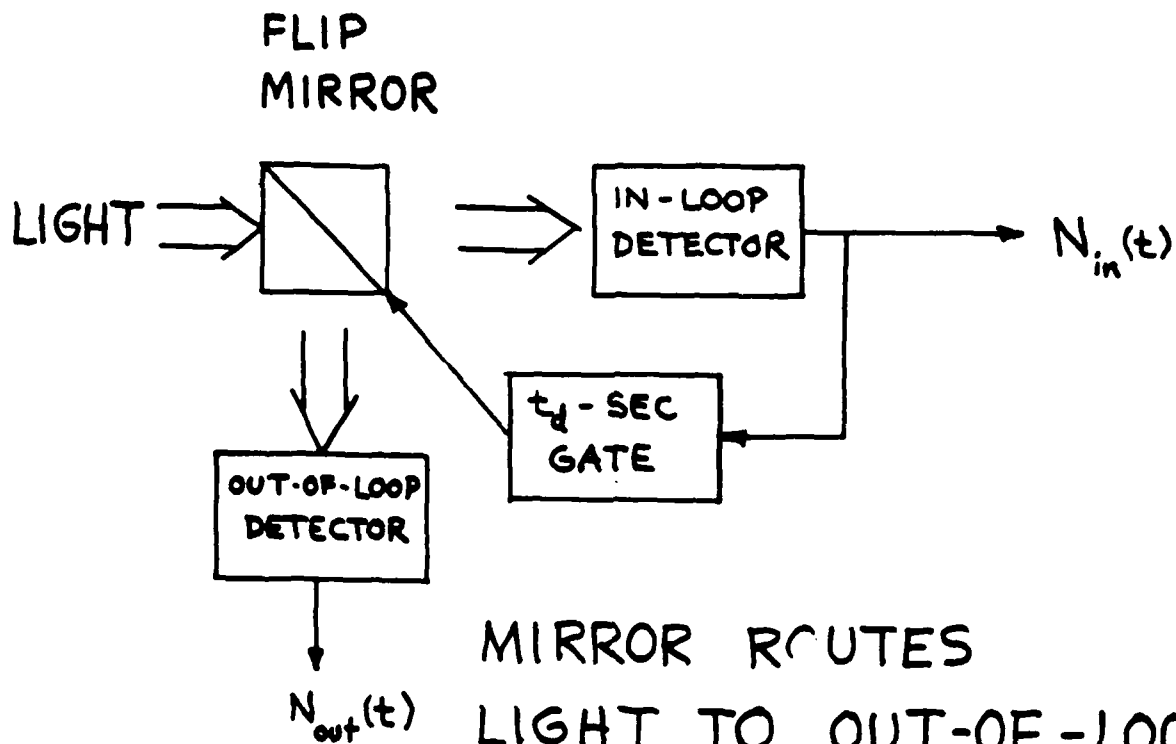
$i(t)$ MEASURES $\eta \int_{A_d} \hat{E}^\dagger(\vec{r}, t) \hat{E}'(\vec{r}, t) d\vec{r}$

$\hat{E}(\vec{r}, t)$ DEPENDS EXPLICITLY ON
PAST MEASUREMENTS

DIRECT DETECTION

- SEMICLASSICAL THEORY IS QUANTITATIVELY CORRECT IF BREAKING THE FEEDBACK LOOP LEAVES THE DETECTOR ILLUMINATED BY A CLASSICAL-STATE DENSITY OPERATOR $\hat{\rho}$
- SUB-POISSONIAN PHOTOCOUNTS
 $\text{VAR}(N(t)) < \langle N(t) \rangle$
POSSIBLE SEMICLASSICALLY
- SUB-SHOT NOISE SPECTRA
 $S_{ii}(f) < g \langle i(t) \rangle$
POSSIBLE SEMICLASSICALLY
- NO UNMISTAKABLE NONCLASSICAL SIGNATURES

DEAD-TIME SYSTEM



MIRROR ROUTES
LIGHT TO OUT-OF-LOOP
DETECTOR FOR t_d -SEC
AFTER EACH IN-LOOP
PHOTOCOUNT

WALKER & JAKEMAN (1985)

DEAD-TIME RESULTS

- SEMICLASSICAL AND QUANTUM THEORIES AGREE
- STEADY-STATE t -SEC COUNTING STATISTICS, $t \gg t_d$

$$\langle N_{in} \rangle \approx \lambda t / (1 + \lambda t_d)$$

$$\langle N_{out} \rangle = \lambda t - \langle N_{in} \rangle$$

$$\text{VAR}(N_{in}) \approx \langle N_{in} \rangle / (1 + \lambda t_d)^2$$

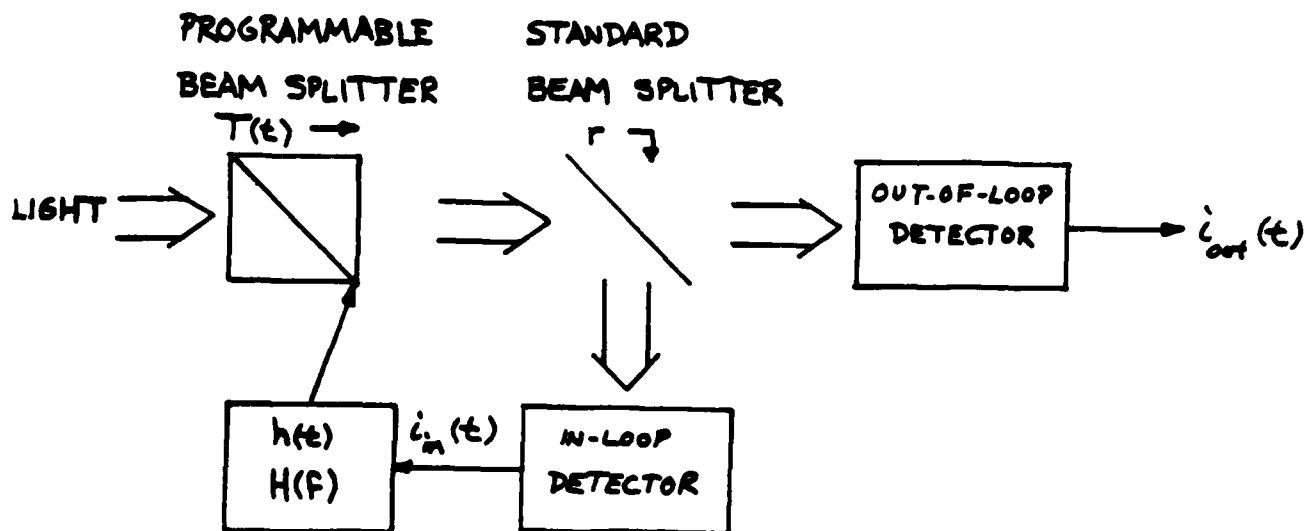
$$\text{VAR}(N_{out}) \approx \langle N_{out} \rangle \left[1 + \lambda t_d / (1 + \lambda t_d)^2 \right]$$

λ = AVERAGE DETECTED PHOTONS/SEC

t_d = DEAD TIME

t = COUNTING INTERVAL DURATION

LINEAR FEEDBACK



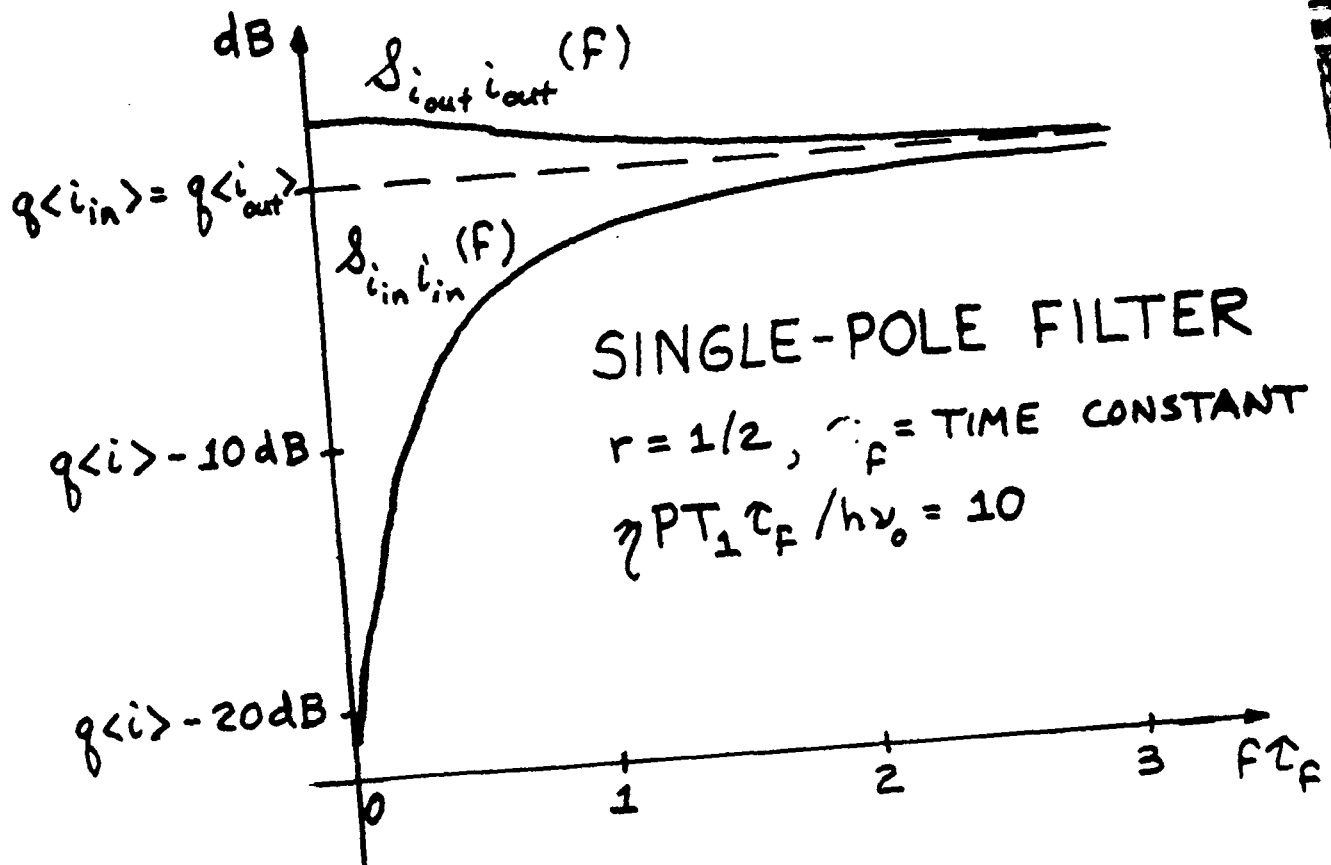
NEGATIVE LINEAR INTENSITY
FEEDBACK IN HIGH SNR REGIME

$$T(t) = T_0 - T_1 \int_{-\infty}^t q^{-1} i_{in}(\tau) h(t-\tau) d\tau$$

YAMAMOTO, IMOTO, & MACHIDA (1986)

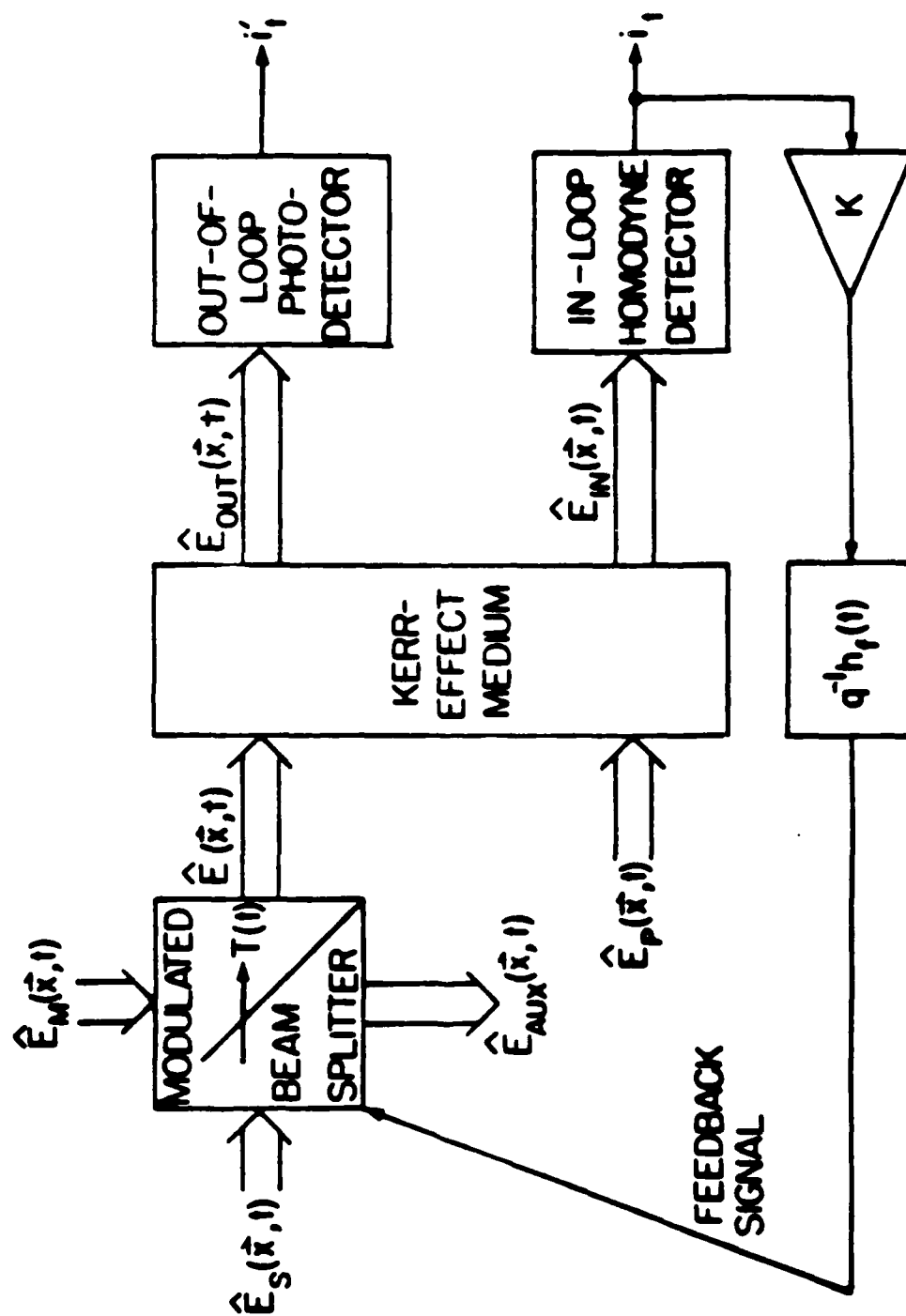
LINEAR FEEDBACK

- SEMICLASSICAL AND QUANTUM THEORIES AGREE

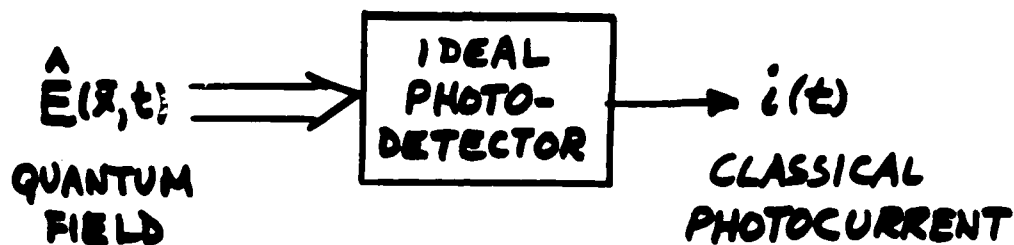


- IN-LOOP QUANTUM FIELD VIOLATES FREE-FIELD UNCERTAINTY PRINCIPLE

SQUEEZED-STATE GENERATION



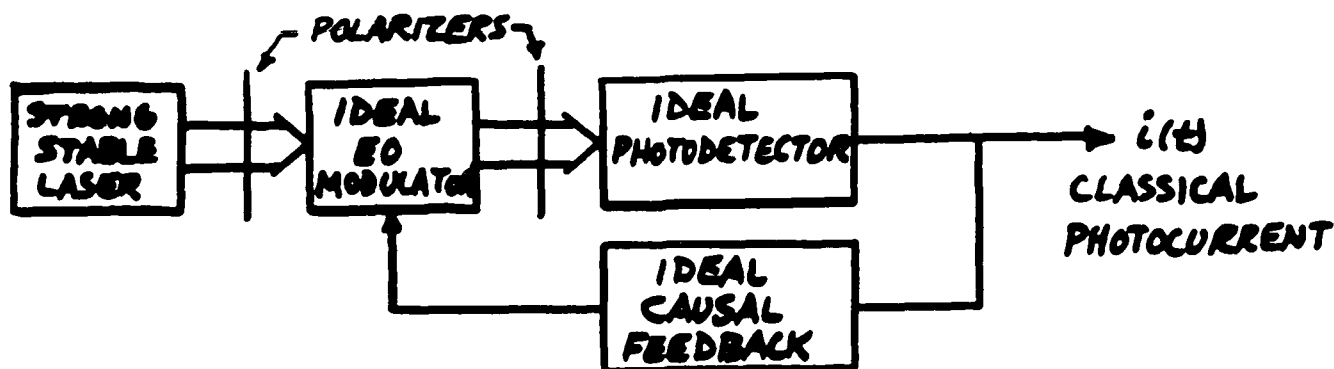
QUANTUM STATE SYNTHESIS



- $\hat{E}(\vec{r}, t)$ IN ARBITRARY STATE $\hat{\rho}$
- DETECTOR IS IDEAL, $\eta = 1$
- $i(t)$ IS SELF-EXCITING IMPULSE PROCESS WITH ARBITRARY CONDITIONAL RATE

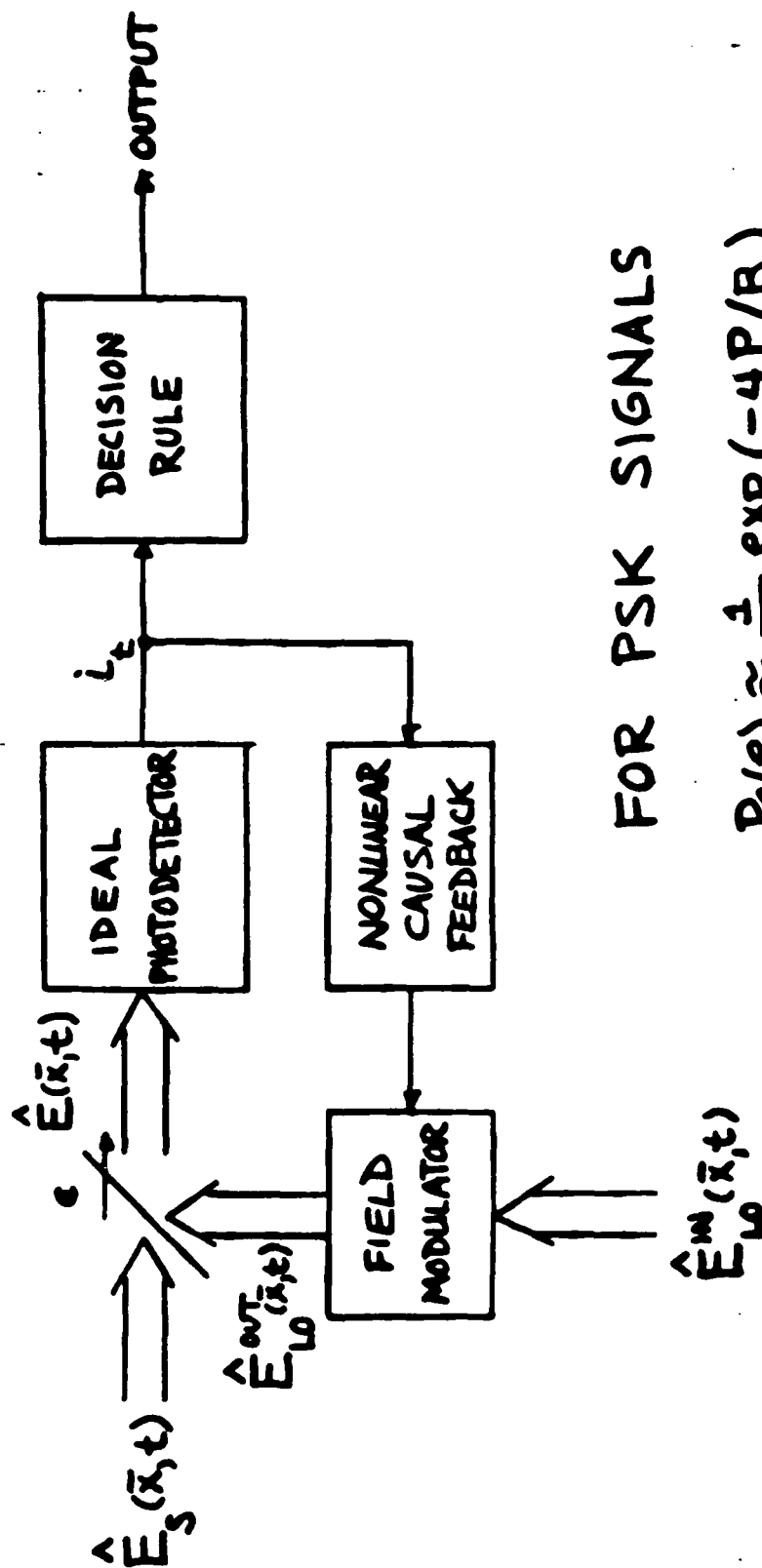
$$\mu(t; \underline{t}, N_t) = \lim_{\Delta t \rightarrow 0} (\Delta t)^{-1} \text{Pr}[\Delta N_t = 1 | \underline{t}, N_t]$$

QUANTUM STATE SYNTHESIS



- CLASSICAL FIELD $E(\vec{x}, t)$ ILLUMINATES DETECTOR
- $i(t)$ IS SELF-EXCITING IMPULSE PROCESS WITH CONDITIONAL RATE $p(t; \underline{x}, N_t)$
- WITH APPROPRIATE FEEDBACK, ANY $p(t; \underline{x}, N_t)$ IS OBTAINABLE
- WITH QND, OPEN LOOP $\hat{E}(\vec{x}, t)$ GIVING ANY $p(t; \underline{x}, N_t)$ IS OBTAINABLE

COHERENT-STATE RECEIVER



FOR PSK SIGNALS

$$Pr(e) \approx \frac{1}{4} \exp(-4P/B)$$

P = AVERAGE PHOTON FLUX

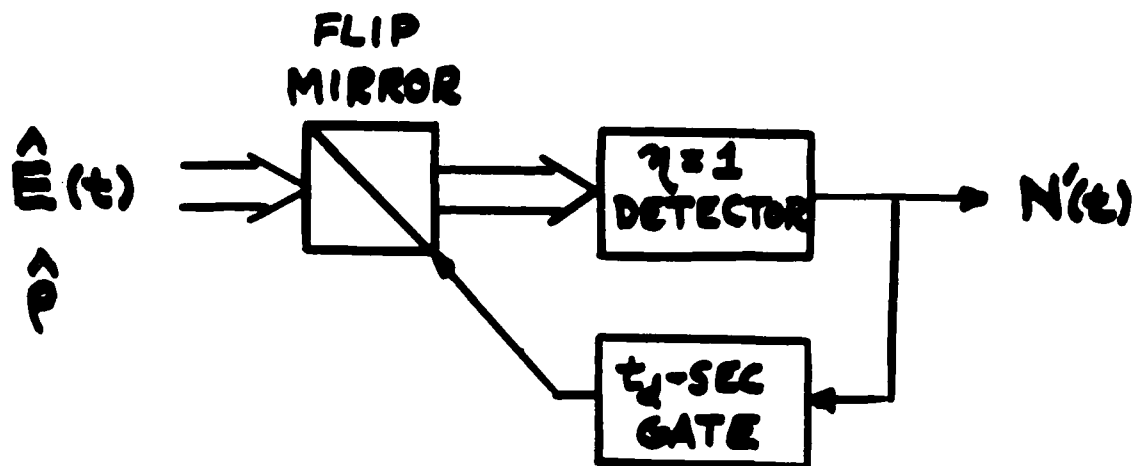
B = BANDWIDTH

DUALITY

- **CLOSED-LOOP SYSTEM AS
STATE SYNTHESIS -
DETECTOR MAKES USUAL
MEASUREMENT,
FEEDBACK TRANSFORMS
INPUT STATE**
- **CLOSED-LOOP SYSTEM AS
MEASUREMENT SYNTHESIS -
INPUT STATE UNCHANGED,
FEEDBACK TRANSFORMS
DETECTOR MEASUREMENT**

DEAD-TIME SYSTEM

• MEASUREMENT SYNTHESIS



$$dN'_t \equiv \lim_{\Delta t \rightarrow 0} \Delta N'_t \quad \text{MEASURES} \quad \int dN'_t |dN_t\rangle \langle dN_t|$$

$|dN_t\rangle = \text{MULTIMODE NUMBER STATE}$

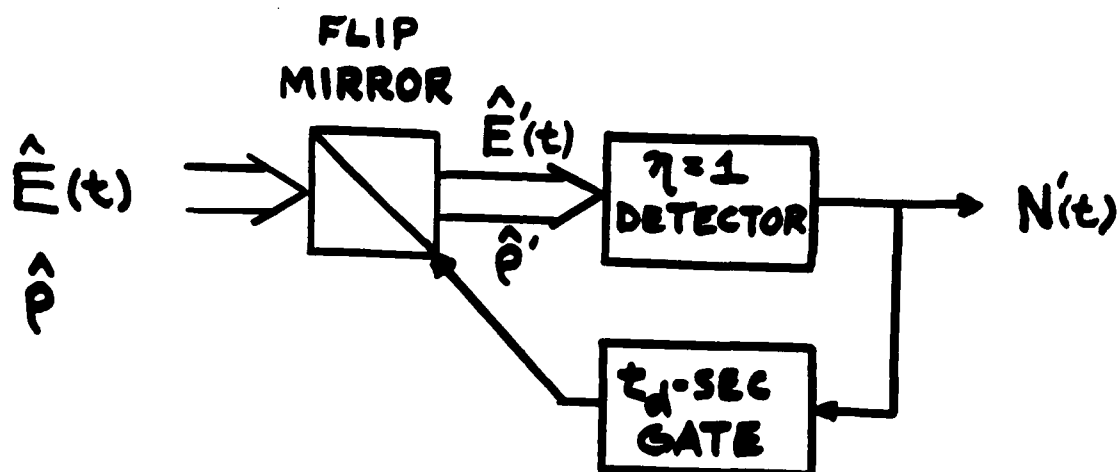
$$dN_t \equiv \{dN_c : t_0 \leq \tau \leq t\}$$

$dN_c = 1$ INDICATES PHOTON AT TIME c

$$dN'_t = \left[1 - u\left(\int_{t-t_d}^t dN_c\right) \right] dN_t$$

DEAD-TIME SYSTEM

• STATE SYNTHESIS



$$dN'_t \equiv \lim_{\Delta t \rightarrow 0} \Delta N'_t \text{ MEASURES } \hat{E}'^T(t) \hat{E}'(t) dt$$

$$\langle dN'_t | \hat{p}' | dN'_t \rangle = \int_{dN_t \in \Theta^{-1}(dN'_t)} \langle dN_t | \hat{p} | dN_t \rangle$$

$$dN_t \xrightarrow{\Theta} dN'_t \text{ IS THE MAP}$$

$$dN'_t = \left[1 - u\left(\int_{t-t_d}^t dN_t\right) \right] dN_t$$

OPEN QUESTIONS

- WHAT MEASUREMENTS CAN BE SYNTHESIZED VIA PHOTODETECTION FEEDBACK?
- WHAT STATES CAN BE SYNTHESIZED VIA PHOTODETECTION FEEDBACK?

REPORT DOCUMENTATION PAGE

1a. REPORT SECURITY CLASSIFICATION Unclassified			1b. RESTRICTIVE MARKINGS A186935		
2a. SECURITY CLASSIFICATION AUTHORITY			3. DISTRIBUTION / AVAILABILITY OF REPORT Approved for public release; distribution unlimited		
2b. DECLASSIFICATION / DOWNGRADING SCHEDULE			4. PERFORMING ORGANIZATION REPORT NUMBER(S)		
6a. NAME OF PERFORMING ORGANIZATION Research Laboratory of Electronics Massachusetts Institute of Technology			7a. NAME OF MONITORING ORGANIZATION		
6b. ADDRESS (City, State, and ZIP Code) 77 Massachusetts Avenue Cambridge, MA 02139			7b. ADDRESS (City, State, and ZIP Code)		
8a. NAME OF FUNDING / SPONSORING ORGANIZATION Office of Naval Research		8b. OFFICE SYMBOL (if applicable)		9. PROCUREMENT INSTRUMENT IDENTIFICATION NUMBER N00014-87-G-0198	
8c. ADDRESS (City, State, and ZIP Code) 800 North Quincy Street Arlington, Virginia 22217 - 5000		10. SOURCE OF FUNDING NUMBERS			
		PROGRAM ELEMENT NO. 41		PROJECT NO. 24502---01	
		TASK NO.		WORK UNIT ACCESSION NO.	
11. TITLE (Include Security Classification) United States - Japan Seminar on Quantum Mechanical Aspects of Quantum Electronics Hilton Inn Resort, Monterey, California - July 21-24, 1987					
12. PERSONAL AUTHOR(S) J. H. Shapiro and H. Takuma, Coordinators					
13a. TYPE OF REPORT Proceedings		13b. TIME COVERED FROM TO		14. DATE OF REPORT (Year, Month, Day) October 1987	
				15. PAGE COUNT 660	
16. SUPPLEMENTARY NOTATION					
17. COSATI CODES			18. SUBJECT TERMS (Continue on reverse if necessary and identify by block number)		
FIELD	GROUP	SUB-GROUP			
19. ABSTRACT (Continue on reverse if necessary and identify by block number)					
<p>These Proceedings represent summaries and viewgraphs from a U.S. - Japan Seminar entitled "Quantum Mechanical Aspects of Quantum Electronics," which was held from July 21 to July 24, 1987 at the Hilton Inn Resort in Monterey, California. The Seminar focused on: neutral atom trapping; ultrahigh stability sources and ultrahigh resolution spectroscopy; squeezed states of light; and nonlinear optics of semiconductors.</p>					
20. DISTRIBUTION / AVAILABILITY OF ABSTRACT <input checked="" type="checkbox"/> UNCLASSIFIED/UNLIMITED <input type="checkbox"/> SAME AS RPT <input type="checkbox"/> DTIC USERS			21. ABSTRACT SECURITY CLASSIFICATION Unclassified		
22a. NAME OF RESPONSIBLE INDIVIDUAL Kyra M. Hall			22b. TELEPHONE (Include Area Code) (617) 253-2569		22c. OFFICE SYMBOL

END

FEB.

1988

DTic